frontiers | Research Topics

Unravelling the complex and multifaceted role of the cerebellum in health and disease

Edited by
Marija Cvetanovic, Paul J. Mathews, Erik Sean Carlson, Anne-Lise Paradis and Krystal Lynn Parker

Published in
Frontiers in Systems Neuroscience
Frontiers in Cellular Neuroscience

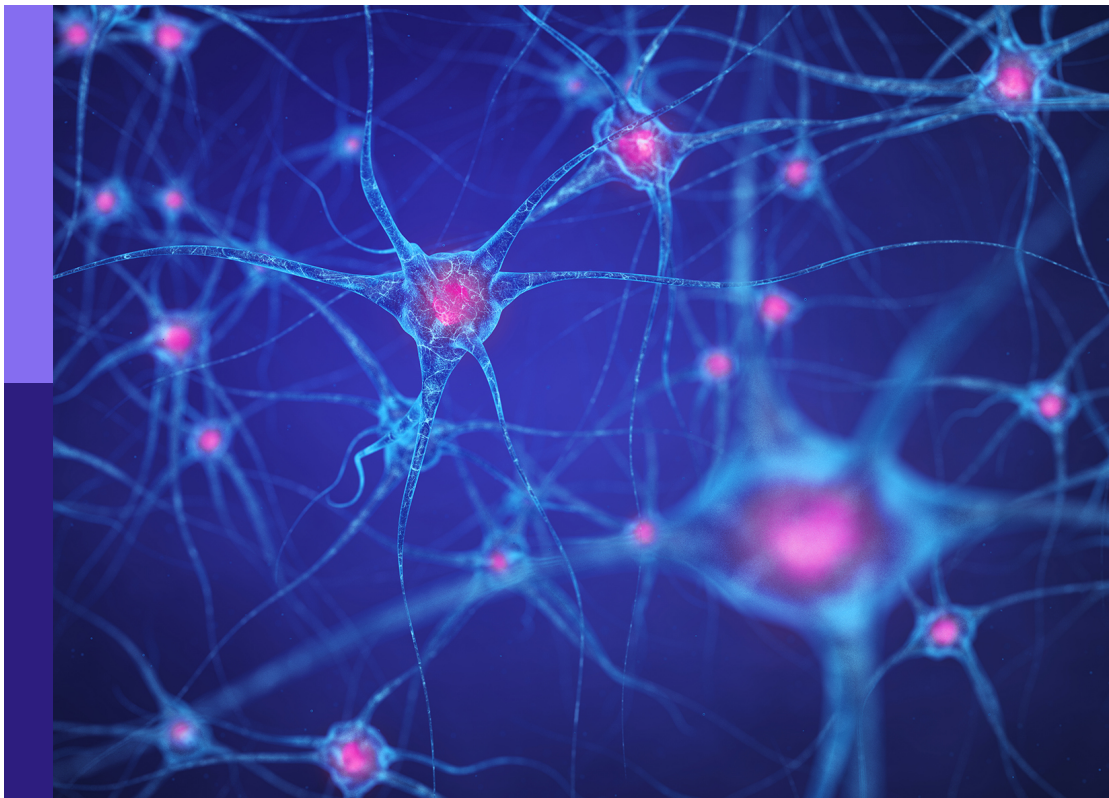

ISSN 1664-8714
ISBN 978-2-83252-109-0
DOI 10.3389/978-2-83252-109-0

About Frontiers

Frontiers is more than just an open access publisher of scholarly articles: it is a pioneering approach to the world of academia, radically improving the way scholarly research is managed. The grand vision of Frontiers is a world where all people have an equal opportunity to seek, share and generate knowledge. Frontiers provides immediate and permanent online open access to all its publications, but this alone is not enough to realize our grand goals.

Frontiers journal series

The Frontiers journal series is a multi-tier and interdisciplinary set of open-access, online journals, promising a paradigm shift from the current review, selection and dissemination processes in academic publishing. All Frontiers journals are driven by researchers for researchers; therefore, they constitute a service to the scholarly community. At the same time, the *Frontiers journal series* operates on a revolutionary invention, the tiered publishing system, initially addressing specific communities of scholars, and gradually climbing up to broader public understanding, thus serving the interests of the lay society, too.

Dedication to quality

Each Frontiers article is a landmark of the highest quality, thanks to genuinely collaborative interactions between authors and review editors, who include some of the world's best academicians. Research must be certified by peers before entering a stream of knowledge that may eventually reach the public - and shape society; therefore, Frontiers only applies the most rigorous and unbiased reviews. Frontiers revolutionizes research publishing by freely delivering the most outstanding research, evaluated with no bias from both the academic and social point of view. By applying the most advanced information technologies, Frontiers is catapulting scholarly publishing into a new generation.

What are Frontiers Research Topics?

Frontiers Research Topics are very popular trademarks of the *Frontiers journals series*: they are collections of at least ten articles, all centered on a particular subject. With their unique mix of varied contributions from Original Research to Review Articles, Frontiers Research Topics unify the most influential researchers, the latest key findings and historical advances in a hot research area.

Find out more on how to host your own Frontiers Research Topic or contribute to one as an author by contacting the Frontiers editorial office: frontiersin.org/about/contact

Unravelling the complex and multifaceted role of the cerebellum in health and disease

Topic editors

Marija Cvetanovic — University of Minnesota Twin Cities, United States
Paul J. Mathews — Lundquist Institute for Biomedical Innovation, United States
Erik Sean Carlson — University of Washington, United States
Anne-Lise Paradis — Sorbonne Université, France
Krystal Lynn Parker — The University of Iowa, United States

Citation

Cvetanovic, M., Mathews, P. J., Carlson, E. S., Paradis, A.-L., Parker, K. L., eds. (2023). *Unravelling the complex and multifaceted role of the cerebellum in health and disease*. Lausanne: Frontiers Media SA. doi: 10.3389/978-2-83252-109-0

Table of contents

frontiers | Frontiers in Systems Neuroscience

TYPE Editorial
PUBLISHED 23 March 2023
DOI 10.3389/fnsys.2023.1155939

OPEN ACCESS

EDITED AND REVIEWED BY
Olivia Gosseries,
University of Liège, Belgium

*CORRESPONDENCE
Paul James Mathews
✉ pmathews@ucla.edu

RECEIVED 01 February 2023
ACCEPTED 28 February 2023
PUBLISHED 23 March 2023

CITATION
Mathews PJ, Paradis A-L, Cvetanovic M, Carlson ES and Parker KL (2023) Editorial: Unravelling the complex and multifaceted role of the cerebellum in health and disease. *Front. Syst. Neurosci.* 17:1155939. doi: 10.3389/fnsys.2023.1155939

Editorial: Unravelling the complex and multifaceted role of the cerebellum in health and disease

Paul James Mathews[1,2]*, Anne-Lise Paradis[3], Marija Cvetanovic[4], Erik Sean Carlson[5,6] and Krystal Lynn Parker[7]

[1]Department of Neurology, University of California, Los Angeles School of Medicine, Los Angeles, Los Angeles, CA, United States, [2]Department of Neurology and Institute for Neurotherapeutics, Lundquist Institute for Biomedical Innovation, Torrance, CA, United States, [3]Neurosciences Paris-Seine, Institut de Biologie Paris-Seine (IBPS), Sorbonne Université, CNRS, Inserm, Paris, France, [4]Department of Neuroscience, Institute for Translational Neuroscience, University of Minnesota Twin Cities, St. Paul, MN, United States, [5]Department of Psychiatry and Behavioral Sciences, University of Washington, Seattle, WA, United States, [6]Geriatric Research, Education, and Clinical Center at the Veteran's Affairs Puget Sound Medical Center, Seattle, WA, United States, [7]Department of Psychiatry and the Iowa Neuroscience Institute, The University of Iowa, Iowa City, IA, United States

KEYWORDS

cerebellum, cerebellum-forebrain connectivity, movement disorders, developmental anomalies, computational modeling, cognition, emotion, pain

Editorial on the Research Topic
Unravelling the complex and multifaceted role of the cerebellum in health and disease

The cerebellum is a fascinating brain area to research. It contains most of the brain's neurons, is composed of a highly structured and stereotypical arrangement of cells, has a similar cortical area as the cerebrum, is highly interconnected with the forebrain and brainstem, and has expanded in size over the course of evolution to sustain increased mental and physical capacity. For over 100 years, specific dysfunction in or damage to the cerebellum has been known to cause dramatic deficits in motor coordination. Now, with novel behavioral assessment and advanced technological tools, including computational modeling, functional neuroimaging, advanced tract tracing methods, neuromodulatory tools, and the ability to directly modify gene expression, mounting evidence has dramatically broadened the fields perspective of the cerebellum's role in healthy behavior, implicating it in regulating cognition, mood, reward, decision making, pain, and addiction.

The purpose of this Editorial Research Topic is to collect new and important research focused on how the interconnectivity of the cerebellum with the rest of the brain shapes a wide breadth of functions underlying typical behavior and may explain disease related dysfunction.

Major advancements in our understanding of the cerebellum's role in behavior derive from advances in tract tracing, neural circuit studies, computational modeling approaches, and functional neuroimaging. In the review by McAfee et al., the authors provide a new perspective on cerebellum-forebrain interaction in which the cerebellum coordinates neuronal communication between multiple cerebral cortical regions in a task dependent manner. The authors review studies supporting the cerebellum's role in coordinating cerebral/forebrain activity by influencing cerebral oscillations. The importance of cerebellum-forebrain interactions is further highlighted by Jung et al., where they report using transneuronal tracing techniques and *ex vivo* optophysiology to demonstrate an indirect cerebellar input to the amygdala. This circuit provides a pathway for the cerebellum to impact emotion and potentially pain as discussed in the article by Wang et al. In their review, they detail several downstream potential targets of the cerebellum, including the

amygdala, where the cerebellum could disrupt normal circuit function to induce perceptions of pain in migraine headaches. Woodward et al. provide another example of what can happen when cerebellum-forebrain communication becomes dysregulated, detailing in their review how changes in the neural signaling dynamics of the cerebello-thalamo-cortical network in a harmaline-induced mouse model may be a key feature of the motor disease, essential tremor. These articles highlight the diverse array of known and still to be discovered areas of the brain in which the cerebellum has the potential to normally or abnormally influence neural activity.

Behavioral and computational/theoretical modeling studies provide complementary insight on how cerebro-cerebellar networks are organized and what type of signal processing they sustain. The review article by Laurens presents a novel theoretical framework built on prior experimental findings. He posits that the nodulus and uvula (NU) of the cerebellum contributes to the perception of head rotation, positional tilt with respect to gravity, translational motion, and helps distinguish self-generated from externally induced involuntary head movements *via* an internal model that predicts otolith activation to provide downstream areas with sensory prediction errors. This computational approach emphasizes the close interaction between motor control loops and sensation, explaining the clinical consequences of NU lesions, such as increased postural disturbance under conditions where motor feedback is altered. This is in line with what is reported by Guinamard et al. in children with cerebellar developmental anomalies, in another cognitive domain: music. In their study they not only observe deficits but also correlations between musical perception, singing performance, and oro-bucco-facial motor control. Using a spiking neural network computation model and simulated cerebellar mediated task, Geminiani et al. elucidate potential contributions of cerebellar dysfunction in the movement disorder dystonia. Thus, combined behavioral and modeling studies can help us in the future to better target which signals are important to emphasize or compensate for in therapeutic development.

Mechanistic studies using cellular physiology and molecular biological approaches can give insights into the function and dysfunction of the cerebellum. Bushart and Shakkottai propose a novel hypothesis to explain why genetic mouse models of human neurodegenerative disease often do not recapitulate the phenotypic neurodegeneration and sometimes ataxia that is a hallmark of the human disorder. They posit an intriguing hypothesis that this may arise from differences in the allometric scaling of the channels within cells of the cerebellum between humans and rodents, usually Purkinje cells (PCs). This enlightening review also provides a compendium of phenotypes of so-called "channelopathies" related to ataxia. Delving further into the mechanisms of neurodegeneration at the molecular level, Borgenheimer et al. detail how pathological changes in PCs in the prototypical spinocerebellar ataxia (SCA) type 1 can pathologically spread to other cell types in the cerebellum, including Bergmann glia, velate astrocytes, and oligodendrocytes. Using an advanced single-nuclei RNA sequencing approach to examine a PC specific mouse model of SCA1, they uncovered that several glial genes involved in shaping PC function were found to be dysregulated, thus suggesting that PC specific changes in function may arise from both cell autonomous and indirect effects. These studies highlight the central role abnormalities at the cellular and molecular level have on generating pathological communication between the cerebellum and forebrain/brainstem.

At the heart of the cerebellum's role across this vast set of behavioral domains is its interconnectivity, receiving and distributing neural information from diverse areas of the brain including the amygdala, basal ganglia, and inferior olive. The studies in this Research Topic offer an insight to cerebellar circuit dysfunction at several levels, point to the possibility of innovative therapeutic approaches by cerebellar modulation or musical training, and may help us in the future to better target areas or sites for clinical remediation.

Author contributions

All authors listed have made a substantial, direct, and intellectual contribution to the work and approved it for publication.

Conflict of interest

The authors declare that the research was conducted in the absence of any commercial or financial relationships that could be construed as a potential conflict of interest.

Publisher's note

frontiers in Systems Neuroscience

HYPOTHESIS AND THEORY
published: 11 January 2022
doi: 10.3389/fnsys.2021.781527

Cerebellar Coordination of Neuronal Communication in Cerebral Cortex

*Samuel S. McAfee[1], Yu Liu[2], Roy V. Sillitoe[3,4,5,6] and Detlef H. Heck[2]**

[1] Department of Diagnostic Imaging, St. Jude Children's Research Hospital, Memphis, TN, United States, [2] Department of Anatomy and Neurobiology, University of Tennessee Health Science Center, Memphis, TN, United States, [3] Department of Pathology and Immunology, Baylor College of Medicine, Houston, TX, United States, [4] Department of Neuroscience, Baylor College of Medicine, Houston, TX, United States, [5] Development, Disease Models & Therapeutics Graduate Program, Baylor College of Medicine, Houston, TX, United States, [6] Jan and Dan Duncan Neurological Research Institute of Texas Children's Hospital, Houston, TX, United States

Cognitive processes involve precisely coordinated neuronal communications between multiple cerebral cortical structures in a task specific manner. Rich new evidence now implicates the cerebellum in cognitive functions. There is general agreement that cerebellar cognitive function involves interactions between the cerebellum and cerebral cortical association areas. Traditional views assume reciprocal interactions between one cerebellar and one cerebral cortical site, *via* closed-loop connections. We offer evidence supporting a new perspective that assigns the cerebellum the role of a coordinator of communication. We propose that the cerebellum participates in cognitive function by modulating the coherence of neuronal oscillations to optimize communications between multiple cortical structures in a task specific manner.

Keywords: cerebellum, cerebrocerebellar communication, coherence, functional connectivity, cognition

OPEN ACCESS

Edited by:
Marija Cvetanovic, University of Minnesota Twin Cities, United States

Reviewed by:
Guy Cheron, Université Libre de Bruxelles, Belgium
Richard Apps, University of Bristol, United Kingdom
Martin Bares, Masaryk University, Czechia
Peter Tsai, University of Texas Southwestern Medical Center, United States

****Correspondence:***
Detlef H. Heck
dheck@uthsc.edu

Received: *22 September 2021*
Accepted: *10 December 2021*
Published: *11 January 2022*

Citation:
McAfee SS, Liu Y, Sillitoe RV and Heck DH (2022) Cerebellar Coordination of Neuronal Communication in Cerebral Cortex. Front. Syst. Neurosci. 15:781527. doi: 10.3389/fnsys.2021.781527

INTRODUCTION

Higher order brain functions, including cognitive processes, involve precisely coordinated neuronal communications between multiple cerebral cortical structures (e.g., Damasio, 1989; Vaadia et al., 1995; Mesulam, 1998; Ayzenshtat et al., 2010). In a seminal publication, Fries (2005) proposed a mechanism for controlling neuronal communications between brain structures through the modulation of coherence of their neuronal oscillations (**Box 1**). Experimental findings have since provided substantial support for the concept of "communication through coherence" (CTC), showing that coherence changes do indeed correlate with changes in the effectiveness of neuronal transmission, and that coherence changes occur in a task-specific manner. CTC has been studied in detail in the context of decision making. In rodents, decision-making in SWM requires the coordinated activity of the medial prefrontal cortex (mPFC) and dorsal hippocampus (Churchwell and Kesner, 2011; Gordon, 2011). Simultaneous electrophysiological recordings in the mPFC and hippocampus during performance of SWM tasks have shown that the decision process is associated with an increase in the coherence of theta oscillations between the mPFC and dorsal hippocampus (Jones and Wilson, 2005; Hyman et al., 2010; Benchenane et al., 2011; Gordon, 2011). A comparison of correct and incorrect decisions revealed that mPFC-hippocampal theta coherence reached higher values during correct compared to incorrect decisions, supporting a functional role of coherence in this task (Jones and Wilson, 2005; Hyman et al., 2010). In order to affect brain function changes in coherence need to affect changes in spike activity. In the context of SWM two studies measured both

BOX 1 | Fundamental principles of the Communication Through Coherence (CTC) theory, and their extension to account for cerebrocerebellar interactions.

- Gamma oscillations (>30 Hz) are generated through rhythmic sequences of excitation and inhibition within a local group of neocortical neurons, creating brief temporal windows of high and low excitability.
- Communication between neuronal groups is most effective when the output of the presynaptic group is aligned with a high-excitability window of the postsynaptic group. Synchronization in the gamma range facilitates this.
- A neuronal group receiving gamma-rhythmic inputs from several different presynaptic groups will preferentially respond to the group best aligned with its high-excitability windows, thereby providing selective communication.
- Selective synchronization of gamma is influenced by "top-down" signals that are typically in the alpha/beta range (5–30 Hz). Alpha is typically inhibitory, but beta can enhance gamma frequency to aid in selective synchronization.
- Gamma amplitude is highest in the supragranular layers which tend to direct their influence to higher cortices. Alpha/beta amplitude is highest in the infragranular layers, which project to lower cortices as well as the cerebellum via the pontine nuclei.
- We propose that the cerebellum encodes rhythms in the alpha/beta range that reflect the topographical pattern of gamma activation in the cerebral cortex and generates feedback to facilitate appropriate gamma-rhythmic synchronization in communicating neuronal groups.
- This gamma-rhythmic synchronization may be accomplished via the direct induction and modulation of neocortical gamma, or the indirect modulation of gamma through alpha/beta rhythms.

spike activity and local field potential (LFP) coherence and showed that an increase in coherence is accompanied by an increase in entrainment of mPFC spike activity to the phase of the coherent mPFC-hippocampal theta oscillations (Jones and Wilson, 2005; Hyman et al., 2010). For additional examples of experimental support for CTC, including an influence of coherence on spike activity see also (Jones and Wilson, 2005; Siegel et al., 2008; Bosman et al., 2012; Brunet et al., 2014; Sigurdsson and Duvarci, 2016; Bonnefond et al., 2017; Palmigiano et al., 2017; McAfee et al., 2018).

Importantly, the CTC theory describes a mechanism for *flexibility* in communication between neuronal groups that allows for selective information flow but does not explain the neuronal mechanism for this selectivity itself. The CTC theory proposes that "top-down" signals arise to modulate the effective transmission from "bottom-up" sources of sensory information, with "top-down" signals emerging as a consequence of internally maintained processes such as cognition or attention. The source(s) of these signals remains unknown in many cases. What is perhaps the most intriguing uncertainty is how changes in coherence selectively occur to result in the appropriate spatiotemporal synchronization for a given task. We propose that this process requires the cerebellum as a coordinator of task specific communication, a role that is consistent with existing interpretations of cerebellar function, like supervised learning and internal modeling of sensory and motor functions.

There is extensive evidence for cerebellar involvement in cognitive functions, such as language processing, working memory, and executive function (Marvel and Desmond, 2010; Brissenden et al., 2018; Ashida et al., 2019; Heleven et al., 2019). Anatomical and imaging studies show extensive connections between the cerebellum and neocortical areas essential for cognitive functions in healthy brains (Ito, 2008; Strick et al., 2009; Buckner, 2013). Posterior fossa syndrome, a condition that often develops after surgical removal of a medulloblastoma – a brain tumor that develops in the posterior fossa region of the brain – is characterized by impairments of cognition, emotion, and expressive language (Schmahmann et al., 2007; Morris et al., 2009). Patay (2015) suggested that the severity of posterior fossa syndrome is determined by the degree of damage to the cerebrocerebellar connection pathways during surgery, rather than to the extent of cerebellar damage (Patay, 2015). The sheer spectrum of cognitive functions now linked to the cerebellum (Rapoport et al., 2000; Schmahmann et al., 2019) suggest that the cerebellar contribution supports a general neuronal principle of cognitive processes rather than a specific contribution to any individual particular function.

Thus, accepting a central, albeit yet undefined role of the cerebellum in cognition, progress toward a complete understanding of normal cognitive brain function and of the neuropathology of mental illnesses must include a more comprehensive understanding of the neuronal mechanisms that comprise the cerebellar involvement in cognition.

Even before there was broad acceptance of a cerebellar role in cognition, it became obvious that cerebellar neuropathology was one of the most common neuropathologies found in the brains of patients with autism spectrum disorder (ASD) (Bauman and Kemper, 1985; Courchesne, 1997; Fatemi et al., 2012; Becker and Stoodley, 2013) or schizophrenia (Weinberger et al., 1980; Jurjus et al., 1994; Picard et al., 2007; Andreasen and Pierson, 2008). More recently, studies have also implicated the cerebellum in dementia and Alzheimer's disease (Schmahmann, 2016; Jacobs et al., 2018). As we review below, these diseases are often associated with changes in coherence of cortical oscillations, indicative of dyscoordination of communication consistent with the cerebellum failing to perform its proposed role as a coordinator of communication.

The new perspective we propose here reconciles some of the prevailing theories in cerebral and cerebellar research. Tracing cerebrocerebellar connectivity using transneuronal transport of neurotropic viruses revealed reciprocal connections between a specific cerebellar region and a specific cerebral cortical site, suggesting a separation of function through closed-loop connections (Middleton and Strick, 2001; Kelly and Strick, 2003; **Figure 1A**). However, newer studies documented considerable convergence and divergence in cerebrocerebellar connectivity, painting a more complex picture that allows for a richer interaction between structures and functions (Henschke and Pakan, 2020). The latter view is more in line with the proposed new perspective of the cerebellum as a coordinator of task-specific neuronal communication between cerebral cortical structures *via* the modulation of coherence of oscillations (**Figure 1B**). We propose, based on recent experimental findings from our labs (McAfee et al., 2019) and from others (Popa et al., 2013; Lindeman et al., 2021), that the cerebellum accomplishes this by encoding the phase relations of ongoing neuronal oscillations in neocortical areas and providing task-appropriate

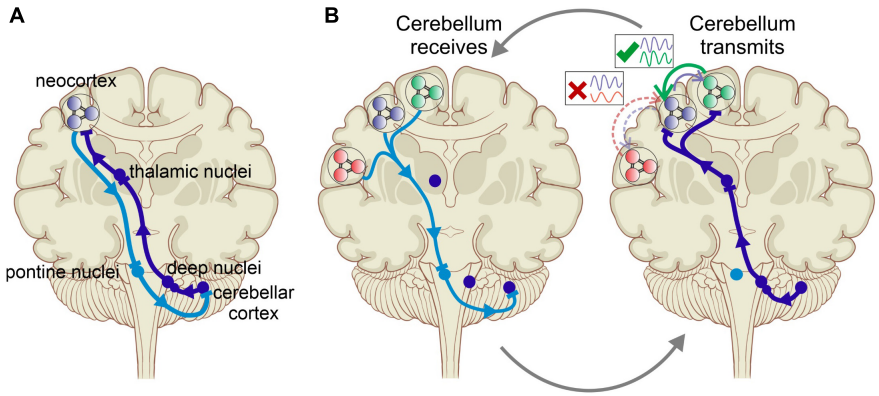

FIGURE 1 | (A) Cerebrocerebellar interaction *via* reciprocal connections between specific cerebral and cerebellar areas. Purkinje cells in the cerebellar cortex project to the neocortical areas *via* the cerebellar nuclei and the thalamus. In what was often described as a closed-loop projection, the neocortex in turn projects back to the cerebellar area of origin *via* the pontine nuclei. This one-to-one interaction scheme is the basis of most approaches to investigating cerebrocerebellar interactions. **(B)** Cerebellar modulation of communication between cerebral cortical areas provides a revised picture of cerebrocerebellar interactions, in which the cerebellum does not primarily modulate the activity in specific cortical areas but rather coordinates the communication between areas by augmenting the coherence of neuronal oscillations in a task specific manner. This occurs cyclically with the cerebellum areas receiving the neuronal "context" of cerebral activity from multiple regions by encoding their oscillations, comparing their timing, and then transmitting the output *via* the thalamus to promote synchrony between task-appropriate cerebral cortical regions.

feedback that promotes specific spatiotemporal patterns of gamma activation. Ultimately, these interactions provide "top-down" selectivity for inter-areal coherence.

Modulation of coherence is a temporal coordination task, requiring similar millisecond-range precision as the temporal coordination of muscle contractions for motor control, for which the cerebellum is known to be crucially important. The unique cerebellar cortical network architecture and cellular properties ideally enable the cerebellum to encode neocortical oscillations and transform this information into task-specific outputs to modulate coherence. This new perspective of cerebrocerebellar interaction also sheds a new light on findings from imaging studies that have identified cerebellar loci as parts of brain-wide networks (Habas et al., 2009; Buckner et al., 2013; Halko et al., 2014; Guell et al., 2018a,b). Assuming a role of the cerebellum as coordinator of cerebral cortical communication, a new approach is to link activity in the cerebellar nodes to the strength of functional connectivity between cerebral cortical nodes of the network. Recent experiments by Halko et al. (2014) provide some support for this notion, showing that stimulation of the cerebellar cortex in humans increased functional connectivity in the default mode network. Looking at known functional and anatomical cerebrocerebellar connectivity patterns with this new perspective provides new opportunities for resolving key questions around the neuronal "language" of cerebrocerebellar interactions.

DYNAMIC COORDINATION OF NEURONAL ACTIVITY IN THE CEREBRAL CORTEX

Cerebral functional networks are defined as such based on robust and consistent spatiotemporal patterns of neuronal activity, often linked to specific brain states and mental operations (Fox and Raichle, 2007; Ayzenshtat et al., 2010; Raichle, 2015). These patterns are manifest in different ways at varying spatial and temporal scales, resulting in distinct but interrelated observations with different imaging modalities. Brain-wide functional networks identified with functional MRI reflect spatial patterns of neuronal activity that is temporally coordinated on the scale of hundreds of milliseconds to seconds. The vasodilation that drives these BOLD signal patterns in the neocortex is tightly linked to the bursting of gamma oscillations (Mateo et al., 2017), which are highly focal in nature and influence communication on the neuronal level (Fries, 2005). Oscillations in the alpha and beta range (5–30 Hz) are more spatially diffuse and effect both the occurrence and coherence of gamma oscillations (Richter et al., 2017). Resting state brain networks can also be captured using magnetoencephalography (MEG), which provides a higher temporal resolution and allows capturing oscillations at higher frequency bands, including alpha and beta rhythms. Brookes et al. (2011) used MEG measurements to recreate the spatial patterns that constitute functional networks in fMRI. This involvement of alpha and beta oscillations in brain wide functional networks together with their modulation of gamma oscillations suggests that they may play a key role in the spatial selectivity of gamma coherence, forming a critical link between communication at the neuronal level and the macroscopic organization of brain-wide functional networks.

In the following sections, we will review evidence that the cerebellum is essential for the coherence of cerebral gamma oscillations within a well-defined functional network, and that the cerebellar activity reflects information about cerebral oscillations within a broad range of frequencies. We propose that these findings, along with a trove of anatomical, physiological, and imaging evidence, supports the idea that the cerebellum plays a key role in the modulation of gamma coherence across different areas of the cerebral cortex. We propose that

this is accomplished through the encoding of sub-gamma cerebral oscillations by the cerebellum, and the subsequent generation of cerebello-cortical feedback. The result of this feedback is the modulation of cerebral gamma and thus its coherence, although it remains to be explored whether gamma is modulated directly or indirectly through the modulation of sub-gamma oscillations.

Experimental Evidence Supporting Cerebellar Coordination of Communication by Coherence

A seminal study by Popa et al. (2013) was the first to suggest a role for the cerebellum in coordinating coherence in the sensorimotor system. They performed simultaneous recordings of neuronal oscillations in the primary sensory (S1) and primary motor cortices (M1) of the mystacial whisker system in freely moving rats. Up to eight electrodes were placed in each area to allow analysis of coherence within S1 and M1 as well as between the two areas. Whenever the rats engaged in active whisker movements, coherence of gamma oscillations within S1 and M1 increased for the duration of the behavior (Popa et al., 2013; **Figure 2A**). A crucial involvement of the cerebellum in this behavior-related coherence increase became clear when the authors used Muscimol to pharmacologically inactivate the interposed nucleus of the cerebellum, i.e., the nucleus that projects to the whisker system *via* the motor thalamus. Inactivation of the interposed nucleus eliminated the increase of S1-M1 gamma coherence during whisking behavior (Popa et al., 2013). Importantly, the generation of gamma oscillations within each structure was not altered by inactivating cerebellar output. Thus, the generation of gamma rhythms *per se* did not require an intact cerebellar output, but between-structure coherence of gamma did. A very recent study supported these findings using optogenetic excitation of Purkinje cells to silence cerebellar output and examined the resulting changes in coherence in greater anatomical and temporal detail. Lindeman et al. (2021) used linear silicon probes to record along the cortical depth of S1 and M1 during sensory stimulation delivered *via* an air puff to the whiskers. Concurrent optical stimulation of Purkinje cells in the contralateral cerebellar hemisphere caused temporary dampening of cerebellar output, resulting in the loss of sensory-evoked S1-M1 coherence in the gamma range (**Figure 2B**). The authors also showed that Purkinje cell stimulation reduced the amplitude of evoked local field potential (LFP) response to whisker stimulation predominantly in the deep cortical layers of both S1 and M1. This effect, as well as the disruption of gamma-band coherence, was largely rescued by delaying the onset of Purkinje cell stimulation by 20 ms relative to the air puff, indicating that the coherence modulation was mediated by a fast, ascending cerebellar pathway. Additionally, Purkinje cell stimulation was accompanied by an increase in S1-M1 coherence within the theta range regardless of concurrent whisker stimulation. This suggests that theta-band coherence was a direct result of the transient cerebellar stimulation and may reflect a mechanism of cerebellar-controlled sub-gamma neuronal activity capable of mediating gamma-band activity. The authors completed the study by creating an *in silico* laminar model of cerebellar, cortical, and subcortical interactions showing that coherent gamma activity likely flowed from S1 to M1, while coherent theta was a top-down signal flowing from M1 to S1 (Lindeman et al., 2021). This is intriguing given the proposed role of theta within the CTC hypothesis – that it acts as a gating rhythm in the target region that modulates the effectiveness of gamma-frequency transmission from a given source (Fries, 2015). The cerebellar stimulation in this study appeared to induce a consistent theta phase relationship with M1 leading S1, which we would not expect to promote gamma-band propagation from S1 to M1.

Signals Received by the Cerebellum: Cerebellar Encoding of Cerebral Oscillations

The findings by Popa et al. (2013) and Lindeman et al. (2021) discussed above are consistent with our proposed role of the cerebellum as a coordinator of coherence, but they do not provide information about the neuronal activity in the cerebellum itself. In order to modulate cortical coherence effectively for a given task, it is essential that the cerebellum can encode the neuronal "context" elicited by the task. This likely includes an array of neuronal oscillations that are commonly observed throughout different sensorimotor (e.g., Baker et al., 1999; Watanabe and Kohn, 2015) and cognition-related cortices (e.g., Osipova et al., 2006; Myers et al., 2014), and which may be offset with meaningful delays. With the majority of subcortically projecting layer V pyramidal neurons sending collaterals to the pontine nuclei (Leergaard and Bjaalie, 2007; Suzuki et al., 2012), information about oscillatory activity throughout the cerebral cortex is likely to reach the cerebellum *via* its mossy fiber (MF) inputs.

Encoding of the oscillatory phase of a cortical region, and calculation of phase difference between two co-active cortical regions, are capabilities that would ideally enable the extraction of the neuronal context associated with a given task. Results from our own studies show that Purkinje cell simple spike activity in cerebellar lobulus simplex (LS) and Crus I of awake mice does indeed represent the instantaneous phases and the phase differences between LFP oscillations in the mPFC and the dorsal hippocampal CA1 region (dCA1) (McAfee et al., 2019). Crus I and LS Purkinje cells differed in their representation of instantaneous phases. In Crus I, Purkinje cells mostly represented the phases of delta oscillations in mPFC and dCA1. In LS, Purkinje cells also represented the phase of delta oscillations, but also the phases of high gamma oscillations in mPFC and dCA1 (**Figure 3**). Interestingly, phase differences between mPFC and dCA1 oscillations were represented equally in both cerebellar lobules for all major frequency bands of neuronal rhythms (delta, theta, beta, and gamma) (McAfee et al., 2019; **Figure 3**). The mPFC and dCA1 are known to show modulations of coherence in the context of spatial working memory tasks (Gordon, 2011; Spellman et al., 2015), suggesting a potential involvement of the cerebellum in the modulation of coherence and the associated spatial working memory task.

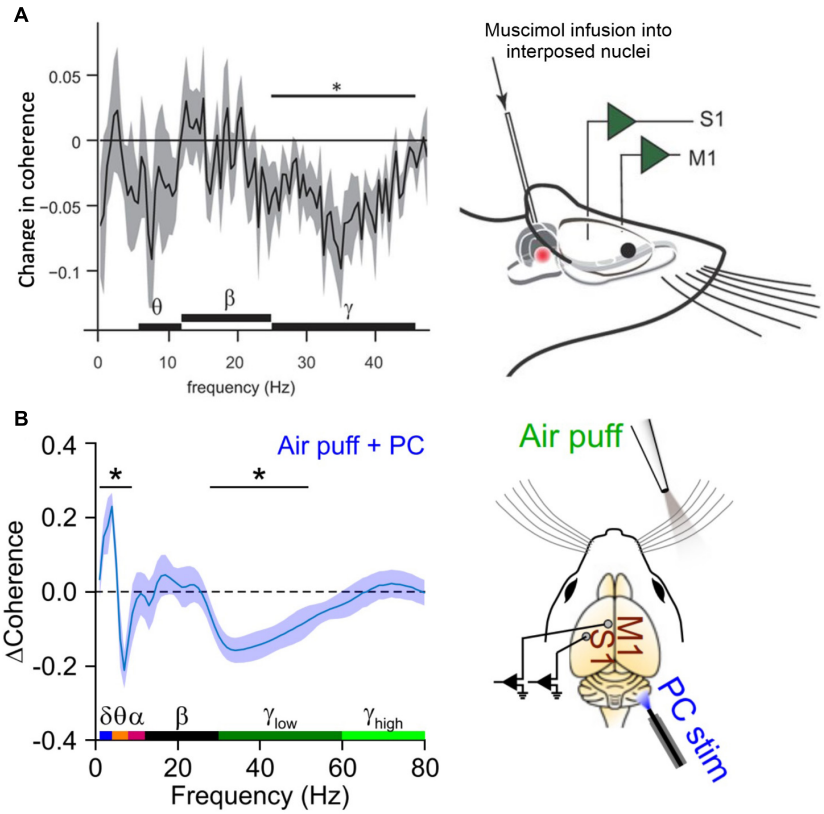

FIGURE 2 | Inactivation of cerebellar output reduces gamma coherence between S1 and M1. **(A)** In an experiment that involved simultaneous measurements of LFPs in S1 and M1 of awake, head fixed rats, Popa et al. (2013) demonstrated that pharmacological inactivation of the interposed nuclei selectively reduced gamma coherence between S1 and M1. The plot on the left shows a change in coherence relative to the control condition in which the interposed was kept intact. The experimental approach is illustrated on the right (from: Popa et al., 2013). **(B)** A similar, recent experiment showing that optogenetic inhibition of cerebellar output (*via* Purkinje cell excitation) significantly reduced the coherence of gamma responses evoked by whisker stimulation. The plot on the left shows estimated effect of Purkinje cell stimulation on coherence between deep layer S1 and superficial layer M1. Theta-range S1–M1 coherence was enhanced with Purkinje cell stimulation (from: Lindeman et al., 2021). *These frequencies were statistically significant ($p < 0.05$).

How does the cerebellar network derive information about oscillatory phase and phase difference at distinct frequencies from the inputs it receives? The largest descending excitatory input to the cerebellar cortex is conveyed *via* neurons in the pontine nuclei that project MFs that synapse with granule cells (GCs) in the cerebellar cortex. Pontine afferents appear to be arranged in such a way as to convey the aggregate activity level of the neuronal field from which they originate. These projection neurons have dense but local dendritic arbors and mutual synaptic connection with neighboring corticopontine neurons (Morishima et al., 2011), and do little to spatially or temporally transform the excitation they receive.

For example, motor cortical efferents remain somatotopically arranged, but non-specific in their synapses – their axons forming numerous branches, with neighboring projections terminating on interlaced fields in the pons (Brodal and Bjaalie, 1992; Schmahmann et al., 2004). This results in a sort of spatial smoothing, and in some cases a mixing of cortical sources, as neuronal signals are transferred from cortical to pontine somatotopy. Pontine inputs from other regions appear to follow the same arrangement.

Despite the diversity of function in the pontine nuclei, pre-cerebellar neurons universally translate their input current into a rate code in a linear fashion (Kolkman et al., 2011; **Figure 4B**). Consequently, oscillatory population activity from the cortex is received by pre-cerebellar neurons in the pons and immediately transformed into phase information *via* firing rate. [Inversely, sustained DC current drives neuronal spiking activity with irregular intervals, making pontine neurons effective responders to oscillatory input, but ineffective generators of sustained oscillatory output (Schwarz et al., 1997).] Recent studies show that GCs receiving this appear to be biophysically tuned to different phase information within this input as well – along the depth of the GC layer, neurons respond preferentially to inputs of increasing frequency, thereby forming a gradient tuned to distinct phases within the ponto-cerebellar signal (Straub et al., 2020; **Figure 4C**). Parallel fibers also exhibit a depth-dependence in conduction velocity, with deeper GCs conducting action potentials at a higher velocity (Straub et al., 2020). Modeling showed that these GC properties together led to more precise Purkinje cell responses to a given spike-frequency-modulated MF input (Straub et al.,

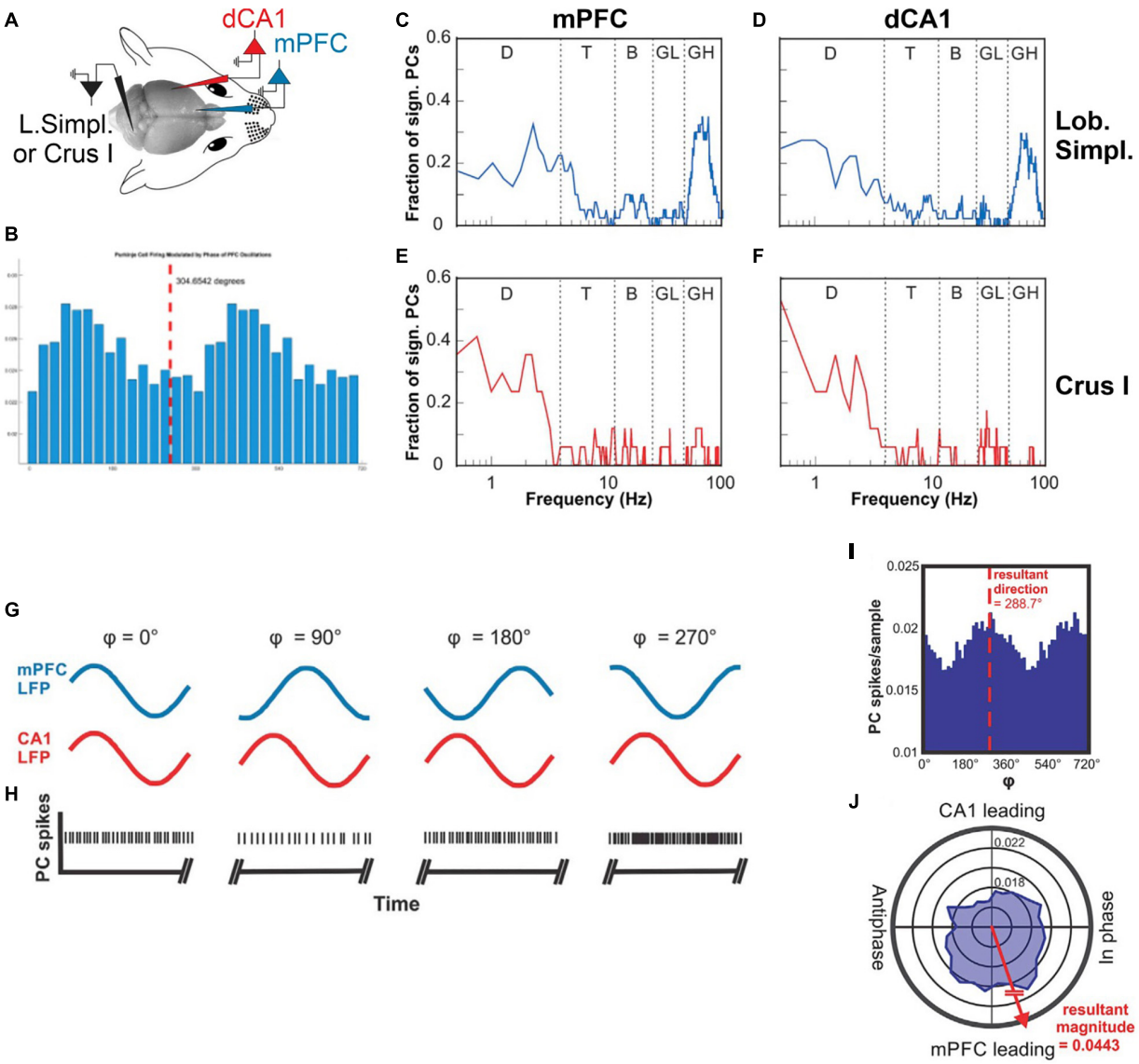

FIGURE 3 | Cerebellar representations of phase and phase differences of oscillations in the mPFC and CA1. **(A)** Illustration of the experimental setup with recording electrodes in the mPFC and dCA1, picking up LFPs and a recording electrode in cerebellar lobulus simplex recording single unit Purkinje cell spike activity. **(B)** Example histogram showing Purkinje cell simple spike rate plotted against the phase of a 10 Hz oscillation recorded in the mPFC. **(C)** Fraction of Purkinje cells in LS (n = 32) whose simple spike activity was significantly correlated with oscillatory phase plotted as a function of mPFC oscillation frequency (plotted on a log-10 scale). The function shows two peaks at the delta frequency range (0.5–4 Hz) and the high gamma range (50–100 Hz). **(D)** As in **(C)** but showing fractions of LS Purkinje cells significantly modulated by the phase of oscillatory activity in CA1. **(E)** Fraction of Purkinje cells in Crus I (n = 17) whose simple spike activity was significantly correlated with the oscillatory phase in mPFC plotted as a function of mPFC oscillation frequency. The function shows a single peak at the delta frequency range (0.5–4 Hz). **(F)** As in **(E)** but showing fractions of Crus I Purkinje cells significantly modulated by the phase of oscillatory activity in CA1. D, delta; T, theta; B, beta; LG, low gamma; HG, high gamma. **(G)** Illustration of hypothetical oscillations at a specific frequency occurring simultaneously in the mPFC (blue traces) and CA1 (red traces) and displaying different phase relationships (4) at different times. The phase relationship 4 is defined as the phase difference relative to the mPFC oscillation. **(H)** Hypothetical Purkinje cell spikes recorded simultaneously with the LFP activity in the mPFC and CA1 shown in **(G)**. The rate modulation of this hypothetical Purkinje cell shows a significant increase in spike firing when the phase difference between mPFC and CA1 oscillations reaches values around 270°. **(I)** Phase histogram of real Purkinje cell simple spike activity. The histogram shows spike activity as a function of mPFC-CA1 phase differences at 11 Hz. The simple spike activity of the Purkinje cell in this example was significantly modulated as a function of mPFC-CA1 phase difference, with a preference of 288.7°. **(J)** Same data as in **(I)** represented in polar coordinates. Vectors composed of the angular value 4 and the magnitude of the spikes per sample were summated to determine the angular preference of Purkinje cell activity. The resultant vector magnitude was taken to quantify the degree of modulation and tested against surrogate results for statistical significance (from McAfee et al., 2019).

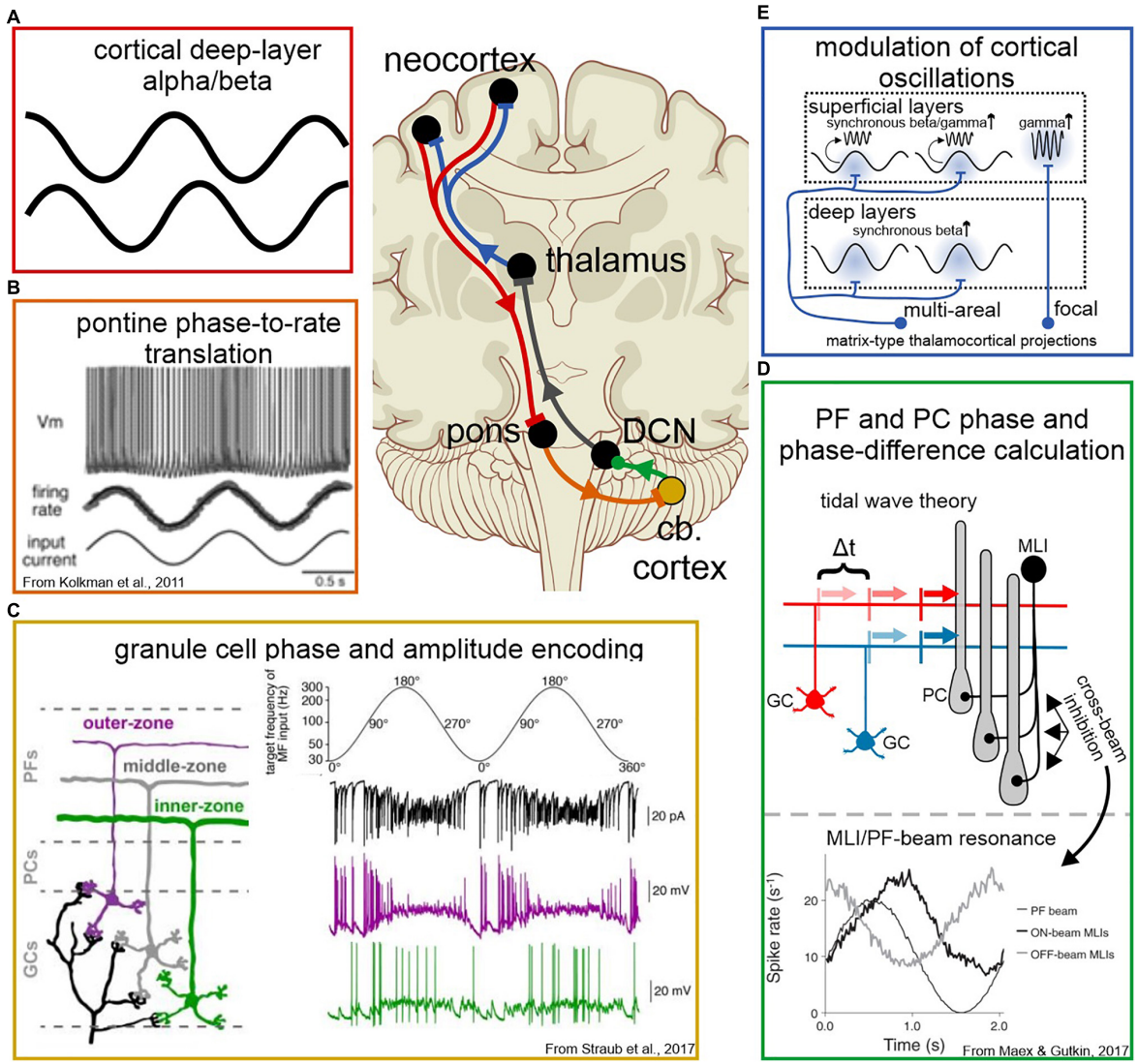

FIGURE 4 | Cellular and network mechanisms of oscillatory encoding and modulation in the cortico-cerebello-cortical circuit. Panel labels are color-coded according to where in the circuit a modulation of the neuronal signal occurs, corresponding to the schematics in the top-center. **(A)** Cortico-cerebellar signals originate in the deep layers of the neocortex, where alpha and beta oscillations predominate. **(B)** Pre-cerebellar neurons in the pons translate a dynamic current input into rate in a linear fashion, thereby translating oscillatory current into a rate code. **(C)** Deep and superficial GCs respond preferentially to different phases of the ponto-cerebellar signal, thereby encoding both phase (*via* time) and amplitude (*via* GC depth) of oscillatory input. **(D)** Phase and phase difference of oscillatory activity is decoded by Purkinje cells, *via* two potential mechanisms. Top: tidal wave theory proposes that a phase difference in a band-limited frequency range can be calculated as a time difference along slow-conducting parallel fibers. Each parallel fiber conveys information about the phase of one cerebral oscillation, and together convey information about the phase relationship of their inputs. Two inputs offset by Δt would arrive simultaneously at the Purkinje cell dendritie. Bottom: simulations show that rhythmic excitation can generate network resonance across parallel fiber beams with a phase shift, due to cross-beam inhibition from MLIs. Rhythmic excitation could augment Purkinje cell responses to input across parallel fiber beams, thereby providing a means to calculate phase differences that are too great to be accounted for in parallel fiber conduction length. **(E)** Feedback to the cortex conveyed *via* thalamocortical projections. Multi-areal matrix-type projections target superficial and deep layers in multiple cortical areas, likely inducing simultaneous beta oscillations that facilitate simultaneous gamma bursts in targeted regions. Focal matrix-type projections preferentially target the superficial layers, suggesting a role in spatially selective augmentation of gamma responses during the bottom-up flow of information.

2020). Altogether, this suggests a role for GCs in isolating phase and amplitude components from the cortico-cerebellar signal before conveying this information to Purkinje cells for temporal comparison.

Interestingly, at least for phase differences of a brief time interval, the cerebellar cortical network architecture is uniquely designed to "calculate" phase difference from oscillatory fiber activity arriving from two different structures (**Figure 4D**). A phase to phase-difference transform occurs along the slow-conducting parallel fibers in a mechanism first proposed by Braitenberg and Atwood (1958) and Braitenberg et al. (1997) as the "tidal wave hypothesis." Phase differences between

oscillations at any given frequency can be expressed in terms of temporal delays. MFs providing inputs that are phase-locked to oscillations at their respective cerebral cortical site of origin, excite neighboring GCs with delays that are proportional to phase differences between cerebral cortical oscillations. As the spike responses elicited in the GCs propagate along the slow conducting GC axons, the parallel arrangement of these fibers uniquely allows for the asynchronous activity to realign to a synchronous volley of inputs to the two-dimensional dendrites of Purkinje cells (**Figure 4D**). During periods of robust oscillation, an array of Purkinje cells could passively encode a range of phase relationships expressed by their inputs, allowing the timing of the teaching signal(s) from the climbing fiber pathway to help distinguish contextually meaningful phase relationships for synaptic modification. That the cerebellar network can indeed transform sequential input arriving at the GC layer into synchronous volleys of parallel fiber spikes and elicit sequence specific Purkinje cell responses was shown in a series of *in vitro* experiments by one of us (Heck, 1993, 1995, 1999; see also Braitenberg et al., 1997).

Within this framework, it is important to consider frequency specificity of MF inputs as an important component of the cerebrocerebellar pathway. Cortico-pontine input is driven by neurons in cortical layer V, which primarily carry sub-gamma frequencies (Castro-Alamancos, 2013; Bastos et al., 2018; **Figure 4A**). For larger phase difference calculation for lower (sub-gamma) frequencies, network resonance properties likely also play a role (**Figure 4D**).

Interestingly, the cerebellar Golgi cell network, which is connected *via* gap junctions, seems ideally designed to prevent large scale synchronization of the cerebellar input layer in response to rhythmic MF activity (Vervaeke et al., 2010). Gap junctions connecting Golgi cells have unique low pass filtering properties, permitting the propagation of the slow after-hyperpolarization component of an action potential while the fast, depolarizing portion has little to no effect on the membrane potential of neighboring Golgi cells (Vervaeke et al., 2010). This results in a functional lateral inhibition and desynchronization of Golgi cell network activity, allowing rhythmic inputs to remain separated in space and frequency.

Cerebellar network modeling suggests that molecular layer interneurons (MLIs; basket cells and stellate cells) impart circuit resonance that would be consequential for the frequency specificity of encoding phase information (Maex and Gutkin, 2017). In these models, MLI inhibition is shown to set an optimal frequency of resonance that can be varied with the strength of inhibition, potentially providing a mechanism for fine tuning the frequency specificity of the cerebellar response to broad band inputs (Maex and Gutkin, 2017). These same network properties also generate on-beam and off-beam excitation/inhibition cycles that are phase-shifted (Maex and Gutkin, 2017). The full implications of this remain to be explored *in vivo*, but nevertheless provide a potential mechanism for oscillation "memory" as well as prediction within a resonating network, depending on whether the phase is shifted in a positive or negative direction, respectively (**Figure 4D**). In this scheme, resonance can occur along separate beams in a phase-shifted manner, remaining mutually reinforcing while augmenting Purkinje cell responses across beams in a phase-relationship specific manner, providing a mechanism for phase-relationship encoding at lower frequencies.

Selective drive of deep cerebellar nuclei (DCN) neurons is the final step in the pathway for the generation of feedback to the cortex. There are four main synaptic influences that determine the activity of DCN neurons: inhibitory input from Purkinje cells, excitatory inputs from collaterals from MFs and climbing fibers, and finally synaptic inputs from other neurons within the DCN network (Perciavalle et al., 2013). The inhibitory influence of Purkinje cells dominated early theories implying cerebellar cortical suppression of DCN activity (e.g., Houk, 1991) despite experimental evidence to the contrary, which suggested a more complex reality (McDevitt et al., 1987). To this date surprisingly little is known about how the interacting synaptic inputs determine the activity of DCN projection neurons (Perciavalle et al., 2013). One of the reasons why the DCN networks and neuronal properties are still poorly understood may be the fact that the physiological properties of the DCN neurons do not easily correspond to morphology, and that there is no reliable way to identify cell types based on extracellularly recorded spike shapes or spike activity patterns (Canto et al., 2016). *In vitro* studies suggest that synchronous Purkinje cell activity is an effective mechanism for controlling DCN activity (Gauck and Jaeger, 2000; Person and Raman, 2012) and task specific synchronized Purkinje cell activity has been observed *in vivo* (Heck et al., 2007). There is however, thus far no demonstration of Purkinje cell synchrony modulating DCN firing in a behaving animal. Observation of DCN activity during behavior show a gradual rate modulation on time scales related to the ongoing behavior, suggesting that rate modulated inputs are driving the changes (Thach, 1970; Lu et al., 2013). Additional experiments are needed to determine the role of synchronized inputs in the control of DCN output. An important property of synchronized inhibition is its ability to induce precisely timed spike activity in the DCN (Gauck and Jaeger, 2000; Person and Raman, 2012), which may play a role in the transmission of phase resetting signals from the DCN to thalamus.

The Cerebellum Transmitting: Cerebellar Coordination of Cerebral Activity

How would cerebellar output influence the coherence of oscillations in two cerebral cortical areas? The thalamus is believed to play a key role in the coordination of cerebral oscillations (Jones, 2001), including the modulation of their coherence (Guillery, 1995; Destexhe et al., 1999; Saalmann, 2014), and notably between the mPFC and dorsal hippocampus (Hallock et al., 2016). Generally, cerebellar outputs terminate on several thalamic nuclei, which contain relay neurons that in turn project throughout the cerebral cortex. Subtypes of thalamic relay neurons can be defined based on which of the cortical layers they target, as these different targets suggest a different influence on cortical activity. A subtype of relay neuron known as matrix-type is thought to play a key role in the modulation of cerebral oscillations (Jones, 2001), and is characterized by widespread lateral axonal arborization in the superficial neocortical layers (Clasca et al., 2012) where gamma oscillations are most

prominent. Matrix-type neurons are common in the intralaminar and mediodorsal thalamic nuclei (Clasca et al., 2012), which are thought to have a particularly important role in the coordination of cerebral cortical oscillations, and which receive excitatory input from the cerebellum (Aumann and Horne, 1996a,b; Melik-Musyan and Fanardjyan, 1998; Saalmann, 2014). Matrix-type relay neurons can be further divided into focal- and multi-areal-targeting groups, which (as the name implies) form dense terminals in either one or multiple cortical regions (Clasca et al., 2012; **Figure 4E**). Interestingly, focal matrix-type relay neurons tend to synapse in the superficial layers exclusively, whereas multi-areal matrix-type neurons target cortical layer V as well (Clasca et al., 2012). Simultaneous excitatory drive to layers I, II/III, and V has been proposed as a mechanism for the generation of beta oscillations in the cortex (Sherman et al., 2016), suggesting that these neurons might modulate inter-areal gamma coherence *via* the induction of gamma-enhancing beta events in multiple regions simultaneously. Many different means of cortical modulation are possible based on cerebello-thalamo-cortical anatomy, yet the exact mechanism(s), or combinations therein, of cerebellar coordination of cerebral cortical oscillations remain to be determined.

It is important to note that the mechanism we propose does not require synchronization of rhythmic neuronal activity between the cerebellum and cerebral cortex. Synchronization of cerebral and cerebellar rhythms have been observed in animals and humans (Ros et al., 2009; Cheron et al., 2016) and have been suggested to reflect ongoing cerebrocerebellar interaction (Cheron et al., 2016). The mechanism we propose here does not require synchronized oscillations between the cerebral and cerebellar cortex. We predict that that cerebellum continually monitors the phase differences between oscillations in two cerebral cortical structures to detect and correct deviations from the optimal phase difference, based on the specific task and the structures involved. Rhythmic Purkinje cell activity synchronized with the cerebral cortex would not necessarily interfere with this function but at the same time the rhythm would not carry any information relevant to the task.

Further clues as to the cerebellar role in the spatiotemporal organization of cerebral cortical activity can be gleaned from functional imaging studies. Resting state fMRI measurements can be used to identify intrinsic cerebral cortical networks that mimic the regional activation observed during various tasks and at rest. Virtually all functional networks (except visual) (Schmahmann et al., 2019) exhibit robust representation in the cerebellum (Buckner, 2013; Guell et al., 2018a; Marek et al., 2018; **Figure 5A**), with seemingly similar roles of the cerebellum in task and rest conditions (Schmahmann et al., 2019). The cerebellar representation of resting-state networks contains redundant functional domains in a center-out pattern that resembles the pattern of bifurcated pontocerebellar axonal targeting in rodents (Biswas et al., 2019). The functional relationship between cortex and cerebellum appears this way in resting-state studies that measure steady-state connectivity, but different patterns emerge when the assumption of stationarity is dropped. For example, one study examined which areas of the brain were co-active with the intraparietal sulcus, an association region considered critical for the integration of multisensory information for spatial processing. Interestingly, this region did not co-activate with a single region of the cerebellum, but instead co-activated with several non-overlapping cerebellar regions, each representing which other cortical region(s) were simultaneously active (Liu and Duyn, 2013; **Figure 5B**). This shows that specific focal activations in the cerebellum correspond to distributed spatial patterns of cerebral cortical co-activation, suggesting that selective inter-areal communication is established between distributed networks in the cerebral cortex when certain cerebellar regions are active. The directionality of this relationship is not known, however, and may represent encoding of cerebral co-activation by the cerebellum, induction of cerebral co-activation by the cerebellum, or an interplay of the two. Investigation of lag between cerebral cortical and cerebellar BOLD signals suggests the former, but the timescale of fMRI is very slow, and the fact that cerebellar BOLD is driven primarily by GC layer input (Diedrichsen et al., 2010) make it difficult to preclude the latter.

The development of whole-brain networks seen in fMRI, especially how the cerebellum is integrated into them, also suggests that the cerebellum could function as a central hub for communication between major cerebral cortical areas (Fair et al., 2009; **Figure 5C**). Early in neural development, intrinsic cortical networks are poorly defined, with each cortical region only exhibiting correlated activation with its immediate neighboring regions (Fair et al., 2009; Power et al., 2010; Kundu et al., 2018). At this stage, the cerebellum does not appear to share substantial functional links with any cortical regions–in this regard, we are referring here specifically to functional links that would have direct resemblance to mature cognitive function. As the brain reaches circuit maturity, intrinsic spatial patterns emerge in the cerebral cortex, forming distributed networks with correlations that are defined functionally rather than anatomically. At this stage, the cerebellum becomes so embedded into the network structure that it seemingly acts as a hub for the coordination of communication between the distributed cortical networks (Fair et al., 2009; Kundu et al., 2018). Additionally, the regions of the cerebellum with the highest inter-subject variance in functional mapping were those that correspond to cerebral cortical areas related to executive function and cognition (Marek et al., 2018). Altogether, this evidence suggests a number of things: that the cerebrocerebellar relationship maintains coordinated inter-areal communication between functionally defined cortical regions, that focal cerebellar activation corresponds to spatially selective cerebral co-activation, and that these spatial relations that come to define cerebral cortical network organization are learned or acquired over the course of development. We argue that these findings strongly support the idea that the cerebellum integrates information from cerebral cortical activity and teaching signals from the inferior olive to adaptively co-activate regions and establish spatially selective coherence, thus leading to meaningful integration within and across cerebral cortical networks over the course of development. Importantly, this new view we present here not only explains the observed patterns of co-activity in the adult cerebrocerebellar system but provides a framework for the investigation of developmental disorders that are known to involve the cerebellum, such as ASDs and schizophrenia.

Compared to fMRI, electroencephalography (EEG) captures brain activity with much lower spatial but far higher temporal resolution, including frequencies in the gamma range (Freeman et al., 2003). EEG has been applied to investigate cerebellar influence on cerebral cortical activity using non-invasive transcranial magnetic stimulation (TMS) to stimulate the cerebellum (for a recent review see Fernandez et al., 2020). While most cerebellar TMS-EEG studies report on evoked potentials in the cerebral cortex, some also investigated oscillatory activity. Findings from these latter studies showed that cerebral cortical oscillations are modulated by TMS applied to the cerebellum. For example, Farzan et al. (2016) applied intermittent theta burst stimulation (iTBS) to the vermis and the Crus I/II region of the right hemisphere of the posterior cerebellum in healthy adults. Post-stimulation power spectral analysis showed an increase in power of beta to low gamma oscillations in frontal and parietal regions following vermal stimulation, and a global reduction in theta and an increase in high gamma oscillations in fronto-temporal areas following stimulation of the hemisphere (Farzan et al., 2016). The spatial arrangement of these findings is consistent with cerebrocerebellar functional connectivity patterns based on fMRI activity maps (Buckner et al., 2011). Similarly, application of high frequency repetitive transcranial magnetic (rTMS) stimulation of the cerebellum combined with EEG revealed a stimulation-site specific modulation of gamma power in frontal cortical regions (Schutter et al., 2003). Stimulation of the vermis resulted in a shift of gamma power from left frontal to right frontal dominance while stimulation of control sites in the occipital cortex and cerebellar hemisphere did not induce this effect (Schutter et al., 2003). Du et al. (2018) were able to show that cerebellar TMS stimulation increased synchrony between left and right prefrontal areas within the theta to gamma frequency range. What sets their study apart is that they were also able to show that cerebellar-evoked increase in bilateral prefrontal synchrony was associated with better working memory performance, linking cerebellar modulation of cerebral cortical oscillations to cognitive function (Du et al., 2018). These studies thus show that activity in specific cerebellar subregions can influence cerebrocortical neuronal dynamics in multiple frequency bands with regional specificity, and that this influence can be linked to cognitive processes.

Cerebellar Involvement in Hippocampal–Prefrontal Interactions

Cerebellar involvement in cognitive functions and cognitive disorders that are associated with cerebellar neuropathology involves cerebellar interactions with frontal cerebral cortical areas (Ramnani, 2006; Schmahmann et al., 2019; Wagner and Luo, 2019). More recently, essential spatial functions, such as spatial

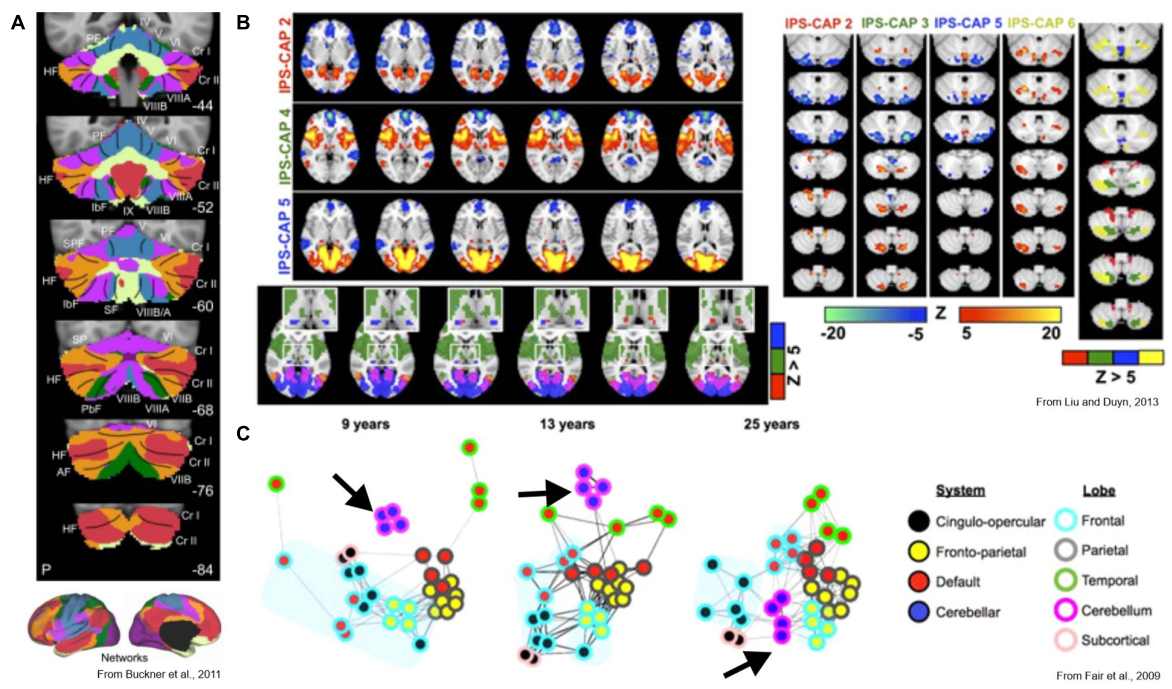

FIGURE 5 | Key functional imaging studies of cerebrocerebellar interaction. **(A)** Voxel-to-network mapping of cerebellar relationship to cerebral intrinsic networks. Most of the cerebellum is most-strongly linked to association and cognitive cerebral areas. **(B)** Co-activation pattern analysis identifies recurring spatial patterns of co-activation in the brain. Left: three unique cerebral co-activation patterns involving the intraparietal sulcus are shown. Lower panel shows unique thalamic foci associated with each pattern as well. Right: corresponding cerebellar activations. Focal activation of cerebellar cortex is linked to complex patterns of co-activation across distributed cerebral cortical networks. The non-overlapping foci suggests a voxel-to-network mapping of cerebellar activity to cortical networks is insufficient to describe the cerebellum's role in distributed brain networks. **(C)** Maturation of brain networks over the course of development. Black arrow indicates cluster of cerebellar nodes at each developmental stage. Early in development, cortical areas are functionally linked to their nearest anatomical neighbors, and the cerebellum has no functional link to the cortex. Once mature however, the cerebellum acts as a hub between distributed functional networks in cortex.

coding by place cells or spatial memory have been shown to require an intact cerebellum (Tomlinson et al., 2014; Lefort et al., 2015, 2019). Accordingly, trans-neuronal tracing showed projections from cerebellar vermal lobule VI and hemisphere lobule Crus I to the dorsal thalamus (Watson et al., 2019). Connections between the hippocampus and Crus I are notable in the context of cerebellar cognitive function, because Crus I also has reciprocal connections with the prefrontal cortex (Middleton and Strick, 2001), which have recently been directly linked to the control of social behavior in mice (Kelly et al., 2020). The prefrontal cortex and dorsal hippocampus are jointly required for spatial working memory function in rodents (Jones and Wilson, 2005; Benchenane et al., 2011; Wirt and Hyman, 2017; Negron-Oyarzo et al., 2018) and their connection with the cerebellum may help explain findings of cerebellar involvement in spatial orientation (Burguiere et al., 2005; Rochefort et al., 2011) and spatial working memory (Tomlinson et al., 2014).

To determine the physiological nature of hippocampal cerebellar interactions, Watson et al. (2019) implanted mice with recording electrodes in the dorsal hippocampus, vermal lobule VI and Crus I. They then trained the mice in a simple goal-directed behavior, requiring the mice to traverse a linear path to receive a reward consisting of an electrical stimulation of the medial forebrain bundle (Carlezon and Chartoff, 2007) at the end of the path (Watson et al., 2019). As mice improved their performance of this goal-directed behavior, coherence of theta oscillations (6–12 Hz) between the dorsal hippocampus and Crus I selectively increased (Watson et al., 2019), suggesting that the communication between Crus I and dorsal hippocampus involves task related coherence of neuronal oscillations (Watson et al., 2019).

IMPLICATIONS FOR COGNITIVE DISORDERS

Cerebellar coordination of neuronal communication predicts that cerebellar pathophysiology would result in deficits in neuronal communication between brain areas and that those deficits would be detectable in measurements of functional connectivity. This should be testable in brain disorders that have a high likelihood of cerebellar neuropathology, such as ASDs and schizophrenia. Interestingly, a hypothesis of brain-wide dysconnection (disordered functional connectivity between brain structures) as a major underlying cause was advanced for both ASDs (Just et al., 2004, 2012; Wass, 2011) and schizophrenia (Stephan et al., 2009; Pettersson-Yeo et al., 2011; Tu et al., 2012). There is, however, no agreement as to the causes of the dysconnectivity; however, they could conceivably occur at the anatomical or functional levels, since such circuit-based disorders often arise due to a combination of circuit miswiring, neuronal degeneration, and functional abnormalities.

Additionally, the inevitable surgical damage to the cerebellum, that occurs during medulloblastoma resection in the posterior fossa region, is known to cause broad cognitive, emotional, and behavioral deficits, particularly in the case of disruption of the cerebellar output tract in children (Morris et al., 2009). The underlying neurobiological causes of this disorder (known as Cerebellar Mutism Syndrome or Posterior Fossa Syndrome) remain unclear, but this disorder highlights the importance of cerebellar output in the development and maintenance of cerebral activity to support normal cognitive function.

Coherence/Functional Connectivity Abnormalities in Autism Spectrum Disorders

Frith (1997) suggested that many of the perceptual and attentional abnormalities in ASDs could be interpreted as "weak central coherence," which she defines as a reduction in the contextual integration of information and a bias toward local rather than global processing, i.e., the inability to integrate pieces of information into a coherent whole. Other authors attributed weak central coherence to an impairment of "temporal binding" between local networks, whereas temporal binding within local networks was presumed to be intact or possibly even enhanced (Brock et al., 2002). Animal studies offer some clues as to the neuronal mechanisms underlying this type of deficit, and how it may result from cerebellar dysfunction. As discussed previously, this type of impairment is analogous to what is observed in the sensorimotor system of rats when cerebellar output nuclei are inhibited, with the coherence between sensory and motor cortices disrupted while local processing remains intact (Popa et al., 2013). Another recent study showed how ASD-like behavior in mice is linked to activity in specific cerebello-thalamo-prefrontal cortical projections (Kelly et al., 2020). Viral tracers were used to drive expression of channelrhodopsin or archaerhodopsin in the polysynaptic projections to mPFC originating from the right Crus I. Increased activity in these terminals *via* optical stimulation increased ASD-like behaviors, while optical inhibition decreased them. Increased activity in this pathway is thought to be linked to the loss of Purkinje cells in the cerebellar cortex that occurs in ASD (Fatemi et al., 2012), resulting in persistent excitatory output. With regard to CTC, dysfunction or loss of Purkinje cells likely results in less opportunity for selective spatiotemporal synchronization, since excitatory output from the cerebellum is normally modulated in response to task-relevant patterns of cerebral activity. Selective synchronization occurs when activation in selected neocortical regions stands out from a background level of neuronal activity, which becomes increasingly difficult as the background level of activity is increased.

In a study of resting state EEG activity that focused specifically on coherence in the low frequency (0.5–3.5 Hz) range, Barttfeld et al. (2011) reported reduced long-range and increased short-range coherence in individuals with ASD. The same study showed that the magnitude of the coherence deficit compared to control subjects scaled with the severity of the ASD phenotype (Barttfeld et al., 2011). Murias et al. (2007) also used EEG recordings and reported increased local and reduced long-distance coherence in individuals with ASD compared to typically behaving control

subjects. Task related functional connectivity, measured with fMRI, was found to be reduced in the visual system of patients with ASD during a task testing working memory of faces (Koshino et al., 2008).

Dinstein et al. (2011) investigated interhemispheric synchronization in toddlers with ASD while they were sleeping in an fMRI. They reported significantly reduced interhemispheric synchronization between language areas and showed that the magnitude of the synchronization was negatively correlated with ASD severity (Dinstein et al., 2011). Supekar et al. (2013) also used fMRI to study an older group of children while they were awake and found that the brains of children with ASD showed brain-wide hyperconnectivity, with the degree of hyperconnectivity predicting the severity of social behavior deficits. Another study by Oldehinkel et al. (2019) examined cerebrocerebellar fMRI connectivity more directly and found that the subjects with ASD exhibited an increase in connectivity between the cerebellum and primary sensory and motor networks. At the same time, the functional connectivity within these networks was abnormally low, with the degree of the connectivity deficit correlated with the severity of symptoms such as sensory processing, repetitive behaviors, and social impairments.

While it is becoming increasingly clear that the cerebellum plays an important role in the development of cerebral functional networks, studies exploring the development of cerebrocerebellar functional connectivity in ASD are lacking. In the meantime, studies of cerebellar cortical development offer some clues as to a functional role of the cerebellum in ASD etiology. Focal gray matter volumes have been found to correlate with performance in specific cognitive domains (Moore et al., 2017) for typically developing children, as well as symptom severity in ASD (D'Mello et al., 2015). Most dramatically, D'Mello et al. (2015) showed that underdevelopment of the right Crus I and Crus II was common in subjects with ASD and associated with higher severity of all symptoms assessed by the Autism Diagnostic Observation Schedule. The authors noted that Crus I/II is functionally connected with the prefrontal and parietal cortices, which are shown to have decreased inter-areal connectivity (hypoconnectivity) in ASD (Washington et al., 2014). This suggests that abnormal development of the gray matter in Crus I/II causes a deficit of selective synchronization between its target nodes, and that this loss of selective synchronization may be a key driver of cognitive and behavioral deficits affecting individuals with ASD.

While the results of these studies show some variability, they consistently show that the brains of individuals with ASD have deficits in intrinsic functional connectivity. Interestingly, these results show an apparent tendency toward low-complexity functional network organization in subjects with ASD (Lai et al., 2010; Rudie et al., 2013) – reflecting either excessive segregation or excessive integration of function (Lord et al., 2017). Such deficits are consistent with Frith's theory of ASD and would be predicted to result from cerebellar pathology and/or pathophysiology if the cerebellum is tasked with the coordination of selective communication between brain areas.

Coherence/Functional Connectivity Abnormalities in Schizophrenia

Schizophrenia or schizophrenia-like symptoms have long been associated with cerebellar neuropathology (Weinberger et al., 1980; Jurjus et al., 1994; Martin and Albers, 1995). A recent study with a sizable and diverse cohort of 983 schizophrenia patients and 1349 healthy controls used MRI to evaluate structural changes in the cerebellum and cerebral cortex (Moberget et al., 2018). In agreement with earlier studies, Moberget et al. (2018) reported a significant reduction of cerebellar gray matter volume in schizophrenia patients compared to control subjects. The largest volume reduction in the cerebellum patients was found in LS, Crus I and Crus II (Moberget et al., 2018). Those same cerebellar areas have previously been shown to be functionally connected with frontoparietal cerebral cortical areas (Buckner et al., 2011). Moberget et al. (2018) found a significant correlation between cerebellar gray matter volume and frontoparietal cortical thickness. Interestingly, this correlation that was strongest in schizophrenia patients, suggesting that the underlying disease jointly affects the cerebellum and cerebral cortex (Moberget et al., 2018).

Karl Friston and Uta Frith proposed dysconnection as a cause of schizophrenia (Friston and Frith, 1995; McGuire and Frith, 1996; Friston, 1999). Results from imaging studies that evaluate functional connectivity in brains of schizophrenia patients and healthy controls largely support the dysconnection hypothesis. For example, the analysis of resting state functional connectivity MRI (rs-fcMRI) showed that patients had deficits in the default-mode network, the fronto-parietal and saliency networks (Orliac et al., 2013; Chang et al., 2014; Sheffield et al., 2015; Goswami et al., 2020), and had abnormal cerebrocerebellar connectivity (Repovs et al., 2011; Tu et al., 2012; Sheffield and Barch, 2016; Kim et al., 2020). At least one study reported that (Moberget et al., 2018) the severity of schizophrenia symptomatology scaled with the magnitude of the deficits in resting state network connectivity (Orliac et al., 2013). There is currently no agreement on the causes of dysconnectivity. Suggestions include reduced white matter connections but also the possibility of abnormal synaptic plasticity (Stephan et al., 2009; Pettersson-Yeo et al., 2011). The role of the cerebellum we propose here adds a crucial third possibility, suggesting that the deficits in network connectivity in schizophrenia are a consequence of loss of cerebellar coordination of CTC.

In an fMRI study that focused on network interactions, Andreasen et al. (1996, 1998) described a dysfunctional prefrontal-thalamic-cerebellar circuitry in schizophrenia patients and proposed that as a result, schizophrenia patients suffer from "cognitive dysmetria." The choice of the term "dysmetria" implicates the cerebellum, as that term commonly describes the inability of cerebellar patients to appropriately control the distance of limb or eye movements. There is no clear specification of how dysmetria applies to cognitive processes, but the proposed coordination of communication by the cerebellum, as we propose here,

relies on principles of precise temporal coordination by the cerebellum that are otherwise ascribed to cerebellar coordination of movements (Diener et al., 1992, 1993). A cerebellar role in coordinating communication between brain areas, and its failure in the brains of schizophrenia patients offers a possible explanation for the findings of dysconnectivity within the cerebral cortex and between the cerebral cortex and the cerebellum. Failed temporal coordination in motor control results in movement dysmetria because the timing of agonist and antagonist activation and inhibition times are no longer appropriately aligned. Applied to cerebral cortical oscillations, failed temporal coordination results in dysmetria of communication because the timing of phase relationships between communication structures is no longer supporting efficient communication.

There is currently no experimental work that would directly show a deficit in cerebellar coordination of CTC in schizophrenia. However, studies using cerebellar stimulation in schizophrenia patients provide evidence that delta and theta oscillation power, which is reduced in the frontal cortex of patients (Parker et al., 2017), can be restored by rhythmic stimulation of the cerebellum (Singh et al., 2019). The influence of the cerebellum on frontal cortical delta activity was reproduced in rats, where delta-activity in the frontal cortex was reduced after locally blocking D1 dopamine receptors, a model that mimics D1 dysfunction in schizophrenia (Parker et al., 2017). The subsequent delta-frequency optogenetic stimulation of thalamic synaptic terminals of afferents from the lateral (dentate) cerebellar nucleus was sufficient to restore delta activity in the frontal cortex (Parker et al., 2017). In this same study, the rats were trained to perform an interval timing task, estimating interval duration of 3 and 12, and blocking frontal cortical D1 receptors reduced the rat's performance in the task. Task performance was again rescued by stimulation of thalamic synaptic terminals of afferents from the lateral (dentate) cerebellar nucleus (Parker et al., 2017). Schizophrenia patients receiving theta burst trans-cranial magnetic stimulation reported significant mood elevations and showed improved memory performance (Demirtas-Tatlidede et al., 2010). Using a similar stimulus for the cerebellum and comparing theta and delta frequency stimuli, Singh et al. (2019) showed an increase in theta oscillation power in the frontal cortex of schizophrenia patients, suggesting the modulation of frontal delta/theta range oscillations by the cerebellum as a possible underlying mechanism for the cognitive and affective improvements observed by Demirtas-Tatlidede et al. (2010).

How the cerebellum modulates delta/theta power in the frontal cortex and how cerebellar neuropathology and its related functional pathophysiological defects would result in diminished delta/theta activity in schizophrenia is unclear. However, several studies have shown that the cerebellum modulates dopamine release in the frontal cortex (Mittleman et al., 2008; Rogers et al., 2011). These findings suggest a direct link between deficits in cerebellar function and deficits in frontal cortical dopamine regulation, which is widely regarded to be a key underlying cause of schizophrenia.

EXISTING VIEWS OF CEREBROCEREBELLAR INTERACTIONS

Cerebrocerebellar interactions have mostly been investigated in the motor domain. We agree with the premise brought forth in recent work (Wagner and Luo, 2019; Li and Mrsic-Flogel, 2020) that the cerebrocerebellar interactions in the cognitive domain are likely analogous to how the cerebellum interacts with motor areas. Thus, it is reasonable to ask how views developed for cerebrocerebellar interaction in motor control can be applied to cerebellar cognitive function and specifically, how they relate to the view we propose here. Several recent studies investigating cerebrocerebellar interactions in the context of preparatory activity provide strong evidence for a cerebellar involvement in the generation of preparatory activity in motor cortical areas (Gao et al., 2018; Chabrol et al., 2019; Li and Mrsic-Flogel, 2020). There is general agreement that the cerebrocerebellar connection loop forms the neuronal basis for cerebellar involvement in the generation of preparatory motor activity. Experimental evidence shows that lesioning of either the neocortex or cerebellum disrupts preparatory activity in the other region, indicating that preparatory activity in the two structures is interdependent (Gao et al., 2018; Chabrol et al., 2019; Li and Mrsic-Flogel, 2020). However, the nature of the neuronal interaction exchanged *via* the cerebrocerebellar loop remains unclear. Li and Mrsic-Flogel (2020) suggest that the cerebellum, through supervised learning, recognizes specific patterns of cerebral cortical inputs and in response returns predictive signals to trigger a state transition in the cerebral cortex shaped to minimize errors in the execution of the next movement segment. Supervised learning is a process by which a system maps input patterns to output patterns based on the observation of consistent input-output pairs, with climbing fiber inputs widely believed to provide error signals (Raymond and Medina, 2018). With regard to movement, the cerebellum is thought to encode neuronal signals related to movement commands as well as their sensory consequences in order to learn their relationship and provide feedback to minimize the difference between expectation and outcome. For a recent review see Raymond and Medina (2018). Alternatively, climbing fibers may generate teaching signals that defy the supervised learning paradigm; it has been shown that under certain conditions teaching signals are scalar, and vary with the predictability of a given stimulus. These features of teaching signals are more consistent with a temporal-difference model of reinforcement learning (Ohmae and Medina, 2015; Lawrenson et al., 2016; Hull, 2020). These hypotheses establish a clear purpose for cerebellar feedback *via* the cerebrocerebellar loop but leave unaddressed the spatiotemporal nature of the signals exchanged, and how they might conform with our current understanding of cortical states. In other words, if corticocerebellar signals need to faithfully represent cortical activity states, and cerebellocortical signals need to be designed to reliably guide cortical activity to the next desired state, then the following key questions arise. How is the oscillatory neuronal activity that defines cortical states represented in MF inputs

and how can this activity be altered *via* cerebellothalamocortical projections?

A recent study by Wagner et al. (2019) provided important new insights into cerebellar representation of cerebrocortical activity states. For their study, head-fixed mice learned to shift a lever to the left or right for a water reward while the activity of layer V (L5) neurons in the forelimb premotor area and GC activity in cerebellar lobule VI were monitored with 2P-calcium imaging throughout the learning process. As task performance improved, the activity patterns of L5 premotor cortical neurons and that of lobule VI GCs become increasingly similar (Wagner et al., 2019). Cerebrocerebellar interaction during a learned motor task thus ultimately may result in cerebral cortical activity states to be represented in the input layer of the cerebellar cortex. Importantly, this is consistent with other studies showing an increase in functional connectivity between the cerebellum and cerebral cortex during motor learning (Mehrkanoon et al., 2016), suggesting that learning facilitates information transmission between cerebral and cerebellar areas involved in the learned task. Both of the above studies focused on cerebellar interaction with a single cerebral cortical area and in the context of motor control (Mehrkanoon et al., 2016; Wagner et al., 2019). If this mechanism holds true for cerebellar interactions with other cerebral cortical areas, it provides a mechanism for the cerebellum to access activity states in cerebral cortical areas with which it interacts in the context of learning. In a more general sense, we argue that the cerebellum encodes a cortical state based on a signature arrangement of distributed neocortical oscillations, and subsequently generates outputs that drive thalamic neurons to modulate oscillatory activity to achieve the desired new cortical state. Specifically, we propose that cerebellar projections to the thalamus are likely to influence thalamic matrix neurons, which terminate preferentially on inhibitory interneurons in cortical layer I (Cruikshank et al., 2012), which play a key role in the generation and modulation of cortical oscillations, especially gamma rhythms (Atallah and Scanziani, 2009; Cardin et al., 2009).

TESTING THE VALIDITY OF THE PROPOSED NEW ROLE OF THE CEREBELLUM

Future animal and clinical (imaging) experiments should be designed to allow the analysis of cerebellar activity and its relationship to coherence between cerebral cortical areas. Currently, all experiments and analyses focus on modulation of activity in individual cerebral and cerebellar areas. The key is to rethink this approach and consider the functional connectivity *via* coherence between cerebral cortical areas as a dependent variable to correlate with cerebellar cortical activity. Human imaging studies lend themselves to this type of analysis but with the limitations that EEG and MEG, which capture fast dynamics, cannot readily access deep cerebellar structures. Magnetic resonance imaging can access activity in brain structures at any location but will only capture slow changes in activation. Animal studies that combine single-unit recordings in the cerebellum, thalamus and cerebral cortex with cell type specific manipulations of cerebrocerebellar connection pathways will be necessary to provide details about the circuits involved, the behaviors affected and the possible influence of neuromodulatory transmitters. The now well documented influence of cerebellar activity on dopamine release in the prefrontal cortex (Mittleman et al., 2008; Rogers et al., 2011) has been suggested to serve reward related functions (Wagner et al., 2017; Carta et al., 2019) but is also likely to influence the power of frontal cortical oscillations in the delta and theta frequency range. Here, we focused our arguments on cognitive function as the most intriguing new role of the cerebellum. However, cerebellar involvement in sensorimotor control is likely to invoke the same principles of task dependent coordination of CTC. After all, cerebellar coordination of coherence in the cerebral cortex was first demonstrated between the primary sensory and motor cortices in rats (Popa et al., 2013) and more recently in the whisker barrel system in mice (Lindeman et al., 2021).

The principle of cerebellar coordination of precisely timed events, as it occurs in the control of muscle contractions to optimize motor coordination, is here applied to the coordination of neuronal oscillations to optimize cerebral cortical communication during cognitive processes. The elegance of this new perspective of cerebrocerebellar interaction lies in its intuitive simplicity that does not require additional assumptions about cerebellar function and can provide a functional interpretation of cerebellar cortical network architecture.

DATA AVAILABILITY STATEMENT

The original contributions presented in the study are included in the article/supplementary material, further inquiries can be directed to the corresponding author.

AUTHOR CONTRIBUTIONS

All authors contributed to the development of the concept. SM and DH wrote and edited the manuscript. YL and RS contributed to writing and editing.

FUNDING

SM was supported by American Lebanese Syrian Associated Charities, St. Jude Children's Research Hospital. DH and YL were supported by R01MH112143, R01MH112143-02S1, and R37MH085726 and the University of Tennessee Neuroscience Institute. RS was supported by R01NS089664, R01NS100874, and 1P50HD103555.

ACKNOWLEDGMENTS

We would like to thank Brittany Correia for valuable comments on earlier versions of the manuscript.

REFERENCES

Andreasen, N. C., O'Leary, D. S., Cizadlo, T., Arndt, S., Rezai, K., Ponto, L. L., et al. (1996). Schizophrenia and cognitive dysmetria: a positron-emission tomography study of dysfunctional prefrontal-thalamic-cerebellar circuitry. *Proc. Natl. Acad. Sci. U.S.A.* 93, 9985–9990. doi: 10.1073/pnas.93.18.9985

Andreasen, N. C., Paradiso, S., and O'Leary, D. S. (1998). "Cognitive dysmetria" as an integrative theory of schizophrenia: A dysfunction in cortical-subcortical-cerebellar circuitry? *Schizophr. Bull.* 24, 203–218.

Andreasen, N. C., and Pierson, R. (2008). The role of the cerebellum in schizophrenia. *Biol. Psychiatry* 64, 81–88.

Ashida, R., Cerminara, N. L., Edwards, R. J., Apps, R., and Brooks, J. C. W. (2019). Sensorimotor, language, and working memory representation within the human cerebellum. *Hum. Brain Mapp.* 40, 4732–4747. doi: 10.1002/hbm.24733

Atallah, B. V., and Scanziani, M. (2009). Instantaneous modulation of gamma oscillation frequency by balancing excitation with inhibition. *Neuron* 62, 566–577. doi: 10.1016/j.neuron.2009.04.027

Aumann, T. D., and Horne, M. K. (1996a). A comparison of the ultrastructure of synapses in the cerebello-rubral and cerebello-thalamic pathways in the rat. *Neurosci. Lett.* 211, 175–178.

Aumann, T. D., and Horne, M. K. (1996b). Ramification and termination of single axons in the cerebellothalamic pathway of the rat. *J. Comp. Neurol.* 376, 420–430.

Ayzenshtat, I., Meirovithz, E., Edelman, H., Werner-Reiss, U., Bienenstock, E., Abeles, M., et al. (2010). Precise spatiotemporal patterns among visual cortical areas and their relation to visual stimulus processing. *J. Neurosci.* 30, 11232–11245.

Baker, S. N., Kilner, J. M., Pinches, E. M., and Lemon, R. N. (1999). The role of synchrony and oscillations in the motor output. *Exp. Brain Res.* 128, 109–117. doi: 10.1007/s002210050825

Barttfeld, P., Wicker, B., Cukier, S., Navarta, S., Lew, S., and Sigman, M. (2011). A big-world network in ASD: dynamical connectivity analysis reflects a deficit in long-range connections and an excess of short-range connections. *Neuropsychologia* 49, 254–263. doi: 10.1016/j.neuropsychologia.2010.11.024

Bastos, A. M., Loonis, R., Kornblith, S., Lundqvist, M., and Miller, E. K. (2018). Laminar recordings in frontal cortex suggest distinct layers for maintenance and control of working memory. *Proc. Natl. Acad. Sci. U.S.A.* 115, 1117–1122. doi: 10.1073/pnas.1710323115

Bauman, M., and Kemper, T. L. (1985). Histoanatomic observations of the brain in early infantile autism. *Neurology* 35, 866–874.

Becker, E. B., and Stoodley, C. J. (2013). Autism spectrum disorder and the cerebellum. *Int. Rev. Neurobiol.* 113, 1–34. doi: 10.1016/B978-0-12-418700-9.00001-0

Benchenane, K., Tiesinga, P. H., and Battaglia, F. P. (2011). Oscillations in the prefrontal cortex: a gateway to memory and attention. *Curr. Opin. Neurobiol* 21, 475–485. doi: 10.1016/j.conb.2011.01.004

Biswas, M. S., Luo, Y., Sarpong, G. A., and Sugihara, I. (2019). Divergent projections of single pontocerebellar axons to multiple cerebellar lobules in the mouse. *J. Comp. Neurol.* 527, 1966–1985. doi: 10.1002/cne.24662

Bonnefond, M., Kastner, S., and Jensen, O. (2017). Communication between Brain areas based on nested oscillations. *eNeuro* 4:ENEURO.0153-16.2017. doi: 10.1523/ENEURO.0153-16.2017

Bosman, C. A., Schoffelen, J. M., Brunet, N., Oostenveld, R., Bastos, A. M., Womelsdorf, T., et al. (2012). Attentional stimulus selection through selective synchronization between monkey visual areas. *Neuron* 75, 875–888. doi: 10.1016/j.neuron.2012.06.037

Braitenberg, V., and Atwood, R. P. (1958). Morphological observations on the cerebellar cortex. *J. Comp. Neurol.* 109, 1–33.

Braitenberg, V., Heck, D. H., and Sultan, F. (1997). The detection and generation of sequences as a key to cerebellar function: experiments and theory. *Behav. Brain Sci.* 20, 229–245.

Brissenden, J. A., Tobyne, S. M., Osher, D. E., Levin, E. J., Halko, M. A., and Somers, D. C. (2018). Topographic Cortico-cerebellar networks revealed by visual attention and working memory. *Curr. Biol.* 28, 3364–3372.e5. doi: 10.1016/j.cub.2018.08.059

Brock, J., Brown, C. C., Boucher, J., and Rippon, G. (2002). The temporal binding deficit hypothesis of autism. *Dev. Psychopathol.* 14, 209–224.

Brodal, P., and Bjaalie, J. G. (1992). Organization of the pontine nuclei. *Neurosci. Res.* 13, 83–118.

Brookes, M. J., Woolrich, M., Luckhoo, H., Price, D., Hale, J. R., Stephenson, M. C., et al. (2011). Investigating the electrophysiological basis of resting state networks using magnetoencephalography. *Proc. Natl. Acad. Sci. U.S.A.* 108, 16783–16788. doi: 10.1073/pnas.1112685108

Brunet, N. M., Bosman, C. A., Vinck, M., Roberts, M., Oostenveld, R., Desimone, R., et al. (2014). Stimulus repetition modulates gamma-band synchronization in primate visual cortex. *Proc. Natl. Acad. Sci. U.S.A.* 111, 3626–3631. doi: 10.1073/pnas.1309714111

Buckner, R. L. (2013). The cerebellum and cognitive function: 25 years of insight from anatomy and neuroimaging. *Neuron* 80, 807–815. doi: 10.1016/j.neuron.2013.10.044

Buckner, R. L., Krienen, F. M., Castellanos, A., Diaz, J. C., and Yeo, B. T. (2011). The organization of the human cerebellum estimated by intrinsic functional connectivity. *J. Neurophysiol.* 106, 2322–2345. doi: 10.1152/jn.00339.2011

Buckner, R. L., Krienen, F. M., and Yeo, B. T. (2013). Opportunities and limitations of intrinsic functional connectivity MRI. *Nat. Neurosci.* 16, 832–837. doi: 10.1038/nn.3423

Burguiere, E., Arleo, A., Hojjati, M., Elgersma, Y., De Zeeuw, C. I., Berthoz, A., et al. (2005). Spatial navigation impairment in mice lacking cerebellar LTD: a motor adaptation deficit? *Nat. Neurosci.* 8, 1292–1294. doi: 10.1038/nn1532

Canto, C. B., Witter, L., and De Zeeuw, C. I. (2016). Whole-cell properties of cerebellar nuclei neurons *in vivo*. *PLoS One* 11:e0165887. doi: 10.1371/journal.pone.0165887

Cardin, J. A., Carlen, M., Meletis, K., Knoblich, U., Zhang, F., Deisseroth, K., et al. (2009). Driving fast-spiking cells induces gamma rhythm and controls sensory responses. *Nature* 459, 663–667. doi: 10.1038/nature08002

Carlezon, W. A. Jr., and Chartoff, E. H. (2007). Intracranial self-stimulation (ICSS) in rodents to study the neurobiology of motivation. *Nat. Protoc.* 2, 2987–2995. doi: 10.1038/nprot.2007.441

Carta, I., Chen, C. H., Schott, A. L., Dorizan, S., and Khodakhah, K. (2019). Cerebellar modulation of the reward circuitry and social behavior. *Science* 363:eaav0581. doi: 10.1126/science.aav0581

Castro-Alamancos, M. A. (2013). The motor cortex: a network tuned to 7-14 Hz. *Front. Neural Circuits* 7:21. doi: 10.3389/fncir.2013.00021

Chabrol, F. P., Blot, A., and Mrsic-Flogel, T. D. (2019). Cerebellar contribution to preparatory activity in motor neocortex. *Neuron* 103, 506–519.e4. doi: 10.1016/j.neuron.2019.05.022

Chang, X., Shen, H., Wang, L., Liu, Z., Xin, W., Hu, D., et al. (2014). Altered default mode and fronto-parietal network subsystems in patients with schizophrenia and their unaffected siblings. *Brain Res.* 1562, 87–99. doi: 10.1016/j.brainres.2014.03.024

Cheron, G., Marquez-Ruiz, J., and Dan, B. (2016). Oscillations, Timing, Plasticity, and Learning in the Cerebellum. *Cerebellum* 15, 122–138. doi: 10.1007/s12311-015-0665-9

Churchwell, J. C., and Kesner, R. P. (2011). Hippocampal-prefrontal dynamics in spatial working memory: interactions and independent parallel processing. *Behav. Brain Res.* 225, 389–395. doi: 10.1016/j.bbr.2011.07.045

Clasca, F., Rubio-Garrido, P., and Jabaudon, D. (2012). Unveiling the diversity of thalamocortical neuron subtypes. *Eur. J. Neurosci.* 35, 1524–1532. doi: 10.1111/j.1460-9568.2012.08033.x

Courchesne, E. (1997). Brainstem, cerebellar and limbic neuroanatomical abnormalities in autism. *Curr. Opin. Neurobiol.* 7, 269–278.

Cruikshank, S. J., Ahmed, O. J., Stevens, T. R., Patrick, S. L., Gonzalez, A. N., Elmaleh, M., et al. (2012). Thalamic control of layer 1 circuits in prefrontal cortex. *J. Neurosci.* 32, 17813–17823. doi: 10.1523/JNEUROSCI.3231-12.2012

Damasio, A. R. (1989). Time-locked multiregional retroactivation: a systems-level proposal for the neural substrates of recall and recognition. *Cognition* 33, 25–62. doi: 10.1016/0010-0277(89)90005-x

Demirtas-Tatlidede, A., Freitas, C., Cromer, J. R., Safar, L., Ongur, D., Stone, W. S., et al. (2010). Safety and proof of principle study of cerebellar vermal theta burst stimulation in refractory schizophrenia. *Schizophr. Res.* 124, 91–100. doi: 10.1016/j.schres.2010.08.015

Destexhe, A., Contreras, D., and Steriade, M. (1999). Cortically-induced coherence of a thalamic-generated oscillation. *Neuroscience* 92, 427–443.

Diedrichsen, J., Verstynen, T., Schlerf, J., and Wiestler, T. (2010). Advances in functional imaging of the human cerebellum. *Curr. Opin. Neurol.* 23, 382–387. doi: 10.1097/WCO.0b013e32833be837

Diener, H. C., Dichgans, J., Guschlbauer, B., Bacher, M., Rapp, H., and Klockgether, T. (1992). The coordination of posture and voluntary movement in patients with cerebellar dysfunction. *Mov. Disord.* 7, 14–22.

Diener, H. C., Hore, J., Ivry, R., and Dichgans, J. (1993). Cerebellar dysfunction of movement and perception. *Can. J. Neurol. Sci.* 20(Suppl. 3), S62–S69.

Dinstein, I., Pierce, K., Eyler, L., Solso, S., Malach, R., Behrmann, M., et al. (2011). Disrupted neural synchronization in toddlers with autism. *Neuron* 70, 1218–1225. doi: 10.1016/j.neuron.2011.04.018

D'Mello, A. M., Crocetti, D., Mostofsky, S. H., and Stoodley, C. J. (2015). Cerebellar gray matter and lobular volumes correlate with core autism symptoms. *Neuroimage Clin.* 7, 631–639. doi: 10.1016/j.nicl.2015.02.007

Du, X., Rowland, L. M., Summerfelt, A., Choa, F. S., Wittenberg, G. F., Wisner, K., et al. (2018). Cerebellar-stimulation evoked prefrontal electrical synchrony is modulated by GABA. *Cerebellum* 17, 550–563. doi: 10.1007/s12311-018-0945-2

Fair, D. A., Cohen, A. L., Power, J. D., Dosenbach, N. U., Church, J. A., Miezin, F. M., et al. (2009). Functional brain networks develop from a "local to distributed" organization. *PLoS Comput Biol* 5:e1000381. doi: 10.1371/journal.pcbi.1000381

Farzan, F., Pascual-Leone, A., Schmahmann, J. D., and Halko, M. (2016). Enhancing the temporal complexity of distributed brain networks with patterned cerebellar stimulation. *Sci. Rep.* 6:23599. doi: 10.1038/srep23599

Fatemi, S. H., Aldinger, K. A., Ashwood, P., Bauman, M. L., Blaha, C. D., Blatt, G. J., et al. (2012). Consensus paper: pathological role of the cerebellum in autism. *Cerebellum* 11, 777–807. doi: 10.1007/s12311-012-0355-9

Fernandez, L., Rogasch, N. C., Do, M., Clark, G., Major, B. P., Teo, W. P., et al. (2020). Cerebral cortical activity following non-invasive cerebellar stimulation-a systematic review of combined TMS and EEG studies. *Cerebellum* 19, 309–335. doi: 10.1007/s12311-019-01093-7

Fox, M. D., and Raichle, M. E. (2007). Spontaneous fluctuations in brain activity observed with functional magnetic resonance imaging. *Nat. Rev. Neurosci.* 8, 700–711. doi: 10.1038/nrn2201

Freeman, W. J., Holmes, M. D., Burke, B. C., and Vanhatalo, S. (2003). Spatial spectra of scalp EEG and EMG from awake humans. *Clin. Neurophysiol.* 114, 1053–1068. doi: 10.1016/S1388-2457(03)00045-2

Fries, P. (2005). A mechanism for cognitive dynamics: neuronal communication through neuronal coherence. *Trends Cogn. Sci.* 9, 474–480.

Fries, P. (2015). Rhythms for cognition: communication through coherence. *Neuron* 88, 220–235.

Friston, K. J. (1999). Schizophrenia and the disconnection hypothesis. *Acta Psychiatr. Scand. Suppl.* 395, 68–79.

Friston, K. J., and Frith, C. D. (1995). Schizophrenia: A disconnection syndrome? *Clin. Neurosci.* 3, 89–97.

Frith, U. (1997). The neurocognitive basis of autism. *Trends Cogn. Sci.* 1, 73–77. doi: 10.1016/S1364-6613(97)01010-3

Gao, Z., Davis, C., Thomas, A. M., Economo, M. N., Abrego, A. M., Svoboda, K., et al. (2018). A cortico-cerebellar loop for motor planning. *Nature* 563, 113–116. doi: 10.1038/s41586-018-0633-x

Gauck, V., and Jaeger, D. (2000). The control of rate and timing of spikes in the deep cerebellar nuclei by inhibition. *J. Neurosci.* 20, 3006–3016.

Gordon, J. A. (2011). Oscillations and hippocampal-prefrontal synchrony. *Curr. Opin. Neurobiol.* 21, 486–491. doi: 10.1016/j.conb.2011.02.012

Goswami, S., Beniwal, R. P., Kumar, M., Bhatia, T., Gur, R. E., Gur, R. C., et al. (2020). A preliminary study to investigate resting state fMRI as a potential group differentiator for schizophrenia. *Asian J. Psychiatr.* 52:102095. doi: 10.1016/j.ajp.2020.102095

Guell, X., Gabrieli, J. D. E., and Schmahmann, J. D. (2018a). Triple representation of language, working memory, social and emotion processing in the cerebellum: convergent evidence from task and seed-based resting-state fMRI analyses in a single large cohort. *Neuroimage* 172, 437–449. doi: 10.1016/j.neuroimage.2018.01.082

Guell, X., Schmahmann, J. D., Gabrieli, J., and Ghosh, S. S. (2018b). Functional gradients of the cerebellum. *eLife* 7:e36652. doi: 10.7554/eLife.36652

Guillery, R. W. (1995). Anatomical evidence concerning the role of the thalamus in corticocortical communication: a brief review. *J. Anat.* 187(Pt 3), 583–592.

Habas, C., Kamdar, N., Nguyen, D., Prater, K., Beckmann, C. F., Menon, V., et al. (2009). Distinct cerebellar contributions to intrinsic connectivity networks. *J. Neurosci.* 29, 8586–8594.

Halko, M. A., Farzan, F., Eldaief, M. C., Schmahmann, J. D., and Pascual-Leone, A. (2014). Intermittent theta-burst stimulation of the lateral cerebellum increases functional connectivity of the default network. *J. Neurosci.* 34, 12049–12056. doi: 10.1523/JNEUROSCI.1776-14.2014

Hallock, H. L., Wang, A., and Griffin, A. L. (2016). Ventral midline thalamus is critical for hippocampal-prefrontal synchrony and spatial working memory. *J. Neurosci.* 36, 8372–8389. doi: 10.1523/JNEUROSCI.0991-16.2016

Heck, D. H. (1993). Rat cerebellar cortex in vitro responds specifically to moving stimuli. *Neurosci. Lett.* 157, 95–98.

Heck, D. H. (1995). Sequential input to guinea pig cerebellar cortex in vitro strongly affects Purkinje cells via parallel fibers. *Naturwissenschaften* 82, 201–203.

Heck, D. H. (1999). Sequential stimulation of rat and guinea pig cerebellar granular cells *in vitro* leads to increasing population activity in parallel fibers. *Neurosci. Lett.* 263, 137–140.

Heck, D. H., Thach, W. T., and Keating, J. G. (2007). On-beam synchrony in the cerebellum as the mechanism for the timing and coordination of movement. *Proc. Natl. Acad. Sci. U.S.A.* 104, 7658–7663.

Heleven, E., van Dun, K., and Van Overwalle, F. (2019). The posterior Cerebellum is involved in constructing Social Action Sequences: an fMRI Study. *Sci. Rep.* 9:11110. doi: 10.1038/s41598-019-46962-7

Henschke, J. U., and Pakan, J. M. (2020). Disynaptic cerebrocerebellar pathways originating from multiple functionally distinct cortical areas. *eLife* 9:e59148. doi: 10.7554/eLife.59148

Houk, J. C. (1991). Red nucleus: role in motor control. *Curr. Opin. Neurobiol.* 1, 610–615. doi: 10.1016/s0959-4388(05)80037-6

Hull, C. (2020). Prediction signals in the cerebellum: beyond supervised motor learning. *eLife* 9:e59148. doi: 10.7554/eLife.54073

Hyman, J. M., Zilli, E. A., Paley, A. M., and Hasselmo, M. E. (2010). Working memory performance correlates with prefrontal-hippocampal theta interactions but not with prefrontal neuron firing rates. *Front. Integr. Neurosci.* 4:2. doi: 10.3389/neuro.07.002.2010

Ito, M. (2008). Control of mental activities by internal models in the cerebellum. *Nat. Rev. Neurosci.* 9, 304–313. doi: 10.1038/nrn2332

Jacobs, H. I. L., Hopkins, D. A., Mayrhofer, H. C., Bruner, E., van Leeuwen, F. W., Raaijmakers, W., et al. (2018). The cerebellum in Alzheimer's disease: evaluating its role in cognitive decline. *Brain* 141, 37–47. doi: 10.1093/brain/awx194

Jones, E. G. (2001). The thalamic matrix and thalamocortical synchrony. *Trends Neurosci.* 24, 595–601. doi: 10.1016/s0166-2236(00)01922-6

Jones, M. W., and Wilson, M. A. (2005). Theta rhythms coordinate hippocampal-prefrontal interactions in a spatial memory task. *PLoS Biol.* 3:e402. doi: 10.1371/journal.pbio.0030402

Jurjus, G. J., Weiss, K. M., and Jaskiw, G. E. (1994). Schizophrenia-like psychosis and cerebellar degeneration. *Schizophr. Res.* 12, 183–184.

Just, M. A., Cherkassky, V. L., Keller, T. A., and Minshew, N. J. (2004). Cortical activation and synchronization during sentence comprehension in high-functioning autism: evidence of underconnectivity. *Brain* 127(Pt 8), 1811–1821. doi: 10.1093/brain/awh199

Just, M. A., Keller, T. A., Malave, V. L., Kana, R. K., and Varma, S. (2012). Autism as a neural systems disorder: a theory of frontal-posterior underconnectivity. *Neurosci. Biobehav. Rev.* 36, 1292–1313. doi: 10.1016/j.neubiorev.2012.02.007

Kelly, E., Meng, F., Fujita, H., Morgado, F., Kazemi, Y., Rice, L. C., et al. (2020). Regulation of autism-relevant behaviors by cerebellar-prefrontal cortical circuits. *Nat. Neurosci.* 23, 1102–1110. doi: 10.1038/s41593-020-0665-z

Kelly, R. M., and Strick, P. L. (2003). Cerebellar loops with motor cortex and prefrontal cortex of a nonhuman primate. *J. Neurosci.* 23, 8432–8444.

Kim, D. J., Moussa-Tooks, A. B., Bolbecker, A. R., Apthorp, D., Newman, S. D., O'Donnell, B. F., et al. (2020). Cerebellar-cortical dysconnectivity in resting-state associated with sensorimotor tasks in schizophrenia. *Hum. Brain Mapp.* 41, 3119–3132. doi: 10.1002/hbm.25002

Kolkman, K. E., McElvain, L. E., and du Lac, S. (2011). Diverse precerebellar neurons share similar intrinsic excitability. *J. Neurosci.* 31, 16665–16674. doi: 10.1523/JNEUROSCI.3314-11.2011

Koshino, H., Kana, R. K., Keller, T. A., Cherkassky, V. L., Minshew, N. J., and Just, M. A. (2008). fMRI investigation of working memory for faces in autism: visual coding and underconnectivity with frontal areas. *Cereb. Cortex* 18, 289–300. doi: 10.1093/cercor/bhm054

Kundu, P., Benson, B. E., Rosen, D., Frangou, S., Leibenluft, E., Luh, W. M., et al. (2018). The integration of functional brain activity from adolescence to adulthood. *J. Neurosci.* 38, 3559–3570. doi: 10.1523/JNEUROSCI.1864-17.2018

Lai, M. C., Lombardo, M. V., Chakrabarti, B., Sadek, S. A., Pasco, G., Wheelwright, S. J., et al. (2010). A shift to randomness of brain oscillations in people with autism. *Biol. Psychiatry* 68, 1092–1099. doi: 10.1016/j.biopsych.2010.06.027

Lawrenson, C. L., Watson, T. C., and Apps, R. (2016). Transmission of predictable sensory signals to the cerebellum via climbing fiber pathways is gated during exploratory behavior. *J. Neurosci.* 36, 7841–7851. doi: 10.1523/JNEUROSCI.0439-16.2016

Leergaard, T. B., and Bjaalie, J. G. (2007). Topography of the complete corticopontine projection: from experiments to principal Maps. *Front. Neurosci.* 1:211–223. doi: 10.3389/neuro.01.1.1.016.2007

Lefort, J. M., Rochefort, C., Rondi-Reig, L., and Group of L.R.R. is member of Bio-Psy Labex and ENP Foundation (2015). Cerebellar contribution to spatial navigation: new insights into potential mechanisms. *Cerebellum* 14, 59–62. doi: 10.1007/s12311-015-0653-0

Lefort, J. M., Vincent, J., Tallot, L., Jarlier, F., De Zeeuw, C. I., Rondi-Reig, L., et al. (2019). Impaired cerebellar Purkinje cell potentiation generates unstable spatial map orientation and inaccurate navigation. *Nat. Commun.* 10:2251. doi: 10.1038/s41467-019-09958-5

Li, N., and Mrsic-Flogel, T. D. (2020). Cortico-cerebellar interactions during goal-directed behavior. *Curr. Opin. Neurobiol.* 65, 27–37. doi: 10.1016/j.conb.2020.08.010

Lindeman, S., Kros, L., Hong, S., Mejias, J. F., Romano, V., Negrello, M., et al. (2021). Cerebellar Purkinje cells can differentially modulate coherence between sensory and motor cortex depending on region and behavior. *Proc. Natl. Acad. Sci. U.S.A.* 118:e2015292118. doi: 10.1073/pnas.2015292118

Liu, X., and Duyn, J. H. (2013). Time-varying functional network information extracted from brief instances of spontaneous brain activity. *Proc. Natl. Acad. Sci. U.S.A.* 110, 4392–4397. doi: 10.1073/pnas.1216856110

Lord, L. D., Stevner, A. B., Deco, G., and Kringelbach, A. L. (2017). Understanding principles of integration and segregation using whole-brain computational connectomics: implications for neuropsychiatric disorders. *Philos. Trans. R. Soc. A Math. Phys. Eng. Sci.* 375:20160283. doi: 10.1098/rsta.2016.0283

Lu, L., Cao, Y., Tokita, K., Heck, D. H., and Boughter, J. D. (2013). Medial cerebellar nuclear projections and activity patterns link cerebellar output to orofacial and respiratory behavior. *Front. Neural Circuits* 7:56. doi: 10.3389/fncir.2013.00056

Maex, R., and Gutkin, B. (2017). Temporal integration and 1/f power scaling in a circuit model of cerebellar interneurons. *J. Neurophysiol.* 118, 471–485. doi: 10.1152/jn.00789.2016

Marek, S., Siegel, J. S., Gordon, E. M., Raut, R. V., Gratton, C., Newbold, D. J., et al. (2018). Spatial and temporal organization of the individual human cerebellum. *Neuron* 100, 977–993.e7. doi: 10.1016/j.neuron.2018.10.010

Martin, P., and Albers, M. (1995). Cerebellum and schizophrenia: a selective review. *Schizophr. Bull.* 21, 241–250.

Marvel, C. L., and Desmond, J. E. (2010). The contributions of cerebrocerebellar circuitry to executive verbal working memory. *Cortex* 46, 880–895. doi: 10.1016/j.cortex.2009.08.017

Mateo, C., Knutsen, P. M., Tsai, P. S., Shih, A. Y., and Kleinfeld, D. (2017). Entrainment of arteriole vasomotor fluctuations by neural activity is a basis of blood-oxygenation-level-dependent "Resting-State" Connectivity. *Neuron* 96, 936–948.e3. doi: 10.1016/j.neuron.2017.10.012

McAfee, S., Liu, Y., Sillitoe, R. V., and Heck, D. H. (2019). Cerebellar lobulus simplex and Crus I differentially represent phase and phase difference of prefrontal cortical and hippocampal oscillations. *Cell Rep.* 27, 2328–2334. doi: 10.1016/j.celrep.2019.04.085

McAfee, S. S., Liu, Y., Dhamala, M., and Heck, D. H. (2018). Thalamocortical communication in the awake mouse visual system involves phase synchronization and rhythmic spike synchrony at high gamma frequencies. *Front. Neurosci.* 12:837. doi: 10.3389/fnins.2018.00837

McDevitt, C. J., Ebner, T. J., and Bloedel, J. R. (1987). Relationships between simultaneously recorded Purkine cells and cerebellar nuclear neurons. *Brain Res.* 425, 1–13.

McGuire, P. K., and Frith, C. D. (1996). Disordered functional connectivity in schizophrenia. *Psychol. Med.* 26, 663–667. doi: 10.1017/s0033291700037673

Mehrkanoon, S., Boonstra, T. W., Breakspear, M., Hinder, M., and Summers, J. J. (2016). Upregulation of cortico-cerebellar functional connectivity after motor learning. *Neuroimage* 128, 252–263. doi: 10.1016/j.neuroimage.2015.12.052

Melik-Musyan, A. B., and Fanardjyan, V. V. (1998). Projections of the central cerebellar nuclei to the intralaminar thalamic nuclei in cats. *Neurophysiology* 30, 39–47. doi: 10.1007/Bf02463111

Mesulam, M. M. (1998). From sensation to cognition. *Brain* 121(Pt 6), 1013–1052.

Middleton, F. A., and Strick, P. L. (2001). Cerebellar projections to the prefrontal cortex of the primate. *J. Neurosci.* 21, 700–712.

Mittleman, G., Goldowitz, D., Heck, D. H., and Blaha, C. D. (2008). Cerebellar modulation of frontal cortex dopamine efflux in mice: relevance to autism and schizophrenia. *Synapse* 62, 544–550.

Moberget, T., Doan, N. T., Alnaes, D., Kaufmann, T., Cordova-Palomera, A., Lagerberg, T. V., et al. (2018). Cerebellar volume and cerebellocerebral structural covariance in schizophrenia: a multisite mega-analysis of 983 patients and 1349 healthy controls. *Mol. Psychiatry* 23, 1512–1520. doi: 10.1038/mp.2017.106

Moore, D. M., D'Mello, A. M., McGrath, L. M., and Stoodley, C. J. (2017). The developmental relationship between specific cognitive domains and grey matter in the cerebellum. *Dev. Cogn. Neurosci.* 24, 1–11. doi: 10.1016/j.dcn.2016.12.001

Morishima, M., Morita, K., Kubota, Y., and Kawaguchi, Y. (2011). Highly differentiated projection-specific cortical subnetworks. *J. Neurosci.* 31, 10380–10391. doi: 10.1523/JNEUROSCI.0772-11.2011

Morris, E. B., Phillips, N. S., Laningham, F. H., Patay, Z., Gajjar, A., Wallace, D., et al. (2009). Proximal dentatothalamocortical tract involvement in posterior fossa syndrome. *Brain* 132(Pt 11), 3087–3095. doi: 10.1093/brain/awp241

Murias, M., Swanson, J. M., and Srinivasan, R. (2007). Functional connectivity of frontal cortex in healthy and ADHD children reflected in EEG coherence. *Cereb. Cortex* 17, 1788–1799. doi: 10.1093/cercor/bhl089

Myers, N. E., Stokes, M. G., Walther, L., and Nobre, A. C. (2014). Oscillatory brain state predicts variability in working memory. *J. Neurosci.* 34, 7735–7743. doi: 10.1523/JNEUROSCI.4741-13.2014

Negron-Oyarzo, I., Espinosa, N., Aguilar-Rivera, M., Fuenzalida, M., Aboitiz, F., and Fuentealba, P. (2018). Coordinated prefrontal-hippocampal activity and navigation strategy-related prefrontal firing during spatial memory formation. *Proc. Natl. Acad. Sci. U.S.A.* 115, 7123–7128. doi: 10.1073/pnas.1720117115

Ohmae, S., and Medina, J. F. (2015). Climbing fibers encode a temporal-difference prediction error during cerebellar learning in mice. *Nat. Neurosci.* 18, 1798–1803. doi: 10.1038/nn.4167

Oldehinkel, M., Mennes, M., Marquand, A., Charman, T., Tillmann, J., Ecker, C., et al. (2019). Altered connectivity between cerebellum, visual, and sensory-motor networks in autism spectrum disorder: results from the EU-AIMS longitudinal european autism project. *Biol. Psychiatry Cogn. Neurosci. Neuroimaging* 4, 260–270. doi: 10.1016/j.bpsc.2018.11.010

Orliac, F., Naveau, M., Joliot, M., Delcroix, N., Razafimandimby, A., Brazo, P., et al. (2013). Links among resting-state default-mode network, salience network, and symptomatology in schizophrenia. *Schizophr. Res.* 148, 74–80. doi: 10.1016/j.schres.2013.05.007

Osipova, D., Takashima, A., Oostenveld, R., Fernandez, G., Maris, E., and Jensen, O. (2006). Theta and gamma oscillations predict encoding and retrieval of declarative memory. *J. Neurosci.* 26, 7523–7531. doi: 10.1523/JNEUROSCI.1948-06.2006

Palmigiano, A., Geisel, T., Wolf, F., and Battaglia, D. (2017). Flexible information routing by transient synchrony. *Nat. Neurosci.* 20, 1014–1022. doi: 10.1038/nn.4569

Parker, K. L., Kim, Y. C., Kelley, R. M., Nessler, A. J., Chen, K. H., Muller-Ewald, V. A., et al. (2017). Delta-frequency stimulation of cerebellar projections can compensate for schizophrenia-related medial frontal dysfunction. *Mol. Psychiatry* 22, 647–655. doi: 10.1038/mp.2017.50

Patay, Z. (2015). Postoperative posterior fossa syndrome: unraveling the etiology and underlying pathophysiology by using magnetic resonance imaging. *Childs Nerv. Syst.* 31, 1853–1858. doi: 10.1007/s00381-015-2796-1

Perciavalle, V., Apps, R., Bracha, V., Delgado-Garcia, J. M., Gibson, A. R., Leggio, M., et al. (2013). Consensus paper: current views

on the role of cerebellar interpositus nucleus in movement control and emotion. *Cerebellum* 12, 738–757. doi: 10.1007/s12311-013-0464-0

Person, A. L., and Raman, I. M. (2012). Purkinje neuron synchrony elicits time-locked spiking in the cerebellar nuclei. *Nature* 481, 502–505. doi: 10.1038/nature10732

Pettersson-Yeo, W., Allen, P., Benetti, S., McGuire, P., and Mechelli, A. (2011). Dysconnectivity in schizophrenia: where are we now? *Neurosci. Biobehav. Rev.* 35, 1110–1124. doi: 10.1016/j.neubiorev.2010.11.004

Picard, H., Amado, I., Mouchet-Mages, S., Olie, J. P., and Krebs, M. O. (2007). The role of the cerebellum in schizophrenia: an update of clinical, cognitive, and functional evidences. *Schizophr. Bull.* 34, 155–172.

Popa, D., Spolidoro, M., Proville, R. D., Guyon, N., Belliveau, L., and Lena, C. (2013). Functional role of the cerebellum in gamma-band synchronization of the sensory and motor cortices. *J. Neurosci.* 33, 6552–6556. doi: 10.1523/JNEUROSCI.5521-12.2013

Power, J. D., Fair, D. A., Schlaggar, B. L., and Petersen, S. E. (2010). The development of human functional brain networks. *Neuron* 67, 735–748. doi: 10.1016/j.neuron.2010.08.017

Raichle, M. E. (2015). The brain's default mode network. *Annu. Rev. Neurosci.* 38, 433–447. doi: 10.1146/annurev-neuro-071013-014030

Ramnani, N. (2006). The primate cortico-cerebellar system: anatomy and function. *Nat. Rev. Neurosci.* 7, 511–522. doi: 10.1038/nrn1953

Rapoport, M., van Reekum, R., and Mayberg, H. (2000). The role of the cerebellum in cognition and behavior: a selective review. *J. Neuropsychiatry Clin. Neurosci.* 12, 193–198. doi: 10.1176/jnp.12.2.193

Raymond, J. L., and Medina, J. F. (2018). Computational principles of supervised learning in the cerebellum. *Annu. Rev. Neurosci.* 41, 233–253. doi: 10.1146/annurev-neuro-080317-061948

Repovs, G., Csernansky, J. G., and Barch, D. M. (2011). Brain network connectivity in individuals with schizophrenia and their siblings. *Biol. Psychiatry* 69, 967–973. doi: 10.1016/j.biopsych.2010.11.009

Richter, C. G., Thompson, W. H., Bosman, C. A., and Fries, P. (2017). Top-Down Beta Enhances Bottom-Up Gamma. *J. Neurosci.* 37, 6698–6711. doi: 10.1523/JNEUROSCI.3771-16.2017

Rochefort, C., Arabo, A., Andre, M., Poucet, B., Save, E., and Rondi-Reig, L. (2011). Cerebellum shapes hippocampal spatial code. *Science* 334, 385–389. doi: 10.1126/science.1207403

Rogers, T. D., Dickson, P. E., Heck, D. H., Goldowitz, D., Mittleman, G., and Blaha, C. D. (2011). Connecting the dots of the cerebrocerebellar role in cognitive function: Neuronal pathways for cerebellar modulation of dopamine release in the prefrontal cortex. *Synapse* 65, 1204–1212. doi: 10.1002/syn.20960

Ros, H., Sachdev, R. N., Yu, Y., Sestan, N., and McCormick, D. A. (2009). Neocortical networks entrain neuronal circuits in cerebellar cortex. *J. Neurosci.* 29, 10309–10320. doi: 10.1523/JNEUROSCI.2327-09.2009

Rudie, J. D., Brown, J. A., Beck-Pancer, D., Hernandez, L. M., Dennis, E. L., Thompson, P. M., et al. (2013). Altered functional and structural brain network organization in autism. *Neuroimage Clin.* 2, 79–94. doi: 10.1016/j.nicl.2012.11.006

Saalmann, Y. B. (2014). Intralaminar and medial thalamic influence on cortical synchrony, information transmission and cognition. *Front. Syst. Neurosci.* 8:83. doi: 10.3389/fnsys.2014.00083

Schmahmann, J. D. (2016). Cerebellum in Alzheimer's disease and frontotemporal dementia: not a silent bystander. *Brain* 139(Pt 5), 1314–1318. doi: 10.1093/brain/aww064

Schmahmann, J. D., Guell, X., Stoodley, C. J., and Halko, M. A. (2019). The Theory and Neuroscience of Cerebellar Cognition. *Annu. Rev. Neurosci.* 42, 337–364. doi: 10.1146/annurev-neuro-070918-050258

Schmahmann, J. D., Rosene, D. L., and Pandya, D. N. (2004). Motor projections to the basis pontis in rhesus monkey. *J. Comp. Neurol.* 478, 248–268. doi: 10.1002/cne.20286

Schmahmann, J. D., Weilburg, J. B., and Sherman, J. C. (2007). The neuropsychiatry of the cerebellum - insights from the clinic. *Cerebellum* 6, 254–267.

Schutter, D. J., van Honk, J., d'Alfonso, A. A., Peper, J. S., and Panksepp, J. (2003). High frequency repetitive transcranial magnetic over the medial cerebellum induces a shift in the prefrontal electroencephalography gamma spectrum: a pilot study in humans. *Neurosci. Lett.* 336, 73–76. doi: 10.1016/s0304-3940(02)01077-7

Schwarz, C., Moeck, M., and Thier, P. (1997). Electrophysiological properties of rat pontine nuclei neurons *in vitro*. I. Membrane potentials and firing patterns. *J. Neurophysiol.* 78, 3323–3337.

Sheffield, J. M., and Barch, D. M. (2016). Cognition and resting-state functional connectivity in schizophrenia. *Neurosci. Biobehav. Rev.* 61, 108–120. doi: 10.1016/j.neubiorev.2015.12.007

Sheffield, J. M., Repovs, G., Harms, M. P., Carter, C. S., Gold, J. M., MacDonald, A. W., et al. (2015). Fronto-parietal and cingulo-opercular network integrity and cognition in health and schizophrenia. *Neuropsychologia* 73, 82–93. doi: 10.1016/j.neuropsychologia.2015.05.006

Sherman, M. A., Lee, S., Law, R., Haegens, S., Thorn, C. A., Hamalainen, M. S., et al. (2016). Neural mechanisms of transient neocortical beta rhythms: converging evidence from humans, computational modeling, monkeys, and mice. *Proc. Natl. Acad. Sci. U.S.A.* 113, E4885–E4894. doi: 10.1073/pnas.1604135113

Siegel, M., Donner, T. H., Oostenveld, R., Fries, P., and Engel, A. K. (2008). Neuronal synchronization along the dorsal visual pathway reflects the focus of spatial attention. *Neuron* 60, 709–719. doi: 10.1016/j.neuron.2008.09.010

Sigurdsson, T., and Duvarci, S. (2016). Hippocampal-prefrontal interactions in cognition, behavior and psychiatric disease. *Front. Syst. Neurosci.* 9:190. doi: 10.3389/fnsys.2015.00190

Singh, A., Trapp, N. T., De Corte, B., Cao, S., Kingyon, J., Boes, A. D., et al. (2019). Cerebellar theta frequency transcranial pulsed stimulation increases frontal theta oscillations in patients with schizophrenia. *Cerebellum* 18, 489–499. doi: 10.1007/s12311-019-01013-9

Spellman, T., Rigotti, M., Ahmari, S. E., Fusi, S., Gogos, J. A., and Gordon, J. A. (2015). Hippocampal-prefrontal input supports spatial encoding in working memory. *Nature* 522, 309–314. doi: 10.1038/nature14445

Stephan, K. E., Friston, K. J., and Frith, C. D. (2009). Dysconnection in schizophrenia: from abnormal synaptic plasticity to failures of self-monitoring. *Schizophr. Bull.* 35, 509–527. doi: 10.1093/schbul/sbn176

Straub, I., Witter, L., Eshra, A., Hoidis, M., Byczkowicz, N., Maas, S., et al. (2020). Gradients in the mammalian cerebellar cortex enable Fourier-like transformation and improve storing capacity. *eLife* 9:e51771. doi: 10.7554/eLife.51771

Strick, P. L., Dum, R. P., and Fiez, J. A. (2009). Cerebellum and nonmotor function. *Annu. Rev. Neurosci.* 32, 413–434. doi: 10.1146/annurev.neuro.31.060407.125606

Supekar, K., Uddin, L. Q., Khouzam, A., Phillips, J., Gaillard, W. D., Kenworthy, L. E., et al. (2013). Brain hyperconnectivity in children with autism and its links to social deficits. *Cell Rep.* 5, 738–747. doi: 10.1016/j.celrep.2013.10.001

Suzuki, L., Coulon, P., Sabel-Goedknegt, E. H., and Ruigrok, T. J. (2012). Organization of cerebral projections to identified cerebellar zones in the posterior cerebellum of the rat. *J. Neurosci.* 32, 10854–10869. doi: 10.1523/JNEUROSCI.0857-12.2012

Thach, W. T. (1970). Discharge of cerebellar neurons related to two maintained postures and two prompt movements. I. Nuclear Cell Output. *J. Neurophysiol.* 33, 527–547.

Tomlinson, S. P., Davis, N. J., Morgan, H. M., and Bracewell, R. M. (2014). Cerebellar contributions to spatial memory. *Neurosci. Lett.* 578, 182–186. doi: 10.1016/j.neulet.2014.06.057

Tu, P. C., Hsieh, J. C., Li, C. T., Bai, Y. M., and Su, T. P. (2012). Cortico-striatal disconnection within the cingulo-opercular network in schizophrenia revealed by intrinsic functional connectivity analysis: a resting fMRI study. *Neuroimage* 59, 238–247. doi: 10.1016/j.neuroimage.2011.07.086

Vaadia, E., Haalman, I., Abeles, M., Bergman, H., Prut, Y., Slovin, H., et al. (1995). Dynamics of neuronal interactions in monkey cortex in relation to behavioural events. *Nature* 373, 515–518.

Vervaeke, K., Lorincz, A., Gleeson, P., Farinella, M., Nusser, Z., and Silver, R. A. (2010). Rapid desynchronization of an electrically coupled interneuron network

with sparse excitatory synaptic input. *Neuron* 67, 435–451. doi: 10.1016/j.neuron.2010.06.028

Wagner, M. J., Kim, T. H., Kadmon, J., Nguyen, N. D., Ganguli, S., Schnitzer, M. J., et al. (2019). Shared cortex-cerebellum dynamics in the execution and learning of a motor task. *Cell* 177, 669–682.e24. doi: 10.1016/j.cell.2019.02.019

Wagner, M. J., Kim, T. H., Savall, J., Schnitzer, M. J., and Luo, L. (2017). Cerebellar granule cells encode the expectation of reward. *Nature* 544, 96–100. doi: 10.1038/nature21726

Wagner, M. J., and Luo, L. (2019). Neocortex-Cerebellum Circuits for Cognitive Processing. *Trends Neurosci.* 43, 42–54. doi: 10.1016/j.tins.2019.11.002

Washington, S. D., Gordon, E. M., Brar, J., Warburton, S., Sawyer, A. T., Wolfe, A., et al. (2014). Dysmaturation of the default mode network in autism. *Hum. Brain Mapp.* 35, 1284–1296. doi: 10.1002/hbm.22252

Wass, S. (2011). Distortions and disconnections: disrupted brain connectivity in autism. *Brain Cogn.* 75, 18–28. doi: 10.1016/j.bandc.2010.10.005

Watanabe, R. N., and Kohn, A. F. (2015). Fast oscillatory commands from the motor cortex can be decoded by the spinal cord for force control. *J. Neurosci.* 35, 13687–13697. doi: 10.1523/JNEUROSCI.1950-15.2015

Watson, T. C., Obiang, P., Torres-Herraez, A., Watilliaux, A., Coulon, P., Rochefort, C., et al. (2019). Anatomical and physiological foundations of cerebello-hippocampal interaction. *eLife* 8, e41896. doi: 10.7554/eLife.41896

Weinberger, D. R., Kleinman, J. E., Luchins, D. J., Bigelow, L. B., and Wyatt, R. J. (1980). Cerebellar pathology in schizophrenia: a controlled postmortem study. *Am. J. Psychiatry* 137, 359–361.

Wirt, R. A., and Hyman, J. M. (2017). Integrating spatial working memory and remote memory: interactions between the medial prefrontal cortex and hippocampus. *Brain Sci.* 7:43. doi: 10.3390/brainsci7040043

Conflict of Interest: The authors declare that the research was conducted in the absence of any commercial or financial relationships that could be construed as a potential conflict of interest.

frontiers | Frontiers in Systems Neuroscience

ORIGINAL RESEARCH
published: 13 May 2022
doi: 10.3389/fnsys.2022.879634

Novel Cerebello-Amygdala Connections Provide Missing Link Between Cerebellum and Limbic System

*Se Jung Jung[1‡], Ksenia Vlasov[1‡], Alexa F. D'Ambra[1], Abhijna Parigi[1†], Mihir Baya[1], Edbertt Paul Frez[1], Jacqueline Villalobos[1], Marina Fernandez-Frentzel[1], Maribel Anguiano[1], Yoichiro Ideguchi[1†], Evan G. Antzoulatos[1,2] and Diasynou Fioravante[1,2]**

[1]Center for Neuroscience, University of California, Davis, Davis, CA, United States, [2]Department of Neurobiology, Physiology and Behavior, University of California, Davis, Davis, CA, United States

The cerebellum is emerging as a powerful regulator of cognitive and affective processing and memory in both humans and animals and has been implicated in affective disorders. How the cerebellum supports affective function remains poorly understood. The short-latency (just a few milliseconds) functional connections that were identified between the cerebellum and amygdala—a structure crucial for the processing of emotion and valence—more than four decades ago raise the exciting, yet untested, possibility that a cerebellum-amygdala pathway communicates information important for emotion. The major hurdle in rigorously testing this possibility is the lack of knowledge about the anatomy and functional connectivity of this pathway. Our initial anatomical tracing studies in mice excluded the existence of a direct monosynaptic connection between the cerebellum and amygdala. Using transneuronal tracing techniques, we have identified a novel disynaptic circuit between the cerebellar output nuclei and the basolateral amygdala. This circuit recruits the understudied intralaminar thalamus as a node. Using *ex vivo* optophysiology and super-resolution microscopy, we provide the first evidence for the functionality of the pathway, thus offering a missing mechanistic link between the cerebellum and amygdala. This discovery provides a connectivity blueprint between the cerebellum and a key structure of the limbic system. As such, it is the requisite first step toward obtaining new knowledge about cerebellar function in emotion, thus fundamentally advancing understanding of the neurobiology of emotion, which is perturbed in mental and autism spectrum disorders.

Keywords: cerebellar nuclei, basolateral amydala, limbic, circuit, electrophysiology, channelrhodopsin, anatomy, mouse

OPEN ACCESS

Edited by:
Krystal Lynn Parker,
The University of Iowa, United States

Reviewed by:
Detlef H. Heck,
University of Tennessee Health Science Center, United States
Mai Fox,
University of Tennessee Health Science Center, United States, in collaboration with reviewer DHH
Nick Garber Hollon,
University of California, San Diego, United States

****Correspondence:***
Diasynou Fioravante
dfioravante@ucdavis.edu

†Present addresses:
Yoichiro Ideguchi,
Department of Molecular Medicine, The Scripps Research Institute, La Jolla, CA, United States
Abhijna Parigi,
10x Genomics, Pleasanton, CA, United States

‡These authors have contributed equally to this work and share first authorship

Received: *20 February 2022*
Accepted: *05 April 2022*
Published: *13 May 2022*

Citation:
Jung SJ, Vlasov K, D'Ambra AF, Parigi A, Baya M, Frez EP, Villalobos J, Fernandez-Frentzel M, Anguiano M, Ideguchi Y, Antzoulatos EG and Fioravante D (2022) Novel Cerebello-Amygdala Connections Provide Missing Link Between Cerebellum and Limbic System. Front. Syst. Neurosci. 16:879634. doi: 10.3389/fnsys.2022.879634

INTRODUCTION

The cerebellum is increasingly recognized as a regulator of limbic functions (Strick et al., 2009; Buckner, 2013; Reeber et al., 2013; Strata, 2015; Adamaszek et al., 2017; Schmahmann, 2019; Liang and Carlson, 2020; Hull, 2020). The human cerebellum is activated in response to aversive or threatening cues, upon remembering emotionally charged events, and during social behavior,

reward-based decision making, and violation of expectations (Ploghaus et al., 1999; Damasio et al., 2000; Ernst, 2002; Ahs et al., 2009; Moulton et al., 2010, 2014; Guo et al., 2013; Van Overwalle et al., 2014; Guell et al., 2018; Ernst et al., 2019). Consistent with this, deficits in cerebellar function are associated with impaired emotional attention and perception, as seen in depression, anxiety, schizophrenia, and post-traumatic stress disorder (Yin et al., 2011; Roy et al., 2013; Parker et al., 2014; Phillips et al., 2015), as well as cognitive and emotional disturbances collectively known as cerebellar cognitive affective syndrome (Schmahmann and Sherman, 1998). Animal models have recapitulated some of these findings, with selective mutations, damage or inactivation of the rodent cerebellum resulting in altered acquisition or extinction of learned defensive responses, and impaired social and goal-directed behavior, without motor deficits (Supple et al., 1987; Supple and Leaton, 1990; Sebastiani et al., 1992; Bauer et al., 2011; Lorivel et al., 2014; Otsuka et al., 2016; Xiao et al., 2018; Carta et al., 2019; Frontera et al., 2020; Han et al., 2021; Baek et al., 2022; Lawrenson et al., 2022).

The limited understanding of the anatomical and functional circuits that connect the cerebellum to limbic centers has impeded mechanistic insight into the neural underpinnings of cerebellar limbic functions, which have begun to be dissected only recently (Xiao et al., 2018; Carta et al., 2019; Frontera et al., 2020; Kelly et al., 2020; Low et al., 2021). Moreover, a neuroanatomical substrate for the functional connections between the cerebellum and a key affective center, the amygdala (Janak and Tye, 2015), has yet to be provided, even though these connections were observed more than 40 years ago (Heath and Harper, 1974; Snider and Maiti, 1976; Heath et al., 1978). The purpose of the present work was to generate a mesoscale map of functional neuroanatomical connectivity between the cerebellum and amygdala. We focused on connections between the deep cerebellar nuclei (DCN), which give rise to most cerebellar output pathways (Ito, 2006), and the basolateral amygdala (BLA), which is known to process affect-relevant salience and valence information (Janak and Tye, 2015; O'Neill et al., 2018; Yizhar and Klavir, 2018), and which was targeted in the early electrophysiological studies of Heath and Harper (1974) and Heath et al. (1978).

MATERIALS AND METHODS

Mice

C57Bl/6J mice of both sexes were used in accordance with National Institute of Health guidelines. All procedures were reviewed and approved by the Institutional Animal Care and Use Committee of the University of California, Davis. Mice were maintained on a 12-h light/dark cycle with ad libitum access to food and water. For anatomical tracing experiments, postnatal day P45–65 (at the time of injection) mice were used (N = 11 mice). For slice optophysiology, P18–25 (at the time of injection) mice were used.

Virus and Tracer Injections

For stereotaxic surgeries, mice were induced to a surgical plane of anesthesia with 5% isoflurane and maintained at 1%–2% isoflurane. Mice were placed in a stereotaxic frame (David Kopf Instruments, Tujunga, CA) on a feedback-controlled heating pad. Following the skin incision, small craniotomies were made above the target regions with a dental drill. The following coordinates (in mm) were used (from bregma): for medial DCN: −6.4 AP, ± 0.75 ML, −2.2 DV; for interposed DCN: −6.3 AP, ± 1.6 ML, −2.2 DV; for lateral DCN: −5.7 AP, ± 2.35 ML, −2.18 DV. For basolateral amygdala: −0.85 AP, ± 3.08 ML, −4.5 DV. For limbic thalamus: −0.85 AP, ± 0.3 ML, −3.3 DV, and −1.2 AP, ± 0.5 ML, −3.5 DV. A small amount of tracer (50–100 nl for DCN, 300–500 nl for thalamus) was pressure-injected in the targeted site with a UMP3–1 ultramicropump (WPI, Sarasota, FL) and glass pipettes (Wiretrol II, Drummond; tip diameter: 25–50 μm) at a rate of 30 nl/min. The pipette was retracted 10 min after injection, the skin was sutured (Ethilon P-6 sutures, Ethicon, Raritan, NJ) and/or glued (Gluture, Abbott Labs, Abbott Park, IL) and the animal was allowed to recover completely prior to returning to the home cage. Preoperative analgesia consisted of a single administration of local lidocaine (VetOne, MWI, Boise, ID; 1 mg/kg) and Meloxicam (Covetrus, Portland, ME; 5 mg/kg), both SC. Postoperative analgesia consisted of a single administration of Buprenex (AmerisourceBergen Drug Corp, Sacramento, CA; 0.1 mg/kg) and Meloxicam 5 mg/kg, both SC, followed by Meloxicam at 24 and 48 h. The following adeno-associated viruses (AAV) and tracers were used: AAV8-CMV-TurboRFP (UPenn Vector Core, $1.19*10^{14}$ gc/ml), AAV9-CAG-GFP (UNC Vector Core, 2×10^{12} gc/ml), AAV2-retro-CAG-GFP (Addgene, 7×10^{12} gc/ml), AAV2-retro-AAV-CAG-tdTomato (Addgene, 7×10^{12} gc/ml), Cholera toxin subunit B CF-640 (Biotium, 2 mg/ml, 100 nl), AAV1-hSyn-Cre-WPRE-hGH (Addgene, 10^{13} gc/ml, diluted 1:5), AAV5-CAG-FLEX-tdtomato (UNC Viral Core, $7.8*10^{12}$ gc/ml, diluted 1:5), AAV9-EF1a-DIO-hChR2(H134R)-EYFP (Addgene, $1.8*10^{13}$ gc/ml, diluted 1:10), AAV2-hSyn-hChR2(H134R)-EYFP (UNC Vector Core, 5.6×10^{12} gc/ml, diluted 1:2). Three to 5 weeks were allowed for viral expression/labeling.

Histology and Imaging

Following deep anesthesia (anesthetic cocktail: 100 mg/kg ketamine, 10 mg/kg xylazine, 1 mg/kg acepromazine, IP) mice were paraformaldehyde-fixed (4% paraformaldehyde in 0.1 M phosphate buffer, pH 7.4, EMS Diasum, Hatfield, PA) through transcardial perfusion. Brains were post-fixed overnight, cryo-protected with 30% sucrose in PBS, and sliced coronally on a sliding microtome at 60–100 μm thickness. Slices were mounted on slides with Mowiol-based mounting media and scanned using an Olympus VS120 Slide Scanner (Olympus, Germany; resolution with 10× 0.4 N.A. lens at 488 nm: 645 nm in x, y). For immunohistochemistry, slices were blocked with 10% normal goat serum (NGS, Millipore, Burlington, MA) in PBST (0.3% Triton X-100 in PBS) for 1 h. Slices were incubated with primary antibodies (anti-Cre IgG1, Millipore, 1:1,000; anti-NEUN, Cell Signaling, Danvers, MA, 1:1,000; anti-vGLUT2,

Synaptic Systems, Goettingen, Germany, 1:700; anti-PSD-95, Neuromab, Davis, CA, 1:500) in 2% NGS-PBST overnight at 4°C. After 4× 20-min rinses with PBST, secondary antibodies (Alexa fluor-568 goat anti-mouse 1:1,000 IgG1; Alexa fluor-488 goat anti-rabbit 1:1,000; Dylight-405 goat anti-guinea pig 1:200; Alexa fluor-647 goat anti-mouse 1:1,000 IgG2a; Life Technologies, Carlsbad, CA) were applied in 2% NGS-PBST for 1–2 h at room temperature. Following another round of rinses, slices were mounted on slides with Mowiol and scanned on an LSM800 confocal microscope with Airyscan (resolution with 63× 1.4 N.A. oil lens at 488 nm: 120 nm in x, y, 350 nm in z; Zeiss, Germany). Maximal projections of optical *z*-stacks were obtained with Zen software (Zeiss) or ImageJ and used for analysis.

Preparation of Brain Slices for Electrophysiology

Mice of either sex (P39–60) were anesthetized through intraperitoneal injection of ketamine/xylazine/acepromazine anesthetic cocktail and transcardially perfused with ice-cold artificial cerebrospinal fluid (aCSF; in mM: 127 NaCl, 2.5 KCl, 1.25 NaH_2PO_4, 25 $NaHCO_3$, 1 $MgCl_2$, 2 $CaCl_2$, 25 glucose; supplemented with 0.4 sodium ascorbate and 2 sodium pyruvate; ∼310 mOsm). Brains were rapidly removed, blocked, and placed in choline slurry (110 choline chloride, 25 $NaHCO_3$, 25 glucose, 2.5 KCl, 1.25 NaH_2PO_4, 7 $MgCl_2$, 0.5 $CaCl_2$, 11.6 sodium ascorbate, 3.1 sodium pyruvate; ∼310 mOsm). Coronal sections (250 μm) containing the thalamus were cut on a vibratome (Leica VT1200S) and allowed to recover in aCSF at 32°C for 25 min before moving to room temperature until further use. All solutions were bubbled with 95% O_2–5% CO_2 continuously. Chemicals were from Sigma.

Electrophysiology

Slices were mounted onto poly-l-lysine-coated glass coverslips and placed in a submersion recording chamber perfused with aCSF (2–3 ml/min) at near-physiological temperature (30°C–32°C). Whole-cell voltage-clamp recordings were made from tdTomato+ (**Figures 3**, **5**) or CtB+ (**Figure 6**) cells in the thalamus using borosilicate glass pipettes (3–5 MΩ) filled with internal solution containing (in mM): $CsMSO_3$ 120, CsCl 15, NaCl 8, TEA-Cl 10, HEPES 10, EGTA 0.5, QX314 2, MgATP 4 and NaGTP 0.3, biocytin 0.3. Recordings were acquired in pClamp11 using a Multiclamp 700B amplifier (Molecular Devices, San Jose, CA), digitized at 20 kHz, and low-pass filtered at 8 kHz. Membrane potential was maintained at −70 mV. Series resistance and leak current were monitored and recordings were terminated if either of these parameters changed by more than 50%. Optical stimulation of ChR2+ fibers surrounding tdTomato+ or CtB+ thalamic neurons was performed under a 60x water immersion lens (1.0 N.A.) of an Olympus BX51W microscope, using an LED system (Excelitas X-cite; or Prizmatix UHP-T) mounted on the microscope and driven by a Master9 stimulator (AMPI). Optical stimulation consisted of 488 nm light pulses (1–5 ms duration). Power density was set to 1.5–2× threshold (max: 0.25 mW/mm^2). A minimum of five response-evoking trials (inter-trial interval: 60 s) were delivered and traces were averaged. To confirm monosynaptic inputs, action potentials were blocked with TTX (1 μM), followed by TTX+ 4AP (100 μM) to prolong ChR2-evoked depolarization. A connection is monosynaptic if prolonged ChR2-induced presynaptic depolarization in TTX+4AP is sufficient to evoke release (Petreanu et al., 2009).

Data Analysis

Analysis of *ex vivo* recordings was performed using custom MATLAB R2019b scripts (MathWorks, Natick, MA). Postsynaptic current (PSC) amplitude was computed from the maximum negative deflection from baseline within a time window (2.5–40 ms) from stimulus onset. Onset latency was measured at 10% of peak amplitude. Cell location was confirmed through biocytin-streptavidin Alexa fluor staining. For slice registration, the Paxinos Brain Atlas (Paxinos and Franklin, 2001) and the Allen Brain Atlas (ABA_v3) were used. The location of injection sites was identified and experiments were excluded if there was a spill into neighboring nuclei. Cell counting and immunofluorescence intensity analyses were done by raters blind to the experimental hypotheses using ImageJ (Fiji, National Institutes of Health, Bethesda, MD) and Abode Illustrator. Overlap in x- and y-axes between DCN axons and BLA-projecting thalamic neurons was determined through

TABLE 1 | Anatomical abbreviations (in alphabetical order) and antero-posterior coordinates (in mm, from bregma).

Abbreviation	Structure	AP coordinates
BLA	Basolateral amygdaloid nucleus	−0.67 mm to −3.07
CeA	Central amygdala	−0.57 mm to −2.07
CL	Central lateral nucleus of the thalamus	−0.97 mm to −1.97
CM	Central medial nucleus of the thalamus	−0.67 mm to −1.97
DCN	Deep cerebellar nuclei	
IAM	Interanteromedial thalamic nucleus	−0.77 mm to −1.07
IMD	Intermediodorsal nucleus of the thalamus	−0.87 mm to −2.07
Int	Interposed cerebellar nucleus	−6.64 mm to −5.8
IntA	-anterior part	
IntDL	-dorsolateral part	
IntP	-posterior part	
La	Lateral amygdaloid nucleus	−0.87 mm to −2.47
Lat	Lateral cerebellar nucleus	−6.36 mm to −5.68
LP	Lateral posterior thalamic nucleus	−1.27 mm to −3.17
Med	Medial cerebellar nucleus	−6.84 mm to −5.88
MD	Mediodorsal nucleus of the thalamus	−0.57 mm to −1.97
NAc	Nucleus accumbens	
PC	Paracentral nucleus of the thalamus	−1.07 mm to −1.87
PF	Parafascicular nucleus	−1.97 mm to −2.37
PVT	Paraventicular thalamus	−0.17 mm to −2.07
PO	Posterior thalamic nucleus	−1.27 mm to 2.37
PrL	Prelimbic cortex	
RE	Reuniens thalamic nucleus	−0.37 mm to −1.77
RH	Rhomboid thalamic nucleus	−0.77 mm to −1.67
SPA	Subparafascicular area	−2.07 mm to −2.27
VL	Ventrolateral thalamic nucleus	−0.67 mm to −2.27
VM	Ventromedial thalamic nucleus	−0.67 mm to −2.07

visual inspection of epifluorescence images and evaluated by two independent raters. We note that the resolution of epifluorescence imaging is too low to allow firm conclusions about overlap in the *z*-axis. Statistical analysis was performed in Matlab (Mathworks) and Prism (GraphPad), with significance set at $p < 0.05$. Please see **Table 1** for anatomical abbreviations.

RESULTS

Putative Disynaptic Pathways Between Cerebellar Nuclei and BLA Through the Limbic Thalamus

Given that microstimulation of DCN elicits short-latency responses in the BLA (Heath and Harper, 1974; Snider and Maiti, 1976; Heath et al., 1978), we hypothesized that an anatomical pathway exists between the two regions that involve at most two synapses. Initial anatomical tracing experiments did not support a direct DCN-BLA connection (not shown). We, therefore, performed simultaneous injections of an anterograde tracer virus (AAV8-CMV-TurboRFP) bilaterally in the DCN and a retrograde tracer virus (AAV2-retro-CAG-GFP) unilaterally in the BLA (**Figures 1A,B**) to identify potential regions of overlap. In epifluorescence images of brain slices across different animals ($N = 6$), the limbic thalamus consistently emerged as a prominent site of overlap (**Figures 1C1–C3**). We use the term "limbic thalamus" to refer to a collection of non-sensorimotor thalamic nuclei, including the mediodorsal (MD), midline, and intralaminar (IL) nuclei, with diverse projections to cortical (mainly medial prefrontal) and/or subcortical limbic structures (Groenewegen and Witter, 2004; Morgane et al., 2005; Jones, 2007; Vertes et al., 2015). Registration of images to the Allen Brain Atlas localized BLA-projecting thalamic neurons in multiple nuclei of the limbic thalamus (**Figure 1D**), in agreement with known connectivity patterns (Van der Werf et al., 2002; Vertes et al., 2015; Amir et al., 2019; Hintiryan et al., 2021). Visual inspection of diffraction-limited epifluorescence images identified overlapping DCN axonal projections and BLA-projecting neurons in several (but not all) of these thalamic nuclei, including the parafascicular (PF) n. and subparafascicular area (SPA), the centromedial (CM) and MD nuclei, and other midline nuclei (**Figure 1E**). No BLA-projecting neurons were observed in DCN, and no direct DCN projections were observed in BLA (not

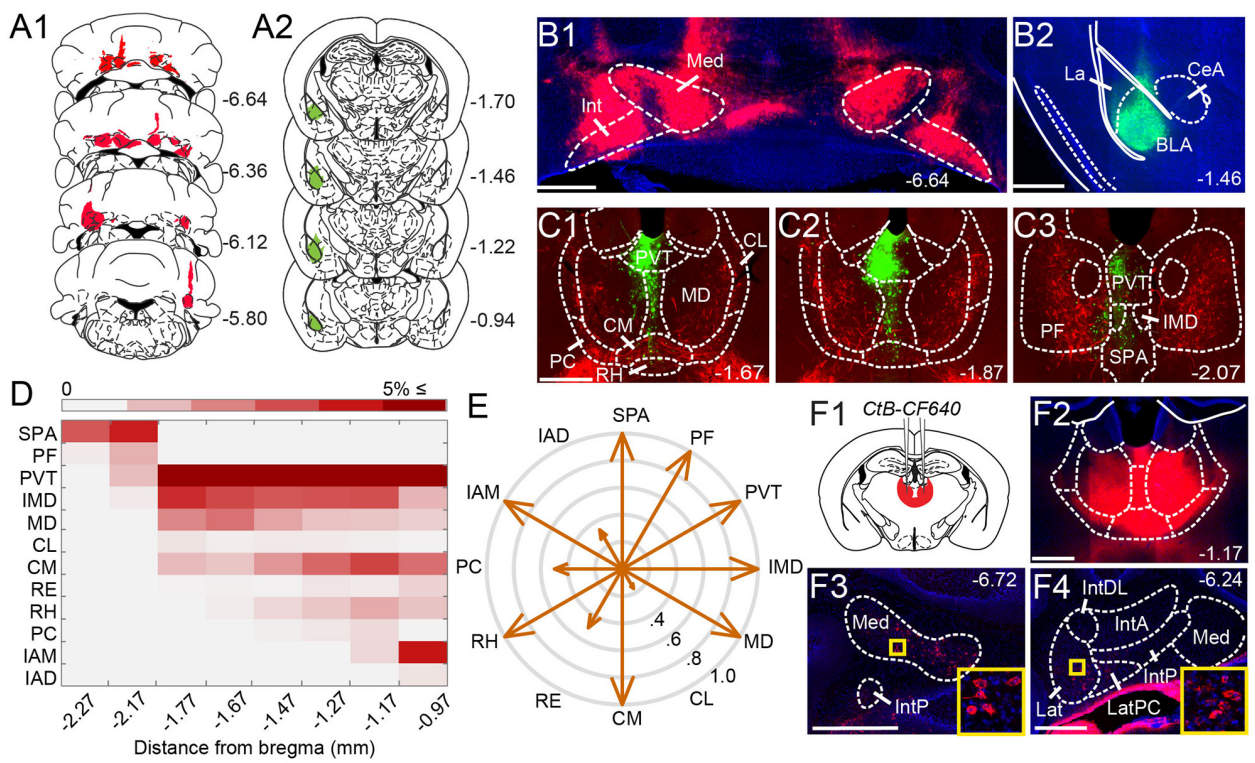

FIGURE 1 | Anatomical tracing uncovers putative disynaptic pathways from the cerebellum to basolateral amygdala. **(A)** Injection sites for anterograde viral tracer in DCN (**A1**, *red*) and retrograde viral tracer in BLA (**A2**, *green*). **(B)** Mosaic epifluorescence image of injection sites in DCN **(B1)** and BLA **(B2)**. **(C1–C3)** Mosaic epifluorescence images of overlapping DCN axons (red) and BLA-projecting neurons (green) in limbic thalamus. **(D)** Relative distribution of BLA-projecting neurons across nuclei of the limbic thalamus, normalized to the total number of labeled neurons and averaged across experiments, as a function of distance from bregma. Antero-posterior coordinates for each nucleus are given in **Table 1**. **(E)** Quantification of overlap between DCN axons and BLA-projecting thalamic neurons. Arrow length in compass plot indicates proportion (0.0–1.0) of experiments with overlap in each thalamic nucleus. **(F1,F2)** Schematic and confocal image of injection site for retrograde tracer CtB CF-640 in limbic thalamus. **(F3,F4)** CtB-labeled projection neurons (red) in DCN at different distances from bregma. Insets show high-magnification images of areas in yellow squares. For all panels, numbers denote distance (in mm) from bregma. Blue: DAPI. Scale bars: 500 μm.

shown). Injection of the tracer cholera toxin subunit B (CtB)-CF640 in the limbic thalamus retrogradely labeled neurons in all DCN (**Figure 1F**), confirming the DCN-limbic thalamus connectivity.

Transneuronal Anatomical Tracing and Optophysiology Establish Synaptic Connectivity Between Cerebellar Nuclei and Limbic Thalamus

To spatially resolve synaptic connectivity between DCN and BLA-projecting thalamic nuclei, we adopted an AAV-based transneuronal approach (Zingg et al., 2017). AAV1-Cre in presynaptic neurons is known to propagate across the synapse and induce expression of a floxed tag in postsynaptic neurons, thus identifying synaptic partners (**Figure 2A**). We injected AAV1-Cre bilaterally in DCN and AAV-FLEX-tdTomato in the thalamus ($N = 5$) and quantified the relative distribution of tdTomato+ neurons in intralaminar and midline thalamic nuclei. Injection coverage for DCN was indicated by Cre immunofluorescence (**Figures 2B1,B2**) and included all cerebellar nuclei. Great care was taken to avoid spill to extracerebellar areas, which resulted in denser coverage of caudal DCN (**Figure 2B3**). TdTomato+ neurons were observed throughout the limbic thalamus, confirming adequate coverage, and extended into ventromedial nuclei (**Figure 2C**), which served as positive control (Gornati et al., 2018; Habas et al., 2019). Averaging the relative distribution of tdTomato+ neurons across five successful experiments revealed that the intralaminar cluster, comprised of centrolateral (CL), paracentral (PC), CM,

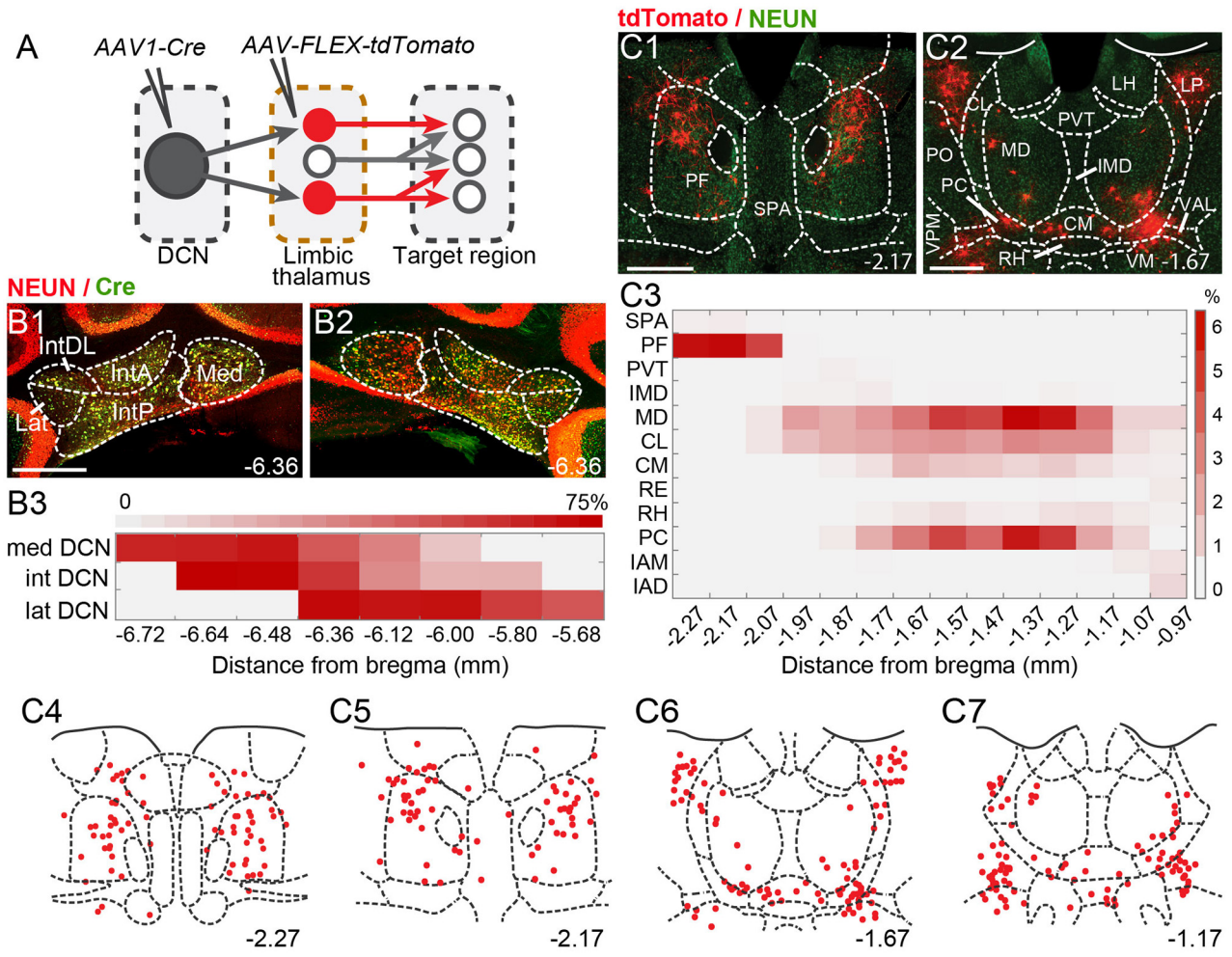

FIGURE 2 | The intralaminar and mediodorsal nuclei are major cerebellar postsynaptic targets in the limbic thalamus. **(A)** Schematic of experimental approach for disynaptic pathway tracing. **(B1,B2)** Example images of bilateral Cre expression in DCN. Red: immunofluorescence for NeuN neural marker; Green: anti-Cre immunoreactivity; Yellow: merge. **(B3)** Heatmap of Cre immunofluorescence in DCN, normalized to NeuN signal and averaged across experiments, as a function of distance (in mm) from bregma. **(C1,C2)** Example images of thalamic neurons conditionally expressing tdTomato (red) upon transneuronal transfer of Cre from cerebellar presynaptic axons. Green: NeuN immunofluorescence. **(C3)** Heatmap of the relative distribution of tdTomato+ neurons across thalamic nuclei, normalized to the total number of labeled neurons and averaged across experiments, as a function of distance from bregma. **(C4–C7)** Example registration of tdTomato+ neurons to the Allen mouse brain atlas. Numbers at the bottom denote distance (in mm) from bregma. Antero-posterior coordinates for each nucleus can be found in **Table 1**. Scale bars: 500 μm.

and PF nuclei (Van der Werf et al., 2002), and MD nucleus encompassed most (∼95%) tagged neurons (**Figure 2C3**), suggesting that these nuclei reliably receive most cerebellar inputs to limbic thalamus. The paraventricular (PVT) nucleus, even though it projects heavily to BLA (**Figure 1C**) and features overlap between DCN axons and BLA-projecting neurons (**Figure 1E**), did not appear to receive robust direct DCN input (**Figure 2C3**).

To confirm that thalamic targets identified with the transneuronal Cre method receive cerebellar synaptic input, we performed optophysiological experiments in acute thalamic slices from mice injected with AAV1-Cre in the DCN and AAV-FLEX-tdTomato in the thalamus (N = 14; **Figure 3A**). To activate cerebellar inputs, channelrhodopsin (ChR2-H134R) was conditionally expressed in DCN through AAV-DIO-ChR2-EYFP injection. DCN axonal projections were stimulated in the thalamus with 488-nm light pulses applied through the objective. Light-evoked synaptic responses were monitored in whole-cell voltage-clamp recordings (V_m = −70 mV) from thalamic neurons, which were selected based on tdTomato expression, their anatomical location, and position in the slice, i.e., surrounded by ChR2-EYFP-expressing axons. In all thalamic nuclei examined (n = 29 cells), light stimulation elicited synaptic responses (mean response in pA: IL: 311.7 ± 100; MD: 105.7 ± 32.3; midline: 565.8 ± 209.8; VM/VPM: 347.5 ± 112.3; LP: 91.8 ± 2.7; **Figure 3B1**) with short latencies (mean latency in ms: IL: 2.5 ± 0.28; MD: 3.3 ± 0.6; midline: 4.2 ± 0.7; VM/VPM: 3.2 ± 0.2; LP: 2.9 ± 0.8; **Figure 3B2**). These data support the specificity of the anatomical connectivity and establish the existence of active DCN terminals (as opposed to just passing axons) across the limbic thalamus.

Thalamic Neurons Receiving Cerebellar Input Project to BLA

If the thalamus is a functional node of the disynaptic DCN-BLA circuit, then we would expect to find axons of DCN input-receiving thalamic neurons in BLA. To this end, we imaged BLA-containing slices from transsynaptic Cre experiments (N = 5; **Figure 4A**). We detected tdTomato+ axons at several antero-posterior distances from bregma (**Figures 4B1–B6**). Using immunohistochemistry with antibodies against pre- and postsynaptic markers of excitatory synapses (vesicular glutamate transporter, vGLUT2; postsynaptic density protein-95, PSD-95), and super-resolution airyscan confocal imaging, we found

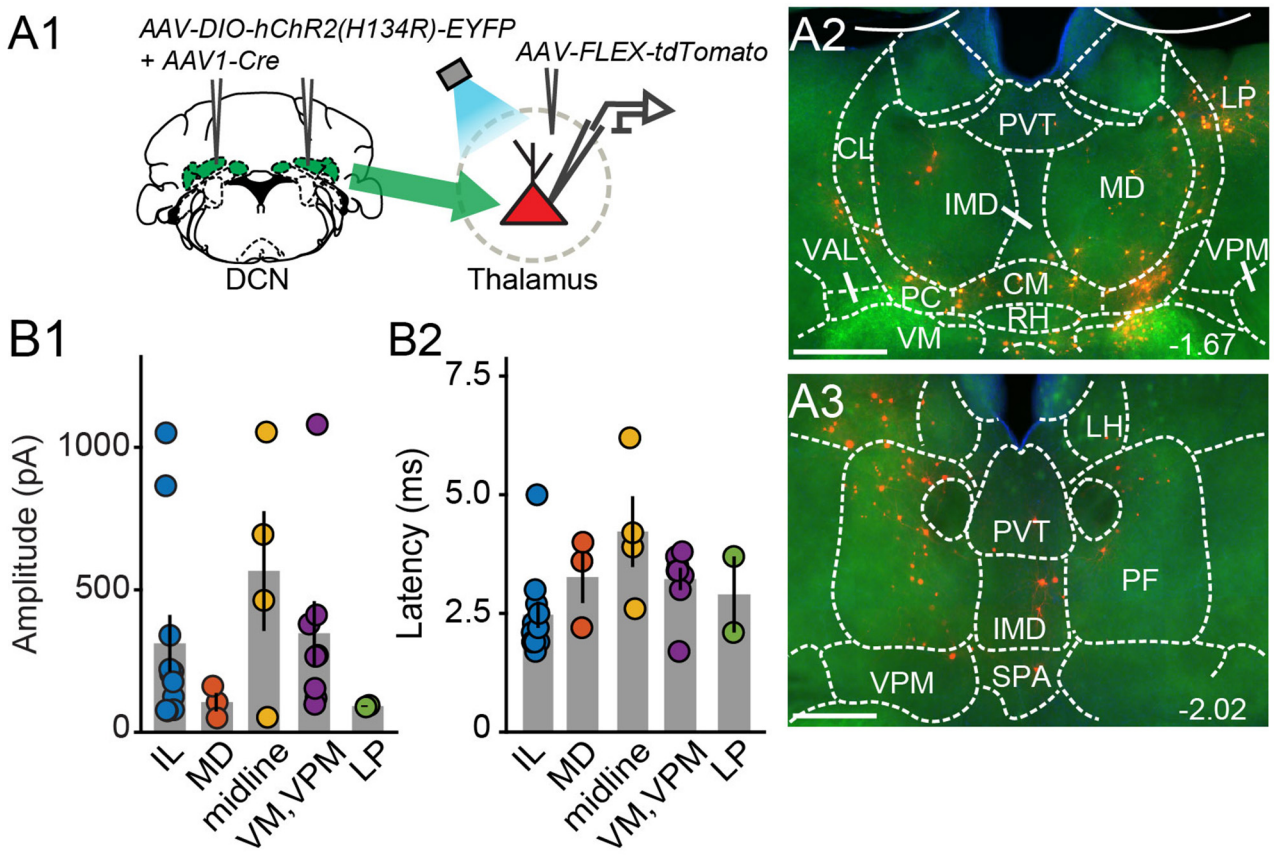

FIGURE 3 | Electrophysiological validation of virally-identified cerebello-thalamic connectivity. **(A1)** Schematic of experimental approach for *ex vivo* optophysiology. **(A2,A3)** Epifluorescence images of anterior **(A2)** and posterior **(A3)** thalamic slices acutely prepared for recordings. DCN input-receiving neurons are tdTomato+. Scale bars: 500 μm. **(B)** Average (± SEM) amplitude **(B1)** and onset latency **(B2)** of ChR2-evoked synaptic currents as a function of recording location in the thalamus. Intralaminar (IL) group: CL, PC, CM, and PF; midline group: IMD and RH.

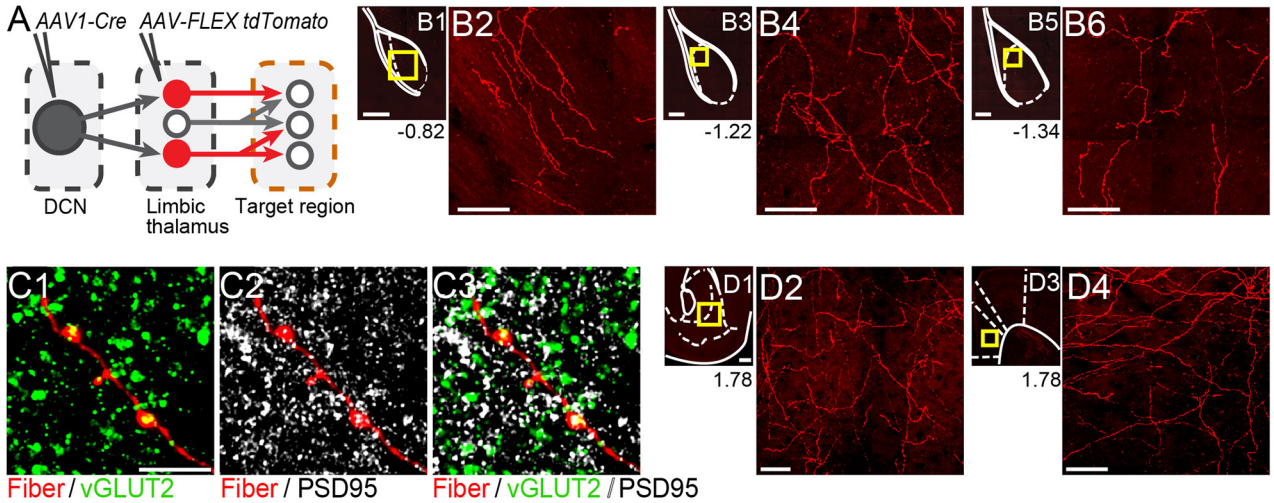

FIGURE 4 | Thalamic neurons receiving cerebellar input form synapses in the basolateral amygdala and also target the nucleus accumbens and prelimbic cortex. **(A)** Schematic diagram of the experimental approach. Targets of tdTomato+ axons of thalamic neurons receiving cerebellar input were identified through imaging. **(B)** Mosaic confocal images of tdTomato+ axons along the anterior-posterior axis of the BLA. **(C)** High resolution airyscan confocal images of tdTomato+ axons in the BLA colocalizing with presynaptic (vGLUT2) **(C1)** and postsynaptic (PSD95) **(C2)** markers of excitatory synapses. Green: vGLUT2, gray: PSD95, yellow/white in **(C3)**: overlay. **(D)** tdTomato+ axons in nucleus accumbens **(D1,D2)** and prelimbic cortex **(D3,D4)**. Yellow squares in **(B1,B3,B5,D1,D3)** show zoom-in areas for **(B2,B4,B6,D2,D4)** images, respectively. Numbers at the bottom of images indicate the distance (in mm) from bregma. Scale bars: **(B1,B3,B5,D1,D3)**: 200 μm; **(B2,B4,B6,D2,D4)**: 50 μm; **(C1–C3)**: 5 μm.

tight colocalization between tdTomato+ axonal varicosities, vGLUT2 and PSD-95, an example of which is shown in **Figure 4C**. This finding suggests that axons of thalamic neurons receiving cerebellar input form morphological synapses in the BLA. Axonal projections of DCN input-receiving thalamic neurons were also observed in other limbic regions including the nucleus accumbens core and shell (**Figures 4D1,D2**) and anterior cingulate/prelimbic cortex (**Figures 4D3,D4**).

The Centromedial and Parafascicular Nuclei Emerge as Functional Nodes in Cerebello-Amygdala Circuit

Our tracer overlap studies pointed to multiple thalamic nuclei as potential relays of cerebellar signals to BLA (**Figure 1E**). Among them, the MD, CM, and PF nuclei showed a higher relative distribution of both BLA-projecting neurons and neurons that receive DCN input (**Figures 1D**, **2C**, **5A**). Further inspection of MD images revealed that, despite clear instances of overlap across experiments, DCN input-receiving neurons localized mostly laterally in MD, and BLA-projecting neurons localized mostly medially. Therefore, to maximize chances of success, for the remainder of this study we focused on CM and PF nuclei and sought to substantiate their role as anatomical and functional relays of DCN-BLA connectivity through super-resolution microscopy and optophysiology.

Airyscan confocal imaging of slices from dual-tracer experiments (**Figure 1**) revealed fluorescently labeled DCN axons (red) in contact with neurons that were retrogradely labeled from the BLA (green) in both CM (**Figures 5B1,B2**) and PF (**Figures 5B3–B5**) nuclei. The existence of functional monosynaptic DCN-CM/PF connections was tested in the subset of electrophysiological experiments from **Figure 3** that targeted CM/PF neurons (**Figure 5C**). Under basal conditions, CM/PF neurons received synaptic inputs from the DCN (at Vm = −70 mV; average amplitude ± SEM: −197.5 pA ± −80.14, n = 6; **Figures 5D1,D5**) with short onset latency (average latency ± SEM: 2.4 ms ± 0.18; **Figure 5D6**), which is consistent with direct monosynaptic connections. Application of the sodium channel blocker tetrodotoxin (TTX) abolished the inputs (average amplitude ± SEM: −5.1 pA ± −2.03; **Figures 5D2,D4,D5**), which recovered upon addition of the potassium channel blocker 4-AP (average amplitude ± SEM: −151.8 pA ± −39.52; **Figures 5D3–D5**; Friedman's non-parametric repeated measures ANOVA: $x^2_r = 9$, n = 6, p = 0.008; Dunn's multiple comparison test: Baseline vs. TTX: p = 0.02, Baseline vs. TTX+4AP: p = 0.99, TTX vs. TTX+4AP: p = 0.01), confirming their monosynaptic nature.

Finally, we tested whether BLA is a target of DCN input-receiving CM/PF neurons (**Figure 6**). We virally expressed ChR2 in DCN and stimulated cerebellar axonal projections in thalamic slices while recording from BLA-projecting CM/PF neurons (whole-cell voltage clamp mode, V_m = −70 mV), which were retrogradely labeled with CtB-CF568 in BLA (**Figures 6A,B**). Optogenetic stimulation elicited reliable DCN-CM/PF synaptic responses (average amplitude ± SEM: −104.1 pA ± −37.1, n = 8; **Figures 6C,D1**) with short latency (3.35 ms ± 0.25; **Figure 6D2**). Combined with the imaging findings (**Figure 5**), our electrophysiological results argue strongly for a DCN-BLA disynaptic circuit that recruits CM/PF nuclei as a node.

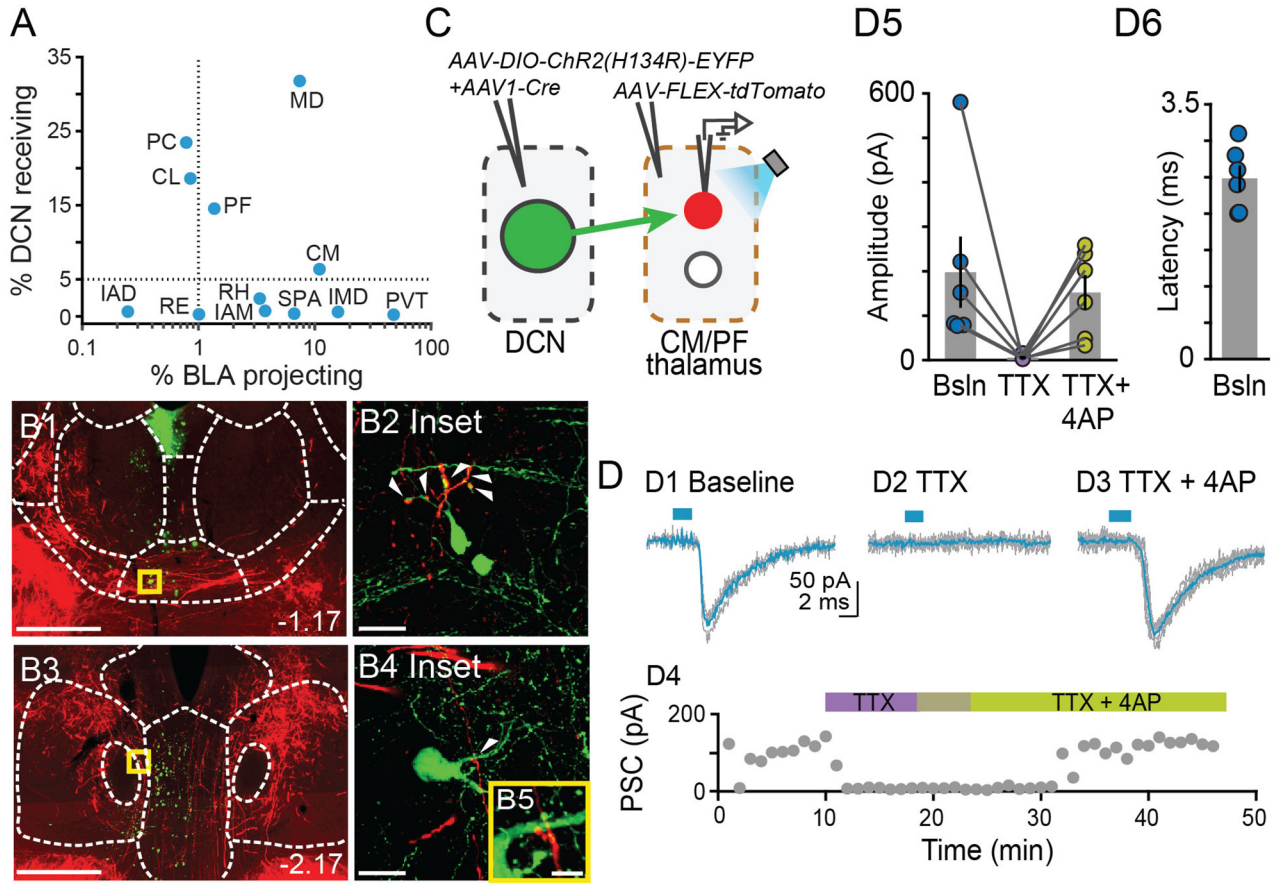

FIGURE 5 | Centromedial and parafascicular neurons project to the basolateral amygdala and receive functional monosynaptic input from the cerebellum. **(A)** Scatterplot of % neurons receiving DCN input vs. % neurons projecting to BLA, for limbic thalamus nuclei. **(B1–B4)** Airyscan confocal images of DCN axons (red) and BLA-projecting neurons (green) in the centromedial (CM; **B1**) and parafascicular (PF; **B3**) thalamic nuclei. **(B2,B4,B5)** Zoomed-in areas in yellow squares from **(B1,B3)**. Scale bars: **(B1,B3)**: 500 μm; **(B2,B4)**: 20 μm; **(B5)**: 5 μm. **(C)** Schematic diagram of *ex vivo* optophysiology approach to test for monosynaptic connections between DCN and CM/PF thalamic n. **(D1–D3)** Average ChR2-evoked synaptic current (teal), overlaid onto single trial responses (gray), at baseline **(D1)**; upon addition of the action potential blocker tetrodotoxin (TTX, 1 μm; **D2**); after further addition of the potassium channel blocker 4-aminopyridine (4AP, 100 μm; **D3**). **(D4)** Time course of the wash-in experiment for the same example cell. **(D5)** Summary of effects on amplitude (mean ± SEM) of ChR2-evoked synaptic responses for the indicated conditions. Bsln: baseline. **(D6)** Average (± SEM) onset latency of ChR2-evoked responses at baseline.

DISCUSSION

Cerebellar connections with the amygdala have been posited previously but the neuroanatomical substrate of this connectivity has been elusive (Strick et al., 2009; D'Angelo and Casali, 2013; Adamaszek et al., 2017). Here, we obtained insight into cerebello-amygdala circuitry by combining various tracing approaches with advanced imaging and optophysiology. We established the existence of a disynaptic circuit between cerebellar nuclei and BLA, thus providing the first blueprint of cerebello-amygdala connectivity at the mesoscale level. The circuit recruits at least the centromedial and parafascicular thalamic nuclei (**Figures 5**, **6**), and most likely also other nuclei of the limbic thalamus (**Figure 1**), as relay nodes. In addition, we identified the intralaminar thalamic cluster and MD nucleus as recipients of the majority of cerebellar inputs to the limbic thalamus (**Figure 2**). Finally, and in addition to BLA, we identified axonal projections of DCN input-receiving thalamic neurons in limbic regions such as nucleus accumbens core and shell and anterior cingulate/prelimbic cortex (**Figure 4**).

The Limbic Thalamus as a Target of Cerebellar Inputs

We targeted the limbic thalamus as a conduit of cerebello-amygdala communication because several of its nuclei foster BLA-projecting neurons in close proximity to DCN axons (**Figure 1**). DCN projections to limbic thalamus have been observed before (Hendry et al., 1979; Haroian et al., 1981; Ichinohe et al., 2000; Fujita et al., 2020; Judd et al., 2021) but the existence of functional synaptic terminals has only been validated for centrolateral and PF intralaminar nuclei (Gornati et al., 2018; Xiao et al., 2018), and never on amygdala-projecting neurons. Our optophysiological experiments also provided the first evidence for the presence of active synaptic connections (as opposed to just passing axons) in paracentral and centromedial (part of intralaminar group), intermediodorsal and rhomboid

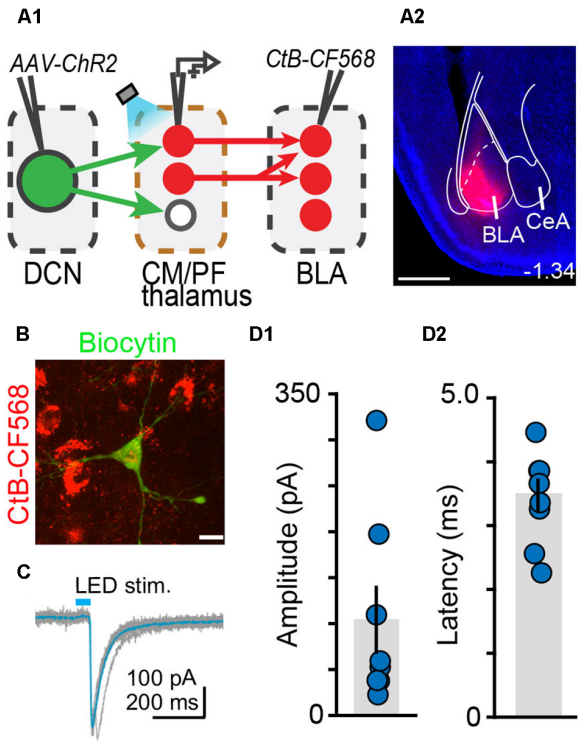

FIGURE 6 | The centromedial and parafascicular thalamus is a functional node of the cerebello-amygdala circuit. **(A)** Experimental approach **(A1)** and example CtB-CF568 injection in amygdala **(A2)**. Blue: DAPI. Scale bar: 500 μm. **(B)** BLA-projecting neuron in centromedial (CM) thalamus retrogradely labeled with CtB CF-568 (red) is also labeled with biocytin (green) through the patch pipette. Scale bar: 10 μm. **(C)** Example ChR2-evoked synaptic response. Average trace (teal) overlaid onto single trials (gray). **(D1,D2)** Average (± SEM) amplitude **(D1)** and onset latency **(D2)** of ChR2-evoked synaptic currents at DCN-CM/PF synapses.

(part of midline group), and mediodorsal nuclei (**Figure 3**), expanding the repertoire of non-motor cerebellar targets and paving the way for causal manipulations.

Technical Considerations

To chart cerebello-amygdala neuroanatomical connections, we used powerful circuit mapping tools including anterograde and retrograde tracer viruses and the transneuronal AAV1-Cre approach (Tervo et al., 2016; Zingg et al., 2017, 2020; Nectow and Nestler, 2020). A distinct advantage of our approach, which combined AAV1-Cre with viral injections of conditionally expressed fluorescent tracers (as opposed to reporter mouse lines), is the ability to definitively point to the thalamus as the source of the observed axonal projections in BLA, nucleus accumbens, and prelimbic cortex—as opposed to e.g., the VTA, which also receives DCN inputs and projects to these regions (Phillipson, 1979; Kuroda et al., 1996; Beier et al., 2015; Breton et al., 2019; D'Ambra et al., 2020). Thus, our approach enabled a conclusive interpretation of anatomical connectivity results. On the other hand, injection coverage/spill and viral tropism (Nectow and Nestler, 2020) need to be considered. Tropism, in particular, could skew the interpretation of disynaptic inputs, as some cell groups in the limbic thalamus might be more efficiently infected by AAVs. Tropism could also explain why recent efforts to trace di- and tri-synaptic cerebellar efferent pathways with herpes simplex viruses did not identify the CM/PF pathway to BLA (Pisano et al., 2021). Lastly, one potential concern could be the propensity of AAVs to be transported in the retrograde direction at high titers (Rothermel et al., 2013; Zingg et al., 2017). To remediate these concerns, we used strict inclusion criteria for injection sites; employed a combination of viral and non-viral anterograde and retrograde tracers; optimized viral titers to minimize retrograde transport; and confirmed circuit connections with slice optophysiology.

Proposed Functions of the DCN-BLA Circuit

Our discovery of the DCN-BLA connection through the CM/PF thalamic nuclei provides an essential map for future investigation of circuit function. The circuit, which could account for the previously observed short-latency cerebello-amygdala responses (Heath and Harper, 1974), could convey cerebellar information about prediction, salience, and/or valence to BLA, shaped by the intrinsic, synaptic, and integrative properties of the nodes. Indeed, the cerebellum is known to encode such information (Ohmae and Medina, 2015; Wagner et al., 2017; Hull, 2020; Ma et al., 2020; Bina et al., 2021; Shuster et al., 2021), which is also seen in BLA (Paton et al., 2006; Adolphs, 2010; Janak and Tye, 2015; Sengupta et al., 2018; Zhang and Li, 2018; Gründemann et al., 2019; Brockett et al., 2021), and which is thought to be used by CM and PF during aversive conditioning, observational learning and reward-seeking behavior (Jeon et al., 2010; Sengupta and McNally, 2014; Vertes et al., 2015; Xiao et al., 2018; Cover and Mathur, 2021; Rizzi et al., 2021).

We have provided morphological evidence for synaptic connections between cerebello-thalamic axons and BLA neurons (**Figure 4**). The functional properties of these synapses remain to be determined, as do the cellular identities of the BLA targets. These targets likely include at least BLA principal neurons, which are the major recipients of CM input (Ahmed et al., 2021). The patterns of BLA ensemble activity triggered by distinct cerebello-thalamic inputs could serve different aspects of cerebellum-dependent emotional functionality, which includes modulation of anxiety and learned fear (Sacchetti et al., 2007; Duvarci and Pare, 2014; Tovote et al., 2015; Otsuka et al., 2016; Frontera et al., 2020; Rudolph et al., 2020); the processing of facial emotional expressions (Wang et al., 2017; Ferrari et al., 2018); regulation of emotional reactivity (Turner et al., 2007; Machado et al., 2009); and even reward-driven motivated behavior (Murray, 2007; Bauer et al., 2011; Peterson et al., 2012; Carta et al., 2019).

The BLA is not the sole nucleus in the amygdala complex that receives cerebellar signals (Magal and Mintz, 2014). Similarly, it is unlikely that the CM and PF are the only nuclei serving cerebello-amygdala communication (our findings; and Kang et al., 2021). Further studies are warranted to delineate the complete neuroanatomical and functional landscape of cerebello-amygdala connectivity. Our findings constitute the first step toward this goal.

DATA AVAILABILITY STATEMENT

The raw data supporting the conclusions of this article will be made available by the authors upon request.

ETHICS STATEMENT

The animal study was reviewed and approved by Institutional Animal Care and Use Committee of the University of California, Davis.

AUTHOR CONTRIBUTIONS

SJ, KV, and DF designed the study. SJ, KV, AD, AP, and YI performed experiments. SJ, KV, EA, and DF analyzed data. MB, EF, JV, MF-F, and MA assisted with cell counting. SJ, KV, AD, and DF wrote the manuscript with input from authors. All authors contributed to the article and approved the submitted version.

FUNDING

This work was supported by R21MH114178, NSF1754831, R01MH128744, a NARSAD Young Investigator Grant, Brain Research Foundation grant BRFSG-2017-02, and a Whitehall Foundation research award to DF; a NARSAD 2018 Young Investigator Grant to EA; a UC Davis Provost's undergraduate fellowship to MA; a NIMH T32MH112507 fellowship to KV; a NIH T32GM007377 and a UC Davis Dean's Distinguished Graduate Fellowships to AD.

ACKNOWLEDGMENTS

We thank Dr. Brian Wiltgen of UC Davis for access to imaging equipment; and Fioravante lab members for comments on a previous version of the manuscript, which has appeared as pre-print on BioRxiv (https://doi.org/10.1101/2022.02.07.479043).

REFERENCES

Adamaszek, M., D'Agata, F., Ferrucci, R., Habas, C., Keulen, S., Kirkby, K. C., et al. (2017). Consensus paper: cerebellum and emotion. *Cerebellum* 16, 552–576. doi: 10.1007/s12311-016-0815-8

Adolphs, R. (2010). What does the amygdala contribute to social cognition? *Ann. N Y Acad. Sci.* 1191, 42–61. doi: 10.1111/j.1749-6632.2010.05445.x

Ahmed, N., Headley, D. B., and Paré, D. (2021). Optogenetic study of central medial and paraventricular thalamic projections to the basolateral amygdala. *J. Neurophysiol.* 126, 1234–1247. doi: 10.1152/jn.00253.2021

Ahs, F., Pissiota, A., Michelgård, A., Frans, O., Furmark, T., Appel, L., et al. (2009). Disentangling the web of fear: amygdala reactivity and functional connectivity in spider and snake phobia. *Psychiatry Res.* 172, 103–108. doi: 10.1016/j.pscychresns.2008.11.004

Amir, A., Paré, J., Smith, Y., and Paré, D. (2019). Midline thalamic inputs to the amygdala: ultrastructure and synaptic targets. *J. Comp. Neurol.* 527, 942–956. doi: 10.1002/cne.24557

Baek, S. J., Park, J. S., Kim, J., Yamamoto, Y., and Tanaka-Yamamoto, K. (2022). VTA-projecting cerebellar neurons mediate stress-dependent depression-like behaviors. *eLife* 11:e72981. doi: 10.7554/eLife.72981

Bauer, D. J., Kerr, A. L., and Swain, R. A. (2011). Cerebellar dentate nuclei lesions reduce motivation in appetitive operant conditioning and open field exploration. *Neurobiol. Learn. Mem.* 95, 166–175. doi: 10.1016/j.nlm.2010.12.009

Beier, K. T., Steinberg, E. E., DeLoach, K. E., Xie, S., Miyamichi, K., Schwarz, L., et al. (2015). Circuit architecture of VTA dopamine neurons revealed by systematic input-output mapping. *Cell* 162, 622–634. doi: 10.1016/j.cell.2015.07.015

Bina, L., Romano, V., Hoogland, T. M., Bosman, L. W. J., and De Zeeuw, C. I. (2021). Purkinje cells translate subjective salience into readiness to act and choice performance. *Cell Rep.* 37:110116. doi: 10.1016/j.celrep.2021.110116

Breton, J. M., Charbit, A. R., Snyder, B. J., Fong, P. T. K., Dias, E. V., Himmels, P., et al. (2019). Relative contributions and mapping of ventral tegmental area dopamine and GABA neurons by projection target in the rat. *J. Comp. Neurol.* 527, 916–941. doi: 10.1002/cne.24572

Brockett, A. T., Vázquez, D., and Roesch, M. R. (2021). Prediction errors and valence: from single units to multidimensional encoding in the amygdala. *Behav. Brain Res.* 4040:113176. doi: 10.1016/j.bbr.2021.113176

Buckner, R. L. (2013). The cerebellum and cognitive function: 25 years of insight from anatomy and neuroimaging. *Neuron* 80, 807–815. doi: 10.1016/j.neuron.2013.10.044

Carta, I., Chen, C. H., Schott, A. L., Dorizan, S., and Khodakhah, K. (2019). Cerebellar modulation of the reward circuitry and social behavior. *Science* 363:eaav0581. doi: 10.1126/science.aav0581

Cover, K. K., and Mathur, B. N. (2021). Rostral intralaminar thalamus engagement in cognition and behavior. *Front. Behav. Neurosci.* 15:652764. doi: 10.3389/fnbeh.2021.652764

Damasio, A. R., Grabowski, T. J., Bechara, A., Damasio, H., Ponto, L. L. B., Parvizi, J., et al. (2000). Subcortical and cortical brain activity during the feeling of self-generated emotions. *Nat. Neurosci.* 3, 1049–1056. doi: 10.1038/79871

D'Ambra, A., Jung, S. J., Ganesan, S., Antzoulatos, E. G., and Fioravante, D. (2020). Cerebellar activation bidirectionally regulates nucleus accumbens shell and core. *bioRxiv* [Preprint]. doi: 10.1101/2020.09.28.283952

D'Angelo, E., and Casali, S. (2013). Seeking a unified framework for cerebellar function and dysfunction: from circuit operations to cognition. *Front. Neural Circuits* 6:116. doi: 10.3389/fncir.2012.00116

Duvarci, S., and Pare, D. (2014). Amygdala microcircuits controlling learned fear. *Neuron* 82, 966–980. doi: 10.1016/j.neuron.2014.04.042

Ernst, M. (2002). Decision-making in a risk-taking task A PET study. *Neuropsychopharmacology* 26, 682–691. doi: 10.1016/S0893-133X(01)00414-6

Ernst, T. M., Brol, A. E., Gratz, M., Ritter, C., Bingel, U., Schlamann, M., et al. (2019). The cerebellum is involved in processing of predictions and prediction errors in a fear conditioning paradigm. *eLife* 8:e46831. doi: 10.7554/eLife.46831

Ferrari, C., Oldrati, V., Gallucci, M., Vecchi, T., and Cattaneo, Z. (2018). The role of the cerebellum in explicit and incidental processing of facial emotional expressions: a study with transcranial magnetic stimulation. *Neuroimage* 169, 256–264. doi: 10.1016/j.neuroimage.2017.12.026

Frontera, J. L., Baba Aissa, H., Sala, R. W., Mailhes-Hamon, C., Georgescu, I. A., Léna, C., et al. (2020). Bidirectional control of fear memories by cerebellar neurons projecting to the ventrolateral periaqueductal grey. *Nat. Commun.* 11:5207. doi: 10.1038/s41467-020-18953-0

Fujita, H., Kodama, T., and du Lac, S. (2020). Modular output circuits of the fastigial nucleus for diverse motor and nonmotor functions of the cerebellar vermis. *eLife* 9:e58613. doi: 10.7554/eLife.58613

Gornati, S. V., Schäfer, C. B., Eelkman Rooda, O. H. J., Nigg, A. L., De Zeeuw, C. I., and Hoebeek, F. E. (2018). Differentiating cerebellar impact on thalamic nuclei. *Cell Rep.* 23, 2690–2704. doi: 10.1016/j.celrep.2018.04.098

Groenewegen, H. J., and Witter, M. P. (2004). "Chapter 17 - Thalamus," in *The Rat Nervous System*, 3rd Edn., ed George Paxinos (Academic Press), 407–453. doi: 10.1016/B978-012547638-6/50018-3

Gründemann, J., Bitterman, Y., Lu, T., Krabbe, S., Grewe, B. F., Schnitzer, M. J., et al. (2019). Amygdala ensembles encode behavioral states. *Science* 364:eaav8736. doi: 10.1126/science.aav8736

Guell, X., Gabrieli, J. D. E., and Schmahmann, J. D. (2018). Triple representation of language, working memory, social and emotion processing in the cerebellum:

convergent evidence from task and seed-based resting-state fMRI analyses in a single large cohort. *Neuroimage* 172, 437–449. doi: 10.1016/j.neuroimage.2018.01.082

Guo, Z., Chen, J., Liu, S., Li, Y., Sun, B., and Gao, Z. (2013). Brain areas activated by uncertain reward-based decision-making in healthy volunteers. *Neural Regen. Res.* 8, 3344–3352. doi: 10.3969/j.issn.1673-5374.2013.35.009

Habas, C., Manto, M., and Cabaraux, P. (2019). The cerebellar thalamus. *Cerebellum* 18, 635–648. doi: 10.1007/s12311-019-01019-3

Han, J.-K., Kwon, S.-H., Kim, Y. G., Choi, J., Kim, J.-I., Lee, Y.-S., et al. (2021). Ablation of STAT3 in Purkinje cells reorganizes cerebellar synaptic plasticity in long-term fear memory network. *eLife* 10:e63291. doi: 10.7554/eLife.63291

Haroian, A. J., Massopust, L. C., and Young, P. A. (1981). Cerebellothalamic projections in the rat: an autoradiographic and degeneration study. *J. Comp. Neurol.* 197, 217–236. doi: 10.1002/cne.901970205

Heath, R. G., Dempesy, C. W., Fontana, C. J., and Myers, W. A. (1978). Cerebellar stimulation: effects on septal region, hippocampus and amygdala of cats and rats. *Biol. Psychiatry* 13, 501–529.

Heath, R. G., and Harper, J. W. (1974). Ascending projections of the cerebellar fastigial nucleus to the hippocampus, amygdala and other temporal lobe sites: evoked potential and histological studies in monkeys and cats. *Exp. Neurol.* 45, 268–287. doi: 10.1016/0014-4886(74)90118-6

Hendry, S. H. C., Jones, E. G., and Graham, J. (1979). Thalamic relay nuclei for cerebellar and certain related fiber systems in the cat. *J. Comp. Neurol.* 185, 679–713. doi: 10.1002/cne.901850406

Hintiryan, H., Bowman, I., Johnson, D. L., Korobkova, L., Zhu, M., Khanjani, N., et al. (2021). Connectivity characterization of the mouse basolateral amygdalar complex. *Nat. Commun.* 12:2859. doi: 10.1038/s41467-021-22915-5

Hull, C. (2020). Prediction signals in the cerebellum: beyond supervised motor learning. *eLife* 9:e54073. doi: 10.7554/eLife.54073

Ichinohe, N., Mori, F., and Shoumura, K. (2000). A di-synaptic projection from the lateral cerebellar nucleus to the laterodorsal part of the striatum via the central lateral nucleus of the thalamus in the rat. *Brain Res.* 880, 191–197. doi: 10.1016/s0006-8993(00)02744-x

Ito, M. (2006). Cerebellar circuitry as a neuronal machine. *Prog. Neurobiol.* 78, 272–303. doi: 10.1016/j.pneurobio.2006.02.006

Janak, P. H., and Tye, K. M. (2015). From circuits to behaviour in the amygdala. *Nature* 517, 284–292. doi: 10.1038/nature14188

Jeon, D., Kim, S., Chetana, M., Jo, D., Ruley, H. E., Lin, S.-Y., et al. (2010). Observational fear learning involves affective pain system and Cav1.2 Ca2+ channels in ACC. *Nat. Neurosci.* 13, 482–488. doi: 10.1038/nn.2504

Jones, E. G. (2007). *The Thalamus*. Cambridge, MA: Cambridge University Press.

Judd, E. N., Lewis, S. M., and Person, A. L. (2021). Diverse inhibitory projections from the cerebellar interposed nucleus. *eLife* 10:e66231. doi: 10.7554/eLife.66231

Kang, S., Jun, S., Baek, S. J., Park, H., Yamamoto, Y., and Tanaka-Yamamoto, K. (2021). Recent advances in the understanding of specific efferent pathways emerging from the cerebellum. *Front. Neuroanat.* 15:759948. doi: 10.3389/fnana.2021.759948

Kelly, E., Meng, F., Fujita, H., Morgado, F., Kazemi, Y., Rice, L. C., et al. (2020). Regulation of autism-relevant behaviors by cerebellar-prefrontal cortical circuits. *Nat. Neurosci.* 23, 1102–1110. doi: 10.1038/s41593-020-0665-z

Kuroda, M., Murakami, K., Igarashi, H., and Okada, A. (1996). The convergence of axon terminals from the mediodorsal thalamic nucleus and ventral tegmental area on pyramidal cells in layer V of the rat prelimbic cortex. *Eur. J. Neurosci.* 8, 1340–1349. doi: 10.1111/j.1460-9568.1996.tb01596.x

Lawrenson, C., Paci, E., Pickford, J., Drake, R. A., Lumb, B. M., and Apps, R. (2022). Cerebellar modulation of memory encoding in the periaqueductal grey and fear behaviour. *eLife* 11:e76278. doi: 10.7554/eLife.76278

Liang, K. J., and Carlson, E. S. (2020). Resistance, vulnerability and resilience: a review of the cognitive cerebellum in aging and neurodegenerative diseases. *Neurobiol. Learn. Mem.* 170:106981. doi: 10.1016/j.nlm.2019.01.004

Lorivel, T., Roy, V., and Hilber, P. (2014). Fear-related behaviors in Lurcher mutant mice exposed to a predator. *Genes Brain Behav.* 13, 794–801. doi: 10.1111/gbb.12173

Low, A. Y. T., Goldstein, N., Gaunt, J. R., Huang, K.-P., Zainolabidin, N., Yip, A. K. K., et al. (2021). Reverse-translational identification of a cerebellar satiation network. *Nature* 600, 269–273. doi: 10.1038/s41586-021-04143-5

Ma, M., Futia, G. L., de Souza, F. M. S., Ozbay, B. N., Llano, I., Gibson, E. A., et al. (2020). Molecular layer interneurons in the cerebellum encode for valence in associative learning. *Nat. Commun.* 11:4217. doi: 10.1038/s41467-020-18034-2

Machado, C. J., Kazama, A. M., and Bachevalier, J. (2009). Impact of amygdala, orbital frontal, or hippocampal lesions on threat avoidance and emotional reactivity in nonhuman primates. *Emotion* 9, 147–163. doi: 10.1037/a0014539

Magal, A., and Mintz, M. (2014). Inhibition of the amygdala central nucleus by stimulation of cerebellar output in rats: a putative mechanism for extinction of the conditioned fear response. *Eur. J. Neurosci.* 40, 3548–3555. doi: 10.1111/ejn.12714

Morgane, P., Galler, J., and Mokler, D. (2005). A review of systems and networks of the limbic forebrain/limbic midbrain. *Prog. Neurobiol.* 75, 143–160. doi: 10.1016/j.pneurobio.2005.01.001

Moulton, E. A., Elman, I., Becerra, L. R., Goldstein, R. Z., and Borsook, D. (2014). The cerebellum and addiction: insights gained from neuroimaging research. *Addict. Biol.* 19, 317–331. doi: 10.1111/adb.12101

Moulton, E. A., Schmahmann, J. D., Becerra, L., and Borsook, D. (2010). The cerebellum and pain: passive integrator or active participator? *Brain Res. Rev.* 65, 14–27. doi: 10.1016/j.brainresrev.2010.05.005

Murray, E. A. (2007). The amygdala, reward and emotion. *Trends Cogn. Sci.* 11, 489–497. doi: 10.1016/j.tics.2007.08.013

Nectow, A. R., and Nestler, E. J. (2020). Viral tools for neuroscience. *Nat. Rev. Neurosci.* 21, 669–681. doi: 10.1038/s41583-020-00382-z

O'Neill, P.-K., Gore, F., and Salzman, C. D. (2018). Basolateral amygdala circuitry in positive and negative valence. *Curr. Opin. Neurobiol.* 49, 175–183. doi: 10.1016/j.conb.2018.02.012

Ohmae, S., and Medina, J. F. (2015). Climbing fibers encode a temporal-difference prediction error during cerebellar learning in mice. *Nat. Neurosci.* 18, 1798–1803. doi: 10.1038/nn.4167

Otsuka, S., Konno, K., Abe, M., Motohashi, J., Kohda, K., Sakimura, K., et al. (2016). Roles of Cbln1 in non-motor functions of mice. *J. Neurosci.* 36, 11801–11816. doi: 10.1523/JNEUROSCI.0322-16.2016

Parker, K. L., Narayanan, N. S., and Andreasen, N. C. (2014). The therapeutic potential of the cerebellum in schizophrenia. *Front. Syst. Neurosci.* 8:163. doi: 10.3389/fnsys.2014.00163

Paton, J. J., Belova, M. A., Morrison, S. E., and Salzman, C. D. (2006). The primate amygdala represents the positive and negative value of visual stimuli during learning. *Nature* 439, 865–870. doi: 10.1038/nature04490

Paxinos, G., and Franklin, K. B. J. (2001). *The Mouse Brain in Stereotaxic Coordinates*, 2nd Edn. San Diego, CA: Academic Press.

Peterson, T. C., Villatoro, L., Arneson, T., Ahuja, B., Voss, S., and Swain, R. A. (2012). Behavior modification after inactivation of cerebellar dentate nuclei. *Behav. Neurosci.* 126, 551–562. doi: 10.1037/a0028701

Petreanu, L., Mao, T., Sternson, S. M., and Svoboda, K. (2009). The subcellular organization of neocortical excitatory connections. *Nature* 457, 1142–1145. doi: 10.1038/nature07709

Phillips, J. R., Hewedi, D. H., Eissa, A. M., and Moustafa, A. A. (2015). The cerebellum and psychiatric disorders. *Front. Public Health* 3:66. doi: 10.3389/fpubh.2015.00066

Phillipson, O. T. (1979). Afferent projections to the ventral tegmental area of Tsai and interfascicular nucleus: a horseradish peroxidase study in the rat. *J. Comp. Neurol.* 187, 117–143. doi: 10.1002/cne.901870108

Pisano, T. J., Dhanerawala, Z. M., Kislin, M., Bakshinskaya, D., Engel, E. A., Hansen, E. J., et al. (2021). Homologous organization of cerebellar pathways to sensory, motor and associative forebrain. *Cell Rep.* 36:109721. doi: 10.1016/j.celrep.2021.109721

Ploghaus, A., Tracey, I., Gati, J. S., Clare, S., Menon, R. S., Matthews, P. M., et al. (1999). Dissociating pain from its anticipation in the human brain. *Science* 284, 1979–1981. doi: 10.1126/science.284.5422.1979

Reeber, S. L., Otis, T. S., and Sillitoe, R. V. (2013). New roles for the cerebellum in health and disease. *Front. Syst. Neurosci.* 7:83. doi: 10.3389/fnsys.2013.00083

Rizzi, G., Li, Z., Hogrefe, N., and Tan, K. R. (2021). Lateral ventral tegmental area GABAergic and glutamatergic modulation of conditioned learning. *Cell Rep.* 34:108867. doi: 10.1016/j.celrep.2021.108867

Rothermel, M., Brunert, D., Zabawa, C., Diaz-Quesada, M., and Wachowiak, M. (2013). Transgene expression in target-defined neuron populations mediated by retrograde infection with adeno-associated viral vectors. *J. Neurosci.* 33, 15195–15206. doi: 10.1523/JNEUROSCI.1618-13.2013

Roy, A. K., Fudge, J. L., Kelly, C., Perry, J. S. A., Daniele, T., Carlisi, C., et al. (2013). Intrinsic functional connectivity of amygdala-based networks in

adolescent generalized anxiety disorder. *J. Am. Acad. Child Adolesc. Psychiatry* 52, 290–299.e2. doi: 10.1016/j.jaac.2012.12.010

Rudolph, S., Guo, C., Pashkovski, S. L., Osorno, T., Gillis, W. F., Krauss, J. M., et al. (2020). Cerebellum-specific deletion of the $GABA_A$ receptor δ subunit leads to sex-specific disruption of behavior. *Cell Rep.* 33:108338. doi: 10.1016/j.celrep.2020.108338

Sacchetti, B., Sacco, T., and Strata, P. (2007). Reversible inactivation of amygdala and cerebellum but not perirhinal cortex impairs reactivated fear memories. *Eur. J. Neurosci.* 25, 2875–2884. doi: 10.1111/j.1460-9568.2007.05508.x

Schmahmann, J. D., and Sherman, J. C. (1998). The cerebellar cognitive affective syndrome. *Brain* 121, 561–579. doi: 10.1093/brain/121.4.561

Schmahmann, J. D. (2019). The cerebellum and cognition. *Neurosci. Lett.* 688, 62–75. doi: 10.1016/j.neulet.2018.07.005

Sebastiani, L., La Noce, A., Paton, J. F., and Ghelarducci, B. (1992). Influence of the cerebellar posterior vermis on the acquisition of the classically conditioned bradycardic response in the rabbit. *Exp. Brain Res.* 88, 193–198. doi: 10.1007/BF02259141

Sengupta, A., and McNally, G. P. (2014). A role for midline and intralaminar thalamus in the associative blocking of Pavlovian fear conditioning. *Front. Behav. Neurosci.* 8:148. doi: 10.3389/fnbeh.2014.00148

Sengupta, A., Yau, J. O. Y., Jean-Richard-Dit-Bressel, P., Liu, Y., Millan, E. Z., Power, J. M., et al. (2018). Basolateral amygdala neurons maintain aversive emotional salience. *J. Neurosci.* 38, 3001–3012. doi: 10.1523/JNEUROSCI.2460-17.2017

Shuster, S. A., Wagner, M. J., Pan-Doh, N., Ren, J., Grutzner, S. M., Beier, K. T., et al. (2021). The relationship between birth timing, circuit wiring and physiological response properties of cerebellar granule cells. *Proc. Natl. Acad. Sci. U S A* 118:e2101826118. doi: 10.1073/pnas.2101826118

Snider, R. S., and Maiti, A. (1976). Cerebellar contributions to the Papez circuit. *J. Neurosci. Res.* 2, 133–146. doi: 10.1002/jnr.490020204

Strata, P. (2015). The emotional cerebellum. *Cerebellum* 14, 570–577. doi: 10.1007/s12311-015-0649-9

Strick, P. L., Dum, R. P., and Fiez, J. A. (2009). Cerebellum and nonmotor function. *Annu. Rev. Neurosci.* 32, 413–434. doi: 10.1146/annurev.neuro.31.060407.125606

Supple, W. F., Jr., and Leaton, R. N. (1990). Cerebellar vermis: essential for classically conditioned bradycardia in the rat. *Brain Res.* 509, 17–23. doi: 10.1016/0006-8993(90)90303-s

Supple, W. F., Jr., Leaton, R. N., and Fanselow, M. S. (1987). Effects of cerebellar vermal lesions on species-specific fear responses, neophobia and taste-aversion learning in rats. *Physiol. Behav.* 39, 579–586. doi: 10.1016/0031-9384(87)90156-9

Tervo, D. G. R., Hwang, B.-Y., Viswanathan, S., Gaj, T., Lavzin, M., Ritola, K. D., et al. (2016). A designer AAV variant permits efficient retrograde access to projection neurons. *Neuron* 92, 372–382. doi: 10.1016/j.neuron.2016.09.021

Tovote, P., Fadok, J. P., and Lüthi, A. (2015). Neuronal circuits for fear and anxiety. *Nat. Rev. Neurosci.* 16, 317–331. doi: 10.1038/nrn3945

Turner, B. M., Paradiso, S., Marvel, C. L., Pierson, R., Boles Ponto, L. L., Hichwa, R. D., et al. (2007). The cerebellum and emotional experience. *Neuropsychologia* 45, 1331–1341. doi: 10.1016/j.neuropsychologia.2006.09.023

Van der Werf, Y. D., Witter, M. P., and Groenewegen, H. J. (2002). The intralaminar and midline nuclei of the thalamus. Anatomical and functional evidence for participation in processes of arousal and awareness. *Brain Res. Brain Res. Rev.* 39, 107–140. doi: 10.1016/s0165-0173(02)00181-9

Van Overwalle, F., Baetens, K., Mariën, P., and Vandekerckhove, M. (2014). Social cognition and the cerebellum: a meta-analysis of over 350 fMRI studies. *Neuroimage* 86, 554–572. doi: 10.1016/j.neuroimage.2013.09.033

Vertes, R. P., Linley, S. B., and Hoover, W. B. (2015). Limbic circuitry of the midline thalamus. *Neurosci. Biobehav. Rev.* 54, 89–107. doi: 10.1016/j.neubiorev.2015.01.014

Wagner, M. J., Kim, T. H., Savall, J., Schnitzer, M. J., and Luo, L. (2017). Cerebellar granule cells encode the expectation of reward. *Nature* 544, 96–100. doi: 10.1038/nature21726

Wang, S., Yu, R., Tyszka, J. M., Zhen, S., Kovach, C., Sun, S., et al. (2017). The human amygdala parametrically encodes the intensity of specific facial emotions and their categorical ambiguity. *Nat. Commun.* 8:14821. doi: 10.1038/ncomms14821

Xiao, L., Bornmann, C., Hatstatt-Burklé, L., and Scheiffele, P. (2018). Regulation of striatal cells and goal-directed behavior by cerebellar outputs. *Nat. Commun.* 9:3133. doi: 10.1038/s41467-018-05565-y

Yin, Y., Li, L., Jin, C., Hu, X., Duan, L., Eyler, L. T., et al. (2011). Abnormal baseline brain activity in posttraumatic stress disorder: a resting-state functional magnetic resonance imaging study. *Neurosci. Lett.* 498, 185–189. doi: 10.1016/j.neulet.2011.02.069

Yizhar, O., and Klavir, O. (2018). Reciprocal amygdala-prefrontal interactions in learning. *Curr. Opin. Neurobiol.* 52, 149–155. doi: 10.1016/j.conb.2018.06.006

Zhang, X., and Li, B. (2018). Population coding of valence in the basolateral amygdala. *Nat. Commun.* 9:5195. doi: 10.1038/s41467-018-07679-9

Zingg, B., Chou, X., Zhang, Z., Mesik, L., Liang, F., Tao, H. W., et al. (2017). AAV-mediated anterograde transsynaptic tagging: mapping corticocollicular input-defined neural pathways for defense behaviors. *Neuron* 93, 33–47. doi: 10.1016/j.neuron.2016.11.045

Zingg, B., Peng, B., Huang, J., Tao, H. W., and Zhang, L. I. (2020). Synaptic specificity and application of anterograde transsynaptic AAV for probing neural circuitry. *J. Neurosci.* 40, 3250–3267. doi: 10.1523/JNEUROSCI.2158-19.2020

Conflict of Interest: The authors declare that the research was conducted in the absence of any commercial or financial relationships that could be construed as a potential conflict of interest.

Publisher's Note: All claims expressed in this article are solely those of the authors and do not necessarily represent those of their affiliated organizations, or those of the publisher, the editors and the reviewers. Any product that may be evaluated in this article, or claim that may be made by its manufacturer, is not guaranteed or endorsed by the publisher.

frontiers | Frontiers in Systems Neuroscience

REVIEW
published: 09 June 2022
doi: 10.3389/fnsys.2022.908569

Vulnerability of Human Cerebellar Neurons to Degeneration in Ataxia-Causing Channelopathies

*David D. Bushart[1] and Vikram G. Shakkottai[2]**

[1] Ohio State University College of Medicine, Columbus, OH, United States, [2] Department of Neurology, University of Texas Southwestern Medical Center, Dallas, TX, United States

Mutations in ion channel genes underlie a number of human neurological diseases. Historically, human mutations in ion channel genes, the so-called channelopathies, have been identified to cause episodic disorders. In the last decade, however, mutations in ion channel genes have been demonstrated to result in progressive neurodegenerative and neurodevelopmental disorders in humans, particularly with ion channels that are enriched in the cerebellum. This was unexpected given prior rodent ion channel knock-out models that almost never display neurodegeneration. Human ataxia-causing channelopathies that result in even haploinsufficiency can result in cerebellar atrophy and cerebellar Purkinje neuron loss. Rodent neurons with ion channel loss-of-function appear to, therefore, be significantly more resistant to neurodegeneration compared to human neurons. Fundamental differences in susceptibility of human and rodent cerebellar neurons in ataxia-causing channelopathies must therefore be present. In this review, we explore the properties of human neurons that may contribute to their vulnerability to cerebellar degeneration secondary to ion channel loss-of-function mutations. We present a model taking into account the known allometric scaling of neuronal ion channel density in humans and other mammals that may explain the preferential vulnerability of human cerebellar neurons to degeneration in ataxia-causing channelopathies. We also speculate on the vulnerability of cerebellar neurons to degeneration in mouse models of spinocerebellar ataxia (SCA) where ion channel transcript dysregulation has recently been implicated in disease pathogenesis.

Keywords: ion channel, channelopathies, ataxia and cerebellar disorders, neurodegeneration, Purkinje cell

OPEN ACCESS

Edited by:
Erik Sean Carlson, University of Washington, United States

Reviewed by:
Paul J. Mathews, Lundquist Institute for Biomedical Innovation, United States
Albert I. Chen, Scintillon Institute, United States

****Correspondence:***
Vikram G. Shakkottai
Vikram.Shakkottai@UTSouthwestern.edu

Received: *30 March 2022*
Accepted: *20 May 2022*
Published: *09 June 2022*

Citation:
Bushart DD and Shakkottai VG (2022) Vulnerability of Human Cerebellar Neurons to Degeneration in Ataxia-Causing Channelopathies. Front. Syst. Neurosci. 16:908569. doi: 10.3389/fnsys.2022.908569

INTRODUCTION

Ion channels play a central role in human health and disease. Historically, mutations in ion channel genes have been associated with episodic neurological disorders, such as episodic ataxia, familial migraine, and seizure disorders (Russell et al., 2013). Recent advances using next-generation sequencing approaches have recognized that ion channels are key contributors to pathology in a variety of neurological disorders, even when a ion channel gene mutation is not the primary driver of disease (Bushart and Shakkottai, 2019). These include the spinocerebellar ataxias (SCAs), a group of autosomal-dominant neurodegenerative disorders affecting primarily the cerebellum and its associated pathways. In marked contrast to the lack of neurodegeneration in episodic disorders

that result from mutant ion channels, mutations or changes in expression of ion channels produce prominent cerebellar degeneration in human SCAs, suggesting a causal role for ion channel dysfunction in the degenerative process. However, in many animal models of channelopathy, structural changes are often absent. While this may reflect fundamental challenges of modeling human disease in murine models, it may also reflect a unique vulnerability of human neurons to ion channel dysfunction.

Many of the ion channel genes that cause known channelopathies are expressed widely, and in overlapping patterns, throughout the central nervous system. Neurons are highly specialized in their ability to process information, with different neuronal subtypes requiring ion channels that possess specific voltage or temporal properties to maintain normal function. These restraints could make neurons susceptible to perturbations in function, or to neurodegeneration, when they harbor mutant or inactive ion channels. It is hypothesized that overlapping properties and expression of ion channels with similar biophysical properties, which is termed "degeneracy," might allow neurons to retain relatively normal function when individual ion channels are lost. This reflects a potential of ion channels with overlapping roles and expression to compensate for other ion channels that undergo a loss-of-function mutation (Goaillard and Marder, 2021). This process of degeneracy and compensation appears to be a plausible mechanism of resistance to neurodegeneration secondary to ion channel loss-of-function in mice. In humans, however, ion channel gene mutations that result even in haploinsufficiency can have profound behavioral and neurodegenerative consequences. This suggests that the same rules of degeneracy and compensation may not apply equally to mice and humans, and that fundamental differences in the vulnerability of human and mouse neurons may exist for the channelopathies.

In addition to progressive motor impairment, a hallmark of the ataxia-causing channelopathies in humans is cerebellar atrophy or a loss of cerebellar volume on brain imaging. Cerebellar atrophy is most commonly associated with the loss of cerebellar Purkinje neurons. Purkinje neurons are thought to be vulnerable to dysfunction and degeneration due to several of their unique features, including a high autonomous firing rate that requires the coordinated action of many different ion channels (Bushart and Shakkottai, 2019). Remarkably, ion channel loss-of-function has also been identified in the autosomal dominant cerebellar ataxias that are not directly caused by mutations in ion channel genes. Ataxia-causing loss-of-function mutations in ion channel genes in humans were initially described to solely produce a late onset, slowly progressive phenotype. More recently identified ion channel gene mutations can, however, produce an early onset phenotype with progressive cerebellar atrophy in the first and second decades of life (see below). Despite clear structural and functional consequences of channelopathies in human neurons, loss of cerebellar Purkinje neurons is not a prominent pathological feature in ion channel knock-out mice. The lack of neurodegeneration is particularly puzzling in ion channel knock-out mice where mutation in the respective disease-causing ion channel gene produces an early onset degenerative phenotype in humans. For the purposes of this review, we define neurodegeneration as is conventional for human disease; namely, either identification of frank loss of cerebellar neurons in autopsy samples or evidence of a macroscopic reduction in cerebellar volume with brain imaging, or both. In human disease, loss of cerebellar brain volume or atrophy is associated with loss of cerebellar Purkinje neurons at autopsy. The current review will discuss vulnerability of human neurons in relation to murine Purkinje neurons regarding degeneration due to mutations in ion channel genes. In addition, we will speculate on the relative resistance to degeneration in mouse models of SCA where ion channel transcript dysregulation, rather than a mutation in an ion channel gene, is associated with disease.

MEMBRANE CHARACTERISTICS OF NEURONS IN HUMAN AND OTHER MAMMALIAN SPECIES USED TO MODEL HUMAN DISEASE

In recent years, knowledge of human neuron membrane physiology has grown significantly with the use of resected cortical tissue. Tissue that is resected for several neurosurgical indications, including temporal lobe epilepsy and tumor, has been successfully used in preparations for patch-clamp recording. Tissue resections generally contain neurons that are representative of healthy human cortical neurons *in vivo*. This process has allowed researchers to make direct comparisons of active and passive membrane properties between neurons from human and model species, along with assessing structure-function relationships in human neurons. From these studies, is has become clear that human neurons are not simply "scaled-up" versions of neurons from other mammalian species; rather, they possess unique structural and functional properties (Mohan et al., 2015; Deitcher et al., 2017; Beaulieu-Laroche et al., 2021).

Several studies have highlighted clear differences between the input-output properties of human cortical neurons and those of model species. A comparative study of layer 5 (L5) cortical pyramidal neurons across multiple mammalian species demonstrated that human neurons diverge from a conserved electrophysiological pattern that is observed in other mammals (Beaulieu-Laroche et al., 2021). As cell size increases, with humans possessing the largest somatic size in L5 cortical pyramidal neurons, ionic conductance generally increases proportionally. However, human neurons break this pattern, exhibiting a much smaller conductance than would be predicted (Beaulieu-Laroche et al., 2021). For example, human cortical L5 neuronal somata are located at a fourfold greater depth (the depth of the soma is correlated with membrane surface area) than corresponding mouse neurons. In spite of being approximately fourfold larger than mouse neurons, the peak voltage-gated potassium current and HCN current in

distal dendritic and somatic outside-out membrane patches in human neurons is similar in amplitude to that of mouse neurons. This suggests that the density of these ion channels is approximately fourfold lower than what would be predicted in humans based on the allometric scaling of these conductances in other mammalian species (Beaulieu-Laroche et al., 2021). The human cortex also contains a much higher neuronal density than predicted for the same degree of expansion in brain size from non-human primates, as compared to other mammals (Herculano-Houzel, 2009, 2012). Additionally, human neurons likely utilize distinct sets of ion channels alongside differences in passive membrane properties, including a specific membrane capacitance that is 50% lower than predicted (Eyal et al., 2016). Human cortical neurons appear to rely more heavily on HCN channels, which generate a subthreshold cation current that can greatly influence signal integration, than mouse cortical neurons (Kalmbach et al., 2018). Other ion channels have not yet been studied in great detail, but differences in somatic and dendritic spike morphology across species (Beaulieu-Laroche et al., 2021) suggest that human neurons likely place emphasis on a subset of ion channels that may be distinct from other species.

Significant differences in dendrite structure and function are also present between human cortical neurons and those from other species. Human L2–L3 cortical pyramidal neurons are much longer and have more complex branching than mouse cortical neurons (Mohan et al., 2015; Deitcher et al., 2017). Functionally, human L2–L3 neurons appear capable of producing graded calcium-mediated action potentials, which theoretically allows a much more dynamic encoding of synaptic input than simple all-or-none spikes (Gidon et al., 2020). This type of graded dendritic spike has not been described in other species, suggesting divergent function in human neurons. In human L5 cortical pyramidal neurons, increased dendritic volume and reduced dendritic ion channel density contribute to an increased input resistance and enhanced somato-dendritic coupling compared to mouse (Beaulieu-Laroche et al., 2018, 2021). In the context of low specific membrane capacitance, which has been proposed to enhance the filtering capacity of human cortical dendrites (Eyal et al., 2016), these features would alter the structure-function relationship in human dendrites. Therefore, dendritic signaling appears to be a major driver of the unique computational features of human neurons.

At present, no physiological data is available from resected human cerebellar tissue. However, a comparative study has shown that human cerebellar neuron density is higher than would be predicted by scaling to other mammals (Herculano-Houzel et al., 2015), a relationship that is also seen in human cortical neurons (Herculano-Houzel, 2009). This raises the possibility that the allometric structure-function relationship of L5 cortical pyramidal neurons that is different in humans (Beaulieu-Laroche et al., 2021) might also extend to cerebellar neurons. If this holds true, a lower-than-predicted current density in human cerebellar neurons might underlie a fundamental susceptibility to perturbances in ion channel function. In turn, further reduced current density upon channelopathy may drive structural changes in an attempt to preserve function, as has been proposed to be a mechanism of neurodegeneration in a mouse model of SCA (Dell'Orco et al., 2015).

ATAXIA-CAUSING CHANNELOPATHIES DUE TO LOSS OF ION CHANNEL FUNCTION IN HUMANS AND MICE

In humans, a number of ion channelopathies cause various forms of episodic ataxia and autosomal dominant SCA. Heterozygous mutations in ion channel genes are sufficient to cause disease, and haploinsufficiency of the causative ion channel is the putative mechanism in many cases. In the last decade, several ion channelopathies, particularly in potassium channel genes, have been identified to result in widespread neurodegeneration of cerebellar and sometimes cortical and other deep brain structures. These disorders are often associated with behavioral alterations and motor dysfunction, although clinical heterogeneity is observed. However, when equivalent ion channel haploinsufficiency or even full channel knockout models in mice are generated, murine models are often resistant to motor and morphological alterations (**Table 1**). This section will highlight the clinical and morphological sequelae of ataxia-causing channelopathies in humans in comparison to what is observed in rodents.

GENE: *KCNMA1*, ION CHANNEL: BK OR LARGE-CONDUCTANCE CALCIUM-ACTIVATED POTASSIUM CHANNEL

KCNMA1 encodes the large conductance calcium-activated potassium channel, also known as the BK or $K_{Ca}1.1$ channel. Mutations in *KCNMA1* cause Liang–Wang syndrome, comprised of developmental delay, cerebellar ataxia, and variable neurological features including seizures and dystonia (Liang et al., 2019), with visceral malformations and death in infancy in the most severe cases. Variable neurodegeneration is also noted on MRI, with early onset of progressive atrophy of the cerebellar hemispheres and vermis in the first and seconds decades of life in multiple patients (Liang et al., 2019, 2022; Du et al., 2020). In a heterologous expression system, BK channel mutations result in loss of BK channel current, with postulated haploinsufficiency and dominant-negative mechanisms (Liang et al., 2019, 2022; Du et al., 2020).

The G354S *KCNMA1* mutation introduced systemically using AAV9 results in gait dysfunction in mice (Du et al., 2020). No neurodegeneration was reported in AAV9-G354S *KCNMA1* mice (Du et al., 2020). G354S *KCNMA1* has been hypothesized to induce mitochondrial dysfunction as the mechanism for disease. Immunogold labeling for *Kcnma1* in mice indicates, however, that BK channels in mice are mostly located at the plasma membrane rather than intracellularly (Kaufmann et al., 2009). This suggests that BK channel function at the plasma membrane is likely a primary mechanism of motor impairment and

TABLE 1 | Phenotypic and structural alterations in human and mouse ion channel gene loss-of-function mutations.

Gene name (channel name)	Citations	Observed phenotype in human	Structural changes in humans (on brain imaging unless otherwise specified)	Observed phenotype in mouse	Structural changes in mouse
KCNMA1 (BK, $K_{Ca}1.1$)	Meredith et al., 2004; Sausbier et al., 2004; Liang et al., 2019; Du et al., 2020; Liang et al., 2022	Liang–Wang syndrome: Death in early onset cases due to a multiple visceral malformation syndrome, craniofacial dysmorphism Developmental delay with speech delay, and ataxia in milder cases	Progressive cerebellar atrophy that is variable but sometimes severe Mild cerebral atrophy Thin corpus callosum	Tremor Abnormal gait Decreased time to fall (rotarod) Overactive bladder	None noted in *Kcnma1* knockout
KCNN2 (SK, $K_{Ca}2.2$)	Callizot et al., 2001; Shakkottai et al., 2004; Szatanik et al., 2008; Mochel et al., 2020	Developmental delay Early onset cerebellar ataxia Extrapyramidal symptoms	Diffuse periventricular white matter changes Cerebellar atrophy (Mochel personal communication in initially identified case)	Frissonnant: Decreased time to fall (rotarod) Decreased locomotor activity Tremor *Kcnn2* knockout: Tremor *Kcnn2* dominant-negative suppression: Decreased time to fall (rotarod) Gait ataxia Tremor	None noted in any model
KCNC3 ($K_v3.3$)	Herman-Bert et al., 2000; Espinosa et al., 2001; Waters et al., 2006; Hurlock et al., 2008	Childhood-onset ataxia or late-onset ataxia Cognitive delay	Global cerebellar volume loss	Decreased time to fall (rotarod) Myoclonus Ethanol hypersensitivity	None noted in *Kcnc3* knockout
KCND3 ($K_v4.3$)	Niwa et al., 2008; Duarri et al., 2012; Lee et al., 2012	Slowly progressive cerebellar ataxia Urinary urgency, incontinence	Mild cerebellar atrophy, Purkinje neuron loss at autopsy (one case)	No neurologic deficits	None noted in *Kcnd3* knockout
ITPR1 (IP3 receptor 1)	Matsumoto et al., 1996; Miyoshi et al., 2001; van de Leemput et al., 2007; Iwaki et al., 2008; Sugawara et al., 2013	Cerebellar ataxia Head tremor	Cerebellar atrophy without brainstem involvement	Early death in global knockout with ataxia and seizures Cerebellar ataxia in Purkinje neuron specific knockout	No structural changes noted Increase in dendritic spine density with simplification of dendrites in Purkinje neuron specific deletion
CACNA1G ($Ca_v3.1$)	Chemin et al., 2018; Coutelier et al., 2015; Morino et al., 2015; Kimura et al., 2017; Li et al., 2018; Hashiguchi et al., 2019; Barresi et al., 2020	Infantile or childhood-onset cerebellar ataxia, global developmental delay in gain-of-function mutations Late onset ataxia with loss-of-function mutations	Childhood-onset cerebellar atrophy Cerebellar atrophy with Purkinje neuron loss at autopsy	Decreased time to fall (rotarod) Increased gait width	Late Purkinje cell loss in loss-of-function mutation
CACNA ($Ca_v2.1$)	Ophoff et al., 1996; Zhuchenko et al., 1997; Jun et al., 1999; Fletcher et al., 2001; Pietrobon, 2002; Du et al., 2013; Reinson et al., 2016; Jen and Wan, 2018	Episodic ataxia type 2: episodes that respond to acetazolamide and spontaneously remit in later life Allelic with Familial hemiplegic and Spinocerebellar ataxia type 6	Variable and selective atrophy of the cerebellar vermis in some cases late in life	Low body weight Decreased lifespan Decreased time to fall (rotarod) Ataxia Seizure	Early Purkinje, granule and Golgi cell loss

cerebellar degeneration in humans, but that mice are resistant to BK channel-dysfunction mediated neurodegeneration. In separate mouse models, complete knockout of *Kcnma1* produces profound ataxia and Purkinje neuron firing impairment in mice, yet cerebellar degeneration is not observed (Meredith et al., 2004; Sausbier et al., 2004). Together, these studies suggest that BK channels play a very important role for cerebellar function in both humans and mice, but that humans are much more vulnerable to both motor impairment (haploinsufficiency in humans vs. complete null in mice) and cerebellar neurodegeneration due to BK channel mutations.

GENE: *KCNN2*, ION CHANNEL: SK2 OR SMALL-CONDUCTANCE CALCIUM-ACTIVATED POTASSIUM CHANNEL 2

KCNN2 encodes the small conductance calcium-activated potassium channel, known as SK2 or $K_{Ca}2.2$. Recently, point mutations in *KCNN2* have been described to result in a spectrum of neurodevelopmental movement disorders (Mochel et al., 2020). Patients generally experience intellectual disability, motor delay, and language delay, along with behavioral comorbidities. Additionally, movement disorders with early age-of-onset are present in many patients, including cerebellar ataxia and extrapyramidal symptoms. White matter abnormalities were observed in three patients out of six for whom MRI data was available, while cerebellar atrophy is also observed in at least one case (Mochel et al., 2020) (Mochel personal communication). The SK2 channel variants are postulated to cause disease through haploinsufficiency.

Interestingly, spontaneous *Kcnn2* mutations have been identified in several mouse strains (Callizot et al., 2001; Szatanik et al., 2008). These mouse strains show tremor and behavioral dysfunction but are not reported to undergo neurodegeneration. Additionally, a mouse model that utilizes a dominant-negative SK channel construct to functionally silence SK channels in the brain also does not display neurodegeneration despite demonstrating prominent motor impairment (Shakkottai et al., 2004). Overall, SK channel loss-of-function appears to induce cerebellar atrophy (in one case) and structural changes in human white matter but does not induce neurodegeneration in mice.

GENE: *KCNC3*, ION CHANNEL: Kv3.3 OR VOLTAGE-GATED POTASSIUM CHANNEL OF THE Kv3 FAMILY

KCNC3 encodes a member of the voltage-gated potassium channel in the Kv3 family. Loss-of-function mutations in *KCNC3* produces a neurological disorder ranging from abnormal neurodevelopment to an adult-onset neurodegenerative disorder (Waters et al., 2006), now termed SCA13. Cerebellar atrophy and slow disease progression, even in early onset cases, is a prominent feature of disease. A putative dominant negative loss-of-function of this ion channel that is enriched in the cerebellum is the postulated mechanism of disease.

Kv3.3 null mice were initially described to have no overt phenotype (Espinosa et al., 2001). Subsequent to the identification of SCA13 due to *KCNC3* mutations, Kv3.3 null mice were identified to have a mild motor phenotype, with primarily increased lateral deviation while ambulating and foot slips when traversing a narrow beam (Hurlock et al., 2008). Nevertheless, no progressive or degenerative phenotype is seen even in mice in which both Kv3.3 and the related Kv3.1 channel are deleted, despite a much more severe ataxic phenotype in Kv3.1/Kv3.3 double null mice compared to Kv3.3 null mice (Espinosa et al., 2001).

GENE: *KCND3*, ION CHANNEL: Kv4.3 OR VOLTAGE-GATED POTASSIUM CHANNEL OF THE Kv4 FAMILY

KCND3 encodes a voltage-gated potassium channel of the Kv4 family. Heterozygous loss-of-function mutations in Kv4.3 results in a late-onset SCA that was identified independently by two separate groups, and is now termed SCA19/22 (Duarri et al., 2012; Lee et al., 2012). Slowly progressive ataxia in mid-life with cerebellar atrophy is characteristic of disease. Cerebellar Purkinje neuron loss is seen in the one described individual with SCA19 who has gone to autopsy (Duarri et al., 2012).

Kv4.3 null mice are described to be indistinguishable from wild-type mice (Niwa et al., 2008). Recording from cardiac ventricular myocytes, an area where Kv4.3 is highly expressed, was also found to be normal *via* cardiac electrophysiology (Niwa et al., 2008).

GENE: *ITPR1*, ION CHANNEL: IP3 RECEPTOR 1

ITPR1 encodes an intracellular calcium channel, the IP3 receptor, that is highly enriched in the cerebellum. Deletions in one copy of the *ITPR1* gene results in autosomal dominant SCA15/16 (van de Leemput et al., 2007; Iwaki et al., 2008), suggesting that haploinsufficiency is sufficient to cause human disease. SCA15/16 presents as slowly progressive, relatively pure cerebellar ataxia with age of onset in the 4th decade of life. Prominent cerebellar atrophy without brainstem involvement is a hallmark of disease (Miyoshi et al., 2001).

Homozygous deletion of *Itpr1* in mice results in death *in utero*, with surviving mice displaying ataxia and epileptic seizures with death by the weaning period (Matsumoto et al., 1996). Although brains of *Itpr1* null mice are smaller, they are histologically indistinguishable from wild-type mice (Matsumoto et al., 1996). Heterozygous *Itpr1* deficient mice are described to have no obvious defects (Matsumoto et al., 1996). Mice with a Purkinje neuron specific deletion of *Itpr1* display progressive ataxia. These mice have normal overall cerebellar morphology, including the organization of the cerebellar cortical layer and Purkinje neuron counts at 10 weeks, but display fewer Purkinje neuron dendritic

branch points and a greater spine density (Sugawara et al., 2013). This suggests that *Itpr1* plays a functional role in the cerebellum in both mice and humans, but only humans exhibit neurodegeneration secondary to loss of the type 1 IP3 receptor.

GENE: *CACNA1G*, ION CHANNEL: CaV3.1 OR T-TYPE VOLTAGE-GATED CALCIUM CHANNEL

CACNA1G encodes $Ca_V3.1$, a T-type voltage-gated calcium channel. Putative gain-of-function, *de novo* point mutations in *CACNA1G* are associated with a neurodevelopmental disorder that includes motor delay, cerebellar ataxia, apraxia, strabismus, and dysmorphic features (Chemin et al., 2018; Barresi et al., 2020). Extensive cerebellar atrophy, mainly in the vermis but sometimes globally, is observed in these patients, while brainstem and cerebral cortex are largely unaffected (Chemin et al., 2018; Barresi et al., 2020). On the other hand, a loss-of-function mutation, p.Arg1715His, causes the autosomal-dominant spinocerebellar ataxia SCA42 (Coutelier et al., 2015; Morino et al., 2015; Kimura et al., 2017). SCA42 results in onset of ataxia and cerebellar atrophy in mid-life and a recurrent p.Arg1715His mutation in Cav3.1 in reported in individuals in France and Japan. An additional mutation in individuals in a family in China with onset of ataxia in mid-life has been reported due to a p.Met1574Lys mutation in Cav3.1 (Li et al., 2018).

In a mouse model of SCA42, knock-in of the mutation analogous to p.Arg1715His (p.Arg1723His in mice) induces motor impairment at 10 weeks that is stable. Mild Purkinje neuron loss is not evident until 50 weeks, without progression of motor impairment (Hashiguchi et al., 2019). In the case of *CACNA1G*, a mouse model of disease recapitulates some of the motor impairment and neurodegeneration observed in human disease, although there is a disconnect, as seen in other channelopathies, between the onset and degree of motor impairment and cerebellar degeneration.

GENE: *CACNA1A*, ION CHANNEL: CaV2.1 OR P/Q TYPE VOLTAGE-GATED CALCIUM CHANNEL

CACNA1A has emerged as an important disease gene that causes a range of episodic disorders and autosomal dominant SCA. *CACNA1A* encodes $Ca_V2.1$, a P/Q type voltage-gated calcium channel that is enriched in presynaptic terminals and in Purkinje neuron cell bodies. *CACNA1A* mutations are the cause of episodic ataxia type 2 (EA2) (Ophoff et al., 1996), familial hemiplegic migraine (FHM) (Ophoff et al., 1996), and spinocerebellar ataxia type 6 (SCA6), a CAG triplet repeat expansion disorder (Zhuchenko et al., 1997). Progressive cerebellar neurodegeneration and motor impairment are present in SCA6, although the mechanism of disease remains unclear. While loss-of-function of CaV2.1 may underlie disease, growing evidence suggests that α1ACT, a separately translated portion of the channel that contains its C-terminal fragment, plays an important role in the disease process (Du et al., 2013). Therefore, it is difficult to speculate on the role of ion channel loss-of-function vs. α1ACT C-terminal toxicity specifically in SCA6. However, in EA2, point mutations in *CACNA1A* lead to early onset of episodes of unsteady gait, slurred speech, and incoordination, in infancy or childhood and sometimes accompanied by progressive ataxia between episodes and variable late cerebellar atrophy (Jen and Wan, 2018). Biallelic *CACNA1A* mutations cause an epileptic encephalopathy, with developmental delay and progressive cerebral and cerebellar atrophy (Reinson et al., 2016).

In mice, Purkinje cell-specific knockout of *Cacna1a* induces motor impairment and causes Purkinje neuron loss beginning at post-natal day 30 (Todorov et al., 2012). A number of other recessive loss-of-function mutations in *Cacna1a* (termed *tottering*, *leaner*, *rolling Nagoya*, and *rocker*) produce a phenotype of ataxia, seizures, and dystonia/dyskinesia in mice. In the *leaner* cerebellum, there is an early and significant loss of cerebellar granule, Golgi, and Purkinje cells (Pietrobon, 2002). *Cacna1a* null mice exhibit a phenotype of ataxia and degeneration of cerebellar neurons, including Purkinje cells, (Jun et al., 1999; Fletcher et al., 2001) similar to *leaner* mice. Thus, *Cacna1a* mutations may be the exception to the general observation that loss-of-function mutations in ion channel genes do not produce degeneration in mouse models. Paradoxically, however, the degenerative phenotype resulting from *Cacna1a* loss-of-function is more prominent in mice as compared to humans where it causes primarily an episodic disorder with variable and late onset of cerebellar atrophy.

ION CHANNEL RESERVE AND DEGENERACY AS A VULNERABILITY FACTOR IN CEREBELLAR DISEASE

As outlined above, human ataxia-causing channelopathies and mouse models of ion channel knockout, particularly for potassium channel genes, show diverging patterns of neurodegeneration and even a complete lack of degeneration in some mouse models. A simplistic argument could be that murine Purkinje neurons are merely more resistant to degeneration. Also, the cerebellum is not uniformly vulnerable to degeneration in human disease, and is resistant to degeneration in canonical age related human neurodegenerative disease (Liang and Carlson, 2020). The idea that mouse Purkinje neurons are more resistant to degeneration is contradicted by several rodent models of human cerebellar ataxia where Purkinje neurons are in fact very vulnerable to degeneration in both mice and humans. For example, in a mouse model of Neiman-Pick C, cerebellar Purkinje neurons undergo profound neurodegeneration, similar to human disease (Elrick et al., 2010), with an almost complete loss of neurons by post-natal week 22. Interestingly, in this study, Purkinje neuron intrinsic excitability (a marker of ion channel dysfunction) was unaffected even in the presence of marked Purkinje neuron atrophy. In marked contrast to the mutations in ion channel genes where the previously developed ion channel-knockout mice displayed no degeneration, *pcd*

mice were identified over four decades ago to have loss of virtually all cerebellar Purkinje cells during the third and fourth post-natal week (Landis and Mullen, 1978). Biallelic variants of the homologous gene, *AGTPBP1*, which codes for a metallocarboxypeptidase that mediates protein deglutamylation of tubulin and non-tubulin target proteins, were recently identified to cause childhood-onset neurodegeneration with profound cerebellar atrophy (Shashi et al., 2018; Sheffer et al., 2019). It is interesting to speculate that the divergence between mouse and human Purkinje neurons in the vulnerability to degeneration is unique to cerebellar disorders of ion channel dysfunction. Rules of compensation and degeneracy may be a key difference in ion channel regulation in humans vs. mice compared to other genes. This is supported by studies in human cortical neurons where the rules of allometric scaling of ion channel density shows clear divergence between human neurons and all other species (Beaulieu-Laroche et al., 2021). Human cerebellar neurons may, therefore, be particularly vulnerable to disease processes that reduce ion channel density, including channelopathies.

In cases of ion channel loss-of-function or knockout, degeneracy or substitution with a different ion channel may compensate for loss of an ion channel. Increased functional reliance on an ion channel that has a similar, but incompletely, overlapping function to the channel that has become non-functional is a mechanism to preserve function. This is perhaps most clearly observed in a knockout mouse model of *Kcnc* channels (K_v3 family members), where genetic knockout of *Kcnc3* fails to induce phenotypic features of disease if the compensatory gene *Kcnc1* is present (Hurlock et al., 2009). However, when *Kcnc1* is knocked out alongside *Kcnc3*, electrophysiologic dysfunction and motor impairment both appear. This is likely due to the similar functional properties of $K_v3.1$ and $K_v3.3$ that enable full compensation of function when $K_v3.3$ is lost. Interestingly, this same mechanism of compensation does not appear to prevent phenotypic features of disease in humans, as *KCNC3* mutations cause SCA13, in which cerebellar neurodegeneration and progressive motor dysfunction are observed (Waters et al., 2006). In other experimental models, ion channel compensation has been hypothesized to involve more functionally distinct channels that preserve a level of neuronal function, although function may become slightly altered (Drion et al., 2015; Goaillard and Marder, 2021).

An alternative compensatory mechanism to the ion channel substitution/degeneracy described above is compensation for partial loss of ion channels through functional reserve. The baseline ion channel density, and how much ion channel exists in excess of what is needed, may predicate how much ion channel protein must be lost before there is impairment in function. Differences in ion channel density may explain differences in vulnerability of human and mouse neurons to neurodegeneration in channelopathies. This concept is outlined in **Figure 1**. A reduced baseline ion channel density in human cerebellar neurons, as has been observed in human cortical neurons (Beaulieu-Laroche et al., 2021), may make them more sensitive to perturbations in ion channel expression or function. In mice, reduced ion channel expression may be tolerated if it does not surpass the level of ion channel reserve needed to maintain normal function. Even in cases of full ion channel knockout, a compensatory ion channel may then act to preserve normal neuronal function.

Despite lack of neurodegeneration in many mouse models of ion channel knockout, cerebellar neurodegeneration is observed in mouse models of SCA that model human SCAs due to a polyglutamine encoding, CAG repeat-expansion in the respective disease genes (so-called polyglutamine ataxia). In mouse models of SCA1 (Dell'Orco et al., 2015; Bushart et al., 2021), SCA2 (Kasumu et al., 2012; Hansen et al., 2013; Dell'Orco et al., 2017), SCA3 (Shakkottai et al., 2011), SCA6 (Jayabal et al., 2016), and SCA7 (Stoyas et al., 2020), onset of motor impairment is concurrent with Purkinje neuron intrinsic firing abnormalities and in many cases long precedes the onset of Purkinje neuron loss. In these diseases, where the respective disease-causing mutations do not reside in ion channels, transcriptional alterations are the likely driver of disease. Remarkably, a reduction in transcript levels of ion channels that drive electrophysiologic dysfunction are shared across several of these disorders (Chopra et al., 2020; Stoyas et al., 2020). In murine models of disease, reduced transcripts for *Kcnma1*, *Cacna1g*, *Trpc3*, and *Itpr1* are seen (Chopra et al., 2020). Interestingly, pharmacologic inhibition of any of these individual ion channels fails to induce spiking abnormalities in wild-type Purkinje neurons, yet inhibition of two or more of these channels simultaneously is sufficient to induce the changes in Purkinje neuron spiking that are observed in mouse models of disease (Chopra et al., 2020; Stoyas et al., 2020). Restoring ion channel expression or function attenuates neurodegeneration in mouse models of SCA1 (Dell'Orco et al., 2015; Chopra et al., 2018) and SCA2 (Kasumu et al., 2012), suggesting that a reduction in ion channel transcripts is a driver of neurodegeneration. If ion channel dysfunction is a driver of neurodegeneration in these disorders, is this an apparent contradiction to the lack of neurodegeneration that is observed in mouse knock-out models of individual ion channel genes? It is possible that by affecting several ion channel transcripts simultaneously, the redundancy and ability to compensate for loss of individual ion channels in mouse Purkinje neurons is now no longer possible. Neurodegeneration in the polyglutamine ataxias in rodent models of disease requires very high overexpression of the mutant protein in transgenic models, or repeat expansion lengths far greater than what is normally observed in human disease in knock-in models of disease. Consistent with the hypothesis that ion channels may be an important driver of neurodegeneration in the polyglutamine ataxias, the degree of binding of the mutant protein in SCA1 is polyglutamine length-dependent, and simultaneously reduces transcripts of several of the channels involved in ataxia-causing channelopathy (Hansen et al., 2013). This may explain the need for overexpression of disease-causing polyglutamine expanded protein to cause sufficient ion channel transcript suppression, therefore overcoming greater ion channel reserve in mice for individual ion channels.

Is the allometric scaling and vulnerability to degeneration of human cerebellar neurons unique to ion channel dysfunction? While there are instances of Purkinje degeneration that occurs

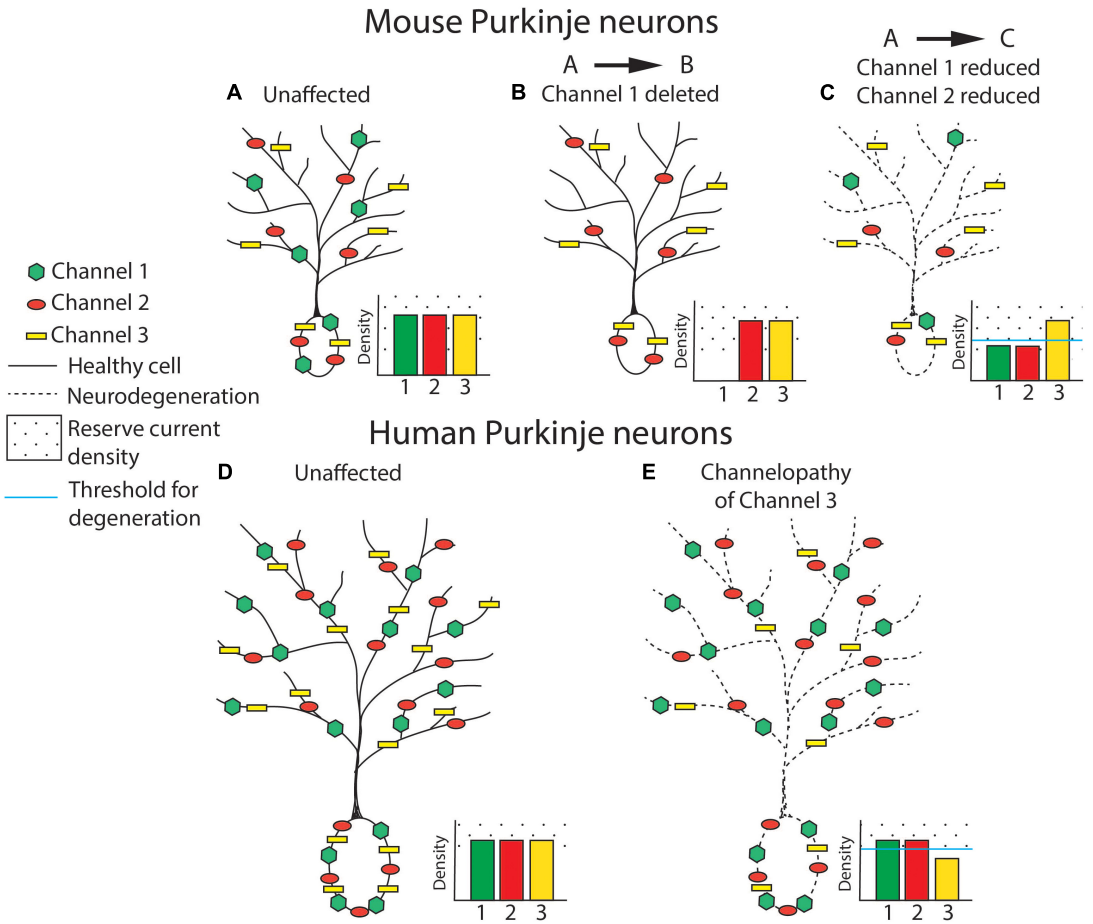

FIGURE 1 | Ion channel loss differentially influences cerebellar neurodegeneration in mice and humans. Ion channel density is represented in cerebellar Purkinje neurons from mouse **(A–C)** and human **(D,E)**. In this basic model, ion channel types are hypothesized to be relatively equivalent for their influence on neurodegeneration and are therefore represented generically as Channel 1 (green hexagon), Channel 2 (red circle), and Channel 3 (yellow rectangle). For each panel, density of expression for each ion channel is represented in a bar plot on the inset of each neuron, with the threshold of channel loss needed to produce neurodegeneration represented by a solid blue line and ion channel "reserve density" noted with a dotted background. Note that the level of reserve ion channel density to produce channel dysfunction is higher in mice for each channel, and that the baseline ion channel density is similar in human and mouse neurons. **(A)** An unaffected wild-type mouse neuron is represented with normal expression of channels 1, 2, and 3. **(B)** Full knockout of an individual ion channel (channel 1) produces no Purkinje neuron degeneration in mice, possibly due to increased function of overlapping or compensatory ion channels. **(C)** Partial reduction of multiple ion channels within the same excitability pathway, as has been observed in mouse models of spinocerebellar ataxia (SCA), is sufficient to produce Purkinje neuron atrophy and neurodegeneration despite each individual channel remaining within a "reserve" level of expression. Degeneration is represented as a cell membrane with a dashed line. **(D)** An unaffected, normal human neuron is represented with normal expression of channels 1, 2, and 3. The density of ion channels is the same as in mouse neurons in spite of a considerable increase in cell size. **(E)** In humans, haploinsufficiency of a single ion channel is sufficient to induce clinical symptoms and Purkinje neuron degeneration. Degeneration is represented as a dashed cell membrane.

in a similar fashion both mice and in humans as outlined above, there are other causes of ataxia, such as in disorders of DNA repair, which also appear to have a disconnect between degeneration that is profound in human disease yet is absent in mouse knockout models. In models of ataxia telangiectasia and ataxia with oculomotor apraxia type 1, complete knockout of the proteins ATM (Lavin, 2013) and APTX (Ahel et al., 2006), respectively, fails to produce motor impairment, cerebellar atrophy, or Purkinje neuron loss (Lavin, 2013; Perez et al., 2021). In a recently developed mouse model, a combination of a biallelic human *ATM* mutation and knockout of *APTX* produces motor impairment and cerebellar volume loss without loss of Purkinje neurons by post-natal day 400. Surprisingly, the progressive motor impairment is associated with slowed Purkinje neuron firing in this model of ataxia-telangiectasia reminiscent of the changes in firing seen in the models of SCA described previously. The ionic basis for the reduction in Purkinje neuron firing in this model of ataxia-telangiectasia remains unexplored. Alterations in Purkinje neuron spiking are also seen in a different DNA break repair disorder. *Xrcc1* knockout mice, a model for an autosomal recessive cerebellar ataxia due to biallelic loss-of-function mutations in the homologous human gene, display slowed Purkinje neuron spiking (Hoch et al., 2017). This somewhat unexpected finding of altered Purkinje neuron

spiking in these models is consistent with the idea that even in disorders of DNA break-repair, the underlying mechanism for degeneration may in fact be secondary to ion channel dysregulation. While there may be other biological processes other than ion channel density that do not scale with the increase in human neuron size, ion channel density is clearly worth investigating as a unique vulnerability factor for degeneration of human cerebellar neurons.

The mechanism for how ion channel dysfunction leads to neurodegeneration in cerebellar disorders remains unclear. A plausible hypothesis is that it is related to aberrant calcium homeostasis. Purkinje neurons are unusual in that the inward calcium current is completely masked by an outward potassium current (Raman and Bean, 1999). Rapid clearance of intracellular calcium is needed in the interspike interval of Purkinje neurons that exhibit high rates of firing (Fierro et al., 1998). Clearance of cellular calcium requires plasma membrane calcium pumps and the sodium-calcium exchanger, also located on the plasma membrane (Fierro et al., 1998). Since the volume of the cell that is cleared of calcium scales as an order of magnitude greater than the surface area of the cell, it may explain the observed increase in ion channel density with increased cell size in most mammalian species. Humans appear to not have sufficient reserve for the increase in calcium clearance mechanisms with the increase in cell size, at least in cortical neurons.

SUITABILITY OF MOUSE MODELS FOR ATAXIA-CAUSING CHANNELOPATHIES

This review presents an argument that ion channel loss-of-function produces distinct patterns of neurodegeneration in humans that are not replicated in mouse models of disease. In complex neurodegenerative conditions where ion channel mutations are not the primary drivers of disease, such as in the polyglutamine SCAs, widespread transcriptional alterations appear to be associated with disease. In these cases, a shared reduction in transcripts of several ion channel genes contributes to neurodegeneration. However, neurodegeneration is not observed in any potassium channel knockout mice. As outlined above, single ion channel deletion appears to be well compensated in mouse Purkinje neurons due to ion channel reserve and overlapping functional roles of similar ion channel genes. While ion channel knockout models have been valuable for understanding the major electrophysiological and behavioral roles of these ion channels, they do not model the neurodegeneration seen in human ataxia causing channelopathies.

CONCLUSION

Human ion channelopathies are closely associated with cerebellar neurodegeneration. Despite this association, ion channel knockout in mice rarely causes neurodegeneration that mirrors human cerebellar disease. This review has presented key differences in cortical neuron function between human and model species. If true also of cerebellar neurons, it suggests that fundamental differences in cerebellar neuron function may make human cerebellar neurons more vulnerable to perturbations in ion channel function. In cases where there is a disconnect in cerebellar degeneration between mouse models and human disease, it may be worth looking for ion channel dysfunction as the basis for cerebellar neurodegeneration.

AUTHOR CONTRIBUTIONS

DB and VS wrote and edited the manuscript. Both authors contributed to the article and approved the submitted version.

FUNDING

This work was supported by National Institutes of Health R01 NS085054 (VS).

REFERENCES

Ahel, I., Rass, U., El-Khamisy, S. F., Katyal, S., Clements, P. M., McKinnon, P. J., et al. (2006). The neurodegenerative disease protein aprataxin resolves abortive DNA ligation intermediates. *Nature* 443, 713–716. doi: 10.1038/nature05164

Barresi, S., Dentici, M. L., Manzoni, F., Bellacchio, E., Agolini, E., Pizzi, S., et al. (2020). Infantile-onset syndromic cerebellar ataxia and CACNA1G mutations. *Pediatr. Neurol.* 104, 40–45. doi: 10.1016/j.pediatrneurol.2019.09.005

Beaulieu-Laroche, L., Brown, N. J., Hansen, M., Toloza, E. H. S., Sharma, J., Williams, Z. M., et al. (2021). Allometric rules for mammalian cortical layer 5 neuron biophysics. *Nature* 600, 274–278. doi: 10.1038/s41586-021-04072-3

Beaulieu-Laroche, L., Toloza, E. H. S., van der Goes, M. S., Lafourcade, M., Barnagian, D., Williams, Z. M., et al. (2018). Enhanced dendritic compartmentalization in human cortical neurons. *Cell* 175, 643–651.e14. doi: 10.1016/j.cell.2018.08.045

Bushart, D. D., Huang, H., Man, L. J., Morrison, L. M., and Shakkottai, V. G. (2021). A chlorzoxazone-baclofen combination improves cerebellar impairment in spinocerebellar ataxia type 1. *Mov. Disord.* 36, 622–631. doi: 10.1002/mds.28355

Bushart, D. D., and Shakkottai, V. G. (2019). Ion channel dysfunction in cerebellar ataxia. *Neurosci. Lett.* 688, 41–48. doi: 10.1016/j.neulet.2018.02.005

Callizot, N., Guenet, J. L., Baillet, C., Warter, J. M., and Poindron, P. (2001). The frissonnant mutant mouse, a model of dopamino-sensitive, inherited motor syndrome. *Neurobiol. Dis.* 8, 447–458. doi: 10.1006/nbdi.2001.0393

Chemin, J., Siquier-Pernet, K., Nicouleau, M., Barcia, G., Ahmad, A., Medina-Cano, D., et al. (2018). *De novo* mutation screening in childhood-onset cerebellar atrophy identifies gain-of-function mutations in the CACNA1G calcium channel gene. *Brain* 141, 1998–2013. doi: 10.1093/brain/awy145

Chopra, R., Bushart, D. D., Cooper, J. P., Yellajoshyula, D., Morrison, L. M., Huang, H., et al. (2020). Altered Capicua expression drives regional Purkinje neuron vulnerability through ion channel gene dysregulation in spinocerebellar ataxia type 1. *Hum. Mol. Genet.* 29, 3249–3265. doi: 10.1093/hmg/ddaa212

Chopra, R., Bushart, D. D., and Shakkottai, V. G. (2018). Dendritic potassium channel dysfunction may contribute to dendrite degeneration in spinocerebellar ataxia type 1. *PLoS One* 13:e0198040. doi: 10.1371/journal.pone.0198040

Coutelier, M., Blesneac, I., Monteil, A., Monin, M. L., Ando, K., Mundwiller, E., et al. (2015). A recurrent mutation in CACNA1G alters Cav3.1 T-type calcium-channel conduction and causes autosomal-dominant cerebellar ataxia. *Am. J. Hum. Genet.* 97, 726–737. doi: 10.1016/j.ajhg.2015.09.007

Deitcher, Y., Eyal, G., Kanari, L., Verhoog, M. B., Atenekeng Kahou, G. A., Mansvelder, H. D., et al. (2017). Comprehensive morpho-electrotonic analysis

shows 2 distinct classes of L2 and L3 pyramidal neurons in human temporal cortex. *Cereb. Cortex* 27, 5398–5414. doi: 10.1093/cercor/bhx226

Dell'Orco, J. M., Pulst, S. M., and Shakkottai, V. G. (2017). Potassium channel dysfunction underlies Purkinje neuron spiking abnormalities in spinocerebellar ataxia type 2. *Hum. Mol. Genet.* 26, 3935–3945. doi: 10.1093/hmg/ddx281

Dell'Orco, J. M., Wasserman, A. H., Chopra, R., Ingram, M. A., Hu, Y. S., Singh, V., et al. (2015). Neuronal atrophy early in degenerative ataxia is a compensatory mechanism to regulate membrane excitability. *J. Neurosci.* 35, 11292–11307. doi: 10.1523/JNEUROSCI.1357-15.2015

Drion, G., O'Leary, T., and Marder, E. (2015). Ion channel degeneracy enables robust and tunable neuronal firing rates. *Proc. Natl. Acad. Sci. U. S. A.* 112, E5361–E5370. doi: 10.1073/pnas.1516400112

Du, X., Carvalho-de-Souza, J. L., Wei, C., Carrasquel-Ursulaez, W., Lorenzo, Y., Gonzalez, N., et al. (2020). Loss-of-function BK channel mutation causes impaired mitochondria and progressive cerebellar ataxia. *Proc. Natl. Acad. Sci. U. S. A.* 117, 6023–6034. doi: 10.1073/pnas.1920008117

Du, X., Wang, J., Zhu, H., Rinaldo, L., Lamar, K. M., Palmenberg, A. C., et al. (2013). Second cistron in CACNA1A gene encodes a transcription factor mediating cerebellar development and SCA6. *Cell* 154, 118–133. doi: 10.1016/j.cell.2013.05.059

Duarri, A., Jezierska, J., Fokkens, M., Meijer, M., Schelhaas, H. J., den Dunnen, W. F., et al. (2012). Mutations in potassium channel kcnd3 cause spinocerebellar ataxia type 19. *Ann. Neurol.* 72, 870–880. doi: 10.1002/ana.23700

Elrick, M. J., Pacheco, C. D., Yu, T., Dadgar, N., Shakkottai, V. G., Ware, C., et al. (2010). Conditional Niemann-Pick C mice demonstrate cell autonomous Purkinje cell neurodegeneration. *Hum. Mol. Genet.* 19, 837–847. doi: 10.1093/hmg/ddp552

Espinosa, F., McMahon, A., Chan, E., Wang, S., Ho, C. S., Heintz, N., et al. (2001). Alcohol hypersensitivity, increased locomotion, and spontaneous myoclonus in mice lacking the potassium channels Kv3.1 and Kv3.3. *J. Neurosci.* 21, 6657–6665. doi: 10.1523/JNEUROSCI.21-17-06657.2001

Eyal, G., Verhoog, M. B., Testa-Silva, G., Deitcher, Y., Lodder, J. C., Benavides-Piccione, R., et al. (2016). Unique membrane properties and enhanced signal processing in human neocortical neurons. *Elife* 5:e16553. doi: 10.7554/eLife.16553

Fierro, L., DiPolo, R., and Llano, I. (1998). Intracellular calcium clearance in Purkinje cell somata from rat cerebellar slices. *J. Physiol.* 510(Pt 2), 499–512. doi: 10.1111/j.1469-7793.1998.499bk.x

Fletcher, C. F., Tottene, A., Lennon, V. A., Wilson, S. M., Dubel, S. J., Paylor, R., et al. (2001). Dystonia and cerebellar atrophy in Cacna1a null mice lacking P/Q calcium channel activity. *FASEB J.* 15, 1288–1290. doi: 10.1096/fj.00-0562fje

Gidon, A., Zolnik, T. A., Fidzinski, P., Bolduan, F., Papoutsi, A., Poirazi, P., et al. (2020). Dendritic action potentials and computation in human layer 2/3 cortical neurons. *Science* 367, 83–87. doi: 10.1126/science.aax6239

Goaillard, J. M., and Marder, E. (2021). Ion channel degeneracy, variability, and covariation in neuron and circuit resilience. *Annu. Rev. Neurosci.* 44, 335–357. doi: 10.1146/annurev-neuro-092920-121538

Hansen, S. T., Meera, P., Otis, T. S., and Pulst, S. M. (2013). Changes in Purkinje cell firing and gene expression precede behavioral pathology in a mouse model of SCA2. *Hum. Mol. Genet.* 22, 271–283. doi: 10.1093/hmg/dds427.dds427

Hashiguchi, S., Doi, H., Kunii, M., Nakamura, Y., Shimuta, M., Suzuki, E., et al. (2019). Ataxic phenotype with altered CaV3.1 channel property in a mouse model for spinocerebellar ataxia 42. *Neurobiol. Dis.* 130:104516. doi: 10.1016/j.nbd.2019.104516

Herculano-Houzel, S. (2009). The human brain in numbers: a linearly scaled-up primate brain. *Front. Hum. Neurosci.* 3:31. doi: 10.3389/neuro.09.031.2009

Herculano-Houzel, S. (2012). The remarkable, yet not extraordinary, human brain as a scaled-up primate brain and its associated cost. *Proc. Natl. Acad. Sci. U. S. A.* 109(Suppl. 1), 10661–10668. doi: 10.1073/pnas.1201895109

Herculano-Houzel, S., Catania, K., Manger, P. R., and Kaas, J. H. (2015). Mammalian brains are made of these: a dataset of the numbers and densities of neuronal and non-neuronal cells in the brain of glires, primates, scandentia, eulipotyphlans, afrotherians and artiodactyls, and their relationship with body mass. *Brain Behav. Evol.* 86, 145–163. doi: 10.1159/000437413

Herman-Bert, A., Stevanin, G., Netter, J. C., Rascol, O., Brassat, D., Calvas, P., et al. (2000). Mapping of spinocerebellar ataxia 13 to chromosome 19q13.3–q13.4 in a family with autosomal dominant cerebellar ataxia and mental retardation. *Am. J. Hum. Genet.* 67, 229–235. doi: 10.1086/302958

Hoch, N. C., Hanzlikova, H., Rulten, S. L., Tetreault, M., Komulainen, E., Ju, L., et al. (2017). XRCC1 mutation is associated with PARP1 hyperactivation and cerebellar ataxia. *Nature* 541, 87–91. doi: 10.1038/nature20790

Hurlock, E. C., Bose, M., Pierce, G., and Joho, R. H. (2009). Rescue of motor coordination by Purkinje cell-targeted restoration of Kv3.3 channels in Kcnc3-null mice requires Kcnc1. *J. Neurosci.* 29, 15735–15744. doi: 10.1523/JNEUROSCI.4048-09.2009

Hurlock, E. C., McMahon, A., and Joho, R. H. (2008). Purkinje-cell-restricted restoration of Kv3.3 function restores complex spikes and rescues motor coordination in Kcnc3 mutants. *J. Neurosci.* 28, 4640–4648. doi: 10.1523/JNEUROSCI.5486-07.2008

Iwaki, A., Kawano, Y., Miura, S., Shibata, H., Matsuse, D., Li, W., et al. (2008). Heterozygous deletion of ITPR1, but not SUMF1, in spinocerebellar ataxia type 16. *J. Med. Genet.* 45, 32–35. doi: 10.1136/jmg.2007.053942

Jayabal, S., Chang, H. H., Cullen, K. E., and Watt, A. J. (2016). 4-aminopyridine reverses ataxia and cerebellar firing deficiency in a mouse model of spinocerebellar ataxia type 6. *Sci. Rep.* 6:29489. doi: 10.1038/srep29489

Jen, J. C., and Wan, J. (2018). Episodic ataxias. *Handb. Clin. Neurol.* 155, 205–215. doi: 10.1016/B978-0-444-64189-2.00013-5

Jun, K., Piedras-Renteria, E. S., Smith, S. M., Wheeler, D. B., Lee, S. B., Lee, T. G., et al. (1999). Ablation of P/Q-type Ca(2 +) channel currents, altered synaptic transmission, and progressive ataxia in mice lacking the alpha(1A)-subunit. *Proc. Natl. Acad. Sci. U. S. A.* 96, 15245–15250. doi: 10.1073/pnas.96.26.15245

Kalmbach, B. E., Buchin, A., Long, B., Close, J., Nandi, A., Miller, J. A., et al. (2018). h-channels contribute to divergent intrinsic membrane properties of supragranular pyramidal neurons in human versus mouse cerebral cortex. *Neuron* 100, 1194–1208.e5. doi: 10.1016/j.neuron.2018.10.012

Kasumu, A. W., Hougaard, C., Rode, F., Jacobsen, T. A., Sabatier, J. M., Eriksen, B. L., et al. (2012). Selective positive modulator of calcium-activated potassium channels exerts beneficial effects in a mouse model of spinocerebellar ataxia type 2. *Chem. Biol.* 19, 1340–1353. doi: 10.1016/j.chembiol.2012.07.013.S1074-5521(12)00266-9

Kaufmann, W. A., Ferraguti, F., Fukazawa, Y., Kasugai, Y., Shigemoto, R., Laake, P., et al. (2009). Large-conductance calcium-activated potassium channels in purkinje cell plasma membranes are clustered at sites of hypolemmal microdomains. *J. Comp. Neurol.* 515, 215–230. doi: 10.1002/cne.22066

Kimura, M., Yabe, I., Hama, Y., Eguchi, K., Ura, S., Tsuzaka, K., et al. (2017). SCA42 mutation analysis in a case series of Japanese patients with spinocerebellar ataxia. *J. Hum. Genet.* 62, 857–859. doi: 10.1038/jhg.2017.51

Landis, S. C., and Mullen, R. J. (1978). The development and degeneration of Purkinje cells in pcd mutant mice. *J. Comp. Neurol.* 177, 125–143. doi: 10.1002/cne.901770109

Lavin, M. F. (2013). The appropriateness of the mouse model for ataxia-telangiectasia: neurological defects but no neurodegeneration. *DNA Repair* 12, 612–619. doi: 10.1016/j.dnarep.2013.04.014

Lee, Y. C., Durr, A., Majczenko, K., Huang, Y. H., Liu, Y. C., Lien, C. C., et al. (2012). Mutations in KCND3 cause spinocerebellar ataxia type 22. *Ann. Neurol.* 72, 859–869. doi: 10.1002/ana.23701

Li, X., Zhou, C., Cui, L., Zhu, L., Du, H., Liu, J., et al. (2018). A case of a novel CACNA1G mutation from a Chinese family with SCA42: a case report and literature review. *Medicine* 97:e12148. doi: 10.1097/MD.0000000000012148

Liang, K. J., and Carlson, E. S. (2020). Resistance, vulnerability and resilience: a review of the cognitive cerebellum in aging and neurodegenerative diseases. *Neurobiol. Learn. Mem.* 170:106981. doi: 10.1016/j.nlm.2019.01.004

Liang, L., Li, X., Moutton, S., Schrier Vergano, S. A., Cogne, B., de Saint-Martin, A., et al. (2019). *De novo* loss-of-function KCNMA1 variants are associated with a new multiple malformation syndrome and a broad spectrum of developmental and neurological phenotypes. *Hum. Mol. Genet.* 28, 2937–2951. doi: 10.1093/hmg/ddz117

Liang, L., Liu, H., Bartholdi, D., van Haeringen, A., Fernandez-Jaen, A., Peeters, E. E. A., et al. (2022). Identification and functional analysis of two new *de novo* KCNMA1 variants associated with Liang-Wang syndrome. *Acta Physiol.* 235:e13800. doi: 10.1111/apha.13800

Matsumoto, M., Nakagawa, T., Inoue, T., Nagata, E., Tanaka, K., Takano, H., et al. (1996). Ataxia and epileptic seizures in mice lacking type 1 inositol 1,4,5-trisphosphate receptor. *Nature* 379, 168–171. doi: 10.1038/379168a0

Meredith, A. L., Thorneloe, K. S., Werner, M. E., Nelson, M. T., and Aldrich, R. W. (2004). Overactive bladder and incontinence in the absence of the BK large

conductance Ca2 + -activated K + channel. *J. Biol. Chem.* 279, 36746–36752. doi: 10.1074/jbc.M405621200

Miyoshi, Y., Yamada, T., Tanimura, M., Taniwaki, T., Arakawa, K., Ohyagi, Y., et al. (2001). A novel autosomal dominant spinocerebellar ataxia (SCA16) linked to chromosome 8q22.1-24.1. *Neurology* 57, 96–100. doi: 10.1212/wnl.57.1.96

Mochel, F., Rastetter, A., Ceulemans, B., Platzer, K., Yang, S., Shinde, D. N., et al. (2020). Variants in the SK2 channel gene (KCNN2) lead to dominant neurodevelopmental movement disorders. *Brain* 143, 3564–3573. doi: 10.1093/brain/awaa346

Mohan, H., Verhoog, M. B., Doreswamy, K. K., Eyal, G., Aardse, R., Lodder, B. N., et al. (2015). Dendritic and axonal architecture of individual pyramidal neurons across layers of adult human neocortex. *Cereb. Cortex* 25, 4839–4853. doi: 10.1093/cercor/bhv188

Morino, H., Matsuda, Y., Muguruma, K., Miyamoto, R., Ohsawa, R., Ohtake, T., et al. (2015). A mutation in the low voltage-gated calcium channel CACNA1G alters the physiological properties of the channel, causing spinocerebellar ataxia. *Mol. Brain* 8:89. doi: 10.1186/s13041-015-0180-4

Niwa, N., Wang, W., Sha, Q., Marionneau, C., and Nerbonne, J. M. (2008). Kv4.3 is not required for the generation of functional Ito,f channels in adult mouse ventricles. *J. Mol. Cell Cardiol.* 44, 95–104. doi: 10.1016/j.yjmcc.2007.10.007

Ophoff, R. A., Terwindt, G. M., Vergouwe, M. N., van Eijk, R., Oefner, P. J., Hoffman, S. M., et al. (1996). Familial hemiplegic migraine and episodic ataxia type-2 are caused by mutations in the Ca2 + channel gene CACNL1A4. *Cell* 87, 543–552. doi: 10.1016/s0092-8674(00)81373-2

Perez, H., Abdallah, M. F., Chavira, J. I., Norris, A. S., Egeland, M. T., Vo, K. L., et al. (2021). A novel, ataxic mouse model of ataxia telangiectasia caused by a clinically relevant nonsense mutation. *Elife* 10:e64695. doi: 10.7554/eLife.64695

Pietrobon, D. (2002). Calcium channels and channelopathies of the central nervous system. *Mol. Neurobiol.* 25, 31–50. doi: 10.1385/MN:25:1:031

Raman, I. M., and Bean, B. P. (1999). Ionic currents underlying spontaneous action potentials in isolated cerebellar Purkinje neurons. *J. Neurosci.* 19, 1663–1674. doi: 10.1523/JNEUROSCI.19-05-01663.1999

Reinson, K., Oiglane-Shlik, E., Talvik, I., Vaher, U., Ounapuu, A., Ennok, M., et al. (2016). Biallelic CACNA1A mutations cause early onset epileptic encephalopathy with progressive cerebral, cerebellar, and optic nerve atrophy. *Am. J. Med. Genet. A* 170, 2173–2176. doi: 10.1002/ajmg.a.37678

Russell, J. F., Fu, Y. H., and Ptacek, L. J. (2013). Episodic neurologic disorders: syndromes, genes, and mechanisms. *Annu. Rev. Neurosci.* 36, 25–50. doi: 10.1146/annurev-neuro-062012-170300

Sausbier, M., Hu, H., Arntz, C., Feil, S., Kamm, S., Adelsberger, H., et al. (2004). Cerebellar ataxia and Purkinje cell dysfunction caused by Ca2 + -activated K + channel deficiency. *Proc. Natl. Acad. Sci. U. S. A.* 101, 9474–9478. doi: 10.1073/pnas.0401702101040170210 1

Shakkottai, V. G., Chou, C. H., Oddo, S., Sailer, C. A., Knaus, H. G., Gutman, G. A., et al. (2004). Enhanced neuronal excitability in the absence of neurodegeneration induces cerebellar ataxia. *J. Clin. Invest.* 113, 582–590. doi: 10.1172/JCI20216

Shakkottai, V. G., do Carmo Costa, M., Dell'Orco, J. M., Sankaranarayanan, A., Wulff, H., and Paulson, H. L. (2011). Early changes in cerebellar physiology accompany motor dysfunction in the polyglutamine disease spinocerebellar ataxia type 3. *J. Neurosci.* 31, 13002–13014. doi: 10.1523/JNEUROSCI.2789-11.2011

Shashi, V., Magiera, M. M., Klein, D., Zaki, M., Schoch, K., Rudnik-Schoneborn, S., et al. (2018). Loss of tubulin deglutamylase CCP1 causes infantile-onset neurodegeneration. *EMBO J.* 37:e100540. doi: 10.15252/embj.2018100540

Sheffer, R., Gur, M., Brooks, R., Salah, S., Daana, M., Fraenkel, N., et al. (2019). Biallelic variants in AGTPBP1, involved in tubulin deglutamylation, are associated with cerebellar degeneration and motor neuropathy. *Eur. J. Hum. Genet.* 27, 1419–1426. doi: 10.1038/s41431-019-0400-y

Stoyas, C. A., Bushart, D. D., Switonski, P. M., Ward, J. M., Alaghatta, A., Tang, M. B., et al. (2020). Nicotinamide pathway-dependent sirt1 activation restores calcium homeostasis to achieve neuroprotection in spinocerebellar ataxia type 7. *Neuron* 105, 630–644.e9. doi: 10.1016/j.neuron.2019.11.019

Sugawara, T., Hisatsune, C., Le, T. D., Hashikawa, T., Hirono, M., Hattori, M., et al. (2013). Type 1 inositol trisphosphate receptor regulates cerebellar circuits by maintaining the spine morphology of purkinje cells in adult mice. *J. Neurosci.* 33, 12186–12196. doi: 10.1523/JNEUROSCI.0545-13.2013

Szatanik, M., Vibert, N., Vassias, I., Guenet, J. L., Eugene, D., de Waele, C., et al. (2008). Behavioral effects of a deletion in Kcnn2, the gene encoding the SK2 subunit of small-conductance Ca^{2+} -activated K + channels. *Neurogenetics* 9, 237–248. doi: 10.1007/s10048-008-0136-2

Todorov, B., Kros, L., Shyti, R., Plak, P., Haasdijk, E. D., Raike, R. S., et al. (2012). Purkinje cell-specific ablation of Cav2.1 channels is sufficient to cause cerebellar ataxia in mice. *Cerebellum* 11, 246–258. doi: 10.1007/s12311-011-0302-1

van de Leemput, J., Chandran, J., Knight, M. A., Holtzclaw, L. A., Scholz, S., Cookson, M. R., et al. (2007). Deletion at ITPR1 underlies ataxia in mice and spinocerebellar ataxia 15 in humans. *PLoS Genet.* 3:e108. doi: 10.1371/journal.pgen.0030108

Waters, M. F., Minassian, N. A., Stevanin, G., Figueroa, K. P., Bannister, J. P., Nolte, D., et al. (2006). Papazian and S. M. Pulst. Mutations in voltage-gated potassium channel KCNC3 cause degenerative and developmental central nervous system phenotypes. *Nat. Genet.* 38, 447–451. doi: 10.1038/ng1758

Zhuchenko, O., Bailey, J., Bonnen, P., Ashizawa, T., Stockton, D. W., Amos, C., et al. (1997). Autosomal dominant cerebellar ataxia (SCA6) associated with small polyglutamine expansions in the alpha 1A-voltage-dependent calcium channel. *Nat. Genet.* 15, 62–69. doi: 10.1038/ng0197-62

Conflict of Interest: The authors declare that the research was conducted in the absence of any commercial or financial relationships that could be construed as a potential conflict of interest.

Publisher's Note: All claims expressed in this article are solely those of the authors and do not necessarily represent those of their affiliated organizations, or those of the publisher, the editors and the reviewers. Any product that may be evaluated in this article, or claim that may be made by its manufacturer, is not guaranteed or endorsed by the publisher.

frontiers | Frontiers in Systems Neuroscience

ORIGINAL RESEARCH
published: 16 June 2022
doi: 10.3389/fnsys.2022.919761

Cerebellum Involvement in Dystonia During Associative Motor Learning: Insights From a Data-Driven Spiking Network Model

*Alice Geminiani[1], Aurimas Mockevičius[1], Egidio D'Angelo[1,2] and Claudia Casellato[1]**

[1] Department of Brain and Behavioral Sciences, University of Pavia, Pavia, Italy, [2] Brain Connectivity Center, IRCCS Mondino Foundation, Pavia, Italy

Dystonia is a movement disorder characterized by sustained or intermittent muscle contractions causing abnormal, often repetitive movements, postures, or both. Although dystonia is traditionally associated with basal ganglia dysfunction, recent evidence has been pointing to a role of the cerebellum, a brain area involved in motor control and learning. Cerebellar abnormalities have been correlated with dystonia but their potential causative role remains elusive. Here, we simulated the cerebellar input-output relationship with high-resolution computational modeling. We used a data-driven cerebellar Spiking Neural Network and simulated a cerebellum-driven associative learning task, Eye-Blink Classical Conditioning (EBCC), which is characteristically altered in relation to cerebellar lesions in several pathologies. In control simulations, input stimuli entrained characteristic network dynamics and induced synaptic plasticity along task repetitions, causing a progressive spike suppression in Purkinje cells with consequent facilitation of deep cerebellar nuclei cells. These neuronal processes caused a progressive acquisition of eyelid Conditioned Responses (CRs). Then, we modified structural or functional local neural features in the network reproducing alterations reported in dystonic mice. Either reduced olivocerebellar input or aberrant Purkinje cell burst-firing resulted in abnormal learning curves imitating the dysfunctional EBCC motor responses (in terms of CR amount and timing) of dystonic mice. These behavioral deficits might be due to altered temporal processing of sensorimotor information and uncoordinated control of muscle contractions. Conversely, an imbalance of excitatory and inhibitory synaptic densities on Purkinje cells did not reflect into significant EBCC deficit. The present work suggests that only certain types of alterations, including reduced olivocerebellar input and aberrant PC burst-firing, are compatible with the EBCC changes observed in dystonia, indicating that some cerebellar lesions can have a causative role in the pathogenesis of symptoms.

Keywords: cerebellum, dystonia, learning, motor dysfunction, modeling, spiking neural networks, simulations

OPEN ACCESS

Edited by:
Paul J. Mathews, Lundquist Institute for Biomedical Innovation, United States

Reviewed by:
Gen Ohtsuki, Kyoto University, Japan
Varun B. Chokshi, Johns Hopkins University, United States

****Correspondence:***
Claudia Casellato
claudia.casellato@unipv.it

Received: *13 April 2022*
Accepted: *24 May 2022*
Published: *16 June 2022*

Citation:
Geminiani A, Mockevičius A, D'Angelo E and Casellato C (2022) Cerebellum Involvement in Dystonia During Associative Motor Learning: Insights From a Data-Driven Spiking Network Model. Front. Syst. Neurosci. 16:919761. doi: 10.3389/fnsys.2022.919761

INTRODUCTION

In the sensorimotor system, the cerebellum plays a key role in motor learning and control (Ito, 2000). Thanks to synaptic plasticity at multiple connection sites (Hansel et al., 2001), the cerebellar output adapts and fine-tunes the amplitude and timing of motor responses in changing and perturbed environments (Marr, 1969; Albus, 1971). A typical cerebellum-driven protocol is Eye-Blink Classical Conditioning (EBCC), where a neutral stimulus, e.g., a sound, is provided (Conditioned Stimulus – CS), followed by a time-locked aversive stimulus, e.g., an air puff on the eye (Unconditioned Stimulus – US), causing a motor response – eye closure. After repeated paired presentations of these stimuli, the cerebellum drives the anticipation of the motor response before the US onset (Conditioned Response – CR; Freeman and Steinmetz, 2011). EBCC is widely used to investigate the neural correlates of cerebellum-driven behavior and also as a clinical biomarker of diseases involving the cerebellar circuit (Steinmetz et al., 2001). For example, EBCC is impaired in spinocerebellar ataxia, but also in pathologies not thought to involve cerebellar regions. Patients with Alzheimer's Disease or neurodevelopmental disorders show impaired EBCC learning, suggesting instead that cerebellar alterations may play a role in these pathologies (Woodruff-Pak et al., 1996; Reeb-Sutherland and Fox, 2015). For other brain diseases, the involvement of the cerebellum is still debated. This is the case of dystonia, a neurological motor disorder characterized by sustained or intermittent muscle contractions that generate repetitive movements, abnormal fixed postures, or both (Albanese et al., 2013). Dystonic movements are typically patterned, twisting, or tremulous, and are often initiated or worsened by voluntary action. It is estimated that dystonia is the third most common movement disorder after Parkinson's disease and essential tremor (Defazio, 2010), and it can have a significant negative impact on the general functioning and quality of life (Camfield et al., 2002). Understanding the pathological neural mechanisms that underlie dystonia is essential to design precise treatment strategies.

Dystonia and the Cerebellum

Although typically associated with dysfunctional basal ganglia (Tarsy and Simon, 2009), dystonia is now commonly regarded as a network disorder (Neychev et al., 2011), involving multiple brain areas and their connections. One of them is the cerebellum (Shakkottai et al., 2016), which is a fundamental part of the motor control system (Marr, 1969; Albus, 1971). In humans, imaging studies have shown cerebellar abnormalities in dystonic patients, and impairments in EBCC learning curves have been reported (Teo et al., 2009; Bologna and Berardelli, 2017). EBCC alterations in dystonia are debated and may not be discriminant of dystonia itself, but might be specific to some dystonia types (Sadnicka et al., 2022).

In rodents, pharmacological and genetic manipulations altering the cerebellum can result in dystonic movements (Isaksen et al., 2017). Damages to signal transmission from the inferior olive to Purkinje cells cause severe motor impairment, and multiple features of dystonia were observed in mouse models where olivocerebellar transmission was silenced (White and Sillitoe, 2017). In other rodent models of dystonia, aberrant firing patterns or synaptic alterations of Purkinje cells have been reported (Fremont et al., 2015; Vanni et al., 2015).

At present, a multi-regional motor network model for dystonia has been proposed stating that dystonia can arise from disruptions in multiple different brain regions, including the basal ganglia, the cerebellum and the motor cortex along with their connections (Prudente et al., 2014; Schirinzi et al., 2018). Cerebellar alterations may play a distinctive role in the generation of dystonic movements or could induce aberrant activity in the basal ganglia through subcortical connections. Otherwise, cerebellar changes in dystonia may represent a compensation to dysfunctions in other areas. Therefore, the exact role of cerebellar alterations still remains to be elucidated.

Computational Models of the Cerebellum

Computational models embedding realistic neuronal network properties and reproducing motor functions provide a new tool to investigate the neural mechanisms of behaviors in physiological and pathological conditions. Plastic cerebellar spiking models embedded in closed-loop control systems can simulate cerebellum-driven sensorimotor tasks by using the underlying neurophysiological mechanisms (Yamazaki and Tanaka, 2007; Antonietti et al., 2016; Geminiani et al., 2019b). Specific lesions can be applied to these data-driven Spiking Neural Networks (SNNs) to investigate the causal relationships between neural alterations and the disease symptoms. For example, simulations predicted that alterations of synaptic plasticity in the cerebellar cortex could impair EBCC in different forms of cerebellar ataxia and that synaptic plasticity in the deep cerebellar nuclei was a possible compensatory mechanism (Geminiani et al., 2018a). Moreover, in autism spectrum disorder, simulations suggested that a higher CR learning rate could reflect a reduced number of Purkinje cells (Trimarco et al., 2021).

Here, we applied this approach to investigate the involvement of the cerebellum in dystonia through simulations of EBCC driven by a bioinspired SNN model of the cerebellum. The aim is to understand how specific cerebellar alterations impact EBCC in controlling stimuli association and timing (Teo et al., 2009). Three types of alterations observed in rodent models of dystonia were modeled: (i) reduced olivocerebellar connectivity (Ledoux and Lorden, 2002; White and Sillitoe, 2017), (ii) aberrant Purkinje cell firing (burst-firing; Ledoux and Lorden, 2002; Hisatsune et al., 2013), (iii) imbalanced synapse density on Purkinje cells (Vanni et al., 2015).

MATERIALS AND METHODS

Olivocerebellar Spiking Neural Network

The cerebellar model was a Spiking Neural Network (SNN) including the cerebellar cortex, the deep cerebellar nuclei (DCN) and the inferior olive (IO), forming a cerebellar microcomplex. It reproduces a microcomplex with Zebrine-negative Purkinje cells (characterized by a higher intrinsic excitability), which

is considered the primary mechanism responsible for EBCC learning (Wu et al., 2019).

The network architecture was built through a data-driven reconstruction process using the Brain Scaffold Builder (BSB; RRID:SCR_008394, version 3.8+). Neurons were placed in the defined volume and connected based on spatial information (cell densities, oriented morphologies and synapse densities; de Schepper et al., 2021). In the resulting SNN, at the input stage, mossy fibers (*mfs*) excite Granule Cells (GrCs) and Golgi cells (GoCs); GrCs provide excitatory input to GoCs and to Purkinje cells (PCs) through ascending axons (*aas*) and parallel fibers (*pfs*), and excitatory input to Molecular Layer Interneurons (MLIs) through *pfs*. MLIs in turn inhibit PCs. DCN contains two neural populations, (i) GAD-negative large cells (DCN), which are large glutamatergic neurons projecting outside the cerebellum, and (ii) DCN-GABA, which are GABAergic neurons forming the olivo-cerebellar loop. The output of the cerebellum, DCN neurons, receives direct excitation from *mfs* and inhibition from PCs. IO neurons trigger burst-pause responses in PCs through excitatory climbing fibers (*cfs*) which also excite DCN and DCN-GABA (**Figure 1**). Neurons were modeled as Extended-Generalized Leaky Integrate and Fire point neurons (E-GLIF) with parameters optimized as in Geminiani et al. (2018b, 2019a). Neural connections were modeled as conductance-based synapses, with delays extracted from literature and weights tuned to reproduce physiological firing rates in mice at rest (Geminiani et al., 2019b). Connections between *pfs* and PCs were plastic, according to an *ad hoc* Spike Timing Dependent Plasticity rule, driven by the IO teaching signal (Casellato et al., 2014; Luque et al., 2016): concurrent spikes at *pfs* and IOs caused Long-Term Depression (LTD) at the corresponding *pf*-PC synapses, while *pfs* spikes alone caused Long-Term Potentiation (LTP), consistently with experimental observations (Sakurai, 1987; Coesmans et al., 2004).

Simulations were run in NEST (version 2.18), a software simulator for spiking neural networks (Gewaltig and Diesmann, 2007; Eppler et al., 2009; Jordan et al., 2019; RRID:SCR_002963). All simulations were carried out on a PC provided with Intel® Core™ i7-8750H CPU @ 2.20GHz with 16.0 GB RAM in the Operating System Ubuntu 20.04.2 LTS.

EyeBlink Classical Conditioning Protocol

To simulate EBCC, the cerebellar SNN was embedded in a closed-loop control system, with learning intrinsically driven by synaptic plasticity (Antonietti et al., 2016). The sensory and motor signals were encoded in the corresponding cerebellar neural populations according to experimental evidence. *Mfs* conveyed the CS, which was simulated as a non-recurrent 40-Hz spike train delivered to each individual *mf*, lasting 280 ms. The pattern was chosen to generate GrC low-frequency sparse coding which is supposed to be fundamental for cerebellar learning (Schweighofer et al., 2001). The US was delivered to IOs as a 500-Hz burst lasting 30 ms and co-terminating with the CS.

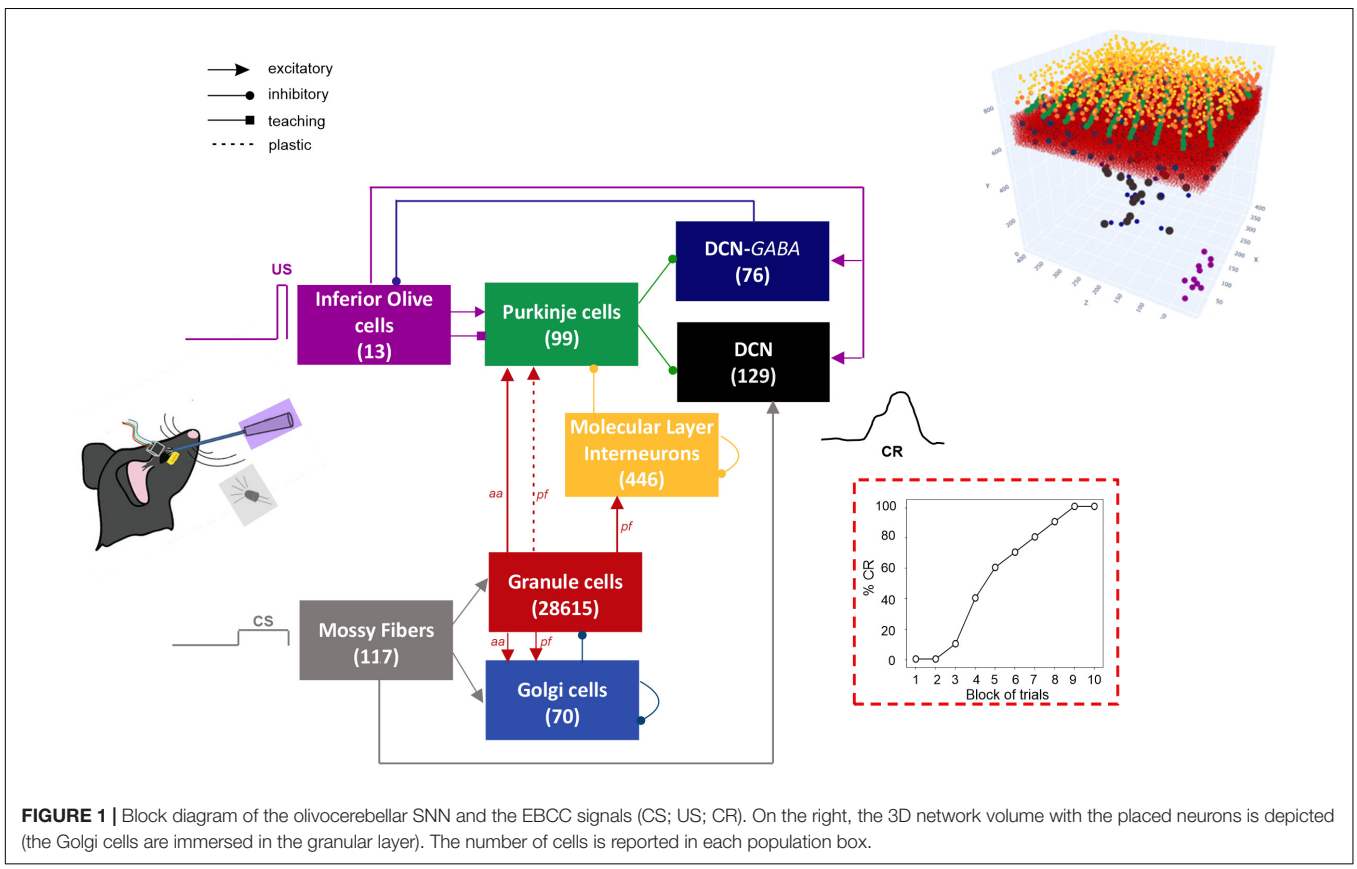

FIGURE 1 | Block diagram of the olivocerebellar SNN and the EBCC signals (CS; US; CR). On the right, the 3D network volume with the placed neurons is depicted (the Golgi cells are immersed in the granular layer). The number of cells is reported in each population box.

The eyelid closure signal was decoded from DCN spikes (see paragraph below *Data Analysis*).

The protocol included 100 trials (10 blocks of 10 trials each) in a row, with 280 ms of stimulation and a 720-ms pause of baseline activity (total trial duration of 1000 ms).

Simulations of Cerebellar Alterations in Dystonia

Three specific localized lesions were applied to the control model.

(i) Reduced olivocerebellar input. Studies in mutant dystonic (dt) rats suggest that reduced IO signaling could be related to dystonia (Stratton and Lorden, 1991; Ledoux and Lorden, 2002). Specifically, decreased PC complex spike firing was observed from single cell recordings (Ledoux and Lorden, 2002), which would result from reduced IO activity. In a more recent study, White and Sillitoe devised a mouse model with genetic silencing of IO, causing the elimination of PC complex spikes as well as severe dystonia (White and Sillitoe, 2017). Complete silencing of IO input would be expected to abolish EBCC acquisition (Zbarska et al., 2007), as it is crucial for the US circuitry and for *pf*-PC plasticity. This type of alteration was modeled in our cerebellar SNN by re-tuning two factors at the same time, (a) by disconnecting the IO teaching signal from a subset of PCs, (b) by reducing the strength in all the synapses between IOs and PCs. Three levels of damage were simulated: 25, 50, and 75% reduction on both factors.

(ii) Aberrant burst-firing pattern of PCs. It has been observed in a number of dystonic rodent models (Ledoux and Lorden, 2002; Hisatsune et al., 2013; Fremont et al., 2015; Washburn et al., 2019). Specifically, PC simple spike burst-firing was reported in dt rats (Ledoux and Lorden, 2002) and PC burst-firing with excessive and repetitive complex spike firing was observed in cerebellum-specific IP3R1 knock-out dystonic mice, which also exhibited increased IO activity (Hisatsune et al., 2013). Both types of burst-firing alterations were modeled in our cerebellar SNN. In one case (intrinsic burst-firing), PC burst-firing was obtained by directly stimulating PCs with intermittent 20-ms spike trains with random 20 or 30 ms pauses, as in experiments, and by reducing PC intrinsic firing. In the other case (IO-induced burst-firing), intermittent stimulation was provided to all IO neurons using 40-ms spike trains with 40 ms pauses, causing increased IO activity and inducing PC bursting as reported in IP3R1 knock-out mouse model of dystonia.

(iii) Imbalanced PC synaptic densities (from MLIs, *pf*s and IOs). It was reported in a mouse model of early-onset isolated dystonia, DYT1 (Vanni et al., 2015). This type of alteration was modeled in our cerebellar SNN by reducing the synapse density between *pf*-PC and MLI-PC, and increasing the synapse density between IO-PC, with proportions as in the experimental study. Two levels of impairment were explored (mild and severe): (a) %14 decrease in *pf*-PC, %39 decrease in MLI-PC,%32 increase in IO-PC, (b) %25 decrease in pf-PC, %71 decrease in MLI-PC, %57 increase in IO-PC. When computing the ratio between the number of excitatory and inhibitory synapses onto PCs (structural E/I balance), these mild and severe alterations corresponded to an increase from 62.3 in the control condition to 88.6 and 110.9, respectively.

Data Analysis

The activity of PCs and DCN was monitored along task repetitions, as these two neuronal populations underwent firing changes driven by *pf*-PC plasticity. To assess intrinsic firing properties (firing rate and irregularity, respectively), we computed the number of spikes and the Coefficient of Variation of the Inter-Spike Intervals (CV_{ISI}) in the baseline time window of the first trial, i.e., from the end of CS to the end of trial (from 280 to 1000 ms). To assess firing modulation, we computed the Spike Density Function (SDF) as the convolution of each cell's spikes in every trial, with a Gaussian kernel of 20 and 10 ms for PCs and DCN, respectively (Dayan and Abbott, 2001). SDFs of the two populations were then computed by averaging SDFs of individual cells. We evaluated the population SDF in the CR time window, i.e., between 100 ms from the CS onset to the co-termination of CS and US (i.e., 280 ms from CS onset). Furthermore, to quantify learning in terms of neural activity, an index of *SDF change* was computed as the time-integral of SDF in the CR time window of the last block (averaged across the last 10 trials) subtracting the average activity in the first 100 ms after the CS onset. This quantifies the time-locked rate change, i.e., the modulation in the inter-stimuli-interval within each trial.

The motor output response (eyelid closure) was derived by applying a moving average filter with a 100-ms time window to SDF of the DCN population, obtaining a *filtered SDF*. A CR was detected when this motor output signal reached a fixed threshold of 4 Hz in the CR time window and remained above the threshold. The CR time window did not include the first 100 ms from the CS onset because non-EBCC related responses are supposed to occur there, according to experimental evidence (ten Brinke et al., 2015). The CR threshold was set at 4 Hz to have 70% of CRs in the 6th block of learning, as in EBCC experiments on control mice (de Oude et al., 2021).

We computed %CR in each block of 10 trials, and the timing of the CR onset (advance with respect to the US onset). The CR onset was defined as the time instant when the motor output began monotonically rising.

For SDF change, baseline firing rate and CV_{ISI} distributions, outliers were excluded as the values falling outside the interval between Q1 – 1.5 * IQR and Q3 + 1.5 * IQR, where Q1 is the 1st quartile, Q3 is the 3rd quartile, IQR is the Inter-Quartile Range.

The Wilcoxon statistical test was applied to compare CR onset, SDF change, baseline firing rate and CV_{ISI} values between simulations of control and pathological conditions, with statistical significance at $p < 0.01$. The McNemar's test with $p < 0.01$ was applied to %CR.

RESULTS

Simulation of Physiological Conditions

In physiological conditions, the model was able to reproduce the EBCC learning curve obtained in mice experiments (de Oude et al., 2021). In the first trial, PC spike pattern at the CS onset

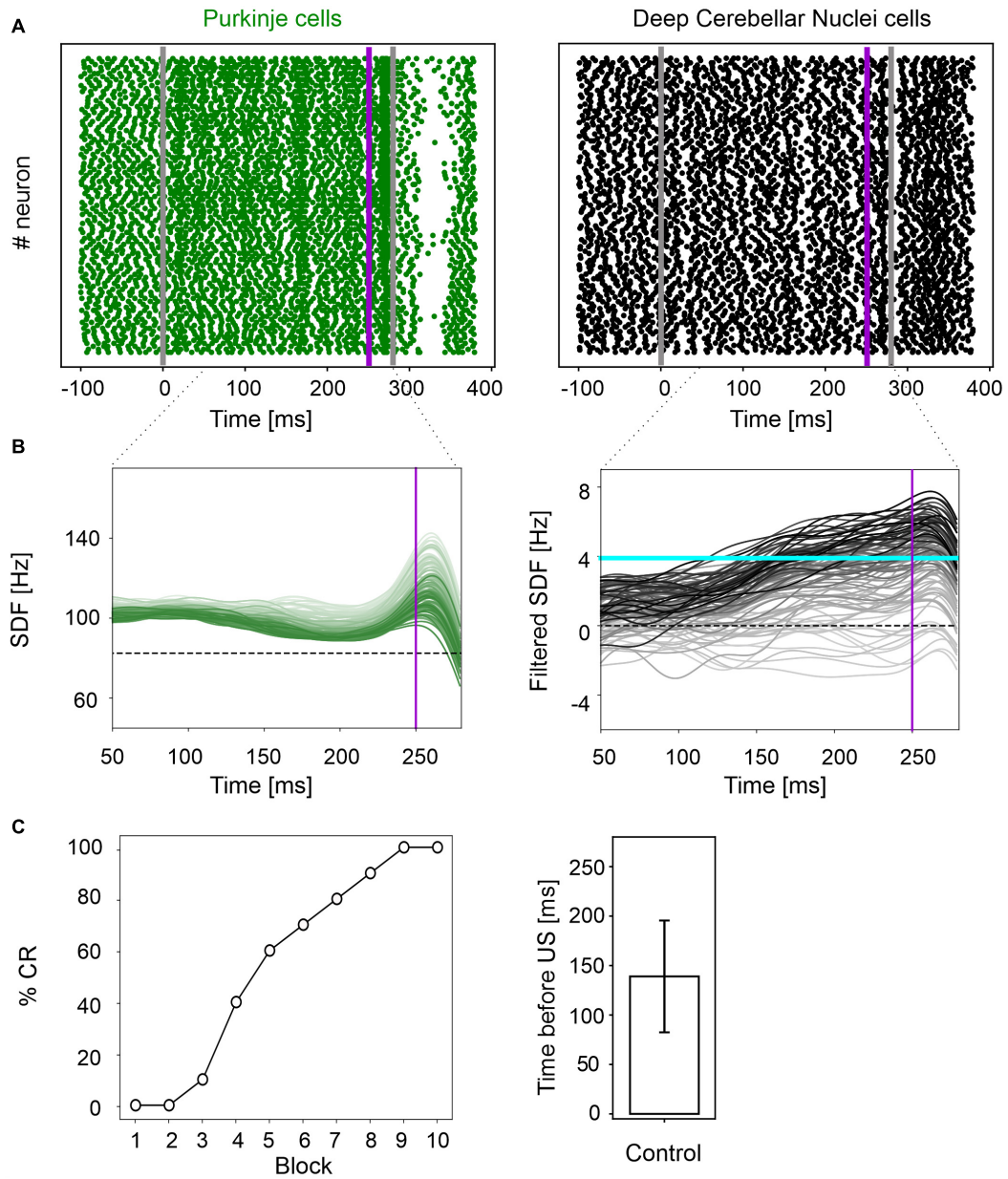

FIGURE 2 | EBCC simulations in the control condition. **(A)** Exemplificative raster plots showing spiking activity of each cell (y axis) within PC (green) and DCN (black) populations in the first trial. Gray vertical lines represent the CS onset and end, purple line marks the US onset (which co-terminates with CS). **(B)** SDF in PC population and DCN motor output (averaging across cell SDFs) for each trial (0 ms is aligned with the CS onset). Increasing darkness of the lines corresponds to subsequent trials (the lightest is the first trial, the darkest is the last trial). Dashed horizontal line indicates baseline activity, solid horizontal cyan line (right panels) represents the CR threshold. Purple vertical line corresponds to US onset time. **(C)** Behavioral EBCC outcome: %CR along trial blocks (left panel), and CR timing with respect to US onset (right panel). Error bar indicates the standard deviation.

increased from basal discharge and remained constant during the entire inter-stimuli interval; then, during the US, a burst was generated, followed by a pause. PC pause released DCN neurons, which fired strongly, generating a blink after the US (**Figure 2A** and **Supplementary Figure 1**). Thanks to *pf*-PC LTD in the time window before the US, PC firing rate decreased throughout trials due to a progressive accentuation of the spike suppression (**Figure 2B** left, and **Supplementary Figure 1**). This caused a gradual release of DCN firing (i.e., DCN facilitation; **Figure 2B** right, and **Supplementary Figure 1**). Along the learning process, PC suppression became more and more evident. In the last trial, most of PCs (39 out of 99) underwent a significant suppression in the second half of the CR time window, while a few PCs (14 out of 99), due to LTP and intrinsic neuronal mechanisms, moved to an upstate at the beginning of the CR time window (**Supplementary Figure 2**).

Consequently, along the learning process, DCN facilitation yielded a progressive increase of the cerebellar motor output, triggering eye closures before the US onset (**Figure 2C** left). The resulting %CR curve matched the values obtained in experimental studies, reaching 70% in the 6th block of learning, and 100% in the 9th block. Also, the response timing was in the physiological range, with a CR onset of 139 ± 57 ms before the US (**Figure 2C** right).

Simulation of Reduced Olivocerebellar Input

A reduced IO input to PCs caused insufficient modulation of PC and DCN activity, as well as a slower and reduced %CR learning curve. By further increasing the amount of damage, the behavioral dysfunction became more severe.

In all three tested damage levels, baseline properties of PCs and DCN were not altered, indicating a normal intrinsic neuron firing: firing rate and irregularity were not significantly different with respect to the control simulations (**Supplementary Figure 3**). With 25% decrease in IO-PC signaling, PC spike suppression was slightly less pronounced, resulting in a reduced DCN facilitation (**Figure 3A**). Overall, the SDF changes were comparable to control simulations (**Figure 3D**). Consequently, the model was still able to produce CRs, even if the acquisition was slower and more unstable than in the control network, with the maximum %CR reaching 70% (**Figure 4A**). As expected, compromising half of the IO-PC signaling amplified the effects (**Figure 3B**): PC and DCN SDF changes were significantly smaller than in control simulations (**Figure 3D**) and the motor output rarely reached the CR threshold. Consequently, CR acquisition was compromised, reaching a maximum of 40% (**Figure 4A**). With the highest level of damage, the activity of PC and DCN populations remained constant throughout the whole EBCC training protocol (**Figure 3C**). PC SDF change, on average, was close to 0, while mean DCN SDF change was even negative (**Figure 3D**). The motor output never reached the CR threshold before US onset, thus, no CRs were produced throughout the entire task (**Figure 4A**).

CR curves were significantly lower than in controls in all three levels of damage (total number of CRs in control = 56; in 25% damage = 30; in 50% damage = 17; in 75% damage = 0; McNemar's $p < 0.01$ in all damage cases vs. control). Regression analysis proved a significant linear relationship between the damage level and the number of CRs ($R^2 = 0.98$ and $p = 0.01$). CR onset was delayed but the difference did not reach statistical significance (in control = 139 ± 57 ms; in 25% damage = 126 ± 69 ms; in 50% damage = 101 ± 62 ms; in 75% damage: N/A. $p > 0.01$ in all damage cases vs. control; **Figure 4B**).

Simulation of Aberrant Burst-Firing Pattern of PCs

The applied modifications to the cerebellar SNN transformed PC simple spike activity into burst-firing (**Supplementary Figure 4**). In the simulations with intrinsic PC burst-firing, PC activity was characterized by short intervals of increased spiking activity, separated by pauses. This led to a significant increase in mean PC CV_{ISI} when compared to the control condition (**Supplementary Figure 5**). Moreover, due to the altered PC firing, DCN also exhibited a corresponding burst-firing pattern and increased irregularity (**Supplementary Figure 5**). Baseline firing rates were statistically different from the control condition, but still in the physiological ranges for the activity of PCs and DCN of EBCC-related cerebellar modules (de Zeeuw and Ten Brinke, 2015; Beekhof et al., 2021).

The population firing of PCs and the DCN motor output showed irregular oscillations (**Figure 5A**). PCs and DCN were more variable in the impaired than in the control model, but the difference was not statistically significant (**Figure 5C**). The motor output in some trials exceeded threshold already in the first 100 ms, i.e., before the plausible time window for CRs. This improperly timed response was not considered as CR. Consequently, CR acquisition was impaired (**Figure 5D**), as the proportion of trials with detected CR was significantly different between control and impaired conditions (control: 56; impaired: 26, McNemar's $p < 0.01$). The maximum %CR was 60% in the 8th block. When generated, the CRs were significantly delayed (control: 139 ± 57 ms, impaired: 113 ± 33 ms, before US onset; $p < 0.01$).

In the simulations with IO-induced PC burst-firing, excessive olivocerebellar signaling resulted in PC burst-firing patterns: sharp increases in PC firing induced by IO input were present, which were followed by pauses (**Supplementary Figure 4**). This PC burst-firing contributed to abnormal burst-firing patterns of DCN, which showed pauses during increased PC activity as well as increased firing during PC pauses. Thus, the irregularity of PC and DCN neurons was significantly higher than in the healthy network; PC baseline activity was similar and DCN baseline was slightly different from the control condition (**Supplementary Figure 5**), but still in the physiological ranges reported for the activity of DCN in EBCC-related cerebellar modules (de Zeeuw and Ten Brinke, 2015; Beekhof et al., 2021).

PC and DCN firing patterns during trials were highly disorganized in the burst-firing intervals, with DCN also exhibiting increased firing rates with improper modulation (**Figure 5B**). PC and DCN SDF changes were more variable in the impaired model when compared to the control one, but not resulting in significant differences (**Figure 5C**). No CR acquisition was observed in this condition (**Figure 5D**).

Simulation of Imbalanced PC Synaptic Densities

A mild damage on PC synaptic densities was implemented with 14% reduction in *pf*-PC, 39% reduction in MLI-PC and 32% increase in IO-PC. The model produced comparable results as in the control condition (**Figure 6**). PC suppression and DCN facilitation were not significantly different from control simulations (**Figure 6C**). CR acquisition was intact (control: 56; impaired: 55, McNemar's $p = 0.66$). No significant differences were found in CR onset latencies (control: 139 ± 57 ms; impaired: 156 ± 57 ms, $p = 0.23$). PC and DCN intrinsic

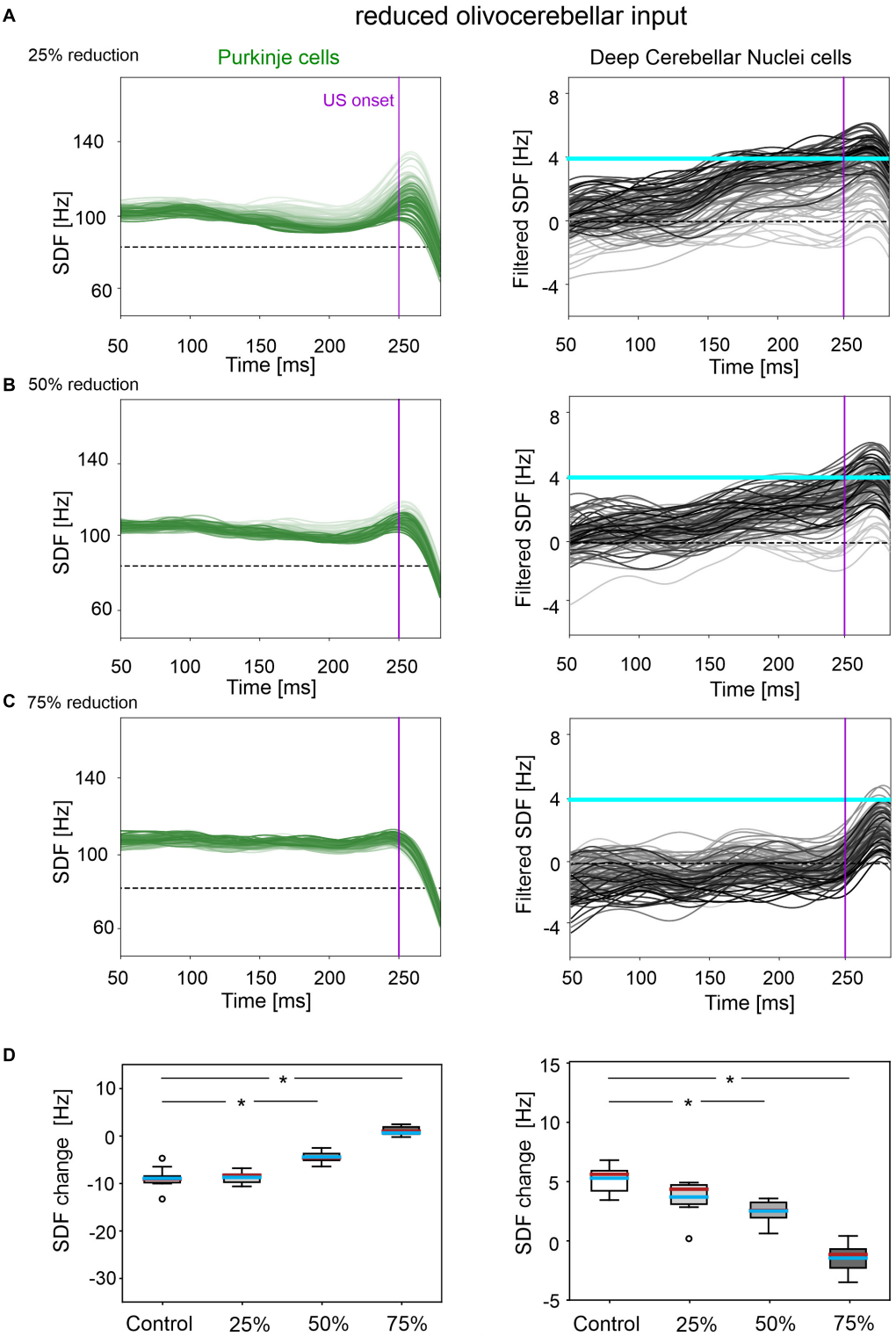

FIGURE 3 | Neural activity underlying EBCC in the case of reduced olivocerebellar input by 25% **(A)**, 50% **(B)**, 75% **(C)**. SDF in PC population and DCN motor output (averaging across cell SDFs) for each trial (0 ms is aligned with the CS onset). Increasing darkness of the lines corresponds to subsequent trials (the lightest is the first trial, the darkest is the last trial). Dashed horizontal line indicates baseline activity, solid horizontal cyan line (right panels) represents CR threshold. Purple vertical line corresponds to US onset time. **(D)** SDF change in PC (left) and DCN (right) populations from the 10 trials in the last block, with respect to SDF value in the first 100 ms from CS onset. Cyan horizontal line indicates the mean, red horizontal line the median, box edges the 1st and 3rd quartile, whiskers the minimum and maximum accepted values, excluding outliers (indicated as circles). * corresponds to $p < 0.01$ in the Wilcoxon test.

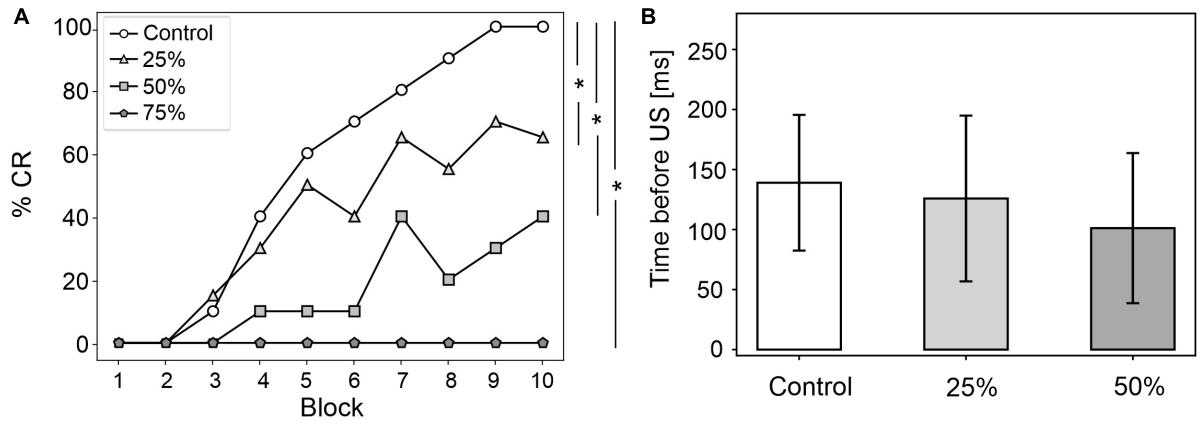

FIGURE 4 | EBCC behavior in the case of reduced olivocerebellar input (25%, 50 and 75%), compared to the control condition. **(A)** %CR along trial blocks. **(B)** CR timing with respect to US onset. Error bars indicate the standard deviation. Impaired condition with 75% IO-PC reduction is not represented in B) as no CRs were acquired during the simulation. * corresponds to $p < 0.01$ in the McNemar's test for %CR and the Wilcoxon test for the CR onset timing.

firing properties were similar between control and pathological simulations (**Supplementary Figure 6**).

Even imposing a more severe impairment on PC synaptic densities (25% reduction in *pf*-PC, 71% reduction in MLI-PC and 57% increase in IO-PC), baseline PC and DCN firing properties were unaltered (**Supplementary Figure 6**), and behavioral results were similar to the control condition were produced (**Figure 6D**).

DISCUSSION

In this work we used advanced SNN models to investigate whether different types of cerebellar lesions could modify EBCC in dystonia. The main observation is that specific cerebellar cortical lesions associated with dystonia, e.g., reduced olivocerebellar input and aberrant PC firing, can compromise EBCC learning. Conversely, other lesions, e.g., a change in the excitatory/inhibitory balance on PCs, were ineffective. These results support the concept that, although originally associated with basal ganglia dysfunction, dystonia might involve the cerebellum and can be regarded as a network disorder (Neychev et al., 2011; Shakkottai et al., 2016) affecting multiple brain areas and their connections. The fact that cerebellar microcircuit alterations demonstrated a causal role in some, but not in all cases, is akin to clinical reports showing inconstant EBCC changes in dystonia (Sadnicka et al., 2022) and suggests heterogeneity in the microscopic underpinnings of the disease.

Reduced Olivocerebellar Input

IO spikes are thought to convey motor error signals to the cerebellum and are also implicated in the control of motor response timing (Marr, 1969; Albus, 1971; Jacobson et al., 2008). Thus, a reduced olivocerebellar input to PCs probably leads to impaired motor learning and abnormal temporal processing of somatosensory inputs conveyed from cortical regions to the cerebellum (Latorre et al., 2020). Indeed, our cerebellar SNN model predicted a deficit in CR generation and a delayed CR timing in simulations with reduced IO-PC communication, and the deficit significantly linearly increased with damage severity.

Aberrant Burst-Firing Pattern in PCs

An altered PC burst-firing is known as a potential mechanism impairing cerebellar motor control and learning. The cerebellum is involved in the control of agonist and antagonist muscles, supposedly correlated with increase and decrease in DCN firing. From a physiological point of view, dystonia is characterized by abnormal co-contraction of agonist and antagonist muscles (Berardelli et al., 1998; Shakkottai, 2014). Therefore, an irregular PC and DCN activity caused by inappropriate burst-firing patterns might alter the timing of muscle contraction. We argue that, if normal PC tonic firing is transformed into abnormal burst-firing, certain muscles could be incorrectly facilitated due to DCN disinhibition, resulting in the simultaneous activation of agonist and antagonist muscles, causing dystonic movements. In EBCC, this might (at least partially) be reflected by the inappropriate timing of eyelid closure. This was indeed the case in simulations with our SNN model when PCs generated intrinsic burst-firing. The motor output crossed the threshold before the CR window and lost its proper shape consisting of alternating rising and decay phases. In other simulations, PC burst-firing was exaggerated by increasing the IO input. Again, this made DCN unstable, preventing the generation of proper and timed motor responses. In general, enhanced and unstable DCN activity could hinder the separation of signals to agonist and antagonist muscle, causing co-contractions and preventing efficient movement control with the consequent emergence of dystonic movements (Shakkottai, 2014).

Imbalanced PC Synaptic Densities

In our SNN simulations, a partial imbalance in PC afferents from MLIs, *pfs* and IOs did not markedly affect EBCC, predicting that neuronal changes reported in dystonic mice (Vanni et al., 2015) would not induce CR learning alterations. Indeed, baseline firing properties, neural modulation and EBCC motor output

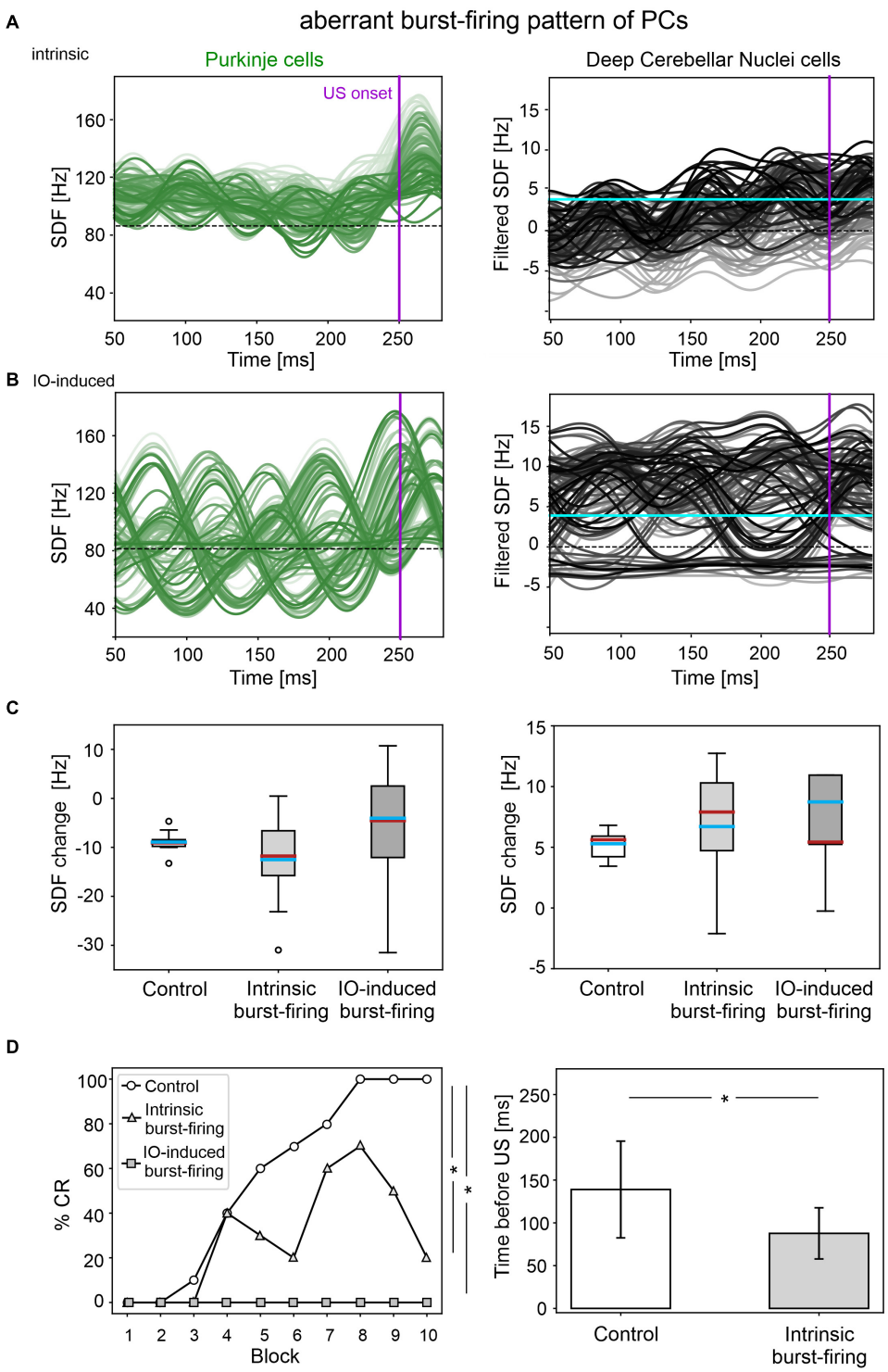

FIGURE 5 | EBCC simulations in the case of aberrant burst-firing pattern of PCs. SDF in PC population and DCN motor output (averaging across cell SDFs) for each trial (0 ms is aligned with the CS onset), with intrinsic PC burst-firing **(A)** and IO-induced PC burst-firing **(B)**. Increasing darkness of the lines corresponds subsequent trials (the lightest is the first trial, the darkest is the last trial). Dashed horizontal line indicates baseline activity, solid horizontal cyan line (right panels) represents CR threshold. Purple vertical line corresponds to US onset time. **(C)** SDF change in PC (left) and DCN (right) populations from the 10 trials in the last block, computed in the CR window with respect to SDF value in the first 100 ms from CS onset; * corresponds to $p < 0.01$ in the Wilcoxon test. **(D)** Behavioral EBCC outcome, i.e., %CR along trial blocks (left panel), and CR timing with respect to US onset (right panel), compared to the control condition. Error bars indicate the standard deviation. CR onset is not represented for the IO-induced PC burst-firing case, as no CRs were acquired during the simulation. * corresponds to $p < 0.01$ in the McNemar's test for %CR and the Wilcoxon test for the CR onset timing.

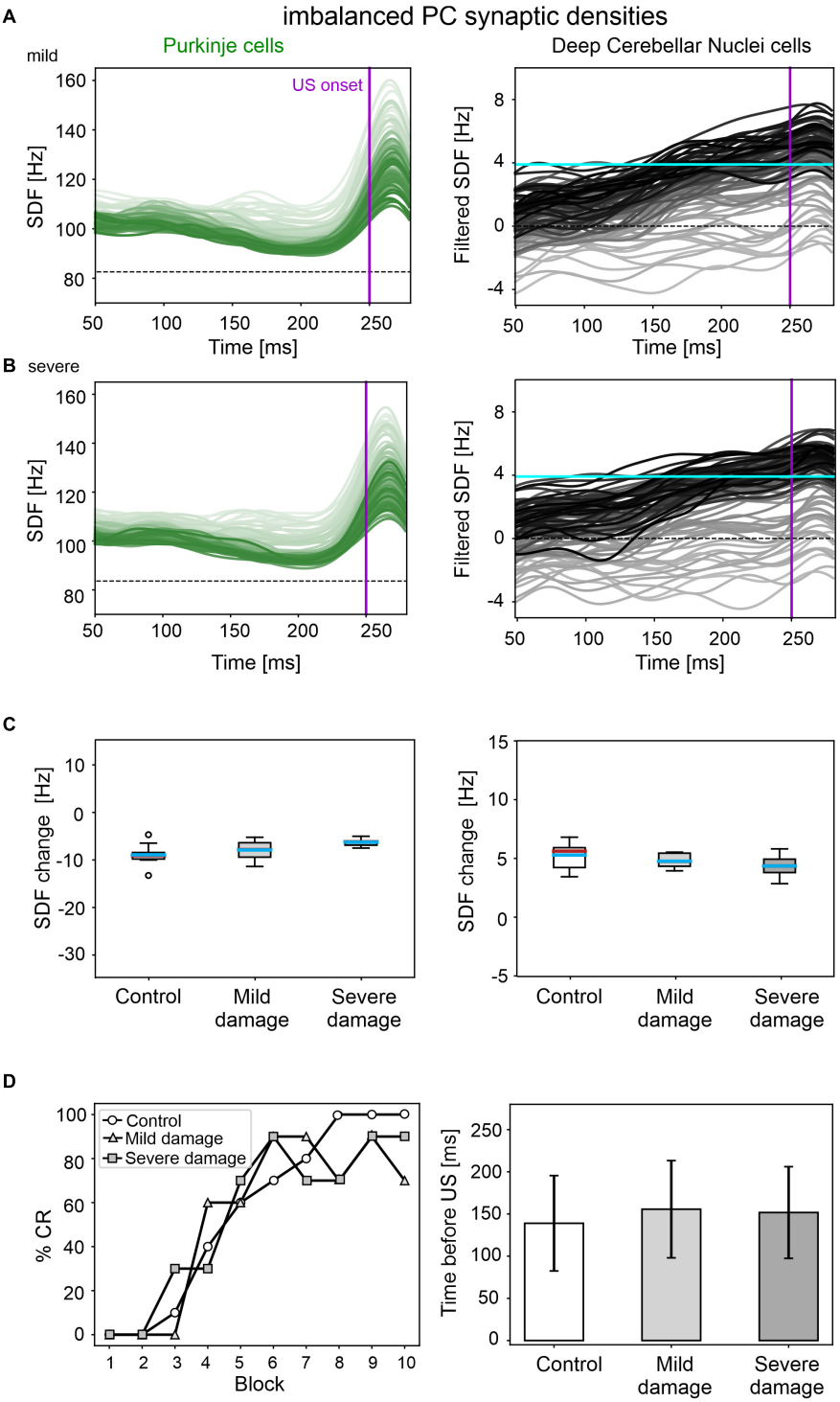

FIGURE 6 | EBCC simulations in the case of imbalanced PC synaptic densities. SDF in PC population and DCN motor output (averaging across cell SDFs) for each trial (0 ms is aligned with the CS onset), with mild **(A)** and severe damage **(B)**. Increasing darkness of the lines corresponds to subsequent trials (the lightest is the first trial, the darkest is the last trial). Dashed horizontal line indicates baseline activity, solid horizontal cyan line (right panels) represents CR threshold. Purple vertical line corresponds to US onset time. **(C)** SDF change in PC (left) and DCN (right) populations from the 10 trials in the last block, with respect to SDF value in the first 100 ms from CS onset. Cyan horizontal line indicates the mean, red horizontal line the median, box edges the 1st and 3rd quartile, whiskers the minimum and maximum accepted values, excluding outliers (indicated as circles). **(D)** Behavioral EBCC outcome, i.e., %CR along trial blocks (left panel), and CR timing with respect to US onset (right panel), compared to the control condition. Error bars indicate the standard deviation.

were similar between control and pathological simulations. We hypothesize that this type of low-level modification in the cerebellum is associated with some types of dystonia where no EBCC alterations have been observed (Sadnicka et al., 2015).

The unchanged EBCC outcomes may be explained by the fact that the increased E/I balance on PCs, induced by altering the number of excitatory and inhibitory synapses, was counterbalanced by a stronger *pf*-PC LTD due to a stronger teaching signal from IO. Therefore, even if more excitatory synapses were present with respect to the inhibitory ones, the potentiated excitatory effect was depressed along the learning process, producing a CR curve comparable to the control condition.

Impacts, Limitations and Future Work

Computational modeling provided us with a unique opportunity to evaluate the causal relationship between various microcircuit lesions (mostly identified in the experimental animals), network dysfunction, and emerging dystonic symptoms.

Nonetheless, spatial aspects of cerebellar lesions could not be considered, since our SNN model did not reproduce any specific cerebellar area but rather demonstrated a pathophysiological principle. Further work will be needed to differentiate the cerebellar regions according to detailed brain atlases and to address the impact of regional alterations. Indeed, Bologna and Berardelli suggested that a dysfunction of the whole cerebellum may cause abnormal movements and postures in many body parts, thus resembling generalized dystonia (Bologna and Berardelli, 2017), while topographically localized alterations of the cerebellum could be related to one affected body area in focal dystonia. Supporting this hypothesis, Raike and colleagues showed that limited regional damage to the cerebellum in mice induced focal dystonia, while extensive cerebellar damage led to generalized dystonia (Raike et al., 2013). In the present work, the cerebellar SNN model was used to simulate EBCC. Thus, it could correspond to cerebellar areas involved in eye movement control, e.g., the vermis of lobules V-VI (Cheng et al., 2014; Diedrighsen and Bastian, 2014). Impaired cerebellar function in the regions related to eye movement control could be associated with blepharospasm, a type of focal dystonia affecting eyelid movements. Indeed, structural (Ramdhani et al., 2014) and functional (Hutchinson et al., 2000; Kerrison et al., 2003) imaging studies report cerebellar changes in patients with blepharospasm. Eyelid CR acquisition during EBCC would be expected to be heavily compromised due to involuntary eyelid spasms. This is predicted in our simulations with IO-induced PC burst-firing, which produced unmodulated output and no CR acquisition. Accordingly, Valls-Sole and Defazio argue that no reports of EBCC are available in patients with blepharospasm since an abnormal eyeblink would interfere with EBCC training (Valls-Sole and Defazio, 2016). Conversely, in the types of dystonia affecting other body parts, functionalities of the cerebellar areas involved in eyelid movement control might be unaffected, resulting in normal EBCC acquisition. For example, DYT1 dystonia is characterized by an onset in one limb with task-specific dystonia at first, which later becomes less task-specific and progresses to other areas, becoming multifocal or generalized (Ozelius and Lubarr, 2016); however, the spread of dystonic symptoms to craniocervical muscles is rare, which could explain why EBCC is unimpaired in DYT1 patients (Sadnicka et al., 2015). In summary, the region-function mapping could be tested by using full-scale cerebellar model, applying region-specific lesions, and investigating the involvement of different cerebellar lobules in the various forms of dystonia.

We argue that a better understanding of the cerebellar role in dystonic motor networks would be fundamental to devise effective treatment strategies. In some studies, cerebellar transcranial magnetic stimulation (TMS) has shown positive effects on dystonic symptoms (Koch et al., 2014; Bradnam et al., 2015). However, as Miterko and colleagues argue, it is not clear when the cerebellum should be considered as a treatment target in dystonia (Miterko et al., 2019). For instance, TMS over the cerebellum would be a less invasive alternative to, for example, the deep brain stimulation (DBS) of the globus pallidus (Wichmann and DeLong, 2011). Again, the focality of TMS and the design of the applied pattern may play a crucial role that remains to be addressed.

Regardless of whether cerebellar abnormalities are primary or secondary to the compensation of neurodegeneration processes, the different types of cerebellar impairment during associative learning might help to distinguish dystonia forms. More extensive experiments, combined with the simulations described here (**Table 1**), could allow to define a more robust link between EBCC and different types of dystonia. Thus, EBCC could be used as a clinical non-invasive marker, as shown for other pathologies. For example, it was shown that EBCC outcomes could differentiate between Alzheimer's Disease and cerebrovascular dementia (Woodruff-Pak et al., 1996).

A limitation of this study is that plasticity was modeled only at *pf*-PC synapses. However, plasticity at *pf*-MLI, PC-DCN and *mf*-DCN connections is also implicated in EBCC learning (Ohyama et al., 2006; Boele et al., 2018). Thus, a multiple-plasticity network could provide a more comprehensive view into EBCC learning abnormalities due to cerebellar dysfunctions associated with dystonia. For example, reductions in MLI-PC connections as in Vanni et al. (2015) might result in more evident EBCC impairments than in our simulations if MLI synapses were plastic. A further test could be to model, during EBCC, both Z- and Z+ PCs, which have different intrinsic excitability and are likely to undergo either simple spike suppression or facilitation, respectively (de Zeeuw, 2021).

Moreover, the simplified point neurons used here could be replaced by multicompartmental morphology-based models (Masoli et al., 2015; Masoli and D'Angelo, 2017), in order to focus on PC subcellular structural and functional abnormalities (Llinás and Sugimori, 1980; Stuart and Häusser, 1994; Womack and Khodakhah, 2004; Ohtsuki et al., 2012), which are often quite subtle in dystonia. PCs showed shortened primary dendrites and decreased spines on the distal dendrites (Zhang et al., 2011). In addition, specific ionic channels can be responsible for dystonic dysfunctionalities. The irregular spiking of mutant

TABLE 1 | Summary table of experimental models of dystonia and corresponding in silico models.

Experimental model			In silico model	
References	**Animal model**	**Observed abnormalities**	**Applied lesions in the SNN model ("pathology model")**	**Effects of lesions in pathological simulations compared to control**
Ledoux and Lorden, 2002; White and Sillitoe, 2017	Genetically dystonic (*dt*) rats; $Ptf1a^{Cre}$;$Vglut2^{fx/fx}$ mice.	Reduced olivocerebellar input	Reduced IO-PC weight and reduced IO-PC number of connections (by 25%, 50% or 75%).	PC baseline = DCN baseline = PC irregularity = DCN irregularity = PC suppression ↓ DCN facilitation ↓ %CR ↓ CR time before US =
Ledoux and Lorden, 2002	Genetically dystonic (*dt*) rats	PC burst-firing pattern	Direct injection of intermittent spike trains in all PCs, during the whole simulation: 20 ms spike trains with 20–30 ms pauses; Reduced PC intrinsic current for basal discharge.	PC baseline: ↑ DCN baseline: ↓ PC irregularity: ↑ DCN irregularity: ↑ PC suppression: = DCN facilitation: = %CR: ↓ CR time before US: ↓
Hisatsune et al., 2013	*Itpr1* knockout mice	PC burst-firing with increased IO activity	Direct injection of intermittent spike trains to all IOs, during the whole simulation: 40 ms spike trains with 40 ms pauses.	PC baseline: = DCN baseline: ↑ PC irregularity: ↑ DCN irregularity: ↑ PC suppression: - DCN facilitation: - %CR: ↓ CR time before US: -
Vanni et al., 2015	Heterozygous torsinA knockout mice (Tor1a + /–) and human ΔGAG mutant torsinA transgenic mice (hMT)	Reduced *pf* synaptic contacts on PC distal dendrites; Increased IO synaptic contacts on PCs; Reduced GABAergic input to PCs.	Removed 14%, 25% of *pf*-PC connections; Increased 32%, 57% of IO-PC connections; Removed 39%, 71% of MLI-PC connections.	PC baseline: = DCN baseline: = PC irregularity: = DCN irregularity: = PC suppression: = DCN facilitation: = %CR: = CR time before US: =

Specifically, reference experimental studies along with the animal models and observed neural abnormalities are reported on the left; equivalent lesions applied to the SNN model and effects during simulations are listed on the right. Pathological simulation outcomes are indicated as modifications of parameters related to neural activity and behavior (e.g., firing rate irregularity and %CR) with respect to control simulations: increased (↑), decreased (↓), unchanged (=), not available (-).

Purkinje cells found in cell-attached recording may be due to an alteration of calcium channels, Ca^{2+}-dependent K^{+} currents, or both (Liu et al., 2020), or to the alteration of Na^{+}-related mechanisms (Fremont et al., 2015). Consideration of these molecular mechanisms would pave the way to explore PCs as a therapeutic target (Cook et al., 2021): manipulating PC firing and cerebellar output may show great promise for treating dystonia (Liu et al., 2020).

Furthermore, our model included the cerebellar circuit only. This allowed to isolate the cerebellar contribution in the disorder and understand the impact of specific lesions. However, to investigate the role of the cerebellum in dystonia as a motor network disorder (Neychev et al., 2011), more complex systems involving multiple brain nodes could be used, e.g., including the basal ganglia and the motor cortex. By inducing impairments in the cerebellum, such brain models could provide insight into whether and how dysfunctional cerebellum affects the integrity of the full motor network. In addition, cerebellar neuromodulation treatments (e.g., DBS or TMS), for instance, specifically targeting altered PC activity with DBS (Brown et al., 2020), might be modeled, allowing us to monitor signal propagation through the whole motor network. This could help to better understand how the cerebellum modulates the activity of the basal ganglia through their subcortical connections (Bostan et al., 2010; Chen et al., 2014), or vice versa, and how it could be directly related to dystonia.

DATA AVAILABILITY STATEMENT

The datasets presented in this study can be found in online repositories. The names of the repository/repositories and accession number(s) can be found in the article/ **Supplementary Material**. The code for running simulations and analyzing results from this article are available at the following repository: https://github.com/dbbs-lab/dystonia_ebcc.

AUTHOR CONTRIBUTIONS

AG designed the system and performed the simulations, analyzed the simulated data, and wrote the manuscript. AM performed the simulations, prepared the figures, and contributed in writing. ED'A supported in interpreting the results and defined the physiological aspects. CC coordinated the work, supported the design of the system and of the simulations, and wrote the manuscript. All authors contributed to the article and approved the submitted version.

FUNDING

This research has received funding from the European Union's Horizon 2020 Framework Program for Research and Innovation under the Specific Grant Agreement No. 945539 (Human Brain Project SGA3).

ACKNOWLEDGMENTS

Special acknowledgment to EBRAINS and FENIX for informatic support and infrastructure.

SUPPLEMENTARY MATERIAL

The Supplementary Material for this article can be found online at: https://www.frontiersin.org/articles/10.3389/fnsys.2022.919761/full#supplementary-material

Supplementary Figure 1 | SDFs in PC population **(A)** and DCN motor output **(B)**, averaging across cell SDFs, for each trial. Increasing darkness of the lines corresponds to subsequent trials (the lightest is the first trial, the darkest is the last trial). Each trial starts with the CS onset and last 1000 ms in total. At 250 ms the US is delivered (purple vertical line) and co-terminates with CS at 280 ms (gray vertical line). The US causes a burst-pause in PCs, which then return to baseline; consequently, a pause-burst response is triggered in the DCN motor output, before the return to baseline. The signals change in the time window before US throughout learning, thanks to synaptic plasticity. Note that first 50 ms are cut since artifacts of SDF analysis. Dashed horizontal line indicates the baseline activity (in the first 100 ms), solid horizontal cyan line (right panel) represents the CR threshold.

Supplementary Figure 2 | SDFs of downstate **(A)** and upstate **(B)** individual PCs, undergoing a significant SDF change (suppression/facilitation), in the last trial with respect to initial state (first 100 ms from CS onset) in the control condition. The thicker lines represent the average across cells. The frequency values are normalized with respect to the initial state activity (horizontal dashed lines at 0 Hz).

Supplementary Figure 3 | Baseline firing rate **(A)**, and irregularity measured through the CV_{ISI} **(B)** of PCs (left) and DCN (right) in the case of reduced olivocerebellar input for the three damage levels, compared to the control condition. Cyan horizontal line indicates the mean, red horizontal line indicates the median, box edges – 1st and 3rd quartile, whiskers – minimum and maximum accepted values, excluding outliers (indicated as circles).

Supplementary Figure 4 | Raster plots showing spiking activity of each cell (y axis) within PC population in the first trial of simulations with aberrant PC burst-firing, intrinsic **(A)** and IO-induced **(B)**. Gray vertical lines represent the CS onset and end, purple line marks the US onset.

Supplementary Figure 5 | Baseline firing rate **(A)** and irregularity measured through the CV_{ISI} **(B)** of PC (left) and DCN cells (right) in the case of intrinsic and IO-induced PC burst-firing, compared to the control condition. Cyan horizontal line indicates the mean, red horizontal line indicates the median, box edges – 1st and 3rd quartile, whiskers – minimum and maximum accepted values, excluding outliers (indicated as circles).

Supplementary Figure 6 | Baseline firing rate **(A)** and irregularity measured through the CV_{ISI} **(B)** of PC (left) and DCN cells (right) in the case of imbalanced PC synaptic densities, for mild and severe damage levels, compared to the control condition. Cyan horizontal line indicates the mean, red horizontal line indicates the median, box edges – 1st and 3rd quartile, whiskers – minimum and maximum accepted values, excluding outliers (indicated as circles).

REFERENCES

Albanese, A., Bhatia, K., Bressman, S. B., Delong, M. R., Fahn, S., Fung, V. S. C., et al. (2013). Phenomenology and classification of dystonia: a consensus update. *Move. Disord.* 28, 863–873. doi: 10.1002/MDS.25475

Albus, J. S. (1971). A theory of cerebellar function. *Mathe. Biosci.* 10, 25–61. doi: 10.1016/0025-5564(71)90051-4

Antonietti, A., Casellato, C., Garrido, J. A., Luque, N. R., Naveros, F., Ros, E., et al. (2016). Spiking Neural Network with distributed plasticity reproduces cerebellar learning in Eye Blink Conditioning paradigms. *IEEE Trans. Biomed. Eng.* 63, 210–219. doi: 10.1109/TBME.2015.2485301

Beekhof, G. C., Gornati, S. V., Canto, C. B., Libster, A. M., Schonewille, M., Zeeuw, C. I. D., et al. (2021). Activity of Cerebellar Nuclei Neurons Correlates with ZebrinII Identity of Their Purkinje Cell Afferents. *Cells* 10:2686. doi: 10.3390/CELLS10102686

Berardelli, A., Rothwell, J. C., Hallett, M., Thompson, P. D., Manfredi, M., and Marsden, C. D. (1998). The pathophysiology of primary dystonia. *Brain* 121, 1195–1212. doi: 10.1093/BRAIN/121.7.1195

Boele, H., Peter, S., Ten Brinke, M. M., Verdonschot, L., Ijpelaar, A. C. H., Rizopoulos, D., et al. (2018). Impact of parallel fiber to Purkinje cell long-term depression is unmasked in absence of inhibitory input. *Sci. Adv.* 4:eaas9426. doi: 10.1126/sciadv.aas9426

Bologna, M., and Berardelli, A. (2017). Cerebellum: an explanation for dystonia? *Cerebell. Ataxias* 4:6. doi: 10.1186/S40673-017-0064-8

Bostan, A. C., Dum, R. P., and Strick, P. L. (2010). The basal ganglia communicate with the cerebellum. *Proc. Natl. Acad. Sci. U.S.A.* 107, 8452–8456. doi: 10.1073/PNAS.1000496107

Bradnam, L. V., Graetz, L. J., McDonnell, M. N., and Ridding, M. C. (2015). Anodal transcranial direct current stimulation to the cerebellum improves handwriting and cyclic drawing kinematics in focal hand dystonia. *Front. Hum. Neurosci.* 9:286. doi: 10.3389/FNHUM.2015.00286

Brown, E. G., Bledsoe, I. O., Luthra, N. S., Miocinovic, S., Starr, P. A., and Ostrem, J. L. (2020). Cerebellar Deep Brain Stimulation for Acquired Hemidystonia. *Move. Disord. Clin. Pract.* 7, 188–193. doi: 10.1002/MDC3.12876

Camfield, L., Ben-Shlomo, Y., and Warner, T. T. (2002). Impact of cervical dystonia on quality of life. *Move. Disord.* 17, 838–841. doi: 10.1002/MDS.10127

Casellato, C., Antonietti, A., Garrido, J. A., Carrillo, R. R., Luque, N. R., Ros, E., et al. (2014). Adaptive robotic control driven by a versatile spiking cerebellar network. *PLoS One* 9:e112265. doi: 10.1371/journal.pone.0112265

Chen, C. H., Fremont, R., Arteaga-Bracho, E. E., and Khodakhah, K. (2014). Short latency cerebellar modulation of the basal ganglia. *Nat. Neurosci.* 17, 1767–1775. doi: 10.1038/NN.3868

Cheng, F. B., Feng, J. C., Ma, L. Y., Miao, J., Ott, T., Wan, X. H., et al. (2014). Combined occurrence of a novel TOR1A and a THAP1 mutation in primary dystonia. *Mov. Disord.* 29, 1079–1083. doi: 10.1002/MDS.25921

Coesmans, M., Weber, J. T., de Zeeuw, C. I., and Hansel, C. (2004). Bidirectional Parallel Fiber Plasticity in the Cerebellum under Climbing Fiber Control. *Neuron* 44, 691–700. doi: 10.1016/J.NEURON.2004.10.031

Cook, A. A., Fields, E., and Watt, A. J. (2021). Losing the Beat: Contribution of Purkinje Cell Firing Dysfunction to Disease, and Its Reversal. *Neuroscience* 462, 247–261. doi: 10.1016/J.NEUROSCIENCE.2020.06.008

Dayan, P., and Abbott, L. F. (2001). *Theoretical Neuroscience: Computational and Mathematical Nodeling of Neural Systems*. Cambridge, Mass: MIT Press.

de Oude, N. L., Hoebeek, F. E., Ten Brink, M. M., de Zeeuw, C. I., and Boele, H. J. (2021). Pavlovian eyeblink conditioning is severely impaired in tottering mice. *J. Neurophysiol.* 125, 398–407. doi: 10.1152/JN.00578.2020/ASSET/IMAGES/MEDIUM/JN-00578-2020R01.PNG

de Schepper, R., Geminiani, A., Masoli, S., Rizza, M. F., Antonietti, A., Casellato, C., et al. (2021). Scaffold modelling captures the structure-function-dynamics relationship in brain microcircuits. *bioRxiv* [Preprint]. doi: 10.1101/2021.07.30.454314

de Zeeuw, C. I., and Ten Brinke, M. M. (2015). The Cerebellum and Motor Learning. *Cold Spring Harbor Perspect. Biol.* 7:a021683.

de Zeeuw, C. I. (2021). Bidirectional learning in upbound and downbound microzones of the cerebellum. *Nat. Rev. Neurosci.* 22, 92–110. doi: 10.1038/S41583-020-00392-X

Defazio, G. (2010). The epidemiology of primary dystonia: current evidence and perspectives. *Eur. J. Neurol.* 17, 9–14. doi: 10.1111/J.1468-1331.2010.03053.X

Diedrighsen, J., and Bastian, A. (2014). "Cerebellar function," in *The Cognitive Neurosciences*, eds M. S. Gazzaniga and G. R. Mangun (Cambridge: MIT Press).

Eppler, J. M., Helias, M., Muller, E., Diesmann, M., Gewaltig, M., and Stewart, T. C. (2009). PyNEST?: a convenient interface to the NEST simulator. *Front. Neuroinform.* 2:12. doi: 10.3389/neuro.11.012.2008

Freeman, J. H., and Steinmetz, A. B. (2011). Neural circuitry and plasticity mechanisms underlying delay eyeblink conditioning. *Learn. Mem.* 19, 666–677. doi: 10.1101/lm.2023011

Fremont, R., Tewari, A., and Khodakhah, K. (2015). Aberrant Purkinje cell activity is the cause of dystonia in a shRNA-based mouse model of Rapid Onset Dystonia–Parkinsonism. *Neurobiol. Dis.* 82, 200–212. doi: 10.1016/J.NBD.2015.06.004

Geminiani, A., Casellato, C., Antonietti, A., D'Angelo, E., and Pedrocchi, A. (2018a). A multiple-plasticity Spiking Neural Network embedded in a closed-loop control system to model cerebellar pathologies. *Int. J. Neural Syst.* 28:1750017. doi: 10.1142/S0129065717500174

Geminiani, A., Casellato, C., Locatelli, F., Prestori, F., Pedrocchi, A., and D'Angelo, E. (2018b). Complex dynamics in simplified neuronal models: reproducing Golgi cell electroresponsiveness. *Front. Neuroinform.* 12:88. doi: 10.3389/fninf.2018.00088

Geminiani, A., Pedrocchi, A., D'Angelo, E., and Casellato, C. (2019b). Response dynamics in an olivocerebellar spiking neural network with nonlinear neuron properties. *Front. Comput. Neurosci.* 13:68. doi: 10.3389/fncom.2019.00068

Geminiani, A., Casellato, C., D'Angelo, E., and Pedrocchi, A. (2019a). Complex electroresponsive dynamics in olivocerebellar neurons represented with extended-generalized leaky integrate and fire models. *Front. Comput. Neurosci.* 13:35. doi: 10.3389/fncom.2019.00035

Gewaltig, M.-O., and Diesmann, M. (2007). NEST (NEural Simulation Tool). *Scholarpedia* 2:1430. doi: 10.4249/scholarpedia.1430

Hansel, C., Linden, D. J., and D'Angelo, E. (2001). Beyond parallel fiber LTD: the diversity of synaptic and non-synaptic plasticity in the cerebellum. *Nat. Neurosci.* 4, 467–475. doi: 10.1038/87419

Hisatsune, C., Miyamoto, H., Hirono, M., Yamaguchi, N., Sugawara, T., Ogawa, N., et al. (2013). IP3R1 deficiency in the cerebellum/brainstem causes basal ganglia-independent dystonia by triggering tonic Purkinje cell firings in mice. *Front. Neural Circuits* 7:156. doi: 10.3389/FNCIR.2013.00156/ABSTRACT

Hutchinson, P. J., O'Connell, M. T., Al-Rawi, P. G., Maskell, L. B., Kett-White, R., Gupta, A. K., et al. (2000). Clinical cerebral microdialysis: a methodological study. *J. Neurosurg.* 93, 37–43. doi: 10.3171/JNS.2000.93.1.0037

Isaksen, T. J., Kros, L., Vedovato, N., Holm, T. H., Vitenzon, A., Gadsby, D. C., et al. (2017). Hypothermia-induced dystonia and abnormal cerebellar activity in a mouse model with a single disease-mutation in the sodium-potassium pump. *PLoS Genet.* 13:e1006763. doi: 10.1371/JOURNAL.PGEN.1006763

Ito, M. (2000). Mechanisms of motor learning in the cerebellum. *Brain Res.* 886, 237–245. doi: 10.1016/S0006-8993(00)03142-5

Jacobson, S. W., Stanton, M. E., Molteno, C. D., Burden, M. J., Fuller, D. S., Hoyme, H. E., et al. (2008). Impaired Eyeblink Conditioning in Children with Fetal Alcohol Syndrome. *Alcoholism* 32, 365–372. doi: 10.1111/j.1530-0277.2007.00585.x

Jordan, J., Mørk, H., Vennemo, S. B., Terhorst, D., Peyser, A., Ippen, T., et al. (2019). NEST 2.18.0. *Zenodo* doi: 10.5281/ZENODO.2605422

Kerrison, J. B., Lancaster, J. L., Zamarripa, F. E., Richardson, L. A., Morrison, J. C., Holck, D. E. E., et al. (2003). Positron emission tomography scanning in essential blepharospasm. *Am. J. Ophthalmol.* 136, 846–852. doi: 10.1016/S0002-9394(03)00895-X

Koch, G., Porcacchia, P., Ponzo, V., Carrillo, F., Cáceres-Redondo, M. T., Brusa, L., et al. (2014). Effects of two weeks of cerebellar theta burst stimulation in cervical dystonia patients. *Brain Stimul.* 7, 564–572. doi: 10.1016/J.BRS.2014.05.002

Latorre, A., Rocchi, L., Magrinelli, F., Mulroy, E., Berardelli, A., Rothwell, J. C., et al. (2020). Unravelling the enigma of cortical tremor and other forms of cortical myoclonus. *Brain* 143, 2653–2663. doi: 10.1093/BRAIN/AWAA129

Ledoux, M. S., and Lorden, J. F. (2002). Abnormal spontaneous and harmaline-stimulated Purkinje cell activity in the awake genetically dystonic rat. *Exp. Brain Res.* 145, 457–467. doi: 10.1007/S00221-002-1127-4

Liu, Y., Xing, H., Wilkes, B. J., Yokoi, F., Chen, H., Vaillancourt, D. E., et al. (2020). The abnormal firing of Purkinje cells in the knockin mouse model of DYT1 dystonia. *Brain Res. Bull.* 165, 14–22. doi: 10.1016/J.BRAINRESBULL.2020.09.011

Llinás, R., and Sugimori, M. (1980). Electrophysiological properties of in vitro Purkinje cell dendrites in mammalian cerebellar slices. *J. Physiol.* 305, 197–213. doi: 10.1113/JPHYSIOL.1980.SP013358

Luque, N. R., Garrido, J. A., Naveros, F., Carrillo, R. R., D'Angelo, E., and Ros, E. (2016). Distributed Cerebellar Motor Learning: A Spike-Timing-Dependent Plasticity Model. *Front. Comput. Neurosci.* 10:17. doi: 10.3389/fncom.2016.00017

Marr, D. (1969). A theory of cerebellar cortex. *J. Physiol.* 202, 437–470. doi: 10.1113/jphysiol.1969.sp008820

Masoli, S., and D'Angelo, E. (2017). Synaptic activation of a detailed Purkinje cell model predicts voltage-dependent control of burst-pause responses in active dendrites. *Front. Cell. Neurosci.* 11:278. doi: 10.3389/fncel.2017.00278

Masoli, S., Solinas, S., and Angelo, E. D. (2015). Action potential processing in a detailed Purkinje cell model reveals a critical role for axonal compartmentalization. *Front. Cell. Neurosci.* 9:47. doi: 10.3389/fncel.2015.00047

Miterko, L. N., Baker, K. B., Beckinghausen, J., Bradnam, L. V., Cheng, M. Y., Cooperrider, J., et al. (2019). Consensus Paper: Experimental Neurostimulation of the Cerebellum. *Cerebellum* 18, 1064–1097. doi: 10.1007/S12311-019-01041-5

Neychev, V. K., Gross, R. E., Lehéricy, S., Hess, E. J., and Jinnah, H. A. (2011). The functional neuroanatomy of dystonia. *Neurobiol. Dis.* 42, 185–201. doi: 10.1016/J.NBD.2011.01.026

Ohtsuki, G., Piochon, C., Adelman, J. P., and Hansel, C. (2012). SK2 channel modulation contributes to compartment-specific dendritic plasticity in cerebellar Purkinje cells. *Neuron* 75, 108–120. doi: 10.1016/J.NEURON.2012.05.025

Ohyama, T., Nores, W. L., Medina, J. F., Riusech, F. A., and Mauk, M. D. (2006). Learning-Induced Plasticity in Deep Cerebellar Nucleus. *J. Neurosci.* 26, 12656–12663. doi: 10.1523/JNEUROSCI.4023-06.2006

Ozelius, L., and Lubarr, N. (2016). *DYT1 Early-Onset Isolated Dystonia. GeneReviews§* . Available online at: https://www.ncbi.nlm.nih.gov/books/NBK1492/ (accessed on Mar 24, 2022).

Prudente, C. N., Hess, E. J., and Jinnah, H. A. (2014). Dystonia as a network disorder: what is the role of the cerebellum? *Neuroscience* 260, 23–35. doi: 10.1016/J.NEUROSCIENCE.2013.11.062

Raike, R. S., Pizoli, C. E., Weisz, C., van den Maagdenberg, A. M., Jinnah, H. A., and Hess, E. J. (2013). Limited regional cerebellar dysfunction induces focal dystonia in mice. *Neurobiol. Dis.* 49, 200–210. doi: 10.1016/J.NBD.2012.07.019

Ramdhani, R. A., Kumar, V., Velickovic, M., Frucht, S. J., Tagliati, M., and Simonyan, K. (2014). What's special about task in dystonia? A voxel-based morphometry and diffusion weighted imaging study. *Mov. Disord.* 29, 1141–1150. doi: 10.1002/MDS.25934

Reeb-Sutherland, B. C., and Fox, N. A. (2015). Eyeblink Conditioning: A Non-invasive Biomarker for Neurodevelopmental Disorders. *J. Autism Dev. Disord.* 45, 376–394. doi: 10.1007/s10803-013-1905-9

Sadnicka, A., Rocchi, L., Latorre, A., Antelmi, E., Teo, J., Pareés, I., et al. (2022). A Critical Investigation of Cerebellar Associative Learning in Isolated Dystonia. *Mov. Disord.* [Epub ahead of print]. doi: 10.1002/MDS.28967

Sadnicka, A., Teo, J. T., Kojovic, M., Pareés, I., Saifee, T. A., Kassavetis, P., et al. (2015). All in the blink of an eye: new insight into cerebellar and brainstem function in DYT1 and DYT6 dystonia. *Eur. J. Neurol.* 22, 762–767. doi: 10.1111/ENE.12521

Sakurai, M. (1987). Synaptic modification of parallel fibre-Purkinje cell transmission in in vitro guinea-pig cerebellar slices. *J. Physiol.* 394, 463–480. doi: 10.1113/JPHYSIOL.1987.SP016881

Schirinzi, T., Sciamanna, G., Mercuri, N. B., and Pisani, A. (2018). Dystonia as a network disorder: a concept in evolution. *Curr. Opin. Neurol.* 31, 498–503. doi: 10.1097/WCO.0000000000000580

Schweighofer, N., Doya, K., and Lay, F. (2001). Unsupervised learning of granule cell sparse codes enhances cerebellar adaptive control. *Neuroscience* 103, 35–50. doi: 10.1016/s0306-4522(00)00548-0

Shakkottai, V. G. (2014). Physiologic changes associated with cerebellar dystonia. *Cerebellum* 13, 637–644. doi: 10.1007/S12311-014-0572-5

Shakkottai, V. G., Batla, A., Bhatia, K., Dauer, W. T., Dresel, C., Niethammer, M., et al. (2016). Current Opinions and Areas of Consensus on the Role of the Cerebellum in Dystonia. *Cerebellum* 16, 577–594. doi: 10.1007/S12311-016-0825-6

Steinmetz, J. E., Tracy, J. A., and Green, J. T. (2001). Classical eyeblink conditioning: clinical models and applications. *Integrat. Physiol. Behav. Sci.* 36, 220–238. doi: 10.1007/BF02734095

Stratton, S. E., and Lorden, J. F. (1991). Effect of harmaline on cells of the inferior olive in the absence of tremor: differential response of genetically dystonic and harmaline-tolerant rats. *Neuroscience* 41, 543–549. doi: 10.1016/0306-4522(91)90347-Q

Stuart, G., and Häusser, M. (1994). Initiation and spread of sodium action potentials in cerebellar Purkinje cells. *Neuron* 13, 703–712. doi: 10.1016/0896-6273(94)90037-X

Tarsy, D., and Simon, D. K. (2009). Dystonia. *N. Engl. J. Med.* 355, 818–829. doi: 10.1056/NEJMRA055549

ten Brinke, M. M., Boele, H. J., Spanke, J. K., Potters, J. W., Kornysheva, K., Wulff, P., et al. (2015). Evolving Models of Pavlovian Conditioning: Cerebellar Cortical Dynamics in Awake Behaving Mice. *Cell Rep.* 13, 1977–1988. doi: 10.1016/j.celrep.2015.10.057

Teo, J., van de Warrenburg, B. P. C., Schneider, A., Rothwell, J., and Bhatia, K. (2009). Neurophysiological evidence for cerebellar dysfunction in primary focal dystonia. *J. Neurol. Neurosurg. Psychiatr.* 80, 80–83. doi: 10.1136/jnnp.2008.144626

Trimarco, E., Mirino, P., and Caligiore, D. (2021). Cortico-Cerebellar Hyper-Connections and Reduced Purkinje Cells Behind Abnormal Eyeblink Conditioning in a Computational Model of Autism Spectrum Disorder. *Front. Syst. Neurosci.* 15:666649. doi: 10.3389/FNSYS.2021.666649/BIBTEX

Valls-Sole, J., and Defazio, G. (2016). Blepharospasm: Update on Epidemiology, Clinical Aspects, and Pathophysiology. *Front. Neurol.* 7:45. doi: 10.3389/FNEUR.2016.00045

Vanni, V., Puglisi, F., Bonsi, P., Ponterio, G., Maltese, M., Pisani, A., et al. (2015). Cerebellar synaptogenesis is compromised in mouse models of DYT1 dystonia. *Exp. Neurol.* 271, 457–467. doi: 10.1016/J.EXPNEUROL.2015.07.005

Washburn, S. G., Fremont, R., Moreno, M. C., Angueyra, C., and Khodakhah, K. (2019). Acute cerebellar knockdown of Sgce reproduces salient features of myoclonus-dystonia (DYT11) in mice. *Elife* 8:e52101. doi: 10.7554/ELIFE.52101

White, J. J., and Sillitoe, R. V. (2017). Genetic silencing of olivocerebellar synapses causes dystonia-like behaviour in mice. *Nat. Commun.* 8:14912. doi: 10.1038/ncomms14912

Wichmann, T., and DeLong, M. R. (2011). Deep-Brain Stimulation for Basal Ganglia Disorders. *Basal Ganglia* 1, 65–77. doi: 10.1016/J.BAGA.2011.05.001

Womack, M. D., and Khodakhah, K. (2004). Dendritic Control of Spontaneous Bursting in Cerebellar Purkinje Cells. *J. Neurosci.* 24, 3511–3521. doi: 10.1523/JNEUROSCI.0290-04.2004

Woodruff-Pak, D. S., Papka, M., Romano, S., and Li, Y.-T. (1996). Eyeblink Classical Conditioning in Alzheimer' s Disease and Cerebrovascular Dementia. *Neurobiol. Aging* 17, 505–512.

Wu, B., Blot, F. G. C., Wong, A. B., Osório, C., Adolfs, Y., Pasterkamp, R. J., et al. (2019). TRPC3 is a major contributor to functional heterogeneity of cerebellar Purkinje cells. *Elife* 8:e45590. doi: 10.7554/ELIFE.45590

Yamazaki, T., and Tanaka, S. (2007). A spiking network model for passage-of-time representation in the cerebellum. *Eur. J. Neurosci.* 26, 2279–2292. doi: 10.1111/j.1460-9568.2007.05837.x

Zbarska, S., Holland, E. A., Bloedel, J. R., and Bracha, V. (2007). Inferior olivary inactivation abolishes conditioned eyeblinks: extinction or cerebellar malfunction? *Behav. Brain Res.* 178, 128–138. doi: 10.1016/j.bbr.2006.12.012

Zhang, L., Yokoi, F., Jin, Y. H., DeAndrade, M. P., Hashimoto, K., Standaert, D. G., et al. (2011). Altered Dendritic Morphology of Purkinje cells in Dyt1 ΔGAG Knock-In and Purkinje Cell-Specific Dyt1 Conditional Knockout Mice. *PLoS One* 6:e18357. doi: 10.1371/JOURNAL.PONE.0018357

Conflict of Interest: The authors declare that the research was conducted in the absence of any commercial or financial relationships that could be construed as a potential conflict of interest.

Publisher's Note: All claims expressed in this article are solely those of the authors and do not necessarily represent those of their affiliated organizations, or those of the publisher, the editors and the reviewers. Any product that may be evaluated in this article, or claim that may be made by its manufacturer, is not guaranteed or endorsed by the publisher.

frontiers | Frontiers in Systems Neuroscience

ORIGINAL RESEARCH
published: 28 July 2022
doi: 10.3389/fnsys.2022.899446

Cerebello-Thalamo-Cortical Network Dynamics in the Harmaline Rodent Model of Essential Tremor

Kathryn Woodward[1], *Richard Apps*[1], *Marc Goodfellow*[2,3] *and Nadia L. Cerminara*[1]*

[1]School of Physiology, Pharmacology and Neuroscience, University of Bristol, Bristol, United Kingdom, [2]Department of Engineering, Mathematics and Physical Sciences, University of Exeter, Exeter, United Kingdom, [3]Living Systems Institute, University of Exeter, Exeter, United Kingdom

Essential Tremor (ET) is a common movement disorder, characterised by a posture or movement-related tremor of the upper limbs. Abnormalities within cerebellar circuits are thought to underlie the pathogenesis of ET, resulting in aberrant synchronous oscillatory activity within the thalamo-cortical network leading to tremors. Harmaline produces pathological oscillations within the cerebellum, and a tremor that phenotypically resembles ET. However, the neural network dynamics in cerebellar-thalamo-cortical circuits in harmaline-induced tremor remains unclear, including the way circuit interactions may be influenced by behavioural state. Here, we examined the effect of harmaline on cerebello-thalamo-cortical oscillations during rest and movement. EEG recordings from the sensorimotor cortex and local field potentials (LFP) from thalamic and medial cerebellar nuclei were simultaneously recorded in awake behaving rats, alongside measures of tremor using EMG and accelerometery. Analyses compared neural oscillations before and after systemic administration of harmaline (10 mg/kg, I.P), and coherence across periods when rats were resting vs. moving. During movement, harmaline increased the 9–15 Hz behavioural tremor amplitude and increased thalamic LFP coherence with tremor. Medial cerebellar nuclei and cerebellar vermis LFP coherence with tremor however remained unchanged from rest. These findings suggest harmaline-induced cerebellar oscillations are independent of behavioural state and associated changes in tremor amplitude. By contrast, thalamic oscillations are dependent on behavioural state and related changes in tremor amplitude. This study provides new insights into the role of cerebello-thalamo-cortical network interactions in tremor, whereby neural oscillations in thalamocortical, but not cerebellar circuits can be influenced by movement and/or behavioural tremor amplitude in the harmaline model.

Keywords: essential tremor, harmaline, cerebellum, thalamus, motor cortex, LFP

OPEN ACCESS

Edited by:
Paul J. Mathews, Lundquist Institute for Biomedical Innovation, United States

Reviewed by:
Joshua J. White, Erasmus Medical Center, Netherlands
Zhenyu Gao, Erasmus Medical Center, Netherlands

***Correspondence:**
Nadia L. Cerminara
n.cerminara@bristol.ac.uk

Received: *18 March 2022*
Accepted: *22 June 2022*
Published: *28 July 2022*

Citation:
Woodward K, Apps R, Goodfellow M and Cerminara NL (2022) Cerebello-Thalamo-Cortical Network Dynamics in the Harmaline Rodent Model of Essential Tremor. Front. Syst. Neurosci. 16:899446. doi: 10.3389/fnsys.2022.899446

INTRODUCTION

Essential tremor (ET) is a pathological tremor that affects an estimated ∼1% of the population, or 4.6% of those aged 65 years and above (Louis and Ferreira, 2010). ET is characterised as an action tremor—a tremor typically produced by voluntary contraction of muscles and present during sustained posture or voluntary movement (Thenganatt and Jankovic, 2016; Bhatia et al., 2018).

ET tremor frequency in humans is usually around 6–12 Hz and the tremor typically affects the arms and hands but can also affect the head and voice. The pathophysiology underlying ET is unclear, although it is increasingly recognised as a heterogenous disease or syndrome, where there may be several underlying aetiologies producing the clinical phenotype of ET. Converging research suggests that a common feature is abnormalities in activity within the cerebellum which are propagated through the cerebello-thalamo-cortical network. A cardinal symptom of cerebellar dysfunction is intention tremor; a tremor that worsens with goal-directed movement, resulting from disturbances to cerebellar output pathways (Holmes, 1939; Fahn, 1984) and intention tremor has been associated with severe or advanced cases of ET (Deuschl et al., 2000; Louis et al., 2009; Sternberg et al., 2013). Similarly, ataxia—another cardinal sign of cerebellar dysfunction—can be present in ET (Singer et al., 1994; Stolze et al., 2001; Duval et al., 2006; Arkadir and Louis, 2013). Patients with ET have also shown impaired performance on cerebellar-dependent behaviours, such as eye-blink conditioning (Kronenbuerger et al., 2007, 2008), and visuo-motor adaptation (Hanajima et al., 2016). Neuropathological changes have also been observed in the cerebellum of ET patients, including Purkinje cell loss, changes in Purkinje cell morphology and connectivity (e.g., Kuo et al., 2011, 2017a; Yu et al., 2012; Babij et al., 2013; Louis et al., 2014) and redistribution of climbing fibre synapses on the Purkinje cell dendritic arbour, with a greater number of climbing fibre synapses found on distal dendritic spines (Lin et al., 2014; Kuo et al., 2017b; Lee D. et al., 2018; Pan et al., 2020). Clinical studies describing cerebellar abnormalities have, therefore, been closely associated with ET.

A major outflow path of the cerebellum is its projection to the sensorimotor cortex *via* the ventrolateral thalamus (VL), including a subregion termed the ventral intermediate nucleus (VIM, Lierse, 1993). Hua et al. (1998) identified cells within VIM that fire periodically at rates that correlate with tremors. Furthermore, deep brain stimulation of VIM can provide symptomatic relief to ET (Vaillancourt et al., 2003). And thalamic stimulation at a near-to-tremor frequency can entrain the frequency of the tremor, as well as amplify or suppress tremor amplitude, depending on the phase of tremor oscillation when the stimulation is applied (Cagnan et al., 2013). Taken together these findings suggest the thalamus plays an important role in propagating tremor oscillations through the cerebello-thalamo-cortical pathway.

Harmaline is a pharmacological model of tremor, that involves the administration of the β-carboline alkaloid harmaline, which is a reversible inhibitor of monoamine oxidase-A (Hoon et al., 1997). Harmaline-induced tremor is characterised as an action tremor, akin to ET, with the frequency of tremor varying slightly across species (10–16 Hz in mice, 8–12 Hz in rats, 7–12 Hz in monkeys, and 10–16 Hz in pigs; Lamarre et al., 1975; Martin et al., 2005; Lee J. et al., 2018). Harmaline tremor shares similar underlying neural pathways as ET (Handforth, 2012). For example, electrical stimulation within the thalamus in harmaline-treated mice and rats significantly reduces the amplitude of harmaline-induced tremor, akin to the effects of deep brain stimulation observed in ET patients (Bekar et al., 2008; Lee and Chang, 2019). Harmaline induces a temporary increase in the frequency of rhythmic activity in the brainstem inferior olivary (IO) complex, predominantly within the caudal medial accessory olive and caudal dorsal accessory olive (De Montigny and Lamarre, 1973; Lamarre et al., 1975). This in turn, increases the regularity and synchrony of climbing fibre evoked complex spikes in the cerebellar cortex, particularly within the vermis and paravermis, with a complete suppression of simple spikes (De Montigny and Lamarre, 1973; Bernard et al., 1984).

It has previously been hypothesised that tremor-onset with action in ET is due to disrupted cerebellar output (Buijink et al., 2015). The cerebellar nuclei transmit integrated sensorimotor signals to the wider motor network (e.g., Giuffrida et al., 1981; Armstrong and Edgley, 1984; Rowland and Jaeger, 2005; Becker and Person, 2019). Bilateral rhythmic optogenetic stimulation of the interpositus nucleus has been shown to induce a tremor in mice at the same frequency of the stimulation (Brown et al., 2020). This underscores the importance of increased cerebellar nuclear rhythmicity in generating and propagating tremorgenic rhythms. Neuropathological changes in ET may disrupt normal movement-related oscillations in the cerebellum, which in turn may disrupt cerebellar output from the cerebellar nuclei during movement (Pellerin and Lamarre, 1997; Hartmann and Bower, 1998; Courtemanche et al., 2002; Dugué et al., 2009; Baumel et al., 2021). Research to date, however, has not examined the impact of harmaline on cerebellar projections to ascending thalamo-cortical pathways, nor whether movement modulates activity in these pathways. Our aim was to examine harmaline's effect on the cerebello-thalamo-cortical network in the awake behaving rat by recording local field potential (LFP) oscillations at the tremor frequency across the network and using coherence analysis to examine how these neural network interactions are modulated by movement. Cross-correlation analysis was carried out to examine the functional connectivity of oscillations between nodes of the tremor network. We observed that harmaline-induced tremor can be characterised as an action tremor associated with coherent tremor frequency oscillations across the cerebello-thalamo-cortical network, suggesting propagation of tremor oscillations across the network. Furthermore, harmaline induced prominent pathological oscillations in the cerebellum, and cerebellar coherence with tremor were observed when the animals were resting/immobile and moving. In contrast, thalamic coherence with tremor was modulated by movement. These findings provide evidence that harmaline-induced tremor involves comparable electrophysiological correlates to those reported in ET. Additionally, these findings suggest that the neural oscillations in the cerebellum and thalamus have different roles in modulating tremor, as thalamus but not cerebellar oscillations are influenced by movement and/or behavioural tremor amplitude in the harmaline model.

MATERIALS AND METHODS

Animals

All procedures were performed in accordance with the United Kingdom Animals (Scientific Procedures) Act 1986 and the University of Bristol Animal Welfare and Ethical Review Body. Experiments were performed on 14 adult male Lister Hooded rats (300–600 g). All animals were housed in groups under normal environmental conditions (∼20°C and 45%–65% humidity), maintained on a 12/12 h light/dark reverse lighting cycle and provided with food and water ad libitum. Rats were handled daily for at least 1 week prior to surgery. Following surgery, the animals were housed separately, and their health was monitored closely with observational assessments and monitoring of weight.

Surgery

Rats were anaesthetised with a combination of ketamine (50%) and medetomidine (30%) in saline (20%) delivered via i.p. injection at a dose of 1 ml/kg, and then placed in a stereotaxic frame and secured with atraumatic ear bars coated with local anaesthetic lidocaine (10% Xylocaine®). Occasionally an additional dose of 0.1 ml of the ketamine/medetomidine/saline solution was given to maintain surgical levels of anaesthesia, as evidenced by pedal and eye blink reflexes. Core body temperature was maintained at 36–37°C through a rectal thermometer and heat mat.

Previous research has shown the firing rate and rhythmic activity of cells within the medial cerebellar nucleus show a stronger response to harmaline than cells within the interpositus or lateral cerebellar nuclei (Batini et al., 1981; Lorden et al., 1992). Furthermore, the harmaline-induced rhythmic firing of IO neurons occurs mainly in the caudal medial accessory olive and caudal dorsal accessory olive, which provide climbing fibre projections to the vermal A and B zones which then project to the medial cerebellar nuclei and lateral vestibular nucleus (De Montigny and Lamarre, 1973; Llinás and Volkind, 1973; Batini et al., 1981). Therefore, the medial cerebellar nucleus was targeted in these experiments. Rats were implanted with microdrives targeting the medial cerebellar nuclei (1 mm lateral and 11.3 mm posterior from bregma, and 4.1 mm ventral from the surface of the cerebellum) and the ventral anterior and ventral lateral (VA/VL) complex of the thalamus (1.8 mm lateral, 2.28 mm posterior from bregma, and 5.1 mm ventral from the surface of the cerebral cortex), also known as the "motor thalamus" (Nakamura et al., 2014) with two-to-four tetrodes per brain site (impedance 80–400 kΩ at 1 kHz). Two EEG screws were implanted over either side of the motor cortex (3 mm lateral and 2 mm anterior from bregma), and two EEG screws were implanted over either side of the sensory cortex (3 mm lateral and 0.5 mm anterior to bregma).

For 7 out of 14 rats, one of the cerebellar tetrodes was cut ∼2 mm shorter to simultaneously target the cerebellar cortex. All tetrodes were coated with fluorescent marker DiI (3% in absolute ethanol) before implantation. Pairs of flexible stainless-steel wires (Cooner wire, USA) were implanted and sutured into the neck EMG and either the triceps brachii or biceps femoris muscles to record EMG. A reference screw pre-soldered to the insulated silver wire was fixed into the right parietal skull plate, and a support screw was fixed into the left parietal skull plate. A ground screw soldered to an insulated silver wire was fixed over the right occipital skull plate. Following the completion of surgery, 1 ml dose of analgesic carprofen (5% in saline) was given subcutaneously followed by 0.1 ml of atipamezole (20% in saline) given *via* i.p. injection, to reverse the effects of the medetomidine.

Neurophysiological Recordings

After recovery from surgery, differential recordings were made using a tethered CerePlex μ Headstage and a Cereplex acquisition system (Blackrock Microsystems). Raw data were continuously recorded at a sampling rate of 30 kHz and all data were analysed off-line (see the section on "Data Processing"). Low pass filtered EEG and EMG data (<500 Hz) were sampled at 2 kHz. The Blackrock CerePlex μ Headstage also enabled 3-axis accelerometer recordings, which were low pass filtered (<500 Hz) and sampled at 2 kHz. Data were collected before (i.e., pre-harmaline) and after administration of harmaline hydrochloride (10 mg/kg, i.p.). Neural and EMG signals were sampled while rats were quietly at rest or moved freely around their home cage. Baseline data were collected across 2–5 days. After harmaline administration, data were continuously recorded until any visible deficits in motor function (e.g., tremor, ataxia) were completely recovered.

Histology

Upon completion of the experiment, animals were deeply anaesthetised with Euthatal (1 ml, i.p.) and an electrolytic lesion (3 μA for 30 s) made at the tetrode recording site with the greatest signal-to-noise ratio (SNR). Rats were then transcardially perfused with 0.9% saline, followed by 0.1 M phosphate buffer (PB) that contained 4% paraformaldehyde. Neural tissue was post-fixed in 4% paraformaldehyde for 24–72 h, and then transferred into 30% sucrose solution for 3–4 days before cutting and mounting sections. Cerebellar tissue was cut sagittally at a thickness of either 40 μm (n = 10 rats) or 100 μm (n = 6 rats). The thalamus was sectioned either in the coronal (n = 5 rats; 100 μm section thickness) or sagittal plane (n = 10 rats; 40 μm section thickness). Additional verification of tetrode placement within the cerebellum and thalamus was obtained by identifying histological tissue tracks of tetrodes marked with DiI. These were visualised with a fluorescent Axioskop 2 Plus microscope (Zeiss) fitted with a CoolLED pE-100 excitation system and images acquired using AxioVision software.

Data Processing

Processing of raw data was performed offline using MATLAB (2018) version 9.4.0.813654 (R2018a) Natick, Massachusetts: The MathWorks Inc. Bipolar referencing configurations were used for all EMG, EEG, and tetrode LFP recordings. Where multiple tetrodes were inserted into a single brain region, the tetrode with the greatest SNR of multiunit activity was selected for group analysis. Data were band-pass filtered between 1 and 49 Hz, and then down-sampled to 1 kHz.

A principal component analysis was performed on tri-accelerometer data to combine measurements in three directions into one principal component or axis to capture the axis with maximal variance for subsequent spectral analysis.

To examine how neural network interactions are modulated by movement, electrophysiological data were divided into epochs where the rats were quietly resting vs. moving. This was achieved by applying a global movement-threshold value to a measure of total acceleration, which was the absolute magnitude of acceleration in any direction and was taken as a proxy of overall movement, to distinguish between any periods of resting vs. moving. Total acceleration, *A*, was calculated as:

$$A = \sqrt{x^2 + y^2 + z^2} \quad (1)$$

Here, *x*, *y*, and *z* represent the three axes of the accelerometer. Total acceleration was then smoothed using a moving average filter with a window size of 100 samples. A global movement threshold of 1 m/s^2 was then applied to the measure of total acceleration to distinguish periods of resting/immobility from movement (Pasquet et al., 2016; Meyer et al., 2018; Guitchounts et al., 2020). This threshold was verified against video recordings and performed well at identifying time points when rats begin to move around the cage or move to adjust their resting position. Electrophysiological data were then categorised into "resting" or "moving", whereby rats were classified as either resting or moving if total acceleration, *A*, was below or above the threshold for the entire two-second non-overlapping epoch duration, respectively. Classified epochs were visually verified against the video recordings.

A trade-off between frequency resolution and the number of epochs was introduced when choosing epoch length. A shorter epoch size increased the number of total epochs, whereas a longer epoch size increased the low-frequency resolution of recorded signals but decreased the number of epochs in total. A 2-s-long epoch was chosen as it captured eight cycles of 4 Hz, which is the lowest tremor frequency recorded in patients, as well as providing a good number of epochs for analysis (average = 642 ± 330 epochs per condition per rat). Neural data were collated across baseline and harmaline conditions and collated data were z-score normalised to allow comparison of spectral amplitude across conditions and rats. Epochs containing data points larger than or equal to four standard deviations (SD) of the mean were rejected from further analysis to remove large amplitude artefacts (West et al., 2018).

Spectral Analysis

For analysis of EMG, accelerometer, and LFP oscillations at the tremor frequency, fast Fourier transforms (FFT) were applied to each 2-s epoch (2,000 data points per epoch). Accelerometer amplitude ratio was defined as the signal amplitude within the tremor frequency range (9–15 Hz) divided by the total amplitude in the low-frequency range (0–15 Hz), calculated for each epoch as follows:

$$Amplitude\ ratio = \frac{\sum Sxx\,(9-15Hz\ bins)}{\sum Sxx\,(0-15Hz\ bins)} \quad (2)$$

Here *Sxx* represents the absolute magnitude obtained from the FFT. Similar methods have been previously employed to examine changes in the distribution of power at tremor-specific frequencies (Iseri et al., 2011). Signal frequency coherence was computed by examining the magnitude-squared coherence (*Cxy*) for each epoch using the "mscohere" function in MATLAB:

$$Cxy = \frac{|Pxy\,(f)|^2}{Pxx\,(f)\,Pyy\,(f)} \quad (3)$$

Here *Cxy* represents coherence, *Pxy* represents the cross-spectrum of the two signals and *Pxx* and *Pyy* represent the separate amplitude spectrum of the two signals.

In order to account for levels of coherence solely due to chance, we used a surrogate corrected version of the coherence. We focused on coherence in the tremor frequency band by averaging coherence values in the interval 9–15 Hz. Next, for each epoch, 99 surrogate datasets were generated using the iterative amplitude adjusted fast Fourier transform algorithm (IAAFFT) using MATLAB (Venema et al., 2016). Coherence was computed on each of the 99 surrogate epochs, and the statistical significance of coherence was examined by comparing mean coherence at the tremor frequency (9–15 Hz) for each recorded epoch against the mean coherence at 9–15 Hz for the 99 surrogate epochs. Finally, surrogate-corrected mean coherence values, C, were calculated as Rummel et al. (2010):

$$C = \frac{P - P\,(surr)}{1 - P\,(surr)} S \quad (4)$$

Here *P* represents the mean coherence coefficient across the tremor frequency coherence bins (9–15 Hz) of the real data, and *P* (surr) represents the mean coherence at the tremor frequency across 99 surrogate epochs. If *P* is greater than *P* (surr), then the null hypothesis that the two signals are independent can be rejected, and S takes a value of 1. Else, the null cannot be rejected, S takes the value of 0.

Cross-Correlations

Time-lagged relationships between LFP recorded from each brain region, as well as with EMG, were calculated using cross-correlation analysis. Data were first band-pass filtered at the tremor frequency range (9–15 Hz) before dividing into epochs as described above. Epochs recorded during harmaline conditions when the rat was categorised as "moving" were selected for further analysis. Cross-correlations were calculated using the "xcorr" function in MATLAB. Time-lags showing maximum correlation coefficients were pooled across epochs, and the normalised probability of maximum cross-correlation at binned time-lags was calculated (±100 ms lags with a 2 ms bin width). Peak probability was calculated as the summed probability at the highest bin and the two adjacent probability bins (i.e., the sum at the peak). Peak probabilities that surpassed a threshold value of 0.1 were included within summary statistics examining time-lagged relationships between tremor signals recorded across the network.

Changes in Coherence Across the Neural Network

To examine changes in coherence across the recorded neural network, statistical analyses compared the area under the mean coherence curve at the tremor frequency (9–15 Hz) between the recorded and surrogate datasets using one-tailed paired *t*-tests. Holm-Bonferroni adjusted p-values were applied to control for multiple coherence comparisons per condition.

Multilevel Regression Models

Multilevel regression models were fit using MLwiN (v3.05, Centre for Multilevel Modelling, University of Bristol, UK), to investigate the impact of harmaline on LFP amplitude at the tremor frequency and the impact of movement on LFP coherence at the tremor frequency in the harmaline treated rat. Models were specified with the amplitude ratio or surrogate-corrected mean coherence at 9–15 Hz as the response variable, with responses for each epoch (level 1) nested under each rat (level 2). A null model (no explanatory variables) was compared to a random intercepts model which specified a dichotomous explanatory variable for harmaline (harmaline vs. baseline) or movement (movement vs. resting). The random intercepts model was then compared to a random slopes model, which allows the relationship (i.e., slope) between the explanatory and response variables to vary across rats. The inclusion of this level 2 variation can provide a more accurate estimate of the standard error when random-slope variation is present (Bell et al., 2019).

Models are presented in equations 5–7 below, where y_{ij} is the response variable for rat j at sampled epoch i. The null model estimates the grand mean of the y, represented by β_0, and the variability in the grand mean across rats, u_{0j}, and sampled epochs e_{ij}. Model 2 and 3 additionally includes a regression coefficient β_1 for the dummy coded explanatory variable, $x, \{0, 1\}$. The regression coefficient for the intercept β_{0ij} represents the reference group, which is either the control condition when harmaline is included as the explanatory variable, x, or resting when movement is included as the explanatory variable, x. If the random intercepts models provided a significantly better fit than the null, the random intercepts model (model 2) was then statistically compared to the random slopes model (model 3).

$$\begin{aligned} \text{Model 1: Null} \quad & \text{Level 1:} \quad y_{ij} = \beta_{0ij} \\ & \text{Level 2:} \quad \beta_{0ij} = \beta_0 + u_{0j} + e_{ij} \end{aligned} \tag{5}$$

$$\begin{aligned} \text{Model 2: Random intercepts} \quad & \text{Level 1:} \quad y_{ij} = \beta_{0ij} + \beta_1 x_{ij} \\ & \text{Level 2:} \quad \beta_{0ij} = \beta_0 + u_{0j} + e_{ij} \end{aligned} \tag{6}$$

$$\begin{aligned} \text{Model 3: Random slopes} \quad & \text{Level 1:} \quad y_{ij} = \beta_{0ij} + \beta_{1j} x_{ij} \\ & \text{Level 2:} \quad \beta_{0ij} = \beta_0 + u_{0j} + e_{ij} \\ & \qquad\quad \beta_{1j} = \beta_1 + u_{1j} \end{aligned} \tag{7}$$

If diagnostic checks revealed a non-normal distribution of the residuals in the model, a generalised linear model with an approximate Poisson distribution of the response data was applied and the model was re-run (Leyland and Groenewegen, 2020). Wald chi-squared tests were applied to statistically examine the significance of the effects, testing the null hypothesis that the coefficient for the explanatory variable equals the coefficient for the baseline variable. This statistically compares the standardised regression coefficients for harmaline vs. control or for moving vs. resting.

RESULTS

Harmaline Induces a Tremor at 9–15 Hz in Awake Rats

A whole-body tremor in response to systemic harmaline administration was observed within 5–15 min of intraperitoneal injection of harmaline and lasted for up to 3 h. The tremor could be readily identified in the raw EMG and accelerometer traces (**Figures 1A,B**). Harmaline induced a tremor at 9–15 Hz with a peak at 11 Hz, as shown in the EMG and accelerometer amplitude spectrum (shaded grey region; **Figures 1C,D**), where the peak tremor frequency remained relatively stable over time (**Supplementary Figure 1**). A Wald chi-square test showed the estimated coefficients for EMG and accelerometer amplitude ratio at 9–15 Hz were significantly greater for harmaline (EMG: mean = 0.36, 95% CI [0.33 0.39], Accelerometer: mean = 0.53, 95% CI [0.48 0.58]) than pre-harmaline conditions (EMG: mean = 0.24, 95% CI [0.21 0.26], $\chi^2_{(1)} = 4.385$, $p = 0.036$, $n = 7$ rats, Accelerometer: mean = 0.30, 95% CI [0.28 0.32], $\chi^2_{(1)} = 75.633$, $p < 0.001$, $n = 12$ rats; **Figures 1E,F**). These observations are in agreement with previous studies on harmaline-induced tremor in awake rodents (Pan et al., 2018, 2020).

Harmaline Induces a Change in Neural Rhythms in Cerebellar Circuits

Post-mortem histology of the recording site location confirmed that from a total of 14 animals, five animals had cerebellar tetrode recording sites located in the medial cerebellar nucleus, five animals had tetrode recording sites located within the vermal cerebellar cortex and four animals had tetrode recording sites located in both the medial cerebellar nucleus and the vermal cerebellar cortex (**Figures 2A–C**). The LFP recorded from the cerebellar cortex and cerebellar nuclei across rats during pre-harmaline and harmaline conditions are shown in **Figures 2D,E**. An increase in rhythmic activity in the tremor frequency range (9–15 Hz; peak 11 Hz, shaded grey region) was seen in both the cerebellar cortex and medial cerebellar nucleus during harmaline compared to the pre-harmaline condition (**Figures 2F,G**). Smaller amplitude harmonic oscillations are also present at twice the tremor frequency (∼23 Hz). Quantitatively, harmaline significantly increased the LFP amplitude ratio at 9–15 Hz in the cerebellar cortex and in the medial cerebellar nuclei (**Figures 2H,I**, cerebellar cortex: mean = 0.35, 95% CI [0.30 0.39], medial cerebellar nuclei: mean = 0.27, 95% CI [0.24 0.29]) compared to the control condition (cerebellar cortex: mean = 0.22, SE = 0.01, $\chi^2_{(1)} = 32.14$, $p < 0.01$, $n = 9$ rats, medial cerebellar nuclei: mean = 0.23, 95% CI [0.22 0.24], $\chi^2_{(1)} = 8.32$, $p = 0.004$, $n = 8$). One rat was excluded from the medial cerebellar nuclei analysis as the mean LFP amplitude for harmaline was

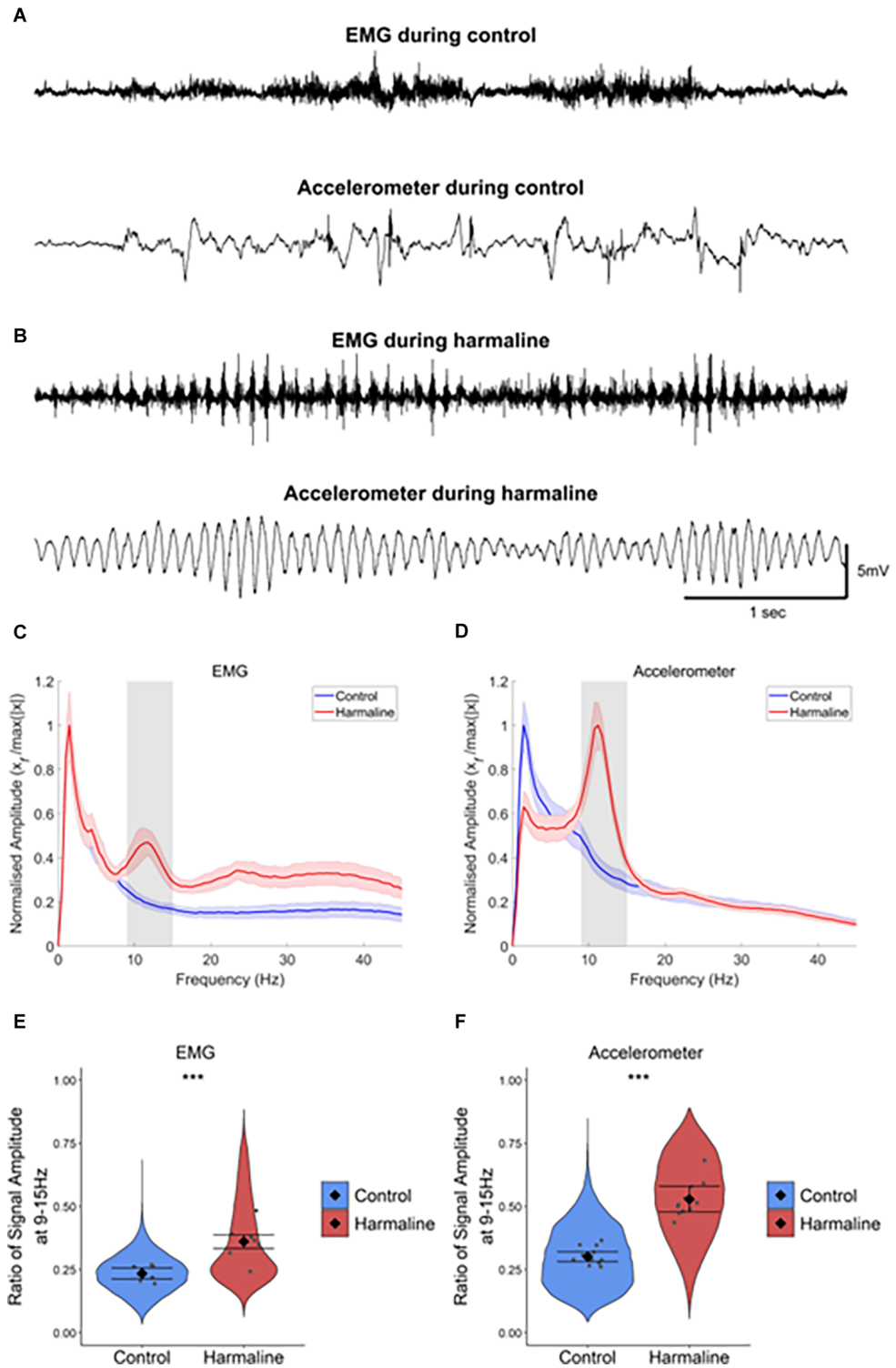

FIGURE 1 | Harmaline induces a 9–15 Hz tremor. **(A,B)** Representative example EMG and accelerometer recording from a rat during **(A)** control and **(B)** harmaline. The upper trace is EMG, and the lower trace is accelerometer. **(C,D)** Mean (±SE) amplitude spectrum for **(C)** EMG (n = 7 rats) and **(D)** accelerometer (n = 12 rats) during control and harmaline. The solid line represents mean amplitude, and the coloured shaded areas represent SE. The grey area represents the tremor frequency (9–15 Hz). **(E,F)** Ratio of amplitude at the tremor peak for **(E)** EMG and **(F)** accelerometer, where the violin plots show the distribution of this ratio across all epochs (pooled across rats). Individual grey data points represent the mean per rat. Fixed effects parameter estimates (±CI) representing predicted mean estimates are shown by ♦ and corresponding error bars. *** indicates $p < 0.001$.

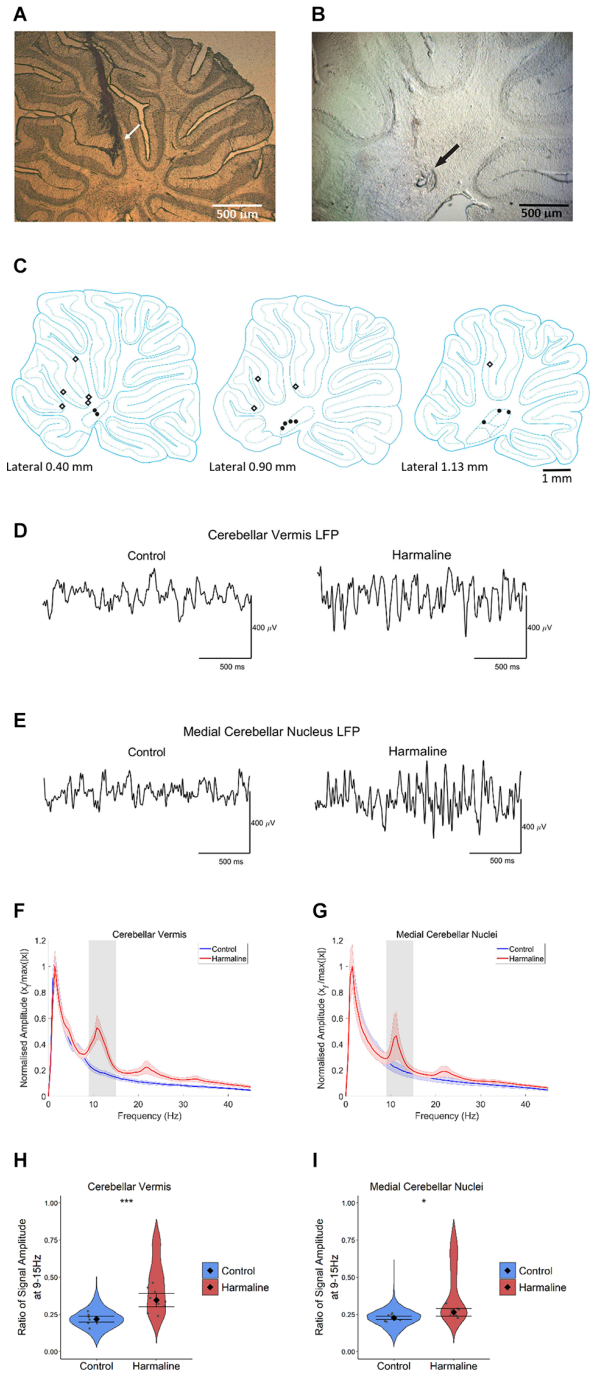

FIGURE 2 | Harmaline increases oscillatory activity in the cerebellum at the tremor frequency. **(A,B)** Examples of sagittal cerebellar sections with tetrode tracts in the **(A)** cerebellar vermis and **(B)** medial cerebellar nuclei from two different rats. Arrows indicate the approximate positions of the tetrode tips. **(C)** Summary diagram illustrating approximate electrode positions on sagittal sections of the cerebellum (adapted from Paxinos and Watson, 2005). Black dots represent approximate electrode positioning per rat in the medial cerebellar nuclei, and diamond symbols represent approximate electrode positions per rat in the cerebellar cortex. **(D,E)** Representative LFP traces from **(D)** cerebellar vermis and **(E)** medial cerebellar nuclei during pre-harmaline control and harmaline. **(F,G)** Mean (±SE) amplitude spectrum for **(F)** cerebellar vermis (n = 9) and **(G)** medial cerebellar nuclei (n = 9) during control and harmaline. The solid line represents mean amplitude, and the coloured shaded areas represent SE. The grey area represents the tremor frequency. **(H,I)** Ratio of amplitude at the tremor peak for **(H)** cerebellar vermis (n = 9) and **(I)** medial cerebellar nuclei (n = 8), where the violin plots show the distribution of this ratio across all epochs (pooled across rats). Individual grey points represent the mean per rat. Fixed effects parameter estimates (±CI) representing predicted mean estimates are shown by ♦ and corresponding error bars. *** indicates $p < 0.001$, and * indicates $p < 0.05$ **(E,F)**.

greater than two standard deviations of the group mean. Taken together these results suggest that harmaline induces tremor frequency (9–15 Hz) oscillations in the vermal cortex and medial cerebellar nuclei.

Harmaline Was Not Found to Significantly Increase the Amplitude of Tremor Rhythms in Thalamocortical Circuits

To examine the impact of harmaline on neural activity in thalamocortical circuits, the amplitude spectrum of LFP recorded from the motor region of the thalamus and subdural EEG (**Figures 3C,D**) recorded over the sensorimotor cortex were assessed. In a total of 10 animals, histological identification of tetrode tracks (**Figures 3A,B**) indicated that recordings were located within the VL/VA complex of the thalamus, also known as the "motor thalamus", and we use this term to refer to the VL/VA thalamus complex. Prior to harmaline, a small peak in oscillatory activity at around 7 Hz was observed in both the motor thalamus and the EEG (vertical blue dotted line in **Figures 3E,F**). However, during harmaline, this 7 Hz oscillation was replaced by a smaller amplitude oscillation at 5 Hz (vertical red dotted line in **Figures 3E,F**). No distinct peaks in oscillatory activity were detected at the tremor frequency range (9–15 Hz, grey shaded regions in **Figures 3E,F**).

A Wald test revealed no significant difference in motor thalamus LFP amplitude ratio at 9–15 Hz for harmaline (mean = 0.24, 95% CI [0.22 0.25]) vs. control (mean = 0.23, 95% CI [0.21 0.24], $\chi^2_{(1)} = 0.84$, $p = 0.359$, $n = 9$; **Figure 3G**). However, there was a small but significant decrease in EEG amplitude ratio at 9–15 Hz during harmaline (mean = 0.25, 95% CI [0.23 0.26]) compared to the pre-harmaline condition (mean = 0.26, 95% CI [0.25 0.27]), ($\chi^2_{(1)} = 3.85$, $p = 0.05$, $n = 9$; **Figure 3H**). These findings illustrate a change in the rhythmicity of thalamocortical activity during harmaline vs. control conditions, where there is a shift from 7 Hz to 5 Hz.

Harmaline-Induced Tremor Amplitude Is Modulated by Movement

As harmaline tremor is reported to be an action tremor that resembles ET (Pan et al., 2018, 2020), it is of interest to examine how activity and interactions within the tremor-related neural network are modulated by movement. To examine whether harmaline-induced tremor changes in severity during movement, accelerometer activity was compared during periods of movement vs. resting, which was defined by total acceleration falling above or below a threshold of 1 m/s^2, respectively, for

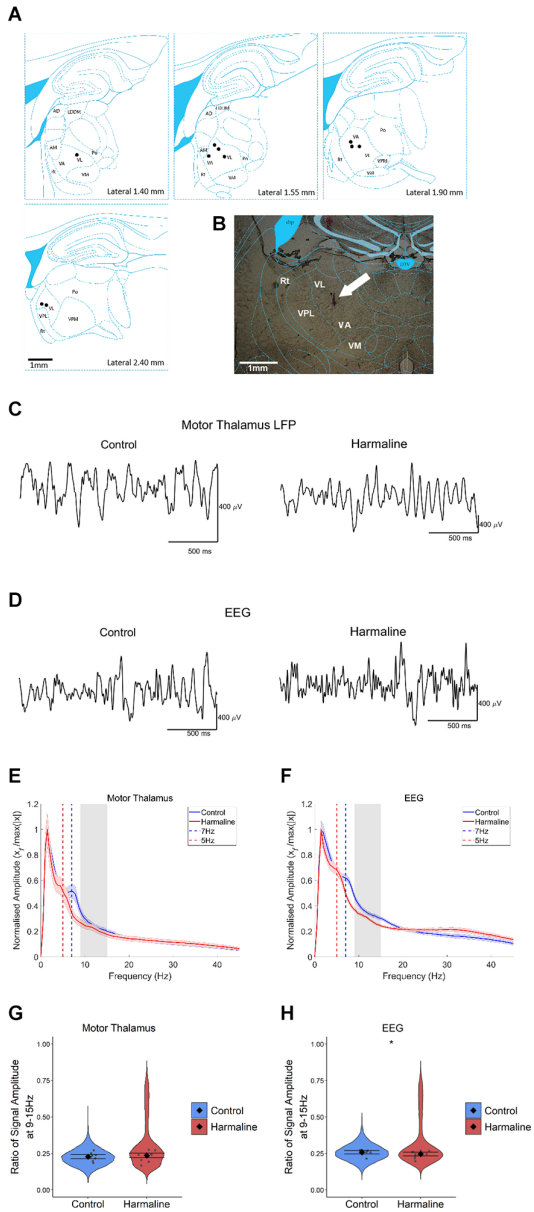

FIGURE 3 | The amplitude of oscillations at the tremor frequency in the thalamocortical circuits. **(A)** Summary diagram illustrating approximate electrode positions on sagittal sections of the thalamus (adapted from Paxinos and Watson, 2005), where each black dot represents the approximate electrode positioning per rat and the VA/VL complex of the thalamus (i.e., motor thalamus). **(B)** Example coronal section from one rat with electrode approximately located in the VA/VL complex of the thalamus. The arrow indicates the approximate position of the tetrode tip. **(C,D)** Representative LFP traces from **(C)** motor thalamus and **(E)** EEG during pre-harmaline control and harmaline. **(E,F)** Mean (±SE) amplitude spectrum for **(E)** motor thalamus (n = 9 rats) and **(F)** EEG (n = 9 rats) during control and harmaline. The solid line represents mean amplitude, and the coloured shaded areas represent SE. The grey area represents the tremor frequency. **(G,H)** Ratio of amplitude at the tremor peak for **(G)** motor thalamus and **(H)** EEG, where the violin plots show the distribution of this ratio across all epochs (pooled across rats). Individual grey points represent the mean per rat. Fixed effects parameter estimates (±CI) representing predicted mean estimates are shown by ♦ and corresponding error bars. * indicates $p < 0.05$.

the entire epoch duration (**Figure 4A**). In both behavioural states, the accelerometer spectrum has a distinct peak at the tremor frequency range (9–15 Hz, grey banded section of each panel (**Figure 4B**). A Wald test showed that total accelerometer amplitude at the tremor frequency was significantly greater during movement (mean = 2.35, 95% CI [2.07 2.62]) than during rest (mean = 0.51, 95% CI [0.39 0.63], $\chi^2_{(1)} = 166.42$, $p < 0.001$, $n = 12$; **Figure 4C**).

Figure 4B also illustrates that across the entire spectrum (<45 Hz) accelerometer amplitude was greater during movement than during rest. To ensure that the difference in tremor frequency amplitude between resting and moving was not related to the generalised increase in accelerometer amplitude during movement, the amplitude ratio at the tremor frequency was also examined (see "Methods" Section) to compare the relative amplitude of oscillations at 9–15 Hz (**Figure 4D**). This revealed a significant increase in the ratio of accelerometer tremor frequency amplitude for rest (mean = 0.57, 95% CI [0.054 0.61]) compared to movement (mean = 0.46, 95% CI [0.42 0.50], $\chi^2_{(1)} = 31.66$, $p < 0.001$, $n = 12$; **Figure 4E**), indicating that the increase in total accelerometer amplitude during movement was not specific to the tremor frequency range.

In summary, these results, therefore, suggest that harmaline-induced tremor is present when rats are at rest and also during movement, but the amplitude of rhythmic activity across the frequency spectrum studied (0–45 Hz) increases significantly with movement. This corresponds with the visual inspection of tremor, where a low amplitude tremor was visible during resting, but the tremor became much more pronounced when the rat moved around the cage.

In addition to harmaline producing a significant action tremor in rats, general ataxia was also observed 5–15 min following the intraperitoneal injection and could last for up to 3 h. This included a loss of coordination, an unsteady gait, and an increased spreading of the paws and foot slips during walking. There was also an absence of rearing and an increase in occurrences where the rat was lying down or leaning on the side of the cage. However, when the percentage of time rats spent actively moving vs. being quietly at rest was compared there was no statistically significant difference between pre-harmaline (median = 62.0%) and harmaline (median = 59.6%, $z = -0.408$, $p = 0.683$, $r = -0.109$, $n = 14$ rats). This suggests that harmaline has little or no effect on overall activity levels in rats (**Figure 4F**). However, rats' movements were, significantly slower (on average by 28%) during harmaline [mean = 2.79 m/s^2, SD = 0.28] in comparison to control conditions [mean = 3.87 m/s^2, SD = 0.38, $t_{(13)} = 9.883$, $p < 0.001$, $n = 14$ rats; **Figure 4G**].

Harmaline-Induced Changes in Coherence During Movement and Rest

To examine the degree to which neural oscillations across the cerebello-thalamo-cortical network correlate with harmaline-induced behavioural tremor, coherence between the neural activity recorded from each of the three brain regions under investigation and tremor activity measured *via* the accelerometer were assessed during rest and movement following harmaline administration.

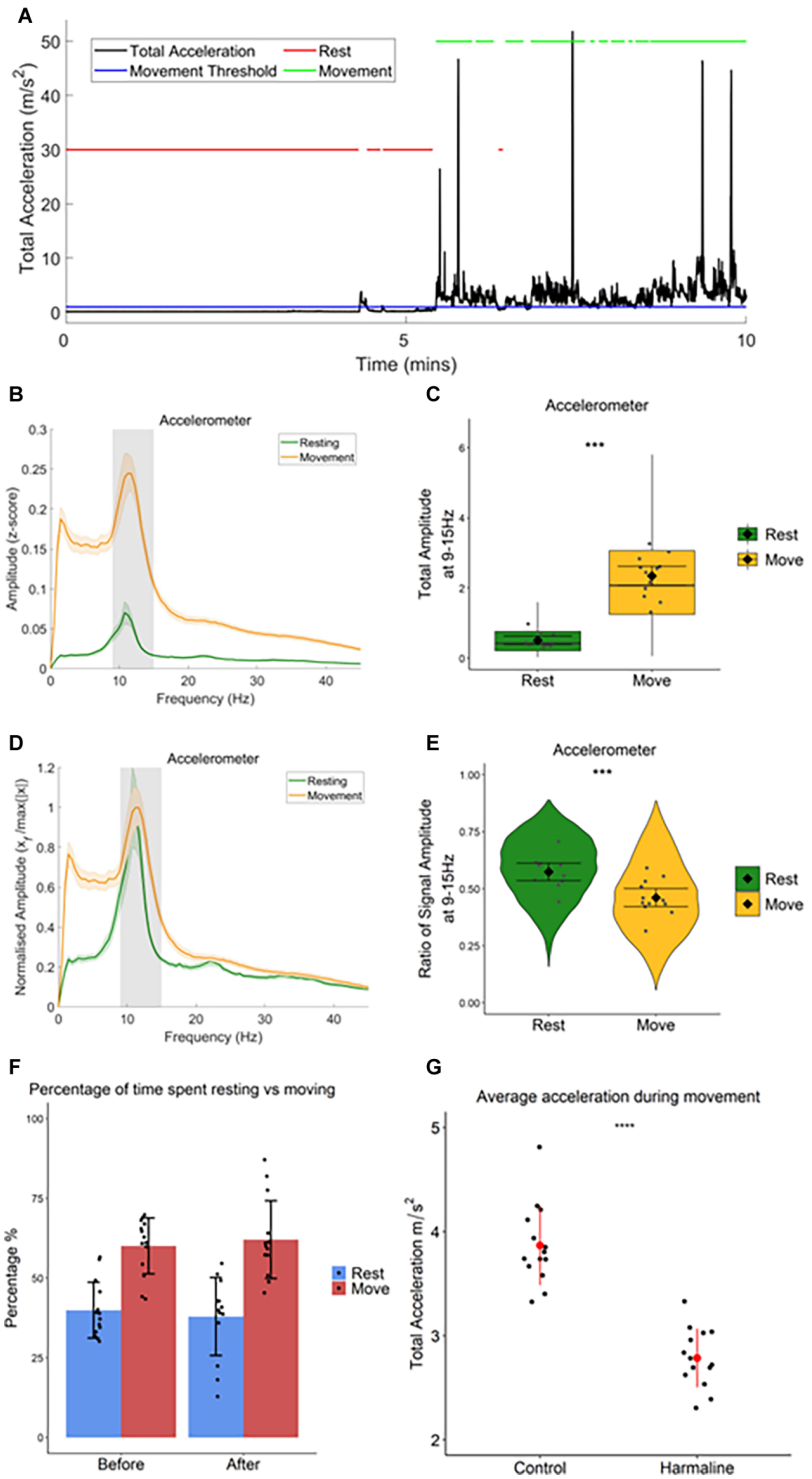

FIGURE 4 | Total amplitude of harmaline-induced tremor increases with movement. **(A)** Movement threshold (1 ms^{-2}; blue horizontal line) applied to total acceleration data (black) to distinguish periods of rest and movement. Red lines demonstrate time points categorised as "rest", and green lines demonstrate time points categorised as "movement". **(B)** Total (±SE) and **(D)** relative (±SE) amplitude accelerometer spectrum (n = 12 rats) during rest and movement. The solid line represents the mean, and the coloured shaded areas represent SE. The grey area represents the tremor frequency. **(C)** Total accelerometer amplitude and **(E)** ratio of accelerometer amplitude at the tremor peak, across all epochs (pooled across rats). Individual grey points represent the mean per rat. Fixed effects parameter estimates (±CI) representing predicted mean estimates are shown by ♦ and corresponding error bars. *** indicates $p < 0.001$. **(F)** Percentage of time spent resting and moving during baseline (before) and harmaline conditions. Each dot represents one rat. Error bars represent ±SD. **(G)** Average total acceleration during movement before (control) and after harmaline treatment. Each dot represents one rat. Error bars represent ± SD. *** indicates $p < 0.001$.

During rest and movement, a peak in coherence between the accelerometer and the cerebellar vermis LFP (**Figure 5A**), and the accelerometer and medial cerebellar nuclear LFP (**Figure 5B**) was evident at the tremor frequency (9–15 Hz, grey shaded area). A harmonic peak in coherence at double the tremor frequency (∼23 Hz) is also evident, which is likely due to a non-sinusoidal neural oscillation at the tremor rhythm. Surrogate analysis revealed that 76.6% of epochs showed significant cerebellar vermis-kinematic coherence at 9–15 Hz in comparison to the surrogate dataset (n = 8,142 out of 10,632 epochs, which included 76.2% of epochs classified as "resting", and 77.0% of epochs classified as "moving"). The analysis also revealed that 65.0% of epochs also showed significant medial cerebellar nuclear-kinematic coherence at 9–15 Hz (n = 6,478 out of 9,963, this included 64.7% of epochs classified as "resting", and 65.0% of epochs classified as "moving"). Overall, this shows average coherence at 9–15 Hz was greater for the recorded data (**Figures 5A,B**, green and yellow lines) compared to surrogate datasets (**Figures 5A,B**, blue and purple lines).

Model coefficients for surrogate-corrected mean coherence were compared across resting and movement (**Figures 5C,D**). This revealed no difference in surrogate-corrected mean coherence at the tremor frequency across resting and movement, for either cerebellar vermis-kinematic coherence (Rest: mean = 0.20, 95% CI [0.15 0.25], Movement: mean = 0.22, 95% CI [0.10 0.34], $\chi^2_{(1)} = 0.28$, $p = 0.599$, $n = 8$) nor medial cerebellar-nuclei-kinematic coherence (Rest: log mean = −1.93, 95% CI [−1.19 −1.68], mean = 0.14, 95% CI [0.10, 0.18] Movement: log mean = −1.84, 95% CI [−1.91, −1.58], mean = 0.16, 95% CI [0.10, 0.22], $\chi^2_{(1)} = 0.16$, $p = 0.684$, $n = 7$).

Together, the surrogate analysis, therefore suggests that tremor-frequency oscillations in the cerebellar vermis and medial cerebellar nuclei are significantly correlated with kinematic measures of tremor in harmaline-treated rats for the majority of epochs (76.2% for the cerebellar cortex, 65.0% for the cerebellar nuclei). Furthermore, epochs showing statistically significant coherence are distributed equally across resting and movement, and the strength of coherence is not modulated by movement.

Equivalent analysis of the motor thalamus and EEG data also revealed a peak in coherence between the accelerometer and motor thalamic LFP (**Figure 5E**), and the accelerometer and EEG (**Figure 5F**) at the tremor frequency (9–15 Hz, grey shaded area) during rest and movement. However, the peak coherence was lower than that found for the cerebellar vermis and medial cerebellar nuclei. Broader peaks in coherence were also observed at double the tremor frequency (∼24 Hz). Surrogate analysis revealed that 54.5% of epochs showed significant motor thalamo-kinematic coherence at 9–15 Hz in comparison to the surrogate dataset (n = 5,597 out of 10,267 epochs, 49.0% of "resting" epochs, 61.8% of "moving" epochs), where average motor thalamo-kinematic coherence was greater for recorded data compared to surrogate datasets (**Figure 5E**). Comparison of surrogate-corrected mean coherence coefficients also revealed a significant increase in tremor frequency coherence for movement (log mean = −1.93, 95% CI [−2.25, −1.29], mean = 0.15, 95% CI [0.11, 0.28]) compared to resting (log mean = −2.41, 95% CI [−2.53, −2.30], mean = 0.09, 95% CI [0.08, 0.10], $\chi^2_{(1)} = 28.07$, $p < 0.001$, $n = 8$; **Figure 5G**). Surrogate analysis also showed 52.3% of epochs showed significant EEG-kinematic coherence at 9–15 Hz in comparison to the surrogate dataset (n = 6,402 out of 12,249 epochs, 50.82% of "resting" epochs, 54.0% of "moving" epochs). However, there was no significant difference in surrogate-corrected mean coherence coefficients at the tremor frequency for movement (log mean = −2.26, 95% CI [−2.29, −1.97], mean = 0.10, 95% CI [0.09, 0.12]) vs. resting epochs (log mean = −2.382, 95% CI [−2.52, −2.24], mean = 0.09, 95% CI [0.08, 0.10]), $\chi^2_{(1)} = 2.47$, $p = 0.116$, $n = 9$; **Figure 5H**).

A similar pattern was seen when examining average coherence values at the tremor frequency for medial cerebellar nuclei-thalamic and motor thalamus-EEG coherence (**Figures 6** and **7**). A peak in medial cerebellar nucleo-motor thalamic coherence was observed at the tremor frequency (**Figure 6A**), with coherence at this frequency greater for recorded data compared to surrogate datasets during movement only, and not during rest (**Figures 6C,D**). A total of 47.3% of epochs showed significant medial cerebellar nucleo-motor thalamic coherence at 9–15 Hz in comparison to the surrogate dataset (n = 3,635 out of 7,681 epochs, 44.7% of "resting" epochs, 49.2% of "moving" epochs). There was also a significant increase in surrogate-corrected medial cerebellar nucleo-motor thalamic coherence for movement (log mean = −2.31, 95% CI [−2.36, −1.74], mean = 0.10, 95% CI [0.08, 0.13]) compared to resting (log mean = −2.58, 95% CI [−2.77, −2.39], mean = 0.08, 95% CI [0.07, 0.08], $\chi^2_{(1)} = 5.79$, $p = 0.016$, $n = 6$; **Figure 6B**). In addition to the peak in medial cerebellar nucleo-motor thalamic coherence at the tremor frequency, a small peak was also observed at approximately half the tremor frequency during movement (grey and green dotted lines, **Figure 6D**). During the control condition, a peak in medial cerebellar nucleo-motor thalamic coherence was observed at ∼8 Hz, during movement only (green vertical dotted line; **Figure 6F**) and not during rest (**Figure 6E**), which may reflect an intrinsic movement-related oscillation.

When examining motor thalamus-EEG coherence, a small peak in coherence was also found at the tremor frequency range (9–15 Hz; **Figure 7A**, grey dotted line **Figures 7C,D**), where coherence was greater for recorded data compared to surrogate datasets. A total of 52.6% of epochs showed significant motor thalamus-EEG coherence at 9–15 Hz in comparison to the surrogate dataset (n = 5,685 out of 10,802 epochs, 52.1% of "resting" epochs, 53.1% of "moving" epochs). However, there was no significant difference in surrogate-corrected mean coherence coefficients at the tremor frequency for movement (log mean = −2.36, 95% CI [−2.62, −2.26], mean = 0.09, 95% CI [0.07, 0.11]) compared to rest (log mean = −2.28, 95% CI [−2.46, −2.10], mean = 0.10, 95% CI [0.09, 0.12], $\chi^2_{(1)} = 0.21$, $p = 0.646$, $n = 8$; **Figure 7B**). In addition to the small 9–15 Hz peak in motor thalamus-EEG coherence, a much larger peak in coherence was evident at 4.5–6 Hz, which may reflect an intrinsic thalamocortical oscillation or a sub-harmonic of the tremor frequency. This peak was more prominent during movement than rest (green dotted line, **Figures 7C,D**). To examine whether the 4.5–6 Hz oscillation

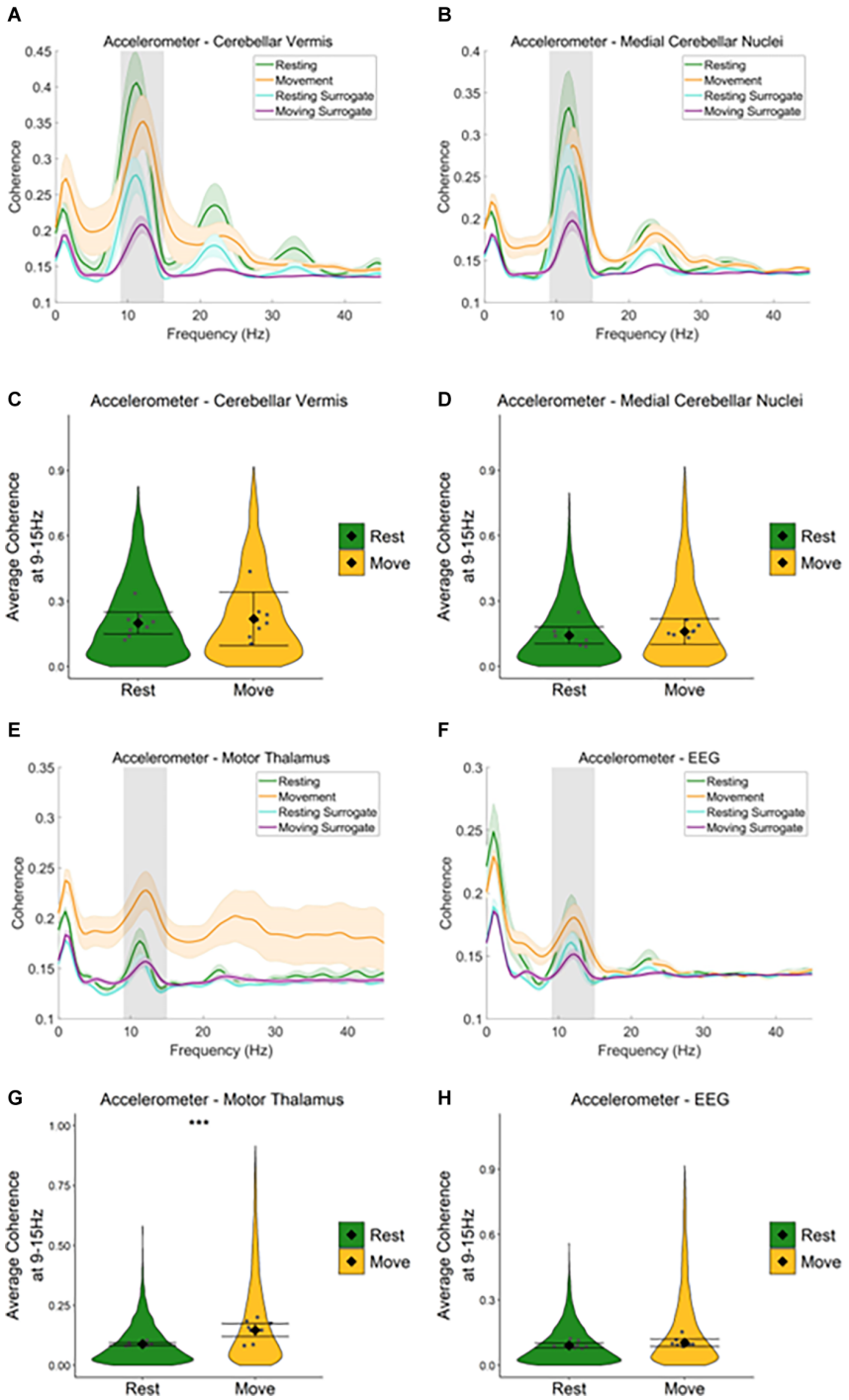

FIGURE 5 | Neural oscillations across the cerebello-thalamo-cortical network correlate with harmaline-induced behavioural tremor. **(A,B)** Mean (±SE) **(A)** cerebellar cortex-kinematic (n = 8 rats), **(B)** cerebellar nuclei-kinematic (n = 7 rats) during resting and movement for real and surrogate datasets. The solid line represents mean coherence, and the coloured shaded areas represent SE. The grey area represents the tremor frequency. **(C,D)** Average surrogate-corrected **(C)** cerebellar cortex-kinematic, **(D)** cerebellar nuclei-kinematic coherence at the tremor peak across all epochs with significant coherence (pooled across rats). Individual grey points represent the mean per rat. Fixed effects parameter estimates (±CI) representing predicted mean estimates are shown by ♦ and corresponding error bars. *** indicates $p < 0.001$ **(E)** thalamic-kinematic ((textitn = 8 rats), and **(F)** cortico-kinematic (textitn = 6 rats) coherence during resting and movement for real and surrogate datasets. The solid line represents mean coherence, and the coloured shaded areas represent SE. The grey area represents the tremor frequency. **(G,H)** Average surrogate-corrected **(G)** thalamic-kinematic and (H) cortico-kinematic coherence at the tremor peak across all epochs with significant coherence (pooled across rats). Individual grey points represent the mean per rat. Fixed effects parameter estimates (±CI) representing predicted mean estimates are shown by ♦ and corresponding error bars. *** indicates $p < 0.001$.

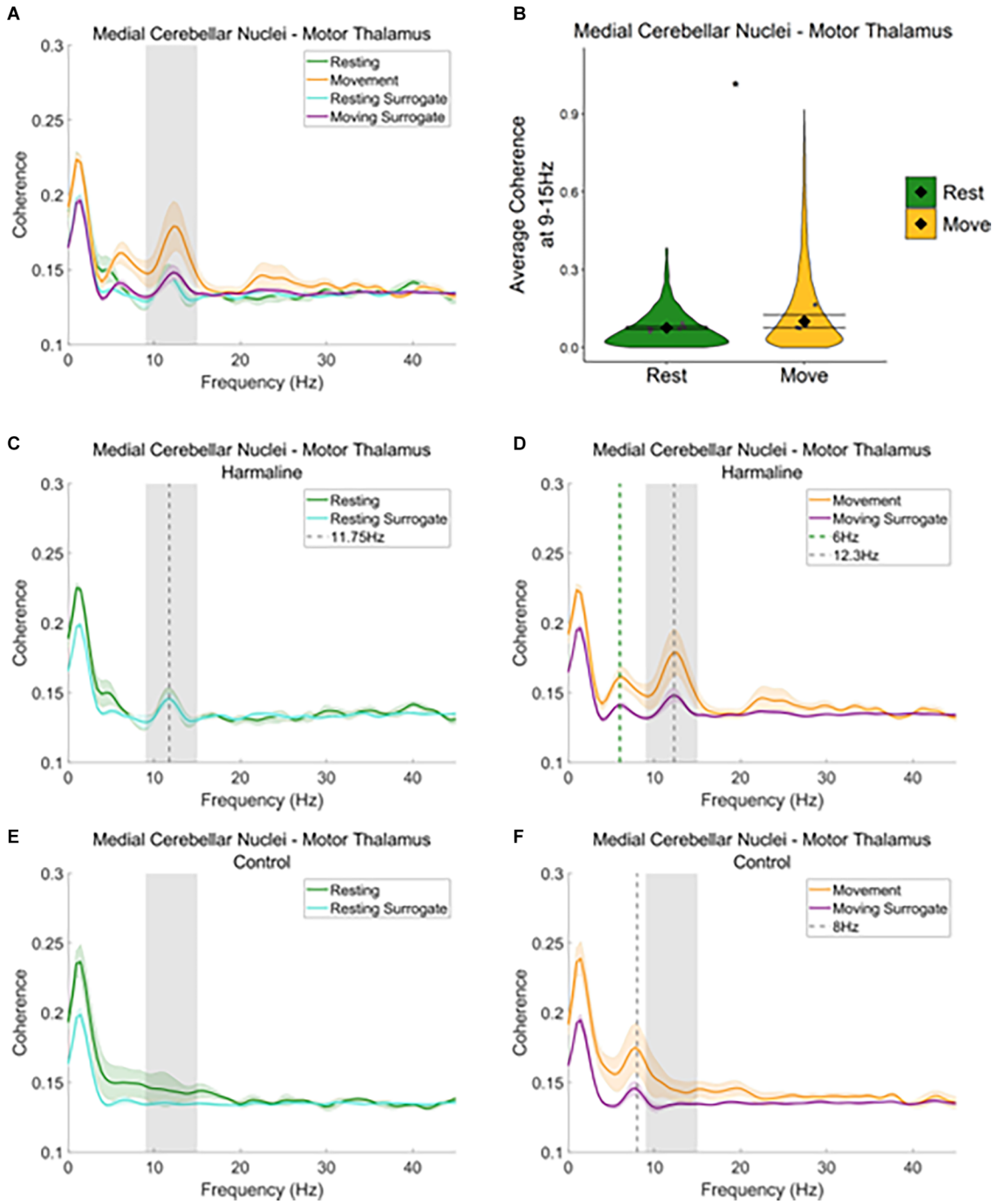

FIGURE 6 | Cerebello-thalamic coherence in the harmaline model. **(A)** Mean (±SE) **(A)** cerebellar nuclei-thalamic (n = 6) coherence during resting and movement for real and surrogate datasets. The solid line represents mean coherence, and the coloured shaded areas represent SE. The grey area represents the tremor frequency. **(B)** Average surrogate-corrected cerebellar nuclei-thalamic coherence at the tremor peak across all epochs with significant coherence (pooled across rats). Individual grey points represent the mean per rat. Fixed effects parameter estimates (±CI) representing predicted mean estimates are shown by ♦ and corresponding error bars. * indicates $p < 0.05$. **(C–F)** Mean (±SE) cerebellar nuclei-thalamic (n = 6); coherence in harmaline model **(C,D)** and control **(E,F)** during resting **(C,E)** and movement **(D,F)** for real and surrogate datasets. The solid line represents mean coherence, and the coloured shaded areas represent SE. The grey area represents the tremor frequency.

was related to harmaline-induced tremor, or an intrinsic thalamocortical oscillation, thalamocortical coherence during baseline control conditions for both movement and rest was also inspected (**Figures 7E,F**). During the control condition, a peak in motor thalamus-EEG coherence was observed at ∼8 Hz, where coherence at this frequency is greater during

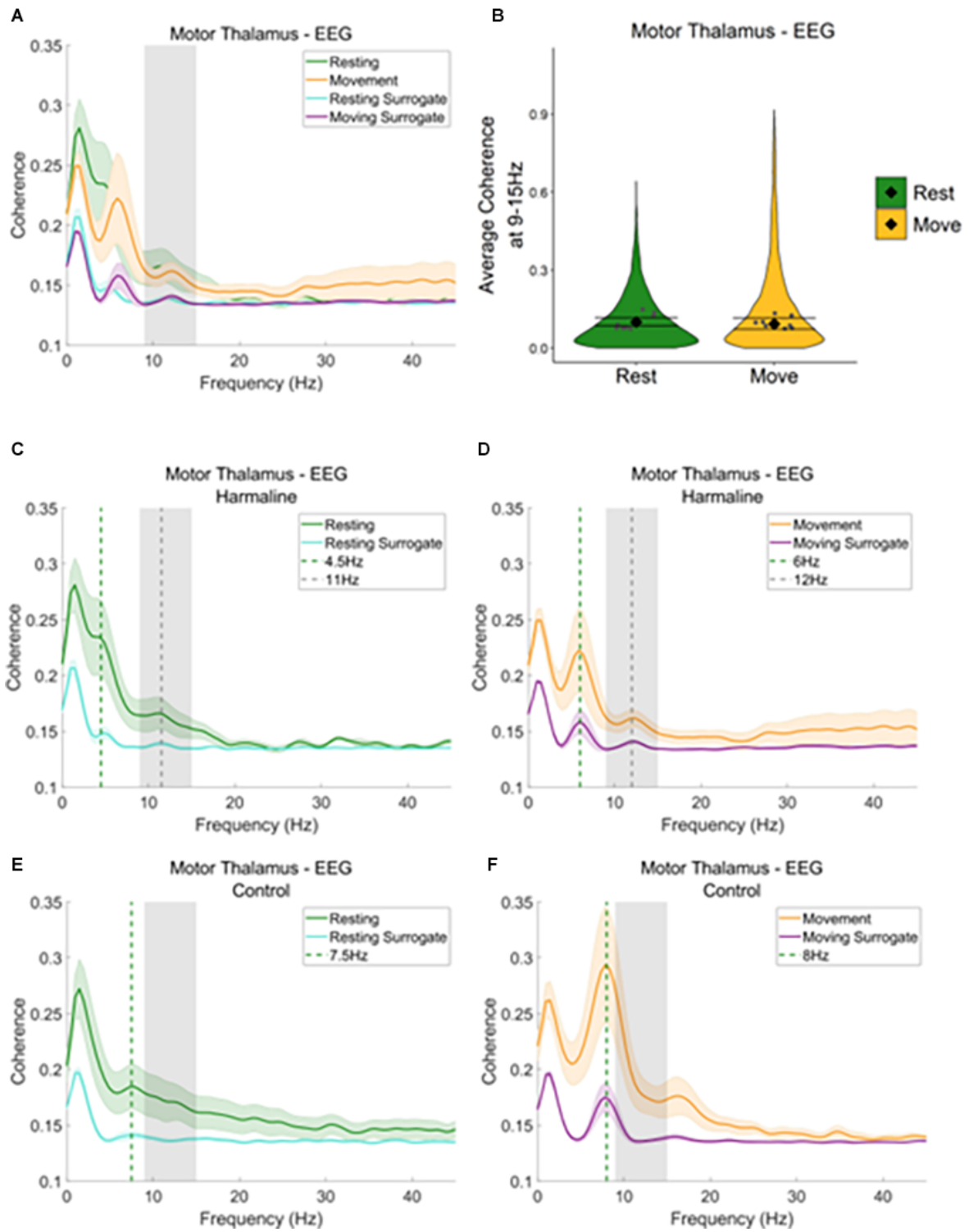

FIGURE 7 | Thalamocortical coherence in the harmaline model. **(A)** Mean (±SE) thalamocortical coherence (n = 8) during resting and movement for real and surrogate datasets. The solid line represents mean coherence, and the coloured shaded areas represent SE. The grey area represents the tremor frequency. **(B)** Average surrogate-corrected thalamocortical coherence at the tremor peak across all epochs with significant coherence (pooled across rats). Individual grey points represent mean per rat. Fixed effects parameter estimates (±CI) representing predicted mean estimates are shown by ♦ and corresponding error bars. **(C–F)** Mean (±SE) thalamocortical coherence (n = 8); coherence in harmaline model **(C,D)** and control **(E,F)** during resting **(C,E)** and movement **(D,F)** for real and surrogate datasets. The solid line represents mean coherence, and the coloured shaded areas represent SE. The grey area represents the tremor frequency.

movement than rest (green vertical dotted line; **Figures 7E,F**). This suggests the presence of an intrinsic thalamo-cortical oscillation at ∼8 Hz during control conditions, which is modulated by motor activity. During harmaline tremor, the frequency of this oscillation shifts to ∼4.5–6 Hz (**Figure 7D**; green vertical dotted line), which could be an intrinsic thalamocortical oscillation or reflect a sub-harmonic of the tremor frequency.

In sum, these findings illustrate significant motor thalamo-kinematic coherence at the tremor frequency for 54.5% of epochs (**Figure 5G**) that was significantly modulated by movement despite the absence of a peak in thalamic oscillatory LFP activity at the tremor frequency during harmaline conditions compared to control (**Figure 3E**). Furthermore, the strength of medial cerebellar nuclear-motor thalamic coherence was significantly modulated by movement (**Figure 6B**), even though the strength of medial cerebellar nuclear-kinematic coherence at the tremor frequency was not modulated by movement (**Figure 5D**). Significant sensorimotor EEG-kinematic coherence and motor thalamus-EEG coherence at the tremor frequency was also found, but this was not significantly modulated by movement, with evidence suggesting that harmaline can induce a change in the frequency of intrinsic thalamocortical rhythms, whereby a ∼8 Hz rhythm is shifted to 4.5–6 Hz rhythm. Together these findings suggest a role for thalamic involvement in harmaline-tremor rhythms during motor activity.

Changes in Motor Thalamic LFP During Movement

As significant motor thalamic-kinematic coherence was observed during harmaline conditions, and as this coherence significantly increased during movement vs. rest, the amplitude spectrum of motor thalamic LFP during harmaline conditions was also compared across rest and movement epochs (**Figure 8A**). A Wald test revealed no significant difference in motor thalamus LFP amplitude ratio at 9–15 Hz for rest (mean = 0.23, 95% CI [0.21 0.26]) vs. movement (mean = 0.24, 95% CI [0.18 0.29], $\chi^2_{(1)}$ = 2.66, p = 0.064, n = 9; **Figure 8B**). The lack of changes in LFP amplitude at the tremor frequency was further explored by comparing LFP amplitude during rest and movement during pre-harmaline control and harmaline conditions (**Figures 8C,D**). An oscillation at ∼7 Hz was found to be present during the pre-harmaline control condition when the rats were moving (**Figure 8D**, grey dotted line) but not when the rats were resting (**Figure 8C**, blue line). During harmaline, this ∼7 Hz oscillation during movement shifted to a ∼5 Hz oscillation (**Figure 8D**, green dotted line). A smaller peak at approximately 5 Hz could also be seen during rest for harmaline conditions (**Figure 8C**). This shift in oscillation frequencies may be due to an intrinsic 7–8 Hz movement-related oscillation which is entrained to a sub-harmonic of the tremor frequency during harmaline.

Changes in Network Coherence

To examine differences in the mean magnitude of coherence at the tremor frequency at a network level, statistical analyses were applied to compare the mean area under the coherence curve at 9–15 Hz for real and surrogate datasets (**Table 1**), and the results are summarised graphically in **Figure 9A**. During control (i.e., no harmaline) conditions, there was no statistically significant coherence in the motor network at the tremor frequency range when the rats were quietly at rest. However, motor activity under control conditions (without tremor) was associated with significant 9–15 Hz coherence between the kinematic measure and: (1) the sensorimotor cortex (EEG); (2) the medial cerebellar nuclei; and (3) the motor thalamus, as well as thalamocortical (motor thalamus-EEG) coherence. Coherence at this frequency range in the absence of tremor suggests the presence of an intrinsic movement-related neural oscillation in the motor network occurs within a similar frequency range as harmaline-induced tremor. This corresponds with data presented in **Figure 7F**, which identified a thalamocortical oscillation occurring within the theta frequency range (∼8 Hz) during movement for control (non-tremor) conditions.

Following administration of harmaline, statistically significant coherence at the tremor frequency (9–15 Hz) was evident at rest between all brain regions and the kinematic measure of tremor. However, no statistically significant tremor-related activity was present within the cerebello-thalamo-cortical pathway at rest. By comparison, during movement, statistically significant tremor-related coherence was found across the entire network. In sum, both motor activity and harmaline-induced tremor are associated with increased coherence at 9–15 Hz, but coherence across the medial cerebellar nuclear-motor thalamo-cortical pathway is dependent on the presence of tremor during active movement (**Figure 9A**).

To examine the time-lags of oscillations within the tremor network, cross-correlations were performed. Normalised probability histograms of time-lags with max cross-correlation were computed per rat (see "Methods" Section), and the time-lags with peak probability surpassing the probability threshold of 0.1 were extracted. Time lags with the maximum cross-correlation (−1 or 1) represent the time lag with the best fit between the two time-series (**Figure 9C**). This is estimated by shifting the recorded time-series from one node of the tremor network either forwards or backwards relative to another node in the network, which gives a positive or negative time-lag, respectively. Time-lags of the max-correlation are, therefore, classified as being in a positive or negative direction, which indicates whether one time-series may lead or trail the other, to examine the directionality of oscillations and estimate how long it takes for an oscillation to propagate from one region to another (**Figure 9C**). **Figure 9B** displays examples of normalised probability histograms of time-lags for different network connections in two different rats. Importantly, these histograms show clear peaks in the probability of max correlation at certain time-lags (arrows in **Figure 9B**).

The mean (±SD) time-lags for each connection within the tremor network were examined across rats summarised in **Figure 9D**). In seven out of nine rats, estimated time-lags of simultaneous cerebellar LFP-EMG recordings suggest tremor oscillations travelled from the cerebellum to the muscle

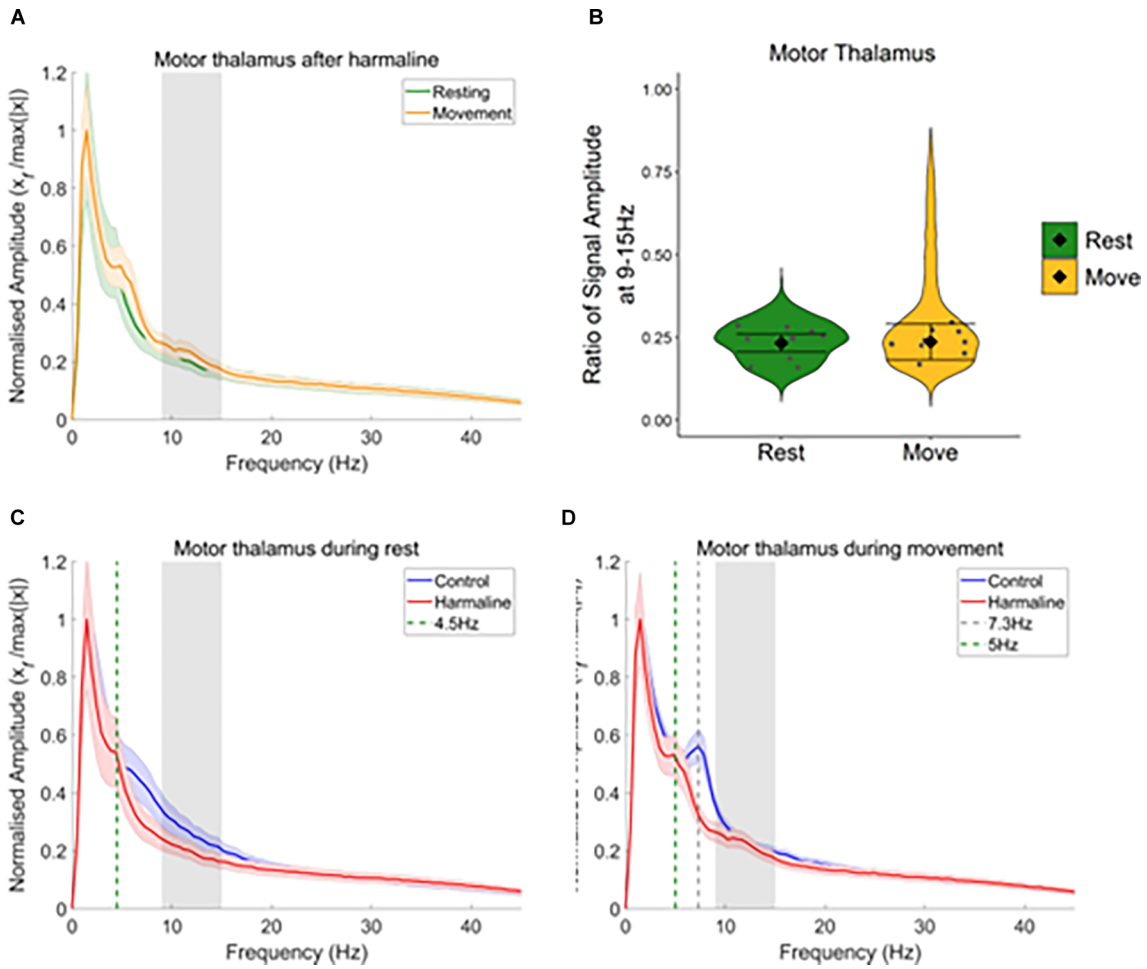

FIGURE 8 | Harmaline changes the frequency of thalamus rhythms during movement. **(A)** Mean (±SE) amplitude spectrum for the motor thalamus (n = 9) during rest and movement during harmaline. The solid line represents mean amplitude, and the coloured shaded areas represent SE. The grey area represents the tremor frequency. **(B)** Ratio of amplitude at the tremor frequency range for the motor thalamus, where the violin plots show the distribution of this ratio across all epochs. Individual grey points represent the mean per rat. Fixed effects parameter estimates (±CI) representing predicted mean estimates are shown by ♦ and corresponding error bars. **(C,D)** Mean (±SE) amplitude spectrum for the motor thalamus (n = 9) during **(C)** rest and **(D)** movement during control and harmaline. The solid line represents mean amplitude, and the coloured shaded areas represent SE. The grey area represents the tremor frequency.

TABLE 1 | Surrogate analysis of coherence at the tremor frequency (9–15 Hz).

Paired Connection	Control				Harmaline				
	During resting		During movement		During resting		During movement		
	t	*p*	*t*	*P*	*t*	*p*	*t*	*p*	*N*
Cb—Acc	2.73	0.015	2.28	0.028	5.45	<0.001*	3.86	0.003*	8
CN—Acc	1.29	0.122	3.29	0.008*	3.38	0.007*	7.80	<0.001*	7
Thal—Acc	−1.23	0.871	3.50	0.005*	2.71	0.015*	4.41	0.002*	8
EEG—Acc	0.83	0.215	7.01	<0.001*	3.37	0.005*	4.18	0.002*	9
CN—Thal	1.23	0.136	1.84	0.062	0.53	0.308	2.31	0.034*	6
Thal—EEG	2.20	0.032	3.29	0.012*	3.38	0.034	3.18	<0.001*	8

*Paired one-tailed t-tests were applied to statistically examine whether the area under the mean coherence curve at the tremor frequency was greater than the area under the mean coherence curve at the tremor frequency from surrogate datasets. N, number of rats included in analysis; Acc, Accelerometer; Cb, Cerebellar cortex; CN, Medial Cerebellar nuclei; Thal, Thalamus. *Significant following Holm-Bonferroni-adjusted p-values to control for family-wise error rate.*

(i.e., positive time-lags suggesting forward connection). Five out of seven rats showed positive time-lags between tremor oscillations recorded simultaneously from the cerebellum and motor thalamus LFP, and five out of seven rats also showed positive time-lags between tremor oscillations recorded from motor thalamus LFP and EEG. This suggests that the direction of tremor oscillations largely follows the direction of information flow within the cerebello-motor thalamo-cortical pathway.

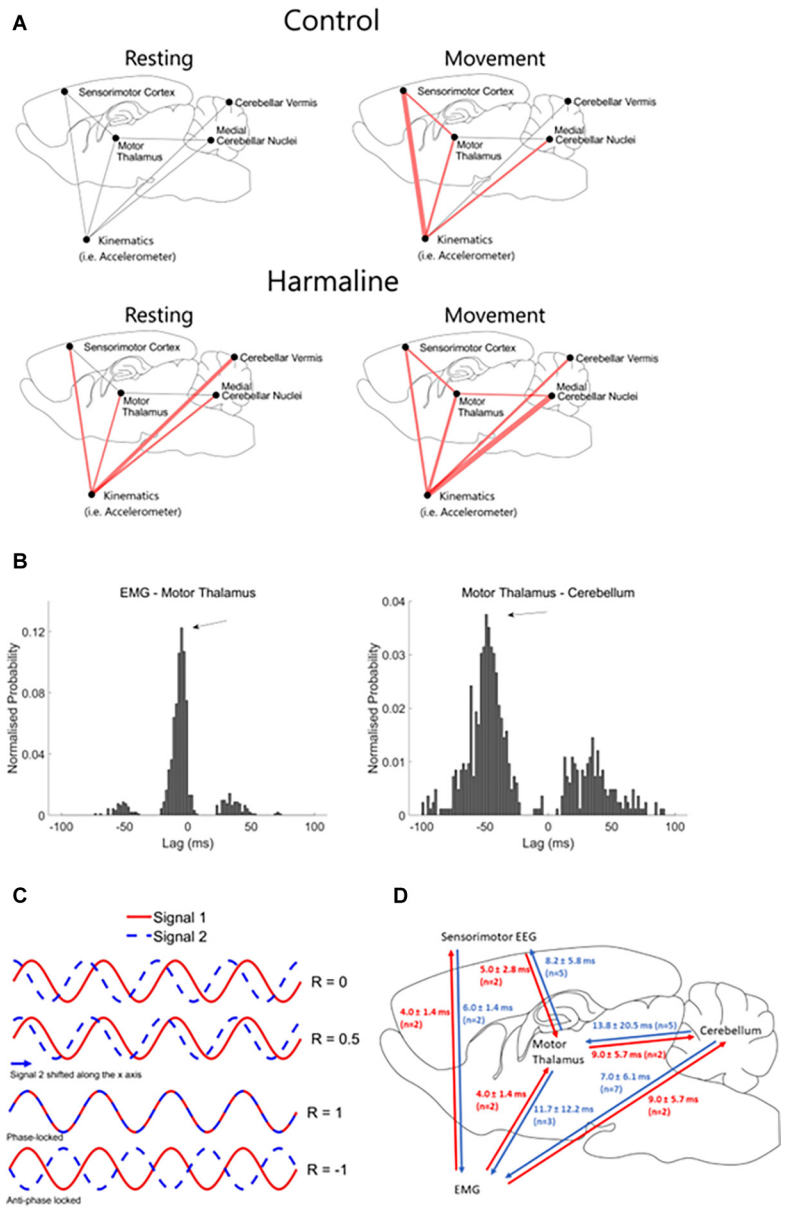

FIGURE 9 | Changes in connectivity across the medial cerebellar-motor thalamus-cortical network. **(A)** Surrogate analysis of coherence at the tremor frequency (9–15 Hz) during control (rest and move) and harmaline (rest and move). Red lines indicate significantly greater coherence at 9–15 Hz for the recorded neural data compared to the mean from 99 surrogate datasets generated using IAAFT, with Holm-Bonferroni adjusted significance levels for multiple comparisons. The width of the red line corresponds with the size of the t-statistic of the one-tailed paired *t*-tests comparing surrogate and original datasets, where the thicker the line the larger the effect-size. **(B)** Example histogram displaying the probability of time-lags (ms) with max cross-correlation across 2-s epochs taken during motor activity after harmaline administration for a single rat. Examples are from two different rats, and negative lags correspond to a backward connection between the name pairs. Arrows indicate time-lags with peak probability of max cross-correlation. **(C)** Schematic of cross-correlation at different time lags for two perfect sine waves at the same frequency. Shifting one signal (e.g., signal 2) relative to the other (e.g., signal 1) influences the correlation coefficient (R), which varies between −1 (negative correlation) and 1 (positive correlation). A perfect positive correlation is found when the signals are perfectly phase-locked (i.e., perfect alignment of the two sine waves). A perfect negative correlation between these two signals is found when signals are perfectly locked in an anti-phase direction (i.e., the peaks of signal 1 aligning with troughs of signal 2, and vice versa). **(D)** Schematic showing mean time delays of tremor frequency oscillations across each recording node in the tremor-network. N corresponds to the number of rats included in the summary statistic.

However, estimated time-lags of oscillations simultaneously recorded across the thalamus LFP-EMG and EEG-EMG, suggest a more complex combination of efferent and afferent inputs of tremor oscillations, as ∼50% of these connections showed a positive time-lag, and ∼50% showed a negative time-lag.

DISCUSSION

Our results demonstrate that harmaline-tremor in rats is associated with significant coherence across the medial cerebellar nuclear-motor thalamo-cortical network at the tremor frequency (9–15 Hz). This corresponds with electrophysiological findings from ET patients, which demonstrated that neural oscillations in the thalamus and EEG correlate with behavioural tremor (Hua et al., 1998; Schnitzler et al., 2009). Harmaline is known to increase oscillatory activation of the olivo-cerebellar pathway. Therefore, these results suggest that increased oscillatory activation of this pathway in rats is associated with similar electrophysiological correlates of tremor in ET. The experiments reported here also showed that movement is associated with significantly increased coherence of motor thalamic neural oscillations with harmaline-induced behavioural tremor. Conversely, medial cerebellar nuclear and vermal cerebellar cortex neural tremor oscillations were not modulated by movement or increased tremor amplitude.

Harmaline as a Model of ET

Previous research has qualitatively described harmaline-induced tremor as an action tremor (Placantonakis et al., 2004; Handforth, 2012), akin to the action tremor phenotype observed with ET (Bhatia et al., 2018). Our results support this observation, demonstrating that harmaline tremor significantly increases in amplitude during movement compared to rest. However, a significant harmaline-induced behavioural tremor was also present during rest/immobility. This could be attributed to either a resting tremor (i.e., a tremor occurring when muscles are completely relaxed), or to a postural tremor, as the threshold used to distinguish rest vs. movement could not differentiate between rest with and without postural muscle control of the head, body, or limbs. Harmaline would therefore seem to provide a good model of action tremor, although there are phenotypic differences from ET. This includes the tremor frequency (9–15 Hz in the harmaline rodent model, and 4–12 Hz in ET; Bhidayasiri, 2005), and the body parts affected by tremor, as harmaline induces a whole-body tremor whereas ET typically affects only the upper limbs and sometimes the head (Bhatia et al., 2018).

Our results also show that harmaline-induced tremor shares similar electrophysiological correlates to ET. Harmaline was shown to induce significant coherence of tremor frequency oscillations across the cerebello-thalamo-cortical network. Previous studies examining cerebral cortico-muscular coupling in ET patients using simultaneous EEG (or MEG) and EMG recordings, as well as direct thalamic electrophysiological recordings, suggest that ET is a disorder involving hyper-synchronous activity across the cerebello-thalamo-cortical circuit (Schnitzler et al., 2006; Muthuraman et al., 2012; Pedrosa et al., 2014). The results reported here, therefore, highlight that harmaline-induced tremor can also be characterised by increased coupling across the cerebello-thalamo-cortical network at the tremor frequency during movement, which suggests propagation of neural tremor oscillations across this pathway.

Although harmaline-induced tremor and ET show similarities in their phenotype and electrophysiological correlates, differences in the aetiology of tremor remain. Harmaline has been well-documented to produce a tremor by increasing the rhythmicity and frequency of olivo-cerebellar inputs (for a review see Handforth, 2012). However, there is little evidence for the involvement of hyper-oscillatory olivo-cerebellar activity in ET. Although there is some neuroimaging evidence indicating overactivity of portions of the brainstem, possibly reflecting the inferior olive (IO, Hallett and Dubinsky, 1993; Boecker et al., 1996), this has not been replicated in other studies (Wills et al., 1994). A post-mortem analysis also failed to reveal any detectable differences in IO cell packing density or evidence of IO neuronal damage in ET compared to controls (Louis et al., 2013). However, gross anatomical differences may not be apparent given that pathophysiological hyperactivity of the IO is thought to underlie the tremor. On the other hand, there is accumulating evidence of heterogeneous Purkinje cell-related pathologies in ET (see Section "Introduction"), indicating a clear role for cerebellar abnormalities in ET (Louis, 2016). These abnormalities may arise from a complex range of degenerative and compensatory changes in cerebellar circuits that would lead to dysregulation and/or increased oscillatory cerebellar nuclei output. This in turn could alter nucleo-olivary projections, which modulate the synchrony and timing of IO neurons (Lefler et al., 2014). Changes in cerebellar nuclei output could also lead to pathological rhythms transmitted to the cerebello-thalamo-cortical pathway, which is hypothesised to be involved in ET (Hua et al., 1998; Buijink et al., 2015). Therefore, despite the likelihood that ET develops due to a complex range of degenerative and compensatory changes in cerebellar circuits, the findings reported here show that the harmaline model provides good construct validity as it increases rhythmic cerebellar output and generates tremor correlated neural oscillations in the thalamocortical network, as well as generating an action tremor.

Overall, our findings show that harmaline-induced tremor is associated with increased oscillatory medial cerebellar nuclear output and tremor-correlated neural oscillations in the motor thalamo-cortical network. However, it is also important to note that the effect of harmaline on the central and peripheral nervous system are non-specific, and little is known about its influence on the wider nervous system. Harmaline is a mono-amine-oxidase inhibitor for group A amines, and therefore inhibits the breakdown of mono-amine neurotransmitters (e.g., noradrenaline, serotonin), which can affect multiple and distributed neural systems (Chen and Shih, 1997; Herraiz et al., 2010). Harmaline may also have acetylcholinesterase inhibitor effects (Udenfriend et al., 1958); acetylcholine receptors are widespread in the cerebellum, and some motor dysfunctions have been related to cerebellar cholinergic dysfunctions (Zhang et al., 2016). Therefore, in addition to inducing tremor *via* its effects on the olivo-cerebellar circuit, harmaline may be inducing unknown effects on the wider nervous system.

Thalamic Involvement in Tremor

Our results illustrate that harmaline was associated with significant motor thalamo-kinematic coherence at the tremor frequency, indicating thalamic oscillations correlated with behavioural tremor. This is despite a lack of harmaline-induced changes in motor thalamic LFP oscillations at the tremor frequency. Previous research has shown electrical stimulation of the VA/VL nuclei of the thalamus in harmaline-treated mice and rats significantly reduces the amplitude of harmaline-induced tremor, akin to the effects of deep brain stimulation observed in ET patients (Bekar et al., 2008; Lee and Chang, 2019). Harmaline tremor amplitude is also significantly reduced by intra-thalamic infusion of the GABA receptor agonist muscimol, suggesting inhibition of thalamic activity reduces tremor (Bekar et al., 2008). Furthermore, inactivation of adenosine A1 receptors blocked the therapeutic effect of thalamic stimulation on harmaline-treated mice, suggesting that the release of ATP and activation of adenosine A1 receptors may be key to the depression of excitatory transmission in the thalamus and reduction of tremor in response to thalamic stimulation (Bekar et al., 2008). A selective adenosine A1 receptor agonist has been shown to significantly reduce extracellular levels of glutamate in VA/VL thalamic nuclei in rats, as well as significantly reduce the amplitude of harmaline-induced tremor (Kosmowska et al., 2020). Taken together, this suggests the thalamus may play an important role in modulating the amplitude of harmaline-induced tremor in rats.

Our results also show that motor thalamo-kinematic coherence was significantly modulated by movement or increased tremor amplitude in response to movement. This is consistent with findings in ET patients which showed thalamo-muscular coherence occurred after tremor onset (Pedrosa et al., 2014), and that tremor-related rhythmic activity of neurons in the ventral thalamus was only present during tremor induced by sustained posture and not during resting (Hua and Lenz, 2005). This suggests tremor-related oscillations in the thalamus occur after the onset of action tremor, and that thalamo-muscular coherence may be a consequence of tremor rather than a driver. Functional mapping of the ventral thalamus in ET patients revealed that thalamic neurons which burst in correlation with tremor included neurons that responded to sensory input as well as neurons responding to voluntary movements (Hua and Lenz, 2005). This suggests peripheral sensory inputs may be involved in modulating or amplifying tremor-related activity in the thalamus. Therefore, increased motor thalamo-kinematic coherence during movement compared to resting may be at least partly related to sensory feedback of behavioural tremor.

By comparison, medial cerebellar nuclear-kinematic coherence and vermal cerebellar cortex-kinematic coherence were equally strong during movement and rest. As total tremor amplitude significantly increased during movement, this may suggest an extra-cerebellar source is involved in the modulation of tremor amplitude and thalamic tremor-oscillations with movement. For example, afferent feedback of behavioural tremor may amplify thalamic tremor-oscillations. Mechanoreceptors in the skin, muscle, and joints receive information on touch, vibration and proprioception, and these receptors project *via* the dorsal column medial-lemniscal pathway to the dorsal column nuclei complex (DCN), which comprises the gracile and cuneate nuclei (Loutit et al., 2021). The DCN complex in turn has excitatory projections to the ventral posterior lateral and ventral posterior medial (i.e., somatosensory) nuclei of the thalamus (Kramer et al., 2017; Uemura et al., 2020), as well as projections to the zona incerta, red nucleus, cerebellar cortex, and IO (Boivie, 1971; Robinson et al., 1987; McCurdy et al., 1998; Quy et al., 2011). Therefore, the combination of somatosensory feedback of tremor and direct cerebellar-thalamic projections may contribute to the amplification or spread of tremor oscillations in the thalamus during movement.

Harmaline Induces a Shift in Thalamocortical Oscillation Frequencies

Our findings also show a shift in neural oscillation frequencies identified within the motor thalamus LFP and EEG amplitude spectra in response to harmaline, where oscillations at ∼7 Hz in the motor thalamus LFP and EEG during pre-harmaline control conditions are shifted to oscillations at around ∼5 Hz during harmaline tremor. In addition, when examining medial cerebellar nuclear-motor thalamus coherence, and thalamocortical coherence, a peak in coherence was observed at 8 Hz during pre-harmaline control, which shifted to a peak at 4.5–6 Hz during harmaline tremor. This shift in the frequency of thalamocortical neural oscillations in response to harmaline could be due to the entrainment of intrinsic ∼7–8 Hz rhythms to a sub-harmonic of the tremor frequency, as 5–6 Hz is approximately half the tremor frequency. This would provide further support for thalamic involvement in harmaline tremor pathways and may account for the lack of changes observed in thalamic-EEG coherence at the tremor frequency, as tremor-frequency-related oscillations may instead manifest at a sub-harmonic of the tremor frequency.

We also observed a ∼7–8 Hz oscillations during pre-harmaline control conditions in motor thalamus LFP when rats were moving and not resting. A recent study by Baumel and Cohen (2021) demonstrated that a 7–8 Hz theta oscillation in the cerebellar nuclei was higher in power when the animals were moving compared to rest. Therefore, cerebellar output during movement may shape thalamic oscillations and may account for the intrinsic movement related cerebellar nuclear oscillations that we observed, although the functional relevance of this interaction is unknown.

Roles of the Cerebellum and Thalamus in Modulating Tremor

As the findings presented in this study show that thalamic but not cerebellar oscillations are associated with tremor amplitude, this may indicate that different parts of the cerebello-thalamo-cortical loop have different roles in modulating tremor. Evidence from brain stimulation studies suggests that the cerebellum may be responsible for maintaining the frequency of tremor in ET. For example, transcranial alternating currents applied over the cerebellum at the same frequency as the patient's

tremor did not affect the amplitude of the tremor but could entrain the tremor frequency, i.e., influence the phase and instantaneous frequency of the tremor (Brittain et al., 2015). Research has also shown that tremor frequency in ET is more tuned to a central frequency compared to PD, where tremor frequency can vary over a broader range (Di Biase et al., 2017). In the harmaline model, the frequency of the tremor is also tightly centred on a narrow-frequency range, and *in vivo* electrophysiological studies have shown that this frequency is paced by olivo-cerebellar rhythms (De Montigny and Lamarre, 1973; Llinás and Volkind, 1973). Taken together, this suggests that abnormalities occurring within olivo-cerebellar circuits can produce very regular pathological rhythmic oscillations that are tightly coupled with tremor frequency but are independent of behavioural state.

Comparatively, studies suggest that thalamic oscillations may be tightly coupled with tremor amplitude. For example, thalamic oscillations in the harmaline model were associated with changes in tremor amplitude with movement, and previous clinical research has shown that tremor amplitude in ET was amplified or suppressed depending on the phase of thalamic stimulation at frequencies close to the tremor frequency (Cagnan et al., 2013). Furthermore, DBS applied to the thalamus is used as a chronic treatment for ET, where high frequency (e.g., 150 Hz) stimulation is applied to disrupt or mask tremor oscillations in the thalamus (Kiss et al., 2002; Karas et al., 2013). Taken together, this may suggest abnormal tremor-related neural oscillations in the cerebellum, and possibly descending pathways from the brainstem that receive cerebellar input (e.g., rubrospinal, vestibulospinal, reticulospinal), may play an important role in the timing or pacing of tremor rhythms. However, changes in the synchronisation of thalamo-cortical oscillations to the behavioural tremor rhythm may be important for modulating the amplitude of behavioural tremor, where increased synchronisation at the tremor frequency exacerbates tremor. Sensory feedback may represent one mechanism driving the synchronisation of thalamic oscillations to the behavioural tremor during movement (Hua and Lenz, 2005; Pedrosa et al., 2014). This is counter to traditional theories of ET neural networks, which suggest that the cerebello-thalamo-cortical pathway plays a key role in peripheral tremor (Manto, 2008; Buijink et al., 2015; Muthuraman et al., 2018). However, the findings reported here demonstrated that coherence between the motor thalamus and tremor was modulated by movement, whereas coherence between the cerebellum (medial cerebellar nuclei and cerebellar vermis) and tremor was not, and suggests that whilst the frequency of the tremor may be governed by the cerebellum, thalamic oscillations relate to the amplitude of the behavioural tremor.

DATA AVAILABILITY STATEMENT

The raw data supporting the conclusions of this article will be made available by the authors, without undue reservation.

ETHICS STATEMENT

The animal study was reviewed and approved by University of Bristol Animal Welfare and Ethical Review Body.

AUTHOR CONTRIBUTIONS

NC, RA, and MG conceived and designed the experiment. KW acquired and analysed the data. KW and NC prepared the first draft of the manuscript and the figures. All authors reviewed the manuscript for intellectual content. All authors contributed to the article and approved the submitted version.

FUNDING

This work was supported by the Medical Research Council UK (G1100626) and the BBSRC (BB/P000959/1) to NC and RA. This work was supported in part by grant MR/N0137941/1 for the GW4 BIOMED MRC DTP, awarded to the Universities of Bath, Bristol, Cardiff and Exeter from the Medical Research Council (MRC)/UKRI.

SUPPLEMENTARY MATERIAL

The Supplementary Material for this article can be found online at: https://www.frontiersin.org/articles/10.3389/fnsys.2022.899446/full#supplementary-material.

Supplementary Figure 1 | Changes in tremor amplitude over time. Mean accelerometer amplitude spectrum for one rat at different time points following systemic administration of harmaline (10 mg/kg, I.P).

REFERENCES

Arkadir, D., and Louis, E. D. (2013). The balance and gait disorder of essential tremor: what does this mean for patients? *Ther. Adv. Neurol. Disord.* 6, 229–236. doi: 10.1177/1756285612471415

Armstrong, D. M., and Edgley, S. A. (1984). Discharges of nucleus interpositus neurones during locomotion in the cat. *J. Physiol.* 351, 411–432. doi: 10.1113/jphysiol.1984.sp015253

Babij, R., Lee, M., Cortés, E., Vonsattel, J. P. G., Faust, P. L., and Louis, E. D. (2013). Purkinje cell axonal anatomy: quantifying morphometric changes in essential tremor versus control brains. *Brain* 136, 3051–3061. doi: 10.1093/brain/awt238

Batini, C., Bernard, J. F., Buisseret-Delmas, C., Conrath-Verrier, M., and Horcholle-Bossavit, G. (1981). Harmaline-induced tremor - II. Unit activity correlation in the interposito-rubral and oculomotor systems of cat. *Exp. Brain Res.* 42, 383–391. doi: 10.1007/BF00237503

Baumel, Y., and Cohen, D. (2021). State-dependent entrainment of cerebellar nuclear neurons to the local field potential during voluntary movements. *J. Neurophysiol.* 126, 112–122. doi: 10.1152/jn.00551.2020

Baumel, Y., Yamin, H.G., and Cohen, D. (2021). Cerebellar nuclei neurons display aberrant oscillations during harmaline-induced tremor. *Heliyon* 7:e08119. doi: 10.1016/j.heliyon.2021.e08119

Becker, M. I., and Person, A. L. (2019). Cerebellar control of reach kinematics for endpoint precision. *Neuron* 103, 335–348.e5. doi: 10.1016/j.neuron.2019.05.007

Bekar, L., Libionka, W., Tian, G. F., Xu, Q., Torres, A., Wang, X., et al. (2008). Adenosine is crucial for deep brain stimulation-mediated attenuation of tremor. *Nat. Med.* 14, 75–80. doi: 10.1038/nm1693

Bell, A., Fairbrother, M., and Jones, K. (2019). Fixed and random effects models: making an informed choice. *Qual. Quant.* 53, 1051–1074. doi: 10.1007/s11135-018-0802-x

Bernard, J. F., Buisseret-Delmas, C., Compoint, C., and Laplante, S. (1984). Harmaline induced tremor III. A combined simple units, horseradish peroxidase and 2-deoxyglucose study of the olivocerebellar system in the rat. *Exp. Brain Res.* 57, 128–137. doi: 10.1007/BF00231139

Bhatia, K. P., Bain, P., Bajaj, N., Elble, R. J., Hallett, M., Louis, E. D., et al. (2018). Consensus Statement on the classification of tremors. from the task force on tremor of the international Parkinson and movement disorder society. *Mov. Disord.* 33, 75–87. doi: 10.1002/mds.27121

Bhidayasiri, R. (2005). Differential diagnosis of common tremor syndromes. *Postgrad. Med. J.* 81, 756–762. doi: 10.1136/pgmj.2005.032979

Brittain, J. S., Cagnan, H., Mehta, A. R., Saifee, T. A., Edwards, M. J., and Brown, P. (2015). Distinguishing the central drive to tremor in Parkinson's disease and essential tremor. *J. Neurosci.* 35, 795–806. doi: 10.1523/JNEUROSCI.3768-14.2015

Boecker, H., Wills, A. J., Ceballos-Baumann, A., Samuel, M., Thompson, P. D., Findley, L. J., et al. (1996). The effect of ethanol on alcohol—responsive essential tremor: a positron emission tomography study. *Ann. Neurol.* 39, 650–658. doi: 10.1002/ana.410390515

Boivie, J. (1971). The termination of the spinothalamic tract in the cat. An experimental study with silver impregnation methods. *Exp. Brain Res.* 112, 331–353. doi: 10.1007/BF00234489

Brown, A. M., White, J. J., van der Heijden, M. E., Zhou, J., Lin, T., and Sillitoe, R. V. (2020). Purkinje cell misfiring generates high-amplitude action tremors that are corrected by cerebellar deep brain stimulation. *eLife* 9:e51928. doi: 10.7554/eLife.51928

Buijink, A. W. G., van der Stouwe, A. M., Broersma, M., Sharifi, S., Groot, P. F., Speelman, J. D., et al. (2015). Motor network disruption in essential tremor: a functional and effective connectivity study. *Brain* 138, 2934–2947. doi: 10.1093/brain/awv225

Cagnan, H., Brittain, J. S., Little, S., Foltynie, T., Limousin, P., Zrinzo, L., et al. (2013). Phase dependent modulation of tremor amplitude in essential tremor through thalamic stimulation. *Brain* 136, 3062–3075. doi: 10.1093/brain/awt239

Chen, K., and Shih, J. C. (1997). Monoamine oxidase A and B: structure, function and behavior. *Adv. Pharmacol.* 42, 292–296. doi: 10.1016/s1054-3589(08)60747-4

Courtemanche, R., Pellerin, J. P., and Lamarre, Y. (2002). Local field potential oscillations in primate cerebellar cortex: modulation during active and passive expectancy. *J. Neurophysiol.* 88, 771–782. doi: 10.1152/jn.2002.88.2.771

De Montigny, C., and Lamarre, Y. (1973). Rhythmic activity induced by harmaline in the olivo-cerebello-bulbar system of the cat. *Brain Res.* 53, 81–95. doi: 10.1016/0006-8993(73)90768-3

Deuschl, G., Wenzelburger, R., Löffler, K., Raethjen, J., and Stolze, H. (2000). Essential tremor and cerebellar dysfunction clinical and kinematic analysis of intention tremor. *Brain* 123, 1568–1580. doi: 10.1093/brain/123.8.1568

Di Biase, L., Brittain, J. S., Sha, S. A., Pedrosa, D. J., Cagnan, H., Mathy, A., et al. (2017). Tremor stability index: a new tool for differential diagnosis in tremor syndromes. *Brain* 140, 1977–1986. doi: 10.1093/brain/awx104

Dugué, G. P., Brunel, N., Hakim, V., Schwartz, E., Chat, M., Lévesque, M., et al. (2009). Electrical coupling mediates tunable low-frequency oscillations and resonance in the cerebellar Golgi cell network. *Neuron* 61, 126–139. doi: 10.1016/j.neuron.2008.11.028

Duval, C., Sadikot, A. F., and Panisset, M. (2006). Bradykinesia in patients with essential tremor. *Brain Res.* 1115, 213–216. doi: 10.1016/j.brainres.2006.07.066

Fahn, S. (1984). "Cerebellar tremor: clinical aspects," in *Movement Disorders: Tremor*, eds L. J. Findley, and R. Capildeo (UK: Palgrave Macmillan). doi: 10.1007/978-1-349-06757-2_26

Giuffrida, R., Volsi, G. L., Perciavalle, V., Santangelo, F., and Urbano, A. (1981). Influences of precerebellar systems triggering movement on single cells of the interpositus nucleus of the cat. *Neuroscience* 6, 1625–1631. doi: 10.1016/0306-4522(81)90228-1

Guitchounts, G., Masis, J., Wolff, S. B., and Cox, D. (2020). Encoding of 3d head orienting movements in the primary visual cortex. *Neuron* 108, 512–525.e4. doi: 10.1016/j.neuron.2020.07.014

Hallett, M., and Dubinsky, R. M. (1993). Glucose metabolism in the brain of patients with essential tremor. *J. Neurol. Sci.* 114, 45–48. doi: 10.1016/0022-510x(93)90047-3

Hanajima, R., Tsutsumi, R., Shirota, Y., Shimizu, T., Tanaka, N., and Ugawa, Y. (2016). Cerebellar dysfunction in essential tremor. *Mov. Disord.* 31, 1230–1234. doi: 10.1002/mds.26629

Handforth, A. (2012). Harmaline tremor: underlying mechanisms in a potential animal model of essential tremor. *Tremor Other Hyperkinet. Mov. (NY)* 2:2. doi: 10.7916/D8TD9W2P

Hartmann, M. J., and Bower, J. M. (1998). Oscillatory activity in the cerebellar hemispheres of unrestrained rats. *J. Neurophysiol.* 80, 1598–1604. doi: 10.1152/jn.1998.80.3.1598

Herraiz, T., Gonzáleza, D., Ancín-Azpilicuetac, C., Aránb, H., and Guilléna, V. J. (2010). β-Carboline alkaloids in *Peganum harmala* and inhibition of human monoamine oxidase (MAO). *Food Chem. Toxicol.* 48, 839–845. doi: 10.1016/j.fct.2009.12.019

Holmes, G. (1939). The cerebellum of man. *Brain* 62, 1–30. doi: 10.1093/brain/62.1.1

Hoon, K., Sablin, S., and Ramsay, R. (1997). Inhibition of monoamine oxidase A by β-carboline derivatives. *Arch. Biochem. Biophys.* 337, 137–142. doi: 10.1006/abbi.1996.9771

Hua, S. E., and Lenz, F. A. (2005). Posture-related oscillations in human cerebellar thalamus in essential tremor are enabled by voluntary motor circuits. *J. Neurophysiol.* 93, 117–127. doi: 10.1152/jn.00527.2004

Hua, S. E., Lenz, F. A., Zirh, T. A., Reich, S. G., and Dougherty, P. M. (1998). Thalamic neuronal activity correlated with essential tremor. *J. Neurol. Neurosurg. Psychiatry* 64, 273–276. doi: 10.1136/jnnp.64.2.273

Iseri, P. K., Karson, A., Gullu, K. M., Akman, O., Kokturk, S., and Yardýmoglu, M. (2011). The effect of memantine in harmaline-induced tremor and neurodegeneration. *Neuropharmacology* 61, 715–723. doi: 10.1016/j.neuropharm.2011.05.015

Karas, P. J., Mikell, C. B., Christian, E., Liker, M. A., and Sheth, S. A. (2013). Deep brain stimulation: a mechanistic and clinical update. *Neurosurg. Focus* 35:E1. doi: 10.3171/2013.9.FOCUS1338

Kiss, Z. H. T., Mooney, D. M., Renaud, L., and Hu, B. (2002). Neuronal response to local electrical stimulation in rat thalamus: physiological implications for mechanisms of deep brain stimulation. *Neuroscience* 113, 137–143. doi: 10.1016/s0306-4522(02)00122-7

Kosmowska, B., Ossowska, K., Konieczny, J., Lenda, T., Berghauzen-Maciejewska, K., and Wardas, J. (2020). Inhibition of excessive glutamatergic transmission in the ventral thalamic nuclei by a selective adenosine A1 receptor agonist, 5′-chloro-5′-deoxy-(±)-ENBA underlies its tremorolytic effect in the harmaline-induced model of essential tremor. *Neuroscience* 429, 106–118. doi: 10.1016/j.neuroscience.2019.12.045

Kramer, P. R., Strand, J., Stinson, C., Bellinger, L. L., Kinchington, P. R., Yee, M. B., et al. (2017). Role for the ventral posterior medial/posterior lateral thalamus and anterior cingulate cortex in affective/motivation pain induced by varicella zoster virus. *Front. Integr. Neurosci.* 11:27. doi: 10.3389/fnint.2017.00027

Kronenbuerger, M., Gerwig, M., Brol, B., Block, F., and Timmann, D. (2007). Eyeblink conditioning is impaired in subjects with essential tremor. *Brain* 130, 1538–1551. doi: 10.1093/brain/awm081

Kronenbuerger, M., Tronnier, V. M., Gerwig, M., Fromm, C., Coenen, V. A., Reinacher, P., et al. (2008). Thalamic deep brain stimulation improves eyeblink conditioning deficits in essential tremor. *Exp. Neurol.* 211, 387–396. doi: 10.1016/j.expneurol.2008.02.002

Kuo, S. H., Erickson-Davis, C., Gillman, A., Faust, P. L., Vonsattel, J. P. G., and Louis, E. D. (2011). Increased number of heterotopic Purkinje cells in essential tremor. *J. Neurol. Neurosurg. Psychiatry* 82, 1038–1040. doi: 10.1136/jnnp.2010.213330

Kuo, S. H., Wang, J., Tate, W. J., Pan, M. K., Kelly, G. C., Gutierrez, J., et al. (2017a). Cerebellar pathology in early onset and late onset essential tremor. *Cerebellum* 16, 473–482. doi: 10.1007/s12311-016-0826-5

Kuo, S. H., Lin, C. Y., Wang, J., Sims, P. A., Pan, M. K., Liou, J. Y., et al. (2017b). Climbing fiber-Purkinje cell synaptic pathology in tremor and cerebellar degenerative diseases. *Acta Neuropathol.* 133, 121–138. doi: 10.1007/s00401-016-1626-1

Lamarre, Y., Joffroy, A. J., Dumont, M., De Montigny, C., Grou, F., and Lund, J. P. (1975). Central mechanisms of tremor in some feline and primate models. *Can. J. Neurol. Sci.* 2, 227–233. doi: 10.1017/s0317167100020321

Lee, J., and Chang, S. (2019). Altered primary motor cortex neuronal activity in a rat model of harmaline-induced tremor during thalamic deep brain stimulation. *Front. Cell. Neurosci.* 13:448. doi: 10.3389/fncel.2019.00448

Lee, D., Gan, S. R., Faust, P. L., Louis, E. D., and Kuo, S. H. (2018). Climbing fiber-Purkinje cell synaptic pathology across essential tremor subtypes. *Parkinsonism Relat. Disord.* 51, 24–29. doi: 10.1016/j.parkreldis.2018.02.032

Lee, J., Kim, I., Lee, J., Knight, E., Cheng, L., Kang, S. I., et al. (2018). Development of harmaline-induced tremor in a swine model. *Tremor Other Hyperkinet. Mov. (N Y)* 8:532. doi: 10.7916/D8J68TV7

Lefler, Y., Yarom, Y., and Uusisaari, M. Y. (2014). Cerebellar inhibitory input to the inferior olive decreases electrical coupling and blocks subthreshold oscillations. *Neuron* 81, 1389–1400. doi: 10.1016/j.neuron.2014.02.032

Leyland, A. H., and Groenewegen, P. P. (2020). "Multilevel linear regression using MLwiN: mortality in England wales, 1979–1992," in *Multilevel Modelling for Public Health and Health Services Research*, (Cham: Springer), 173–254. doi: 10.1007/978-3-030-34801-4_11

Lierse, W. (1993). "Functional anatomy of the thalamus," in *Basic Mechanisms of the EEG*, eds S. Zschocke and E. J. Speckmann (Boston, MA: Birkhäuser), 121–128. doi: 10.1007/978-1-4612-0341-4_9

Lin, C. Y., Louis, E. L., Faust, P. L., Koeppen, A. H., Vonsattel, J. P. G., and Kuo, S. H. (2014). Abnormal climbing fibre-Purkinje cell synaptic connections in the essential tremor cerebellum. *Brain* 137, 3149–3159. doi: 10.1093/brain/awu281

Llinás, R., and Volkind, R. A. (1973). The olivo-cerebellar system: functional properties as revealed by harmaline-induced tremor. *Exp. Brain Res.* 18, 69–87. doi: 10.1007/BF00236557

Lorden, J. F., Lutes, J., Michela, V. L., and Ervin, J. (1992). Abnormal cerebellar output in rats with an inherited movement disorder. *Exp. Neurol.* 118, 95–104. doi: 10.1016/0014-4886(92)90026-m

Louis, E. D., Babij, R., Cortés, E., Vonsattel, J. P. G., and Faust, P. L. (2013). The inferior olivary nucleus: a postmortem study of essential tremor cases versus controls. *Mov. Disord.* 28, 779–786. doi: 10.1002/mds.25400

Louis, E. D., Lee, M., Babij, R., Ma, K., Cortés, E., Vonsattel, J. P. G., et al. (2014). Reduced Purkinje cell dendritic arborization and loss of dendritic spines in essential tremor. *Brain* 137, 3142–3148. doi: 10.1093/brain/awu314

Louis, E. D. (2016). Linking essential tremor to the cerebellum: neuropathological evidence. *Cerebellum* 15, 235–242. doi: 10.1007/s12311-015-0692-6

Louis, E. D., and Ferreira, J. J. (2010). How common is the most common adult movement disorder? Update on the worldwide prevalence of essential tremor. *Mov. Disord.* 25, 534–541. doi: 10.1002/mds.22838

Louis, E. D., Frucht, S. J., and Rios, E. (2009). Intention tremor in essential tremor: prevalence and association with disease duration. *Mov. Disord.* 24, 626–627. doi: 10.1002/mds.22370

Loutit, A. J., Vickery, R. M., and Potas, J. R. (2021). Functional organization and connectivity of the dorsal column nuclei complex reveals a sensorimotor integration and distribution hub. *J. Comp. Neurol.* 529, 187–220. doi: 10.1002/cne.24942

Manto, M. (2008). Tremorgenesis: a new conceptual scheme using reciprocally innervated circuit of neurons. *J. Transl. Med.* 6:71. doi: 10.1186/1479-5876-6-71

Martin, F. C., Thu Le, A., and Handforth, A. (2005). Harmaline-induced tremor as a potential preclinical screening method for essential tremor medications. *Mov. Disord.* 20, 298–305. doi: 10.1002/mds.20331

McCurdy, M. L., Houk, J. C., and Gibson, A. R. (1998). Organization of ascending pathways to the forelimb area of the dorsal accessory olive in the cat. *J. Comp. Neurol.* 392, 115–133. doi: 10.1002/(SICI)1096-9861(19980302)392:1%3C115::AID-CNE8%3E3.0.CO;2-5

Meyer, A. F., Poort, J., O'Keefe, J., Sahani, M., and Linden, J. F. (2018). A head-mounted camera system integrates detailed behavioral monitoring with multichannel electrophysiology in freely moving mice. *Neuron* 100, 46–60.e7. doi: 10.1016/j.neuron.2018.09.020

Muthuraman, M., Heute, U., Arning, K., Anwar, A. R., Elble, R., Deuschl, G., et al. (2012). Oscillating central motor networks in pathological tremors and voluntary movements. What makes the difference? *Neuroimage* 60, 1331–1339. doi: 10.1016/j.neuroimage.2012.01.088

Muthuraman, M., Raethjen, J., Koirala, N., Anwar, A. R., Mideksa, K. G., Elble, R., et al. (2018). Cerebello-cortical network fingerprints differ between essential, Parkinson's and mimicked tremors. *Brain* 141, 1770–1781. doi: 10.1093/brain/awy098

Nakamura, K. C., Sharott, A., and Magill, P. J. (2014). Temporal coupling with cortex distinguishes spontaneous neuronal activities in identified basal ganglia-recipient and cerebellar-recipient zones of the motor thalamus. *Cereb. Cortex* 24, 81–97. doi: 10.1093/cercor/bhs287

Pan, M. K., Li, Y. S., Wong, S. B., Ni, C. L., Wang, Y. M., Liu, Y. C., et al. (2020). Cerebellar oscillations driven by synaptic pruning deficits of cerebellar climbing fibers contribute to tremor pathophysiology. *Sci. Transl. Med.* 12:eaay1769. doi: 10.1126/scitranslmed.aay1769

Pan, M. K., Ni, C. L., Wu, Y. C., Li, Y. S., and Kuo, S. H. (2018). Animal models of tremor: relevance to human tremor disorders. *Tremor Other Hyperkinet. Mov. (N Y)* 8:587. doi: 10.7916/D89S37MV

Pasquet, M. O., Tihy, M., Gourgeon, A., Pompili, M. N., Godsil, B. P., Léna, C., et al. (2016). Wireless inertial measurement of head kinematics in freely-moving rats. *Sci. Rep.* 6:35689. doi: 10.1038/srep35689

Paxinos, G., and Watson, C. (2005). *The Rat Brain Stereotaxic Coordinates*. Sydney, NSW: Academic Press.

Pedrosa, D. J., Quatuor, E. L., Reck, C., Amande, K., Pauls, M., Huber, C. A., et al. (2014). Thalamomuscular coherence in essential tremor: hen or egg in the emergence of tremor? *J. Neurosci.* 34, 14475–14483. doi: 10.1523/JNEUROSCI.0087-14.2014

Pellerin, J. P., and Lamarre, Y. (1997). Local field potential oscillations in primate cerebellar cortex during voluntary movement. *J. Neurophysiol.* 78, 3502–3507. doi: 10.1152/jn.1997.78.6.3502

Placantonakis, D. G., Bukovsky, A. A., Zeng, X. H., Kiem, H. P., and Welsh, J. P. (2004). Fundamental role of inferior olive connexin 36 in muscle coherence during tremor. *Proc. Natl. Acad. Sci. U S A* 101, 7164–7169. doi: 10.1073/pnas.0400322101

Quy, P. N., Fujita, H., Sakamoto, Y., Na, J., and Sugihara, I. (2011). Projection patterns of single mossy fiber axons originating from the dorsal column nuclei mapped on the aldolase C compartments in the rat cerebellar cortex. *J. Comp. Neurol.* 519, 874–899. doi: 10.1002/cne.22555

Robinson, F. R., Houk, J. C., and Gibson, A. R. (1987). Limb specific connections of the cat magnocellular red nucleus. *J. Comp. Neurol.* 257, 553–577. doi: 10.1002/cne.902570406

Rowland, N. C., and Jaeger, D. (2005). Coding of tactile response properties in the rat deep cerebellar nuclei. *J. Neurophysiol.* 94, 1236–1251. doi: 10.1152/jn.00285.2005

Rummel, C., Müller, M., Baierd, G., Amora, F., and Schindlera, K. (2010). Analyzing spatio-temporal patterns of genuine cross-correlations. *J. Neurosci. Methods* 191, 94–100. doi: 10.1016/j.jneumeth.2010.05.022

Schnitzler, A., Münks, C., Butz, M., Timmermann, L., and Gross, J. (2009). Synchronized brain network associated with essential tremor as revealed by magnetoencephalography. *Mov. Disord.* 24, 1629–1635. doi: 10.1002/mds.22633

Schnitzler, A., Timmermann, L., and Gross, J. (2006). Physiological and pathological oscillatory networks in the human motor system. *J. Physiol. Paris* 99, 3–7. doi: 10.1016/j.jphysparis.2005.06.010

Singer, C., Sanchez-Ramos, J., and Weiner, W. J. (1994). Gait abnormality in essential tremor. *Mov. Disord.* 9, 193–196. doi: 10.1002/mds.870090212

Sternberg, E. J., Alcalay, R. N., Levy, O. A., and Louis, E. D. (2013). Postural and intention tremors: a detailed clinical study of essential tremor vs. Parkinson's disease. *Front. Neurol.* 4:51. doi: 10.3389/fneur.2013.00051

Stolze, H., Petersen, G., Raethjen, J., Wenzelburger, R., and Deuschl, G. (2001). The gait disorder of advanced essential tremor. *Brain* 124, 2278–2286. doi: 10.1093/brain/124.11.2278

Thenganatt, M. A., and Jankovic, J. (2016). The relationship between essential tremor and Parkinson's disease. *Parkinsonism Relat. Disord.* 22, S162–S165. doi: 10.1016/j.parkreldis.2015.09.032

Udenfriend, S., Witkop, B., Redfield, B. G., and Weissbach, H. (1958). Studies with reversible inhibitors of monoamine oxidase: harmaline and related compounds. *Biochem. Pharmacol.* 1, 160–165. doi: 10.1016/0006-2952(58)90025-X

Uemura, Y., Haque, T., Sato, F., Tsutsumi, Y., Ohara, H., Oka, A., et al. (2020). Proprioceptive thalamus receiving forelimb and neck muscle spindle inputs via the external cuneate nucleus in the rat. *Brain Struct. Funct.* 225, 2177–2192. doi: 10.1007/s00429-020-02118-2

Vaillancourt, D. E., Sturman, M. M., Metman, L. V., Bakay, R. A. E., and Corcos, D. M. (2003). Deep brain stimulation of the VIM thalamic nucleus modifies several features of essential tremor. *Neurology* 61, 919–925. doi: 10.1212/01.wnl.0000086371.78447.d2

Venema, V., Ament, F., and Simmer, C. (2016). A stochastic iterative amplitude adjusted Fourier Transform algorithm with improved accuracy. *Nonlin. Processes Geophys.* 13, 321–328. doi: 10.5194/npg-13-321-2006

West, T. O., Berthouze, L., Halliday, D. M., Litvak, V., Sharott, A., Magill, P. J., et al. (2018). Propagation of beta/gamma rhythms in the cortico-basal ganglia circuits of the Parkinsonian rat. *J. Neurophysiol.* 119, 1608–1628. doi: 10.1152/jn.00629.2017

Wills, A. J., Jenkins, I. H., Thompson, P. D., Findley, L. J., and Brooks, D. J. (1994). Red nuclear and cerebellar but no olivary activation associated with essential tremor: a positron emission tomoraphic study. *Ann. Neurol.* 36, 636–642. doi: 10.1002/ana.410360413

Yu, M., Ma, K., Faust, P. L., Honig, L. S., Cortés, E., Vonsattel, J. P. G., et al. (2012). Increased number of Purkinje cell dendritic swellings in essential tremor. *Eur. J. Neurol.* 19, 625–630. doi: 10.1111/j.1468-1331.2011.03598.x

Zhang, C., Zhou, P., and Yuan, T. (2016). The cholinergic system in the cerebellum: from structure to function. *Rev. Neurosci.* 27, 769–776. doi: 10.1515/revneuro-2016-0008

Conflict of Interest: The authors declare that the research was conducted in the absence of any commercial or financial relationships that could be construed as a potential conflict of interest.

Publisher's Note: All claims expressed in this article are solely those of the authors and do not necessarily represent those of their affiliated organizations, or those of the publisher, the editors and the reviewers. Any product that may be evaluated in this article, or claim that may be made by its manufacturer, is not guaranteed or endorsed by the publisher.

frontiers | Frontiers in Systems Neuroscience

TYPE Original Research
PUBLISHED 18 August 2022
DOI 10.3389/fnsys.2022.886427

OPEN ACCESS

EDITED BY
Krystal Lynn Parker,
The University of Iowa, United States

REVIEWED BY
Thenille Braun Janzen,
Federal University of ABC, Brazil
Markus Christiner,
University of Graz, Austria

*CORRESPONDENCE
Antoine Guinamard
antoine.guinamard@univ-lille.fr
Delphine Dellacherie
delphine.dellacherie@univ-lille.fr

RECEIVED 28 February 2022
ACCEPTED 15 July 2022
PUBLISHED 18 August 2022

CITATION
Guinamard A, Clément S, Goemaere S, Mary A, Riquet A and Dellacherie D (2022) Musical abilities in children with developmental cerebellar anomalies. *Front. Syst. Neurosci.* 16:886427. doi: 10.3389/fnsys.2022.886427

Musical abilities in children with developmental cerebellar anomalies

Antoine Guinamard[1,2]*, Sylvain Clément[1], Sophie Goemaere[2,3], Alice Mary[2], Audrey Riquet[2] and Delphine Dellacherie[1,2]*

[1]Univ. Lille, ULR 4072 – PSITEC – Psychologie: Interactions, Temps, Émotions, Cognition, Lille, France, [2]CHU Lille, Centre de Référence Malformations et Maladies Congénitales du Cervelet, Lille, France, [3]CHU Lille, Centre Régional de Diagnostic des Troubles d'Apprentissage, Lille, France

Developmental Cerebellar Anomalies (DCA) are rare diseases (e.g., Joubert syndrome) that affect various motor and non-motor functions during childhood. The present study examined whether music perception and production are affected in children with DCA. Sixteen children with DCA and 37 healthy matched control children were tested with the Montreal Battery for Evaluation of Musical Abilities (MBEMA) to assess musical perception. Musical production was assessed using two singing tasks: a pitch-matching task and a melodic reproduction task. Mixed model analyses showed that children with DCA were impaired on the MBEMA rhythm perception subtest, whereas there was no difference between the two groups on the melodic perception subtest. Children with DCA were also impaired in the melodic reproduction task. In both groups, singing performance was positively correlated with rhythmic and melodic perception scores, and a strong correlation was found between singing ability and oro-bucco-facial praxis in children with DCA. Overall, children with DCA showed impairments in both music perception and production, although heterogeneity in cerebellar patient's profiles was highlighted by individual analyses. These results confirm the role of the cerebellum in rhythm processing as well as in the vocal sensorimotor loop in a developmental perspective. Rhythmic deficits in cerebellar patients are discussed in light of recent work on predictive timing networks including the cerebellum. Our results open innovative remediation perspectives aiming at improving perceptual and/or production musical abilities while considering the heterogeneity of patients' clinical profiles to design music-based therapies.

KEYWORDS

cerebellum, developmental cerebellar anomalies, ataxia, music perception, music production, singing, children, rhythm

Introduction

Developmental Cerebellar Anomalies (DCA) are rare diseases characterized by a quantitative and/or qualitative abnormality of the cerebellum that is present at birth or manifests in early childhood, and persists into adulthood. These abnormalities in most cases lead to the presence of congenital cerebellar ataxia, which refers to a lack of coordination and balance disorders occurring from birth or in the first months of life. Initially manifested by the presence of hypotonia and psychomotor retardation, cerebellar ataxia may improve or remain stable during development, without regression. The most well-known congenital ataxia is Joubert syndrome, a genetic disorder characterized by a specific cerebellar malformation known as the "molar tooth sign" on brain imaging. Other congenital ataxias are associated with hypoplasia, dysgenesis, or atrophy of the cerebellar vermis and/or cerebellar hemispheres or brainstem. Brain imaging may, however, appear normal, and in many cases the etiology of these congenital cerebellar ataxias remains unknown (Steinlin et al., 1998; Garel et al., 2011; Musselman et al., 2014; Bertini et al., 2018). In addition to the well-known motor (balance and coordination) disorders caused by cerebellar motor syndrome, children with DCA may have a variety of cognitive and socio-emotional deficits affecting non-motor functions (Schmahmann and Sherman, 1998; Steinlin et al., 1999; Tavano et al., 2007). Among these deficits, timing abilities may be affected in these patients, particularly rhythmic abilities (Dennis et al., 2004, 2009; Hopyan et al., 2009; Bégel et al., 2022a), but it is not known whether musical abilities are more generally affected, and whether these difficulties affect only musical perception or whether production disorders are also found. However, there is growing evidence that the development of musical skills is important for the development of higher functions (Flaugnacco et al., 2014; Lense et al., 2021). A better understanding of the impact of childhood cerebellar pathologies on musical abilities should lead to improved diagnosis and remediation of DCA patients.

Musical perception and production abilities emerge early and develop spontaneously in children (Winkler et al., 2009; Perani et al., 2010; Stadler Elmer, 2012; Provasi et al., 2014a), such that the majority of the general population have sophisticated music perception abilities (Bigand, 2003) and are able to sing in tune and in time, without formal musical training (Dalla Bella et al., 2007; Dalla Bella and Berkowska, 2009; Berkowska and Dalla Bella, 2013). Musical ability is comprised of complex skills and involves a distributed brain network, including the cerebellum (Peretz and Zatorre, 2005; Chen et al., 2008; Herholz and Zatorre, 2012; Herholz et al., 2012).

The involvement of the cerebellum is reported in various aspects of musical perception and production. While for a long time the cerebellum was mainly considered to play a role in motor functions, theories have evolved in recent decades to include its role in higher cognitive functions (Schmahmann and Sherman, 1998; Schmahmann, 2019) and in more fundamental tasks related to sensory functions (Baumann et al., 2015). Thus, the cerebellum is active in purely sensory auditory processing and is involved in both passive listening and pitch discrimination tasks, especially as the difficulty of the task increases (Parsons et al., 2009; Petacchi et al., 2011; Lega et al., 2016). In addition to pitch processing, sound duration processing also engages the cerebellum (Belin et al., 2002), and cerebellar gray matter volumes are positively related to beat interval discrimination abilities (Paquette et al., 2017). It is therefore not surprising that neuroimaging studies have demonstrated its activation during music listening (Brown et al., 2004b). For instance, listening to musical rhythms, even passively, recruits the cerebellum along with other motor regions of the brain (Chen et al., 2008; Gordon et al., 2018) and cerebellar activations are greater during rhythmic than during melodic tasks (Parsons, 2001; Thaut et al., 2014). Some studies suggest also that the cerebellum has a role in working memory for rhythm (Jerde et al., 2011; Konoike et al., 2012; Teki and Griffiths, 2016) whereas its involvement in melodic working memory has not been reported to date.

Like music perception, music production involves several processes that rely in part on the cerebellum. Whether one is singing or playing an instrument, producing the desired pitch sequence and rhythmic structure requires precise motor control and auditory-motor integration, with feedforward and feedback components, which in turn involves the cerebellum (Wolpert et al., 1998; Bastian, 2006; Zatorre et al., 2007; Kleber and Zarate, 2014; Johnson et al., 2019; Peng et al., 2021). Neuroimaging studies have shown that the networks involved in singing and playing an instrument partially overlap (Segado et al., 2018) and in both cases have shown that the cerebellum is activated (Zatorre et al., 2007; Zarate and Zatorre, 2008; Kleber and Zarate, 2014; Brown et al., 2015; González-García et al., 2016). The cerebellum is involved in motor rhythm reproduction tasks, especially when rhythms are complex or novel (Penhune et al., 1998) and it is particularly active when musicians make and correct errors while performing (Pfordresher et al., 2014). Singing single notes (Perry et al., 1999) as well as short melodies with or without words also activates the cerebellum (Brown et al., 2004a; Kleber et al., 2007), and the more experienced the singer, the more active the cerebellum becomes during singing (Kleber et al., 2010). Singing seems to involve especially the lobule VI of the posterior cerebellum, which somatotopically represents the lips and tongue and is also activated during speech (Callan et al., 2007). These activations are not surprising knowing that the cerebellum is involved in motor control of vocal muscles (Grabski et al., 2012). More broadly, the cerebellum is involved in the vocal sensorimotor loop (Berkowska and Dalla Bella, 2009), with a crucial role in motor-to-auditory and self-initiated sounds

predictions (Knolle et al., 2012, 2013) and in auditory feedback control (Li et al., 2019; Peng et al., 2021).

One of the cerebellum's roles common to both musical perception and production is its participation in timing processes. The cerebellum is part of a distributed neural network, including the basal ganglia, the motor cortex and the premotor cortex, all of which enable temporal processing (Coull and Nobre, 2008; Coull et al., 2011; Bareš et al., 2018). The cerebellum has a recognized role in absolute duration-based timing (Grube et al., 2010b; Teki et al., 2011; Breska and Ivry, 2016) and it is also known to play a notable role in predictive timing, i.e., the ability to develop temporal expectations about upcoming events based on previous temporal information (Bastian, 2006; Schwartze and Kotz, 2013, 2016; Kotz et al., 2014). Predictive timing abilities are particularly useful when coordinating one's action with rhythmic events such as music, which has a very regular and predictable structure (Dalla Bella et al., 2013). The cerebellum is therefore active in sensorimotor synchronization tasks (synchronized finger tapping) in adults (Rao et al., 1997; Jäncke et al., 2000; Stoodley et al., 2012) and in children (Rivkin et al., 2003; De Guio et al., 2012), but could also be very important when we are singing previously listened tunes, in particular when they are familiar, since it involves anticipating the rhythmic structure of the sequence to be sung.

Further support for the involvement of the cerebellum in music processing comes from studies of patients with cerebellar lesions, most of which have been conducted on patients with acquired lesions. First, sound duration perception deficits were found in adults with various cerebellar damages such as stroke, tumor or cerebellar degeneration (Ivry and Keele, 1989) and in children with cerebellar degeneration in the context of ataxia telangiectasia (Mostofsky et al., 2000). Such deficits have also been reported in temporal duration reproduction tasks in children after cerebellar tumor resection (Droit-Volet et al., 2013). Moreover, in addition to duration perception or reproduction deficits, rhythm perception and production has also been shown to be impaired in patients with cerebellar damages. According to an electroencephalography study, cerebellar lesions may have a specific impact on rhythm processing when played at a fast pace as it require more resources for accurate encoding of events (Nozaradan et al., 2017). This complements studies that have shown deficits in tempo change detection tasks in adult patients with cerebellar damage (Molinari et al., 2003; Schwartze et al., 2016). Studies involving rhythmic production have also shown that adult and children patients with cerebellar lesions exhibit greater variability in tapping tasks than control participants, both in spontaneous tapping and in tapping synchronized with auditory sequences of isochronous stimuli or in adaptive tasks, consistent with a cerebellar role in predictive timing (Ivry and Keele, 1989; Provasi et al., 2014b; Schwartze et al., 2016). However, some studies reported also preserved rhythm perception abilities in acquired cerebellar disorder (Grube et al., 2010a; Provasi et al., 2014b). Indeed, children with acquired cerebellar lesions following tumor resection showed preserved abilities in a tempo discrimination task (Provasi et al., 2014b). Similarly, adults with spino-cerebellar ataxia performed similarly to controls on rhythmic tasks despite deficits for absolute timing perception of single intervals (Grube et al., 2010a). The question of whether the temporal deficits related to a cerebellum lesion only concern durations or extend to rhythmic skills is therefore still controversial.

To our knowledge, only one clinical study has investigated both rhythmic and melodic musical perception in a group of adult patients with cerebellar acquired disorders (Tölgyesi and Evers, 2014) in the context of a degenerative affection (i.e., Machado-Joseph disease) or of cerebellar stroke. All the patients were significantly impaired in melody perception tested with a melody comparison task, and the group of patients with cerebellar degeneration also showed impairment in the ability to recognize familiar melodies. In addition, the authors proposed a rhythm reproduction task in which participants were asked to reproduce short rhythmic sequences by tapping with a pen on a table while the examiner scored the correctness of the rhythm and the meter. Patients with cerebellar damage performed similarly to controls in reproducing the rhythmic pattern but had significantly lower scores for the meter component, suggesting that rhythm production deficits were due to difficulties in maintaining a stable tempo rather than in reproduction rhythmic pattern *per se*. Melodic production was not investigated in this study, so it is not known whether this ability is affected in these patients. Singing, a widespread popular practice, most often requires the production of both rhythmic and melodic patterns (Dalla Bella et al., 2007). Only one pilot study has recently addressed the issue of singing abilities in adult patients with cerebellar disorders (Zúñiga et al., 2020). In this case study, the authors examined the speech and singing abilities of two ataxic patients with cerebellar dysarthria, a speech disorder resulting from motor coordination impairments in the context of cerebellar damage (Ackermann et al., 1992). For both patients, the authors reported alterations in basic motor processes concerning breathing, phonation and prosody. Moreover, speech and singing abilities were related to the degree of dysarthria, highlighting the potential influence of cerebellar coordination disorders on music production abilities. The patients' music perception abilities were not assessed in this study.

The aforementioned clinical studies were conducted in patients with acquired cerebellar lesions and, to our knowledge, very few studies to date have explored some partial aspects of musical abilities in developmental cerebellar anomalies, which are characterized by cerebellar disorders present from birth or very early in development. None of them has explored in a comprehensive way the musical abilities by looking at both the melodic and rhythmic sides as well as the perceptual and productive aspects. In a study of children with

DCA associated with spina bifida meningomyelocele, Dennis et al. (2004) reported impaired duration but preserved pitch perception around 3,000 Hz using discrimination tasks. The authors also reported greater variability in a synchronization-continuation tapping task when children were required to continue tapping rhythmically after the rhythmic stimulus had stopped, suggesting that predictive timing could be affected in these patients. Rhythm perception has also been studied in this same population (Hopyan et al., 2009). The authors showed that in comparison to healthy controls, children with DCA displayed a deficit in rhythm perception when comparing pairs of non-syncopated rhythms produced by drum sound. Dennis et al. (2009) replicated these findings in a larger sample and showed an association between rhythm perception deficits and cerebellar volumes. More recently, in a multiple-case study designed to evaluate the therapeutic benefit of dance interventions, deficits in sensorimotor synchronization to the metronome and/or music were found in six out of seven children with DCA (Bégel et al., 2022a). Taken together, these studies suggest that DCA patients present a musical deficit of rhythm that could be at least partially linked to predictive timing difficulties. However, none of these studies explored melody in addition to rhythm perception in the same children with DCA, and the only production component explored was synchronized finger tapping.

The primary objective of this novel study was therefore to examine music perception and production (singing) abilities in children with DCA. A secondary objective was to explore, in both groups of participants, the relationship between singing abilities and rhythmic and melodic perceptual abilities, as well as the relationship between singing and oro-bucco-facial praxis which is typically impaired in cerebellar syndrome. For this purpose, sixteen children with DCA were compared to 37 healthy controls matched for age and non-verbal intelligence. Music perception abilities were assessed using the abbreviated version of the Montreal Music Ability Assessment Battery (MBEMA) (Peretz et al., 2013). This battery assesses melodic and rhythmic perception, as well as musical memory. Music production abilities were evaluated using two singing tasks, a pitch matching task and a melodic reproduction task (Clément et al., 2015). The melodic reproduction task involved either familiar or unfamiliar stimuli. In addition, oro-bucco-facial praxis was assessed using the Hénin-Dulac test in which children had to reproduce different movements involving the oral region (Hénin, 1981).

We expected that children with DCA would perform worse than healthy controls in both perception and music production. We also expected that patients' deficits would be more pronounced in rhythmic perception than in melodic perception. For the melodic reproduction task, as observed by Clément et al. (2015), we expected a condition effect in the control group, with an advantage for singing melodies from familiar songs over melodies from familiar tunes, and an advantage for singing the latter over unfamiliar melodies. Finally, we hypothesized positive correlations between perceptual abilities (melodic or rhythmic) and melodic singing on the one hand, and between oro-bucco-facial praxis abilities and melodic singing on the other hand. Because individuals with DCA have different types of cerebellar anomalies and this is a source of principled variability within the group, we were also interested in performing individual analyses to highlight potential differences in profiles or potential dissociations.

Materials and methods

Participants

Patients

Twenty-nine patients with developmental cerebellar anomalies (DCA group) were first selected at the Centre national de référence Malformations et Maladies Congénitales du Cervelet (C2M2C, Lille University Hospital). In order to isolate the specific contribution of the cerebellum to musical abilities, the following exclusion criteria were applied: (1) supratentorial abnormalities visible on MRI, (2) progressive cerebellar pathology, (3) epileptic seizures or febrile convulsions, (4) uncorrected auditory deficit, (5) intellectual disability determined by an intelligence quotient (IQ) < 70, measured by the Wechsler Intelligence Scale (Wechsler, 2005, 2016). After applying the exclusion criteria, sixteen children with congenital cerebellar ataxia participated in this study (nine boys and seven girls, aged from 8.0 to 13.0 years). All patients had a clinical cerebellar syndrome evaluated during a neurological examination performed by a specialist neuropediatrician and they all benefited from a neuropsychological evaluation. Patient 1 was diagnosed with cerebellar ataxia in the context of a Coffin-Siris syndrome linked to a mutation in the ARID1B gene, Patient 11 in the context of a Joubert syndrome linked to mutations in the CC2D2A gene, and Patient 15 in the context of mutations in the CACNA1A gene. For the thirteen other patients, the diagnosis of DCA was of unknown etiology. In 12 patients, cerebellar ataxia was associated with abnormalities observable with magnetic resonance imaging (MRI 3 Tesla), while in the other four patients, no abnormality was visible on MRI. At the moment of the study, 10 of the patients were or had been followed up by a speech therapist for speech and/or language difficulties (Patient 1, 3, 4, 10, 11, 12, 13, 14, 15, 16). A detailed description of patient characteristics is available in **Supplementary Table 1**.

Controls

A group of 37 typically developing children (CONTROL group; 13 boys and 24 girls, aged 7.8–13.1 years) was recruited from different schools in Hauts-de-France. None of the children in the control group had any known neurological, psychiatric

or developmental disorder or hearing impairment at the time of the study. In order to check their general functioning, the children in the control group were assessed with four subtests of the WISC IV battery (Wechsler, 2005). These subtests assessed non-verbal intelligence (Matrix), working memory (Digit Span), and processing speed (Coding and Symbol Search). No children with deficits in any of these tests were included in the study.

The two groups of children were matched for age and non-verbal intelligence (standard score on the Matrix subtest). The CONTROL and DCA groups did not differ in either age [$t_{(51)} = -0.402$; $p > 0.05$] or non-verbal intelligence score [$t_{(51)} = -0.856$; $p > 0.05$]. In both groups, the first language was French for all children. None of the children had received more than 1 year of formal music or dance training. All participants and their parents signed informed consent in accordance with the Declaration of Helsinki to participate in the study.

Material and procedure

Musical perception assessment

Musical perception abilities were assessed using the short version of the MBEMA (Peretz et al., 2013). It consists of three subtests, each with twenty items. In the first two subtests, each item consists of a target melody and a comparison melody separated by an interval of 1.5 s, and the child must decide whether they are similar or not. The comparison melodies can differ either melodically (subtest "Melody") or rhythmically (subtest "Rhythm"). In the last subtest "Memory" the child hears 20 melodies, 10 of which were part of the two previous subtests and has to decide whether the melody has been heard before or not. The stimuli used in the abbreviated MBEMA can be downloaded from the website of Isabelle Peretz.[1]

Musical production assessment

Each participant played a computer-game "goose game," created by Clément et al. (2015), against the experimenter. Through this game, the children and the experimenter were prompted to perform two singing tasks: a pitch-matching task and a melodic reproduction task. The game was designed so that the children would always win, and so that each child would have the same number of productions. The order of all the stimuli to be sung during the game (single notes and melodies) was randomized and identical for all the children. Presenting these singing tasks as a game allowed for motivating competition between the child and the experimenter.

In the "pitch-matching" trials, a piano note was played twice, and after each presentation, the participant had to sing back the note on the syllable /*la*/. Over the entire game, children had to reproduce all 12 degrees of the tempered scale from C4 (f0 = 261.23 Hz) to B4 (f0 = 493.88 Hz). Stimuli were produced using the virtual instrument "Steinway Grand Piano" in Apple Logic Pro 9 software and had an average duration of 1.4 s.

In the "melodic reproduction" trials, a short melody was played twice on the piano, and the participants had to sing it on the syllable /*la*/ after each presentation. There was a total of six melodies to sing: two familiar songs melodies that are usually associated with lyrics and learnt in early childhood (FAM-SONG condition: "Brother John," "Au Clair de la Lune"), two familiar melodies from movies or cartoons, not associated with lyrics and not learned explicitly in childhood (FAM-TUNE condition: "Pink Panther theme," "Mission: Impossible"), and two unknown melodies composed for the study (UNFAM-TUNE condition: "Unknown A," "Unknown B"). The familiar melodies consisted of the first musical phrase of the main theme, 4–5 bars in length. The unknown melodies were similar in length, had the same rhythmic and melodic complexity, and used the same pitch range as the familiar melodies. The scores of the melodies are available as **Supplementary Figure 1**. In the FAM-SONG and FAM-TUNE (familiar melodies) conditions, the title of the melody was announced to the child before the listening to the sample. After the experiment, we verified that all children indeed knew the familiar melodies by asking them about their knowledge of where the melodies came from and whether they had heard them often before. Stimuli were produced with the same configuration as for the single notes. All melodies were created with a fixed MIDI velocity of 80 and a tempo of 100 bpm, resulting in an average duration of 7.02 s ($SD = 1.9$ s).

During the game, all the stimuli were presented through headphones (Sennheiser HD 265 linear), and all the sung productions were recorded with a Zoom H2 digital audio recorder (uncompressed WAV file type, 16-bit/44.1 kHz) placed in front of the children.

Oro-bucco-facial praxis assessment

Each participant's oro-bucco-facial praxis was assessed with the clinical test of oro-bucco-facial praxis (Hénin, 1981). In this test, the experimenter describes and performs a series of movements of the lips, tongue, cheeks, and mandibles, or eyes and forehead, and participants are asked to reproduce each of them successively. Each movement correctly reproduced in one or two trials was considered a success.

All children were assessed individually in a quiet room. Music perception and production abilities were tested, followed by an assessment of oro-bucco-facial praxis. The protocol lasted approximately 45 min. The children were offered a break between each task.

1 http://www.peretzlab.ca/

Measures

Musical perception

For the three tests of the abbreviated MBEMA ("Melody," "Rhythm," and "Memory"), a score out of 20 is assigned to the child according to the number of correct answers provided (Peretz et al., 2013).

Musical production

All sung productions (single notes and melodies) were extracted from the continuous recording using Audacity version 2.2.1 recording and editing software (Audacity Team, 2019) for evaluation. To measure the pitch-matching accuracy, the pitch of each note was calculated using the algorithm provided by the "Pitchtrack" function of the phonTools package (Barreda, 2015) for R software (R Core Team, 2021). For each note, "Pitchtrack" measures the fundamental frequency every 10 ms. Of these measurements, only those of quantiles 2 and 3 are kept and averaged. The pitch obtained in Hertz (Hz) is compared to the theoretical pitch of the expected notes. This comparison allows for octave transpositions: if a participant had to sing an "A" at 440 Hz and sings a note at 830 Hz, the lower octave will be used (830/2 = 415 Hz) and the error is measured between 415 Hz and the target of 440 Hz. This error is expressed in cents (hundredths of semitones).

To assess melodic reproductions, as in Clément et al. (2015), we chose a subjective assessment method rather than a computerized analysis because some singing productions of children with DCA were severely impaired, so much so that it was not possible to recognize the original melody. Subjective rating is a method that has been validated and has been found to have a high congruence with objective measurements of vocal accuracy (Larrouy-Maestri et al., 2013). All melodic reproductions of the children were sorted by tune and presented in a random order to 10 healthy judges (five males and five females; age: mean = 25.9 years, *SD* = 2.2 years; musical background: mean = 2.4 years, *SD* = 3.0 yrs) using PsychoPy software (Peirce et al., 2019). For each trial, they heard the piano example, followed by a child's song. They were then asked to give an overall score to the child's production by clicking on a continuous scale from 0 (very poor performance) to 10 (very good performance), considering all musical parameters such as pitch and rhythm. They were also explicitly asked to ignore any global transposition of the melodies. Each judge was asked to rate all 636 productions (53 children; two trials per tune, six tunes). To avoid fatigue effects, the ratings were conducted in several sessions spread over several days. The judges were unaware of the presence of recordings of children with cerebellar disorders and were therefore blind to group affiliation. The ratings of the 10 judges were then averaged for each child's production.

Oro-bucco-facial praxis

For each movement successfully completed in one or two trials, the participant receives one point. For each of the four movement categories assessed ("lips", "tongue", "cheeks and mandibles", "eyes and forehead"), the score is transformed to a score out of 10 that can be compared to norms. We then calculated an overall Oro-bucco-facial praxis score for each child by adding these four scores, obtaining an overall score out of 40.

Statistical analyses

Data processing and statistical analyses were performed using R studio software version 4.1.2 (R Core Team, 2021). To investigate the relationship between music perception abilities (MBEMA scores) and group (DCA, CONTROL), and the relationship between melody singing ability and group, linear mixed models were fit using the packages Lme4 version1.1-29 (Bates et al., 2015) and LmerTest version 3.1-3 (Kuznetsova et al., 2017). For all models, a Satterthwaite adjustment was used to compute the degrees of freedom. *Post-hoc* tests were computed with Holm–Bonferroni correction using the emmeans package version 1.7.4-1 (Lenth et al., 2022). Additionally, inter-rater agreement was assessed for the subjective ratings of the melodies, using Intraclass Correlation Coefficient (ICC) computed with the SimplyAgree R package version 0.0.3 (Caldwell, 2022).

Spearman correlation tests were used to explore the relationships between music perception, singing, and oro-buccofacial praxis, assuming that these relations may not be linear. To avoid an increase in Type I error due to multiple testing, Holm-Bonferroni corrections were applied to the results.

Individual analyses were performed in order to estimate the proportion of children with DCA who were impaired in each task and to examine, for each patient, the presence of a concomitant deficit in the Melody and Rhythm subtests of the MBEMA and/or the Oro-Bucco-Facial praxis. As the sample of the CONTROL group (n = 37) did not allow us to use the z-score method, we used the Bayesian Test of Deficit proposed by Crawford et al. (2011) allowing us to compare each patient to the CONTROL group, controlling for the effects of age as a covariate. These comparisons were done using the "BTD_cov" software published by the authors.

Results

Musical perception

The mean scores on the three MBEMA subtests are presented in **Figure 1**. A linear mixed model was built to analyze MBEMA scores as a function of participant group

and subtest. A "full model" was built including Group (DCA, Control), Subtest (Melody, Rhythm, Memory) and the Group-by-Subtest interaction as fixed effects together with a random intercept for Subjects.

This full model was compared to four reduced models by successively removing interaction term and then either Group or Subtest predictors. All four models were first fitted with maximum likelihood method (ML) to enable comparisons. Based on Likelihood Ratio Tests (LRT) and Akaike's Information Criterion (AIC) (Akaike, 1974; Bozdogan, 1987), the full model was identified as the best fitting model. Details of the model comparisons are available in **Supplementary Table 2**.

The final model was then fit with Restricted Maximum Likelihood method (REML) (Marginal R^2 = 0.194, Conditional R^2 = 0.574). Visual inspection of the residuals plots as well as the random effects deviation plots did not reveal any obvious deviation from normality. Equation and coefficient of the model are presented in **Table 1**.

Fixed effects omnibus Anova (Type III) was performed with Satterthwaite method for degrees of freedom. This revealed an significant Group by Subtest interaction [$F(2, 102) = 5.91$; $p = 0.004$] as well as significant main effects of Group [$F(1, 51) = 11.00$; $p = 0.002$] and Subtest [$F(2, 102) = 7.75$; $p < 0.001$].

Post hoc analysis with Holm-Bonferroni correction revealed that patients with DCA obtained significantly lower scores than healthy controls on the Rhythm subtest ($p < 0.001$) whereas there was no significant difference between the two groups for the Melody ($p = 0.209$) and Memory ($p = 0.067$) subtests.

Musical Production

Pitch-matching

A mean pitch error was computed for each group by averaging the absolute pitch errors. Since the assumption of normality of the distributions was not validated, the Mann Whitney *U*-test was used to compare these means. There was no significant difference between the mean pitch errors of DCA and CONTROL participants ($W = 228$; $p = 0.097$; mean error: DCA group = 233 cents; CONTROL group = 198 cents).

Melodic singing

Figure 2 shows the average ratings given by judges in the melodic reproduction (singing) task for the two groups of participants (DCA and CONTROL) as a function of condition (FAM-SONG; FAM-TUNE; UNFAM-TUNE). Ratings of the 10 blind judges were averaged for each children's production.

We used a linear mixed model to evaluate the effect of group on the ability to sing melodies. There were two melodies per condition, and each of the 53 children sang twice for each melody, so there were 636 observations.

A random slope and intercept model was built with a by-subjects random intercept as well as a by-subject random slope for the effect of condition, assuming correlation between the random intercept and slope. Group (DCA, CONTROL), Condition (FAM-SONG, FAM-TUNE, UNFAM-TUNE) and the interaction between Group and Condition was entered as fixed effects. This full model was compared to the reduced model with no interaction, and to the two reduced models with only group or condition as a fixed effect. We also compared the full model to a random intercept by subject model with the same fixed effects. For comparisons, models with different fixed effects were fit with ML method and model with different random effects were fit with REML method. Model comparisons base on LRT and AIC identified the full model with random slope and intercept as the best fitting model. Details of the model comparisons are available in **Supplementary Table 3**.

The final model was then fit with REML (Marginal R^2 = 0.279 Conditional R^2 = 0.794). Visual inspection of the residuals plots as well as the random effects deviation plots did not reveal any obvious deviation from normality. Equation and coefficients of the model are presented in **Table 2**.

Fixed effects omnibus anova (Type III) with Satterthwaite method for degrees of freedom highlighted an effect of Group [$F(1, 51) = 23.381$; $p \leq 0.001$], Condition [$F(2, 51) = 7.75$; $p < 0.001$] and a Group by Condition interaction [$F(2, 51) = 5.91$; $p = 0.001$].

Post hoc analysis with Holm-Bonferroni correction showed that in the CONTROL group, performance was significantly better in the FAM-SONG condition than in the FAM-TUNE condition ($p < 0.001$), which were themselves significantly better than in the UNFAM-TUNE condition ($p < 0.001$). In contrast, in the DCA group, no significant difference was found between the FAM-SONG and FAM-TUNE condition ($p = 0.753$) and between the FAM-TUNE and UNFAM-TUNE condition ($p = 0.441$).

We also verified inter-rater reliability of the production ratings using ICC based on a single rater, absolute agreement, two-way random effects model (Koo and Li, 2016). We found a moderate to good agreement between the 10 judges [ICC(2, 1) = 0.7529, lower bound = 0.7238, upper bound = 0.7794].

Correlations between musical perception and production

Links between music perception and production abilities in each group of participants were explored with Spearman correlations tests between MBEMA Melody and Rhythm subtests scores and the average melodic singing scores. In each of the two groups of participants, we found two positive correlations between scores on the music perception subtests (Melody and Rhythm) of the MBEMA and performance in the melodic singing task (respectively, for the Melody subtest: DCA: $\rho = 0.644$, $p = 0.011$; CONTROL: $\rho = 0.668$; $p < 0.001$ and for the Rhythm subtest: DCA: $\rho = 0.702$, $p = 0.002$; CONTROL:

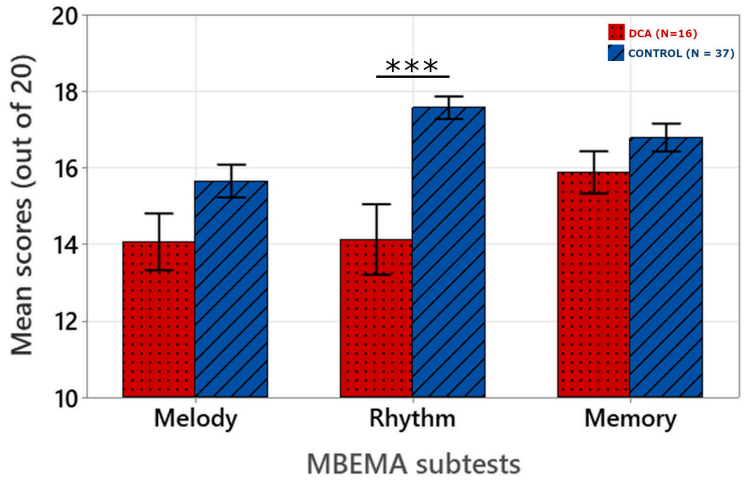

FIGURE 1
Mean scores obtained for each subtest of the MBEMA. Origin is set at chance level (10/20). The error bars correspond to the standard error of the mean. ***$p < 0.001$.

TABLE 1 Summary of the final linear mixed model for MBEMA analyses.

Final model equation: MBEMA_score ~ 1 + group + subtest + group:subtest + (1 | Subject)

Fixed effects						
	Estimate	**Std. Error**	**95% CI lower**	**95% CI upper**	**t**	***p***
Intercept	16.67	0.33	6.024	17.309	5.84	<0.001
GroupCEREB	−1.98	0.60	−3.149	−0.810	−3.38	0.002
Subtest 1	−1.02	0.24	−1.493	−0.543	−4.20	<0.001
Subtest 2	0.18	0.24	−0.357	0.591	0.48	0.630
GroupCEREB × Subtest 1	0.39	0.44	−0.471	1.257	0.89	0.376
GroupCEREB × Subtest 2	1.07	0.44	0.207	1.934	2.43	0.017
Random effects						
		Variance			Std Deviation	
Participant (intercept)		2.89			1.70	
Model fit						
		Marginal			Conditional	
R^2		0.194			0.573	

Sum-coding contrast method was used. p-values for fixed effects have been calculated using Satterthwaites approximations. Confidence Intervals have been calculated using the Wald method.

$\rho = 0.529$; $p < 0.001$). Figures 3, 4 display the scatter plots of these correlations.

Oro-bucco-facial praxis

We compared the global score of oro-bucco-facial praxis of the DCA and CONTROL groups. Mann Whitney *U*-test was used as the normality assumption was not validated. As expected, given their motor coordination disorders, the results showed that the DCA group scored significantly lower than the CONTROL group in the Oro-Bucco-Facial Praxia test (DCA: mean score = 31.7, *SD* = 7.92; CONTROL: mean score = 38.9, SD = 1.33; *W* = 58.0; $p < 0.001$).

We calculated correlations between the oro-bucco-facial praxis score and melodic singing performance, highlighting a strong positive correlation between the overall oro-bucco-facial praxis scores and mean scores on the melodic singing

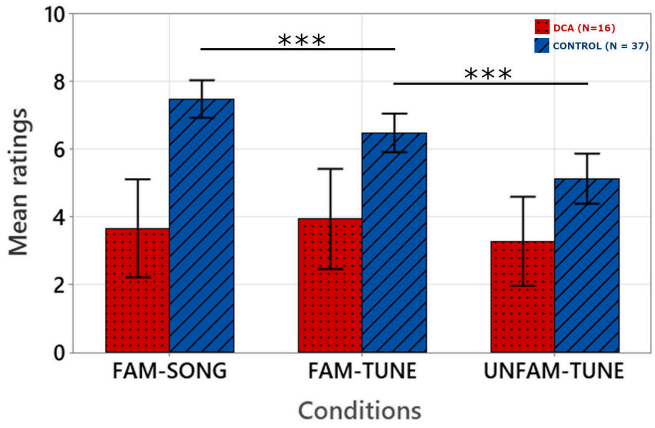

FIGURE 2
Mean ratings on the melodic reproduction task as a function of experimental conditions. The error bars correspond to the standard error of the mean. Ratings were given by 10 blind judges on a continuous scale from 0 (very poor performance) to 10 (very good performance) and were then averaged. ***$p < 0.001$.

TABLE 2 Summary of the final Linear Mixed Model for the melodic reproduction task analyses.

Final model equation:melody_rating ~ 1 + group + condition + group:condition + (1 + condition | Subject)

Fixed effects						
	Estimate	**Std. Error**	**95% CI lower**	**95% CI upper**	**t**	***p***
Intercept	6.35	0.31	5.745	6.962	2.47	<0.001
GroupCEREB	−2.73	0.56	−3.838	−1.624	−4.84	<0.001
Condition 1	1.11	0.16	0.810	1.418	7.17	<0.001
Condition 2	0.12	0.13	−0.132	0.369	0.92	0.360
GroupCEREB × condition 1	−1.08	0.28	−1.635	−0.527	−3.82	<0.001
GroupCEREB × condition 2	0.19	0.23	−0.262	0.650	0.83	0.409
Random effects						
	Variance			Std Deviation		
Participant (intercept)	3.43			1.85		
condition1	0.67			0.79		
Condition2	0.33			0.57		
Model fit						
	Marginal			Conditional		
R^2	0.279			0.794		

Sum-coding contrast method was used. p-values for fixed effects have been calculated using Satterthwaites approximations. Confidence Intervals have been calculated using the Wald method.

reproduction task in the DCA group (DCA: $\rho = 0.728$, $p < 0.001$) but not in the CONTROL group ($\rho = 0.314$, $p = 0.087$).

Individual analyses

Bayesian Tests of Deficit (Crawford et al., 2011) revealed that eight out of sixteen patients with DCA, i.e., half of them, had a deficit in music perception, including seven patients with a rhythmic deficit and two patients with a melodic deficit (Table 3). Only one patient was impaired in both the Rhythm and Melody subtests of the MBEMA. Although all sixteen patients in the DCA group were able to sing the single notes correctly, 10 out of sixteen patients were impaired in the melodic singing task when compared to the children of the CONTROL group. These singing deficits were systematically associated with

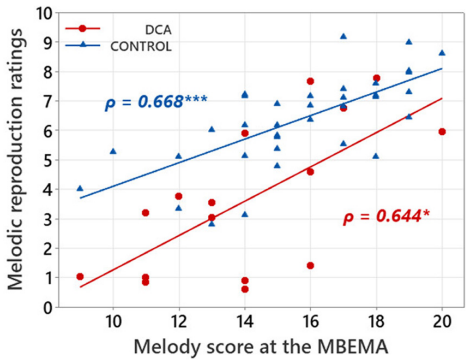

FIGURE 3
Scatterplot illustrating the correlations between mean ratings in melodic reproduction task and scores on the MBEMA Melody subtest. Regression lines are fitted for each group and the Spearman's ρ are indicated. *$p < 0.05$ and ***$p < 0.001$.

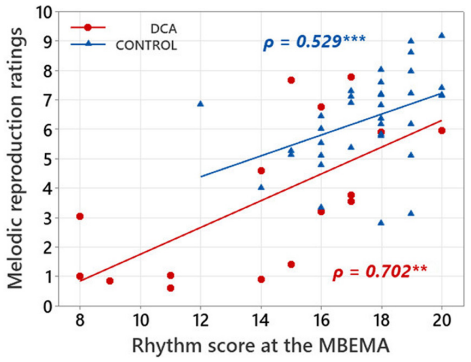

FIGURE 4
Scatterplot illustrating the correlations between mean ratings in melody singing and scores on the MBEMA Rhythm subtest. Regression lines are fitted for each group and the Spearman's ρ are indicated. **$p < 0.01$ and ***$p < 0.001$.

a deficit also found in music perception (rhythm and/or melody) and/or oro-bucco-facial praxis. Concerning the praxis, 12 out of sixteen patients had a very low score in the Oro-Bucco-Facial Praxis test. Finally, four out of the sixteen patients with DCA had no deficit in any of the tasks of our study.

The aim of these individual analyses was to explore possible dissociations between perception and production. Interestingly, three patients (Patient 4, 11, 14) were impaired in the melodic singing task without having an associated deficit in music perception, but these three patients had deficits in oro-bucco-facial praxis. Conversely, one patient (Patient 5) had a perceptual deficit in the Rhythm subtest associated with a deficit in the Oro-Bucco-Facial praxis, but without any singing impairment, and another patient had a deficit in the Oro-Bucco-Facial praxis without any deficit in music perception or singing (patient 3). The two patients with a perceptual deficit in the Melody subtest had a pathological performance in singing as well (patients 1 and 16).

Discussion

The purpose of this study was to explore music perception and production abilities in children with DCA. Music perception abilities were assessed using the MBEMA (Peretz et al., 2013), and music production abilities were assessed using two singing tasks presented via a playful and motivating computer game created by Clément et al. (2015). In addition, oro-bucco-facial praxis was assessed using the Hénin-Dulac test (Hénin, 1981). Results showed that children with DCA performed lower in rhythm perception and in singing short melodies, as well as in the oro-bucco-facial praxis test.

Regarding the music perception tasks, our mixed model analyses and *post hoc* tests showed that children with DCA scored significantly lower than healthy control children in the rhythm subtest of the MBEMA. In contrast, we did not find any significant difference between the two groups of participants in the melody comparison task or in the memory subtest of the MBEMA. These results bring further evidence of the important role of the cerebellum in rhythm processing already suggested by neuroimaging studies (Parsons, 2001; Chen et al., 2008; Thaut et al., 2014) and by studies showing rhythmic deficits in patients with cerebellar damages (Tölgyesi and Evers, 2014; Schwartze et al., 2016; Bégel et al., 2022a). In addition, these results provide a developmental perspective that has been little studied to date, suggesting a cerebellar role in the development of rhythmic abilities in children. Our findings complement those obtained in the two studies that reported rhythmic perception deficits in children with DCA in the specific case of spina bifida meningomyelocele (Dennis et al., 2009; Hopyan et al., 2009). Further, our results highlight the specificity of rhythmic perceptual deficits compared to melodic deficits and thus suggest that the musical difficulties experienced by children with DCA are not global. Our results also extend these findings of rhythmic deficits to other conditions with DCA, strengthening the evidence for a cerebellar role in the development of rhythm perception. The cerebellum is part of a distributed network that enables timing processes, including basal ganglia, the motor and premotor cortices (Grahn and Brett, 2007; Coull and Nobre, 2008; Coull et al., 2011; Breska and Ivry, 2016; Bareš et al., 2018). Its involvement is notable in predictive timing processes (Bastian, 2006; Schwartze and Kotz, 2013; Kotz et al., 2014; Schwartze et al., 2016) and in the neural tracking of beat and rhythm (Nozaradan et al., 2017). While the basal ganglia and associated cortico-striato-thalamo-cortical circuits seem to be specifically involved in rhythm processing that suppose high demand on internally generated beat, the cerebellum is thought to work in parallel to this circuit and contribute to this process

TABLE 3 Summary of the individual analyses results for each task.

	P-Values at the Bayesian test of deficit					
	Musical production (Singing tasks, Clément et al., 2015)		Musical perception (MBEMA short version, Peretz et al., 2013)			Oro-Bucco-Facial Praxis (Hénin-Dulac Test, Hénin, 1981)
	Pitch-matching task	Melodic reproduction task	Melody subtest	Rhythm subtest	Memory subtest	
Patient 1	0.110	0.001	0.007	<0.001	0.472	<0.001
Patient 2	0.401	0.259	0.137	0.240	0.169	0.085
Patient 3	0.398	0.434	0.317	0.331	0.074	0.036
Patient 4	0.120	0.001	0.440	0.077	0.357	<0.001
Patient 5	0.393	0.087	0.423	0.011	0.138	<0.001
Patient 6	0.062	<0.001	0.245	0.021	0.495	<0.001
Patient 7	0.213	0.002	0.464	0.003	0.408	<0.001
Patient 8	0.407	0.286	0.317	0.210	0.225	0.202
Patient 9	0.397	0.169	0.394	0.101	0.343	0.372
Patient 10	0.333	0.002	0.109	<0.001	0.441	0.001
Patient 11	0.078	0.020	0.081	0.198	0.441	0.040
Patient 12	0.381	0.032	0.230	<0.001	0.374	<0.001
Patient 13	0.093	0.496	0.414	0.109	0.153	0.496
Patient 14	0.107	0.042	0.069	0.326	0.268	<0.001
Patient 15	0.082	0.001	0.054	<0.001	0.056	<0.001
Patient 16	0.081	0.020	0.033	0.159	<0.001	<0.001

Each patient was compared to the entire control group, controlling for age as a covariate for each test. The null hypothesis is that the case's score is an observation of the control population's scores. The p-value calculated is also the estimated proportion of controls with the same value on the covariate that are expected to obtain a lower score than the case (Crawford et al., 2011). All significant *p*-values are highlighted in grey ($\alpha = 0.05$).

via a precise encoding and rapid transmission of an event-based representation of the temporal structure (Schwartze and Kotz, 2013, 2016; Nozaradan et al., 2017). The rhythm subtest of the MBEMA involves pairs of short melodies that are likely to differ in the duration of two adjacent tones but maintain the same meter and tempo. Thus, this task requires rhythmic grouping skills that rely on a precise encoding of the temporal events, and require the ability to correctly predict the onset of upcoming event based on previous information. This task could therefore particularly involve the cerebellum. This task also requires working memory, and our findings are in line with studies that suggest a specific involvement of the cerebellum in working memory for rhythms and for time interval embedded in rhythmic sequences (Jerde et al., 2011; Teki and Griffiths, 2016).

Moreover, individual analyses revealed heterogeneity within the patient group. While the group of patients performed significantly lower in rhythm perception than the group of healthy control children, of the sixteen patients, only eight were impaired in at least one subtest of music perception, including seven patients with a deficient score in rhythm perception. Heterogeneity is commonly reported in neurodevelopmental disorders and especially in DCA (Tavano et al., 2007; Jissendi-Tchofo et al., 2011), but the fact that half of the patients did not show any deficit in music perception is of particular interest. One explanation for this disparity in results may lie in the diversity of cerebellar anomalies within the patient group and the fact that rhythm processing involves specific parts of the cerebellum. Especially, in children with DCA associated to spina bifida meningomyelocele, Dennis et al. (2009) showed that rhythm perception deficits were associated with specific volumetric variations in the cerebellum. We did not investigate cerebellar volumes in this study, and it is therefore possible that children without rhythmic deficits have different volumetric variations. It might also be possible that some children have developed compensatory mechanisms. Cerebral plasticity is a phenomenon that is a source of variability in the development of children with neurodevelopmental disorders and could thus also explain part of the observed heterogeneity. Functional outcomes depend on several interacting factors, such as differences in genes, socioeconomic status, and differences in support and care (Dennis et al., 2013, 2014). In particular, cerebellar volumes and sensorimotor skills may vary with music or dance training from an early age (Baer et al., 2015; Nigmatullina et al., 2015).

Thus, each child's individual development may be influenced by many of these factors. It should also be noted that studies of adult cerebellar patients with acquired lesions have also reported controversial results regarding the involvement of the cerebellum in rhythm perception and prediction abilities (Grube et al., 2010a; Breska and Ivry, 2016, 2018, 2020). Future studies should therefore further investigate the individual variability of rhythmic skills in cerebellar disorders to better understand its source.

With regard to music production abilities, mixed model analyses revealed that children with DCA were impaired in singing short melodies. Our melodic singing task had three conditions: melodies were either those of familiar songs, familiar tunes, or melodies that were new and therefore unknown. Whereas control children showed superior performance on familiar songs and familiar tunes over unknown melodies, children with DCA did not benefit from prior knowledge of melodies. Singing disorders were expected because of the known involvement of the cerebellum in different processes of the vocal sensorimotor loop (Berkowska and Dalla Bella, 2009). Especially, it generates motor-to-auditory predictions (Knolle et al., 2012) and contributes to the prediction of self-initiated sounds (Knolle et al., 2013). The cerebellum is also involved in motor control of vocal muscles (Grabski et al., 2012) and in the auditory feedback control of vocal production (Li et al., 2019; Peng et al., 2021). Therefore, cerebellar anomalies can impair singing production at different levels.

The fact that children with DCA were impaired in melodic singing but were able to sing single notes as well as controls suggests that the singing deficit is revealed by the melodic nature of the task. Singing melodies requires not only the matching of desired pitches, but also the production of accurate rhythms, and therefore requires both rhythmic and melodic perception skills. As expected, in both groups, strong correlations were found between the MBEMA melody and rhythm subtests and the melodic singing scores. Given that children in the DCA group were mostly impaired in rhythm perception, they may have encountered difficulties in singing the melodies with a correct rhythm. Indeed, individual analyses revealed that six of the seven patients impaired in the rhythm subtest were also impaired in singing melodies.

In addition, motor impairments associated with cerebellar dysfunction (Ackermann et al., 1992; Mariën et al., 2014) could also have altered production of melodies, as singing involves a precise coordination of the vocal muscles, as well as the precise coordination of the muscles of the respiratory and phonatory apparatus. Within the patient group, a strong correlation was found between the score at the oro-bucco-facial praxis test (Hénin, 1981) and the mean rating at melodic singing. Moreover, our individual analyses revealed that all the children who were impaired in melodic singing were also impaired in oro-bucco-facial praxis. Ataxic dysarthria is part of the cerebellar syndrome and is mainly manifested by articulatory deficits and slowed speech tempo (Ackermann et al., 1992). It is often also accompanied by respiratory and phonatory disorder which can cause irregular alterations of voice quality and loudness (Mariën et al., 2014). Therefore, it is not surprising that patients who displayed a deficit in oro-bucco-facial praxis were also impaired in the melodic singing task. These findings can be related to those of a recent study (Zúñiga et al., 2020) which suggest links between dysarthria and singing abilities in two patients suffering a cerebellar stroke.

Taken together, our findings suggest an important role of the cerebellum in the development of singing abilities, with impairments found in patients on both the perceptive and motor components of the vocal sensorimotor loop. To further investigate the results, we examined individual performance on the different tasks of the experiment, which allowed us to highlight performance dissociations. Three patients (patients 4, 11, 14) had melodic singing deficits in the presence of preserved perceptual abilities, suggesting that good perceptual musical abilities are not sufficient for the development of singing skills. This dissociation had already been documented in the literature (Berkowska and Dalla Bella, 2009). However, these three patients had a deficit of the oro-bucco-facial praxis, which could explain the singing deficit despite the preservation of musical perception. On the other hand, interestingly, a patient with an oro-bucco-facial praxis deficit (patient 3), and another patient (patient 5, also impaired in rhythm) showed correct performance in the singing task despite the presence of oro-bucco-facial praxis deficit, suggesting that the development of the ability to sing melodies correctly is still possible in the presence of such praxis deficits. Finally, four patients did not show any deficits in any tasks. All these findings suggest that singing abilities could depend both on the development of musical perception as well as of the oro-buccal praxis. Different developmental trajectories are possible in the presence of DCA, which is probably due to the presence of compensation mechanisms in some cases.

Understanding of the mechanisms underlying musical deficits in relation to DCA in the present study is limited by some shortcomings. First, the subjective assessment procedure for melodic singing does not allow to distinguish between rhythmic or melodic impairment. As in a previous study by Clément et al. (2015), we chose this method because some of the patients' productions were impaired to the point that they contained only a few notes and were not recognizable. To unravel the impacts of rhythmic, melodic, and praxis deficits on music production abilities, future studies could use paradigms with conditions that specifically vary these parameters or consider new methods of singing analysis. Furthermore, it is not clear which specific mechanisms of rhythmic perception and/or production are affected. This study therefore calls for a more comprehensive assessment of rhythmic perception, production, and rhythm-based prediction abilities in the presence of DCA, varying conditions such as tempo, meter, or syncopation. Finally, it is worth reminding that all participants had received less than 1 year of formal music or dance instruction. However,

non-formal music practice may vary among participants, and future studies should control for music and dance exposure. Similarly, we were not able to clearly control the different care paths of the patients. However, these differences in care may have had an impact on the development and implementation of compensatory mechanisms, which could partly explain the observed heterogeneity. Further studies should also investigate the links between speech and language and musical deficits in children with DCA. To explore these mechanisms and the underlying brain substrates, neuroimaging studies could provide interesting information, both from a structural and functional perspective.

Conclusion and implications

Overall, our results suggest that DCA are associated with deficits in the musical sphere, especially in rhythmic perception and melodic singing. Further research will be needed to unravel the links between rhythmic, praxis, and singing deficits found in children with DCA. The impairment of rhythmic abilities is consistent with studies that have shown that rhythmic impairments are common in neurodevelopmental disorders (Lense et al., 2021), particularly in dyslexia (Bégel et al., 2022b) and ADHD (Puyjarinet et al., 2017), for which an involvement of the cerebellum has been highlighted (Stoodley, 2016; Sathyanesan et al., 2019). Rhythmic deficits are often associated with cognitive and social deficits, and therapeutic approaches based on rhythm and audio-motor synchronization such as dance are a promising tool for children with DCA as they seem to improve rhythmic abilities as well as cognitive functions (Bégel et al., 2022a). Our study provides new evidence regarding the involvement of the cerebellum in singing abilities and may pave the way for music-based remediation including singing training. Moreover, the heterogeneity of musical performance in this population must be considered before considering such interventions. Indeed, the different profiles observed suggest that various mechanisms may be affected in DCA, which should lead to a detailed assessment of musical abilities in these patients in order to orient them toward the intervention that will be most adapted to their needs.

Data availability statement

The raw data supporting the conclusions of this article will be made available by the authors, without undue reservation.

Ethics statement

Ethical review and approval was not required for the study on human participants in accordance with the local legislation and institutional requirements. Written informed consent to participate in this study was provided by the participants' legal guardian/next of kin.

Author contributions

AG, SC, and DD contributed to the analysis of the results. AG and DD contributed to the writing of the manuscript. All authors approved the submitted version, contributed to the design, and implementation of the research.

Funding

CHU Lille, Lille, France supported all publication fees and Univ. Lille, ULR 4072—PSITEC—Psychologie : Interactions Temps Émotions Cognition, Lille, France supported proofreading fees. This work was supported by the University of Lille to AG.

Acknowledgments

We are grateful to Vadleen Lowenski for her help in data collection, and to the judges who rated the sung melodies. We also thank all the children who participated in this study.

Conflict of interest

The authors declare that the research was conducted in the absence of any commercial or financial relationships that could be construed as a potential conflict of interest.

Publisher's note

Supplementary material

The Supplementary Material for this article can be found online at: https://www.frontiersin.org/articles/10.3389/fnsys.2022.886427/full#supplementary-material

References

Ackermann, H., Vogel, M., Petersen, D., and Poremba, M. (1992). Speech deficits in ischaemic cerebellar lesions. *J. Neurol.* 239, 223–227. doi: 10.1007/BF00839144

Akaike, H. (1974). A new look at the statistical model identification. *IEEE Trans. Automat. Control* 19, 716–723. doi: 10.1109/TAC.1974.1100705

Audacity Team (2019). *Audacity(R): Free audio editor and recorder (2.2.1) [Computer software]*. Available online at: https://www.audacityteam.org

Baer, L. H., Park, M. T. M., Bailey, J. A., Chakravarty, M. M., Li, K. Z. H., and Penhune, V. B. (2015). Regional cerebellar volumes are related to early musical training and finger tapping performance. *Neuroimage* 109, 130–139. doi: 10.1016/j.neuroimage.2014.12.076

Bareš, M., Apps, R., Avanzino, L., Breska, A., D'Angelo, E., Filip, P., et al. (2018). Consensus paper: Decoding the contributions of the cerebellum as a time machine. From neurons to clinical applications. *Cerebellum* 18, 266–286. doi: 10.1007/s12311-018-0979-5

Barreda, S. (2015). *phonTools: Tools for phonetic and acoustic analyses (0.2-2.1) [R-Package]*. Available online at: https://CRAN.R-project.org/package=phonTools

Bastian, A. J. (2006). Learning to predict the future: The cerebellum adapts feedforward movement control. *Curr. Opin. Neurobiol.* 16, 645–649. doi: 10.1016/j.conb.2006.08.016

Bates, D., Mächler, M., Bolker, B., and Walker, S. (2015). Fitting linear mixed-effects models using lme4. *J. Stat. Softw.* 67, 1–48. doi: 10.18637/jss.v067.i01

Baumann, O., Borra, R. J., Bower, J. M., Cullen, K. E., Habas, C., Ivry, R. B., et al. (2015). Consensus paper: The role of the cerebellum in perceptual processes. *Cerebellum* 14, 197–220. doi: 10.1007/s12311-014-0627-7

Bégel, V., Bachrach, A., Dalla Bella, S., Laroche, J., Clément, S., Riquet, A., et al. (2022a). Dance improves motor, cognitive, and social skills in children with developmental cerebellar anomalies. *Cerebellum* 21, 264–279. doi: 10.1007/s12311-021-01291-2

Bégel, V., Dalla Bella, S., Devignes, Q., Vandenbergue, M., Lemaître, M.-P., and Dellacherie, D. (2022b). Rhythm as an independent determinant of developmental dyslexia. *Dev. Psychol.* 58, 339–358. doi: 10.1037/dev0001293

Belin, P., McAdams, S., Thivard, L., Smith, B., Savel, S., Zilbovicius, M., et al. (2002). The neuroanatomical substrate of sound duration discrimination. *Neuropsychologia* 40, 1956–1964. doi: 10.1016/s0028-3932(02)00062-3

Berkowska, M., and Dalla Bella, S. (2009). Acquired and congenital disorders of sung performance: A review. *Adv. Cogn. Psychol.* 5, 69–83. doi: 10.2478/v10053-008-0068-2

Berkowska, M., and Dalla Bella, S. (2013). Uncovering phenotypes of poor-pitch singing: The Sung Performance Battery (SPB). *Front. Psychol.* 4:714. doi: 10.3389/fpsyg.2013.00714

Bertini, E., Zanni, G., and Boltshauser, E. (2018). "Chapter 6—Nonprogressive congenital ataxias," in *Handbook of clinical neurology*, Vol. 155, eds M. Manto and T. A. G. M. Huisman (Amsterdam: Elsevier), 91–103. doi: 10.1016/B978-0-444-64189-2.00006-8

Bigand, E. (2003). More about the musical expertise of musically untrained listeners. *Ann. N. Y. Acad. Sci.* 999, 304–312. doi: 10.1196/annals.1284.041

Bozdogan, H. (1987). Model selection and Akaike's Information Criterion (AIC): The general theory and its analytical extensions. *Psychometrika* 52, 345–370. doi: 10.1007/BF02294361

Breska, A., and Ivry, R. B. (2016). Taxonomies of timing: Where does the cerebellum fit in? *Curr. Opin. Behav. Sci.* 8, 282–288. doi: 10.1016/j.cobeha.2016.02.034

Breska, A., and Ivry, R. B. (2018). Double dissociation of single-interval and rhythmic temporal prediction in cerebellar degeneration and Parkinson's disease. *Proc. Natl. Acad. Sci. U.S.A.* 115, 12283–12288. doi: 10.1073/pnas.1810596115

Breska, A., and Ivry, R. B. (2020). Context-specific control over the neural dynamics of temporal attention by the human cerebellum. *Sci. Adv.* 6:eabb1141. doi: 10.1126/sciadv.abb1141

Brown, R. M., Zatorre, R. J., and Penhune, V. B. (2015). Expert music performance: Cognitive, neural, and developmental bases. *Prog. Brain Res.* 217, 57–86. doi: 10.1016/bs.pbr.2014.11.021

Brown, S., Martinez, M. J., and Parsons, L. M. (2004b). Passive music listening spontaneously engages limbic and paralimbic systems. *NeuroReport* 15, 2033–2037. doi: 10.1097/00001756-200409150-00008

Brown, S., Martinez, M. J., Hodges, D. A., Fox, P. T., and Parsons, L. M. (2004a). The song system of the human brain. *Brain Res. Cogn. Brain Res.* 20, 363–375. doi: 10.1016/j.cogbrainres.2004.03.016

Caldwell, A. R. (2022). SimplyAgree: An R package and jamovi module for simplifying agreement and reliability analyses. *J. Open Sour. Softw.* 7:4148. doi: 10.21105/joss.04148

Callan, D. E., Kawato, M., Parsons, L., and Turner, R. (2007). Speech and song: The role of the cerebellum. *Cerebellum* 6, 321–327. doi: 10.1080/14734220601187733

Chen, J. L., Penhune, V. B., and Zatorre, R. J. (2008). Listening to musical rhythms recruits motor regions of the brain. *Cereb. Cortex* 18, 2844–2854. doi: 10.1093/cercor/bhn042

Clément, S., Planchou, C., Béland, R., Motte, J., and Samson, S. (2015). Singing abilities in children with Specific Language Impairment (SLI). *Front. Psychol.* 6:420. doi: 10.3389/fpsyg.2015.00420

Coull, J., Cheng, R.-K., and Meck, W. (2011). Neuroanatomical and neurochemical substrates of timing. *Neuropsychopharmacology* 36, 3–25. doi: 10.1038/npp.2010.113

Coull, J., and Nobre, A. (2008). Dissociating explicit timing from temporal expectation with fMRI. *Curr. Opin. Neurobiol.* 18, 137–144. doi: 10.1016/j.conb.2008.07.011

Crawford, J. R., Garthwaite, P. H., and Ryan, K. (2011). Comparing a single case to a control sample: Testing for neuropsychological deficits and dissociations in the presence of covariates. *Cortex* 47, 1166–1178. doi: 10.1016/j.cortex.2011.02.017

Dalla Bella, S., and Berkowska, M. (2009). Singing proficiency in the majority: Normality and « phenotypes » of poor singing. *Ann. N. Y. Acad. Sci.* 1169, 99–107. doi: 10.1111/j.1749-6632.2009.04558.x

Dalla Bella, S., Białuńska, A., and Sowiński, J. (2013). Why movement is captured by music, but less by speech: Role of temporal regularity. *PLoS One* 8:e71945. doi: 10.1371/journal.pone.0071945

Dalla Bella, S., Giguère, J.-F., and Peretz, I. (2007). Singing proficiency in the general population. *J. Acoust. Soc. Am.* 121, 1182–1189. doi: 10.1121/1.2427111

De Guio, F., Jacobson, S. W., Molteno, C. D., Jacobson, J. L., and Meintjes, E. M. (2012). Functional magnetic resonance imaging study comparing rhythmic finger tapping in children and adults. *Pediatr. Neurol.* 46, 94–100. doi: 10.1016/j.pediatrneurol.2011.11.019

Dennis, M., Edelstein, K., Hetherington, R., Copeland, K., Frederick, J., Blaser, S. E., et al. (2004). Neurobiology of perceptual and motor timing in children with spina bifida in relation to cerebellar volume. *Brain* 127(Pt 6), 1292–1301. doi: 10.1093/brain/awh154

Dennis, M., Hopyan, T., Juranek, J., Cirino, P. T., Hasan, K. M., and Fletcher, J. (2009). Strong-meter and weak-meter rhythm identification in spina bifida meningomyelocele and volumetric parcellation of rhythm-relevant cerebellar regions. *Ann. N. Y. Acad. Sci.* 1169, 84–88. doi: 10.1111/j.1749-6632.2009.04863.x

Dennis, M., Spiegler, B. J., Juranek, J. J., Bigler, E. D., Snead, O. C., and Fletcher, J. M. (2013). Age, plasticity, and homeostasis in childhood brain disorders. *Neurosci. Biobehav. Rev.* 37, 2760–2773. doi: 10.1016/j.neubiorev.2013.09.010

Dennis, M., Spiegler, B. J., Simic, N., Sinopoli, K. J., Wilkinson, A., Yeates, K. O., et al. (2014). Functional plasticity in childhood brain disorders: When, what, how, and whom to assess. *Neuropsychol. Rev.* 24, 389–408. doi: 10.1007/s11065-014-9261-x

Droit-Volet, S., Zélanti, P. S., Dellatolas, G., Kieffer, V., El Massioui, N., Brown, B. L., et al. (2013). Time perception in children treated for a cerebellar medulloblastoma. *Res. Dev. Disabil.* 34, 480–494. doi: 10.1016/j.ridd.2012.09.006

Flaugnacco, E., Lopez, L., Terribili, C., Zoia, S., Buda, S., Tilli, S., et al. (2014). Rhythm perception and production predict reading abilities in developmental dyslexia. *Front. Hum. Neurosci.* 8:392. doi: 10.3389/fnhum.2014.00392

Garel, C., Fallet-Bianco, C., and Guibaud, L. (2011). The fetal cerebellum: Development and common malformations. *J. Child Neurol.* 26, 1483–1492. doi: 10.1177/0883073811420148

González-García, N., González, M. A., and Rendón, P. L. (2016). Neural activity related to discrimination and vocal production of consonant and dissonant musical intervals. *Brain Res.* 1643, 59–69. doi: 10.1016/j.brainres.2016.04.065

Gordon, C. L., Cobb, P. R., and Balasubramaniam, R. (2018). Recruitment of the motor system during music listening: An ALE meta-analysis of fMRI data. *PLoS One* 13:e0207213. doi: 10.1371/journal.pone.0207213

Grabski, K., Lamalle, L., Vilain, C., Schwartz, J.-L., Vallée, N., Tropres, I., et al. (2012). Functional MRI assessment of orofacial articulators: Neural correlates of lip, jaw, larynx, and tongue movements. *Hum. Brain Mapp.* 33, 2306–2321. doi: 10.1002/hbm.21363

Grahn, J. A., and Brett, M. (2007). Rhythm and beat perception in motor areas of the brain. *J. Cogn. Neurosci.* 19, 893–906. doi: 10.1162/jocn.2007.19.5.893

Grube, M., Lee, K.-H., Griffiths, T., Barker, A., and Woodruff, P. (2010b). Transcranial magnetic theta-burst stimulation of the human cerebellum distinguishes absolute, duration-based from relative, beat-based perception of subsecond time intervals. *Front. Psychol.* 1:171. doi: 10.3389/fpsyg.2010.00171

Grube, M., Cooper, F. E., Chinnery, P. F., and Griffiths, T. D. (2010a). Dissociation of duration-based and beat-based auditory timing in cerebellar degeneration. *Proc. Natl. Acad. Sci. U.S.A.* 107, 11597–11601. doi: 10.1073/pnas.0910473107

Hénin, N. (1981). Etude de la motricité et des praxies oro-faciales chez l'enfant de 2;6 ans à 12;6 ans. *Les Cah. D'orl* 15, 809–853.

Herholz, S. C., Halpern, A. R., and Zatorre, R. J. (2012). Neuronal correlates of perception, imagery, and memory for familiar tunes. *J. Cogn. Neurosci.* 24, 1382–1397. doi: 10.1162/jocn_a_00216

Herholz, S. C., and Zatorre, R. J. (2012). Musical training as a framework for brain plasticity: Behavior, function, and structure. *Neuron* 76, 486–502. doi: 10.1016/j.neuron.2012.10.011

Hopyan, T., Schellenberg, E. G., and Dennis, M. (2009). Perception of strong-meter and weak-meter rhythms in children with spina bifida meningomyelocele. *J. Int. Neuropsychol. Soc.* 15, 521–528. doi: 10.1017/S1355617709090845

Ivry, R. B., and Keele, S. W. (1989). Timing functions of the cerebellum. *J. Cogn. Neurosci.* 1, 136–152. doi: 10.1162/jocn.1989.1.2.136

Jäncke, L., Loose, R., Lutz, K., Specht, K., and Shah, N. J. (2000). Cortical activations during paced finger-tapping applying visual and auditory pacing stimuli. *Brain Res. Cogn. Brain Res.* 10, 51–66. doi: 10.1016/s0926-6410(00)00022-7

Jerde, T. A., Childs, S. K., Handy, S. T., Nagode, J. C., and Pardo, J. V. (2011). Dissociable systems of working memory for rhythm and melody. *Neuroimage* 57, 1572–1579. doi: 10.1016/j.neuroimage.2011.05.061

Jissendi-Tchofo, P., Pandit, F., Soto-Ares, G., and Vallee, L. (2011). Neuropsychological evaluation and follow-up of children with cerebellar cortical dysplasia. *Dev. Med. Child Neurol.* 53, 1119–1127. doi: 10.1111/j.1469-8749.2011.04117.x

Johnson, J. F., Belyk, M., Schwartze, M., Pinheiro, A. P., and Kotz, S. A. (2019). The role of the cerebellum in adaptation: ALE meta-analyses on sensory feedback error. *Hum. Brain Mapp.* 40, 3966–3981. doi: 10.1002/hbm.24681

Kleber, B., Birbaumer, N., Veit, R., Trevorrow, T., and Lotze, M. (2007). Overt and imagined singing of an Italian aria. *Neuroimage* 36, 889–900. doi: 10.1016/j.neuroimage.2007.02.053

Kleber, B., Veit, R., Birbaumer, N., Gruzelier, J., and Lotze, M. (2010). The brain of opera singers: Experience-dependent changes in functional activation. *Cereb. Cortex* 20, 1144–1152. doi: 10.1093/cercor/bhp177

Kleber, B., and Zarate, J. M. (2014). "The neuroscience of singing," in *The oxford handbook of singing*, eds G. F. Welch, D. M. Howard, and J. Nix (Oxford: Oxford University Press). doi: 10.1093/oxfordhb/9780199660773.013.015

Knolle, F., Schröger, E., Baess, P., and Kotz, S. A. (2012). The cerebellum generates motor-to-auditory predictions: ERP lesion evidence. *J. Cogn. Neurosci.* 24, 698–706. doi: 10.1162/jocn_a_00167

Knolle, F., Schröger, E., and Kotz, S. A. (2013). Cerebellar contribution to the prediction of self-initiated sounds. *Cortex* 49, 2449–2461. doi: 10.1016/j.cortex.2012.12.012

Konoike, N., Kotozaki, Y., Miyachi, S., Miyauchi, C. M., Yomogida, Y., Akimoto, Y., et al. (2012). Rhythm information represented in the fronto-parieto-cerebellar motor system. *Neuroimage* 63, 328–338. doi: 10.1016/j.neuroimage.2012.07.002

Koo, T. K., and Li, M. Y. (2016). A guideline of selecting and reporting intraclass correlation coefficients for reliability research. *J. Chiropr. Med.* 15, 155–163. doi: 10.1016/j.jcm.2016.02.012

Kotz, S. A., Stockert, A., and Schwartze, M. (2014). Cerebellum, temporal predictability and the updating of a mental model. *Philos. Trans. R. Soc. Lond. Ser. B Biol. Sci.* 369:20130403. doi: 10.1098/rstb.2013.0403

Kuznetsova, A., Brockhoff, P. B., and Christensen, R. H. B. (2017). lmerTest package: Tests in linear mixed effects models. *J. Stat. Softw.* 82, 1–26. doi: 10.18637/jss.v082.i13

Larrouy-Maestri, P., Lévêque, Y., Schön, D., Giovanni, A., and Morsomme, D. (2013). The evaluation of singing voice accuracy?: A comparison between subjective and objective methods. *J. Voice* 27, 259.e1–259.e5. doi: 10.1016/j.jvoice.2012.11.003

Lega, C., Vecchi, T., D'Angelo, E., and Cattaneo, Z. (2016). A TMS investigation on the role of the cerebellum in pitch and timbre discrimination. *Cerebellum Ataxias* 3:6. doi: 10.1186/s40673-016-0044-4

Lense, M. D., Ladányi, E., Rabinowitch, T.-C., Trainor, L., and Gordon, R. (2021). Rhythm and timing as vulnerabilities in neurodevelopmental disorders. *Philos. Trans. R. Soc. B* 376:20200327. doi: 10.1098/rstb.2020.0327

Lenth, R. V., Buerkner, P., Herve, M., Love, J., Miguez, F., Riebl, H., et al. (2022). *emmeans: Estimated marginal means, aka least-squares means (1.7.4-1) [R-Package]*. Available online at: https://CRAN.R-project.org/package=emmeans

Li, W., Zhuang, J., Guo, Z., Jones, J. A., Xu, Z., and Liu, H. (2019). Cerebellar contribution to auditory feedback control of speech production: Evidence from patients with spinocerebellar ataxia. *Hum. Brain Mapp.* 40, 4748–4758. doi: 10.1002/hbm.24734

Mariën, P., Ackermann, H., Adamaszek, M., Barwood, C. H. S., Beaton, A., Desmond, J., et al. (2014). Consensus paper: Language and the cerebellum: An ongoing Enigma. *Cerebellum* 13, 386–410. doi: 10.1007/s12311-013-0540-5

Molinari, M., Leggio, M. G., De Martin, M., Cerasa, A., and Thaut, M. (2003). Neurobiology of rhythmic motor entrainment. *Ann. N. Y. Acad. Sci.* 999, 313–321. doi: 10.1196/annals.1284.042

Mostofsky, S. H., Kunze, J. C., Cutting, L. E., Lederman, H. M., and Denckla, M. B. (2000). Judgment of duration in individuals with ataxia-telangiectasia. *Dev. Neuropsychol.* 17, 63–74. doi: 10.1207/S15326942DN1701_04

Musselman, K. E., Stoyanov, C. T., Marasigan, R., Jenkins, M. E., Konczak, J., Morton, S. M., et al. (2014). Prevalence of ataxia in children: A systematic review. *Neurology* 82, 80–89. doi: 10.1212/01.wnl.0000438224.25600.6c

Nigmatullina, Y., Hellyer, P. J., Nachev, P., Sharp, D. J., and Seemungal, B. M. (2015). The neuroanatomical correlates of training-related perceptuo-reflex uncoupling in dancers. *Cereb. Cortex* 25, 554–562. doi: 10.1093/cercor/bht266

Nozaradan, S., Schwartze, M., Obermeier, C., and Kotz, S. A. (2017). Specific contributions of basal ganglia and cerebellum to the neural tracking of rhythm. *Cortex* 95, 156–168. doi: 10.1016/j.cortex.2017.08.015

Paquette, S., Fujii, S., Li, H. C., and Schlaug, G. (2017). The cerebellum's contribution to beat interval discrimination. *Neuroimage* 163, 177–182. doi: 10.1016/j.neuroimage.2017.09.017

Parsons, L. M. (2001). Exploring the functional neuroanatomy of music performance, perception, and comprehension. *Ann. N. Y. Acad. Sci.* 930, 211–231. doi: 10.1111/j.1749-6632.2001.tb05735.x

Parsons, L. M., Petacchi, A., Schmahmann, J. D., and Bower, J. M. (2009). Pitch discrimination in cerebellar patients: Evidence for a sensory deficit. *Brain Res.* 1303, 84–96. doi: 10.1016/j.brainres.2009.09.052

Peirce, J., Gray, J. R., Simpson, S., MacAskill, M., Höchenberger, R., Sogo, H., et al. (2019). PsychoPy2: Experiments in behavior made easy. *Behav. Res. Methods* 51, 195–203. doi: 10.3758/s13428-018-01193-y

Peng, D., Lin, Q., Chang, Y., Jones, J. A., Jia, G., Chen, X., et al. (2021). A causal role of the cerebellum in auditory feedback control of vocal production. *Cerebellum* 20, 584–595. doi: 10.1007/s12311-021-01230-1

Penhune, V. B., Zattore, R. J., and Evans, A. C. (1998). Cerebellar contributions to motor timing: A PET study of auditory and visual rhythm reproduction. *J. Cogn. Neurosci.* 10, 752–765. doi: 10.1162/089892998563149

Perani, D., Saccuman, M. C., Scifo, P., Spada, D., Andreolli, G., Rovelli, R., et al. (2010). Functional specializations for music processing in the human newborn brain. *Proc. Natl. Acad. Sci. U.S.A.* 107, 4758–4763. doi: 10.1073/pnas.0909074107

Peretz, I., Gosselin, N., Nan, Y., Caron-Caplette, E., Trehub, S. E., and Béland, R. (2013). A novel tool for evaluating children's musical abilities across age and culture. *Front. Syst. Neurosci.* 7:30. doi: 10.3389/fnsys.2013.00030

Peretz, I., and Zatorre, R. (2005). Brain organization for music processing. *Annu. Rev. Psychol.* 56, 89–114. doi: 10.1146/annurev.psych.56.091103.070225

Perry, D. W., Zatorre, R. J., Petrides, M., Alivisatos, B., Meyer, E., and Evans, A. C. (1999). Localization of cerebral activity during simple singing. *Neuroreport* 10, 3979–3984. doi: 10.1097/00001756-199912160-00046

Petacchi, A., Kaernbach, C., Ratnam, R., and Bower, J. M. (2011). Increased activation of the human cerebellum during pitch discrimination: A positron emission tomography (PET) study. *Hear. Res.* 282, 35–48. doi: 10.1016/j.heares.2011.09.008

Pfordresher, P. Q., Mantell, J. T., Brown, S., Zivadinov, R., and Cox, J. L. (2014). Brain responses to altered auditory feedback during musical keyboard production: An fMRI study. *Brain Res.* 1556, 28–37. doi: 10.1016/j.brainres.2014.02.004

Provasi, J., Anderson, D. I., and Barbu-Roth, M. (2014a). Rhythm perception, production, and synchronization during the perinatal period. *Front. Psychol.* 5:1048. doi: 10.3389/fpsyg.2014.01048

Provasi, J., Doyère, V., Zélanti, P. S., Kieffer, V., Perdry, H., El Massioui, N., et al. (2014b). Disrupted sensorimotor synchronization, but intact rhythm discrimination, in children treated for a cerebellar medulloblastoma. *Res. Dev. Disabil.* 35, 2053–2068. doi: 10.1016/j.ridd.2014.04.024

Puyjarinet, F., Bégel, V., Lopez, R., Dellacherie, D., and Dalla Bella, S. (2017). Children and adults with attention-deficit/hyperactivity disorder cannot move to the beat. *Sci. Rep.* 7:11550. doi: 10.1038/s41598-017-11295-w

R Core Team (2021). *R: A language and environment for statistical computing [Computer software]*. Vienna: R Foundation for Statistical Computing.

Rao, S. M., Harrington, D. L., Haaland, K. Y., Bobholz, J. A., Cox, R. W., and Binder, J. R. (1997). Distributed neural systems underlying the timing of movements. *J. Neurosci.* 17, 5528. doi: 10.1523/JNEUROSCI.17-14-05528.1997

Rivkin, M. J., Vajapeyam, S., Hutton, C., Weiler, M. L., Hall, E. K., Wolraich, D. A., et al. (2003). A functional magnetic resonance imaging study of paced finger tapping in children. *Pediatr. Neurol.* 28, 89–95. doi: 10.1016/s0887-8994(02)00492-7

Sathyanesan, A., Zhou, J., Scafidi, J., Heck, D. H., Sillitoe, R. V., and Gallo, V. (2019). Emerging connections between cerebellar development, behaviour and complex brain disorders. *Nat. Rev. Neurosci.* 20, 298–313. doi: 10.1038/s41583-019-0152-2

Schmahmann, J. D. (2019). The cerebellum and cognition. *Neurosci. Lett.* 688, 62–75. doi: 10.1016/j.neulet.2018.07.005

Schmahmann, J. D., and Sherman, J. C. (1998). The cerebellar cognitive affective syndrome. *Brain* 121(Pt 4), 561–579. doi: 10.1093/brain/121.4.561

Schwartze, M., Keller, P. E., and Kotz, S. A. (2016). Spontaneous, synchronized, and corrective timing behavior in cerebellar lesion patients. *Behav. Brain Res.* 312, 285–293. doi: 10.1016/j.bbr.2016.06.040

Schwartze, M., and Kotz, S. A. (2013). A dual-pathway neural architecture for specific temporal prediction. *Neurosci. Biobehav. Rev.* 37, 2587–2596. doi: 10.1016/j.neubiorev.2013.08.005

Schwartze, M., and Kotz, S. A. (2016). Contributions of cerebellar event-based temporal processing and preparatory function to speech perception. *Brain Lang.* 161, 28–32. doi: 10.1016/j.bandl.2015.08.005

Segado, M., Hollinger, A., Thibodeau, J., Penhune, V., and Zatorre, R. J. (2018). Partially overlapping brain networks for singing and cello playing. *Front. Neurosci.* 12:351. doi: 10.3389/fnins.2018.00351

Stadler Elmer, S. (2012). Characteristics of early productive musicality. Problems of music pedagogy, 10, 9-23. *Probl. Music Pedag.* 10, 9–23.

Steinlin, M., Styger, M., and Boltshauser, E. (1999). Cognitive impairments in patients with congenital nonprogressive cerebellar ataxia. *Neurology* 53, 966–973. doi: 10.1212/wnl.53.5.966

Steinlin, M., Zangger, B., and Boltshauser, E. (1998). Non-progressive congenital ataxia with or without cerebellar hypoplasia: A review of 34 subjects. *Dev. Med. Child Neurol.* 40, 148–154. doi: 10.1111/j.1469-8749.1998.tb15438.x

Stoodley, C. J. (2016). The cerebellum and neurodevelopmental disorders. *Cerebellum* 15, 34–37. doi: 10.1007/s12311-015-0715-3

Stoodley, C. J., Valera, E. M., and Schmahmann, J. D. (2012). Functional topography of the cerebellum for motor and cognitive tasks: An fMRI study. *Neuroimage* 59, 1560–1570. doi: 10.1016/j.neuroimage.2011.08.065

Tavano, A., Grasso, R., Gagliardi, C., Triulzi, F., Bresolin, N., Fabbro, F., et al. (2007). Disorders of cognitive and affective development in cerebellar malformations. *Brain* 130(Pt 10), 2646–2660. doi: 10.1093/brain/awm201

Teki, S., and Griffiths, T. D. (2016). Brain bases of working memory for time intervals in rhythmic sequences. *Front. Neurosci.* 10:239. doi: 10.3389/fnins.2016.00239

Teki, S., Grube, M., Kumar, S., and Griffiths, T. D. (2011). Distinct neural substrates of duration-based and beat-based auditory timing. *J. Neurosci.* 31, 3805–3812. doi: 10.1523/JNEUROSCI.5561-10.2011

Thaut, M. H., Trimarchi, P. D., and Parsons, L. M. (2014). Human brain basis of musical rhythm perception: Common and distinct neural substrates for meter, tempo, and pattern. *Brain Sci.* 4, 428–452. doi: 10.3390/brainsci4020428

Tölgyesi, B., and Evers, S. (2014). The impact of cerebellar disorders on musical ability. *J. Neurol. Sci.* 343, 76–81. doi: 10.1016/j.jns.2014.05.036

Wechsler, D. (2005). *WISC-IV: Echelle d'intelligence de Wechsler pour enfants*, 4 Edn. Paris: ECPA.

Wechsler, D. (2016). *WISC-V: Echelle d'intelligence de Wechsler pour enfants*, 5 Edn. Paris: ECPA.

Winkler, I., Háden, G. P., Ladinig, O., Sziller, I., and Honing, H. (2009). Newborn infants detect the beat in music. *Proc. Natl. Acad. Sci. U.S.A.* 106, 2468–2471. doi: 10.1073/pnas.0809035106

Wolpert, D. M., Miall, R. C., and Kawato, M. (1998). Internal models in the cerebellum. *Trends Cogn. Sci.* 2, 338–347. doi: 10.1016/S1364-6613(98)01221-2

Zarate, J. M., and Zatorre, R. J. (2008). Experience-dependent neural substrates involved in vocal pitch regulation during singing. *Neuroimage* 40, 1871–1887. doi: 10.1016/j.neuroimage.2008.01.026

Zatorre, R. J., Chen, J. L., and Penhune, V. B. (2007). When the brain plays music: Auditory-motor interactions in music perception and production. *Nat. Rev. Neurosci.* 8, 547–558. doi: 10.1038/nrn2152

Zúñiga, M. S. S., Espejo, C. H., Navarrete, L. H., Reyes, A. E., and Rivas, D. R. (2020). Speech and singing performance in patients suffering a cerebellar stroke: A case study. *Rev. Investig. Logopedia* 10, 43–51. doi: 10.5209/rlog.64278

frontiers | Frontiers in Systems Neuroscience

TYPE Hypothesis and Theory
PUBLISHED 15 September 2022
DOI 10.3389/fnsys.2022.886284

OPEN ACCESS

EDITED BY
Anne-Lise Paradis,
Center for the National Scientific Research (CNRS), France

REVIEWED BY
David Samuel Zee,
Johns Hopkins University, United States
Marija Cvetanovic,
University of Minnesota Twin Cities, United States

*CORRESPONDENCE
Jean Laurens
jean.laurens@esi-frankfurt.de

RECEIVED 28 February 2022
ACCEPTED 22 August 2022
PUBLISHED 15 September 2022

CITATION
Laurens J (2022) The otolith vermis: A systems neuroscience theory of the Nodulus and Uvula.
Front. Syst. Neurosci. 16:886284.
doi: 10.3389/fnsys.2022.886284

The otolith vermis: A systems neuroscience theory of the Nodulus and Uvula

Jean Laurens*

Ernst Strüngmann Institute (ESI) for Neuroscience in Cooperation with Max Planck Society, Frankfurt, Germany

The Nodulus and Uvula (NU) (lobules X and IX of the cerebellar vermis) form a prominent center of vestibular information processing. Over decades, fundamental and clinical research on the NU has uncovered many aspects of its function. Those include the resolution of a sensory ambiguity inherent to inertial sensors in the inner ear, the otolith organs; the use of gravity signals to sense head rotations; and the differential processing of self-generated and externally imposed head motion. Here, I review these works in the context of a theoretical framework of information processing called the internal model hypothesis. I propose that the NU implements a forward internal model to predict the activation of the otoliths, and outputs sensory predictions errors to correct internal estimates of self-motion or to drive learning. I show that a Kalman filter based on this framework accounts for various functions of the NU, neurophysiological findings, as well as the clinical consequences of NU lesions. This highlights the role of the NU in processing information from the otoliths and supports its denomination as the "otolith" vermis.

KEYWORDS

cerebellum, vestibular, Kalman filter, gravity, internal model

Introduction

Lobules IX and X of the cerebellar vermis, also known as the Nodulus and Uvula (NU) (**Figure 1A**), are a prominent center of vestibular information processing. Over decades of vestibular research, the NU has been studied from many perspectives: anatomical, physiological, clinical, and theoretical. Anatomically, the NU is the recipient of abundant primary and secondary projections (**Figure 1A**, black) from the vestibular organs (**Figure 1B**) that sense head motion in 3D (**Figure 1C**). It also connects with prominent components of the subcortical vestibular network: vestibular nuclei (VN), fastigial nucleus (FN) (**Figure 1A**), and vestibular regions of the inferior olive (IO) (Bernard, 1987; Voogd and Barmack, 2006; Voogd et al., 2012). Physiologically, recordings of Purkinje cells have shown that they participate in a well-defined central computation that separates gravity and translation head motion from signals from the

otoliths (Angelaki et al., 2004; Yakusheva et al., 2007; Laurens et al., 2013b). Clinically, lesions of the NU disrupt the sensing of head rotation by altering a process called velocity storage (VS) (Waespe et al., 1985; Solomon and Cohen, 1994; Angelaki and Hess, 1995a,b; Wearne et al., 1998; Meng et al., 2014). Theoretically, the NU is understood as the neuronal implementation of an internal model of head motion (Merfeld, 1995; Laurens and Angelaki, 2011, 2017; Karmali and Merfeld, 2012).

This multiplicity of viewpoints complicates the effort to understand the role of the NU in vestibular information processing and raises the question of whether the NU performs a unitary function at all. Here, I show that physiological and clinical findings can be explained by a single theoretical concept: that the NU implements an internal model of head motion to predict the activation of the otoliths, and outputs sensory prediction errors that are broadcasted to other brain regions to correct internal estimates of self-motion, or to drive learning. Based on the afferent and efferent connections of the NU, and the physiology of neighboring regions, I discuss the position of this internal model in the anatomical vestibular and cerebellar networks.

This framework indicates that the NU plays a pivotal role in processing information from the otoliths and sends otoliths-based feedback to other brain regions, hence supporting the notion of the NU as the "otolith" vermis.

Tilt/translation discrimination

Tilt/translation discrimination is one of the fundamental steps of central vestibular information processing. It resolves a sensory ambiguity by disambiguating the sensory signals from the otoliths that cannot discriminate tilt from translation. This is easily illustrated by considering the following analogy: the otolith organs are similar to a pendulum fixed to the head that swings relative to the head during tilt or translation motion (**Figure 2A**). Thus, based on otoliths signals alone, it is impossible to distinguish tilt from translational motion (Einstein, 1907).

After a brief summary of the theoretical concepts involved in tilt/translation discrimination, I will review the involvement of the NU and associated vestibular networks:

Theoretical framework

From a physical point of view, the otolith organs sense the gravito-inertial acceleration (GIA), which can be expressed as the sum of gravitational (G) and inertial (A) accelerations (**Figure 2B**). These two accelerations are in fact physically equivalent (Einstein, 1907), and it is therefore impossible to separate them based on otolith cues alone. In this respect, the otolith organs are inherently ambiguous.

How (or whether) the brain deals with this ambiguity has been the subject of considerable attention and debate, both at the experimental and theoretical levels (Mayne, 1974; Angelaki et al., 1999, 2004; Hess and Angelaki, 1999; Merfeld et al., 1999, 2005a,b; Bos and Bles, 2002; Raphan and Cohen, 2002; Laurens and Angelaki, 2011; Yakushin et al., 2017; Jamali et al., 2019). For several decades, two distinct hypotheses existed. The first, called the "frequency segregation" hypothesis (Seidman and Paige, 1996; Raphan and Cohen, 2002), stipulates that the brain does not explicitly distinguish tilt from translation, but separates the low-frequency and high-frequency components of the otolith signals (**Figure 2C**), and interprets the low-frequency component as tilt and the high-frequency component as translation (**Figure 2D**). This framework implies that motion sensation should be identical during tilt and translation: indeed, the brain would interpret otolith signals based on their frequency content alone, and not whether the head is really tilting or translating.

The second hypothesis stipulates that the brain uses semicircular canals information to separate tilt from translation. Indeed, tilt movements are rotations and are sensed by the canals. By integrating rotation velocity signals in three dimensions ("$\int$3D box" in **Figure 2E**), the brain can compute head tilt relative to gravity (**Figure 2E**). Once head tilt is known, translation can be computed by a simple subtraction (A = GIA-G, **Figure 2E**) and the gravito-inertial ambiguity is resolved. This hypothesis is part of a more general framework called the internal model theory, which assumes that the brain uses internal representations of head motion (here tilt and translation) that match sensory signals as well as the physical laws governing head motion (here the causal relationship between rotation and tilt) and the sensory organs (here the physical principle of gravito-inertial ambiguity).

One limitation of this process is that, in the absence of corrective mechanism, the 3D integration would tend to accumulate errors that result from inaccurate rotation signals. To prevent this, most models add a feedback loop that continuously biases the tilt estimate toward the GIA (**Figure 2E**, "somatogravic feedback"). This feedback mitigates the accumulation of errors by imposing the GIA as a reference for tilt at low frequencies. It also implies that low-frequency translations are interpreted as head tilt (**Figure 2F**), and in this respect the discrimination model is similar to the frequency segregation model.

The crucial step in the tilt/translation discrimination model is the 3D integration. This step is developed in detail in **Figures 2G,H**. Mathematically, the 3D integrator computes an estimate of the 3D position of the gravity vector (G) in egocentric coordinates, based on rotation signals (Ω) and on the somatogravic feedback. The somatogravic feedback itself is proportional to the acceleration signal (A = GIA-G) and

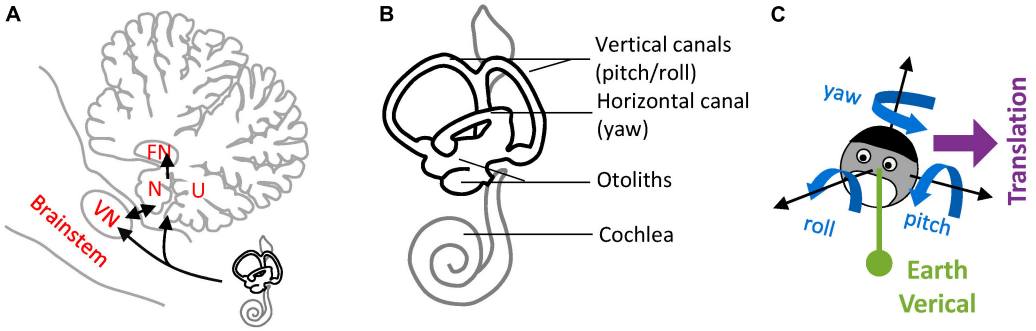

FIGURE 1
Nodulus and Uvula (NU) and brainstem/cerebellar networks that process 3D head motion. **(A)** Drawing of the NU, represented on a sagittal section of the cerebellum through the midline. The Nodulus (N) and Uvula (U) correspond to the Xth and IXth lobules of the vermis, respectively. The VN and FN are also represented. Connections between the vestibular organs and these regions are shown by black arrows. **(B)** Drawing of the vestibular organs (black) and cochlea (gray) in the inner ear. The vertical and horizontal semicircular canals are sensitive to head rotations in 3D, and the otoliths to tilt and translation. **(C)** Variables used to describe 3D head motion. 3D rotations are decomposed into yaw, pitch and roll rotations, expressed in an egocentric frame of reference. Head tilt is expressed as relative to the allocentric earth vertical. Translational motion is expressed as an egocentric 3D vector.

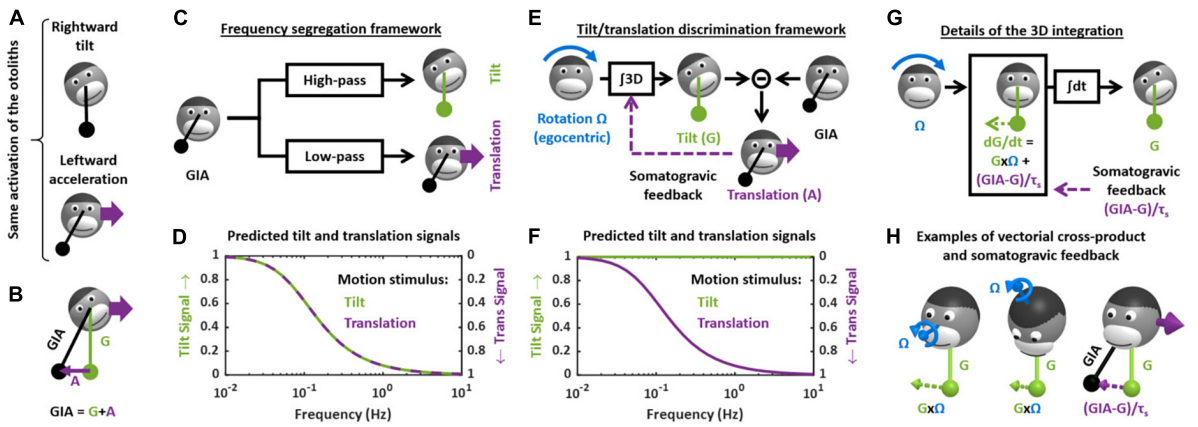

FIGURE 2
Theoretical frameworks for the resolution of the gravito-inertial ambiguity. **(A)** Illustration of the ambiguity: the otolith organs are analogous to a pendulum (black) that swing relative to the head during tilt (top) or translation (bottom). **(B)** Physical model: the otoliths sense the GIA, which is the sum of gravitational (G) and inertial (A) acceleration. **(C)** Outline of the frequency segregation hypothesis. **(D)** Predicted internal tilt and translation signals during tilt (green) and translational (violet) motion, based on the frequency segregation hypothesis. Any given stimulus (i.e., tilt or translation at a given frequency) is decomposed into a tilt and translation signals. The left and right ordinate axes indicate the amplitude of the tilt and translation signals, respectively, relative to the amplitude of the stimulus. Note that, based on the frequency segregation hypothesis, these internal signals are identical during tilt and translational motion. **(E)** Outline of the internal model hypothesis. **(F)** Predicted internal tilt and translation signals based on the internal model hypothesis. **(G)** Decomposition of the 3D integration in two steps: computing dG/dt as a function of rotation signals ($G \times \Omega$) and of the somatogravic feedback [$(GIA-G)/\tau_s$] and temporal integration ($\int dt$). **(H)** Illustration of the vectorial cross-product ($G \times \Omega$) and somatogravic feedback in 3D. The left and middle panels illustrate the cross-product during roll tilt (left) and yaw rotation around a tilted axis (OVAR, middle). The right panel illustrates the somatogravic feedback during leftward acceleration.

can be expressed as $(GIA-G)/\tau_s$, where τ_s is the time constant with which the somatogravic illusion develops during constant linear acceleration. This integration can be divided into two steps. The first step computes how G varies (i.e., dG/dt) based on the rotation signal Ω: this is accomplished by a vectorial cross-product $G \times \Omega$. This is illustrated by two examples in Figure 2H (left and right panel): in both cases, the rotation Ω causes the head to tilt toward the right side. Accordingly, the vectorial cross-product $G \times \Omega$ is a vector that points to the right, indicating that G moves rightward. In addition, dG/dt is computed by adding the somatogravic feedback to $G \times \Omega$. As illustrated in the right panel of Figure 2H, this feedback tends to align G toward the GIA. Finally, dG/dt is integrated over time to compute G.

In agreement with both models, experiments in humans and non-human primates have revealed that low-frequency translation is indeed interpreted as head tilt: this effect is called oculogravic or somatogravic illusion (Graybiel, 1952;

Graybiel et al., 1979; Paige and Tomko, 1991; Curthoys, 1996). Both the frequency filtering and the discrimination model interpret this effect by pointing out that low-frequency accelerations are very infrequent in everyday's life. Therefore, if the brain cannot discriminate low-frequency tilt from translation, it is logic to interpret both as tilt. The two models differ upon the reason why the brain cannot discriminate low-frequency tilt from translation. In the discrimination framework, this is because the integration process accumulates error and therefore becomes unreliable at low frequencies (Laurens and Droulez, 2007; Laurens and Angelaki, 2017). In the filtering model, it is because the brain never discriminates them in the first place.

The crucial experiment to distinguish these frameworks is to test whether the brain can discriminate high-frequency tilt from translation, as predicted by the discrimination model. This model also predicts that artificially activating the canals can induce illusory translation. From the last 90s onward, these predictions were both confirmed by a series behavioral studies in macaques (Angelaki et al., 1999; Hess and Angelaki, 1999; Laurens et al., 2010) and humans (Merfeld et al., 1999; Vingerhoets et al., 2007; Khosravi−Hashemi et al., 2019). These behavioral results, which were themselves conclusive, were followed by a series of neurophysiological studies that firmly confirmed the disambiguation model and identified some of its neuronal correlates, as will be discussed next.

Tilt- and translation-selective neurons

Starting in the early 2000s, a series of studies have uncovered neurons that encode specifically translation or tilt (called translation- and tilt-selective neurons, respectively), thereby providing a direct and compelling confirmation of the discrimination model. These neurons exist in the NU, and in regions closely associated with it, including the fastigial and VN. In the NU, these neurons amount to about two-third of the Purkinje cells and are the only Purkinje cells for which a clearly defined function has been proposed. This suggests that the NU is indeed mainly involved in computation related to tilt/translation discrimination. In this section, I will summarize these experiments and the properties of translation- and tilt-selective cells in the NU.

Most experiments on tilt/translation discrimination use an experimental paradigm where the head is translated in the horizontal plane (**Figure 3A**, translation) or tilted around a horizontal axis (**Figure 3A**, roll tilt). The motion profiles are matched such that the activation of the otoliths is identical during both paradigms (**Figure 3B**, GIA, black). Therefore, these motions may only be discriminated on the basis of semicircular canal signals, which are activated during tilt but not translation (**Figure 3B**, roll velocity, blue). Note that I have illustrated only lateral motion in **Figure 3** for simplicity, but that this protocol can be repeated along multiple directions to establish the cell's spatial tuning. In-depth mathematical analyses of these experiments can be found in Green et al. (2005); Laurens and Angelaki (2016).

In the early 2000s, a series of studies (Angelaki et al., 2004; Shaikh et al., 2005; Yakusheva et al., 2007, 2008, 2010) identified so-called "translation-selective" cells whose firing rate is modulated by translation but much less during tilt (**Figure 3C**). The existence of these cells was a major conceptual advance, since it was the first physiological demonstration that the brain discriminates tilt from translation.

In a more recent series of studies (Laurens et al., 2013b; Stay et al., 2019; Laurens and Angelaki, 2020), we identified so-called "tilt-selective" neurons whose firing rate is modulated by tilt but much less during translation (**Figure 3D**). Subsequently (Laurens and Angelaki, 2020), we established that these tilt-selective cells encode an intermediate computation step in the 3D integration (**Figure 2E**), namely, the computation of dG/dt (**Figure 2G**). Specifically, we found that they encode both transformed rotation signals, i.e., $G \times \Omega$, and the somatogravic feedback [see Laurens and Angelaki (2020) for details].

A crucial element for identifying tilt-selective cells was the use of 3D motion protocols (**Figures 3A–D**, right column). During roll tilt, the egocentric roll velocity (**Figure 3B**) and the allocentric velocity dG/dt (**Figure 3A**, broken line) follow a similar profile: based on this motion alone, we cannot distinguish which is encoded by neurons. To resolve this, we designed an additional tilt protocol where animals rotated at a constant velocity about a tilted axis [off-vertical axis rotation (OVAR)]. This created a periodic tilt stimulus with the same tilt and tilt velocity profiles along the head's lateral axis compared to roll motion (**Figure 3A**, green). Critically, the egocentric velocity was different: we used a sinusoidal rotation during roll and a constant-velocity rotation during OVAR (**Figure 3B**, blue). Therefore, cells that encode egocentric velocity would necessarily respond differently during sinusoidal tilt and OVAR. Instead, we found that tilt-selective cells respond similarly during these motions (**Figure 3D**), thus confirming that they encode allocentric tilt velocity.

In Laurens et al. (2013b), we determined how many Purkinje cells in the NU of macaques are translation-selective, tilt-selective, or encode other variables. About a third of neurons are translation-selective cells, and about a third are tilt-selective cells (**Figures 3E,F**). The remaining third did not have significantly different responses during tilt and translation: we classified them as GIA-selective (when their responses to both stimuli were approximately similar) or composite otherwise. Few neurons responded neither to tilt nor to translation (n.r. in **Figure 3F**). The results of this study were confirmed by independent recordings in our labs, in macaques (Laurens and Angelaki, 2020) and mice (Stay et al., 2019). In addition, one study has found translation-selective neurons in the input layer of the NU, i.e., the granular layer (Meng et al., 2014). Crucially,

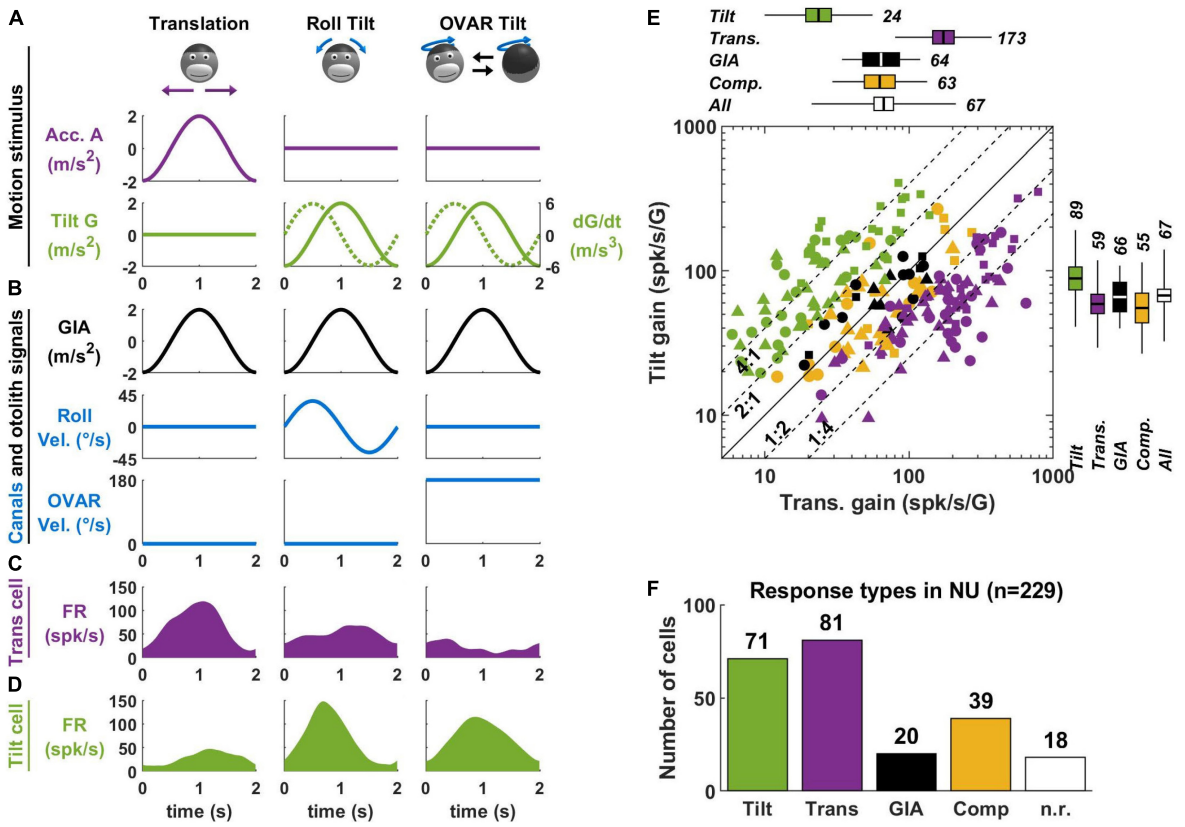

FIGURE 3
Translation- and tilt-selective neurons in the NU. **(A)** Example motion stimuli used in tilt/translation discrimination experiments. **(B)** Sensory signals during these experiments. Roll and OVAR velocity refer to the head's rotation velocity about its naso-occipital and vertical axis, which correspond to the rotations illustrated in panel **(A)**. **(C,D)** Firing rate of example translation-and tilt-selective cells during a cycle of rotation. **(E)** Scatterplot of the response gain during tilt and translation across the NU. Tilt-selective cells (green) respond preferentially to tilt compared to translation and appear above the diagonal. Reciprocally, translation-selective cells (violet) appear below the diagonal. Other cell types (GIA-selective, yellow and composite, black) appear near to the diagonal. **(F)** Distribution of responses types across the NU: about a third (71/229) cells are tilt-selective, and about a third (81/229) are translation-selective. Other cell types form the remaining third: note that 18 non-responsive cells (n.r., white) don't appear in panel **(E)**. Data replotted from Laurens et al. (2013b).

we tested that tilt- and translation-selective cells conformed to predictions of the tilt/translation discrimination framework in Laurens et al. (2013a,b). Together, these studies provide extensive experimental and theoretical support for the concept of tilt/translation discrimination.

Vestibular network for tilt/translation discrimination

To date, neurons involved in tilt/translation discrimination have been identified in three interconnected regions: the NU, as described above, the FN, and the VN. In addition, we found that IO neurons that project to tilt- and translation-selective cells in the NU are translation-selective themselves. By combining these findings with anatomical studies, I propose that tilt/translation discrimination occurs in an anatomical network outlined in this section.

Subregions of the Nodulus and Uvula

First, the NU is not a homogenous region, but can be divided further into subregions innervated by different subnuclei of the IO. The organization of these subregions has been studied and reviewed in detailed by Voogd et al. (1996, 2012, 2013) in several publications; available data indicate that it is well conserved across model species (rat, rabbits, cats, and likely non-human primates). This organization is outlined in **Figure 4A**.

The most prominent subregion of the NU is a large medial region innervated by the group β of the IO (**Figure 4A**, violet diagonal lines). Anatomical reconstructions in Yakusheva et al. (2007, 2010), Laurens et al. (2013b) indicate that tilt- and translation-selective cells are found throughout the NU, in a large region that spans most of the medial portion of the vermis (**Figure 4A**, violet). Therefore, it is likely that this region coincides with the region innervated by the group β. This

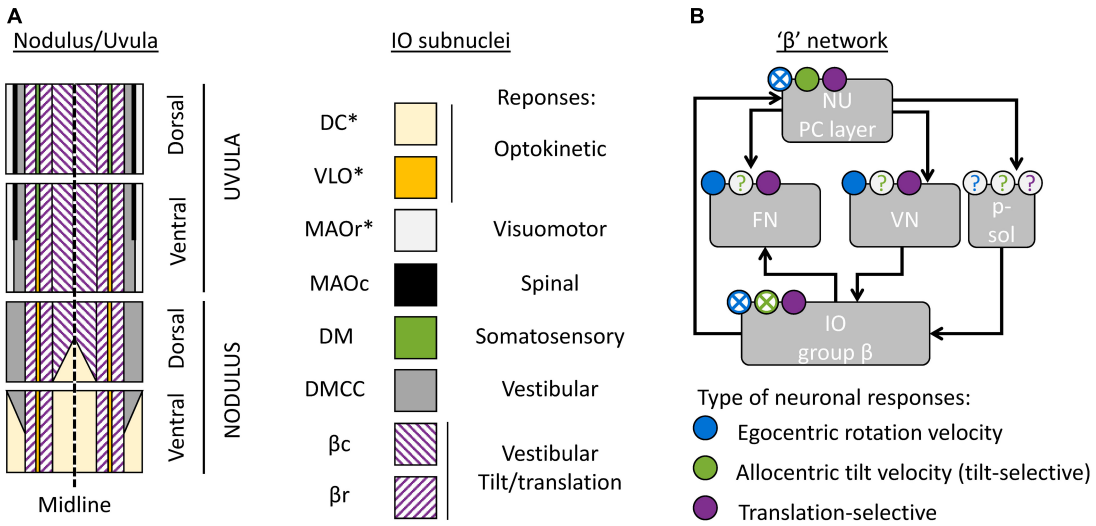

FIGURE 4
Cerebellar and brainstem nuclei involved in tilt/translation discrimination. **(A)** Schematic map of the NU, indicating the regions innervated by distinct IO subnuclei (Voogd et al., 1996, 2013; Voogd and Barmack, 2006). DC, Dorsal Cap; VLO, ventrolateral outgrowth; MAOr/MAOc, rostral/caudal part of the medial accessory olive; DM, dorsomedial group; DMCC, dorsomedial cell column; βc/βr, caudal/rostral part of the group β. Stars indicate IO subnuclei that project to the flocculus and/or paraflocculus. **(B)** Interconnections between cerebellar and brainstem regions connected to the group β. The circular symbols placed above each region indicate the presence of absence of three types of neuronal response (egocentric rotation velocity, tilt-selective and translation-selective responses are color-coded in blue, green and violet respectively). Filled symbols and crosses indicate, respectively, that the presence or absence of the corresponding response type has been established. Question marks indicate that it is still unknown. p-sol: parasolitary nucleus.

conclusion is further supported by other studies that found vestibular responses in this region (Barmack and Shojaku, 1995; Fushiki and Barmack, 1997; Yakhnitsa and Barmack, 2006; Kitama et al., 2014). Although these studies did not investigate tilt/translation discrimination specifically, they found that this region is primarily sensitive to vestibular stimulation. They also further subdivided it into two sagittal bands that preferentially respond to motion along the ipsilateral posterior canal plane (most medially) and ipsilateral anterior canal plane (more laterally). These bands correspond to the caudal and rostral parts of the nucleus β. Note that the dorsal uvula only received sparse projections from the vestibular organs and VN, unlike the rest of the NU (Voogd et al., 1996; Voogd and Barmack, 2006). Yet, there appear to be at least some translation-selective cells in the dorsal uvula (Yakusheva et al., 2007, 2010): current data are insufficient to determine whether these cells are sparser.

What is the function of other subregions of the NU? To date, only a partial answer may be formulated. First, a sizeable portion of the nodulus is innervated by the DC of the IO (**Figure 4A**, yellow), and a narrow band is innervated by the VLO (**Figure 4A**, orange). These two regions of the IO are sensitive to optokinetic stimuli, i.e., to retinal flow. It is likely that the Purkinje cells in these regions are more specialized in the processing of visual stimuli. Accordingly, Yakusheva et al. (2013) have shown that a population of NU neurons respond to visual stimulation, that this population is distinct from tilt- and translation-selective cells, and that it is spatially restricted to a subregion of the NU located anterior and medially, which could match the ventral nodulus. Note that the DC and VLO also project to the flocculus and paraflocculus (Voogd et al., 1996), and therefore these regions may be part of a network involved in oculomotricity.

Finally, the most lateral zones of the NU are innervated by the MAO, DM, and DMCC. These regions of the IO receive projections from a variety of systems: vestibular, spinal, somatosensory, and visuomotor. To date, no recording studies have established the function of these regions.

The "β" network

Anatomical studies have identified subregions of the FN and VN that connect to the group β of the IO or the corresponding regions of the NU. Together, these regions form what may be called a "β" network. I will describe this network here.

First, the NU projects to the ipsilateral FN (**Figure 4B**). Within the FN, projections from the NU terminate in a ventral subdivision (Armstrong and Schild, 1978; Dietrichs, 1983; Bernard, 1987; Ikeda et al., 1989; Fujita et al., 2020). That subdivision is distinct from the most prominent subdivisions of the FN, which are the "rostral" and "caudal" FN: the "rostral" FN is a relay between the anterior vermis and the spinal VN

(Voogd, 2016; Fujita et al., 2020) and the "caudal" FN is an oculomotor subnucleus (Ikeda et al., 1989; Fujita et al., 2020). Projections from the NU terminate in a region located caudally relative to the "rostral" FN and ventrally and somewhat rostral relative to the "caudal" FN. Interestingly, this region may also receive projections from the group β in the IO (Dietrichs and Walberg, 1985). Together, these studies indicate that there is a "β" subnucleus of the FN that likely corresponds to the module F4 described in Fujita et al. (2020).

The NU also projects to the ipsilateral VN (**Figure 4B**; Bernard, 1987; Xiong and Matsushita, 2000). Note however that the exact location of NU target neurons within the VN has never been firmly established.

Finally, the group β of the IO likely receives indirect projections from the NU. Indeed, it receives projection from the VN (Barmack et al., 1993; Balaban and Beryozkin, 1994). Alternatively, the NU may project to the group β through the parasolitary nucleus (**Figure 4B**), which is an anatomical relay between these regions (Barmack et al., 1993, 1998; Balaban and Beryozkin, 1994; Barmack and Yakhnitsa, 2000).

Tilt/translation discrimination through the "β" network

In addition to the NU, several studies have identified neuronal correlates of tilt/translation discrimination through the "β " network.

First, translation-selective neurons have been found in the FN of macaque monkeys (Angelaki et al., 2004; Shaikh et al., 2005; Laurens and Angelaki, 2016; Mackrous et al., 2019). However, there is some uncertainty regarding the exact location of these recordings in respect to NU projections. Although these studies reported that their recordings occurred in the "rostral" FN, they did not perform histological reconstruction. Therefore, they likely could not locate their recordings with enough precision to distinguish between the "rostral" and "β" portions of the FN. Note that (Mackrous et al., 2019) found that a third of neurons are potentially tilt-selective neurons. However, they did not perform recordings during 3D motion (as in **Figures 3A–D**) and it is, therefore, uncertain whether these neurons encode allocentric tilt, as opposed to egocentric rotations.

Translation-selective cells have been identified in the VN (Angelaki et al., 2004; Meng et al., 2014; Mackrous et al., 2019). Importantly, (Meng et al., 2014) recorded 26 VN cells that were targeted by NU projections (and were not eye movement related), and demonstrated that 11 of them were translation-selective, and the rest GIA-selective. Therefore, at least a part of the translation-selective cells in the VN may be targeted by NU projections. However, more detailed studies will be necessary to establish the exact nature and functions of the interconnections between VN and NU.

The velocity storage

As we saw in the previous section, neuronal recording studies indicate that tilt/translation discrimination is a prominent function of the NU. Yet, lesion studies in monkeys (Waespe et al., 1985; Angelaki and Hess, 1995a,b; Wearne et al., 1998) and humans (Hain et al., 1988; Lee et al., 2017), or electric stimulation studies in monkeys (Solomon and Cohen, 1994; Meng et al., 2014) have linked it to a seemingly unrelated function: the control of a phenomenon called VS.

What is the VS? Based on Bayesian modeling theory, it is the central element of a multisensory internal model that senses head rotation velocity optimally (Laurens and Droulez, 2007; Laurens and Angelaki, 2017). In the context of tilt/translation discrimination, it provides the egocentric rotation velocity signal $\boldsymbol{\Omega}$ to the 3D integrator. Prior to this definition, the concept of VS originated in the 70s (Raphan et al., 1979), as a leaky integrator connected to the semicircular canals (**Figure 5A**, blue and orange). In Laurens and Angelaki (2011), we demonstrated how the VS could be connected to the internal model of tilt/translation discrimination to create a full 3D model of vestibular information processing, as shown in **Figure 5A**. In Laurens and Angelaki (2017), we demonstrated that the historic model by Raphan and Cohen (Raphan et al., 1979) is equivalent to an optimal Kalman filter.

Velocity storage during rotations in a horizontal plane

When rotating in complete darkness (and in a horizontal plane), head motion is sensed by the semicircular canals. These canals act as a high-pass filter, with a time constant of ∼4 s. This implies that, during a constant-velocity rotation (**Figure 5B**, gray), their signal will vanish in about 15–20 s (**Figure 5B**, orange). Yet, the brain's sense of rotation will persist for a longer duration, with a time constant of 10–30 s (Raphan et al., 1979; Bertolini et al., 2010; Laurens et al., 2010; **Figure 5B**, blue). This indicates that a central mechanism increases the time constant of rotation sensation compared to the canals. In their textbook model, Raphan et al. (1979), Raphan and Cohen modeled this mechanism as a leaky integrator (**Figure 5B**, black) whose output sums with the canals (Raphan et al., 1979), and this integrator was named VS.

Although the VS increases its time constant, rotation sensation keep high-pass characteristics. A consequence of this is that, when stopping after a long period of constant velocity rotation, one experiences an after-effect that is symmetric to the response to the initial rotation (**Figure 5B**, after t = 60 s). This after-effect is the basis of some experimental protocols discussed in the next section.

When rotating relative to a visual surround, rotation sensation persists indefinitely [**Figure 5C**, note that visual

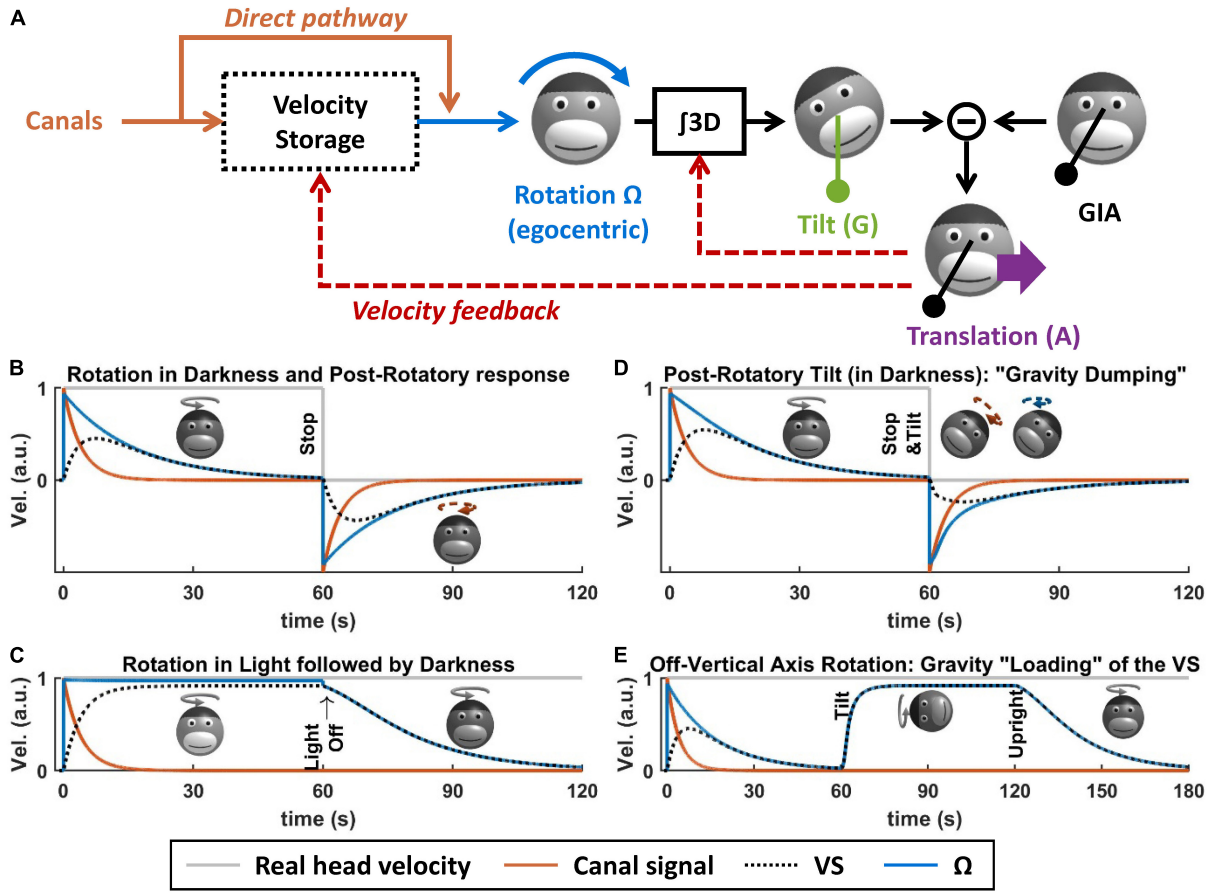

FIGURE 5
Velocity storage. **(A)** Model of the velocity storage during 3D motion (Laurens and Angelaki, 2011). See text for explanations. **(B–E)** Simulations of rotation perception during rotations in darkness or light, and 3D rotations. Head motion is illustrated by monkey heads, drawn in darker shades when the rotation occurs in darkness. The orange broken arrows in panels **(B,D)** represent the post-rotatory canal activation. The blue broken arrows in panel **(D)** represent the post-rotatory rotation signal.

pathways are not shown in **Figure 5A** for simplicity; see Raphan et al. (1979), Laurens and Angelaki (2011, 2017) for details]. If light is extinguished (without altering the subject's rotation), then rotation sensation does not cease immediately but decrease exponentially with the same constant during rotation in darkness. This indicates that the VS also store a signal that originates from the visual system.

Velocity storage during 3D rotations

The previous section described the principles of how the brain processes rotations in a horizontal plane. These principles also apply to rotations in a vertical plane. However, rotating in a vertical plane involves another fundamental mechanism: the interactions between rotation sensation and the otoliths. It is the case because integrating rotation movement is a fundamental part of tilt/translation discrimination, as described above. It is also the case because, reciprocally, otolith signals participate to rotation sensing, as described next.

First, rotation signals can be put in conflict with gravity sensing by the otoliths. A classical paradigm called post-rotatory tilt consists of rotating a subject in darkness, stopping the rotation (as in **Figure 5B**), and then tilting the subject (**Figure 5D**, at t = 60 s) (Benson, 1974; DiZio and Lackner, 1988; Merfeld et al., 1993, 1999; Angelaki and Hess, 1994, 1995b; Furman and Koizuka, 1994; Gizzi et al., 1994; Fetter et al., 1996; Zupan et al., 2000; Yasuda et al., 2002, 2003; Kitama et al., 2004; Fushiki et al., 2006; Laurens et al., 2010). In an egocentric reference frame, the post-rotatory activity of the canals (**Figure 5D**, broken arrow) is identical as in a **Figure 5B**. However, this activity now indicates that the head rotates about a tilted axis. According the internal model framework, this signal is integrated into an estimate of head tilt that varies continuously. However, this estimate will not match the activity of the otoliths since the head is in fact immobile. This mismatch can be resolved by assuming that the head is translating, as has

been shown in Merfeld et al. (1999), Laurens et al. (2013a), Khosravi−Hashemi et al. (2019): this will be discussed further in the next section. In addition to this, this mismatch is resolved by altering the central rotation signal (Ω) in two ways. First, its amplitude and duration are reduced (**Figure 5D**, compare with **Figure 5B**): this phenomenon is called "gravity dumping." Second, after the head is tilted, the axis of the rotation signal gradually shifts spatially until it aligns with earth-vertical. This axis shift occurs centrally: the post-rotatory rotation signal generated by the canals remains head-fixed (this is illustrated by a schematic head in **Figure 5D**, with an orange arrow), but the rotation signal contributed by the VS aligns with earth-vertical (schematic head in **Figure 5D**, with a blue arrow). Gravity dumping and the realignment of the post-rotatory response with gravity have been observed in several species: squirrel monkeys and macaques (Dai et al., 1991; Merfeld et al., 1993; Angelaki and Hess, 1994, 1995b), cats (Yasuda et al., 2002, 2003; Kitama et al., 2004; Fushiki et al., 2006), and humans (Benson, 1974; DiZio and Lackner, 1988; Furman and Koizuka, 1994; Gizzi et al., 1994; Fetter et al., 1996; Merfeld et al., 1999; Zupan et al., 2000): note that gravity dumping and axis realignment are weaker in humans compared to monkeys. Note that post-rotatory responses align with allocentric vertical even when the initial rotation did not occur about a vertical axis (Dai et al., 1991; Jaggi-Schwarz et al., 2000): this rules out the hypothesis that the axis re-alignment is due to a mechanism that encodes rotation in allocentric coordinates and favors the interpretation that it is a conflict resolution mechanism.

Gravity can also be used to sense head rotation. For instance, when rotating about an earth-horizontal axis in darkness, rotation perception and VOR can last indefinitely (Correia and Guedry, 1966; Harris, 1987; Angelaki and Hess, 1996; Angelaki et al., 2000; Kushiro et al., 2002; Laurens et al., 2010). This can be revealed by first rotating around a vertical axis until rotation sensation subsides (**Figures 5E**, $t < 60$ s) and then tilting the head while maintaining the rotation (**Figure 5E**). In this situation, the rotation sensation rapidly resumes (**Figure 5E**, after $t = 60$ s) and stabilizes to a steady-state level called "bias velocity." This rotation sensation is mediated by the VS: this can be shown by re-aligning the head with vertical (**Figure 5E**, at $t = 120$ s). After this, rotation sensation persists and decreases with the typical time constant of the VS (Jaggi-Schwarz et al., 2000; Laurens et al., 2010), indicating that the "bias velocity" signal (until $t = 120$ s) is stored in the VS. The bias velocity can be observed in macaques (Angelaki and Hess, 1996; Angelaki et al., 2000; Kushiro et al., 2002; Laurens et al., 2010), cats (Harris, 1987), and humans (Benson and Bodin, 1966; Correia and Guedry, 1966; Wall and Furman, 1990). Note that the bias velocity varies as a function of tilt angle and saturates or vanishes at high rotation speed (Angelaki et al., 2000; Kushiro et al., 2002; Laurens et al., 2010). Similar to the dumping effect during otolith conflicts, the bias velocity is lower in humans compared to monkeys.

In Laurens and Angelaki (2011), we demonstrated that these results can be explained by the internal model framework, and specifically by a feedback loop from the internal model of tilt/translation discrimination to the VS (**Figure 5A**, velocity feedback). This will be shown in more detail in the next section.

Velocity storage and Nodulus and Uvula

From a theoretical point of view, the VS and the general framework of the internal model are well understood. But how are they related to the NU? To date, the neuronal substrate of the VS is unknown. However, lesion studies have shown that the NU is involved in VS in at least two respects. First, NU lesions abolish the influence of gravity on the VS, both in experimental (Waespe et al., 1985; Angelaki and Hess, 1995a,b; Wearne et al., 1998) and in clinical cases (Hain et al., 1988; Lee et al., 2017). Second, NU lesions also alter the time constant of the VS during rotations in a horizontal plane (Waespe et al., 1985; Angelaki and Hess, 1995a,b; Wearne et al., 1998).

Thus, there appears to be a discrepancy between electrophysiological studies, that point to tilt/translation discrimination as the most obvious function of the NU, and lesions studies that suggest that it is involved in the VS. Furthermore, although the VS computes egocentric rotation signals, NU neurons do not encode egocentric rotation velocity (Fushiki and Barmack, 1997; Kitama et al., 2014), which seems to increase the contradiction between these two putative functions. We will see that theoretical models readily provide an answer to this paradox.

A theoretical framework for Nodulus and Uvula function

I will now propose a theoretical model that conciliates these seemingly dissimilar functions of the NU. This model is grounded in the concept of internal model that was initially proposed in the early 80s (Mayne, 1974; Ormsby and Young, 1977; Oman, 1982; Borah et al., 1988; Young, 2011; Clark et al., 2019) and has evolved into complete 3D models of vestibular information processing (Merfeld, 1995; Bos and Bles, 2002; Laurens and Droulez, 2007; Laurens and Angelaki, 2011, 2017; Karmali and Merfeld, 2012).

Internal model framework

The concept of internal model is largely related to the technique of Kalman filtering used in aerospace (Kalman, 1960; Kalman and Bucy, 1961; **Figure 6A**). It posits that the brain maintains and updates an internal representation of

head motion (**Figure 6A**, black) by two mechanisms. The first is by integrating motor efference copies that encode how the head is expected to move based on voluntary motor activity. The second is a forward model where the brain simulates the sensory organs to anticipate vestibular (and other) sensory efferences (**Figure 6A**, gray). Any discrepancy between the anticipated and received sensory signals leads to a sensory prediction error (**Figure 6A**, red), which updates the internal representation of head motion through feedback loops. This framework has received considerable support from its ability to account for the results of behavioral studies (Merfeld et al., 1993, 1999; Glasauer and Merfeld, 1997; Bos and Bles, 2002; Laurens et al., 2010; Laurens and Angelaki, 2011, 2017; Karmali and Merfeld, 2012). It is also supported by neurophysiological findings, as will be described in the next section.

Internal model for otolith information processing

I will now explain how the internal model framework can explain the multiple functions of the NU. I will use the Kalman filter model in Laurens and Angelaki (2017), and specifically the part of that model dedicated to processing otolith signals (**Figure 6B**).

The model includes three motion variables that are central to vestibular information processing: (1) the angular velocity of the head in egocentric coordinates (**Ω**, blue), the allocentric tilt of the head (G, green), and the linear acceleration (A, violet). Note that head rotation and tilt are linked by a causal relationship: changes in head tilt occur through rotation movements, and therefore head tilt is the 3D integral of **Ω**. These motion variables and the causal relationship between them constitute the internal representation of head motion.

This internal representation can be updated by motor efference copies. Note that this model does not address motor control explicitly. For simplicity, it is assumed that motor centers provide signals that encode self-generated rotations (**Figure 6B**, blue) and translations (**Figure 6B**, violet). Note also that the model does not include a distinct efference copy to encode tilt: this is because tilt movements result from rotations; therefore, self-generated tilt is encoded indirectly by the rotation efference copy.

Next, the model computes sensory prediction and sensory prediction error. From a physical point of view, otoliths sense the sum of tilt and translation (**Figure 2B**). The model mimicks this by summing the internal tilt and translation signals (**Figure 6B**, gray box). This prediction is subtracted from the actual signal from the otolith reafference (GIA, black), and the result of this subtraction is the otolith prediction error (**Figure 6B**, red).

Otolith prediction errors

The concept of otolith prediction error is central to understanding the NU. To fully apprehend it, we may examine when these errors occur or not:

Otolith prediction errors occur during passive or unexpected translations. This is because translations activate the otoliths, but the model does not have any information to anticipate this activation.

Otolith prediction errors occur during canal/otolith conflicts similar to the post-rotatory tilt (**Figure 5D**). This is because, based on rotation signals (**Ω**), the model anticipates that the head rotates relative to gravity, but the head is in fact immobile. Multiple experimental paradigms induce canal/otolith conflicts: post-rotatory tilt (Benson, 1974; DiZio and Lackner, 1988; Dai et al., 1991; Merfeld et al., 1993, 1999; Angelaki and Hess, 1994, 1995b; Jaggi-Schwarz et al., 2000; Zupan et al., 2000; Fushiki et al., 2006; Laurens et al., 2010), tilt movement while rotating (Young, 1971; Dichgans and Brandt, 1973; Guedry and Benson, 1976; Bles, 1998; Dai et al., 2009; Laurens et al., 2013a) and direct stimulation of the canals (Khosravi−Hashemi et al., 2019).

In contrast, otolith prediction errors do not occur during active tilt or translations, because motor efference copies allow anticipating the activation of the otoliths.

Based on (Laurens and Angelaki, 2017), otolith prediction errors do not occur during passive tilt either. This is because passive tilt movement is accomplished by passively rotating the head, which induces canal prediction errors. These prediction errors are taken into account by the internal model of rotation (**Figure 6B**, blue) upstream of the 3D integrator (**Figure 6B**, green). As a consequence, the internal estimate of tilt (G in **Figure 6B**) is accurate during passive tilt, and otolith prediction errors do not occur.

Finally, otolith prediction errors can occur during OVAR, but only when the rotation signal **Ω** does not match the actual rotation of the head. This occurs, for instance, during the first second following head tilt in **Figure 5E** (Laurens et al., 2011). It also occurs during long-duration, high velocity OVAR, where the VS is not sufficient to maintain an accurate rotation estimate (Laurens et al., 2013b).

Feedback loops

Next, sensory prediction errors drive feedback loops that update the internal model of head motion. The optimal organization of these feedback loops can be predicted using the Kalman filter algorithm (Kalman, 1960; Kalman and Bucy, 1961). As a rule, each sensory prediction error should drive a feedback loop to update each motion variable. Therefore, in the simplified model of **Figure 6B**, the otolith prediction error

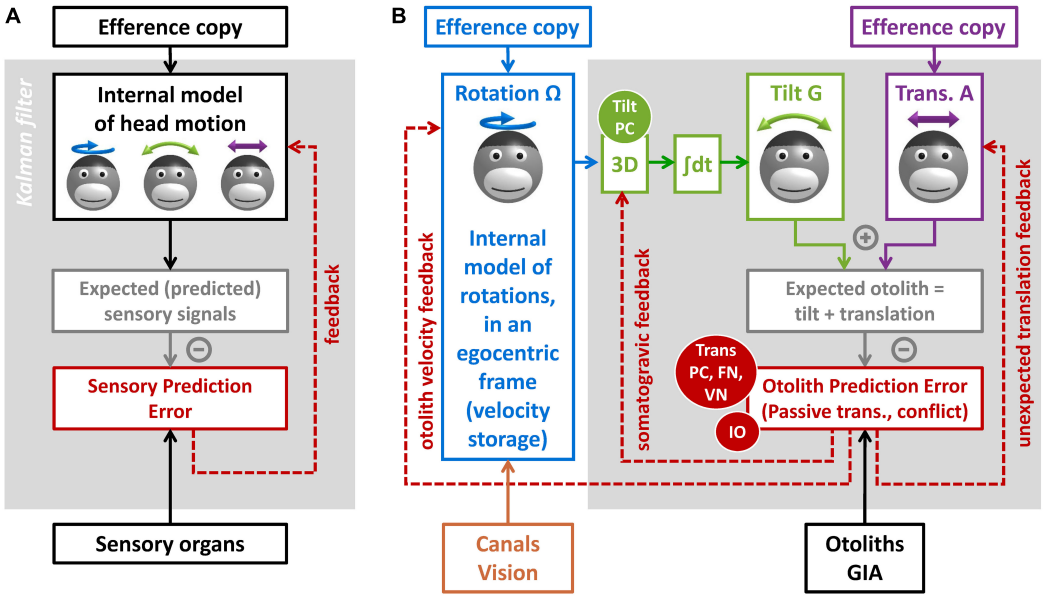

FIGURE 6
Kalman filter models of vestibular information processing. **(A)** Overview of the Kalman filter algorithm. **(B)** Detail of the Kalman filter model in Laurens and Angelaki (2017), focusing on the processing of otolith information.

drives feedback loops to the three motion variables: rotation, tilt, and translation. I will discuss each of these loops.

The feedback to the internal model of translation has gain of 1, and therefore that otolith prediction error is interpreted by the brain as an unexpected translation. This allows the internal model to detect passive translations, during which otolith prediction errors occur. This feedback also implies that canal/otolith conflicts should induce a sense of translation: this important prediction was verified by behavioral experiments in Merfeld et al. (1999), Laurens et al. (2013a), Khosravi−Hashemi et al. (2019) and historically provides an important support to the internal model framework. Finally, a sensation of translation should occur during OVAR when Ω does not match the rotation of the head: this has been verified in Vingerhoets et al. (2007), Laurens et al. (2011).

The feedback to the internal model of tilt is fed to the 3D integrator. As a consequence, this feedback matches exactly the somatogravic feedback in **Figure 2E**. During passive translations, the consequence of this feedback is the somatogravic effect (see Section "Tilt/translation discrimination"). During canal/otolith conflict or during OVAR, this feedback acts to correct the incorrect tilt signals and to decrease the conflict (Laurens et al., 2013a).

Finally, the Kalman filter predicts that the feedback to the rotation estimate is fed to the VS and that it acts to adjust the internal model of rotation to match head motion relative to gravity [see Laurens and Angelaki (2011, 2017)]. As a consequence, this feedback is responsible for the "dumping" (**Figure 5D**) and realignment of the rotation signal during post-rotatory tilt, and it is also responsible for creating a velocity signal in the VS during OVAR (**Figure 5E**).

Note that the models in **Figures 2E**, **5A** are included in the model in **Figure 6B**: the model in **Figure 2E** is implemented by the 3D integrator and the feedback loops to the internal model of translation and tilt, and the model in **Figure 5A** is implemented by adding the feedback loop to the internal model of rotation.

This shows that a wide range of behavioral observations can be explained by a simple mechanism where otolith prediction errors drive corrective feedback loops to the internal model of motion. Next, we will discuss how these loops correspond to neuronal response in the central vestibular network. Before this, we can emphasize an important point: the notions of "translation signal" and "otolith prediction error" are closely associated and practically indistinguishable during passive motion, since otolith prediction errors are always interpreted as passive translations.

The Nodulus and Uvula as a forward model of the otoliths

I will now examine how the internal model frameworks match neuronal responses in the NU and associated regions.

First and foremost, the response of translation-selective cells in the NU and downstream (VN and FN) corresponds precisely

to otolith prediction errors. Indeed, by definition, translation-selective neurons in the NU, VN, and FN respond during passive translations but not passive tilt. Furthermore, translation-selective neurons in the NU respond to canal/otolith conflict (Laurens et al., 2013a), or during OVAR when Ω does not match head motion (Laurens et al., 2013b). Finally, translation-selective cells in the FN respond less to self-generated translation compared to passive translations (Mackrous et al., 2019). Based on this, we can propose that these cells, so far described as "translation-selective," actually encode otolith prediction errors (red oval panel in **Figure 6B**) that drive the three feedback loops in **Figure 6B**.

We have determined in Laurens et al. (2013b), Laurens and Angelaki (2020) that tilt-selective cells encode an allocentric tilt velocity signal (see Section " Tilt- and translation-selective neurons"). Accordingly, we propose that they perform the spatial transformation from egocentric rotation signals (Ω) into tilt velocity, which is represented by the block "3D" in **Figure 6B**. This implies that tilt-selective cells should encode the somatogravic feedback during low-frequency translation: we confirmed this in Laurens et al. (2013a).

Thus, the internal model hypothesis accounts for all known responses in the NU, as well as in the associated regions (**Figure 4B**). At the same time, it accounts for the consequences of NU lesions on the VS. Indeed, this framework predicts that gravity influences the VS (**Figures 2A,D,E**) through that velocity feedback loop (**Figures 5A**, **6B**) that originates from the very computations that discriminate tilt from translation. Therefore, NU lesions would automatically abolish the gravity dependence of the VS (Waespe et al., 1985; Hain et al., 1988; Angelaki and Hess, 1995a,b; Wearne et al., 1998; Lee et al., 2017). Furthermore, by eliminating the tonic input from the NU onto neuronal networks that underlie the VS, NU lesions or stimulations may alter its time constant during rotations in a horizontal plane (Waespe et al., 1985; Solomon and Cohen, 1994; Angelaki and Hess, 1995a,b; Wearne et al., 1998; Meng et al., 2014). Note that the neuronal substrate of the VS is yet unknown.

Interestingly, this framework suggests that the velocity feedback to the VS may be driven by translation-selective neurons themselves. This illustrates that the functions of these neurons may be much wider than simply conveying translation signals. In fact, they may be seen as an output channel of the NU that broadcast feedback signals to regulate multiple variables of the internal model.

In the Kalman filter framework, the function of feedback loops is to correct the internal model of motion online. However, our recent finding that IO neurons project to the NU are translation-selective (Angelaki and Laurens, 2021) indicates that IO activity may also encode otolith prediction errors (**Figure 6B**). Since IO has been involved in cerebellar learning (Lisberger, 1988; Gao et al., 2012), this would point to an additional role where sensory prediction errors are used to control the learning of internal models in the cerebellum.

Conclusion

Through this review, I have summarized a variety of findings regarding the physiology and function of the NU. I have proposed that these findings are explained by the theory that the NU implements a forward internal model of head motion to predict how the otolith organs are activated by movements on the head and broadcasts feedback signals to other brain regions when prediction errors occur. Note that previous theoretical works based on internal model (Merfeld, 1995; Glasauer and Merfeld, 1997; Bos and Bles, 2002; Laurens and Droulez, 2007; Laurens and Angelaki, 2011, 2017; Karmali and Merfeld, 2012) proposed all-encompassing theories of how multiple motion variables are computing by the brain. The present work does not conflict with these models, but stresses out that the NU implements a forward model of one sensory organ, the otolith, and therefore pinpoints the function of the NU with a greater degree of specificity. Notably, this framework accounts for the NU's involvement in tilt/translation discrimination, for physiological studies of the NU, and for the NU influence on the VS. On this basis, I propose that the NU may be seen as a section of the vermis dedicated to the otolith organs, i.e., an "otolith vermis."

The theoretical concept of internal model was initially proposed in the 70s (Mayne, 1974; Ormsby and Young, 1977; Oman, 1982; Borah et al., 1988; Young, 2011; Clark et al., 2019) and evolved into detailed models of vestibular information processing (Merfeld, 1995; Glasauer and Merfeld, 1997; Bos and Bles, 2002; Laurens and Droulez, 2007; Laurens and Angelaki, 2011, 2017; Karmali and Merfeld, 2012). Over the years, it gained strong support based on its ability to explain self-motion perception (Merfeld et al., 1993, 1999; Bos and Bles, 2002; Laurens et al., 2010; Laurens and Angelaki, 2011) and physiological recordings (Angelaki et al., 2004; Cullen, 2012; Laurens et al., 2013a,b). This concept has also gained a wide acceptance in the larger field of motor control (Wolpert et al., 1995; Körding and Wolpert, 2004; Todorov, 2004; Chen-Harris et al., 2008; Sağlam et al., 2014). Here, I have shown that it can account for multiple functions of the NU. This illustrates the predictive power of the internal model framework and supports its use as a normative approach for understanding vestibular function.

It is also worth noting that theoretical models of vestibular information processing were developed and refined based on decades of behavioral data (Merfeld, 1995; Glasauer and Merfeld, 1997; Bos and Bles, 2002; Laurens and Droulez, 2007; Laurens and Angelaki, 2011, 2017; Karmali and Merfeld, 2012). The fact that we now can now identify the neuronal correlates of postulated brain computations illustrates the importance of

grounding systems neuroscience in mathematical models of behavior. In this respect, the vestibular system is a unique field that may pioneer the way for studying the principles of sensory-motor control and cerebellar computations.

Earlier modeling works (Merfeld, 1995; Bos and Bles, 2002; Laurens and Droulez, 2007; Laurens and Angelaki, 2011) emphasized how central vestibular computations transform vestibular signals into final estimates of self-motion. In contrast, the Kalman filter framework stresses that self-motion perception is primarily driven by motor efference copies, and how the vestibular organs are primarily used as an error detector, and to generate corrective feedback (Cullen, 2012; Laurens and Angelaki, 2017). This change of viewpoint, largely driven by a series of work in Kathleen Cullen's laboratory (Cullen, 2012, 2019), is a very significant progress in understanding the vestibular system.

The Kalman filter framework also encourages us to understand the vestibular system in the wider context of motor loops (Wolpert et al., 1995; Körding and Wolpert, 2004; Todorov, 2004; Chen-Harris et al., 2008; Sağlam et al., 2014). By emphasizing the feedback role of the vestibular system, it explains why postural disturbances following vestibular lesions are particularly severe when walking or standing on unstable support that amplify motor errors (McCall and Yates, 2011; Strupp et al., 2016; Sprenger et al., 2017). The optimal estimation framework from which the Kalman filter originates also have the ability to model the consequences of vestibular lesions and sensory substitution (Laurens and Droulez, 2008; Alberts et al., 2018; Angelaki and Laurens, 2020), and is a promising way to study vestibular deficits or vestibular prosthetics.

Recordings in the PC layer of the NU have allowed discovering two components of the internal model highlighted in **Figure 6B**: the translation- and tilt-selective neurons. In contrast, some crucial components remain to be identified. In particular, neurons encoding the internal model of tilt (G) and the predicted otolith signals remain to be discovered. Furthermore, the neuronal mechanism that conveys motor efference copies to the NU is also unknown. Their discovery and characterization will probably be an exciting challenge for vestibular system neuroscience in the following years. Another challenge will be to understand the multiple functions of vestibular feedbacks in ecological conditions, in health and disease.

Data availability statement

The original contributions presented in this study are included in the article/supplementary material, further inquiries can be directed to the corresponding author.

Author contributions

All authors listed have made a substantial, direct, and intellectual contribution to the work, and approved it for publication.

Conflict of interest

The author declares that the research was conducted in the absence of any commercial or financial relationships that could be construed as a potential conflict of interest.

Publisher's note

All claims expressed in this article are solely those of the authors and do not necessarily represent those of their affiliated organizations, or those of the publisher, the editors and the reviewers. Any product that may be evaluated in this article, or claim that may be made by its manufacturer, is not guaranteed or endorsed by the publisher.

References

Alberts, B. B. G. T., Selen, L. P. J., Verhagen, W. I. M., Pennings, R. J. E., and Medendorp, W. P. (2018). Bayesian quantification of sensory reweighting in a familial bilateral vestibular disorder (DFNA9). *J. Neurophysiol.* 119, 1209–1221. doi: 10.1152/jn.00082.2017

Angelaki, D. E., and Hess, B. J. (1994). Inertial representation of angular motion in the vestibular system of rhesus monkeys I. Vestibuloocular reflex. *J. Neurophysiol.* 71, 1222–1249. doi: 10.1152/jn.1994.71.3.1222

Angelaki, D. E., and Hess, B. J. (1995a). Lesion of the nodulus and ventral uvula abolish steady-state off-vertical axis otolith response. *J. Neurophysiol.* 73, 1716–1720. doi: 10.1152/jn.1995.73.4.1716

Angelaki, D. E., and Hess, B. J. (1995b). Inertial representation of angular motion in the vestibular system of rhesus monkeys. II. Otolith-controlled transformation that depends on an intact cerebellar nodulus. *J. Neurophysiol.* 73, 1729–1751. doi: 10.1152/jn.1995.73.5.1729

Angelaki, D. E., and Hess, B. J. (1996). Three-dimensional organization of otolith-ocular reflexes in rhesus monkeys. II. Inertial detection of angular velocity. *J. Neurophysiol.* 75, 2425–2440. doi: 10.1152/jn.1996.75.6.2425

Angelaki, D. E., and Laurens, J. (2020). Time Course of Sensory Substitution for Gravity Sensing in Visual Vertical Orientation Perception following Complete Vestibular Loss. *Eneuro* 7, ENEURO.21–ENEURO.20. doi: 10.1523/ENEURO.0021-20.2020

Angelaki, D. E., and Laurens, J. (2021). Two functionally distinct Purkinje cell populations implement an internal model within a single olivo-cerebellar loop. *bioRxiv* [Preprint]. doi: 10.1101/2021.05.09.443096v2

Angelaki, D. E., McHenry, M. Q., Dickman, J. D., Newlands, S. D., and Hess, B. J. M. (1999). Computation of Inertial Motion: Neural Strategies to Resolve Ambiguous Otolith Information. *J. Neurosci.* 19, 316–327. doi: 10.1523/JNEUROSCI.19-01-00316.1999

Angelaki, D. E., Merfeld, D. M., and Hess, B. J. M. (2000). Low-frequency otolith and semicircular canal interactions after canal inactivation. *Exp. Brain Res.* 132, 539–549. doi: 10.1007/s002210000364

Angelaki, D. E., Shaikh, A. G., Green, A. M., and Dickman, J. D. (2004). Neurons compute internal models of the physical laws of motion. *Nature* 430, 560–564. doi: 10.1038/nature02754

Armstrong, D. M., and Schild, R. F. (1978). An investigation of the cerebellar cortico-nuclear projections in the rat using an autoradiographic tracing method. I. Projections from the vermis. *Brain Res.* 141, 1–19. doi: 10.1016/0006-8993(78)90613-3

Balaban, C. D., and Beryozkin, G. (1994). Organization of vestibular nucleus projections to the caudal dorsal cap of kooy in rabbits. *Neuroscience* 62, 1217–1236. doi: 10.1016/0306-4522(94)90354-9

Barmack, N. H., Fagerson, M., and Errico, P. (1993). Cholinergic projection to the dorsal cap of the inferior olive of the rat, rabbit, and monkey. *J. Comp. Neurol.* 328, 263–281. doi: 10.1002/cne.903280208

Barmack, N. H., Fredette, B. J., and Mugnaini, E. (1998). Parasolitary nucleus: A source of GABAergic vestibular information to the inferior olive of rat and rabbit. *J. Comp. Neurol.* 392, 352–372. doi: 10.1002/(SICI)1096-9861(19980316)392:3<352::AID-CNE6<3.0.CO;2-0

Barmack, N. H., and Shojaku, H. (1995). Vestibular and visual climbing fiber signals evoked in the uvula-nodulus of the rabbit cerebellum by natural stimulation. *J. Neurophysiol.* 74, 2573–2589. doi: 10.1152/jn.1995.74.6.2573

Barmack, N. H., and Yakhnitsa, V. (2000). Vestibular Signals in the Parasolitary Nucleus. *J. Neurophysiol.* 83, 3559–3569. doi: 10.1152/jn.2000.83.6.3559

Benson, A. J. (1974). "Modification of the Response to Angular Accelerations by Linear Accelerations," in *Vestibular System Part 2: Psychophysics, Applied Aspects and General Interpretations*, eds A. J. Benson, N. Bischof, W. E. Collins, A. R. Fregly, A. Graybiel, F. E. Guedry, et al. (Germany: Springer), 281–320. doi: 10.1007/978-3-642-65920-1_6

Benson, A. J., and Bodin, M. A. (1966). Effect of Orientation to the Gravitational Vertical on Nystagmus Following Rotation About A Horizontal Axis. *Acta Laryngol.* 61, 517–526. doi: 10.3109/00016486609127090

Bernard, J.-F. (1987). Topographical organization of olivocerebellar and corticonuclear connections in the rat?An WGA-HRP study: I. Lobules IX, X, and the flocculus. *J. Comp. Neurol.* 263, 241–258. doi: 10.1002/cne.902630207

Bertolini, G., Ramat, S., Laurens, J., Bockisch, C. J., Marti, S., Straumann, D., et al. (2010). Velocity storage contribution to vestibular self-motion perception in healthy human subjects. *J. Neurophysiol.* 105, 209–223.

Bles, W. (1998). Coriolis effects and motion sickness modelling. *Brain Res. Bull.* 47, 543–549. doi: 10.1016/S0361-9230(98)00089-6

Borah, J., Young, L. R., and Curry, R. E. (1988). Optimal Estimator Model for Human Spatial Orientation. *Ann. N. Y. Acad. Sci.* 545, 51–73. doi: 10.1111/j.1749-6632.1988.tb19555.x

Bos, J. E., and Bles, W. (2002). Theoretical considerations on canal-otolith interaction and an observer model. *Biol. Cybern.* 86, 191–207. doi: 10.1007/s00422-001-0289-7

Chen-Harris, H., Joiner, W. M., Ethier, V., Zee, D. S., and Shadmehr, R. (2008). Adaptive control of saccades via internal feedback. *J. Neurosci.* 28, 2804–2813.

Clark, T. K., Newman, M. C., Karmali, F., Oman, C. M., and Merfeld, D. M. (2019).). Mathematical models for dynamic, multisensory spatial orientation perception. *Prog. Brain Res.* 248, 65–90. doi: 10.1016/bs.pbr.2019.04.014

Correia, M. J., and Guedry, F. E. (1966). Modification of Vestibular Responses as a Function of Rate of Rotation About an Earth-Horizontal Axis. *Acta Laryngol.* 62, 297–308. doi: 10.3109/00016486609119575

Cullen, K. E. (2012). The vestibular system: Multimodal integration and encoding of self-motion for motor control. *Trends Neurosci.* 35, 185–196. doi: 10.1016/j.tins.2011.12.001

Cullen, K. E. (2019). Vestibular processing during natural self-motion: Implications for perception and action. *Nat. Rev. Neurosci.* 20, 346–363. doi: 10.1038/s41583-019-0153-1

Curthoys, I. S. (1996). The delay of the oculogravic illusion. *Brain Res. Bull.* 40, 407–410. doi: 10.1016/0361-9230(96)00134-7

Dai, M., Raphan, T., and Cohen, B. (2009). Adaptation of the angular vestibulo-ocular reflex to head movements in rotating frames of reference. *Exp. Brain Res.* 195, 553–567. doi: 10.1007/s00221-009-1825-2

Dai, M. J., Raphan, T., and Cohen, B. (1991). Spatial orientation of the vestibular system: Dependence of optokinetic after-nystagmus on gravity. *J. Neurophysiol.* 66, 1422–1439. doi: 10.1152/jn.1991.66.4.1422

Dichgans, J., and Brandt, Th. (1973). Optokinetic Motion Sickness And Pseudo-Coriolis Effects Induced By Moving Visual Stimuli. *Acta Laryngol.* 76, 339–348. doi: 10.3109/00016487309121519

Dietrichs, E. (1983). The cerebellar corticonuclear and nucleocortical projections in the cat as studied with anterograde and retrograde transport of horseradish peroxidase. *Anat. Embryol.* 167, 449–462.

Dietrichs, E., and Walberg, F. (1985). The cerebellar nucleo-olivary and olivo-cerebellar nuclear projections in the cat as studied with anterograde and retrograde transport in the same animal after implantation of crystalline WGA-HRP: II. The fastigial nucleus. *Anat. Embryol.* 173, 253–261. doi: 10.1007/BF00316306

DiZio, P., and Lackner, J. R. (1988). The effects of gravitoinertial force level and head movements on post-rotational nystagmus and illusory after-rotation. *Exp. Brain Res.* 70, 485–495. doi: 10.1007/BF00247597

Einstein, A. (1907). Über das Relativitätsprinzip und die aus demselben gezogenen Folgerungen. *Jahrbuch der Radioaktivität und Elektronik*. 4, 411–462.

Fetter, M., Heimberger, J., Black, R., Hermann, W., Sievering, F., and Dichgans, J. (1996). Otolith-semicircular canal interaction during postrotatory nystagmus in humans. *Exp. Brain Res.* 108, 463–472. doi: 10.1007/BF00227269

Fujita, H., Kodama, T., and du Lac, S. (2020). Modular output circuits of the fastigial nucleus for diverse motor and nonmotor functions of the cerebellar vermis. *eLife* 9:e58613. doi: 10.7554/eLife.58613

Furman, J. M., and Koizuka, I. (1994). Reorientation of poststimulus nystagmus in tilted humans. *J. Vestib. Res.* 4, 421–428.

Fushiki, H., and Barmack, N. H. (1997). Topography and Reciprocal Activity of Cerebellar Purkinje Cells in the Uvula-Nodulus Modulated by Vestibular Stimulation. *J. Neurophysiol.* 78, 3083–3094. doi: 10.1152/jn.1997.78.6.3083

Fushiki, H., Maruyama, M., and Watanabe, Y. (2006). Efficacy of tilt-suppression in postrotatory nystagmus in cats. *Brain Res.* 1108, 127–132. doi: 10.1016/j.brainres.2006.06.010

Gao, Z., van Beugen, B. J., and De Zeeuw, C. I. (2012). Distributed synergistic plasticity and cerebellar learning. *Nat. Rev. Neurosci.* 13, 619–635. doi: 10.1038/nrn3312

Gizzi, M., Raphan, T., Rudolph, S., and Cohen, B. (1994). Orientation of human optokinetic nystagmus to gravity: A model-based approach. *Exp. Brain Res.* 99, 347–360. doi: 10.1007/BF00239601

Glasauer, S., and Merfeld, D. M. (1997). "Modelling three-dimensional vestibular responses during complex motion stimulation," in *Three-Dimensional Kinematics of Eye, Head and Limb Movements*, (eds) M. Fetter, T. Haslwanter and H. Misslisch, (Milton Park: Routledge), 387–398.

Graybiel, A. (1952). Oculogravic illusion. *AMA Arch. Ophthalmol.* 48, 605–615.

Graybiel, A., Johnson, W., Money, K., Malcolm, R., and Jennings, G. (1979). Oculogravic illusion in response to straight-ahead acceleration of a CF-104 aircraft. *Aviat. Space Environ. Med.* 50, 382–6.

Green, A. M., Shaikh, A. G., and Angelaki, D. E. (2005). Sensory vestibular contributions to constructing internal models of self-motion. *J. Neural Eng.* 2, S164–S179. doi: 10.1088/1741-2560/2/3/S02

Guedry, F. E. Jr., and Benson, A. B. (1976). Coriolis cross-coupling effects: Disorienting and nauseogenic or not. *Aviat. Space Environ. Med.* 49, 29–35. doi: 10.21236/ADA036899

Hain, T. C., Zee, D. S., and Maria, B. L. (1988). Tilt Suppression of Vestibulo-ocular Reflex in Patients with Cerebellar Lesions. *Acta Laryngol.* 105, 13–20. doi: 10.3109/00016488809119440

Harris, L. R. (1987). Vestibular and optokinetic eye movements evoked in the cat by rotation about a tilted axis. *Exp. Brain Res.* 66, 522–532. doi: 10.1007/BF00270685

Hess, B. J. M., and Angelaki, D. E. (1999). Oculomotor Control of Primary Eye Position Discriminates Between Translation and Tilt. *J. Neurophysiol.* 81, 394–398. doi: 10.1152/jn.1999.81.1.394

Ikeda, Y., Noda, H., and Sugita, S. (1989). Olivocerebellar and cerebelloolivary connections of the oculomotor region of the fastigial nucleus in the macaque monkey. *J. Comp. Neurol.* 284, 463–488. doi: 10.1002/cne.902840311

Jaggi-Schwarz, K., Misslisch, H., and Hess, B. J. M. (2000). Canal-Otolith Interactions After Off-Vertical Axis Rotations I. Spatial Reorientation of Horizontal Vestibuloocular Reflex. *J. Neurophysiol.* 83, 1522–1535. doi: 10.1152/jn.2000.83.3.1522

Jamali, M., Carriot, J., Chacron, M. J., and Cullen, K. E. (2019). Coding strategies in the otolith system differ for translational head motion vs. Static orientation relative to gravity. *eLife* 8:e45573. doi: 10.7554/eLife.45573

Kalman, R. E. (1960). Contributions to the theory of optimal control. *Bol. Soc. Mat. Mexicana* 5, 102–119.

Kalman, R. E., and Bucy, R. (1961). New results in linear filtering and prediction theory. *J. Basic Eng.* 83, 95–108.

Karmali, F., and Merfeld, D. M. (2012). A distributed, dynamic, parallel computational model: The role of noise in velocity storage. *J. Neurophysiol.* 108, 390–405. doi: 10.1152/jn.00883.2011

Khosravi—Hashemi, N., Forbes, P. A., Dakin, C. J., and Blouin, J. (2019). Virtual signals of head rotation induce gravity—dependent inferences of linear acceleration. *J. Physiol.* 597, 5231–5246. doi: 10.1113/JP278642

Kitama, T., Komagata, J., Ozawa, K., Suzuki, Y., and Sato, Y. (2014). Plane-specific Purkinje cell responses to vertical head rotations in the cat cerebellar nodulus and uvula. *J. Neurophysiol.* 112, 644–659. doi: 10.1152/jn.00029.2014

Kitama, T., Luan, H., Ishida, M., and Sato, Y. (2004). Effect of side-down tilt on optokinetic nystagmus and optokinetic after-nystagmus in cats. *Neurosci. Res.* 48, 269–283. doi: 10.1016/j.neures.2003.11.007

Körding, K. P., and Wolpert, D. M. (2004). Bayesian integration in sensorimotor learning. *Nature* 427:244.

Kushiro, K., Dai, M., Kunin, M., Yakushin, S. B., Cohen, B., and Raphan, T. (2002). Compensatory and Orienting Eye Movements Induced By Off-Vertical Axis Rotation (OVAR) in Monkeys. *J. Neurophysiol.* 88, 2445–2462. doi: 10.1152/jn.00197.222

Laurens, J., and Angelaki, D. E. (2011). The functional significance of velocity storage and its dependence on gravity. *Exp. Brain Res.* 210, 407–422. doi: 10.1007/s00221-011-2568-4

Laurens, J., and Angelaki, D. E. (2016). How the Vestibulocerebellum Builds an Internal Model of Self-motion. *Neuronal Codes Cereb.* 2016, 97–115. doi: 10.1016/B978-0-12-801386-1.00004-6

Laurens, J., and Angelaki, D. E. (2017). A unified internal model theory to resolve the paradox of active versus passive self-motion sensation. *eLife* 6:e28074. doi: 10.7554/eLife.28074

Laurens, J., and Angelaki, D. E. (2020). Simple spike dynamics of Purkinje cells in the macaque vestibulo-cerebellum during passive whole-body self-motion. *Proc. Natl. Acad. Sci. U.S.A.* 117, 3232–3238. doi: 10.1073/pnas.1915873117

Laurens, J., and Droulez, J. (2007). Bayesian processing of vestibular information. *Biol. Cybern.* 96, 389–404.

Laurens, J., and Droulez, J. (2008). *Bayesian Modelling of Visuo-Vestibular Interactions Probabilistic Reasoning and Decision Making in Sensory-Motor Systems*. Germany: Springer.

Laurens, J., Meng, H., and Angelaki, D. E. (2013b). Neural Representation of Orientation Relative to Gravity in the Macaque Cerebellum. *Neuron* 80, 1508–1518. doi: 10.1016/j.neuron.2013.09.029

Laurens, J., Meng, H., and Angelaki, D. E. (2013a). Computation of linear acceleration through an internal model in the macaque cerebellum. *Nat. Neurosci.* 16, 1701–1708. doi: 10.1038/nn.3530

Laurens, J., Strauman, D., and Hess, B. J. (2011). Spinning versus Wobbling: How the Brain Solves a Geometry Problem. *J. Neurosci.* 31, 8093–8101. doi: 10.1523/JNEUROSCI.5900-10.2011

Laurens, J., Straumann, D., and Hess, B. J. M. (2010). Processing of Angular Motion and Gravity Information Through an Internal Model. *J. Neurophysiol.* 104, 1370–1381. doi: 10.1152/jn.00143.2010

Lee, S.-U., Choi, J.-Y., Kim, H.-J., Park, J.-J., Zee, D. S., and Kim, J.-S. (2017). Impaired Tilt Suppression of Post-Rotatory Nystagmus and Cross-Coupled Head-Shaking Nystagmus in Cerebellar Lesions: Image Mapping Study. *Cerebellum* 16, 95–102. doi: 10.1007/s12311-016-0772-2

Lisberger, S. (1988). The neural basis for learning of simple motor skills. *Science* 242, 728–735. doi: 10.1126/science.3055293

Mackrous, I., Carriot, J., Jamali, M., and Cullen, K. E. (2019). Cerebellar Prediction of the Dynamic Sensory Consequences of Gravity. *Curr. Biol.* 29, 2698–2710.e4. doi: 10.1016/j.cub.2019.07.006

Mayne, R. (1974). "A systems concept of the vestibular organs," in *Vestibular System part 2: Psychophysics, Applied Aspects and General Interpretations*, eds M. Fetter, T. Haslwanter, H. Misslisch, and D. Tweed (Germany: Springer), 493–580.

McCall, A. A., and Yates, B. J. (2011). Compensation Following Bilateral Vestibular Damage. *Front. Neurol.* 2:88. doi: 10.3389/fneur.2011.00088

Meng, H., Blázquez, P. M., Dickman, J. D., and Angelaki, D. E. (2014). Diversity of vestibular nuclei neurons targeted by cerebellar nodulus inhibition: Vestibular neurons targeted by nodulus inhibition. *J. Physiol.* 592, 171–188. doi: 10.1113/jphysiol.2013.259614

Merfeld, D. M. (1995). Modeling the vestibulo-ocular reflex of the squirrel monkey during eccentric rotation and roll tilt. *Exp. Brain Res.* 106, 123–134. doi: 10.1007/BF00241362

Merfeld, D. M., Park, S., Gianna-Poulin, C., Black, F. O., and Wood, S. (2005a). Vestibular Perception and Action Employ Qualitatively Different Mechanisms. I. Frequency Response of VOR and Perceptual Responses During *Translation* and *Tilt*. *J. Neurophysiol.* 94, 186–198. doi: 10.1152/jn.00904.2004

Merfeld, D. M., Park, S., Gianna-Poulin, C., Black, F. O., and Wood, S. (2005b). . Vestibular Perception and Action Employ Qualitatively Different Mechanisms. II. VOR and Perceptual Responses During Combined *Tilt&Translation*. *J. Neurophysiol.* 94, 199–205. doi: 10.1152/jn.00905.2004

Merfeld, D. M., Young, L. R., Paige, G. D., and Tomko, D. L. (1993).). Three dimensional eye movements of squirrel monkeys following postrotatory tilt. *J. Vestib. Res.* 3, 123–139.

Merfeld, D. M., Zupan, L., and Peterka, R. J. (1999). Humans use internal models to estimate gravity and linear acceleration. *Nature* 398, 615–618. doi: 10.1038/19303

Oman, C. M. (1982). A heuristic mathematical model for the dynamics of sensory conflict and motion sickness. *Acta Laryngol.* 94, 4–44.

Ormsby, C. C., and Young, L. R. (1977). Integration of semicircular canal and otolith information for multisensory orientation stimuli. *Math. Biosci.* 34, 1–21. doi: 10.3389/fnint.2014.00044

Paige, G. D., and Tomko, D. L. (1991). Eye movement responses to linear head motion in the squirrel monkey I. Basic characteristics. *J. Neurophysiol.* 65, 1170–1182. doi: 10.1152/jn.1991.65.5.1170

Raphan, T., and Cohen, B. (2002). The vestibulo-ocular reflex in three dimensions. *Exp. Brain Res.* 145, 1–27. doi: 10.1007/s00221-002-1067-z

Raphan, T., Matsuo, V., and Cohen, B. (1979). Velocity storage in the vestibulo-ocular reflex arc (VOR). *Exp. Brain Res.* 35, 229–248. doi: 10.1007/BF00236613

Sağlam, M., Glasauer, S., and Lehnen, N. (2014). Vestibular and cerebellar contribution to gaze optimality. *Brain* 137, 1080–1094. doi: 10.1093/brain/awu006

Seidman, S. H., and Paige, G. D. (1996). Perception and Eye Movement during Low-Frequency Centripetal Acceleration. *Ann. N Y Acad. Sci.* 781, 693–695. doi: 10.1111/j.1749-6632.1996.tb15762.x

Shaikh, A. G., Green, A. M., Ghasia, F. F., Newlands, S. D., Dickman, J. D., and Angelaki, D. E. (2005). Sensory Convergence Solves a Motion Ambiguity Problem. *Curr. Biol.* 15, 1657–1662. doi: 10.1016/j.cub.2005.08.009

Solomon, D., and Cohen, B. (1994). Stimulation of the nodulus and uvula discharges velocity storage in the vestibulo-ocular reflex. *Exp. Brain Res.* 102, 57–68. doi: 10.1007/BF00232438

Sprenger, A., Wojak, J. F., Jandl, N. M., and Helmchen, C. (2017). Postural Control in Bilateral Vestibular Failure: Its Relation to Visual. Proprioceptive, Vestibular, and Cognitive Input. *Front. Neurol.* 8:444. doi: 10.3389/fneur.2017.00444

Stay, T. L., Laurens, J., Sillitoe, R. V., and Angelaki, D. E. (2019). Genetically eliminating Purkinje neuron GABAergic neurotransmission increases their response gain to vestibular motion. *Proc. Natl. Acad. Sci. U.S.A.* 116, 3245–3250. doi: 10.1073/pnas.1818819116

Strupp, M., Feil, K., Dieterich, M., and Brandt, T. (2016). Bilateral vestibulopathy. *Handb Clin Neurol.* 137, 235–240. doi: 10.1016/B978-0-444-63437-5.00017-0

Todorov, E. (2004). Optimality principles in sensorimotor control. *Nat. Neurosci.* 7, 907–915. doi: 10.1038/nn1309

Vingerhoets, R. A. A., Van Gisbergen, J. A. M., and Medendorp, W. P. (2007). Verticality Perception During Off-Vertical Axis Rotation. *J. Neurophysiol.* 97, 3256–3268. doi: 10.1152/jn.01333.2006

Voogd, J. (2016). Deiters'. Nucleus. Its Role in Cerebellar Ideogenesis: The Ferdinando Rossi Memorial Lecture. *Cerebellum* 15, 54–66. doi: 10.1007/s12311-015-0681-9

Voogd, J., and Barmack, N. H. (2006). Oculomotor cerebellum. *Prog. Brain Res.* 151, 231–268. doi: 10.1016/S0079-6123(05)51008-2

Voogd, J., Gerrits, N. M., and Ruigrok, T. J. H. (1996).). Organization of the Vestibulocerebellum. *Ann. N.Y. Acad. Sci.* 781, 553–579. doi: 10.1111/j.1749-6632.1996.tb15728.x

Voogd, J., Schraa-Tam, C. K. L., van der Geest, J. N., and De Zeeuw, C. I. (2012). Visuomotor Cerebellum in Human and Nonhuman Primates. *Cerebellum* 11, 392–410. doi: 10.1007/s12311-010-0204-7

Voogd, J., Shinoda, Y., Ruigrok, T. J. H., and Sugihara, I. (2013). "Cerebellar Nuclei and the Inferior Olivary Nuclei: Organization and Connections," in *Handbook of the Cerebellum and Cerebellar Disorders*, eds M. Manto, J. D. Schmahmann, F. Rossi, D. L. Gruol, and N. Koibuchi (Netherlands: Springer), 377–436. doi: 10.1007/978-94-007-1333-8_19

Waespe, W., Cohen, B., and Raphan, T. (1985). Dynamic modification of the vestibulo-ocular reflex by the nodulus and uvula. *Science* 228, 199–202. doi: 10.1126/science.3871968

Wall, C., and Furman, J. M. R. (1990). Visual-vestibular Interaction in Humans during Earth-horizontal Axis Rotation. *Acta Laryngol.* 109, 337–344. doi: 10.3109/00016489009125153

Wearne, S., Raphan, T., and Cohen, B. (1998). Control of Spatial Orientation of the Angular Vestibulooocular Reflex by the Nodulus and Uvula. *J. Neurophysiol.* 79, 2690–2715. doi: 10.1152/jn.1998.79.5.2690

Wolpert, D. M., Ghahramani, Z., and Jordan, M. I. (1995). An internal model for sensorimotor integration. *Science* 269, 1880–1882.

Xiong, G., and Matsushita, M. (2000). Connections of Purkinje cell axons of lobule X with vestibulocerebellar neurons projecting to lobule X or IX in the rat. *Exp. Brain Res.* 133, 219–228. doi: 10.1007/s002210000372

Yakhnitsa, V., and Barmack, N. H. (2006). Antiphasic Purkinje cell responses in mouse uvula-nodulus are sensitive to static roll–tilt and topographically organized. *Neuroscience* 143, 615–626. doi: 10.1016/j.neuroscience.2006.08.006

Yakusheva, T. A., Blazquez, P. M., and Angelaki, D. E. (2008). Frequency-Selective Coding of Translation and Tilt in Macaque Cerebellar Nodulus and Uvula. *J. Neurosci.* 28, 9997–10009. doi: 10.1523/JNEUROSCI.2232-08.2008

Yakusheva, T. A., Blazquez, P. M., and Angelaki, D. E. (2010). Relationship between Complex and Simple Spike Activity in Macaque Caudal Vermis during Three-Dimensional Vestibular Stimulation. *J. Neurosci.* 30, 8111–8126. doi: 10.1523/JNEUROSCI.5779-09.2010

Yakusheva, T. A., Blazquez, P. M., Chen, A., and Angelaki, D. E. (2013). Spatiotemporal Properties of Optic Flow and Vestibular Tuning in the Cerebellar Nodulus and Uvula. *J. Neurosci.* 33, 15145–15160. doi: 10.1523/JNEUROSCI.2118-13.2013

Yakusheva, T. A., Shaikh, A. G., Green, A. M., Blazquez, P. M., Dickman, J. D., and Angelaki, D. E. (2007). Purkinje Cells in Posterior Cerebellar Vermis Encode Motion in an Inertial Reference Frame. *Neuron* 54, 973–985. doi: 10.1016/j.neuron.2007.06.003

Yakushin, S. B., Raphan, T., and Cohen, B. (2017). Coding of Velocity Storage in the Vestibular Nuclei. *Front. Neurol.* 8:386. doi: 10.3389/fneur.2017.00386

Yasuda, K., Fushiki, H., Maruyama, M., and Watanabe, Y. (2003). The effects of pitch tilt on postrotatory nystagmus in cats. *Brain Res.* 991, 65–70. doi: 10.1016/S0006-8993(03)03536-4

Yasuda, K., Fushiki, H., Wada, R., and Watanabe, Y. (2002). Spatial orientation of postrotatory nystagmus during static roll tilt in cats. *J. Vestib. Res.* 12, 15–23.

Young, L. R. (1971). Cross Coupling Between Effects of Linear and Angular Acceleration on Vestibular nystagmus. *Bibl Ophthalmol.* 82, 116–121.

Young, L. R. (2011). Optimal estimator models for spatial orientation and vestibular nystagmus. *Exp. Brain Res.* 210, 465–476. doi: 10.1007/s00221-011-2595-1

Zupan, L. H., Peterka, R. J., and Merfeld, D. M. (2000). Neural Processing of Gravito-Inertial Cues in Humans. I. Influence of the Semicircular Canals Following Post-Rotatory Tilt. *J. Neurophysiol.* 84, 2001–2015. doi: 10.1152/jn.2000.84.4.2001

frontiers | Frontiers in Systems Neuroscience

TYPE Review
PUBLISHED 13 October 2022
DOI 10.3389/fnsys.2022.984406

OPEN ACCESS

EDITED BY
Jose Antonio Lopez-Escamez,
Universidad de Granada, Spain

REVIEWED BY
Maria Concetta Miniaci,
University of Naples Federico II, Italy
Hirofumi Fujita,
University of Texas Southwestern Medical Center, United States

*CORRESPONDENCE
Levi P. Sowers
levi-sowers@uiowa.edu

RECEIVED 02 July 2022
ACCEPTED 27 September 2022
PUBLISHED 13 October 2022

CITATION
Wang M, Tutt JO, Dorricott NO, Parker KL, Russo AF and Sowers LP (2022) Involvement of the cerebellum in migraine.
Front. Syst. Neurosci. 16:984406.
doi: 10.3389/fnsys.2022.984406.

Involvement of the cerebellum in migraine

Mengya Wang[1], Joseph O. Tutt[2], Nicholas O. Dorricott[2], Krystal L. Parker[3], Andrew F. Russo[4,5,6] and Levi P. Sowers[6,7]*

[1]Department of Neuroscience and Pharmacology, University of Iowa, Iowa City, IA, United States, [2]Department of Biology and Biochemistry, University of Bath, Bath, United Kingdom, [3]Department of Psychiatry, University of Iowa, Iowa City, IA, United States, [4]Department of Molecular Physiology and Biophysics, University of Iowa, Iowa City, IA, United States, [5]Department of Neurology, University of Iowa, Iowa City, IA, United States, [6]Center for the Prevention and Treatment of Visual Loss, Veterans Administration Health Center, Iowa City, IA, United States, [7]Department of Pediatrics, University of Iowa, Iowa City, IA, United States

Migraine is a disabling neurological disease characterized by moderate or severe headaches and accompanied by sensory abnormalities, e.g., photophobia, allodynia, and vertigo. It affects approximately 15% of people worldwide. Despite advancements in current migraine therapeutics, mechanisms underlying migraine remain elusive. Within the central nervous system, studies have hinted that the cerebellum may play an important sensory integrative role in migraine. More specifically, the cerebellum has been proposed to modulate pain processing, and imaging studies have revealed cerebellar alterations in migraine patients. This review aims to summarize the clinical and preclinical studies that link the cerebellum to migraine. We will first discuss cerebellar roles in pain modulation, including cerebellar neuronal connections with pain-related brain regions. Next, we will review cerebellar symptoms and cerebellar imaging data in migraine patients. Lastly, we will highlight the possible roles of the neuropeptide calcitonin gene-related peptide (CGRP) in migraine symptoms, including preclinical cerebellar studies in animal models of migraine.

KEYWORDS

migraine, cerebellum, pain, CGRP, sensory processing

Abbreviations: ACC, Anterior cingulate cortex; AMY1, Amylin subtype 1 receptor; CGRP, Calcitonin gene-related peptide; CLR, Calcitonin receptor-like receptor; CTR, Calcitonin receptor; EEG, electroencephalography; FC, Functional connectivity; FHM, Familial hemiplegic migraine; fMRI, functional magnetic resonance imaging; GMV, Gray matter volume; HCs, Healthy controls; i.p., Intraperitoneal; IS, Inflammatory soup; MN, Medial cerebellar nucleus; NSAIDs, Non-steroidal anti-inflammatory drugs; NTG, Nitroglycerin; PACAP38, Pituitary adenylate cyclase-activating polypeptide-38; PAG, Periaqueductal gray; PBN, Parabrachial nucleus; PET, positron emission tomography; PoT, Posterior thalamus; RAMP1, Receptor activity-modifying protein 1; RCP, Receptor component protein; SpV, Spinal trigeminal nucleus; ZI, Zona incerta.

Introduction

Migraine is a debilitating primary headache disorder commonly characterized by moderate or severe headaches that can be aggravated by routine activity (ICHD-3, 2018). Migraine is often accompanied by sensory abnormalities, such as photophobia, phonophobia, nausea, vertigo, and allodynia. The disorder affects 14.4% of the global population, partitioned into 18.9% of females and 9.8% of males (Stovner et al., 2018). Headache disorders, including migraine, are the second leading global cause of disability (GBD 2017 Disease and Injury Incidence and Prevalence Collaborators, 2018; Stovner et al., 2018). Migraine types include those with and without aura, which can be broadly grouped as episodic or chronic, that is less or greater than 15 headache days a month, respectively. Episodic migraine can evolve into chronic migraine. It was believed that migraine patients improperly filter sensory inputs (e.g., somatosensory, visual, and auditory inputs, which results in migraine symptoms (e.g., head pain, photophobia, and phonophobia, respectively).

The cerebellum is widely known for integrating non-motor sensory signals and controlling motor function (Manto et al., 2012). There is, however, a growing realization indicating cerebellar involvement in perceptual (Baumann et al., 2015), emotional (Adamaszek et al., 2017), and cognitive functions (Koziol et al., 2014; Van Overwalle et al., 2020). Of note, there is mounting evidence to support cerebellar involvement in pain and motor response to pain (Moulton et al., 2010), which are both phenotypes exhibited by migraine patients. In addition to the implication in pain phenotypes, the cerebellum communicates to pain/migraine-related regions; is implicated in the other migraine symptoms; and, more importantly, is altered in the migraine patient imaging studies (Vincent and Hadjikhani, 2007; Kros et al., 2018). The objective of this review is to summarize and update the clinical and preclinical studies that link the cerebellum to migraine. Cerebellar symptoms in migraine patients and a comprehensive summary of imaging studies on the cerebellum in migraine patients with/without exposure to sensory stimuli will be reviewed. The possibility that cerebellar CGRP actions may contribute to migraine will be discussed, along with cerebellar findings in migraine animal models, which may provide insight into migraine pathophysiology.

The current therapeutics for migraine

There are two migraine management goals: acute treatments to relieve attacks or preventive treatments to reduce attack frequency and severity. There are non-specific anti-migraine medications for acute and preventative treatment, e.g., non-steroidal anti-inflammatory drugs (NSAIDs) and antiemetics for abortion, and beta blockers and anticonvulsants for prevention (Mayans and Walling, 2018; Ha and Gonzalez, 2019). There are also specific anti-migraine therapies, including triptans (5-$HT_{1B/1D}$ receptor agonists), ditans (5-HT_{1F} receptor agonists), gepants [calcitonin gene-related peptide (CGRP) receptor antagonists] as abortive drugs, and CGRP and CGRP receptor monoclonal antibodies as preventative treatments (Eigenbrodt et al., 2021). Rimegepant and atogepant, belonging to gepants, were recently approved for migraine prevention (Tao et al., 2022) and eptinezumab for acute use in the emergency department (Benemei et al., 2022). Mechanisms underlying migraine prevention or acute treatment following symptom onset are not clear. However, it has been suggested that CGRP actions contribute to both abortive and prophylaxis management in that CGRP-based drugs can achieve both management goals. Among these anti-migraine drugs, 30%–40% of migraine patients do not respond to triptan (Lombard et al., 2020), 50% do not respond to ditans (Mecklenburg et al., 2020), 50% do not respond to CGRP-based drugs (Edvinsson et al., 2018), and more than 50% do not respond to the non-specific anti-migraine preventative treatments (Deen et al., 2017). Further understanding of migraine pathophysiology is necessary to develop new and more effective therapeutics.

Migraine pathogenesis is multifactorial. The failure of efficacy in the non-responders to current medications suggests that CGRP is not the only cause of migraine and that other neuropeptides are involved; e.g., pituitary adenylate cyclase-activating peptide (PACAP-38) works independently of CGRP or 5-$HT_{1B/1D/1F}$ receptors (Kuburas et al., 2021; Ernstsen et al., 2022). In addition, CGRP-based drugs act on the periphery with low penetration across the blood-brain barrier (Edvinsson and Warfvinge, 2019); eg., a preclinical study reported that galcanezumab, one of the FDA-approved CGRP antibodies targeting the CGRP peptide, demonstrated limited blood-brain barrier penetration when injected peripherally into rats (Johnson et al., 2019). Penetration into the cerebellum was 0.18% of the plasma concentration, and penetration into the hypothalamus, the spinal cord, or the prefrontal cortex was ∼0.3% of the plasma concentration (Johnson et al., 2019). The lack of central penetration may be another reason that some migraine patients do not benefit from current therapeutics. This emphasizes that the central mechanisms underlying migraine pathogenesis should be considered. While central mechanisms contribute to migraine pathophysiology, there is still a significant dearth of understanding about the neuroanatomical correlates in migraine. Central neural circuits controlling sensory perception may play a critical role in this disease state. The cerebellum represents a prime sensory integration center in the brain that may govern some of these pathological phenotypes in migraine.

Cerebellar anatomy controlling motor processing

The cerebellum has three main divisions: the cerebrocerebellum, the vestibulocerebellum, and the spinocerebellum (Purves et al., 2018). It is widely accepted that the cerebellum plays a role in motor function (Manto et al., 2012). The cerebrocerebellum, occupies most of the lateral cerebellar hemisphere and projects primarily to the lateral cerebellar nucleus (also known as the dentate nucleus). The cerebrocerebellum receives signals from cerebral cortical areas and sends signals back to the same areas, and in this manner, engages in motor planning (Purves et al., 2018). The vestibulocerebellum, comprising the caudal lobes of the cerebellum, participates in balance control and vestibuloocular regulation. The spinocerebellum contains the median and paramedian zones of the cerebellar hemispheres. Specifically, the paramedian (also called intermediate) zone, which projects primarily to the interposed nucleus, is involved in distal muscle movements, while the median zone (also called the vermis), which projects to the medial cerebellar nucleus (MN, also known as the fastigial nucleus), is involved in movements of axial and proximal muscles (Purves et al., 2018). In addition, the oculomotor vermis (lobules VI and VII) and the MN control eye movement (Manto et al., 2012).

For motor performance, the cerebellum receives dynamic sensory information and subsequently corrects or optimizes movements *via* outputs to different regions (Jueptner and Weiller, 1998). Specifically, the cerebellum receives vestibular, visual, tactile, or proprioceptive sensory information from the spinal cord, vestibular, trigeminal, and dorsal column nuclei *via* mossy fibers, as well as from the inferior olive *via* climbing fibers (Rondi-Reig et al., 2014); e.g., the vestibulocerebellum receives signals from and sends signals to the vestibular complex to control eye and head movements (Purves et al., 2018). The interposed nucleus receives signals from the red nucleus *via* the inferior olive and signals back to the red nucleus (Siegel and Sapru, 2019; Basile et al., 2021). The red nucleus is a region involved in motor control and nociceptive processing in the brainstem (Basile et al., 2021). The MN receives inputs from and sends projections to the reticular and vestibular complex to modulate the lower motor neurons (Purves et al., 2018; Siegel and Sapru, 2019). It is likely that these circuits are shared between motor functions and sensory processing suggesting that they not only lay a foundation for movement control but also have implications for altered sensory processing in migraine.

Cerebellar role in pain processing

In the previous section, the likely role of the cerebellum in sensory processing is mentioned. Considering that pain is an unpleasant sensory and emotional experience associated with actual or potential tissue damage (Sandkuhler, 2009), several studies have investigated the potential link between the cerebellum and pain processing.

Cerebellar circuitry in sensory and emotional dimensions of pain

The sensory dimension of pain in the body is mainly mediated by the spinothalamic tract, which is composed of the spinal cord to the ventroposterolateral thalamus (Kandel et al., 2021). In the head, it is primarily mediated by the trigeminothalamic tract comprising the trigeminal ganglion to the spinal trigeminal nucleus (SpV) and then to the ventroposteromedial thalamus (Kandel et al., 2021) which is a crucial circuit involved in migraine headache attacks (Burstein et al., 2000; Noseda et al., 2019). The ventroposterolateral and ventroposterormedial thalamus are both posterior thalamic nuclei. In addition, the intralaminar thalamus (including the parafasciculus and centromedian thalamus), the amygdala, and the PAG are all involved in the emotional dimension of pain (Ab Aziz and Ahmad, 2006; Siegel and Sapru, 2019). Indeed, sensitization of the SpV and connected third-order trigeminovascular thalamic neurons contributes to the development of cephalic allodynia and migraine headache (Landy et al., 2004; Burstein et al., 2015; Dodick, 2018).

In this section, we will discuss that the cerebellum is structurally connected to regions involved in processing sensory and emotional aspects of pain (**Figure 1** and **Table 1**). Here we organized the cerebellar connections with other regions into sensory and emotional circuits. While the functional relevance of these connections is, at present, poorly defined, their existence suggests a cerebellar influence on these regions towards behavior relevant to migraine.

Sensory-related connections

Spinal cord and brainstem

The cerebellar cortex—predominantly the vermis—is innervated by multiple spinal cord regions, including the contralateral central cervical nucleus, the ipsilateral dorsal nucleus, the lumbar and sacral precerebellar nuclei, lumbar border precerebellar cells, and dispersed neurons of the deep dorsal horn and laminae 6–8 (Sengul et al., 2015), and the MN sends contralateral projections to the spinal cord (Fujita et al., 2020; **Figure 1** and **Table 1**), highlighting the reciprocal connections of the cerebellum and spinal cord.

Another important region in the ascending pain pathway is the SpV, which receives sensory inputs from the cranial meninges and extracephalic skin and relays these inputs to pain processing regions, the thalamic nuclei (Burstein et al., 2010).

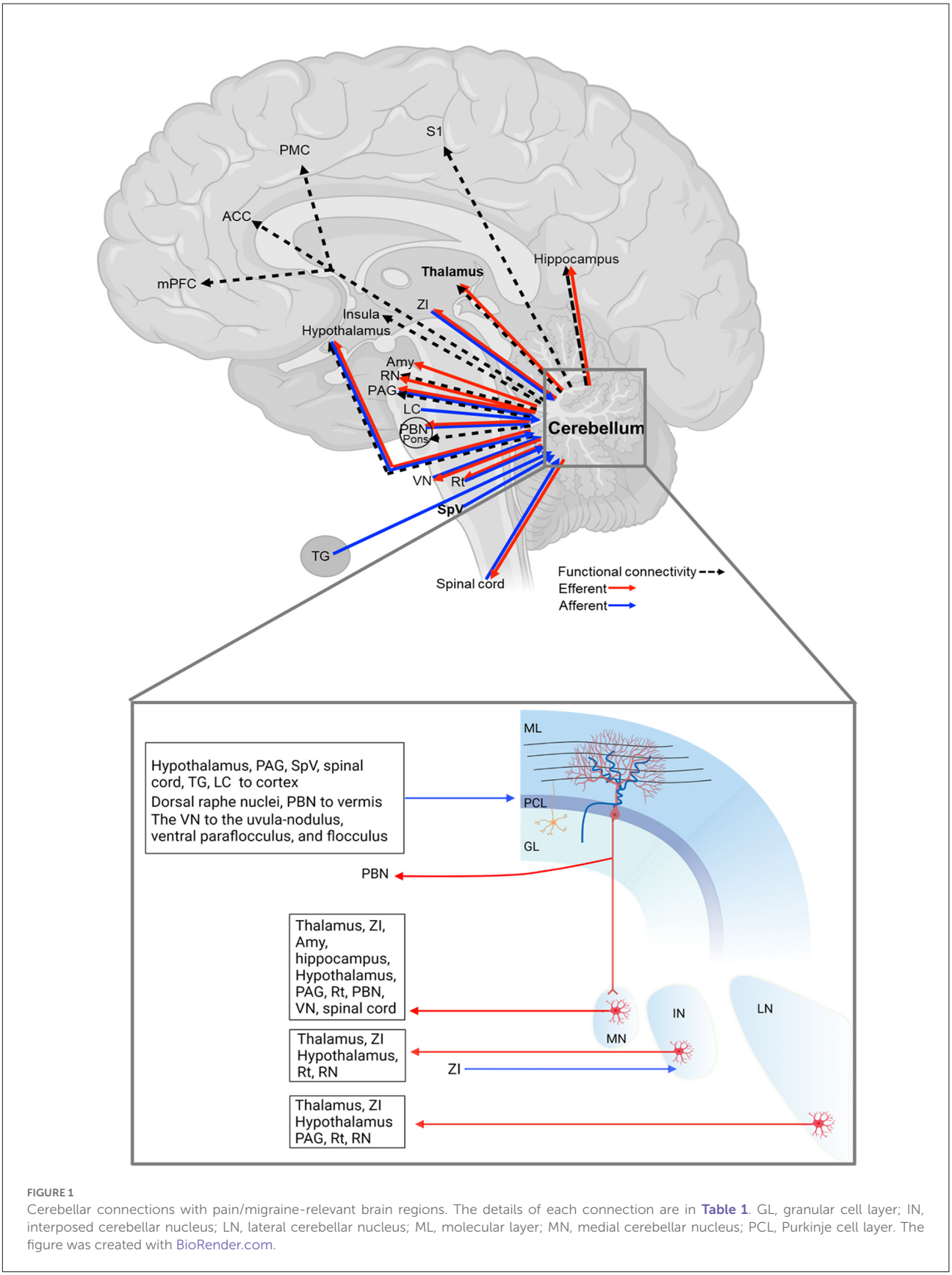

FIGURE 1
Cerebellar connections with pain/migraine-relevant brain regions. The details of each connection are in **Table 1**. GL, granular cell layer; IN, interposed cerebellar nucleus; LN, lateral cerebellar nucleus; ML, molecular layer; MN, medial cerebellar nucleus; PCL, Purkinje cell layer. The figure was created with BioRender.com.

TABLE 1 Cerebellar connections with pain or migraine-relevant brain regions.

Connections	Type	Details	Ref.
Cerebellum-Primary somatosensory cortex (S1)	FC	In migraine patients compared to HCs in the interictal phase • ↓ FC between the right S1 and the right cerebellum posterior lobe (lobule VIIIb)	Zhang et al. (2017)
Cerebellum-Premotor cortex (PMC)	FC	In migraine patients compared to HCs during the interictal phase • ↓ FC between the right dorsal premotor cortex and ipsilateral cerebellar lobule VIII	Qin et al. (2020)
Cerebellum- ACC	FC	Mice receiving IS at low and high frequency; Mice receiving IS at low frequency and NTG • ↑ cerebellar FCs with the ACC	Jia et al. (2019)
Cerebellum-Insula	FC	Mice receiving IS at low and high frequency; Mice receiving IS at low frequency and NTG • ↑ cerebellar FCs with the insula	Jia et al. (2020)
		In migraine patients compared to HCs • ↑ FC between the right posterior insula and the bilateral cerebellum	Ke et al. (2020)
Cerebellum-Medial prefrontal cortex (mPFC)	FC	In migraine patients compared to HCs • ↓ FC between the left Crus I and the default mode network components (including mPFC)	Ke et al. (2020)
		In migraine patients compared to HCs • ↑ FC between the right cerebellum and the right mPFC.	Jin et al. (2013)
Cerebellum-Thalamus	Circuitry→	• The MN → ventromedial, ventrolateral, centrolateral, mediodorsal, parafascicular, supragenicular and posterior thalamic nuclei • The interposed nucleus → the ventrolateral and ventroposterior thalamic nuclei • The lateral cerebellar nucleus → the thalamus	Teune et al. (2000) and Fujita et al. (2020) Teune et al. (2000) and Baldacara et al. (2008) Teune et al. (2000) and Baldacara et al. (2008)
	FC	In migraine patients compared to HCs during the interictal phase. • ↑ FC between the left lateral geniculate nucleus and the ipsilateral cerebellum	Zhang et al. (2020)
	FC	In migraine patients receiving trigeminal stimuli compared to HCs • ↓ FC between Left Crus I (ipsilateral to the stimulation) and the left thalamus and some cortical areas	Mehnert and May (2019)
		Episodic migraine patients administered NTG orally compared to their own baseline • FC change between the right thalamus and the cerebellum during the prodromal and full-blown phase	Martinelli et al. (2021)
Cerebellum- zona incerta (ZI)	Circuitry→ ←	• The MN → ZI	Fujita et al. (2020)
		• The interposed nucleus ↔ (reciprocally) the ZI	Teune et al. (2000) and Ossowska (2020)
		• The lateral nucleus → ZI	Teune et al. (2000)
Cerebellum-Amygdala (Amy)	Circuitry→	• The MN directly → the amygdala (histological degeneration studies)	Heath and Harper (1974)
Cerebellum-Hippocampus	Circuitry→	• The MN directly → the hippocampus (histological degeneration studies)	Heath and Harper (1974)
	FC	In migraine patients compared to HCs during the interictal phase • ↑ FC between the hippocampus and the cerebellum	Wei et al. (2020)
Cerebellum-Hypothalamus	Circuitry→	• Three deep cerebellar nuclei → the hypothalamus contralaterally	Haines and Dietrichs (1984)
		• The MN sends GABAergic fibers → the hypothalamus	Cao et al. (2013)
	←	• The hypothalamus → the cerebellar cortex bilaterally with the ipsilateral preponderance	Dietrichs (1984) and Haines and Dietrichs (1984)

(Continued)

TABLE 1 (Continued)

Connections	Type	Details	Ref.
	FC	In migraine patients compared to HCs during the interictal phase • ↑ FC between the hypothalamus, and cerebellar Crus I&II and lobules V&VI	Moulton et al. (2014)
Cerebellum-periaqueductal gray (PAG)	Circuitry →	• The MN and lateral nucleus →PAG	Teune et al. (2000), Frontera et al. (2020), and Fujita et al. (2020)
	←	• The PAG → the cerebellar cortex	Dietrichs (1983)
	FC	In migraine with ictal allodynia compared to migraine without ictal allodynia • ↑ FC between PAG and the cerebellum	Schwedt et al. (2014b)
Cerebellum-Reticular formation (Rt)	Circuitry →	• The three deep nuclei → the Rt	Teune et al. (2000) and Fujita et al. (2020)
	←	• Dorsal raphe nuclei → the cerebellar vermis	Dietrichs (1985)
		• The Rt → the developing cerebellum *via* serotonergic fibers	Bishop et al. (1988)
Cerebellum-Red nucleus (RN)	Circuitry →	• The interposed and lateral nucleus →the RN	Siegel and Sapru (2019) and Basile et al. (2021)
	FC	In migraine patients compared to HCs during the interictal phase • ↑FC between the right red nucleus and the ipsilateral cerebellum	Huang et al. (2019)
Cerebellum-parabrachial nucleus (PBN)	Circuitry → ←	• The MN and a small number of Purkinje cells in the anterior cerebellar vermis → the PBN	Supple and Kapp (1994), Teune et al. (2000), and Fujita et al. (2020)
		• The PBN sends multilayered fibers →the anterior cerebellar vermis	Supple and Kapp (1994)
	FC	In migraine patients administered NTG to induce a headache, compared to their own baseline. • ↑FC between the pons and the cerebellar tonsils	Karsan et al. (2020)
Cerebellum-Locus coeruleus (LC)	Circuitry ←	• The LC → the cerebellar cortex	Dietrichs (1985, 1988)
Cerebellum-Vestibular nucleus (VN)	Circuitry →	• The paraflocculus, the flocculus, and the uvula-nodulus → the VN	Tabata et al. (2002) and Barmack (2016)
	←	• The VN → the uvula-nodulus, ventral paraflocculus, and flocculus	Barmack (2016)
	→	• The MN → the VN	Bagnall et al. (2009) and Fujita et al. (2020)
Cerebellum-Spinal trigeminal nucleus (SpV)	Circuitry ←	• The SpV and principle sensory nucleus → the cerebellar vermal, medial, and lateral zones	Ikeda (1979), Hayashi et al. (1984), Ohya et al. (1993), and Ge et al. (2014)
		• These trigemino-cerebellar projection neurons predominantly express the vesicular-glutamate transporter 1 (VGLUT1)	Ge et al. (2014)
Cerebellum-Trigeminal ganglion (TG)	Circuitry ←	• The TG → ipsilaterally in Crus I and II, the paramedian lobule, the lateral cerebellar nucleus, and each lobe of the parafloccular cortex	Jacquin et al. (1982)
Cerebellum-spinal cord	Circuitry →	• The MN →the spinal cord	Fujita et al. (2020)
	←	• Spinal cord regions, including the central cervical nucleus, the dorsal nucleus, the lumbar and sacral precerebellar nuclei, lumbar border precerebellar cells, and from dispersed neurons of the deep dorsal horn and laminae 6–8 → the cerebellar cortex, mainly the vermis	Sengul et al. (2015)

HCs, healthy controls; FC, functional connectivity; ACC, the anterior cingulate cortex; IS, inflammatory soup; NTG, nitroglycerin; →←, projecting direction; ↑, increase; ↓, decrease.

Studies also demonstrated that the SpV sends projections to the cerebellar cortex (Ikeda, 1979; Hayashi et al., 1984; Ohya et al., 1993; Ge et al., 2014; **Figure 1** and **Table 1**). These SpV-cerebellar neurons predominantly express the vesicular-glutamate transporter 1 (Ge et al., 2014). It is possible that the cerebellum could be acting to process trigeminal inputs from the SpVefferents and acting as a putative nociceptive processing center (Ruscheweyh et al., 2014). Moreover, an earlier study showed that the primary trigeminal afferents from the trigeminal ganglion terminate in cerebellum regions, including ipsilateral Crus I and II, the paramedian lobule, the lateral cerebellar nucleus, and the paraflocculus (Jacquin et al., 1982; **Figure 1** and **Table 1**). The inputs from the trigeminal sensory neurons highlight this cerebellar connection for a potential role in the processing of sensory input during migraine attacks.

The parabrachial nucleus (PBN) is a region known to modulate multiple aversive behaviors (Palmiter, 2018). The MN sends projections to the PBN (Supple and Kapp, 1994; Teune et al., 2000; Fujita et al., 2020), which relays signals to the cerebellar vermis (Dietrichs, 1985; Supple and Kapp, 1994; **Figure 1** and **Table 1**). Finally, the cerebellum is connected with reticular formation (Bishop et al., 1988; Teune et al., 2000; Fujita et al., 2020), including the dorsal raphe nuclei (Dietrichs, 1985) for pain modulation (Wang and Nakai, 1994), and the red nucleus for motor control and nociceptive processing (Huang et al., 2019; Siegel and Sapru, 2019; Basile et al., 2021; **Figure 1** and **Table 1**) . Together, the vast structural connectivity of the cerebellum with pain processing regions implies a cerebellar hand in sensory evaluation, and dysregulation of these pathways could contribute to the multitude of sensory abnormalities observed during the prodrome and headache phases of migraine.

Thalamus and subthalamus

As mentioned above, the thalamus is the key component in pain modulation, and cerebellar innervation of the thalamic region could contribute to it (**Figure 1** and **Table 1**). The lateral cerebellar nucleus sends projections to the thalamus (Teune et al., 2000; Baldacara et al., 2008). The interposed nucleus innervates the ventrolateral and ventroposterior thalamic nuclei (Teune et al., 2000; Baldacara et al., 2008). The ventroposterior region receives input from ascending trigeminal sensory neurons (Graziano et al., 2008). The MN projects to various thalamic nuclei, including ventromedial, ventrolateral, centrolateral, mediodorsal, parafascicular, suprageniculate thalamic nuclei, and the nucleus in the posterior thalamus (PoT; Teune et al., 2000; Fujita et al., 2020). The PoT integrates signals from the SpV and retinal ganglion cells (Noseda et al., 2010) and is thought to be involved in light-aversive behavior, acutely relevant to migraine (Sowers et al., 2020). Together, cerebellar innervation of the thalamus may contribute to migraine, e.g., thalamic sensitization during migraine.

Moreover, the deep cerebellar nuclei are connected to the zona incerta (ZI), adjacent to the thalamus (Teune et al., 2000; Fujita et al., 2020; Ossowska, 2020). The ZI exerts inhibitory control on all higher-order thalamic nuclei, including the PoT *via* GABAergic projections (Bartho et al., 2002). The ZI acts to gate peripheral inputs into the PoT, depending on the behavioral state (Trageser and Keller, 2004). Interestingly, disinhibition of the trigeminal ZI-PoT- primary somatosensory cortex circuit has been observed in models of chronic pain (Masri et al., 2009) and could be anticipated to accompany migraine (Brennan and Pietrobon, 2018).

Emotion-related regions

The experience of pain contains an emotional-affective dimension, including anxiety and fear. The cerebellum is connected to regions involved in emotional processing (**Figure 1** and **Table 1**) and is thought to be involved in the neural circuitry driving anxiety (Otsuka et al., 2016). The thalamus serves as a hub that regulates both sensory and affective aspects of pain, whose connections to the cerebellum was discussed in section "Sensory-related connections".

The cerebellum is also known to be reciprocally connected to the periaqueductal gray (PAG; Dietrichs, 1983; Teune et al., 2000; Frontera et al., 2020; Fujita et al., 2020), an antinociceptive processing center (Basbaum and Fields, 1978; Morgan et al., 1997). Specifically, the MN and the lateral nucleus project to the PAG (Teune et al., 2000; Frontera et al., 2020; Fujita et al., 2020), and the PAG projects to the cerebellar cortex, including the anterior lobe, the simple lobule, crus I, crus II, the paramedian lobule and the posterior vermis (Dietrichs, 1983). A direct or indirect circuit from the ventrolateral PAG, which modulates fear responses to imminent threats (Vianna and Brandao, 2003; Wright et al., 2019), to the lateral vermal lobule VIII is thought to be necessary for fear-evoked freezing behavior (Koutsikou et al., 2014).

The locus coeruleus, implicated in stress and panic, sends projections to the vermal (Dietrichs, 1985, 1988), intermediate and lateral zones of the cerebellar cortex, with abundant projections in the vermal and intermediate zones (Dietrichs, 1988). In addition, the MN is connected to the hippocampus, the amygdala (Heath and Harper, 1974) implicated in a role in emotional processing (Zhang et al., 2016), and the hypothalamus perhaps related to the development of the autonomic components of the migraine attack (Dietrichs, 1984; Haines and Dietrichs, 1984; Cao et al., 2013). Notedly, even though Heath and Harper reported monosynaptic cerebellar inputs to the hippocampus and amygdala (Heath and Harper, 1974), two recent studies doubted this observation (Watson et al., 2019; Fujita et al., 2020) but the physiological connections are well studied. Furthermore, several psychiatric disorders are comorbid with migraine, including anxiety and depression

(Merikangas and Stevens, 1997; Balaban et al., 2011; Dresler et al., 2019). Given that cerebellar gray matter volume and activity are altered in anxiety patients (Tillfors et al., 2002; Warwick et al., 2008; Bing et al., 2013; Talati et al., 2015; Ke et al., 2016; Wang T. et al., 2016; cerebellar structural abnormalities in migraine patients are detailed in section "Cerebellar volume") and that the cerebellum is structurally connected to multiple affective processing centers, it is feasible that the cerebellum modulates affective aspects of migraine attacks. Dissecting the function of cerebellar circuits in preclinical models is warranted and may provide novel insights for future targeted stimulation-based migraine therapeutics.

Cerebellar impairment alters pain-related symptoms in humans

Pain evaluation was performed in patients with cerebellar infarction. Compared to healthy controls, patients with infarction limited to the cerebellum displayed hyperalgesia to thermal and repeated mechanical stimuli, which were applied to the forearm (Ruscheweyh et al., 2014). The heat hyperalgesia in the ipsilateral side of the infarction site was more prominent (Ruscheweyh et al., 2014). Offset analgesia is a form of endogenous pain inhibition characterized by disproportionately large reductions in pain intensity ratings evoked by small decreases in stimulus intensity (Yelle et al., 2009; Oudejans et al., 2015). In patients with cerebellar infarction in both anterior and posterior areas, offset analgesia was reduced, suggesting deficient descending pain inhibition in patients with cerebellar infarction (Ruscheweyh et al., 2014). In addition, children with resection extending into Crus I/II showed decreased cold pain tolerance compared to healthy controls (Silva et al., 2019). These two studies suggest that cerebellar impairment could lead to hyperalgesia.

Cerebellar manipulation modulates pain in animals

Pain-related behaviors

The presence of cerebellar anatomical connections to pain-related brain regions and observations that cerebellar impairment alters pain in humans suggest a possible cerebellar involvement in pain. However, the causal or modulatory relationship between the cerebellum and pain has yet to be discerned. Preclinical studies provide a valuable avenue to reveal the cerebellar mechanisms underlying pain. While it is impossible to confirm that animals are experiencing pain, methods that assess "pain-like" behaviors have been developed. In general, these methods are divided into two types based on whether the stimulus is applied, e.g., thermal, cold, or mechanical stimulus (Deuis et al., 2017). Widely used stimulus-evoked methods include von Frey, hot plate, and tail-flick tests (Deuis et al., 2017). The non-stimulus, or spontaneous, methods include grimace and burrowing tests (Deuis et al., 2017).

Cutaneous nociception

Approximately 60% of migraine patients reported cutaneous allodynia (Lipton et al., 2008), and here we discuss the evidence linking the cerebellum and cutaneous nociception. Early studies conducted by Russell (1894) and Sprague and Chambers (1959) revealed that cerebellar destruction altered responses to sensory stimuli in animals. Later, the relationship was further explored in awake squirrel monkeys with electrical stimulation of the cerebellar regions in response to tail shock (Siegel and Wepsic, 1974). An increase in nociceptive thresholds was found by electrically stimulating the posterior vermal lobules VI (lobulus simplex) and VII-IX; the anterior intermediate lobules IV-V (culmen); the rostral lateral cerebellar-interpositus nuclear-brachium conjunctivum in intermediate lobe (Siegel and Wepsic, 1974), suggesting that stimulation of these areas is antinociceptive. Among these regions, the anterior intermediate lobules IV-V and rostral lateral cerebellar-interpositus nuclear-brachium conjunctivum in the intermediate lobe displayed dramatic analgesia at stimulation of 0.2 mA (Siegel and Wepsic, 1974). However, when the current was increased to 0.8 mA, stimulation of the bilateral lobules HVIII (the paramedian lobes) decreased the tail shock nociceptive threshold. Altogether, this study suggests a regional specificity of the analgesic effect, which is also dependent upon the stimulation current.

Consistent with this finding, Dey and Ray (1982) later found that electrical stimulation at the culmen or at centralis but close to the culmen region of the anterior cerebellum induced post-stimulation analgesia lasting ∼5–10 min in rats at the intensity of 0.06–0.3 mA (Dey and Ray, 1982). Moreover, administration of morphine into the culmen region of the anterior cerebellum evoked analgesia in rats. This analgesic effect could be blunted by intraperitoneal (i.p.) injection of naloxone, a non-selective opioid receptor antagonist. Ablation of culmen and centralis, shortened analgesia duration after i.p. morphine while lobulus simplex and declive lesion had a trend to prolong i.p. morphine-induced analgesia (Dey and Ray, 1982). These two studies (Siegel and Wepsic, 1974; Dey and Ray, 1982) show a similar result when the culmen is targeted, suggesting that the culmen region is critical in regulating nociception, probably *via* connections with the brainstem reticular formation. Thus, one can speculate that the cerebellum, specifically the culmen, exerts its antinociceptive action by activating the brainstem pain suppression mechanism (Dey and Ray, 1982). In contrast, Hardy found that stimulation of the cerebellar cortex did not induce thermal nociceptive response (Hardy, 1985).

However, the exact region of the cerebellar cortex was not mentioned.

Visceral reflex

The role of the cerebellum in the visceral nociceptive reflex was also studied. Injection of DL-homocysteic acid, an NMDA receptor agonist, into the MN decreased the elicited abdominal reflex (Saab and Willis, 2002). Congruently, the injection of bicuculline, a GABA-A receptor antagonist, into the MN also decreased the reflex (Saab and Willis, 2002). Administration of bicuculline is believed to inhibit Purkinje cells, consequently releasing the MN from its inhibitory influence (Saab and Willis, 2002). In addition, when DL-homocysteic acid was injected into the cerebellar vermal lobule VIII, the reflex was induced, while no effect was observed from DL-homocysteic acid injection into the lateral cerebellar nucleus (Saab and Willis, 2002). This study suggests that the vermal lobule VIII and the MN produced pronociceptive and antinociceptive effects, respectively, in response to the visceral noxious stimulation.

Later, another study demonstrated that administration of glutamate into the MN of rats with chronic visceral hypersensitivity increased the pain threshold, and decreased amplitude and abdominal withdrawal reflex scores (Zhen et al., 2018). This phenotype could be abolished by delivering 3-MPA (a glutamate decarboxylase inhibitor) into the MN, suggesting that glutamate stimulation of the MN exerts a protective action on chronic visceral hypersensitivity (Zhen et al., 2018).

Anxiety

In addition, cerebellar manipulation modulated anxiety. One study using a mutant mouse line with Purkinje cell death reported that mutants spent more time in the open arms of the elevated plus maze, suggesting an anti-anxiety phenotype (Hilber et al., 2004). Bilateral lesion of the MN in juvenile rats was shown to alter anxiety in adulthood although it was not clear whether the anxiety was enhanced or decreased (Helgers et al., 2020), accompanied by enhancement of local field coherence between the medial prefrontal cortex and the sensorimotor cortex (Helgers et al., 2020) and epigenetic dysregulation of the GABAergic system in the nucleus accumbens and the oxytocin system in the prefrontal cortex (Helgers et al., 2021). Cerebellar manipulation can also change fear responses, an affective component of pain. For more details, please refer to Sacchetti et al. (2005).

Neuronal activities in pain-related brain regions

Thalamus

Cerebellar stimulation may manipulate neuronal activities of other regions, including the parafasciculus thalamus, the habenula and the spinal cord, which could contribute to pain. At the circuit level, sciatic nerve stimulation in rats changed the neuronal firing rate in the parafasciculus thalamus, which could be changed by lateral cerebellar nucleus stimulation in an intensity-dependent manner (Liu et al., 1993). For instance, 0.2 mA inhibited most of the nociceptive-on cells (the cells showing an increase in firing rate following the noxious stimulation) in the parafasciculus thalamus, while 0.4 mA activated these neurons (Liu et al., 1993). Considering that the MN and lateral cerebellar nuclei have direct connections to the parafasciculus thalamus (Teune et al., 2000; Fujita et al., 2020), the cerebellum may modulate nociception *via* the parafasciculus thalamus. In addition, cerebellar electrical stimulation also increased the nociceptive-on neuronal responses to tail pinch in the habenula, while transcranial electrostimulation, lateral hypothalamic electrical stimulation, and dorsal raphe electrical stimulation showed opposite effects on nociceptive-on cells in the habenula (Dong et al., 1992).

Spinal cord

The spinal cord is a critical region for regulating pain and headaches. Electrical (0.1–0.15 mA) or DL-homocysteic acid stimulations of the posterior cerebellar vermal lobule VI modulated the neuronal activity of the lumbosacral spinal cord in response to non-noxious and noxious visceral (colorectal distention) or somatic (brush, pressure, and pinch) stimuli: an increase in spinal cord neuronal activity in response to visceral stimuli was observed after cerebellar stimulation, while varied responses to somatic stimuli were seen in rats (Saab et al., 2001). It is possible that the posterior cerebellar vermis exerts its pronociceptive action *via* the inhibition of deep cerebellar nuclei, therefore suppressing the descending pain inhibition pathway.

In contrast, stimulation of the left intermediate hemisphere of the anterior cerebellar cortex significantly decreased the activity of spinal cord dorsal horn neurons bilaterally in response to mechanical stimuli, suggesting the anterior cerebellum may exert an antinociceptive action *via* activating the descending inhibition pathway (Hagains et al., 2011). Altogether, stimulation of the posterior and anterior cerebellum produced opposite effects on spinal cord neuronal activity (Saab et al., 2001; Hagains et al., 2011), and both studies agree that the cerebellum impacts nociception at least in part through the descending pain inhibition pathway.

Furthermore, DL-homocysteic acid injection into the MN increased neuronal responses in dorsal column nuclei to somatic non-noxious stimuli in rats (Saab et al., 2002). The increased neuronal responses in dorsal column nuclei by MN stimulation may be a result of impacting the dorsal column–medial lemniscus pathway directly or the descending pathway indirectly. It should be noted that opposite effects of the MN to pain responses were found after applying innocuous somatic stimuli (increasing activity in dorsal column nuclei indicative of increasing pain; Saab et al., 2002) and noxious

visceral stimuli (decreasing visceral nociceptive reflex indicative of decreasing pain; Saab and Willis, 2002) after stimulation of the MN in a comparable paradigm. This seemingly contradictory finding suggests further exploration is necessary to explain the role of the cerebellum in processing non-noxious and noxious information.

Human studies on the cerebellum and migraine

Migraine is characterized by pulsating and moderate or severe pain on the unilateral side of the head. Migraine patients also reported cutaneous allodynia (pain in response to a non-nociceptive stimulus; Schwedt, 2013; ICHD-3, 2018), and other sensory and motor abnormalities, such as visual, auditory, olfactory, and vestibular hypersensitivity (Schwedt, 2013) with photophobia being the most bothersome symptom other than pain during migraine attacks (Munjal et al., 2020). The cerebellar hand in sensory and pain processing implies a cerebellar influence on head pain, cutaneous allodynia, and sensory abnormalities experienced by migraine patients. In this section, we will talk about the cerebellar symptoms including motor and non-motor dysfunction, imaging studies about cerebellar alterations in migraine patients, and cerebellar manipulations in migraine patients.

Cerebellar symptoms in migraine patients

The cerebellum coordinates both motor and non-motor functions. This section will discuss motor (e.g., motor coordination, vestibular, and oculomotor functions) and non-motor dysfunction in migraine patients.

Motor dysfunction

As mentioned above, vestibular nuclei and the cerebellum are closely connected and work in concert to influence posture, equilibrium, and vestibuloocular eye movements (Purves et al., 2018). Vestibular motor dysfunction was exhibited in migraine patients from the general population. Stabilometric assessment of migraine patients revealed increased body sway relative to healthy controls during both ictal (Anagnostou et al., 2019) and interictal periods (Ishizaki et al., 2002; Anagnostou et al., 2019). However, another study reported no difference in body sway between migraine patients and non-migraine controls (Koppen et al., 2017). Reasons for disparate results are unknown; however, the authors suggest that different sample sizes, patients selected from different cohorts, and a blind design might change the results (Ishizaki et al., 2002; Koppen et al., 2017; Anagnostou et al., 2019). All the same, it was surprising that 8.5% of migraine patients in the second study had ischemic cerebellar lesions located in the posterior lobe (Koppen et al., 2017). These lesions apparently affected fine motor skills but not body sway or other non-motor cerebellar functions (Koppen et al., 2017). Similarly, vestibular symptoms were often predisposed by ischemic or inflammatory lesioning of the cerebellum or brainstem (Kim et al., 2005; Brandt and Dieterich, 2017). Furthermore, a recent study revealed that migraine patients exhibit increased postural sway relative to non-headache controls across a range of light intensities (Pinheiro et al., 2020). This interaction between visual light sensitivity and the corresponding imbalance phenotype suggests a link between the visual system and motor processing in the cerebellum (Pinheiro et al., 2020), but the mechanisms are unclear.

Migraine patients experiencing moderate or severe vestibular symptoms may fall into the diagnostic criteria of vestibular migraine, a subtype of migraine. Vestibular symptoms include positional vertigo, visually-induced vertigo, head motion-induced dizziness with nausea, etc. (ICHD-3, 2018). Approximately 10%–30% of patients in headache and dizziness clinics are diagnosed with vestibular migraine, with the condition affecting about 1%–3% of the total population (Neuhauser et al., 2006; Formeister et al., 2018; Wattiez et al., 2020) and accounting for 10% among migraine patients (ICHD-3, 2018). The current treatments for acute vestibular migraine attacks include triptans (which are effective in 40% of patients) and antiemetic medications (Shen et al., 2020). Prophylactic treatments include selective calcium channel blockers (which reduced vertigo and headaches in ∼65% of patients) and the antiepileptic drug, topiramate (which was effective among 80% of patients; Shen et al., 2020). CGRP-based drugs can improve both migraine and vestibular symptoms in 18 out of 25 patients suffering from vestibular migraine (Hoskin and Fife, 2022). Given the role that the cerebellum and vestibular nuclei play in motor function, targeting the cerebellum may improve the vestibular impairments.

Central ocular motor disorders are a common co-morbidity seen in individuals with vestibular migraine (Neugebauer et al., 2013). This neurological condition is characterized by nystagmus and saccades (Neugebauer et al., 2013). In migraine patients, studies have shown deficiencies in nystagmus and saccadic accuracy, indicative of defective oculomotor function (Harno et al., 2003). The oculomotor vermis is related to saccades and pursuit initiation, and the vestibulocerebellum modulates the vestibularocular reflex (Kheradmand and Zee, 2011; Lal and Truong, 2019). Collectively, these findings suggest that cerebellar deficiencies may partly account for the faulty oculomotor processing displayed by migraine patients.

Motor dysfunction was also exhibited in a subtype of migraine patients, familial hemiplegic migraine (FHM). FHM is an autosomal dominant subtype of migraine with aura characterized by fully reversible motor weakness (ICHD-3, 2018), and displays cerebellar ataxia and nystagmus (Thomsen et al., 2002; Dichgans et al., 2005).

Non-motor dysfunction

Non-motor function in migraine patients may contribute to attack-related disability and interfere with work performance and personal life. However, it is often neglected by clinicians and little is known regarding cognitive dysfunction in migraine patients (Gil-Gouveia and Martins, 2019). Individuals with FHM1, a type of FHM [FHM type will be discussed in detail in Section "Cerebellar changes in familial hemiplegic migraine (FHM)"], were subjected to a series of validated assessment procedures, testing for a range of cerebellar phenotypes (e.g., fine motor skills, vestibular motor function measured by body sway, visuospatial ability, and learning-dependent timing; Koppen et al., 2017). Visuospatial ability and learning-dependent timing require cognitive mechanisms, including working memory, attention, and planning. The cerebrocerebellum is believed to participate in cognitive function (Koppen et al., 2017). Results showed that besides fine motor and vestibular motor dysfunction, FHM1 patients demonstrated defective cerebellar performance in parameters for non-motor function tests (Koppen et al., 2017).

The experience of time is the foundation for information processing and motor behavior, the impairment of which can influence an individual's life (Zhang et al., 2012). Time perception and estimation involve cognitive functions, e.g., perception, attention, and memory (Zhang et al., 2012). A cerebellar role in the performance of timing tasks is well established (Parker, 2015; Ohmae et al., 2017; Tanaka et al., 2021). Migraine patients demonstrated impaired timing estimation in the milliseconds' range (Zhang et al., 2012).

Together, these observations suggest that the cerebellum may have an expansive role in migraine symptomology that extends beyond mere motor output. Future studies will be required to determine whether the specific subregions of the cerebellum and its respective connections are distinctively associated with a specific migraine symptom.

Cerebellar alterations in migraine patients: imaging studies

There is an abundance of imaging studies identifying structural, activity, and functional cerebellar changes in migraine patients. These reports have allowed a glimpse into the cerebellar role in migraine pathophysiology.

Cerebellar structural changes without sensory stimuli application in migraine patients

Cerebellar volume

One interesting finding from imaging studies is the change in cerebellar volume observed in migraine patients. Given that migraine attacks are intermittent, the modification of cerebellar morphology might occur over time. Cerebellar atrophy was observed, and a negative correlation was identified between the migraine disease duration and cerebellar volume (Demir et al., 2016). The majority of the cerebellum is comprised of gray matter, inclusive of the cerebellar cortex and deep cerebellar nuclei. Cerebellar gray matter volume (GMV) decreases were observed in migraine patients, detected during the interictal phase (Jin et al., 2013; Yang et al., 2018; Bonanno et al., 2020; Chou et al., 2021). In contrast, some studies reported an increase in GMV in some cerebellar regions in migraine patients. For example, Mehnert and May demonstrated a GMV increase in lobules VI, VIIb, VIIIa, Crus I, and Crus II in the right cerebellum in migraine patients compared to healthy controls (Mehnert and May, 2019). Furthermore, the GMV decrease in the right VI lobule was correlated with higher attack frequency, and the GMV decrease in the right lobule V was correlated with the disease duration (Mehnert and May, 2019). Another group selectively included patients with high-frequency migraine (10–30 headache days/month). These patients with poor outcomes (<50% reduction in baseline headache days or frequency increase over 2 years) displayed greater GMV in the right Crus II and left Crus I in the cerebellum than healthy controls, and in the bilateral VIIIa and left Crus I in the cerebellum than patients with good outcomes (≥50% reduction over 2 years) during the interictal phase (Liu H. Y. et al., 2020). There was a correlation between the disease duration and GMV in the right cerebellar VIIIa, and between 2-year headache frequencies and GMV in the bilateral VIIIa (Liu H. Y. et al., 2020). This seemingly contrasting data might be attributed to the states when migraine patients were scanned, and the population of migraine patients included in the studies.

In addition to gray matter, the microstructure of white matter is abnormal in migraine patients. Specifically, diffusion tensor imaging (DTI) reveals that the comparison to healthy controls, migraine patients have decreased axonal integrity in vermal lobule VI extending to the bilateral lobules V and VI. These analyses also revealed myelin damage in the right inferior cerebellum peduncle which is composed of cerebellar inputs and outputs (Tae et al., 2018; Qin et al., 2019).

In summary, studies investigating cerebellar structural alterations in migraine patients are not consistent. Longitudinal studies with larger sample sizes and consideration of disease progression would increase the scope for more in-depth analysis moving forward.

Cerebellar activity

Neuronal activity of the cerebellum has been extensively investigated in different migraine conditions with positron emission tomography (PET) and functional magnetic resonance imaging (fMRI) scans. During the interictal phase, regions

in the bilateral posterior lobe in the cerebellum showed spontaneous activity deficiencies in migraine patients compared to healthy controls (Wang J.-J. et al., 2016). The value of spontaneous activity in the left superior cerebellum could discriminate migraine patients from healthy controls, and the value positively correlated with the baseline headache intensity (Yin et al., 2020). When comparing migraine patients with aura to those without aura, the activity amplitude in the bilateral cerebellum was higher in the aura group than in those without aura during the interictal phase (Farago et al., 2017). Importantly, when the migraine phase was taken into consideration, cerebellar activation was observed in female migraine patients in the ictal phase compared to the interictal phase (Afridi et al., 2005). In addition, vestibular migraine patients displayed dramatically increased metabolism in the bilateral cerebellum in the ictal phase compared to the interictal phase (Shin et al., 2014). Vestibular rehabilitation, which aimed to alleviate vestibular symptoms, enhanced the spontaneous activity of the left posterior cerebellum (Liu L. et al., 2020). It suggests that left cerebellar hyperactivity might compensate for the deficits in the vestibular system (Liu L. et al., 2020) and that targeting the cerebellum may be a potential avenue to improving vestibular symptoms in migraine patients. It should be noted that there is no observed consistency in the activation of the specific cerebellar regions between reports. Despite this caveat, studies demonstrated that migraine induces cerebellar activation relative to healthy controls, which is phase-dependent.

Cerebellar functional connectivity

In addition to changes in cerebellar structure and activity in migraine patients, functional connectivity changes are observed (**Figure 1** and **Table 1**). Understanding these functional connectivity changes between the cerebellum and other brain regions will be critical in understanding migraine pathophysiology.

Compared to healthy controls during the interictal phase, functional connectivity increases are observed (**Figure 1** and **Table 1**) between the left lateral geniculate nucleus (the relay center for the visual pathway located in the posterior thalamus) and the ipsilateral cerebellum (Zhang et al., 2020). In addition, functional connectivity was increased in a number of studies in the following locations: between the right red nucleus and the ipsilateral cerebellum (Huang et al., 2019); between the hippocampus and the cerebellum (Wei et al., 2020); between the hypothalamus and cerebellar Crus I and II and lobules V and VI (Moulton et al., 2014); between the right posterior insula and the bilateral cerebellum (Ke et al., 2020); and between the right medial prefrontal cortex and the ipsilateral cerebellum (Jin et al., 2013).

One study found decreased functional connectivity between left Crus I and the default mode network components, including the medial prefrontal cortex in migraine patients compared to healthy controls (Ke et al., 2020). The default mode network has been linked to cognitive and social processing (Li et al., 2014). Functional connectivity between the left Crus I and the left medial prefrontal cortex negatively correlated with migraine frequency (Ke et al., 2020). Du group reported that decreased functional connectivity (**Figure 1** and **Table 1**) was observed between the primary somatosensory cortex and the ipsilateral cerebellar lobule VIIIb (Zhang et al., 2017), and between the right dorsal premotor cortex and the ipsilateral cerebellar lobule VIII in migraine patients compared to healthy controls during the interictal phase (Qin et al., 2020). However, conflicting data was observed as that Qin et al. did not observe changes in the functional connectivity between the primary somatosensory cortex and the cerebellum (Qin et al., 2020). The reason is not clear.

Different ratios of male to female migraine patients or varied migraine phenotypic profiles can affect functional connectivity results. For example, functional connectivity between the PAG and the cerebellum is higher in migraine with ictal allodynia than without ictal allodynia (Schwedt et al., 2014b). These data paint a complex picture of migraine-related functional connectivity and suggest more preclinical studies are necessary to precisely define how specific cerebellar circuits contribute to migraine.

Cerebellar infarcts

Intriguingly, one study showed that migraine patients had a higher risk of subclinical infarcts in the cerebellar posterior circulation territory, and this risk increased with higher attack frequency (Kruit et al., 2004). Notably, there was no significant difference in infarcts in other locations (anterior/carotid circulation, basal ganglia, and corona radiata/centrum semiovale) in migraine patients compared to control subjects (Kruit et al., 2004). Later the same group observed that the cerebellar silent infarcts were always in the posterior lobe in the cerebellar hemispheres and paramedian region (Koppen et al., 2017). The mechanism of infarction remains to be elucidated. Further studies investigating how silent cerebellar infarcts are induced in migraine are necessary, both to further our understanding of migraine pathophysiology and to provide preventive actions for migraine patients with a higher risk of cerebellar infarcts.

Cerebellar changes with sensory stimuli application in migraine patients

Hyperexcitablity in the brain has been reported *via* electroencephalography (EEG) and fMRI techniques which may contribute to hypersensitivity to various sensory modalities like visual, auditory, olfactory, and somatosensory stimuli in patients who experience migraine (Main et al., 1997; Demarquay et al., 2006; Aurora and Wilkinson, 2007; Ashkenazi et al., 2009).

Imaging studies of cerebellar activity and functional connectivity were conducted in migraine patients in response to different stimuli, e.g., visual (Kreczmanski et al., 2019), thermal (Moulton et al., 2011; Maleki et al., 2012, 2021; Russo et al., 2012; Schwedt et al., 2014a), olfactory (Stankewitz and May, 2011), and trigeminal nociceptive (Mehnert and May, 2019) stimuli.

Visual stimuli

Depending on which visual stimulus was used, flickering or static checkerboards activated different cerebellar regions in migraine patients compared to the rest status (Kreczmanski et al., 2019). Moreover, the flickering checkerboard experiment showed higher left cerebellum activity in migraine patients with aura than those without aura, while the static checkerboard experiment showed greater activity in the right cerebellum (Kreczmanski et al., 2019).

Thermal stimuli

The cerebellum was activated in both migraine patients and healthy controls upon reception of painful thermal stimuli to the forearm (Schwedt et al., 2014a) or the face (Moulton et al., 2011; Russo et al., 2012) in the interictal phase. However, the cerebellar regions activated by thermal stimulation on the face between migraine patients and healthy controls were different (Moulton et al., 2011; Russo et al., 2012). Differences in cerebellar region activation were also observed in the interictal and ictal phases when responding to a thermal stimulus applied to the hand (Maleki et al., 2021). Additionally, cerebellar functional connectivity with the temporal pole and the entorhinal cortex was increased in response to thermal stimulation of the forehead in migraine patients compared to healthy controls in the interictal phase (Moulton et al., 2011). Interestingly, female migraine patients showed higher activation in the cerebellum and higher deactivation of cerebellar functional connectivity with the insula than males with noxious heat (Maleki et al., 2012). Altogether, these studies suggest that the cerebellum plays a role in processing visual and painful thermal information in migraine patients.

Olfactory stimuli

May and colleagues observed cerebellar changes during olfactory stimulation in healthy controls and migraine patients. They found that the cerebellum was activated in both healthy controls (Stankewitz et al., 2010) and migraine patients (Stankewitz and May, 2011) who showed higher cerebellar activation in the ictal phase compared to the interictal phase in response to odors (Stankewitz and May, 2011).

Trigeminal stimuli

May group applied trigeminal stimuli to healthy controls (Stankewitz et al., 2010; Mehnert et al., 2017) and migraine patients (Mehnert and May, 2019). In healthy controls, activation was found in the left cerebellar regions (lobules V, VI, VIIIa and Crus I) and the vermal lobule VIIIa, ipsilaterally to the stimulation site. In contrast, less activation was found in the contralateral right cerebellar hemisphere (lobules I–VI; Mehnert et al., 2017). The left SpV showed higher functional connectivity with the left lobules I–IV. The left lobules VI and VIIIa, and vermal lobule VIIIa showed higher functional connectivity with the thalamus or cortical areas (Mehnert et al., 2017). Later, the same stimulation conditions were applied to migraine patients (Mehnert and May, 2019) as in Mehnert et al. (2017). Compared to healthy controls, left Crus I (ipsilateral to the stimulation) of the migraine patient's cerebellum showed increased activity and decreased functional connectivity with the left thalamus and some cortical areas in response to trigeminal nociceptive stimulation (Mehnert and May, 2019; **Figure 1** and **Table 1**). Based on the understanding that the cerebellum is indicated to have an inhibitory role in nociception even though there is uncertainty (discussed in Section "Cerebellar role in pain processing"), it can be speculated that the increase of cerebellar activity is to compensate for the dysfunctional cerebellar functional connectivity to cortical areas in migraine patients (Mehnert and May, 2019). Strikingly, treatment with erenumab, a monoclonal antibody targeting the CGRP receptor, reduced cerebellar activation on both sides in migraine patients in response to trigeminal nociceptive stimuli compared to before erenumab treatment (Ziegeler et al., 2020). This finding indicates that erenumab can have central effects, although these are likely secondary to the peripheral effects, and implies that CGRP may contribute to the cerebellar activity abnormalities observed in migraine. These data highlight the complex functional connectivity of the cerebellum in migraine patients.

Chemical stimuli

In addition to sensory triggers, a peptide trigger, pituitary adenylate cyclase-activating polypeptide-38 (PACAP38), which was reported to induce migraine-like headaches in migraine patients (Schytz et al., 2009; Ghanizada et al., 2020), decreased right cerebellar functional connectivity with default mode network in the early phase of migraine attacks (Amin et al., 2016). Migraine patients administered the migraine trigger nitroglycerin (NTG) can also display a variety of symptoms that closely mirror a migraine attack (Sances et al., 2004). Following NTG administration to migraine patients, the cerebellum showed functional connectivity changes with the right thalamus during the prodromal and full-blown phase (Martinelli et al., 2021), and increased functional connectivity with the pons during the headache phase (Karsan et al., 2020) compared to pre-treatment baseline. These studies suggest that abnormal cerebellar functional connectivity might contribute to the lack of nociceptive modulation in PACAP38- (Amin et al., 2016) and possibly NTG-induced migraine attacks.

Cerebellar changes in familial hemiplegic migraine (FHM)

FHM represents a small portion of migraine patients which may provide insight into migraine as a more general disease through the study of genes contributing to their migraine phenotypes. It can be divided into three subtypes: FHM1, 2, and 3. FHM1 is caused by mutations in the CACNA1A gene, which encodes the α1A subunit of Cav2.1 (P/Q-type) calcium channel. Cav2.1 channel is vital for neurotransmitter release (Catterall, 1998) and is expressed in the brain—cerebellar Purkinje cells in particular (Westenbroek et al., 1995). These mutations usually lead to enhanced glutamatergic neurotransmission (Sutherland et al., 2019). FHM2 is caused by mutations in ATP1A2, which encodes the α2 subunit of a Na^+/K^+ ATPase pump. FHM3 is caused by SCN1A mutations encoding the α1 subunit of the neuronal sodium channel $Na_v1.1$.

Cerebellar atrophy was observed in FHM 1 patients (Vighetto et al., 1988; Joutel et al., 1993; Haan et al., 1994; Elliott et al., 1996; Terwindt et al., 1998; Dichgans et al., 2005; Kono et al., 2014). Atrophy was present in the vermis (Vighetto et al., 1988; Joutel et al., 1993; Elliott et al., 1996; Kono et al., 2014), particularly in the anterior vermis (Vighetto et al., 1988; Elliott et al., 1996). Moreover, studies on one FHM patient (Neligan et al., 1977) or subjects with a family relation to FHM patients (Kors et al., 2001; Takahashi et al., 2005) revealed a possible degenerative mechanism, including Purkinje cell death and abnormal dendritic and axonal morphology. These changes were more apparent in the vermis than in the cerebellar hemisphere (Kors et al., 2001). Deep cerebellar nuclei were relatively intact (Kors et al., 2001). However, the other two studies observed not only changes in Purkinje cells but also gliosis in lateral cerebellar nuclei (Neligan et al., 1977; Takahashi et al., 2005). Together, these observations imply that cerebellar degeneration is involved in FHM. It will be interesting to study cerebellar structural changes in FHM mouse models to further understand the mechanisms of the cerebellum in migraine.

Energy metabolism was also investigated in FHM patients. Compared to healthy controls, FHM1 patients showed a significant reduction in *N*-acetyl aspartate and glutamate, as well as an increase in myo-inositol in the superior cerebellar vermis (Dichgans et al., 2005). These findings indicate impairments in neuronal integrity and glutamatergic neurotransmission, and abnormal proliferation of glial cells, respectively. In addition, *N*-acetyl aspartate in the superior cerebellar vermis was significantly correlated with gait ataxia score (Dichgans et al., 2005). Similarly, another study found that FHM1 and FHM2 patients showed a significant decrease in *N*-acetyl aspartate in the cerebellum compared to healthy controls, with the lowest value in FHM1 patients in the interictal phase (Zielman et al., 2014).

These discoveries point to the importance of the metabolism and neuronal functions of the vermis and Purkinje cells in the FHM cerebellar symptoms. N-acetyl aspartate levels might be an early biomarker for neuronal abnormality or disease progression in FHM (Dichgans et al., 2005; Zielman et al., 2014).

Cerebellar modulations in migraine patients

Studies report that transcranial direct current stimulation of the cerebellum modulated pain intensity in healthy controls (Bocci et al., 2015, 2017). Further, Brighina et al. (2009) applied transcranial magnetic stimulation to migraine patients, with a conditioning stimulus on the right cerebellar cortex and a test stimulus on the left motor cortex. They reported that migraine patients showed a deficit in cerebellar inhibition of the motor cortex compared to healthy controls, which may contribute to the deficit of cortical inhibitory circuits reported in migraine patients (Brighina et al., 2009). Ho et al. (2010) interpreted the cerebellar deficits observed in this study (Brighina et al., 2009) to be a contributor to improper sensory filtering, which is processed in the cortex as painful stimuli. Future studies are necessary to precisely define the mechanisms underlying cerebellar inhibition of cerebral cortical circuits in migraine patients.

The cerebellum contains CGRP and abundant CGRP binding sites

Given the findings described above, it is reasonable to speculate that the cerebellum plays a role in migraine, although whether this is in a causal or merely a regulatory capacity remains to be seen. The underlying mechanisms are unknown. This section discusses the potential contribution of cerebellar CGRP to migraine pathophysiology.

CGRP, a multifunctional neuropeptide, is known to modulate nociception and assist in the onset of migraine. In migraine patients, CGRP levels are elevated in the plasma, cerebrospinal fluid, and saliva, and the infusion of CGRP alone is sufficient to induce a migraine-like headache in 70% of migraine patients (Goadsby et al., 1990; Goadsby and Edvinsson, 1993; Lassen et al., 2002; Juhasz et al., 2005; Petersen et al., 2005; Cady et al., 2009; van Dongen et al., 2017; Russo, 2019). Most notably, CGRP receptor antagonist drugs that block the ligand-receptor binding interaction, are approved by the FDA for the treatment of migraine with efficacy in approximately 50% of sufferers (Olesen et al., 2004; Ho et al., 2008; Connor et al., 2009; Dodick et al., 2018; Reuter, 2018; Skljarevski et al., 2018; Stauffer et al., 2018). Peripheral release of CGRP is suspected to elicit vasodilation and stimulate mast cell degranulation and inflammation in the dural meninges, leading to sustained activation of meningeal nociceptors and causing the prolonged activation of trigeminal

primary afferents (Vecchia and Pietrobon, 2012; Russo, 2015, 2019; Iyengar et al., 2017, 2019; Charles, 2018; Messlinger, 2018). This has been proposed to sensitize trigeminovascular neurons in the thalamus leading to central sensitization that primes the brain for a migraine attack (Vecchia and Pietrobon, 2012; Russo, 2015, 2019; Iyengar et al., 2017, 2019; Charles, 2018). Central sensitization is seemingly also induced by the central release of CGRP, which enhances glutamatergic signaling, increases neuronal excitability, and facilitates synaptic transmission (Han et al., 2005; Seybold, 2009; Russo, 2015). However, the precise sites of CGRP action in the central nervous system that contribute to migraine attacks remain to be fully elucidated. Recent studies have presented the posterior thalamus (Sowers et al., 2020) and the cerebellum (Wang et al., 2022a,b) as candidate sites for CGRP action in migraine pathophysiology.

CGRP expression in the cerebellum

An early study by Kawai et al. (1985) highlighted the presence of CGRP in Purkinje cells in rats. Later, studies updated the distribution of CGRP in the cytoplasm of Purkinje cell bodies as grains and not in dendrites, axons, nor other cells in rats (Edvinsson et al., 2011; Warfvinge and Edvinsson, 2019; Warfvinge et al., 2019). In the rat MN, CGRP is localized in the cell somas of large neurons as grains (Warfvinge and Edvinsson, 2019; **Figure 2**); however, in primates, CGRP is distributed in the cytoplasm of cell bodies and dendrites of Purkinje cells, and cells in the molecular layer (Eftekhari et al., 2013a,b). There is no description of CGRP distribution in the MN of the primate cerebellum (Eftekhari et al., 2013a,b). The difference might be attributed to species, or as suggested by authors, technical reasons (Eftekhari et al., 2013b).

An immunohistochemistry study exploring the fetal development of rats revealed transient expression of CGRP in a subset of inferior olive neurons and established a developmental pattern of CGRP expression in climbing fibers, a subclass of olivocerebellar axons (Chedotal and Sotelo, 1992; Morara et al., 1992, 2001). Specifically, during postnatal development, CGRP-positive climbing fiber terminals were seen to converge onto the cell somas of nearby Purkinje cells (Chedotal and Sotelo, 1992; Morara et al., 1992, 2001; **Figure 2**). An *in-situ* hybridization study demonstrated that the pattern of olivary CGRP mRNA expression coincided with the spatiotemporal distribution of CGRP immunoreactivity in developing neonatal rats, which provides an explanation for transient CGRP expression (Morara et al., 1995). This developmental pattern suggests that CGRP might play a role in reshaping connectivity and stabilizing synapses in the cerebellar circuitry (Morara et al., 1992, 1995). During development, these CGRP-positive climbing fibers can modulate calcium signaling in proximal astrocytes from neonatal mice, enabling CGRP to exert profound effects on neuronal differentiation (Morara et al., 2008).

Interestingly, studies found the distribution of CGRP throughout mossy fibers to the adult cat cerebellar cortex (Sugimoto et al., 1988; Bishop, 1992, 1995). These CGRP-positive mossy fibers were shown to originate from the brainstem precerebellar nuclei (lateral reticular nucleus, external cuneate nucleus, inferior vestibular nucleus, and basilar pons) in adult cats (**Figure 2**), suggesting that these structures may function to regulate input into the cerebellar cortex (Bishop, 1992). Based on this finding, Bishop later investigated the physiological role of CGRP in mossy fibers by exogenous application of CGRP to Purkinje cells of adult cats and reported that CGRP both greatly reduced the sensitivity of Purkinje cells to excitatory amino acids and was able to obstruct synaptic activity following stimulation of the inferior cerebellar peduncle (Bishop, 1995). It was also reported that CGRP within cerebellar mossy fibers and serotoninergic neurons had a synergistic effect on inhibiting Purkinje cell firing in response to glutamate (Bishop, 1995). But one caveat is that CGRP is also expressed in the cerebellar cortex and the MN, not exclusively in the mossy fibers, thus exogenous CGRP application cannot completely mimic CGRP release from mossy fibers. However, one study found that CGRP had a protective effect on the homocysteine-induced neurotoxicity in the cerebellar neurons (Abushik et al., 2017). Homocysteine showed an increased level in migraine patients and thus might play a role in migraine (Isobe and Terayama, 2010; Oterino et al., 2010; Abushik et al., 2014). Further characterization of CGRP action on cerebellar neurons is required.

The expression of CGRP receptors in the cerebellum

The canonical CGRP receptor is a complex of three proteins: receptor activity-modifying protein 1 (RAMP1), calcitonin receptor-like receptor (CLR), and receptor component protein (RCP). Recently, a second CGRP-responsive receptor, amylin subtype 1 receptor (AMY1), which is comprised of RAMP1 and calcitonin receptor (CTR), has also been identified (Hay and Walker, 2017).

Research into the pharmacology of CGRP receptor antagonists revealed that the cerebellum had the most abundant expression of antagonist binding sites (Salvatore et al., 2010; Hostetler et al., 2013). RAMP1 and CLR are reportedly expressed intracellularly in Purkinje cells including their processes, and cells in the molecular layer of the primate cerebellum (Eftekhari et al., 2013b). In the rat cerebellum, RAMP1 was shown to be expressed on the surface of Purkinje cell bodies and their processes, and discovered as fibers in the molecular layer, granular layer, and white matter (**Figure 2**). RAMP1 was also observed as processes, but not in the cell somas in the MN

10.3389/fnsys.2022.984406

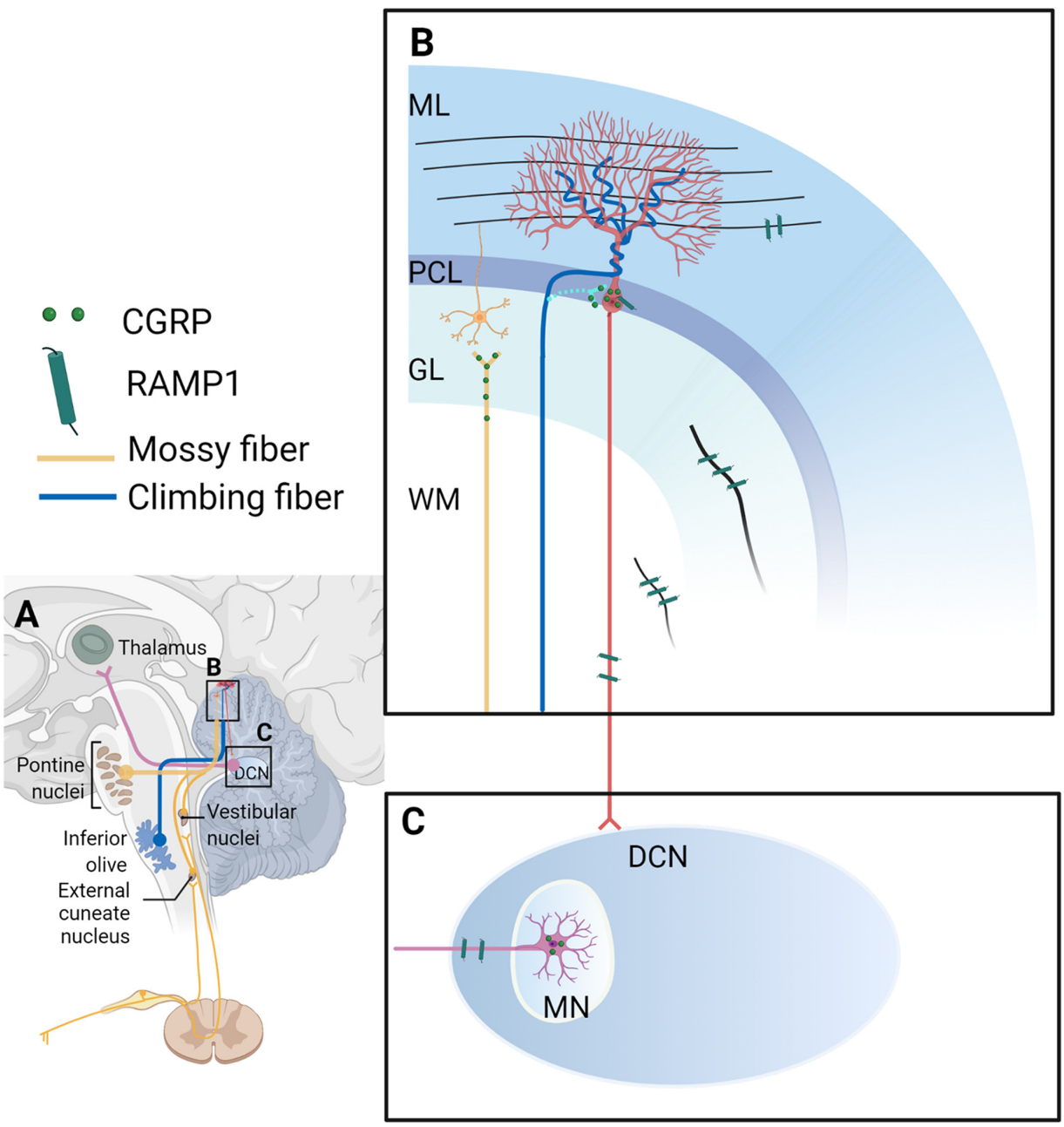

FIGURE 2
Calcitonin gene-related peptide (CGRP)-positive input to the cerebellum and CGRP and RAMP1 expression in the cerebellum. **(A)** Overview of CGRP-positive inputs to the cerebellar cortex from the inferior olive *via* the climbing fiber (blue line), and the pons, vestibular nuclei, and external cuneate nucleus *via* climbing fibers (yellow line). The deep cerebellar nucleus projects to the thalamus (pink line). Magnified and detailed views of box B and box C are displayed in **(B,C)**, respectively. **(B)** Climbing fibers: During postnatal development, CGRP-positive climbing fiber terminals from the inferior olive converge on the cell somas of nearby Purkinje cells (light blue line; these synapses between climbing fibers and Purkinje cell bodies disappear but synaptic contacts between climbing fibers and Purkinje cell dendrites are established in adulthood (dark blue line; Hashimoto and Kano, 2005; Hashimoto et al., 2009). **Mossy fibers**: In adult brains, CGRP-positive mossy fibers were shown to originate from the brainstem precerebellar nuclei (lateral reticular nucleus, external cuneate nucleus, inferior vestibular nucleus, and basilar pons; yellow line). **Purkinje cells**: In rats, CGRP is distributed in the cytoplasm of the Purkinje cell bodies intracellularly as grains, not found in the dendrites/axons nor other cells (red lines and cell). **RAMP1**: In the rat cerebellum, RAMP1 was found on the surface of the Purkinje cell bodies and their processes, and discovered as fibers in the molecular layer, granular layer (the black line in the GL), and white matter (the black line in the WM). Yellow cell: the granular cell; red cell: the Purkinje cell. **(C)** In the MN of the rat brain, CGRP is localized in the cell somas of large neurons as grains. RAMP1 was also found as processes, but not in the cell somas in the MN. It is unclear where CGRP-expressing neurons in the MN project. CGRP, calcitonin gene-related peptide; DCN, deep cerebellar nucleus; GL, granular cell layer; ML, molecular layer; MN, medial cerebellar nucleus; MW, white matter; PCL, Purkinje cell layer; RAMP1, receptor activity-modifying protein 1. The figure was created with BioRender.com.

(Edvinsson et al., 2011, 2020; Warfvinge and Edvinsson, 2019; Warfvinge et al., 2019; **Figure 2**). CLR immunostaining showed inconsistent results detected by the same group—CLR was found on the surface of Purkinje cell bodies and their processes (Edvinsson et al., 2011). Another study by the same group revealed its expression in somas of Purkinje cells, as fibers in the granular layer, and in both the cell somas and fibers in the MN (Warfvinge and Edvinsson, 2019). There are two possible explanations for the inconsistency; it may be attributed to differences in tissue quality; or high levels of receptor expression rendering the observing immunoactivity to appear intracellular (Eftekhari et al., 2013b). Strikingly, stimulation of afferent climbing fibers originating from the inferior olivary complex induced the expression of CGRP receptors in the anterior lobe of the cerebellum in adult rats (Rosina et al., 1990), suggesting that the cerebellar afferents can regulate the expression level of cerebellar CGRP receptors.

In addition to neurons, Morara and colleagues reported the presence of CGRP receptors in Bergmann glia of the developing (Morara et al., 2000) and adult rat cerebellum (Morara et al., 1998), although the exact CGRP receptor subunit was not clarified. Later, they reported the presence of RCP in Bergmann glia in neonatal mice (Morara et al., 2008). Further, the CGRP receptor showed a developmental expression pattern in the developing rat cerebellum (Morara et al., 2000). During the second postnatal week, CGRP receptors were expressed on the surface of Bergmann glia and cytoplasm of Purkinje cells in the rat cerebellum, while after postnatal day 15, CGRP receptors are expressed on the cell surface of Purkinje cells (Morara et al., 2000). However, a later study found that RAMP1 was not in the adult rat cerebellar glial cells, even though RAMP1 and glial cell marker staining were almost identical (Edvinsson et al., 2011).

In total, CGRP receptors appear throughout different cell types in the cerebellum. Combined with the data demonstrating that the cerebellum contains the highest number of binding sites in the primate brain, it is not surprising CGRP could play role in how the cerebellum processes information. Further studies are needed to determine how CGRP and its receptors contribute to behavioral outputs.

Animal studies on the cerebellum and migraine

CGRP and its receptor subunits are expressed in the cerebellum, but their contribution toward migraine pathophysiology is unclear. In addition, what other factors contribute to the abnormality of the cerebellum in migraine? Does the abnormality (in volume, activity, and functional connectivity) of the cerebellum play a causal or modulatory role, or is it the consequence of migraine attacks? In this respect, preclinical studies are necessary to resolve these queries. There are many migraine animal models (for more details, refer to Wang et al., 2021). However, to date, few animal studies have been published that investigate the relationship between the cerebellum and migraine. Despite inherent limitations, these models, coupled with brain imaging and molecular approaches, can provide key mechanistic insights into migraine pathophysiology.

Behavioral studies

Based on the expression of CGRP receptor subunits RAMP1 and CLR in the MN (Warfvinge and Edvinsson, 2019), a recent study investigated the effect of CGRP delivery into the MN on migraine-like behaviors (Wang et al., 2022b). CGRP administration into the MN induced light-aversive behavior in both male and female mice, significant anxiety-like and squinting responses in female mice and more robust tactile hypersensitivity in female mice (Wang et al., 2022b). This discovery suggests that CGRP can act in the cerebellum to induce migraine-like behaviors (Wang et al., 2022b). Later, Wang et al. (2022a) discovered that optical stimulation of CGRP neurons in the MN induced light aversion only in female mice and tactile sensitivity in both sexes. These phenotypes originated from targeting different neuronal populations that are distinct but overlapping. The CGRP administration study targeted CGRP receptor-expressing neurons (Wang et al., 2022b), while the optogenetic study targeted CGRP-expressing neurons (Wang et al., 2022a). It is certainly possible that some CGRP neurons express CGRP receptors, which may result in shared phenotypes. Interestingly, both studies displayed more predominant responses in female mice. Future studies are needed to explore the role of CGRP and CGRP receptors in other cerebellar cells in relation to migraine.

Imaging studies

Using animal models for brain imaging studies can provide an inherently greater homogeneity of observation than is possible in clinical studies; which can help determine the relationship between a brain region and behavior (Hoyer et al., 2014).

Ictal and interictal phases can be easily achieved by applying triggers to animals. The application of NTG or inflammatory soup to animals has been used to model migraine. In a study conducted by Abad et al., male rats showed increased ^{23}Na concentration in the cerebellum ∼2 h after NTG treatment (Abad et al., 2018). This suggests an imbalance of sodium in the cerebellum in this NTG-induced acute migraine model (Abad et al., 2018). Moreover, Jia and colleagues used a mouse migraine model induced by the dural application of inflammatory soup at low and high frequency to mimic episodic and chronic migraine, respectively. The fMRI imaging time was chosen

24 h after the last inflammatory soup treatment to mimic the interictal phase, or 1 h after i.p. injection of NTG to mimic the ictal phase (Jia et al., 2019, 2020). Mice receiving inflammatory soup at low and high frequencies (mimicking the interictal phase) both showed increased cerebellar functional connectivity with the insula (Jia et al., 2020) or anterior cingulate cortex (Jia et al., 2019). Mice receiving inflammatory soup at low frequency and NTG (mimicking ictal phase) also showed an increase in cerebellar functional connectivity with the insula (Jia et al., 2020) or anterior cingulate cortex compared to control mice (Jia et al., 2019). These results support the potential importance of the cerebellum in migraine. It would be interesting to perform imaging such as fMRI to examine the cerebellar activity and functional connectivity in the other migraine models, such as CGRP-induced animal models. These animal models make it feasible to further study molecular mechanisms, including neuronal activities and circuits in the cerebellum.

Electrophysiological studies

Electrical stimulation of the trigeminal ganglion is another animal model of migraine. Trigeminal stimulation of rats decreased the spontaneous firing rate of Purkinje cells in the acute paraflocular slice both contralaterally and ipsilaterally to the stimulation site (Li et al., 2019). The paraflocculus is a cerebellar lobule and sends inputs to vestibular nuclei (Tabata et al., 2002). Given that Purkinje cells in this region synapse onto vestibular nuclei (Tabata et al., 2002), trigeminal ganglion stimulation-induced inhibition of Purkinje cells might contribute to the occurrence of vestibular migraine (Li et al., 2019).

Conclusions

Taken together, the combination of: (1) findings that cerebellar connections with pain/migraine-related regions and manipulations alter pain; (2) cerebellar symptoms in migraine patients and; (3) changes in structure, activity, functional connectivity, and metabolism in migraine patients or migraine animal models, all suggest that the cerebellum plays a role in migraine. Based on reports that cerebellar manipulations affect neuronal activities in pain-related brain regions, we propose that the cerebellum might play a modulatory role in migraine. This could happen by cerebellar modulation of the descending pain pathway *via* the brainstem and/or by modulation of the ascending sensory pathway *via* the dorsal column and thalamus. Moreover, direct ascending projections from both the trigeminal ganglia and the SpV to the cerebellum highlight the likely importance of cerebellar modulation in these sensory pathways.

From clinical and preclinical studies described above, the cerebellar regions that most frequently show abnormalities or have been investigated in pain and migraine are Crus I, Crus II, the vermal lobules VI and VIII, lobules IV–VIII, the MN, and the lateral cerebellar nucleus. Future studies dissecting the specific functions of different cerebellar subregions and their circuits will help reveal cerebellar contributions to migraine pathophysiology. Towards this goal, CGRP and its receptors in the cerebellum might be a possible contributor to migraine. Pharmaceutical and optogenetic approaches to modulate CGRP and its receptors may provide new avenues to reveal cerebellar mechanisms and treat migraine pathophysiology.

Author's note

The contents do not represent the views of Veterans Administration or the United States Government.

Author contributions

MW, JT, and ND drafted the manuscript. KP, AR, and LS critically revised the manuscript. All authors contributed to the article and approved the submitted version.

Funding

This work was supported by the National Institutes of Health (R01 NS075599); VA-ORD (RR&D) MERIT (1 I01 RX003523-0); Career Development Award (IK2 RX002010); and Center for Prevention and Treatment of Visual Loss (VA C6810-C).

Acknowledgments

We thank the VA Center for the Prevention and Treatment of Visual Loss for use of facilities. We thank Thomas L. Duong, Agatha M. Greenway, and Brandon J. Rea for writing assistance.

Conflict of interest

AR is a consultant for Lundbeck, Amgen, Novartis, Eli Lilly, AbbVie, and Schedule 1 Therapeutics.

The remaining authors declare that the research was conducted in the absence of any commercial or financial relationships that could be construed as a potential conflict of interest.

Publisher's note

References

Ab Aziz, C. B., and Ahmad, A. H. (2006). The role of the thalamus in modulating pain. *Malays. J. Med. Sci.* 13, 11–18.

Abad, N., Rosenberg, J. T., Hike, D. C., Harrington, M. G., and Grant, S. C. (2018). Dynamic sodium imaging at ultra-high field reveals progression in a preclinical migraine model. *Pain* 159, 2058–2065. doi: 10.1097/j.pain.0000000000001307

Abushik, P. A., Bart, G., Korhonen, P., Leinonen, H., Giniatullina, R., Sibarov, D. A., et al. (2017). Pro-nociceptive migraine mediator CGRP provides neuroprotection of sensory, cortical and cerebellar neurons via multi-kinase signaling. *Cephalalgia* 37, 1373–1383. doi: 10.1177/0333102416681588

Abushik, P. A., Niittykoski, M., Giniatullina, R., Shakirzyanova, A., Bart, G., Fayuk, D., et al. (2014). The role of NMDA and mGluR5 receptors in calcium mobilization and neurotoxicity of homocysteine in trigeminal and cortical neurons and glial cells. *J. Neurochem.* 129, 264–274. doi: 10.1111/jnc.12615

Adamaszek, M., D'Agata, F., Ferrucci, R., Habas, C., Keulen, S., Kirkby, K. C., et al. (2017). Consensus article: cerebellum and emotion. *Cerebellum* 16, 552–576. doi: 10.1007/s12311-016-0815-8

Afridi, S. K., Giffin, N. J., Kaube, H., Friston, K. J., Ward, N. S., Frackowiak, R. S. J., et al. (2005). A positron emission tomographic study in spontaneous migraine. *Arch. Neurol.* 62, 1270–1275. doi: 10.1001/archneur.62.8.1270

Amin, F. M., Hougaard, A., Magon, S., Asghar, M. S., Ahmad, N. N., Rostrup, E., et al. (2016). Change in brain network connectivity during PACAP38-induced migraine attacks: a resting-state functional MRI study. *Neurology* 86, 180–187. doi: 10.1212/WNL.0000000000002261

Anagnostou, E., Gerakoulis, S., Voskou, P., and Karazizou, E. (2019). Postural instability during attacks of migraine without aura. *Eur. J. Neurol.* 26, 319-e21. doi: 10.1111/ene.13815

Ashkenazi, A., Mushtaq, A., Yang, I., and Oshinsky, M. L. (2009). Ictal and interictal phonophobia in migraine-a quantitative controlled study. *Cephalalgia* 29, 1042–1048. doi: 10.1111/j.1468-2982.2008.01834.x

Aurora, S. K., and Wilkinson, F. (2007). The brain is hyperexcitable in migraine. *Cephalalgia* 27, 1442–1453. doi: 10.1111/j.1468-2982.2007.01502.x

Bagnall, M. W., Zingg, B., Sakatos, A., Moghadam, S. H., Zeilhofer, H. U., and du Lac, S. (2009). Glycinergic projection neurons of the cerebellum. *J. Neurosci.* 29, 10104–10110. doi: 10.1523/JNEUROSCI.2087-09.2009

Balaban, C. D., Jacob, R. G., and Furman, J. M. (2011). Neurologic bases for comorbidity of balance disorders, anxiety disorders and migraine: neurotherapeutic implications. *Expert Rev. Neurother.* 11, 379–394. doi: 10.1586/ern.11.19

Baldacara, L., Borgio, J. G., Lacerda, A. L., and Jackowski, A. P. (2008). Cerebellum and psychiatric disorders. *Braz. J. Psychiatry* 30, 281–289. doi: 10.1590/s1516-44462008000300016

Barmack, N. H. (2016). "Vestibular nuclei and their cerebellar connections," in *Essentials of Cerebellum and Cerebellar Disorders: A Primer For Graduate Students*, eds D. L. Gruol, N. Koibuchi, M. Manto M. Molinari J. D. Schmahmann and Y. Shen (Cham: Springer International Publishing), 69–78.

Bartho, P., Freund, T. F., and Acsady, L. (2002). Selective GABAergic innervation of thalamic nuclei from zona incerta. *Eur. J. Neurosci.* 16, 999–1014. doi: 10.1046/j.1460-9568.2002.02157.x

Basbaum, A. I., and Fields, H. L. (1978). Endogenous pain control mechanisms: review and hypothesis. *Ann. Neurol.* 4, 451–462. doi: 10.1002/ana.410040511

Basile, G. A., Quartu, M., Bertino, S., Serra, M. P., Boi, M., Bramanti, A., et al. (2021). Red nucleus structure and function: from anatomy to clinical neurosciences. *Brain Struct. Funct.* 226, 69–91. doi: 10.1007/s00429-020-02171-x

Baumann, O., Borra, R. J., Bower, J. M., Cullen, K. E., Habas, C., Ivry, R. B., et al. (2015). Consensus article: the role of the cerebellum in perceptual processes. *Cerebellum* 14, 197–220. doi: 10.1007/s12311-014-0627-7

Benemei, S., Bentivegna, E., and Martelletti, P. (2022). Positioning the new drugs for migraine. *Expert Opin. Drug Metab. Toxicol.* 18, 1–3. doi: 10.1080/17425255.2022.2049236

Bing, X., Ming-Guo, Q., Ye, Z., Jing-Na, Z., Min, L., Han, C., et al. (2013). Alterations in the cortical thickness and the amplitude of low-frequency fluctuation in patients with post-traumatic stress disorder. *Brain Res.* 1490, 225–232. doi: 10.1016/j.brainres.2012.10.048

Bishop, G. A. (1992). Calcitonin gene-related peptide in afferents to the cat's cerebellar cortex: distribution and origin. *J. Comp. Neurol.* 322, 201–212. doi: 10.1002/cne.903220206

Bishop, G. A. (1995). Calcitonin gene-related peptide modulates neuronal activity in the mammalian cerebellar cortex. *Neuropeptides* 28, 85–97. doi: 10.1016/0143-4179(95)90080-2

Bishop, G. A., Ho, R. H., and King, J. S. (1988). A temporal analysis of the origin and distribution of serotoninergic afferents in the cerebellum of pouch young opossums. *Anat. Embryol. (Berl)* 179, 33–48. doi: 10.1007/BF00305098

Bocci, T., Barloscio, D., Parenti, L., Sartucci, F., Carli, G., and Santarcangelo, E. L. (2017). High hypnotizability impairs the cerebellar control of pain. *Cerebellum* 16, 55–61. doi: 10.1007/s12311-016-0764-2

Bocci, T., Santarcangelo, E., Vannini, B., Torzini, A., Carli, G., Ferrucci, R., et al. (2015). Cerebellar direct current stimulation modulates pain perception in humans. *Restor. Neurol. Neurosci.* 33, 597–609. doi: 10.3233/RNN-140453

Bonanno, L., Lo Buono, V., De Salvo, S., Ruvolo, C., Torre, V., Bramanti, P., et al. (2020). Brain morphologic abnormalities in migraine patients: an observational study. *J. Headache Pain* 21:39. doi: 10.1186/s10194-020-01109-2

Brandt, T., and Dieterich, M. (2017). The dizzy patient: don't forget disorders of the central vestibular system. *Nat. Rev. Neurol.* 13, 352–362. doi: 10.1038/nrneurol.2017.58

Brennan, K. C., and Pietrobon, D. (2018). A systems neuroscience approach to migraine. *Neuron* 97, 1004–1021. doi: 10.1016/j.neuron.2018.01.029

Brighina, F., Palermo, A., Panetta, M. L., Daniele, O., Aloisio, A., Cosentino, G., et al. (2009). Reduced cerebellar inhibition in migraine with aura: a TMS study. *Cerebellum* 8, 260–266. doi: 10.1007/s12311-008-0090-4

Burstein, R., Jakubowski, M., Garcia-Nicas, E., Kainz, V., Bajwa, Z., Hargreaves, R., et al. (2010). Thalamic sensitization transforms localized pain into widespread allodynia. *Ann. Neurol.* 68, 81–91. doi: 10.1002/ana.21994

Burstein, R., Noseda, R., and Borsook, D. (2015). Migraine: multiple processes, complex pathophysiology. *J. Neurosci.* 35, 6619–6629. doi: 10.1523/JNEUROSCI.0373-15.2015

Burstein, R., Yarnitsky, D., Goor-Aryeh, I., Ransil, B. J., and Bajwa, Z. H. (2000). An association between migraine and cutaneous allodynia. *Ann. Neurol.* 47, 614–624. doi: 10.1002/1531-8249(200005)47:5<614::aid-ana9>3.0.co;2-n

Cady, R. K., Vause, C. V., Ho, T. W., Bigal, M. E., and Durham, P. L. (2009). Elevated saliva calcitonin gene-related peptide levels during acute migraine predict therapeutic response to rizatriptan. *Headache* 49, 1258–1266. doi: 10.1111/j.1526-4610.2009.01523.x

Cao, B. B., Huang, Y., Lu, J. H., Xu, F. F., Qiu, Y. H., and Peng, Y. P. (2013). Cerebellar fastigial nuclear GABAergic projections to the hypothalamus modulate immune function. *Brain Behav. Immun.* 27, 80–90. doi: 10.1016/j.bbi.2012.09.014

Catterall, W. A. (1998). Structure and function of neuronal Ca^{2+} channels and their role in neurotransmitter release. *Cell Calcium* 24, 307–323. doi: 10.1016/s0143-4160(98)90055-0

Charles, A. (2018). The pathophysiology of migraine: implications for clinical management. *Lancet Neurol.* 17, 174–182. doi: 10.1016/S1474-4422(17)30435-0

Chedotal, A., and Sotelo, C. (1992). Early development of olivocerebellar projections in the fetal-rat using Cgrp immunocytochemistry. *Eur. J. Neurosci.* 4, 1159–1179. doi: 10.1111/j.1460-9568.1992.tb00142.x

Chou, K. H., Lee, P. L., Liang, C. S., Lee, J. T., Kao, H. W., Tsai, C. L., et al. (2021). Identifying neuroanatomical signatures in insomnia and migraine comorbidity. *Sleep* 44:zsaa202. doi: 10.1093/sleep/zsaa202

Connor, K. M., Shapiro, R. E., Diener, H. C., Lucas, S., Kost, J., Fan, X., et al. (2009). Randomized, controlled trial of telcagepant for the acute treatment of migraine. *Neurology* 73, 970–977. doi: 10.1212/WNL.0b013e3181b87942

Deen, M., Correnti, E., Kamm, K., Kelderman, T., Papetti, L., Rubio-Beltran, E., et al. (2017). Blocking CGRP in migraine patients - a review of pros and cons. *J. Headache Pain* 18:96. doi: 10.1186/s10194-017-0807-1

Demarquay, G., Royet, J. P., Giraud, P., Chazot, G., Valade, D., and Ryvlin, P. (2006). Rating of olfactory judgements in migraine patients. *Cephalalgia* 26, 1123–1130. doi: 10.1111/j.1468-2982.2006.01174.x

Demir, B. T., Bayram, N. A., Ayturk, Z., Erdamar, H., Seven, P., Calp, A., et al. (2016). Structural changes in the cerebrum, cerebellum and corpus callosum in migraine patients. *Clin. Invest. Med.* 39, S21–S26. doi: 10.25011/cim.v39i6.27495

Deuis, J. R., Dvorakova, L. S., and Vetter, I. (2017). Methods used to evaluate pain behaviors in rodents. *Front. Mol. Neurosci.* 10:284. doi: 10.3389/fnmol.2017.00284

Dey, P. K., and Ray, A. K. (1982). Anterior cerebellum as a site for morphine analgesia and post-stimulation analgesia. *Indian J. Physiol. Pharmacol.* 26, 3–12.

Dichgans, M., Herzog, J., Freilinger, T., Wilke, M., and Auer, D. P. (2005). 1H-MRS alterations in the cerebellum of patients with familial hemiplegic migraine type 1. *Neurology* 64, 608–613. doi: 10.1212/01.WNL.0000151855.98318.50

Dietrichs, E. (1983). Cerebellar cortical afferents from the periaqueductal grey in the cat. *Neurosci. Lett.* 41, 21–26. doi: 10.1016/0304-3940(83)90217-3

Dietrichs, E. (1984). Cerebellar autonomic function—direct hypothalamocerebellar pathway. *Science* 223, 591–593. doi: 10.1126/science.6198719

Dietrichs, E. (1985). Divergent axon collaterals to cerebellum and amygdala from neurons in the parabrachial nucleus, the nucleus locus coeruleus and some adjacent nuclei—a fluorescent double labeling study using rhodamine labeled latex microspheres and fast blue as retrograde tracers. *Anat. Embryol. (Berl)* 172, 375–382. doi: 10.1007/BF00318986

Dietrichs, E. (1988). Cerebellar cortical and nuclear afferents from the feline locus coeruleus complex. *Neuroscience* 27, 77–91. doi: 10.1016/0306-4522(88)90220-5

Dodick, D. W. (2018). A phase-by-phase review of migraine pathophysiology. *Headache* 58, 4–16. doi: 10.1111/head.13300

Dodick, D. W., Silberstein, S. D., Bigal, M. E., Yeung, P. P., Goadsby, P. J., Blankenbiller, T., et al. (2018). Effect of fremanezumab compared with placebo for prevention of episodic migraine a randomized clinical trial. *JAMA* 319, 1999–2008. doi: 10.1001/jama.2018.4853

Dong, W. Q., Wilson, O. B., Skolnick, M. H., and Dafny, N. (1992). Hypothalamic, dorsal raphe and external electrical stimulation modulate noxious evoked responses of habenula neurons. *Neuroscience* 48, 933–940. doi: 10.1016/0306-4522(92)90281-6

Dresler, T., Caratozzolo, S., Guldolf, K., Huhn, J. I., Loiacono, C., Niiberg-Pikksoot, T., et al. (2019). Understanding the nature of psychiatric comorbidity in migraine: a systematic review focused on interactions and treatment implications. *J. Headache Pain* 20:51. doi: 10.1186/s10194-019-0988-x

Edvinsson, L., Eftekhari, S., Salvatore, C. A., and Warfvinge, K. (2011). Cerebellar distribution of calcitonin gene-related peptide (CGRP) and its receptor components calcitonin receptor-like receptor (CLR) and receptor activity modifying protein 1 (RAMP1) in rat. *Mol. Cell Neurosci.* 46, 333–339. doi: 10.1016/j.mcn.2010.10.005

Edvinsson, L., Grell, A. S., and Warfvinge, K. (2020). Expression of the CGRP family of neuropeptides and their receptors in the trigeminal ganglion. *J. Mol. Neurosci.* 70, 930–944. doi: 10.1007/s12031-020-01493-z

Edvinsson, L., Haanes, K. A., Warfvinge, K., and Krause, D. N. (2018). CGRP as the target of new migraine therapies - successful translation from bench to clinic. *Nat. Rev. Neurol.* 14, 338–350. doi: 10.1038/s41582-018-0003-1

Edvinsson, L., and Warfvinge, K. (2019). Recognizing the role of CGRP and CGRP receptors in migraine and its treatment. *Cephalalgia* 39, 366–373. doi: 10.1177/0333102417736900

Eftekhari, S., Salvatore, C. A., Connolly, B. M., O'Malley, S., Miller, P. J., Zeng, Z., et al. (2013a). CGRP and CGRP receptors in human and rhesus monkey cerebellum. *J. Headache Pain* 14:P91. doi: 10.1186/1129-2377-14-s1-p91

Eftekhari, S., Salvatore, C. A., Gaspar, R. C., Roberts, R., O'Malley, S., Zeng, Z., et al. (2013b). Localization of CGRP receptor components, CGRP and receptor binding sites in human and rhesus cerebellar cortex. *Cerebellum* 12, 937–949. doi: 10.1007/s12311-013-0509-4

Eigenbrodt, A. K., Ashina, H., Khan, S., Diener, H. C., Mitsikostas, D. D., Sinclair, A. J., et al. (2021). Diagnosis and management of migraine in ten steps. *Nat. Rev. Neurol.* 17, 501–514. doi: 10.1038/s41582-021-00509-5

Elliott, M. A., Peroutka, S. J., Welch, S., and May, E. F. (1996). Familial hemiplegic migraine, nystagmus and cerebellar atrophy. *Ann. Neurol.* 39, 100–106. doi: 10.1002/ana.410390115

Ernstsen, C., Christensen, S. L., Rasmussen, R. H., Nielsen, B. S., Jansen-Olesen, I., Olesen, J., et al. (2022). The PACAP pathway is independent of CGRP in mouse models of migraine: possible new drug target? *Brain* 145, 2450–2460. doi: 10.1093/brain/awac040

Farago, P., Tuka, B., Toth, E., Szabo, N., Kiraly, A., Csete, G., et al. (2017). Interictal brain activity differs in migraine with and without aura: resting state fMRI study. *J. Headache Pain* 18:8. doi: 10.1186/s10194-016-0716-8

Formeister, E. J., Rizk, H. G., Kohn, M. A., and Sharon, J. D. (2018). The epidemiology of vestibular migraine: a population-based survey study. *Otol. Neurotol.* 39, 1037–1044. doi: 10.1097/MAO.0000000000001900

Frontera, J. L., Aissa, H. B., Sala, R. W., Mailhes-Hamon, C., Georgescu, I. A., Lena, C., et al. (2020). Bidirectional control of fear memories by cerebellar neurons projecting to the ventrolateral periaqueductal grey. *Nat. Commun.* 11:5207. doi: 10.1038/s41467-020-18953-0

Fujita, H., Kodama, T., and du Lac, S. (2020). Modular output circuits of the fastigial nucleus for diverse motor and nonmotor functions of the cerebellar vermis. *eLife* 9:e58613. doi: 10.7554/eLife.58613

GBD 2017 Disease and Injury Incidence and Prevalence Collaborators (2018). Global, regional and national incidence, prevalence and years lived with disability for 354 diseases and injuries for 195 countries and territories, 1990–2017: a systematic analysis for the Global Burden of Disease Study 2017. *Lancet* 392, 1789–1858. doi: 10.1016/S0140-6736(18)32279-7

Ge, S. N., Li, Z. H., Tang, J., Ma, Y. F., Hioki, H., Zhang, T., et al. (2014). Differential expression of VGLUT1 or VGLUT2 in the trigeminothalamic or trigeminocerebellar projection neurons in the rat. *Brain Struct. Funct.* 219, 211–229. doi: 10.1007/s00429-012-0495-1

Ghanizada, H., Al-Karagholi, M. A., Arngrim, N., Olesen, J., and Ashina, M. (2020). PACAP27 induces migraine-like attacks in migraine patients. *Cephalalgia* 40, 57–67. doi: 10.1177/0333102419864507

Gil-Gouveia, R., and Martins, I. P. (2019). Cognition and cognitive impairment in migraine. *Curr. Pain Headache Rep.* 23:84. doi: 10.1007/s11916-019-0824-7

Goadsby, P. J., and Edvinsson, L. (1993). The trigeminovascular system and migraine: studies characterizing cerebrovascular and neuropeptide changes seen in humans and cats. *Ann. Neurol.* 33, 48–56. doi: 10.1002/ana.410330109

Goadsby, P. J., Edvinsson, L., and Ekman, R. (1990). Vasoactive peptide release in the extracerebral circulation of humans during migraine headache. *Ann. Neurol.* 28, 183–187. doi: 10.1002/ana.410280213

Graziano, A., Liu, X. B., Murray, K. D., and Jones, E. G. (2008). Vesicular glutamate transporters define two sets of glutamatergic afferents to the somatosensory thalamus and two thalamocortical projections in the mouse. *J. Comp. Neurol.* 507, 1258–1276. doi: 10.1002/cne.21592

Ha, H., and Gonzalez, A. (2019). Migraine headache prophylaxis. *Am. Fam. Phys.* 99, 17–24. doi: 10.3109/9780203212950-43

Haan, J., Terwindt, G. M., Bos, P. L., Ophoff, R. A., Frants, R. R., and Ferrari, M. D. (1994). Familial hemiplegic migraine in the netherlands dutch migraine genetics research group. *Clin. Neurol. Neurosurg.* 96, 244–249. doi: 10.1016/0303-8467(94)90076-0

Hagains, C. E., Senapati, A. K., Huntington, P. J., He, J. W., and Peng, Y. B. (2011). Inhibition of spinal cord dorsal horn neuronal activity by electrical stimulation of the cerebellar cortex. *J. Neurophysiol.* 106, 2515–2522. doi: 10.1152/jn.00719.2010

Haines, D. E., and Dietrichs, E. (1984). An HRP study of hypothalamo-cerebellar and cerebello-hypothalamic connections in squirrel monkey (*Saimiri sciureus*). *J. Comp. Neurol.* 229, 559–575.

Han, J. S., Li, W., and Neugebauer, V. (2005). Critical role of calcitonin gene-related peptide 1 receptors in the amygdala in synaptic plasticity and pain behavior. *J. Neurosci.* 25, 10717–10728. doi: 10.1523/JNEUROSCI.4112-05.2005

Hardy, S. G. (1985). Analgesia elicited by prefrontal stimulation. *Brain Res.* 339, 281–284. doi: 10.1016/0006-8993(85)90093-9

Harno, H., Hirvonen, T., Kaunisto, M. A., Aalto, H., Levo, H., Isotalo, E., et al. (2003). Subclinical vestibulocerebellar dysfunction in migraine with and without aura. *Neurology* 61, 1748–1752. doi: 10.1212/01.wnl.0000098882.82690.65

Hashimoto, K., Ichikawa, R., Kitamura, K., Watanabe, M., and Kano, M. (2009). Translocation of a "winner" climbing fiber to the purkinje cell dendrite and subsequent elimination of "losers" from the soma in developing cerebellum. *Neuron* 63, 106–118. doi: 10.1016/j.neuron.2009.06.008

Hashimoto, K., and Kano, M. (2005). Postnatal development and synapse elimination of climbing fiber to Purkinje cell projection in the cerebellum. *Neurosci. Res.* 53, 221–228. doi: 10.1016/j.neures.2005.07.007

Hay, D. L., and Walker, C. S. (2017). CGRP and its receptors. *Headache* 57, 625–636. doi: 10.1111/head.13064

Hayashi, H., Sumino, R., and Sessle, B. J. (1984). Functional organization of trigeminal subnucleus interpolaris: nociceptive and innocuous afferent inputs, projections to thalamus, cerebellum and spinal cord and descending modulation from periaqueductal gray. *J. Neurophysiol.* 51, 890–905. doi: 10.1152/jn.1984.51.5.890

Heath, R. G., and Harper, J. W. (1974). Ascending projections of the cerebellar fastigial nucleus to the hippocampus, amygdala and other temporal lobe sites: evoked potential and histological studies in monkeys and cats. *Exp. Neurol.* 45, 268–287. doi: 10.1016/0014-4886(74)90118-6

Helgers, S. O. A., Al Krinawe, Y., Alam, M., Krauss, J. K., Schwabe, K., Hermann, E. J., et al. (2020). Lesion of the fastigial nucleus in juvenile rats deteriorates rat behavior in adulthood, accompanied by altered neuronal activity in the medial prefrontal cortex. *Neuroscience* 442, 29–40. doi: 10.1016/j.neuroscience.2020.06.035

Helgers, S. O. A., Angelov, S., Muschler, M. A. N., Glahn, A., Al-Afif, S., Al Krinawe, Y., et al. (2021). Epigenetic regulation of neural transmission after cerebellar fastigial nucleus lesions in juvenile rats. *Cerebellum* 20, 922–930. doi: 10.1007/s12311-021-01264-5

Hilber, P., Lorivel, T., Delarue, C., and Caston, J. (2004). Stress and anxious-related behaviors in Lurcher mutant mice. *Brain Res.* 1003, 108–112. doi: 10.1016/j.brainres.2004.01.008

Ho, T. W., Edvinsson, L., and Goadsby, P. J. (2010). CGRP and its receptors provide new insights into migraine pathophysiology. *Nat. Rev. Neurol.* 6, 573–582. doi: 10.1038/nrneurol.2010.127

Ho, T. W., Ferrari, M. D., Dodick, D. W., Galet, V., Kost, J., Fan, X., et al. (2008). Efficacy and tolerability of MK-0974 (telcagepant), a new oral antagonist of calcitonin gene-related peptide receptor, compared with zolmitriptan for acute migraine: a randomised, placebo-controlled, parallel-treatment trial. *Lancet* 372, 2115–2123. doi: 10.1016/S0140-6736(08)61626-8

Hoskin, J. L., and Fife, T. D. (2022). New Anti-CGRP medications in the treatment of vestibular migraine. *Front. Neurol.* 12:799002. doi: 10.3389/fneur.2021.799002

Hostetler, E. D., Joshi, A. D., Sanabria-Bohorquez, S., Fan, H., Zeng, Z., Purcell, M., et al. (2013). in vivo quantification of calcitonin gene-related peptide receptor occupancy by telcagepant in rhesus monkey and human brain using the positron emission tomography tracer [^{11}C]MK-4232. *J. Pharmacol. Exp. Ther.* 347, 478–486. doi: 10.1124/jpet.113.206458

Hoyer, C., Gass, N., Weber-Fahr, W., and Sartorius, A. (2014). Advantages and challenges of small animal magnetic resonance imaging as a translational tool. *Neuropsychobiology* 69, 187–201. doi: 10.1159/000360859

Huang, X. B., Zhang, D., Chen, Y. C., Wang, P., Mao, C. N., Miao, Z. F., et al. (2019). Altered functional connectivity of the red nucleus and substantia nigra in migraine without aura. *J. Headache Pain* 20:104. doi: 10.1186/s10194-019-1058-0

ICHD-3 (2018). Headache classification committee of the international headache society (IHS), the international classification of headache disorders, 3rd edition. *Cephalalgia* 38, 1–211. doi: 10.1177/0333102417738202

Ikeda, M. (1979). Projections from the spinal and the principal sensory nuclei of the trigeminal nerve to the cerebellar cortex in the cat, as studied by retrograde transport of horseradish-peroxidase. *J. Comp. Neurol.* 184, 567–585. doi: 10.1002/cne.901840309

Ishizaki, K., Mori, N., Takeshima, T., Fukuhara, Y., Ijiri, T., Kusumi, M., et al. (2002). Static stabilometry in patients with migraine and tension-type headache during a headache-free period. *Psychiatry Clin. Neurosci.* 56, 85–90. doi: 10.1046/j.1440-1819.2002.00933.x

Isobe, C., and Terayama, Y. (2010). A remarkable increase in total homocysteine concentrations in the CSF of migraine patients with aura. *Headache* 50, 1561–1569. doi: 10.1111/j.1526-4610.2010.01713.x

Iyengar, S., Johnson, K. W., Ossipov, M. H., and Aurora, S. K. (2019). CGRP and the trigeminal system in migraine. *Headache* 59, 659–681. doi: 10.1111/head.13529

Iyengar, S., Ossipov, M. H., and Johnson, K. W. (2017). The role of calcitonin gene-related peptide in peripheral and central pain mechanisms including migraine. *Pain* 158, 543–559. doi: 10.1097/j.pain.0000000000000831

Jacquin, M. F., Semba, K., Rhoades, R. W., and Egger, M. D. (1982). Trigeminal primary afferents project bilaterally to dorsal horn and ipsilaterally to cerebellum, reticular formation and cuneate, solitary, supratrigeminal and vagal nuclei. *Brain Res.* 246, 285–291. doi: 10.1016/0006-8993(82)91177-5

Jia, Z. H., Chen, X. Y., Tang, W. J., Zhao, D. F., and Yu, S. Y. (2019). Atypical functional connectivity between the anterior cingulate cortex and other brain regions in a rat model of recurrent headache. *Mol. Pain* 15, 1–9. doi: 10.1177/1744806919842483

Jia, Z., Yu, S., Tang, W., and Zhao, D. (2020). Altered functional connectivity of the insula in a rat model of recurrent headache. *Mol. Pain* 16, 1–8. doi: 10.1177/1744806920922115

Jin, C. W., Yuan, K., Zhao, L. M., Zhao, L., Yu, D. H., von Deneen, K. M., et al. (2013). Structural and functional abnormalities in migraine patients without aura. *NMR Biomed.* 26, 58–64. doi: 10.1002/nbm.2819

Johnson, K. W., Morin, S. M., Wroblewski, V. J., and Johnson, M. P. (2019). Peripheral and central nervous system distribution of the CGRP neutralizing antibody [(125)I] galcanezumab in male rats. *Cephalalgia* 39, 1241–1248. doi: 10.1177/0333102419844711

Joutel, A., Bousser, M. G., Biousse, V., Labauge, P., Chabriat, H., Nibbio, A., et al. (1993). A gene for familial hemiplegic migraine maps to chromosome 19. *Nat. Genet.* 5, 40–45. doi: 10.1038/ng0993-40

Jueptner, M., and Weiller, C. (1998). A review of differences between basal ganglia and cerebellar control of movements as revealed by functional imaging studies. *Brain* 121, 1437–1449. doi: 10.1093/brain/121.8.1437

Juhasz, G., Zsombok, T., Jakab, B., Nemeth, J., Szolcsanyi, J., and Bagdy, G. (2005). Sumatriptan causes parallel decrease in plasma calcitonin gene-related peptide (CGRP) concentration and migraine headache during nitroglycerin induced migraine attack. *Cephalalgia* 25, 179–183. doi: 10.1111/j.1468-2982.2005.00836.x

Kandel, E. R., Koester, J., Mack, S., and Siegelbaum, S. (2021). *Principles of Neural Science*. New York: McGraw Hill

Karsan, N., Bose, P. R., O'Daly, O., Zelaya, F. O., and Goadsby, P. J. (2020). Alterations in functional connectivity during different phases of the triggered migraine attack. *Headache* 60, 1244–1258. doi: 10.1111/head.13865

Kawai, Y., Takami, K., Shiosaka, S., Emson, P. C., Hillyard, C. J., Girgis, S., et al. (1985). Topographic localization of calcitonin gene-related peptide in the rat brain: an immunohistochemical analysis. *Neuroscience* 15, 747–763. doi: 10.1016/0306-4522(85)90076-4

Ke, J., Yu, Y., Zhang, X. D., Su, Y. Y., Wang, X. M., Hu, S., et al. (2020). Functional alterations in the posterior insula and cerebellum in migraine without aura: a resting-state MRI study. *Front. Behav. Neurosci.* 14:567588. doi: 10.3389/fnbeh.2020.567588

Ke, J., Zhang, L., Qi, R. F., Li, W. H., Hou, C. L., Zhong, Y., et al. (2016). A longitudinal fMRI investigation in acute post-traumatic stress disorder (PTSD). *Acta Radiol.* 57, 1387–1395. doi: 10.1177/0284185115585848

Kheradmand, A., and Zee, D. S. (2011). Cerebellum and ocular motor control. *Front. Neurol.* 2:53. doi: 10.3389/fneur.2011.00053

Kim, J. S., Ahn, K. W., Moon, S. Y., Choi, K. D., Park, S. H., and Koo, J. W. (2005). Isolated perverted head-shaking nystagmus in focal cerebellar infarction. *Neurology* 64, 575–576. doi: 10.1212/01.WNL.0000150729.87682.79

Kono, S., Terada, T., Ouchi, Y., and Miyajima, H. (2014). An altered GABA-A receptor function in spinocerebellar ataxia type 6 and familial hemiplegic migraine type 1 associated with the CACNA1A gene mutation. *BBA Clin.* 2, 56–61. doi: 10.1016/j.bbacli.2014.09.005

Koppen, H., Boele, H. J., Palm-Meinders, I. H., Koutstaal, B. J., Horlings, C. G. C., Koekkoek, B. K., et al. (2017). Cerebellar function and ischemic brain lesions in migraine patients from the general population. *Cephalalgia* 37, 177–190. doi: 10.1177/0333102416643527

Kors, E. E., Terwindt, G. M., Vermeulen, F. L., Fitzsimons, R. B., Jardine, P. E., Heywood, P., et al. (2001). Delayed cerebral edema and fatal coma after minor head trauma: role of the CACNA1A calcium channel subunit gene and relationship with familial hemiplegic migraine. *Ann. Neurol.* 49, 753–760. doi: 10.1002/ana.1031

Koutsikou, S., Crook, J. J., Earl, E. V., Leith, J. L., Watson, T. C., Lumb, B. M., et al. (2014). Neural substrates underlying fear-evoked freezing: the periaqueductal grey-cerebellar link. *J. Physiol.* 592, 2197–2213. doi: 10.1113/jphysiol.2013.268714

Koziol, L. F., Budding, D., Andreasen, N., D'Arrigo, S., Bulgheroni, S., Imamizu, H., et al. (2014). Consensus article: the cerebellum's role in movement and cognition. *Cerebellum* 13, 151–177. doi: 10.1007/s12311-013-0511-x

Kreczmanski, P., Wolak, T., Lewandowska, M., and Domitrz, I. (2019). Altered functional brain imaging in migraine patients: BOLD preliminary study in migraine with and without aura. *Neurol. Neurochir. Pol.* 53, 304–310. doi: 10.5603/PJNNS.a2019.0035

Kros, L., Angueyra Aristizabal, C. A., and Khodakhah, K. (2018). Cerebellar involvement in migraine. *Cephalalgia* 38, 1782–1791. doi: 10.1177/0333102417752120

Kruit, M. C., van Buchem, M. A., Hofman, P. A. M., Bakkers, J.T.N., Terwindt, G. M., Ferrari, M. D., et al. (2004). Migraine as a risk factor for subclinical brain lesions. *JAMA* 291, 427–434. doi: 10.1001/jama.291.4.427

Kuburas, A., Mason, B. N., Hing, B., Wattiez, A. S., Reis, A. S., Sowers, L. P., et al. (2021). PACAP induces light aversion in mice by an inheritable mechanism independent of CGRP. *J. Neurosci.* 41, 4697–4715. doi: 10.1523/JNEUROSCI.2200-20.2021

Lal, V., and Truong, D. (2019). Eye movement abnormalities in movement disorders. *Clin. Parkinsonism Relat. Disord.* 1, 54–63. doi: 10.1016/j.prdoa.2019.08.004

Landy, S., Rice, K., and Lobo, B. (2004). Central sensitisation and cutaneous allodynia in migraine: implications for treatment. *CNS Drugs* 18, 337–342. doi: 10.2165/00023210-200418060-00001

Lassen, L. H., Haderslev, P., Jacobsen, V. B., Iversen, H. K., Sperling, B., Olesen, J., et al. (2002). CGRP may play a causative role in migraine. *Cephalalgia* 22, 54–61. doi: 10.1046/j.1468-2982.2002.00310.x

Li, P., Gu, H., Xu, J., Zhang, Z., Li, F., Feng, M., et al. (2019). Purkinje cells of vestibulocerebellum play an important role in acute vestibular migraine. *J. Integr. Neurosci.* 18, 409–414. doi: 10.31083/j.jin.2019.04.1168

Li, W. Q., Mai, X. Q., and Liu, C. (2014). The default mode network and social understanding of others: what do brain connectivity studies tell us. *Front. Hum. Neurosci.* 8:74. doi: 10.3389/fnhum.2014.00074

Lipton, R. B., Bigal, M. E., Ashina, S., Burstein, R., Silberstein, S., Reed, M. L., et al. (2008). Cutaneous allodynia in the migraine population. *Ann. Neurol.* 63, 148–158. doi: 10.1002/ana.21211

Liu, L., Hu, X., Zhang, Y., Pan, Q., Zhan, Q., Tan, G., et al. (2020). Effect of vestibular rehabilitation on spontaneous brain activity in patients with vestibular migraine: a resting-state functional magnetic resonance imaging study. *Front. Hum. Neurosci.* 14:227. doi: 10.3389/fnhum.2020.00227

Liu, H. Y., Lee, P. L., Chou, K. H., Lai, K. L., Wang, Y. F., Chen, S. P., et al. (2020). The cerebellum is associated with 2-year prognosis in patients with high-frequency migraine. *J. Headache Pain* 21:29. doi: 10.1186/s10194-020-01096-4

Liu, F. Y., Qiao, J. T., and Dafny, N. (1993). Cerebellar stimulation modulates thalamic noxious-evoked responses. *Brain Res. Bull.* 30, 529–534. doi: 10.1016/0361-9230(93)90079-q

Lombard, L., Farrar, M., Ye, W., Kim, Y., Cotton, S., Buchanan, A. S., et al. (2020). A global real-world assessment of the impact on health-related quality of life and work productivity of migraine in patients with insufficient versus good response to triptan medication. *J. Headache Pain* 21:41. doi: 10.1186/s10194-020-01110-9

Main, A., Dowson, A., and Gross, M. (1997). Photophobia and phonophobia in migraineurs between attacks. *Headache* 37, 492–495. doi: 10.1046/j.1526-4610.1997.3708492.x

Maleki, N., Linnman, C., Brawn, J., Burstein, R., Becerra, L., and Borsook, D. (2012). Her versus his migraine: multiple sex differences in brain function and structure. *Brain* 135, 2546–2559. doi: 10.1093/brain/aws175

Maleki, N., Szabo, E., Becerra, L., Moulton, E., Scrivani, S. J., Burstein, R., et al. (2021). Ictal and interictal brain activation in episodic migraine: neural basis for extent of allodynia. *PLoS One* 16:e0244320. doi: 10.1371/journal.pone.0244320

Manto, M., Bower, J. M., Conforto, A. B., Delgado-Garcia, J. M., da Guarda, S. N. F., Gerwig, M., et al. (2012). Consensus article: roles of the cerebellum in motor control-the diversity of ideas on cerebellar involvement in movement. *Cerebellum* 11, 457–487. doi: 10.1007/s12311-011-0331-9

Martinelli, D., Castellazzi, G., De Icco, R., Bacila, A., Allena, M., Faggioli, A., et al. (2021). Thalamocortical connectivity in experimentally-induced migraine attacks: a pilot study. *Brain Sci.* 11:165. doi: 10.3390/brainsci11020165

Masri, R., Quiton, R. L., Lucas, J. M., Murray, P. D., Thompson, S. M., Keller, A., et al. (2009). Zona incerta: a role in central pain. *J. Neurophysiol.* 102, 181–191. doi: 10.1152/jn.00152.2009

Mayans, L., and Walling, A. (2018). Acute migraine headache: treatment strategies. *Am. Fam. Physician* 97, 243–251.

Mecklenburg, J., Raffaelli, B., Neeb, L., Sanchez Del Rio, M., and Reuter, U. (2020). The potential of lasmiditan in migraine. *Ther. Adv. Neurol. Disord.* 13:1756286420967847. doi: 10.1177/1756286420967847

Mehnert, J., and May, A. (2019). Functional and structural alterations in the migraine cerebellum. *J. Cereb. Blood Flow Metabol.* 39, 730–739. doi: 10.1177/0271678X17722109

Mehnert, J., Schulte, L., Timmann, D., and May, A. (2017). Activity and connectivity of the cerebellum in trigeminal nociception. *Neuroimage* 150, 112–118. doi: 10.1016/j.neuroimage.2017.02.023

Merikangas, K. R., and Stevens, D. E. (1997). Comorbidity of migraine and psychiatric disorders. *Neurol. Clin.* 15:115. doi: 10.1016/s0733-8619(05)70298-x

Messlinger, K. (2018). The big CGRP flood—sources, sinks and signalling sites in the trigeminovascular system. *J. Headache Pain* 19:22. doi: 10.1186/s10194-018-0848-0

Morara, S., Rosina, A., and Provini, L. (1992). CGRP as a marker of the climbing fibers during the development of the cerebellum in the rat. *Ann. N Y Acad. Sci.* 657, 461–463. doi: 10.1111/j.1749-6632.1992.tb22800.x

Morara, S., Rosina, A., Provini, L., Forloni, G., Caretti, A., and Wimalawansa, S. J. (2000). Calcitonin gene-related peptide receptor expression in the neurons and glia of developing rat cerebellum: an autoradiographic and immunohistochemical analysis. *Neuroscience* 100, 381–391. doi: 10.1016/s0306-4522(00)00276-1

Morara, S., Sternini, C., Provini, L., and Rosina, A. (1995). Developmentally regulated expression of α- and β-calcitonin gene-related peptide mRNA and calcitonin gene-related peptide immunoreactivity in the rat inferior olive. *J. Comp. Neurol.* 354, 27–38. doi: 10.1002/cne.903540104

Morara, S., van der Want, J. J., de Weerd, H., Provini, L., and Rosina, A. (2001). Ultrastructural analysis of climbing fiber-Purkinje cell synaptogenesis in the rat cerebellum. *Neuroscience* 108, 655–671. doi: 10.1016/s0306-4522(01)00433-x

Morara, S., Wang, L. P., Filippov, V., Dickerson, I. M., Grohovaz, F., Provini, L., et al. (2008). Calcitonin gene-related peptide (CGRP) triggers Ca^{2+} responses in cultured astrocytes and in Bergmann glial cells from cerebellar slices. *Eur. J. Neurosci.* 28, 2213–2220. doi: 10.1111/j.1460-9568.2008.06514.x

Morara, S., Wimalawansa, S. J., and Rosina, A. (1998). Monoclonal antibodies reveal expression of the CGRP receptor in Purkinje cells, interneurons and astrocytes of rat cerebellar cortex. *Neuroreport* 9, 3755–3759. doi: 10.1097/00001756-199811160-00034

Morgan, M. M., Grisel, J. E., Robbins, C. S., and Grandy, D. K. (1997). Antinociception mediated by the periaqueductal gray is attenuated by orphanin FQ. *Neuroreport* 8, 3431–3434. doi: 10.1097/00001756-199711100-00003

Moulton, E. A., Becerra, L., Johnson, A., Burstein, R., and Borsook, D. (2014). Altered hypothalamic functional connectivity with autonomic circuits and the locus coeruleus in migraine. *PLos One* 9:e95508. doi: 10.1371/journal.pone.0095508

Moulton, E. A., Becerra, L., Maleki, N., Pendse, G., Tully, S., Hargreaves, R., et al. (2011). Painful heat reveals hyperexcitability of the temporal pole in interictal and ictal migraine States. *Cereb. Cortex* 21, 435–448. doi: 10.1093/cercor/bhq109

Moulton, E. A., Schmahmann, J. D., Becerra, L., and Borsook, D. (2010). The cerebellum and pain: passive integrator or active participator? *Brain Res. Rev.* 65, 14–27. doi: 10.1016/j.brainresrev.2010.05.005

Munjal, S., Singh, P., Reed, M. L., Fanning, K., Schwedt, T. J., Dodick, D. W., et al. (2020). Most bothersome symptom in persons with migraine: results from the migraine in america symptoms and treatment (MAST) study. *Headache* 60, 416–429. doi: 10.1111/head.13708

Neligan, P., Harriman, D. G., and Pearce, J. (1977). Respiratory arrest in familial hemiplegic migraine: a clinical and neuropathological study. *Br. Med. J.* 2, 732–734. doi: 10.1136/bmj.2.6089.732

Neugebauer, H., Adrion, C., Glaser, M., and Strupp, M. (2013). Long-term changes of central ocular motor signs in patients with vestibular migraine. *Eur. Neurol.* 69, 102–107. doi: 10.1159/000343814

Neuhauser, H. K., Radtke, A., von Brevern, M., Feldmann, M., Lezius, F., Ziese, T., et al. (2006). Migrainous vertigo: prevalence and impact on quality of life. *Neurology* 67, 1028–1033. doi: 10.1212/01.wnl.0000237539.09942.06

Noseda, R., Copenhagen, D., and Burstein, R. (2019). Current understanding of photophobia, visual networks and headaches. *Cephalalgia* 39, 1623–1634. doi: 10.1177/0333102418784750

Noseda, R., Kainz, V., Jakubowski, M., Gooley, J. J., Saper, C. B., Digre, K., et al. (2010). A neural mechanism for exacerbation of headache by light. *Nat. Neurosci.* 13, U239–U128. doi: 10.1038/nn.2475

Ohmae, S., Kunimatsu, J., and Tanaka, M. (2017). Cerebellar Roles in Self-Timing for Sub- and Supra-Second Intervals. *J. Neurosci.* 37, 3511–3522. doi: 10.1523/JNEUROSCI.2221-16.2017

Ohya, A., Tsuruoka, M., Imai, E., Fukunaga, H., Shinya, A., Furuya, R., et al. (1993). Thalamic-projecting and cerebellar-projecting interpolaris neuron

responses to afferent inputs. *Brain Res. Bull.* 32, 615–621. doi: 10.1016/0361-9230(93)90163-6

Olesen, J., Diener, H. C., Husstedt, I. W., Goadsby, P. J., Hall, D., Meier, U., et al. (2004). Calcitonin gene-related peptide receptor antagonist BIBN 4096 BS for the acute treatment of migraine. *N. Engl. J. Med.* 350, 1104–1110. doi: 10.1056/NEJMoa030505

Ossowska, K. (2020). Zona incerta as a therapeutic target in Parkinson's disease. *J. Neurol.* 267, 591–606. doi: 10.1007/s00415-019-09486-8

Oterino, A., Toriello, M., Valle, N., Castillo, J., Alonso-Arranz, A., Bravo, Y., et al. (2010). The relationship between homocysteine and genes of folate-related enzymes in migraine patients. *Headache* 50, 99–108. doi: 10.1111/j.1526-4610.2009.01484.x

Otsuka, S., Konno, K., Abe, M., Motohashi, J., Kohda, K., Sakimura, K., et al. (2016). Roles of Cbln1 in non-motor functions of mice. *J. Neurosci.* 36, 11801–11816. doi: 10.1523/JNEUROSCI.0322-16.2016

Oudejans, L. C. J., Smit, J. M., van Velzen, M., Dahan, A., and Niesters, M. (2015). The influence of offset analgesia on the onset and offset of pain in patients with fibromyalgia. *Pain* 156, 2521–2527. doi: 10.1097/j.pain.0000000000000321

Palmiter, R. D. (2018). The parabrachial nucleus: CGRP neurons function as a general alarm. *Trends Neurosci.* 41, 280–293. doi: 10.1016/j.tins.2018.03.007

Parker, K. L. (2015). Timing tasks synchronize cerebellar and frontal ramping activity and theta oscillations: implications for cerebellar stimulation in diseases of impaired cognition. *Front. Psychiatry* 6:190. doi: 10.3389/fpsyt.2015.00190

Petersen, K. A., Lassen, L. H., Birk, S., Lesko, L., and Olesen, J. (2005). BIBN4096BS antagonizes human α-calcitonin gene related peptide-induced headache and extracerebral artery dilatation. *Clin. Pharmacol. Ther.* 77, 202–213. doi: 10.1016/j.clpt.2004.10.001

Pinheiro, C. F., Moraes, R., Carvalho, G. F., Sestari, L., Will-Lemos, T., Bigal, M. E., et al. (2020). The influence of photophobia on postural control in patients with migraine. *Headache* 60, 1644–1652. doi: 10.1111/head.13908

Purves, D., Augustine, G. J., Fitzpatrick, D., Hall, W. C., Mooney, A.-S. L. R. D., Platt, M. L., et al. (2018). *Neuroscience*, Sixth edition. New York: Oxford University Press.

Qin, Z. X., He, X. W., Zhang, J. L., Xu, S., Li, G. F., Su, J. J., et al. (2019). Structural changes of cerebellum and brainstem in migraine without aura. *J. Headache Pain* 20:93. doi: 10.1186/s10194-019-1045-5

Qin, Z. X., Su, J. J., He, X. W., Ban, S. Y., Zhu, Q., Cui, Y. Y., et al. (2020). Disrupted functional connectivity between sub-regions in the sensorimotor areas and cortex in migraine without aura. *J. Headache Pain* 21:47. doi: 10.1186/s10194-020-01118-1

Reuter, U. (2018). A review of monoclonal antibody therapies and other preventative treatments in migraine. *Headache* 58, 48–59. doi: 10.1111/head.13302

Rondi-Reig, L., Paradis, A. L., Lefort, J. M., Babayan, B. M., and Tobin, C. (2014). How the cerebellum may monitor sensory information for spatial representation. *Front. Syst. Neurosci.* 8:205. doi: 10.3389/fnsys.2014.00205

Rosina, A., Morara, S., Provini, L., and Forloni, G. (1990). Modulation of cerebellar CGRP binding sites induced by climbing fibre activation. *Neuroreport* 1, 215–217. doi: 10.1097/00001756-199011000-00010

Ruscheweyh, R., Kuhnel, M., Filippopulos, F., Blum, B., Eggert, T., and Straube, A. (2014). Altered experimental pain perception after cerebellar infarction. *Pain* 155, 1303–1312. doi: 10.1016/j.pain.2014.04.006

Russell, J. S. R. (1894). Experimental researches into the functions of the cerebellum. *Philos. Trans. R Soc. Lond. B Biol. Sci.* 185, 819–861.

Russo, A. F. (2015). Calcitonin gene-related peptide (CGRP): a new target for migraine. *Annu. Rev. Pharmacol. Toxicol.* 55, 533–552. doi: 10.1146/annurev-pharmtox-010814-124701

Russo, A. F. (2019). CGRP-based migraine therapeutics: how might they work, why so safe and what next? *ACS Pharmacol. Transl. Sci.* 2, 2–8. doi: 10.1021/acsptsci.8b00036

Russo, A., Tessitore, A., Esposito, F., Marcuccio, L., Giordano, A., Conforti, R., et al. (2012). Pain processing in patients with migraine: an event-related fMRI study during trigeminal nociceptive stimulation. *J. Neurol.* 259, 1903–1912. doi: 10.1007/s00415-012-6438-1

Saab, C. Y., Garcia-Nicas, E., and Willis, W. D. (2002). Stimulation in the rat fastigial nucleus enhances the responses of neurons in the dorsal column nuclei to innocuous stimuli. *Neurosci. Lett.* 327, 317–320. doi: 10.1016/s0304-3940(02)00379-8

Saab, C. Y., Kawasaki, M., Al-Chaer, E. D., and Willis, W. D. (2001). Cerebellar cortical stimulation increases spinal visceral nociceptive responses. *J. Neurophysiol.* 85, 2359–2363. doi: 10.1152/jn.2001.85.6.2359

Saab, C. Y., and Willis, W. D. (2002). Cerebellar stimulation modulates the intensity of a visceral nociceptive reflex in the rat. *Exp. Brain Res.* 146, 117–121. doi: 10.1007/s00221-002-1107-8

Sacchetti, B., Scelfo, B., and Strata, P. (2005). The cerebellum: synaptic changes and fear conditioning. *Neuroscientist* 11, 217–227. doi: 10.1177/1073858405276428

Salvatore, C. A., Moore, E. L., Calamari, A., Cook, J. J., Michener, M. S., O'Malley, S., et al. (2010). Pharmacological properties of MK-3207, a potent and orally active calcitonin gene-related peptide receptor antagonist. *J. Pharmacol. Exp. Ther.* 333, 152–160. doi: 10.1124/jpet.109.163816

Sances, G., Tassorelli, C., Pucci, E., Ghiotto, N., Sandrini, G., and Nappi, G. (2004). Reliability of the nitroglycerin provocative test in the diagnosis of neurovascular headaches. *Cephalalgia* 24, 110–119. doi: 10.1111/j.1468-2982.2004.00639.x

Sandkuhler, J. (2009). Models and mechanisms of hyperalgesia and allodynia. *Physiol. Rev.* 89, 707–758. doi: 10.1152/physrev.00025.2008

Schwedt, T. J. (2013). Multisensory integration in migraine. *Curr. Opin. Neurol.* 26, 248–253. doi: 10.1097/WCO.0b013e328360edb1

Schwedt, T. J., Chong, C. D., Chiang, C. C., Baxter, L., Schlaggar, B. L., and Dodick, D. W. (2014a). Enhanced pain-induced activity of pain-processing regions in a case-control study of episodic migraine. *Cephalalgia* 34, 947–958. doi: 10.1177/0333102414526069

Schwedt, T. J., Larson-Prior, L., Coalson, R. S., Nolan, T., Mar, S., Ances, B. M., et al. (2014b). Allodynia and descending pain modulation in migraine: a resting state functional connectivity analysis. *Pain Med.* 15, 154–165. doi: 10.1111/pme.12267

Schytz, H. W., Birk, S., Wienecke, T., Kruuse, C., Olesen, J., and Ashina, M. (2009). PACAP38 induces migraine-like attacks in patients with migraine without aura. *Brain* 132, 16–25. doi: 10.1093/brain/awn307

Sengul, G., Fu, Y., Yu, Y., and Paxinos, G. (2015). Spinal cord projections to the cerebellum in the mouse. *Brain Struct. Funct.* 220, 2997–3009. doi: 10.1007/s00429-014-0840-7

Seybold, V. S. (2009). The role of peptides in central sensitization. *Handb. Exp. Pharmacol.* 194, 451–491. doi: 10.1007/978-3-540-79090-7_13

Shen, Y. J., Qi, X. K., and Wan, T. Y. (2020). The treatment of vestibular migraine: a narrative review. *Ann. Indian Acad. Neurol.* 23, 602–607. doi: 10.4103/aian.AIAN_591_19

Shin, J. H., Kim, Y. K., Kim, H. J., and Kim, J. S. (2014). Altered brain metabolism in vestibular migraine: comparison of interictal and ictal findings. *Cephalalgia* 34, 58–67. doi: 10.1177/0333102413498940

Siegel, A. and Sapru, H. N. (2019). *Essential Neuroscience*, 4th edition. Philadelphia, PA: Wolters Kluwer.

Siegel, P., and Wepsic, J. G. (1974). Alteration of nociception by stimulation of cerebellar structures in the monkey. *Physiol. Behav.* 13, 189–194. doi: 10.1016/0031-9384(74)90033-x

Silva, K. E., Rosner, J., Ullrich, N. J., Chordas, C., Manley, P. E., and Moulton, E. A. (2019). Pain affect disrupted in children with posterior cerebellar tumor resection. *Ann. Clin. Transl. Neurol.* 6, 344–354. doi: 10.1002/acn3.709

Skljarevski, V., Matharu, M., Millen, B. A., Ossipov, M. H., Kim, B. K., and Yang, J. Y. (2018). Efficacy and safety of galcanezumab for the prevention of episodic migraine: results of the EVOLVE-2 Phase 3 randomized controlled clinical trial. *Cephalalgia* 38, 1442–1454. doi: 10.1177/0333102418779543

Sowers, L. P., Wang, M. Y., Rea, B. J., Taugher, R. J., Kuburas, A., Kim, Y., et al. (2020). Stimulation of posterior thalamic nuclei induces photophobic behavior in mice. *Headache* 60, 1961–1981. doi: 10.1111/head.13917

Sprague, J. M., and Chambers, W. W. (1959). An analysis of cerebellar function in the cat as revealed by its partial and complete destruction and its interaction with cerebral cortex. *Arch. Ital. Biol.* 97, 68–88. doi: 10.4449/aib.v97i1.1690

Stankewitz, A., and May, A. (2011). Increased limbic and brainstem activity during migraine attacks following olfactory stimulation. *Neurology* 77, 476–482. doi: 10.1212/WNL.0b013e318227e4a8

Stankewitz, A., Voit, H. L., Bingel, U., Peschke, C., and May, A. (2010). A new trigemino-nociceptive stimulation model for event-related fMRI. *Cephalalgia* 30, 475–485. doi: 10.1111/j.1468-2982.2009.01968.x

Stauffer, V. L., Dodick, D. W., Zhang, Q., Carter, J. N., Ailani, J., and Conley, R. R. (2018). Evaluation of galcanezumab for the prevention of episodic migraine the EVOLVE-1 randomized clinical trial. *JAMA Neurol.* 75, 1080–1088. doi: 10.1001/jamaneurol.2018.1212

Stovner, L. J., Nichols, E., Steiner, T. J., Abd-Allah, F., Abdelalim, A., Al-Raddadi, R. M., et al. (2018). Global, regional and national burden of migraine and tension-type headache, 1990-2016: a systematic analysis for the Global Burden of Disease Study 2016. *Lancet Neurol.* 17, 954–976. doi: 10.1016/S1474-4422(18)30322-3

Sugimoto, T., Itoh, K., and Mizuno, N. (1988). Calcitonin gene-related peptide-like immunoreactivity in neuronal elements of the cat cerebellum. *Brain Res.* 439, 147–154. doi: 10.1016/0006-8993(88)91471-0

Supple, W. F., and Kapp, B. S. (1994). Anatomical and physiological relationships between the anterior cerebellar vermis and the pontine parabrachial nucleus in the rabbit. *Brain Res. Bull.* 33, 561–574. doi: 10.1016/0361-9230(94)90082-5

Sutherland, H. G., Albury, C. L., and Griffiths, L. R. (2019). Advances in genetics of migraine. *J. Headache Pain* 20:72. doi: 10.1186/s10194-019-1017-9

Tabata, H., Yamamoto, K., and Kawato, M. (2002). Computational study on monkey VOR adaptation and smooth pursuit based on the parallel control-pathway theory. *J. Neurophysiol.* 87, 2176–2189. doi: 10.1152/jn.00168.2001

Tae, W. S., Ham, B. J., Pyun, S. B., Kang, S. H., and Kim, B. J. (2018). Current clinical applications of diffusion-tensor imaging in neurological disorders. *J. Clin. Neurol.* 14, 129–140. doi: 10.3988/jcn.2018.14.2.129

Takahashi, T., Arai, N., Shimamura, M., Suzuki, Y., Yamashita, S., Iwamoto, H., et al. (2005). Autopsy case of acute encephalopathy linked to familial hemiplegic migraine with cerebellar atrophy and mental retardation. *Neuropathology* 25, 228–234. doi: 10.1111/j.1440-1789.2005.00604.x

Talati, A., Pantazatos, S. P., Hirsch, J., and Schneier, F. (2015). A pilot study of gray matter volume changes associated with paroxetine treatment and response in social anxiety disorder. *Psychiatry Res. Neuroimaging* 231, 279–285. doi: 10.1016/j.pscychresns.2015.01.008

Tanaka, M., Kunimatsu, J., Suzuki, T. W., Kameda, M., Ohmae, S., Uematsu, A., et al. (2021). Roles of the cerebellum in motor preparation and prediction of timing. *Neuroscience* 462, 220–234. doi: 10.1016/j.neuroscience.2020.04.039

Tao, X. Y., Yan, Z. Y., Meng, J. H., Wang, W., Dai, Q. L., Zhou, Q. F., et al. (2022). The efficacy and safety of atogepant for the prophylactic treatment of migraine: evidence from randomized controlled trials. *J. Headache Pain* 23:19. doi: 10.1186/s10194-022-01391-2

Terwindt, G. M., Ophoff, R. A., Haan, J., Vergouwe, M. N., van Eijk, R., Frants, R. R., et al. (1998). Variable clinical expression of mutations in the P/Q-type calcium channel gene in familial hemiplegic migraine. *Neurology* 50, 1105–1110. doi: 10.1212/wnl.50.4.1105

Teune, T. M., van der Burg, J., van der Moer, J., Voogd, J., and Ruigrok, T. J. H. (2000). Topography of cerebellar nuclear projections to the brain stem in the rat. *Prog. Brain Res.* 124, 141–172. doi: 10.1016/S0079-6123(00)24014-4

Thomsen, L. L., Eriksen, M. K., Roemer, S. F., Andersen, I., Olesen, J., and Russell, M. B. (2002). A population-based study of familial hemiplegic migraine suggests revised diagnostic criteria. *Brain* 125, 1379–1391. doi: 10.1093/brain/awf132

Tillfors, M., Furmark, T., Marteinsdottir, I., and Fredrikson, M. (2002). Cerebral blood flow during anticipation of public speaking in social phobia: a PET study. *Biol. Psychiatry* 52, 1113–1119. doi: 10.1016/s0006-3223(02)01396-3

Trageser, J. C., and Keller, A. (2004). Reducing the uncertainty: gating of peripheral inputs by zona incerta. *J. Neurosci.* 24, 8911–8915. doi: 10.1523/JNEUROSCI.3218-04.2004

van Dongen, R. M., Zielman, R., Noga, M., Dekkers, O. M., Hankemeier, T., van den Maagdenberg, A. M. J. M., et al. (2017). Migraine biomarkers in cerebrospinal fluid: a systematic review and meta-analysis. *Cephalalgia* 37, 49–63. doi: 10.1177/0333102415625614

Van Overwalle, F., Manto, M., Cattaneo, Z., Clausi, S., Ferrari, C., Gabrieli, J. D. E., et al. (2020). Consensus article: cerebellum and social cognition. *Cerebellum* 19, 833–868. doi: 10.1007/s12311-020-01155-1

Vecchia, D., and Pietrobon, D. (2012). Migraine: a disorder of brain excitatory-inhibitory balance? *Trends Neurosci.* 35, 507–520. doi: 10.1016/j.tins.2012.04.007

Vianna, D. M. L., and Brandao, M. L. (2003). Anatomical connections of the periaqueductal gray: specific neural substrates for different kinds of fear. *Braz. J. Med. Biol. Res.* 36, 557–566. doi: 10.1590/s0100-879x2003000500002

Vighetto, A., Froment, J. C., Trillet, M., and Aimard, G. (1988). Magnetic resonance imaging in familial paroxysmal ataxia. *Arch. Neurol.* 45, 547–549. doi: 10.1001/archneur.1988.00520290083018

Vincent, M., and Hadjikhani, N. (2007). The cerebellum and migraine. *Headache* 47, 820–833. doi: 10.1111/j.1526-4610.2006.00715.x

Wang, M., Castonguay, W. C., Duong, T. L., Huebner, M. W., Flinn, H. C., Greenway, A. M., et al. (2022a). Stimulation of CGRP-expressing neurons in the medial cerebellar nucleus induces light and touch sensitivity in mice. *Neurobiol. Pain* 12:100098. doi: 10.1016/j.ynpai.2022.100098

Wang, M., Duong, T. L., Rea, B. J., Waite, J. S., Huebner, M. W., Flinn, H. C., et al. (2022b). CGRP Administration into the cerebellum evokes light aversion, tactile hypersensitivity and nociceptive squint in mice. *Front. Pain Res. (Lausanne)* 3:861598. doi: 10.3389/fpain.2022.861598

Wang, J.-J., Chen, X., Sah, S. K., Zeng, C., Li, Y. M., Li, N., et al. (2016). Amplitude of low-frequency fluctuation (ALFF) and fractional ALFF in migraine patients: a resting-state functional MRI study. *Clin. Radiol.* 71, 558–564. doi: 10.1016/j.crad.2016.03.004

Wang, T., Liu, J., Zhang, J., Zhan, W., Li, L., Wu, M., et al. (2016). Altered resting-state functional activity in posttraumatic stress disorder: a quantitative meta-analysis. *Sci. Rep.* 6:27131. doi: 10.1038/srep27131

Wang, Q. P., and Nakai, Y. (1994). The dorsal raphe - an important nucleus in pain modulation. *Brain Res. Bull.* 34, 575–585. doi: 10.1016/0361-9230(94)90143-0

Wang, M., Wattiez, A.-S., and Russo, A. F. (2021). "CGRP antibodies for animal models of primary and secondary headache disorders," in *Monoclonal Antibodies in Headache: From Bench to Patient*, eds A. Maassen van den Brink and P. Martelletti (Cham: Springer International Publishing), 69–97.

Warfvinge, K., and Edvinsson, L. (2019). Distribution of CGRP and CGRP receptor components in the rat brain. *Cephalalgia* 39, 342–353. doi: 10.1177/0333102417728873

Warfvinge, K., Edvinsson, L., Pickering, D. S., and Sheykhzade, M. (2019). The presence of calcitonin gene-related peptide and its receptors in rat, pig and human brain: species differences in calcitonin gene-related peptide pharmacology. *Pharmacology* 104, 332–341. doi: 10.1159/000502471

Warwick, J. M., Carey, P., Jordaan, G. P., Dupont, P., and Stein, D. J. (2008). Resting brain perfusion in social anxiety disorder: a voxel-wise whole brain comparison with healthy control subjects. *Prog. Neuropsychopharmacol. Biol. Psychiatry* 32, 1251–1256. doi: 10.1016/j.pnpbp.2008.03.017

Watson, T. C., Obiang, P., Torres-Herraez, A., Watilliaux, A., Coulon, P., Rochefort, C., et al. (2019). Anatomical and physiological foundations of cerebello-hippocampal interaction. *eLife* 8:e41896. doi: 10.7554/eLife.41896

Wattiez, A. S., O'Shea, S. A., Ten Eyck, P., Sowers, L. P., Recober, A., Russo, A. F., et al. (2020). Patients with vestibular migraine are more likely to have occipital headaches than those with migraine without vestibular symptoms. *Headache* 60, 1581–1591. doi: 10.1111/head.13898

Wei, H. L., Chen, J. A., Chen, Y. C., Yu, Y. S., Zhou, G. P., Qu, L. J., et al. (2020). Impaired functional connectivity of limbic system in migraine without aura. *Brain Imaging Behav.* 14, 1805–1814. doi: 10.1007/s11682-019-00116-5

Westenbroek, R. E., Sakurai, T., Elliott, E. M., Hell, J. W., Starr, T. V. B., Snutch, T. P., et al. (1995). Immunochemical identification and subcellular-distribution of the alpha 1A subunits of brain calcium channels. *J. Neurosci.* 15, 6403–6418. doi: 10.1523/JNEUROSCI.15-10-06403.1995

Wright, K. M., Jhou, T. C., Pimpinelli, D., and McDannald, M. A. (2019). Cue-inhibited ventrolateral periaqueductal gray neurons signal fear output and threat probability in male rats. *eLife* 8:e50054. doi: 10.7554/eLife.50054

Yang, F. C., Chou, K. H., Lee, P. L., Yin, J. H., Chen, S. Y., Kao, H. W., et al. (2018). Patterns of gray matter alterations in migraine and restless legs syndrome. *Ann. Clin. Transl. Neurol.* 6, 57–67. doi: 10.1002/acn3.680

Yelle, M. D., Oshiro, Y., Kraft, R. A., and Coghill, R. C. (2009). Temporal filtering of nociceptive information by dynamic activation of endogenous pain modulatory systems. *J. Neurosci.* 29, 10264–10271. doi: 10.1523/JNEUROSCI.4648-08.2009

Yin, T., Sun, G. J., Tian, Z. L., Liu, M. L., Gao, Y. J., Dong, M. K., et al. (2020). The spontaneous activity pattern of the middle occipital gyrus predicts the clinical efficacy of acupuncture treatment for migraine without aura. *Front. Neurol.* 11:588207. doi: 10.3389/fneur.2020.588207

Zhang, D., Huang, X. B., Su, W., Chen, Y. C., Wang, P., Mao, C. N., et al. (2020). Altered lateral geniculate nucleus functional connectivity in migraine without aura: a resting-state functional MRI study. *J. Headache Pain* 21:17. doi: 10.1186/s10194-020-01086-6

Zhang, J., Su, J., Wang, M., Zhao, Y., Zhang, Q. T., Yao, Q., et al. (2017). The sensorimotor network dysfunction in migraineurs without aura: a resting-state fMRI study. *J. Neurol.* 264, 654–663. doi: 10.1007/s00415-017-8404-4

Zhang, J., Wang, G., Jiang, Y., Dong, W., Tian, Y., and Wang, K. (2012). The study of time perception in migraineurs. *Headache* 52, 1483–1498. doi: 10.1111/j.1526-4610.2012.02222.x

Zhang, X. Y., Wang, J. J., and Zhu, J. N. (2016). Cerebellar fastigial nucleus: from anatomic construction to physiological functions. *Cereb. Ataxias* 3:9. doi: 10.1186/s40673-016-0047-1

Zhen, L. L., Miao, B., Chen, Y. Y., Su, Z., Xu, M. Q., Fei, S. J., et al. (2018). Protective effect and mechanism of injection of glutamate into cerebellum fastigial nucleus on chronic visceral hypersensitivity in rats. *Life Sci.* 203, 184–192. doi: 10.1016/j.lfs.2018.04.043

Ziegeler, C., Mehnert, J., Asmussen, K., and May, A. (2020). Central effects of erenumab in migraine patients: an event-related functional imaging study. *Neurology* 95, e2794–e2802. doi: 10.1212/WNL.0000000000010740

Zielman, R., Teeuwisse, W. M., Bakels, F., Van der Grond, J., Webb, A., van Buchem, M. A., et al. (2014). Biochemical changes in the brain of hemiplegic migraine patients measured with 7 tesla 1H-MRS. *Cephalalgia* 34, 959–967. doi: 10.1177/0333102414527016

frontiers | Frontiers in Cellular Neuroscience

TYPE Original Research
PUBLISHED 15 November 2022
DOI 10.3389/fncel.2022.998408

OPEN ACCESS

EDITED BY
Marco Martina,
Northwestern University, United States

REVIEWED BY
Josef P. Kapfhammer,
University of Basel, Switzerland
Giorgio Grasselli,
University of Genoa, Italy

*CORRESPONDENCE
Marija Cvetanovic
mcvetano@umn.edu

†These authors have contributed equally to this work

SPECIALTY SECTION
This article was submitted to Cellular Neurophysiology, a section of the journal Frontiers in Cellular Neuroscience

RECEIVED 01 August 2022
ACCEPTED 27 October 2022
PUBLISHED 15 November 2022

CITATION
Borgenheimer E, Hamel K, Sheeler C, Moncada FL, Sbrocco K, Zhang Y and Cvetanovic M (2022) Single nuclei RNA sequencing investigation of the Purkinje cell and glial changes in the cerebellum of transgenic Spinocerebellar ataxia type 1 mice. *Front. Cell. Neurosci.* 16:998408. doi: 10.3389/fncel.2022.998408

Single nuclei RNA sequencing investigation of the Purkinje cell and glial changes in the cerebellum of transgenic Spinocerebellar ataxia type 1 mice

Ella Borgenheimer[1†], Katherine Hamel[1†], Carrie Sheeler[1†], Francisco Labrada Moncada[1], Kaelin Sbrocco[1], Ying Zhang[1,2] and Marija Cvetanovic[1,3*]

[1]Department of Neuroscience, University of Minnesota, Minneapolis, MN, United States, [2]Minnesota Supercomputing Institute, University of Minnesota, Minneapolis, MN, United States, [3]Institute for Translational Neuroscience, University of Minnesota, Minneapolis, MN, United States

Glial cells constitute half the population of the human brain and are essential for normal brain function. Most, if not all, brain diseases are characterized by reactive gliosis, a process by which glial cells respond and contribute to neuronal pathology. Spinocerebellar ataxia type 1 (SCA1) is a progressive neurodegenerative disease characterized by a severe degeneration of cerebellar Purkinje cells (PCs) and cerebellar gliosis. SCA1 is caused by an abnormal expansion of CAG repeats in the gene *Ataxin1* (*ATXN1*). While several studies reported the effects of mutant ATXN1 in Purkinje cells, it remains unclear how cerebellar glia respond to dysfunctional Purkinje cells in SCA1. To address this question, we performed single nuclei RNA sequencing (snRNA seq) on cerebella of early stage *Pcp2-ATXN1[82Q]* mice, a transgenic SCA1 mouse model expressing mutant ATXN1 only in Purkinje cells. We found no changes in neuronal and glial proportions in the SCA1 cerebellum at this early disease stage compared to wild-type controls. Importantly, we observed profound non-cell autonomous and potentially neuroprotective reactive gene and pathway alterations in Bergmann glia, velate astrocytes, and oligodendrocytes in response to Purkinje cell dysfunction.

KEYWORDS

cerebellum, SCA1, Purkinje cells, Bergmann glia, oligodendrocytes, velate astrocytes

Introduction

Glial cells play key roles required for normal brain function (Barres, 2008). These roles include maintaining homeostasis of ions, neurotransmitters, and water, providing neurotrophic and energy support, removal of unused synapses, and fast propagation of neuronal potentials (Kofuji and Newman, 2004; Parkhurst et al., 2013; Perea et al., 2014; Verkhratsky and Nedergaard , 2018). In most neurodegenerative diseases, glial cells undergo reactive gliosis: a process that includes gene expression, morphological, and functional changes (Burda and Sofroniew, 2014; Escartin et al., 2021). These glial changes have shown an active role in the pathogenesis of neurodegenerative diseases (Lobsiger and Cleveland, 2007; Sheeler et al., 2020). In some situations, reactive gliosis was beneficial by delaying and ameliorating pathogenesis, but reactive glia may also be harmful and can exacerbate neuronal dysfunction and disease pathogenesis (Heneka et al., 2014; Pekny et al., 2014; Kim et al., 2018). The neuroprotective or harmful nature of reactive glia likely depends on many factors including the stage of disease progression, the signaling that triggers gliosis, and glial gene expression changes.

Glia can become reactive in response to external and/or internal signaling. For instance, in all diseases, glia respond to neuronal dysfunction via external/non-cell autonomous signaling. Additionally, in some neurodegenerative diseases, mutant proteins are expressed within glial cells and can contribute to reactive changes in internal/cell-autonomous manner. Investigating internal (cell–autonomous) and external (non-cell-autonomous) reactive glial gene expression changes and their effect on neurons will lead to a better understanding of the pathogenesis of neurodegenerative diseases.

Spinocerebellar ataxia type-1 (SCA1) is a dominantly inherited neurodegenerative disorder caused by the abnormal expansion of CAG repeats in the *Ataxin-1* (*ATXN1)* gene (Orr et al., 1993). Expansion of 39 or more CAG repeats drives severe pathology of cerebellar Purkinje cells and cerebellar gliosis. SCA1 symptoms include loss of balance and coordination, swallowing and speech difficulties, impairments in cognition and mood, and premature death (Orr and Zoghbi, 2007; Jacobi et al., 2013; Rüb et al., 2013; Moriarty et al., 2016; Diallo et al., 2017, 2019). While *ATXN1*-targeting antisense oligonucleotides (ASOs) show promise in pre-clinical trials (Friedrich et al., 2018), there are currently no disease-modifying treatments available for SCA1. The lack of available treatment options highlights the need for increased understanding of SCA1 pathogenesis. This is particularly relevant when considering early disease stages where the development of effective therapies may lead to the delayed onset, reversal, or slowing of disease phenotypes.

Previous studies used mouse models of SCA1 to demonstrate that mutant ATXN1 causes gene expression changes in Purkinje cells. In addition, we have previously shown that glia undergo reactive gliosis in SCA1 mice and contribute to disease pathogenesis in a stage-of-disease dependent manner. Specifically, we found that glia are neuroprotective early and harmful late in SCA1 disease progression, thus suggesting that glial function could be a key therapeutic target for SCA1 (Kim et al., 2018). Our aim in this work was to investigate the underlying changes occurring in glia across the SCA1 cerebellum and, in doing so, to highlight key pathways that may be important for glial responses to PC dysfunction. To accomplish this, we used the transgenic SCA1 mouse model, *Pcp2- ATXN1[82Q]* line which expresses mutant ATXN1 only the cerebellar Purkinje cells (Burright et al., 1995). This allows us to specifically identify the non-cell autonomous pathways activated in glia by dysfunctional Purkinje cells without the confounding factor of gene expression changes driven by mutant ATXN1 expression within glial cells."

To investigate gene expression changes at the cell-type level we used single-nuclei RNA sequencing. Bulk RNA sequencing has been useful for determining cerebellum-wide changes in the gene expression in SCA1 mouse models (Serra et al., 2004; Ingram et al., 2016a; Driessen et al., 2018). However, bulk RNA sequencing precludes the detection of transcriptional changes at the single-cell level and is also confounded by the possible change in the proportion of cell types (Klein et al., 2015; Lacar et al., 2016; Habib et al., 2017). Previous studies have shown advantages of single nuclei over single cell RNAsequencing. These include preservation of a larger number of cells across multiple subtypes, while minimizing the effects of cell dissociation on gene expression, and enriching for transcripts that are being actively transcribed *in vivo* (Lacar et al., 2016; Habib et al., 2017). Thus, we isolated nuclei from cerebella of SCA1 mice and wild-type controls, and used rigorous analysis to investigate gene expression changes in cerebellar Purkinje cells, and three types of cerebellar glia: Bergmann glia, velate astrocytes, and oligodendrocytes.

Materials and methods

Mice

The creation of the *Pcp2-ATXN1[82Q]* mice was previously described (Burright et al., 1995). We have backcrossed these mice onto the C57BL/6 background for 10 generations. As CAG repeats are unstable and tend to shrink in mice, we periodically sequence the CAG region to evaluate number of repeats (Gatchel and Zoghbi, 2005). At the time of experiments the average number of CAG repeats in our colony was 71. We used 12 week old *Pcp2-ATXN1[82Q]* mice and their littermate wild-type control mice. Animal experimentation was approved by the Institutional Animal Care and Use Committee (IACUC) of University of Minnesota and was conducted in accordance with the National Institutes of Health's (NIH)

Principles of Laboratory Animal Care (86–23, revised 1985), and the American Physiological Society's Guiding Principles in the Use of Animals (National Research Council (Us) Committee for the Update of the Guide for the Care and Use of Laboratory Animals, 2011).

Nuclei isolation

Nuclei for RNA sequencing were isolated using detergent mechanical lysis protocol as previously described (Matson et al., 2018). Briefly, frozen or fresh whole cerebellum was placed into 1.5mL tube with 500uL pre-chilled detergent lysis buffer [low sucrose buffer (LSB) (sucrose 0.32M, 10 mM HEPES, 5mM CaCl2, 3mM MgAc, 0.1mM EDTA, 1mM DTT) with 0.1% Triton-X] and the tissue was homogenized using a mechanical homogenizer. A 40um strainer was placed over a pre-chilled 50mL tube and pre-wetted with 1ml LSB. 1mL of LSB was added to the tube containing the crude nuclei in the lysis buffer and mixed gently by pipetting (2-3 times). Crude nuclei prep was next passed over the 40uM strainer into the pre-chilled 50mL tube, washed with 1 ml LSB, and centrifuged at 3,200 g for 10 min at 4C.

The pellet was resuspended in 3mL of LSB while gently swirling to remove the pellet from the wall, facilitating resuspension, and left on ice for 2 min. The suspension was transferred to an Oak Ridge tube and nuclei were homogenized in LSB for 15-30 s, all while keeping the sample on ice. Using a serological pipette, 12.5mL of density sucrose buffer (sucrose 1M, 10 mM HEPES, 3mM MgAc, 1mM DTT) was layered underneath the LSB homogenate, taking care not to create a bubble which would disrupt the density layer. Samples were then centrifuged at 3,200 g for 20 min at 4C and pelleted nuclei were resuspended in the resuspension solution (PBS, 0.4 mg/ml BSA, 0.2 U/μl RNAse inhibitor). Nuclei were filtered through a 40um pore-size strainer followed by a 30um and 20um pore-size strainers. A small sample of nuclei was pelleted and added to a slide with VectaShield with DAPI to verify single nuclei isolation under fluorescent microscope (**Supplementary Figure 1**). The nuclear suspensions were processed by the Genomic Core at the University of Minnesota using 10X Chromium 3′ GEX Capture to Library Preparation (Chromium Next GEM Single Cell 3′ Reagent Kits v3.1 with Single Cell 3′ v3.1 Gel Beads and Chromium Next GEM Chip G).

Sequencing and analysis

Library quality control was performed using the MiSeq system to estimate average numbers of nuclei per donor mouse. Then all nuclei from 6 donors were multiplexed and sequenced on two independent runs on the Illumina NovaSeq platform, using 1 full lane of S4 chip each time. Sequencing depth ranges from ∼41,000 to ∼120,000 reads per nuclei. Raw, demultiplexed fastq files were analyzed by CellRanger (v5.0.1) using reference genome mm10 (refdata-gex-mm10-2020-A, with the addition of human ATXN1 gene locus), with the option that allows alignment to un-spliced pre-mRNAs (–include-introns). The raw UMI count matrix was cleaned via DIEM algorithm (Alvarez et al., 2020). In summary, DIEM models cell debris using cells with less than 1,000 UMI detected (min_counts = 1,000). In case of overfitting, we increased the threshold to 3,000 (only for the two samples sequenced in the first NovaSeq run). Then the debris scores were manually inspected to exclude true debris. The cleaned gene count table per donor was analyzed with R (v4.1.0) package Seurat (v 4.0.4) for cell type clustering and visualization. Further cell type identification was accomplished with SingleR (v 1.6.1) using DropViz (Saunders et al., 2018). Cerebellum MetaCells reference. We assigned cell types by requiring the same Seurat cluster and the same SingleR annotation.

For identified cell types of Bergmann Cells, Velate Astrocytes, Granule Neurons, Purkinje Neurons, and Oligodendrocytes, scran (v 1.20.1) was used to normalize the single cell expression matrix, followed by limma-trend (v 3.48.3) to test for differential gene expression. Sample batches were considered as an independent factor in the design matrix of the statistical test (design = ∼ genotype + batch). P values were adjusted using Benjamini-Hockberg method. Differential gene expression was determined by an adjusted p-values of 0.05. The lists of differentially expressed genes from different cell types were further analyzed for GO term enrichment using ClusterProfiler (v 4.0.5). Detailed information on the code we used can be found at https://github.com/yingzhang121/snSeq_SCA1.

Visualization of the results was generated using various R packages, including Seurat, ClusterProfiler, enrichplot (v 1.12.2), and ggplot2 (v 3.3.5).

Data is deposited at https://www.ncbi.nlm.nih.gov/geo/query/acc.cgi?acc=GSE215336. To review GEO accession GSE215336 before it becomes public (when results are accepted for publication) please enter token ibqzeqsivrodhkr into the box.

Immunofluorescent staining

IF was performed on a minimum of six different floating 45-μm-thick brain slices from each mouse (six technical replicates per mouse per region or antibody of interest) as we have previously described (Sheeler et al., 2021). We used primary antibody against DNER (Invitrogen, PA5-99872). Confocal images were acquired using a confocal microscope (Olympus FV1000, Leica Stellaris 8) using a 20X oil objective. Z-stacks consisting of twenty non-overlapping 1-μm-thick slices were

10.3389/fncel.2022.998408

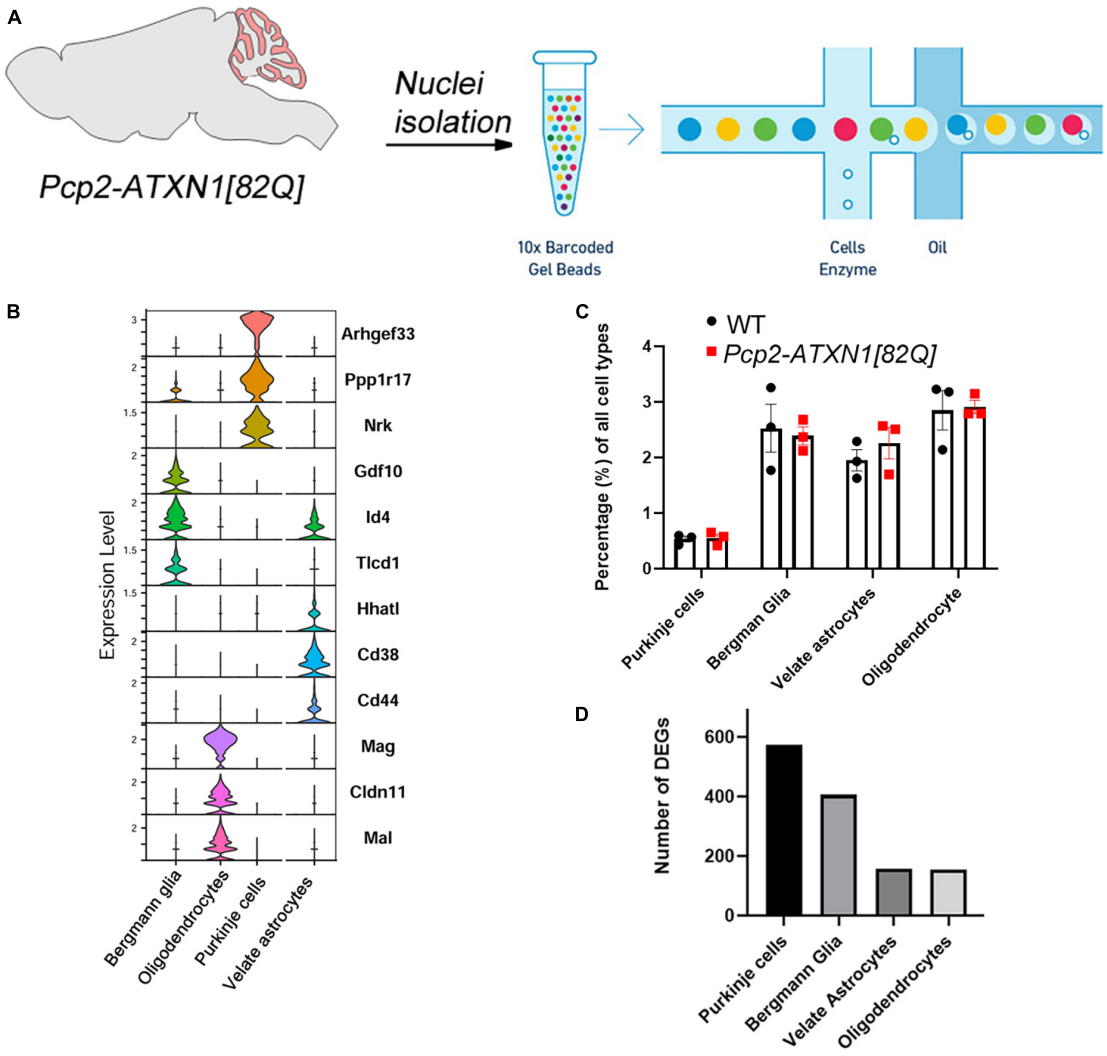

FIGURE 1
Experimental schematics, cell composition and DEGs per cell type in *Pcp2-ATXN1[82Q]* mice. **(A)** Schematic pipeline of SCA1 snRNA-seq and analysis of mouse (*N* = 6 mice) cerebellum (WT *N* = 3, *Pcp2- ATXN1[82Q]* SCA1 *N* = 3). Individual nuclei were isolated from the cerebella of 12 weeks old *Pcp2- ATXN1[82Q]* mice and wild-type littermate controls (*N* = 3 of each). After passing library QC nuclei were sequenced on Illumina NovaSeq platform. **(B)** Normalized violin plots showing expression of cell type-specific marker genes for each mouse cluster to evaluate cell type annotation. 47,894 high-quality, snRNAseq profiles were imported into Seurat for clustering analysis and nuclei were classified into the cell types with SingleR (v 1.6.1) using DropViz Cerebellum MetaCells reference. **(C)** Relative proportions of cell types in WT and SCA1 mice. Average percentages of Purkinje cells (PC), Bergman Glia (BG), velate astrocytes (VA), and oligodendrocytes in *Pcp2- ATXN1[82Q]* mice and wild-type littermate controls (*N* = 3 of each) were calculated as percentage of total cells. Data is presented as mean ± SEM with average values for each mouse represented by a dot. Two-way ANOVA with Sidak's multiple comparison did not detect any significant difference between *Pcp2- ATXN1[82Q]* mice and wild-type littermate controls (**Supplementary Table 2**). **(D)** Total number of differentially expressed genes (DEG) in each cell type. *P* values were adjusted using Benjamini-Hockberg method. Significant differential gene expression was determined by an adjusted p-values ≤ 0.05.

taken of each stained brain slice per brain region (i.e., six z-stacks per mouse, each taken from a different brain slice). The laser power and detector gain were standardized and fixed between mice, and all images for mice within a cohort were acquired in a single imaging session to allow for quantitative comparison. To quantify relative intensity of staining we measured the average signal intensity in the region of interest that included PCs soma and dendrites.

Reverse transcription and quantitative polymerase chain reaction (RTqPCR)

Total RNA was extracted from dissected mouse cerebella, medulla, and hippocampus using TRIzol (Life Technologies), and RT-qPCR was performed as described previously (Lobsiger and Cleveland, 2007). We used IDT Primetime primers for the following genes: *Ptch2*, *Dner* and *Gli*. Relative mRNA levels were

calculated using 18S RNA as a control and wild-type mice as a reference using $2^{-\Delta\Delta Ct}$ as previously described (Lobsiger and Cleveland, 2007).

Statistics

Wherever possible, sample sizes were calculated using power analyses based on the standard deviations from our previous studies, significance level of 5%, and power of 90%. For RNA sequencing data, limma-trend (v 3.48.3) was used to test for differential gene expression. Sample batches were considered as an independent factor in the design matrix of the statistical test (design = ~ genotype + batch). P values were adjusted using Benjamini-Hockberg method. Differential gene expression was determined by an adjusted p-values of 0.05. For all other results, statistical tests were performed with GraphPad Prism 7.0 (GraphPad Software Inc.). Data was analyzed using unpaired Student's t-test with Welch's correction (RTqPCR of cerebellar mRNA from wild-type and *Pcp2-ATXN1[82Q]* mice in **Supplementary Figures 2, 4A, 6B,** and intensity of DNER staining in **Supplementary Figure 4D**), and two-way ANOVA (cell type and genotype) followed by the Sidak's multiple comparison test (relative abundance of each cell type in wild-type and *Pcp2-ATXN1[82Q]* mice, **Figure 1C**) or Tukey's multiple comparison test (percentage of cerebellar cell types expressing endogenous mouse *Atxn1[2Q]* or transgenic human *ATXN1[82Q]* in wild-type and *Pcp2-ATXN1[82Q]* mice, **Supplementary Figure 3**). Outliers were determined using GraphPad PRISM's Robust regression and Outlier removal (ROUT) with a Q = 1% for non-biased selection. Raw data and exact p values are provided in **Supplementary Tables 1–4**.

Results

Mutant ATXN1 expression in Purkinje cells does not alter proportions of cerebellar cells

In this study, we sought to determine the non-cell autonomous reactive gene expression changes in cerebellar glia in response to mutant ATXN1-driven Purkinje cell dysfunction. To ensure that glial cells are affected solely in response to neuronal dysfunction and not because of cell-autonomous expression of expanded ATXN1, we have used a Purkinje cell specific transgenic mouse model of SCA1, *Pcp2-ATXN1[82Q]* mice (Burright et al., 1995). In these mice, mutant *ATXN1* with 82 CAG repeats is selectively expressed under *Purkinje cell protein 2 (Pcp2)* promoter in cerebellar Purkinje cells. We chose to examine glial changes at 12 weeks of age to capture an early stage of SCA1 pathology when disease is still reversible (Zu et al., 2004) and as such therapeutically noteworthy.

Previous bulk RNA sequencing studies showed significant gene expression changes underlying PC dysfunction in the cerebella at 12 weeks, but no detectable PC death (Ingram et al., 2016b; Mellesmoen et al., 2018). We have confirmed that many of these genes, which are considered representative of Purkinje cell pathology in SCA1 by the field, are changed in cerebella of our mice at this time point. These include *Calbindin 1(Calb1)*, *Purkinje cell protein 4* (*Pcp4*), *Regulator of G protein signaling (Rgs8)*, *inositol 1,4,5-trisphosphate receptor* (*ITPR*), *inositol polyphosphate-5-phosphatase (Inpp5)* and *GTPase Activating Rap/RanGAP Domain Like 3 (Garnl3)* (Ingram et al., 2016b). All of these genes were significantly downregulated in our 12 week old mice, indicating that molecular aspects of mutant ATXN1 on PCs were easily detectable in bulk tissue (**Supplementary Figure 2** and **Supplementary Table 1**).

To investigate the gene expression changes attributable to specific cell types, we isolated individual nuclei from the cerebella of six 12 week old SCA1 and littermate control mice (**Figure 1A** and **Supplementary Figure 2**). Nuclei were captured and barcoded followed by single nuclei RNA sequencing (snRNAseq, **Figure 1A**; Klein et al., 2015; Zilionis et al., 2017). After removing debris nuclei using semi-supervised machine learning classifier Debris Identification using Expectation Maximization (DIEM) (Alvarez et al., 2020), we identified a total of 47,894 high-quality, snRNAseq profiles. They were imported into Seurat for clustering analysis and visualization. We then classified nuclei into the cell types with SingleR (v 1.6.1) using DropViz Cerebellum MetaCells reference (Saunders et al., 2018; **Figure 1B**).

First, we wanted to determine whether cellular composition of the cerebellum is altered in SCA1, e.g., whether expression of mutant ATXN1 in Purkinje cells leads to the relative increase or decrease in the numbers of the main cerebellar cell types, including Purkinje cells (PCs), Bergmann glia (BG), velate astrocytes (VA) and oligodendrocytes (OL). We calculated the percentage of each of these cell types by dividing the number of nuclei identified as a specific cell type by the total number of nuclei. Comparing *Pcp2-ATXN1[82Q]* and wild-type mice, we have not found statistically significant difference in the relative percentages of Purkinje cells (0.55 ± 0.068 vs. 0.53 ± 0.052), Bergmann glia (2.39 ± 0.16 vs. 2.52 ± 0.43), velate astrocytes (2.26 ± 0.28 vs. 1.95 ± 0.19), nor oligodendrocytes (2.91 ± 0.12 vs. 2.85 ± 0.35) indicating that at this early disease stage we cannot detect a change in the cerebellar cell type composition in *Pcp2-ATXN1[82Q]* mice (**Figure 1C** and **Supplementary Table 2**).

Additionally, we determined which cerebellar cells express wild-type mouse and mutant human *ATXN1*. We found that endogenous wild-type mouse *Atxn1[2Q]* is expressed in PCs, BG, VA, and OL (**Supplementary Figure 3A** and **Supplementary Table 3**). Furthermore, mutant human *ATXN1[82Q]* is expressed only in PC cells in *Pcp2- ATXN1[82Q]* mice, confirming the Purkinje cell expression specificity of this

line (**Supplementary Figure 3B** and **Supplementary Table 4**). Additionally, no mutant human *ATXN1* expression was found in any cell type in wild-type littermate control mice.

Selective expression of mutant ATXN1 in Purkinje cells causes significant gene expression changes in cerebellar glia

Most gene expression studies to date have focused on understanding how mutant ATXN1 affects Purkinje cells. Here we confirmed that many of the genes considered representative of Purkinje cell-specific pathology are indeed uniquely changed in Purkinje cells. In addition, we investigated gene expression changes in BG, VA and OL in response to PC pathology. Using differential gene expression (DEG) analysis, we identified genes altered in each of these four cell types. We found that each cell type is uniquely affected by ATXN1-driven PC dysfunction and demonstrate different numbers of DEGs (**Figure 1D**). Remarkably, BG and PCs had a comparable number of DEGs (575 and 406, respectively) at 12 weeks despite the fact that mutant ATXN1 is expressed only in PCs in these mice. These significant non-cell autonomous transcriptional alterations in BG may suggest that BG are highly sensitive to perturbation in PCs. Additionally, VA and OL had a notable number of DEGs (157 and 155, respectively, **Figure 1D**). These results indicate that BG, VA and OL all respond to mutant ATXN1 induced dysfunction in PCs.

Single-nuclei analysis confirms previously identified gene expression changes in Purkinje cells and identifies novel and potentially compensatory genes

Previous studies described different sub-populations of PCs based on gene expression profiles and cellular physiology (Zhou et al., 2014; Kozareva et al., 2020). Moreover, several studies have indicated that SCA1 pathology is not uniform across the cerebellum (White et al., 2021). However, most of our understanding of mutant ATXN1 gene expression changes in Purkinje cells is derived from bulk RNA sequencing analysis. This prevents any identification of altered pathology in different sub-types of Purkinje cells which may be more vulnerable or disease resistant (Serra et al., 2004; Ingram et al., 2016b). To address this, we analyzed gene expression changes in PCs and compared the results to previously reported transcriptional alterations in SCA1.

We identified 575 DEGs in Purkinje cells (false discovery rate adjusted p value p.adj/q < 0.05), 56% of which were downregulated and 44% upregulated (**Figure 2A**). This prevalence of downregulated genes is consistent with previous results and is generally thought to reflect the direct repressive effect of mutant ATXN1 on PC gene transcription (Ingram et al., 2016b).

Among the top ten upregulated genes were genes known for their roles in neurodevelopment including *Heparan Sulfate 6-O-Sulfotransferase 3* (*Hs6st3*), *Adhesion G Protein-Coupled Receptor L3* (*Adgrl3*), *Contactin 5* (*Cntn5*), and *Neuregulin 1* (*Nrg1*) (Mei and Xiong, 2008; Cocchi et al., 2016; El Hajj et al., 2017; Moon and Zhao, 2021). In addition, SCA1 PCs had increased expression of *RALY RNA Binding Protein-like (Ralyl),*which is known as an Alzheimer's disease cognitive reserve gene (Zhang et al., 2020) (**Figures 2A–C**).

We also found increased expression of synaptic vesicle genes encoding for vacuolar V-type ATP-ase subunits (*Atp6v0c*, *Atpgv0a1*, and *Atp6v1h*) that provide energy in the form of ATP to fuel transport of neurotransmitters into synaptic vesicles and *Solute carrier family 32a1 (Slc32a1)*, encoding vesicular GABA transporter VGAT (Vesicular GABA and Glycine Transporter). Increased expression of genes providing energy for GABA transport into vesicles as well as increased expression of vesicular GABA transporter could potentially result in higher GABA content per vesicle and increased GABA release from SCA1 PCs.

Previous work has demonstrated marked changes in PC firing in SCA1 which indicate dysfunctions in signaling and cellular physiology (Bushart et al., 2021). In keeping with this, we observed a proportion of gene expression changes suggestive of PCs reduced ability to respond to stimuli. This is indicated by the downregulated expression of genes encoding extracellular matrix proteins (*Mucin3a* (*Muc3a*), *Collagen type 5 alpha1 (Col5a1)*, *Collagen Type 8 Alpha 1 (Col18a*) (Tsai et al., 2021), proteins involved in Wnt and GPCR signaling (*leucine rich repeat containing G protein-coupled receptor 5 (Lgr5)* that enhances Wnt signaling and *phosphodiesterase 10 (Pde10)* that plays a role in signal transduction by regulating the intracellular concentration of cyclic nucleotides cAMP and cGMP) (Carmon et al., 2012), signaling scaffolding protein *Breast cancer anti-estrogen resistance protein 1 (Bcar1)* (Furuichi et al., 2011; Maria del Pilar et al., 2017), and small brain specific non-coding RNA BC1 that regulates dendritic translation (Zhong et al., 2009; Robeck et al., 2016). This perturbed communication of SCA1 PCs is further supported by altered expression of genes involved in calcium and glutamatergic signaling. These downregulated genes encode for calcium voltage gated channels Cav2.1 and Cav3.1 (*calcium voltage-gated channel subunit alpha1 A (Cacna1a), Cacna2d2,* and *Cacna1g*), calcium endoplasmic reticulum pumps SERCA1 and SERCA2 (*ATPase Sarcoplasmic/Endoplasmic Reticulum Ca^{2+} Transporting 2 (Atp2a2)* and *Atp2a3*), ionotropic glutamate receptors (*glutamate ionotropic receptor AMPA type subunit 2 (Gria2), Gria3, glutamate Ionotropic Receptor Delta Type Subunit 2 (Grid2), Grid2 interacting protein(Grid2ip),*

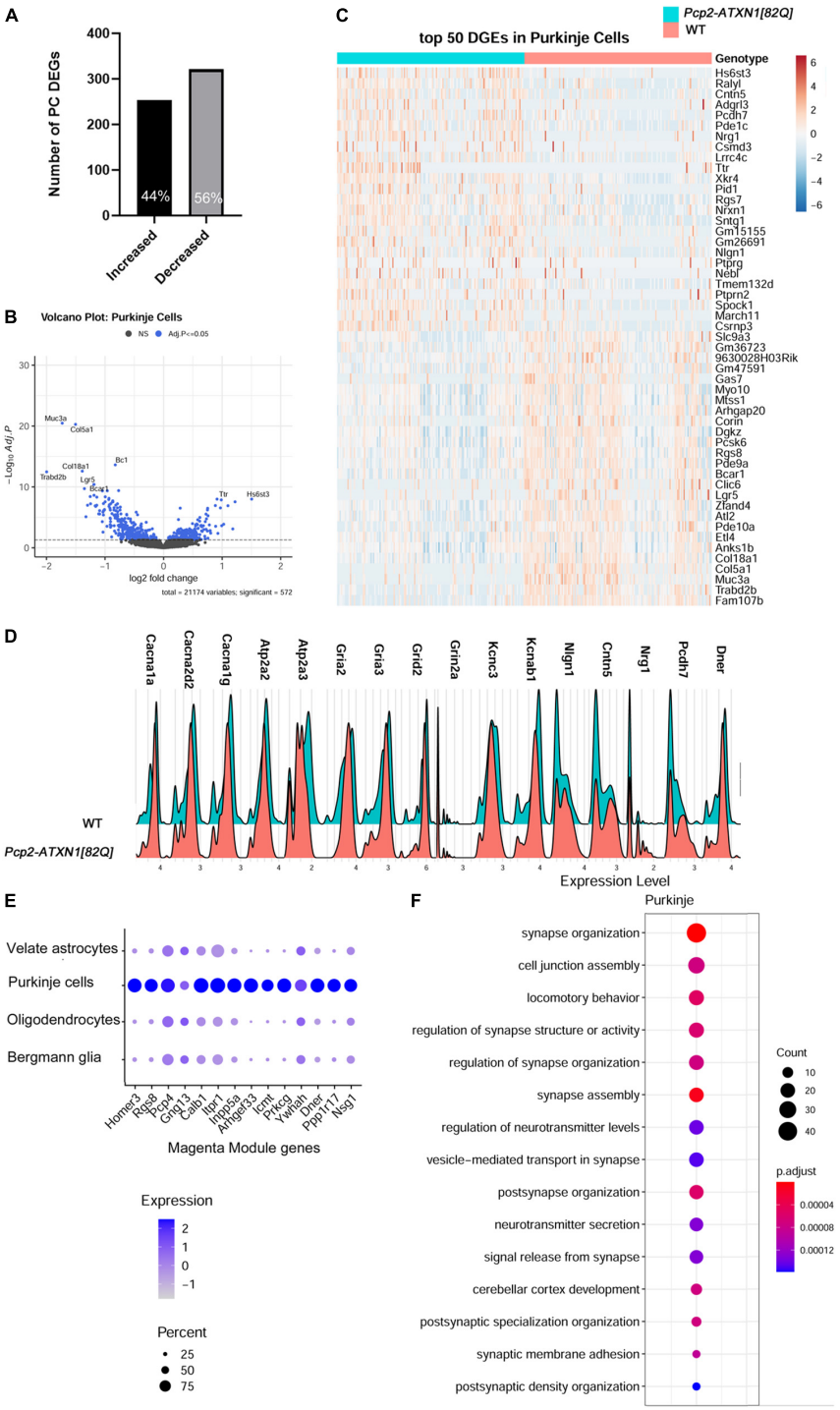

FIGURE 2
Single nuclei analysis identifies SCA1 disease associated transcriptional changes in Purkinje cells. For identified Purkinje Neurons, limma was used to test differential gene abundance between control and *Pcp2-ATXN1[82Q]* samples. *N* = 3 mice of each genotype. *P* values were adjusted using Benjamini-Hockberg method. Differential gene expression was determined by an adjusted p-values of 0.05. **(A)** Number of upregulated and downregulated differentially expressed genes (DEGs) in PCs. **(B)** Volcano plot showing DEGs of PC cluster in *Pcp2-ATXN1[82Q]* SCA1. **(C)** Heatplot displaying expression profiles of top 25 highest upregulated and downregulated PC DEGs in wild-type and *Pcp2-ATXN1[82Q]* samples determined by logFC values with adjusted *p*-values ≤0.05. *N* = 3 mice of each genotype. **(D)** Ridgeplot showing distribution of expression of selected genes in wild-type and *Pcp2-ATXN1[82Q]* Purkinje cells. **(E)** Dot plot of the differential expression of Magenta genes in Purkinje cells, Bergmann glia, velate astrocytes and oligodendrocytes with color of dot depicting expression and size of the dot depicting percentage of cells. All selected genes had adjusted *p*-value ≤ 0.05. **(F)** Pathway analysis of total DEGs between WT and *Pcp2-ATXN1[82Q]* PCs at 12 weeks of age. The color of dots depicts the adjusted *p* values, radius of the dot depicts gene counts (number of genes in the enriched pathway).

glutamate ionotropic receptor NMDA type subunit 2A (*Grin2a*), and potassium channels (*potassium Voltage-Gated Channel Subfamily C Member 3* (*Kcnc3*), associated with SCA13, and *potassium voltage-gated channel subfamily A regulatory beta subunit 1* (*Kcnab1*) (Matsuda et al., 2006; **Figures 2C–D**). These results are consistent with previous studies implicating ion channel, calcium and potassium dysregulation and synaptic dysfunction in SCA1 (Bushart and Shakkottai, 2018). Notably, several of these genes have also been associated with other ataxias including Spinocerebellar ataxia autosomal recessive 18 (*Grid2*) and Episodic Ataxia Type 1 (*Kcnab1*).

SCA1 is a progressive disease worsening with aging. Previous studies used weighted Gene Co-expression Network Analysis (WGCNA) of cerebellar bulk RNA sequencing data from *Pcp2-ATXN1[82Q]* mice to identify a specific module (the Magenta Module) as a gene network significantly correlated with SCA1 disease progression in Purkinje cells (Ingram et al., 2016b). Notably, of the 342 genes identified in the magenta module, the Allen brain atlas suggested that 94 (27%) are PC enriched, 175 genes (51%) are PC exclusive, and 31 genes (9%) belong to multiple cell types (Ingram et al., 2016b). Using single nuclei gene expression analysis, we determined that 103 (30.1%) of the previously identified Magenta Module genes are altered at 12 weeks of age in *Pcp2-ATXN1*(O'Leary et al., 2020) mice. This is consistent with previous bulk RNA sequencing studies that showed that not all of the Magenta Module genes were found to be significantly altered at 12 weeks in *Pcp2-ATXN1*(O'Leary et al., 2020) mice (Ingram et al., 2016b). Of these genes, 74 were exclusively altered in PCs (71.8%), while 29 (28.2%) were also changed in two or more cell types, including BG, VAs and OLs. Most intriguing were 13 Magenta Module genes that were changed in all four cell types (**Figure 2E**). For instance, expression of Magenta genes *Itpr1, Pcp4 and Gng13* was significantly suppressed in PCs and, to a lesser extent, in BG, VAs and OLs. As these genes, respectively, encode for proteins regulating calcium and GPCR signaling (such as inositol 3 phosphate receptor 1 (*ITPR1*) that regulates calcium release from the ER, Purkinje Cell Protein 4 (*PCP4*) that regulates calcium binding to calmodulin, and G Protein Subunit Gamma 13 (*Gng13*) that regulates G protein coupled receptor signaling), this indicates that calcium and G protein signaling are perturbed not only in PCs, as previously described, but also in BG, VAs, and OLs.

Among the genes altered in PCs, but not changed in BG, VAs, or OLs, was *Delta/Notch like EGF Repeat containing* (*Dner*). *Dner* has been previously found to be an important component of PC-BG communication whereby cell surface expression of DNER in Purkinje cells induces morphological differentiation and functional maturation of Bergmann glia. Moreover, loss of *Dner* impairs mouse motor behavior implicating its importance for cerebellar function (Eiraku et al., 2005; Tohgo et al., 2006). Reduced *Dner* expression could be a mechanism by which SCA1 PCs signal changes to BG. Using RT-qPCR, we confirmed decrease in *Dner* mRNA expression in SCA1 cerebella (41% decrease compared to WT controls, **Supplementary Figure 4A** and **Supplementary Table 1**). Furthermore, using immunohistochemistry, we found reduced levels of DNER protein in soma and dendrites of Purkinje cells in *Pcp2-ATXN1[82Q]* mice (0.679 ± 0.006 vs. 0.553 ± 0.041, ∼19% decrease compared to WT controls, **Supplementary Figures 4B–D** and **Supplementary Table 1**).

Using hierarchical enriched pathways analysis of up and downregulated genes in PCs we identified pathways involved in synapse function, including synapse organization, cell junction assembly, regulation of synapse structure or activity, synapse assembly, and regulation of neurotransmitter levels (**Figure 2F**). Among top Gene ontology (GO) pathways associated with the *upregulated* genes were synapse assembly ($q = 3.42 \times 10^{-4}$), synaptic membrane adhesion ($q = 6.1 \times 10^{-4}$), cell junction assembly ($q = 8.8 \times 10^{-4}$), synapse organization ($q = 3.2 \times 10^{-3}$) and cell junction organization ($q = 8.1 \times 10^{-3}$). Kyoto Encyclopedia of Genes and Genomes (KEGG) identified axon guidance ($q = 1.4 \times 10^{-5}$) and synaptic vesicle cycle ($q = 2.9 \times 10^{-3}$) as altered pathways. GO pathway analysis of *downregulated* genes identified calcium binding ($q = 9.8 \times 10^{-3}$), and dendrite and dendritic tree (q values of 1.45 and 1.48×10^{-5}, respectively), while top KEGG pathways of downregulated genes were long-term depression ($q = 4.9 \times 10^{-4}$), cholinergic ($q = 3.2 \times 10^{-3}$), glutamatergic ($q = 3.3 \times 10^{-3}$), serotoninergic ($q = 5.2 \times 10^{-3}$) and dopaminergic ($q = 5.5 \times 10^{-3}$) synapse and retrograde endocananbinoid signaling ($q = 7.1 \times 10^{-3}$). Alterations in calcium and glutamatergic signaling are consistent with previous results from bulk RNAseq in SCA1 cerebella. Our results build upon those previous studies by confirming that ATXN1 is driving these changes specifically in PCs. Moreover, our results indicate upregulation of pathways associated with synapse formation as potential compensatory pathways for signaling disruptions in SCA1 PCs.

Notably, most of the observed gene expression changes seem to be present only in a portion of PCs (**Figures 2C,D**). Consistent with previous studies that suggested intracerebellar differences in the expression of *hATXN1* and in PCs pathology in SCA1 mice (Chopra et al., 2020; Kozareva et al., 2020; White et al., 2021), our analysis indicated that only portion of PCs (∼25%) express detectable levels of mutant human *ATXN1* mRNA in this line (**Supplementary Figure 3B**). We named these cells *hATXN1*+ PCs, while the cells in which we did not detect human ATXN1 we named *hATXN1*- PCs. It is possible that our analysis may underestimate the number of *hATXN1*+ PCs by not detecting low human ATXN1 expression. With that caveat in mind, we next analyzed gene expression changes in SCA1 *hATXN1*+ PCs (31 cells) and *hATXN1*- PCs (110 cells) compared to PCs from wild-type mice (132 cells).

In this limited analysis, we could only identify a handful of DEGs (35) between *hATXN1*+ and *hATXN1*- PCs with at

most 1.6 fold change. We have also identified 531 DEGs in *hATXN1+* PCs and 370 DEG in *hATXN1-* PC cells compared to WT. Notably, 76.5% of the DEG in *hATXN1+* PCs were upregulated, e.g., out of 531 DEGs 406 genes were upregulated (**Supplementary Figure 5** and **Supplementary Table 5**). All of the 125 downregulated *hATXN1+* PCs genes were also downregulated in *hATXN1-* PCs. However, out of the 406 genes that were upregulated in *hATXN1+* PCs, only 47 were upregulated in *hATXN1-* PCs. Among shared upregulated and downregulated genes were previously mentioned top DEGs (**Figures 2B,C**), but the relative fold change in their expression was larger in *hATXN1+* PCs (**Supplementary Figure 5B** and **Supplementary Table 5**). For instance, log2FC for *Hs6st3*, and *Ralyl* were 2.4 and 1.7 in hATXN1+ *PCs,* and 1.2 and 1.08 in *hATXN1-* PCs. Among upregulated genes that were unique to *hATXN1+* PCs was *Gabrg2* (*gamma-aminobutyric acid type A receptor subunit gamma2*), which encodes for ionotropic GABA receptor A subunit.

In conclusion, we confirmed changes in PC gene expression previously found using bulk RNA sequencing. These included a number of genes underlying pathways associated with changes in ion transport and synapse function in SCA1 Purkinje cells. We also identified novel genes that deepen our understanding of altered signaling responsiveness of SCA1 PCs. Moreover, we identified novel genes that are upregulated in PCs early in disease progression. These genes may provide compensatory roles, including added support to extracellular matrix underlying synapse structures and added support to signaling strength, such as the increased expression of synaptic vesicle gene *Slc32a1* which may restore inhibitory/excitatory balance in the cerebellar network. Intriguingly, we showed that PCs differ in the expression of mutant ATXN1 and that PCs expressing the highest, and therefore most detectable, levels of mutant ATXN1 show a high degree of gene upregulation. This is in stark contrast to the *hATXN1-* PCs from SCA1 cerebella with undetectable levels of mutant *ATXN1* or total PCs in which most DEGs are downregulated.

Disrupted Bergmann glia-Purkinje cell signaling via sonic hedgehog in Spinocerebellar ataxia type 1

Bergmann glia are a special type of radial astrocytes which are intimately connected with Purkinje cells, both structurally and functionally. BG cell bodies surround the somas of PCs and their radial processes envelop PCs synapses in the molecular layer. This close morphological interaction is mirrored in the functional interdependence of BG and PCs. BG are essential for PCs function and viability through their many roles including maintenance of potassium homeostasis, removal of synaptic glutamate and provision of neurotrophic support (Rothstein et al., 1996; Grosche et al., 1999; Custer et al., 2006; Djukic et al., 2007; Miyazaki et al., 2017). Similarly, PCs signaling is important for the ongoing function of BG. In particular, sonic hedgehog (Shh) signaling from PCs to BG drives the development and maintenance of Bergmann glia character (Eiraku et al., 2005; Farmer et al., 2016).

With such close interactions, BG are perfectly poised to sense and respond to PC dysfunction in SCA1. Indeed, we have previously shown both that BG undergo reactive gliosis in patients with SCA1 and in SCA1 mouse models (Cvetanovic et al., 2015; Rosa et al., 2021) and that they contribute to disease pathogenesis in SCA1 mice. Thus, we next wanted to investigate molecular changes in BG that underlie their response to PC dysfunction early in SCA1 progression.

We identified 406 DEGs (p.adj $< = 0.05$) in Bergmann glia. Out of these 151 (37.2%) were downregulated and 255 (62.8%) upregulated (**Figure 3A**).

Glial fibrillary acidic protein (*Gfap*) expression was increased, indicating a reactive glial phenotype similar to what we have found in previous work. In addition, we have found increased expression of several genes that have been attributed neuroprotective roles including *secreted protein acidic and rich in cysteine like 1 (Sparcl1), fibroblast growth factor 12 (Fgf12), platelet derived growth factor D (Pdgfd)*, and *Cystatin 3* (*Cst3)* (**Figures 3B,C**). SPARCL1 promotes excitatory synapse formation. One of the early signs of SCA1 is loss of excitatory VGLUT2+ synapses on PCs (Kim et al., 2018). Increased *Sparcl1* expression in SCA1 BG could thus be a compensatory mechanism to promote formation of new excitatory synapses as these signaling structures are lost. Expression of growth factors, such as Fibroblast growth factor (*Fgf) 12*, and *Platelet Derived Growth Factor D (PdgfD)* was also increased in SCA1 BG. Fibroblast growth factors (FGFs) via their receptors (FGFRs) modulate important cellular processes such as cell proliferation, and death. FGF12 interacts with all four major FGFR and protects cells from apoptosis (Sochacka et al., 2020). In response to injury or various stresses, PDGFs modulate neuronal excitability by affecting ion channels, and stimulate survival signals rescuing cells from apoptosis (Funa and Sasahara, 2014). Increased expression of *Fgf12* and *PdgfD* in BG is likely to be neuroprotective and delay dysfunction and cell death of PCs (Chopra et al., 2018). In addition, BG may be serving a neuroprotective role by upregulating the expression of the *Cystatin 3* (*Cst3*), the most abundant extracellular inhibitor of cysteine proteases. Cysteine proteases are upregulated in neurodegenerative and neuroinflammatory conditions and can lead to ECM breakdown and cell death (Hook et al., 2015). Inhibitors of cysteine proteases including Cst3 have been shown to be neuroprotective in neurodegenerative diseases (Kaur and Levy, 2012; Zou et al., 2017). Thus, increase in *Cst3* in BG could be neuroprotective by preventing deleterious ECM changes. Together, increased expression of these neuro-supportive genes indicates potential mechanisms by which reactive SCA1 BG exert beneficial effects during the early stages of disease.

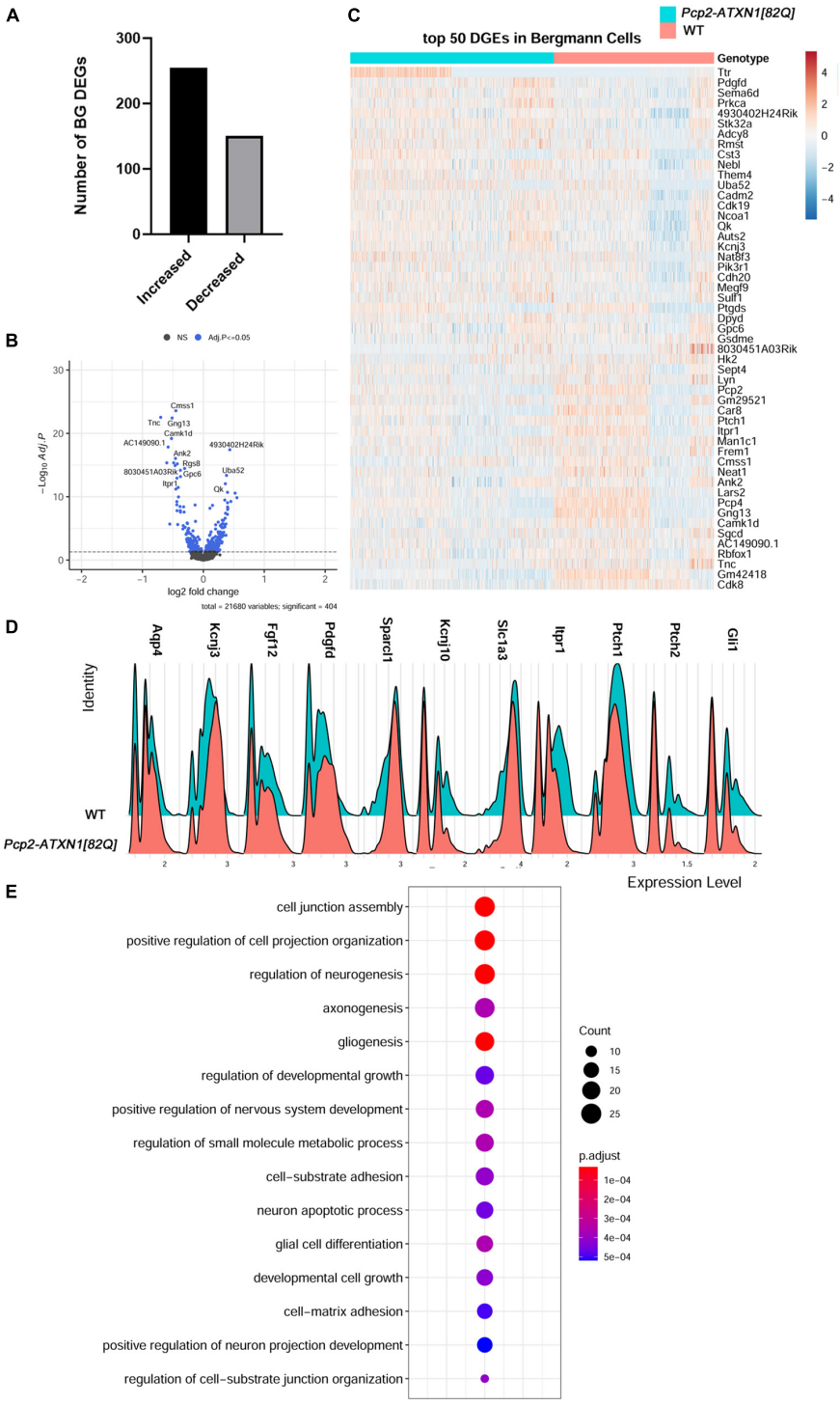

FIGURE 3
Mutant ATXN1 causes significant non-cell autonomous gene expression perturbations in SCA1 Bergmann glia. **(A)** For identified Bergmann glia, limma was used to test differential gene abundance between control and *Pcp2-ATXN1[82Q]* samples. *N* = 3 mice of each genotype. *P* values were adjusted using Benjamini-Hockberg method. Differential gene expression was determined by an adjusted *p*-values of 0.05. **(A)** Number of upregulated and downregulated differentially expressed genes (DEGs) in BG. **(B)** Volcano plot showing DEGs of BG cluster in *Pcp2-ATXN1[82Q]* SCA1. **(C)** Heatplot displaying expression profiles of top 25 highest upregulated and downregulated DEGs in wild-type and *Pcp2-ATXN1[82Q]* Bergmann glia determined by logFC values with adjusted *p*-values $\leq$ 0.05. *N* = 3 mice of each genotype. **(D)** Ridgeplot showing distribution of expression of selected genes in wild-type and *Pcp2-ATXN1[82Q]* Bergmann glia. **(E)** Dot plot of the pathway analysis of total DEGs between WT and *Pcp2-ATXN1[82Q]* Bergmann glia at 12 weeks of age. The color of dots depicts the adjusted *p* values, radius of the dot depicts gene counts (number of genes in the enriched pathway).

We have also observed changes in the expression of homeostatic BG genes responsible for regulating neuronal function. We found that expression of *Kcnj10* (**Figure 3D**), encoding the potassium inward rectifier Kir4.1, is decreased in BG at this stage of disease. Kir4.1 regulates extracellular potassium ion levels and, subsequently, PC excitability and firing rate. Previous work has shown that the firing rate of PCs is decreased early in SCA1 (Dell'Orco et al., 2015). This observed decrease in *Kcnj10* expression is expected to moderate PC firing rate (Djukic et al., 2007). BG may also moderate PC synaptic signaling via reduced expression of *Solute carrier family 1 Member 3 (Slc1a3). Slc1a3* encodes for the plasma membrane glutamate aspartate transporter (GLAST) that is responsible for synaptic glutamate removal. Decreased *Slc1a3* expression may result in slower and less efficient glutamate removal, thus prolonging glutamate signaling on PCs.

Our results also provide insight into how are BG genes altered in SCA1. Previous studies have found that PCs regulate BG character via Sonic hedgehog (Shh) signaling (Farmer et al., 2016). For instance, Shh signaling from PCs regulates higher expression of *Kcnj10* and lower expression of *aquaporin 4* (*Aqp4)* in BG compared to velate astrocytes. Interestingly, we found that expression of Shh receptors *Patched 1* and *2* (*Ptch1, Ptch2*) (Adolphe et al., 2014) is decreased in BG in *Pcp2-ATXN1[82Q]* cerebella indicating one critical way in which PC-BG communication is impacted in SCA1. Loss of PC-BG Shh signaling could affect BG function in several ways, including decreased expression of *Kcnj10* and increased expression of *Aqp4,* both changes that we indeed observed in SCA1 BG. Expression of Shh downstream transcriptional activator *Gli1* is also decreased, further supporting dysfunctional Shh PC-BG signaling in SCA1 (**Figure 3D**). We investigated whether these changes in Shh signaling occur widely or only in the subset of BG, such as the ones residing next to *hATXN1+* PCs. Most BG observed in this study showed decreased expression of *Ptch1, Ptch2,* and *Gli1* (**Supplementary Figure 6A**). We confirmed reduced expression of *Ptch2* and *Gli1* using RT-qPCR of whole *Pcp2-ATXN1[82Q]* cerebellar extracts (**Supplementary Figure 6B** and **Supplementary Table 1**). As the most logical cause of this reduced BG expression is decreased expression of ligand *Shh* from PCs, we assessed *Shh* expression in identified PC populations. However, we found no significant change in *Shh* expression in total PCs, *hATXN1+*, or *hATXN1-* PCs (**Supplementary Figure 6C** and **Supplementary Table 5**). This may suggest either altered post-transcriptional regulation of Shh in PCs or broader changes in PC signaling capabilities that are disrupting this crucial mechanism.

We further investigated the expression of genes that may regulate BG response to PC dysfunction. Calcium regulated adenylate cyclase *(Adcy8)* controls neuroinflammation by increasing the production of cyclic adenosine monophosphate (cAMP), an important negative regulator of inflammation (Wieczorek et al., 2012; Wang et al., 2020). We have found increased expression of *Adcy8* in BG that may moderate their pro-inflammatory response in SCA1. Sox2 is a transcriptional regulator of BG reactivity. The long non-coding RNA (lncRNA) *Rmst* is known for its role in facilitating activation of Sox2. We observed increased expression of *Rmst* that may play a role in facilitating Sox2-regulation of reactive glial response in SCA1 BG (Ng et al., 2013; Cerrato et al., 2018).

Hierarchical enriched pathways analysis of the DEGs in BG identified pathways involved in development, including cell junction assembly, positive regulation of cell projection organization, regulation of neurogenesis, axonogenesis, gliogenesis, small molecule metabolic processes and neuron apoptotic processes (**Figure 3E**). Among top GO pathways associated with the upregulated genes were nervous system development ($q = 1.2 \times 10^{-9}$), regulation of biological quality ($q = 1.5 \times 10^{-9}$), cell adhesion ($q = 9.8 \times 10^{-9}$), organonitrogen compound metabolic processes ($q = 3.8 \times 10^{-7}$) and cell projection organization ($q = 5 \times 10^{-8}$). KEGG identified circadian entrainment ($q = 3.6 \times 10^{-2}$) as dysregulated pathway in BG. This is very intriguing considering the role the cerebellum has in sleep and sleep disturbances in SCA patients (Pedroso et al., 2011; DelRosso and Hoque, 2014). GO pathway analysis of downregulated genes identified transmembrane transporter binding ($q = 7 \times 10^{-3}$), smoothened binding and hedgehog receptor activity ($q = 4.9 \times 10^{-2}$), cell to cell signaling ($q = 6.4 \times 10^{-7}$), apoptotic processes ($q = 1.3 \times 10^{-2}$) and synapse ($q = 5 \times 10^{-14}$). KEGG analysis of downregulated genes identified retrograde endocannabinoid signaling ($q = 1 \times 10^{-3}$), glutamatergic ($q = 2 \times 10^{-3}$) and dopaminergic synapses ($q = 4.3 \times 10^{-2}$), long-term depression ($q = 8.1 \times 10^{-3}$) and Spinocerebellar ataxias ($q = 8.4 \times 10^{-3}$).

Our analysis supports the hypothesis that SCA1 BG increase their neuroprotective support in response to PC dysfunction. It confirms the reactive SCA1 phenotype previously observed through the upregulation of *Gfap* and suggests an ongoing regulation of neuroinflammatory response through the expression of *Adcy8* and *Rmst.* More importantly, these results implicate altered PC-BG Shh signaling as one of the mechanisms by which BG function is perturbed in SCA1.

Increased expression of genes that promote neurogenesis, gliogenesis, and synaptogenesis indicates compensatory gene expression changes in velate astrocytes

Velate astrocytes (VAs) are a type of cerebellar astrocytes that reside in the granule cell layer. As such, they are surrounded by the most numerous neurons in the brain and are the only astrocytes in the brain that are largely outnumbered by neurons they are associated with (Herculano-Houzel, 2014). However, very little is known about the response of velate

astrocytes to cerebellar pathology, including SCA1. Therefore, we next investigated genes and pathways altered in SCA1 velate astrocytes.

We have identified 157 DEGs (p.adj $<$ = 0.05) in SCA1 velate astrocytes compared to those of their wild-type littermate controls. A majority (114 or 72.6%) of the identified DEGs were upregulated (**Figures 4A–D**). Notably, one of genes with increased expression was *Vimentin* (*Vim*). *Vim* encodes for the intermediate filament predominantly found in astrocytes. Vimentin is upregulated in reactive astrogliosis (Janeczko, 1993; O'Leary et al., 2020), indicating that VAs, like BG, undergo reactive gliosis in SCA1 (**Figure 4D**). *Apolipoprotein E* (*ApoE*) also plays a role in reactive astrogliosis (Ophir et al., 2003; Sen et al., 2017). Increased expression of *ApoE* in VAs further indicates reactive velate astrogliosis in SCA1.

A previous study identified two different types of reactive astrocytes that were termed "A1" and "A2," respectively (Liddelow et al., 2017). A1 astrocytes are thought to be harmful as they up-regulate classical complement cascade genes previously shown to be destructive to synapses, while A2 astrocytes are thought to be neuroprotective due to increased expression of neurotrophic factors. To determine whether reactive BG and VAs are more like A1 or A2 astrocytes, we examined the expression of A1 and A2 astrocyte genes in VA and BG. While we found increased expression of panreactive genes *Gfap*, *Vim*, and *CD44*, we found no clear pattern or distinction in A1 or A2 type gene expression in BG or VAs (**Figure 4E**).

Among the top upregulated VA genes were genes involved in neurogenesis, gliogenesis, and synapse maintenance including *Neural Cell adhesion molecule 2* (*Ncam2*), *Sema6D*, *Quaking (Qk)*, *Serpine E2*, *Clusterin (Clu)* and *CUB And Sushi Multiple Domains 1* (*Csmd1*). NCAM2 is involved in many roles in the brain including neurogenesis, neuronal migration, neuronal differentiation, synaptogenesis, calcium signaling, and maintenance of presynaptic and postsynaptic compartments in adult brains. In addition, it has been proposed that a decrease in NCAM2 levels is associated with loss of synaptic structure in the early stages of neurodegenerative diseases (Parcerisas et al., 2021). Quaking (Qk) is an RNA binding protein residing in astrocyte processes and promotes astrocyte maturation (Sakers et al., 2021). Astrocyte secreted Clu co-localizes with presynaptic puncta of excitatory neurons and loss of *Clu* led to impaired presynaptic function and reduced spine density *in vivo* (Chen et al., 2021). On the other hand, overexpression of *Clu* in astrocytes reduced pathology and restored synaptic function in mouse model of Alzheimer's disease (Chen et al., 2021). Recently, *CUB And Sushi Multiple Domains 1*(*Csmd1*) was suggested to oppose the complement cascade that facilitates synaptic loss in neurodegeneration (Baum et al., 2020). Therefore, it is reasonable to assume that increased expression of *Ncam2*, *Qk*, *Clu* and *Csmd1* in velate astrocytes may be neuroprotective in SCA1 by promoting astrocyte maturation and synaptic function.

VEGF is a neurotrophic factor whose decrease was previously shown to contribute to Purkinje cell pathology in SCA1 (Cvetanovic et al., 2011). We found a reduced expression of *vascular endothelial growth factor* (*VEGF)* suggesting that velate astrocytes contribute to a VEGF reduction in SCA1 (**Figure 4D**).

Pathway analysis of all VA DEGs identified developmental pathways including regulation of neurogenesis, gliogenesis, positive regulation of projection organization, regulation of nervous system development, and regulation of protein catabolic process (**Figure 4F**). Breaking this down into pathways unique to up and downregulated genes, we found that GO pathway analysis of only upregulated genes highlighted many developmental pathways including cell morphogenesis, regulation of neuron projection development, positive regulation of gliogenesis, and glial differentiation (q values of 3.2×10^{-6}, 1.5×10^{-5}, 3.9×10^{-5}, and 4.5×10^{-5}, respectively). Further, GO pathway analysis of the downregulated genes identified calcium ion binding ($q = 3.1 \times 10^{-3}$), vesicle mediated transport in synapse ($q = 3.5 \times 10^{-2}$), negative regulation of neuronal death ($q = 4.1 \times 10^{-2}$), glutamatergic synapse ($q = 4.5 \times 10^{-4}$), Spinocerebellar ataxia ($q = 1.3 \times 10^{-3}$), retrograde endocannabinoid signaling ($q = 2.4 \times 10^{-2}$), and long-term depression ($q = 2.7 \times 10^{-2}$).

Together, these results indicate that VAs exhibit a reactive astrocyte phenotype in SCA1 that is characterized by the expression of genes regulating synapse structure and maintenance. Furthermore, reduction in *Vegf* expression in VAs seems to implicate VAs as an important contributor to reduced VEGF expression in the SCA1 cerebellum, suggesting that they may play a role in PC pathology. As this model represents a non-cell autonomous response of these cells to PC dysfunction this could indicate a negative feedback mechanism that could contribute to progressive worsening of cellular pathology over time.

Gene expression analysis indicates reactive activation in Spinocerebellar ataxia type 1 oligodendrocytes

Oligodendrocytes (OL) envelop axons with myelin and maintain long-term axonal integrity (Bradl and Lassmann, 2010). Cells of the oligodendrocyte lineage are important for cerebellar development and motor learning (Mathis et al., 2003; McKenzie et al., 2014). Previous studies have found significant changes in the cerebellar white matter in SCA1 patients and in *Pcp2-ATXN1[82Q]* mice, indicating that oligodendrocytes (OLs) may be affected in SCA1 (Liu et al., 2018; Park et al., 2020). Moreover, a recent study found a decrease in oligodendrocyte numbers in human post-mortem samples from patients with SCA1 (Tejwani et al., 2021) and a decreased

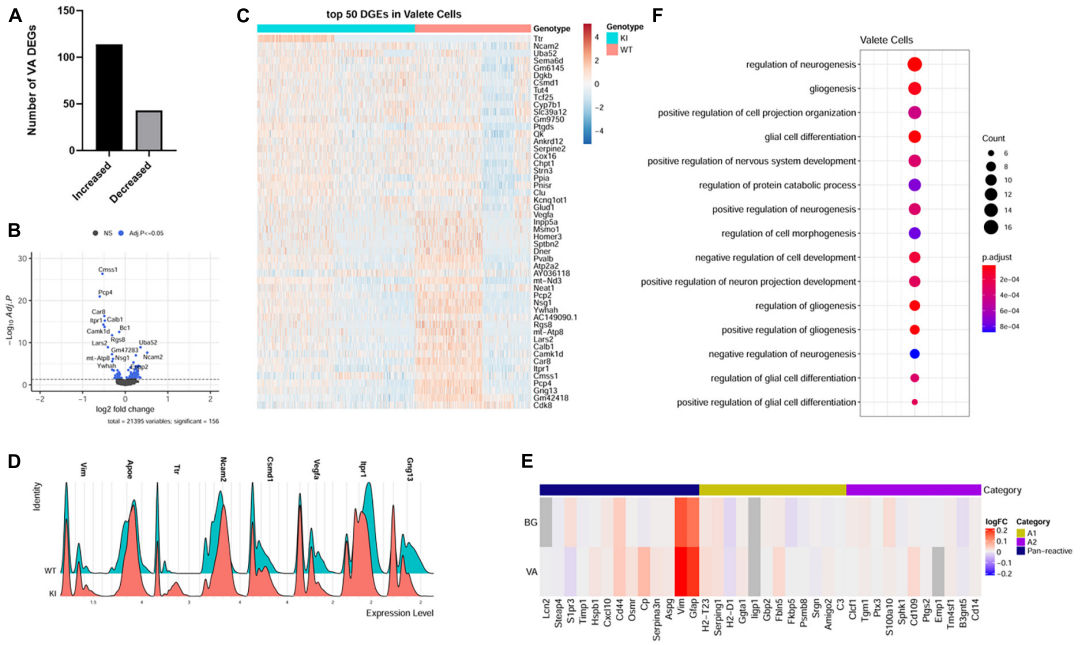

FIGURE 4
Velate astrocytes gene expression changes in SCA1. For identified velate astrocytes limma was used to test differential gene abundance between control and *Pcp2-ATXN1[82Q]* samples. *N* = 3 mice of each genotype. *P* values were adjusted using Benjamini-Hockberg method. Differential gene expression was determined by an adjusted *p*-values of 0.05. **(A)** Number of upregulated and downregulated differentially expressed genes (DEGs) in VA. **(B)** Volcano plot showing DEGs of VA cluster in *Pcp2-ATXN1[82Q]* SCA1. **(C)** Heatplot displaying expression profiles of top 25 highest upregulated and downregulated DEGs in wild-type and *Pcp2-ATXN1[82Q]* VA determined by logFC values with adjusted p-values $\leq$ 0.05. *N* = 3 mice of each genotype. **(D)** Ridgeplot showing distribution of expression of selected genes in wild-type and *Pcp2-ATXN1[82Q]* VAs. **(E)** Heatplot of normalized expression of astrocyte A1/A2 genes in BG and VA at 12 weeks of age. Color indicates logFC. **(F)** Dot plot of the pathway analysis of total DEGs between WT and *Pcp2-ATXN1[82Q]* VA at 12 weeks of age. The color of dots depicts the adjusted p values, radius of the dot depicts gene counts (number of genes in the enriched pathway).

expression of mature oligodendrocyte genes, including *Myelin Oligodendrocyte Glycoprotein* (*Mog*) in a knock-in mouse model of SCA1, *Atxn1*$^{154Q/2Q}$ mice (Tejwani et al., 2021). In *Atxn1*$^{154Q/2Q}$ mice mutant Atxn1 is expressed widely, including in oligodendrocyte precursor cells (OPC) and OLs.

To gain insight into which of these gene expression changes are induced in response to PC pathogenesis alone, we examined genes and pathways altered in oligodendrocyte nuclei from *Pcp2-ATXN1[82Q]* mice compared to littermate controls. We found 154 DEGs in oligodendrocytes in *Pcp2-ATXN1[82Q]* cerebella, with the majority (94 DEG or 61%) of these genes being upregulated (**Figure 5A**). While the percentage of OLs identified in our SCA1 samples is not significantly different from WT controls, the expression of several oligodendrocyte marker genes including *Transferrin* (*Trf*), *Mog*, *Claudin 11* (*Cldn11*) and *Reticulon 4* (*Rtn4*) was increased (**Figures 5B–D**; Bradl and Lassmann, 2010).

Increased expressions of *Crystallin Alpha B* (*Cryab*) and *apolipoprotein E* (*ApoE*) have been associated with protective reactive gliosis in neurodegenerative diseases such as Parkinson's disease (PD), Alzheimer's disease (AD), and Multiple Sclerosis (MS) (Ophir et al., 2003; Ousman et al., 2007; Liu et al., 2015; Kuipers et al., 2017; D'Agostino et al., 2019). We found increased expression of *Cryab* and *ApoE* indicating protective reactive oligodendrogliosis in SCA1.Notably, we observed increased expression of transcriptional factor *JunD*, which is a functional component of activated protein 1 (AP1) complex. The AP1 complex regulates many OL inflammatory and immune genes, suggesting that AP1 may modulate a non-cell autonomous reactive OL response in SCA1 pathogenesis (Behmoaras et al., 2008).

We also found altered expression of many genes important for oligodendrocyte function (**Figure 5E**). Among them is increased expression of *Glutamate-Ammonia Ligase* (*Glul*) encoding for glutamine synthetase (GS) This molecule serves as a key glutamate-catabolizing enzyme that catalyzes the conversion of glutamate to glutamine. Previous studies demonstrated that OLs support neuronal glutamatergic transmission via expression of GS (Xin et al., 2019). Moreover, *Glul* expression in OLs is increased in chronic pathological conditions including amyotrophic lateral sclerosis (ALS) and MS (Ben Haim et al., 2021). As glutamate signaling is perturbed in SCA1, it is possible that OLs increase GS expression to compensate for these changes in glutamate metabolism in SCA1.

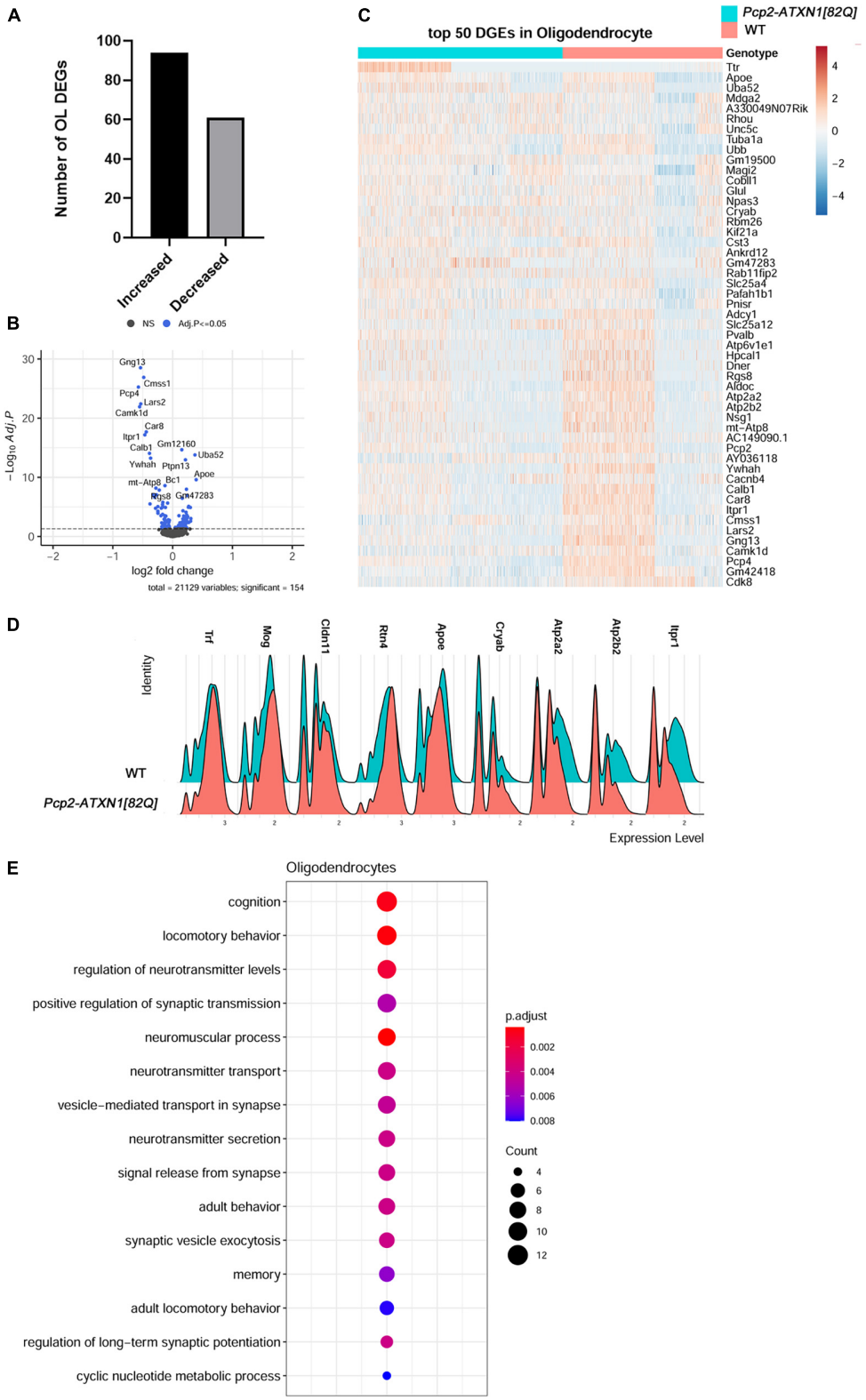

FIGURE 5
Gene expression changes in SCA1 oligodendrocytes. Limma was used to test differential gene abundance in oligodendrocytes between control and *Pcp2-ATXN1[82Q]* samples. *N* = 3 mice of each genotype. *P* values were adjusted using Benjamini-Hockberg method. Differential gene expression was determined by an adjusted *p*-values of 0.05. **(A)** Number of upregulated and downregulated differentially expressed genes

(Continued)

FIGURE 5 (Continued)
(DEGs) in OL. **(B)** Volcano plot showing DEGs of OL cluster in *Pcp2-ATXN1[82Q]* SCA1. **(C)** Heatplot displaying expression profiles of top 25 highest upregulated and downregulated DEGs in wild-type and *Pcp2-ATXN1[82Q]* oligodendrocytes determined by logFC values with adjusted *p*-values $\leq$0.05. *N* = 3 mice of each genotype. **(D)** Ridgeplot showing distribution of expression of selected genes in wild-type and *Pcp2-ATXN1[82Q]* OL. **(E)** Dot plot of the pathway analysis of total DEGs between WT and *Pcp2-ATXN1[82Q]* OL at 12 weeks of age. The color of dots depicts the adjusted p values, radius of the dot depicts gene counts (number of genes in the enriched pathway).

Genes downregulated in SCA1 OLs included *Atp2a2* and *Atp2a3* which encode for the calcium endoplasmic reticulum pumps SERCA1 and SERCA2, respectively. This implicates a reduced ability of OLs endoplasmic reticula (ER) to buffer calcium. In addition, reduced expression of *Atp2b2* that encodes for Plasma Membrane Calcium-Transporting ATPase is expected to reduce plasma membrane calcium buffering. Together these results indicate perturbed calcium homeostasis as a feature of reactive SCA1 OLs (**Figures 5B-D**).

Intriguingly, the top two pathways of OLs DEGs identified were cognition and locomotor behavior, implicating that molecular pathway alterations in SCA1 oligodendrocytes could be associated with the broader symptomology of SCA1. Pathway analysis of all OLs DEGs also identified regulation of neurotransmitter levels, positive regulation of synaptic transmission, vesicle-mediated transport in synapses and neurotransmitter secretion, potentially implicating OL in modulating synaptic transmission in SCA1 (**Figure 5E**).

Breaking this analysis down into pathways unique to up and downregulated genes, we found that GO pathway analysis of only downregulated genes identified pathways involved in transport and binding of ions including inorganic cation transmembrane transporter activity ($q = 7.5 \times 10^{-6}$), calcium binding ($q = 9.3 \times 10^{-6}$), P-type calcium transporter activity ($q = 4.2 \times 10^{-4}$), synaptic signaling ($q = 1.6 \times 10^{-7}$), modulation of chemical synaptic transmission ($q = 5.4 \times 10^{-6}$), glutamatergic synapse ($q = 6.4 \times 10^{-6}$), and Spinocerebellar ataxia ($q = 2.9 \times 10^{-5}$). Moreover, pathway analysis of OLs upregulated DEGs identified movement of cell or subcellular component ($q = 9.4 \times 10^{-5}$), cell migration ($q = 8.8 \times 10^{-4}$), myelin sheath ($q = 2.4 \times 10^{-7}$), and synapse ($q = 1.4 \times 10^{-4}$).

Together, these analyses indicate that oligodendrocytes respond to PC dysfunction in SCA1 by becoming reactive. Reactive response of SCA1 OLs is characterized by increased expression of *Cryab*, *ApoE, and Glul,* and may be regulated by transcriptional factor AP1. While this may allow for increased neuroprotection, such as compensatory glutamate buffering, reactive OLs response may impact their calcium homeostasis.

Discussion

Through this work we sought to increase our understanding of the cell-type specific changes during the early stages of SCA1. Furthermore, by using a model in which the pathological mutation was restricted to PCs, we aimed to provide insight into how these pathogenic processes within PCs affect non-cell autonomous gene expression and signaling pathways within other cerebellar cells. To accomplish this, we have employed single nuclei RNA sequencing to investigate transcriptional changes in individual cerebellar cell types in "early stage" 12 week old animals, a time point which represents a phase of SCA1 in which symptoms are beginning to become apparent but before the progressive cell death of PCs within the cerebellum.

There are several important findings from our study. First, mutant ATXN1 expression in Purkinje cells causes profound transcriptional alterations in cerebellar glia in a non-cell autonomous manner. Mutant ATXN1 expression in PCs alone caused altered gene expression in every glial subtype analyzed, often driving an increase in gene expression (Bergmann glia (62.8%), velate astrocytes (72.6%) and oligodendrocytes (61%). As at this early disease stage there is no detectable Purkinje cell loss in *Pcp2-ATXN1[82Q]* mice, we propose that these glial transcriptome changes are in direct response to ATXN1-driven Purkinje cell dysfunction (Bell et al., 2010; Ingram et al., 2016b).

Second, we identified novel transcriptional changes in PCs that may be relevant to disease pathogenesis. These potentially compensatory gene expression changes include increased expression of *Ralyl*, *Atp6v0c*, *Atpgv0a1*, *Atp6v1h*, Atp6v and *Slc32a1*. *Ralyl* is an RNA binding protein known for its neuroprotective role in Alzheimer's (Zhang et al., 2020). Increased expression of three vacuolar V-type ATP-ase subunits (*Atp6v0c*, *Atpgv0a1*, and *Atp6v1h*) that provide electrochemical gradient to fill synaptic vesicles with GABA, and *Slc32a1*, encoding vesicular GABA and Glycine Transporter (VGAT) that transports GABA in the vesicles may suggest increased GABA content in PCs synaptic vesicle. As spontaneous firing rate of PCs is decreased in *Pcp2-ATXN1[82Q]* mice (Dell'Orco et al., 2015), an increase in GABA loading per vesicle may represent compensatory change to restore or ameliorate synaptic transmission by increasing the total amount of GABA released at PC terminals.

Third, because previous work in this mouse model suggested altered levels of mutant ATXN1 in PCs across the cerebellum, we assessed the relative expression of human ATXN1 within our SCA1 PCs. In doing so, we identified two populations-those that were expressing detectable ATXN1 (~25%) and those that had no detectable ATXN1. It is likely that we underestimated the number of mutant ATXN1 expressing PCs

due to the rigor of our analysis. It is unclear whether PCs with undetectable mutant *hATXN1* have reduced production of mutant ATXN1 mRNA or are more efficient in transporting it out of the nucleus and/or degrading it. Intriguingly, in contrast to prevalent gene downregulation in total PCs and *hATXN1- PCs,* majority of DEGs were upregulated in *hATXN1+* cells. It is possible that these upregulated genes provide resistance to SCA1, and it will be important for future studies to distinguish whether *hATXN1+* or – cells are more affected in SCA1. This result also indicates that some of the ATXN1 –induced gene expression changes may be missed when comparing total SCA1 to WT PCs. Furthermore, out of 370 DEGs in *hATXN1- PCs,* 355 were also present when comparing total SCA1 to WT PCs. Thus majority (64%) of DEGs identified in comparison of total SCA1 and WT PCs are genes with altered expression in PCs in which we could not detect mutant *hATXN1.*

Fourth, our results support perturbed Shh signaling as one of contributors to BG molecular alterations in SCA1. Sonic hedgehog (Shh) signaling is one of the key communication pathways by which PCs regulate BG character (Farmer et al., 2016). We found that the expression of Shh receptors *Patched 1* and 2 and Shh signaling downstream transcription factor *Gli1* are reduced in SCA1 BG. Previous studies have shown that Shh-Ptch2 communication regulates expression of homeostatic genes *Slc1a3*, *Kcnj10*, and *Aqp4* in Bergmann glia (Farmer et al., 2016). We also validated a previously reported decrease in the expression of glutamate transporter *Slc1a3* in Bergmann glia (Cvetanovic, 2015), and identified additional perturbations in the expression of homeostatic genes such as *Kcnj10 and Aqp4* that are critical for PC function (Djukic et al., 2007; Nicita et al., 2018). Therefore, we propose that decreased Shh signaling contributes to reduced expression of S*lc1a3* and *Kcnj10* and increased expression of *Aqp4* that we found in SCA1 BG.

Fifth, we provide evidence that reactive response in velate astrocytes includes increased expression of several neuroprotective genes such as *ApoE, Ncam2*, *Clu* and *Csmd1*. ApoE, among other roles, contributes to astrocyte activation and increases BDNF secretion. Increased ApoE in SCA1 VAs may contribute to increased BDNF that is neuroprotective in SCA1 (Ophir et al., 2003; Sen et al., 2017; Mellesmoen et al., 2018; Sheeler et al., 2021). *Ncam2, Clu* and *Csmd1* are protective against loss of synapses (Baum et al., 2020; Parcerisas et al., 2021), and their increased expression in SCA1 VAs may compensate for loss of synapses seen in SCA1. These results also increase our limited understanding of VAs reactive gliosis in cerebellar disease.

Six, we identified intriguing transcriptional changes in SCA1 oligodendrocytes indicative of reactive oligodendrogliosis that may be regulated by increased expression of JunD. While OLs numbers do not seem to be altered at 12 weeks in *Pcp2-ATXN1[82Q]* cerebellum, we have found increased expression of OL marker genes and neurosupportive genes including *Trf*, *Mog*, *Cldn11*, *Rtn4*, *Glul, Cryab* and *ApoE*. These results indicate neuroprotective effects of reactive cerebellar OLs in SCA1.

Finally, we identified shared DEGs and pathways that are altered in all four analyzed cell types in SCA1 cerebella and as such are promising candidates for future therapies. Transthyretin (Ttr) is a protein that binds and distributes retinol and thyroid hormones. Retinol is important for cerebellar function (Tafti and Ghyselinck, 2007) where it binds retinoic acid receptor-related orphan receptors (ROR). Previous studies identified the importance of retinol in SCA1 (Serra et al., 2006), by demonstrating reduced expression of RORa–regulated genes in cerebella of SCA1 mice, and that partial loss of RORa enhances PCs pathology (Serra et al., 2006). Recent studies found that Ttr plays important roles in other cells such as OPC, cerebellar granule neurons and astrocytes. For example, Ttr regulates proliferation and survival of OPCs (Alshehri et al., 2020), δ-GABAA-R expression in cerebellar granule neurons (Zhou et al., 2019), and glycolysis in astrocytes (Zawişlak et al., 2017). We found that *Ttr* expression is increased in SCA1 PCs, BG, VA and OL. It is likely that this increase in *Ttr* expression is beneficial for PCs, OLs, astrocytes and granule neurons, and compensates for reduced RORa function in SCA1. It will be important to understand the mechanism of *Ttr* upregulation, and whether exogenous Ttr is therapeutically beneficial in SCA1.

In addition, several Magenta module genes, including genes involved in calcium homeostasis, such as *Atp2a2* and *Itpr1* were reduced in all four cell types, indicating that restoring calcium homeostasis may be another good target for SCA1 therapeutic approaches.

Selective neuronal vulnerability is a feature shared by many neurodegenerative diseases. In the case of SCA1, although mutant ATXN1 is expressed throughout the brain, cerebellar Purkinje cells (PCs) are most affected (Servadio et al., 1995). Severe vulnerability of PCs in SCA1 is likely brought about by the combination of the toxic effects of mutant ATXN1 within PCs and the changes in PCs microenvironment, including glial cell alterations. In this respect, it is important to note that glial cells in the cerebellum are found to have distinct transcriptomes compared to the glial cells in other brain regions (Grabert et al., 2016; Soreq et al., 2017; Boisvert et al., 2018). Uniqueness of cerebellar glia gets even more pronounced during aging (Grabert et al., 2016; Boisvert et al., 2018; Clarke et al., 2018). Yet, while neurodegeneration associated glial gene expression changes have been studied intensively in the other brain regions, less is known about gene expression changes in cerebellar glia during neurodegeneration. Our results provide much needed insight into gene expression changes of cerebellar Bergmann glia, velate astrocytes and oligodendrocytes in response to PC dysfunction.

It is likely that some of the molecular changes we identified are compensatory, allowing for continued cerebellar function, and that some may be pathogenic, promoting disease progression.

Our results provide a framework to investigate how individual pathogenic processes contribute to the sequence of progressive cerebellar dysfunctions in SCA1. Our results are freely available and we hope that they will stimulate future studies to causally investigate how these gene and pathway perturbations contribute to SCA1 pathogenesis as well as facilitate development of novel therapeutic approaches.

Data availability statement

All the data from this study are available from the authors. RNA sequencing data are deposited at https://www.ncbi.nlm.nih.gov/geo/query/acc.cgi?acc=GSE215336.

Ethics statement

Animal experimentation was approved by Institutional Animal Care and Use Committee (IACUC) of University of Minnesota.

Author contributions

MC conceptualized the study. EB, CS, KH, FLM, and KS performed the experiments. YZ and MC analyzed the data. MC, EB, CS, KH, FLM, KS, and YZ wrote the manuscript. All authors contributed to the article and approved the submitted version.

Funding

This work was supported by a National Institute of Health NINDS awards (R01 NS107387 and NS109077 to MC).

Acknowledgments

We acknowledge all the members of Orr and Cvetanovic laboratories for thoughtful discussions and feedback on the study. Work in this study was aided by the Single Cell Services of the University of Minnesota Genomics Center.

Conflict of interest

The authors declare that the research was conducted in the absence of any commercial or financial relationships that could be construed as a potential conflict of interest.

Publisher's note

Supplementary material

The Supplementary Material for this article can be found online at: https://www.frontiersin.org/articles/10.3389/fncel.2022.998408/full#supplementary-material

SUPPLEMENTARY FIGURE 1
Example of isolated nuclei showing absence of clumping and spherical, non-damaged nuclei. Nuclei for RNA sequencing were isolated from the mouse cerebella using detergent mechanical lysis protocol, and stained with DAPI. Scale bar = 100 μm.

SUPPLEMENTARY FIGURE 2
Reduced expression of Purkinje cell genes in *Pcp2-ATXN1[82Q]* mice. Quantitative RT-PCR of bulk cerebellar lysates was used to evaluate expression of Purkinje cell genes *Calb1*, *Pcp4*, *Homer3*, *Rgs8*, *ITPR*, *Inpp5* and *Garnl3*. Data is presented as mean ± SEM with average values for each mouse represented by a dot. N = 6 -7 mice per genotype (WT and *Pcp2-ATXN1[82Q]*) $^*p < 0.05$ unpaired t test with Welch's correction.

SUPPLEMENTARY FIGURE 3
Expression of endogenous mouse *Atxn1[2Q]* and mutant human *ATXN1[82Q]* in cerebellar cells. **(A)** Percentage of cerebellar cells expressing endogenous mouse *Atxn1[2Q]* in wild-type and *Pcp2-ATXN1[82Q]* mice. **(B)** Percentage of cerebellar cells expressing mutant human *hATXN1[82Q]* in wild-type and *Pcp2-ATXN1[82Q]* mice. Data is presented as mean ± SEM with average values for each mouse represented by a dot. N = 3. $^*P < 0.05$ Two way ANOVA with Tukey's multiple comparisons tests.

SUPPLEMENTARY FIGURE 4
Decreased expression of *Dner* mRNA and protein in Purkinje Cells. **(A).** Quantitative RT-PCR of bulk cerebellar lysates from 12 weeks old wild-type and *Pcp2-ATXN1[82Q]* mice was used to evaluate expression of *Dner*. Data is presented as mean ± SEM with average values for each mouse represented by a dot. N = 7, $^*p < 0.05$ unpaired t test with Welch's correction. **(B,C)** Cerebellar slices from 12 week old wild-type and *Pcp2-ATXN1[82Q]* mice were stained with DNER antibody. **(D)** Confocal images and Image J were used to quantify DNER expression in soma and dendrites of PCs (right). Data is presented as mean ± SEM with values for each mouse analyzed represented by a dot. N = 3 wild-type and N = 5 *Pcp2-ATXN1[82Q]* mice$^*p < 0.05$ unpaired t-test with Welch's correction. Scale bars = 50 μm.

SUPPLEMENTARY FIGURE 5
Gene expression changes in *hATXN1* + and *hATXN1*- Purkinje cells. For identified *hATXN1* + and *hATXN1*- Purkinje cells limma was used to test differential expression between control and *Pcp2-ATXN1[82Q]* samples. **(A)** Number of upregulated and downregulated differentially expressed genes (DEGs) in *hATXN1* + and *hATXN1*- *PCs*. N = 3 mice of each genotype. P values were adjusted using Benjamini-Hockberg method. Differential gene expression was determined by an adjusted p-values ≤ 0.05. **(B)** Heatplot displaying expression profiles of selected upregulated and downregulated DEGs in wild-type PCs and *hATXN1* + and *hATXN1*- PCs from *Pcp2-ATXN1[82Q]* cerebella determined by logFC values with adjusted p-values ≤ 0.05. N = 3 mice of each genotype.

SUPPLEMENTARY FIGURE 6
Changes in Shh signaling in Bergmann glia. **(A)** Ridgeplots showing distribution of expression of *Ptch1, Ptch2,* and *Gli1* in BG population in wild-type and *Pcp2-ATXN1[82Q]* mice ($N = 3$ of each). *P* values adjusted using Benjamini-Hockberg method ≤ 0.05 for all three genes. **(B)** Quantitative RT-PCR of bulk cerebellar lysates from 12 weeks old wild-type and *Pcp2-ATXN1[82Q]* mice was used to evaluate expression of *Ptch2* and *Gli1 mRNA*. Data is presented as mean ± SEM with average values for each mouse represented by a dot. $N = 7$, $^*p < 0.05$ unpaired t test with Welch's correction. **(C)** Ridgeplot showing distribution of *Shh* expression in *hATXN1* + and *hATXN1*- PCs. *P* value adjusted using Benjamini-Hockberg method ≥ 0.05.

SUPPLEMENTARY TABLE 1
Raw data from RTqPCR of PC and BG Genes, DNER intensity.

SUPPLEMENTARY TABLE 2
Percentage of cells per genotype.

SUPPLEMENTARY TABLE 3
Percentage of Cell Expressing Endogenous *Atxn1[2Q]*.

SUPPLEMENTARY TABLE 4
Percentage of cells expressing mutant human *ATXN1[82Q]*.

SUPPLEMENTARY TABLE 5
DEG in PCs with detectable and not detectable expression of mutant human *ATXN1*.

References

Adolphe, C., Nieuwenhuis, E., Villani, R., Li, Z. J., Kaur, P., Hui, C. C., et al. (2014). Patched 1 and patched 2 redundancy has a key role in regulating epidermal differentiation. *J. Invest. Dermatol.* 134, 1981–1990. doi: 10.1038/jid.2014.63

Alshehri, B., Pagnin, M., Lee, J. Y., Petratos, S., and Richardson, S. J. (2020). The Role of Transthyretin in Oligodendrocyte Development. *Sci. Rep.* 10:4189.

Alvarez, M., Rahmani, E., Jew, B., Garske, K. M., Miao, Z., Benhammou, J. N., et al. (2020). Enhancing droplet-based single-nucleus RNA-seq resolution using the semi-supervised machine learning classifier DIEM. *Sci. Rep.* 10:11019. doi: 10.1038/s41598-020-67513-5

Barres, B. A. (2008). The Mystery and Magic of Glia: A Perspective on Their Roles in Health and Disease. *Neuron* 60, 430–440. doi: 10.1016/j.neuron.2008.10.013

Baum, M. L., Wilton, D. K., Muthukumar, A., Fox, R. G., Carey, A., Crotty, W., et al. (2020). CUB and Sushi Multiple Domains 1 (CSMD1) opposes the complement cascade in neural tissues. *Biorxiv* [Preprint]. doi: 10.1101/2020.09.11.291427

Behmoaras, J., Bhangal, G., Smith, J., McDonald, K., Mutch, B., Lai, P. C., et al. (2008). Jund is a determinant of macrophage activation and is associated with glomerulonephritis susceptibility. *Nat. Genet.* 40, 553–559.

Bell, J. J. L., Lordkipanidze, T., and Cobb, N. (2010). Bergmann glial ensheathment of dendritic spines regulates synapse number without affecting spine motility. *Neuron Glia Biol.* 6, 193–200. doi: 10.1017/S1740925X10000165

Ben Haim, L., Schirmer, L., Zulji, A., Sabeur, K., Tiret, B., Ribon, M., et al. (2021). Evidence for glutamine synthetase function in mouse spinal cord oligodendrocytes. *Glia* 69, 2812–2827.

Boisvert, M. M., Erikson, G. A., Shokhirev, M. N., and Allen, N. J. (2018). The Aging Astrocyte Transcriptome from Multiple Regions of the Mouse Brain. *Cell Rep.* 22, 269–285.

Bradl, M., and Lassmann, H. (2010). Oligodendrocytes: Biology and pathology. *Acta Neuropathol.* 119, 37–53.

Burda, J. E., and Sofroniew, M. V. (2014). Reactive gliosis and the multicellular response to CNS damage and disease. *Neuron* 81, 229–248. doi: 10.1016/j.neuron.2013.12.034

Burright, E. N., Clark, B. H., Servadio, A., Matilla, T., Feddersen, R. M., Yunis, W. S., et al. (1995). SCA1 transgenic mice: A model for neurodegeneration caused by an expanded CAG trinucleotide repeat. *Cell* 82, 937–948. doi: 10.1016/0092-8674(95)90273-2

Bushart, D. D., and Shakkottai, V. G. (2018). Ion channel dysfunction in cerebellar ataxia. *Neurosci. Lett.* 688, 41–48. doi: 10.1016/j.neulet.2018.02.005688: 41-48

Bushart, D. D., Huang, H., Man, L. J., Morrison, L. M., and Shakkottai, V. G. A. (2021). Chlorzoxazone-Baclofen Combination Improves Cerebellar Impairment in Spinocerebellar Ataxia Type 1. *Mov. Disord.* 36, 622–631. doi: 10.1002/mds.28355

Carmon, K. S., Lin, Q., Gong, X., Thomas, A., and Liu, Q. (2012). LGR5 Interacts and Cointernalizes with Wnt Receptors To Modulate Wnt/β-Catenin Signaling. *Mol. Cell. Biol.* 32, 2054–2064.

Cerrato, V., Mercurio, S., Leto, K., Fucà, E., Hoxha, E., Bottes, S., et al. (2018). Sox2 conditional mutation in mouse causes ataxic symptoms, cerebellar vermis hypoplasia, and postnatal defects of Bergmann glia. *Glia* 66, 1929–1946. doi: 10.1002/glia.23448

Chen, F., Swartzlander, D. B., Ghosh, A., Fryer, J. D., Wang, B., and Zheng, H. (2021). Clusterin secreted from astrocyte promotes excitatory synaptic transmission and ameliorates Alzheimer's disease neuropathology. *Mol. Neurodegener.* 16:5. doi: 10.1186/s13024-021-00426-7

Chopra, R., Bushart, D. D., and Shakkottai, V. G. (2018). Dendritic potassium channel dysfunction may contribute to dendrite degeneration in spinocerebellar ataxia type 1. *PLoS One* 13:e0198040. doi: 10.1371/journal.pone.0198040

Chopra, R., Bushart, D. D., Cooper, J. P., Yellajoshyula, D., Morrison, L. M., Huang, H., et al. (2020). Altered Capicua expression drives regional Purkinje neuron vulnerability through ion channel gene dysregulation in spinocerebellar ataxia type 1. *Hum. Mol. Genet.* 29, 3249–3265. doi: 10.1093/hmg/ddaa212

Clarke, L. E., Liddelow, S. A., Chakraborty, C., Münch, A. E., and Heiman, M. (2018). Normal aging induces A1-like astrocyte reactivity. *Proc. Natl. Acad. Sci. U. S. A.* 115, E1896–E1905.

Cocchi, E., Fabbri, C., Han, C., Lee, S. J., Patkar, A. A., Masand, P. S., et al. (2016). Genome-wide association study of antidepressant response: Involvement of the inorganic cation transmembrane transporter activity pathway. *BMC Psychiatry* 16:106. doi: 10.1186/s12888-016-0813-x

Custer, S. K., Garden, G. A., Gill, N., Rueb, U., Libby, R. T., Schultz, C., et al. (2006). Bergmann glia expression of polyglutamine-expanded ataxin-7 produces neurodegeneration by impairing glutamate transport. *Nat. Neurosci.* 9, 1302–1311. doi: 10.1038/nn1750

Cvetanovic, M. (2015). Decreased Expression of Glutamate Transporter GLAST in Bergmann Glia Is Associated with the Loss of Purkinje Neurons in the Spinocerebellar Ataxia Type 1. *Cerebellum* 14, 8–11. doi: 10.1007/s12311-014-0605-0

Cvetanovic, M., Ingram, M., Orr, H., and Opal, P. (2015). Early activation of microglia and astrocytes in mouse models of spinocerebellar ataxia type 1. *Neuroscience* 289, 289–299.

Cvetanovic, M., Patel, J. M., Marti, H. H., Kini, A. R., and Opal, P. (2011). Vascular endothelial growth factor ameliorates the ataxic phenotype in a mouse model of spinocerebellar ataxia type 1. *Nat. Med.* 17, 1445–1447. doi: 10.1038/nm.2494

D'Agostino, M., Scerra, G., Cannata Serio, M., Caporaso, M. G., Bonatti, S., and Renna, M. (2019). Unconventional secretion of α-Crystallin B requires the Autophagic pathway and is controlled by phosphorylation of its serine 59 residue. *Sci. Rep.* 9:16892. doi: 10.1038/s41598-019-53226-x

Dell'Orco, J. M., Wasserman, A. H., Chopra, R., Ingram, M. A. C., Hu, Y. S., Singh, V., et al. (2015). Neuronal Atrophy Early in Degenerative Ataxia Is a Compensatory Mechanism to Regulate Membrane Excitability. *J. Neurosci.* 35, 11292–11307. doi: 10.1523/JNEUROSCI.1357-15.2015

DelRosso, L. M., and Hoque, R. (2014). The cerebellum and sleep. *Neurol. Clin.* 32, 893–900. doi: 10.1016/j.ncl.2014.07.003

Diallo, A., Jacobi, H., Cook, A., Giunti, P., Parkinson, M. H., Labrum, R., et al. (2019). Prediction of Survival With Long- Term Disease Progression in Most Common Spinocerebellar Ataxia. *Mov. Disord.* 34, 1220–1227. doi: 10.1002/mds.27739

Diallo, A., Jacobi, H., Schmitz-Hubsch, T., Cook, A., Labrum, R., Durr, A., et al. (2017). Body Mass Index Decline Is Related to Spinocerebellar Ataxia Disease Progression. *Mov. Disord.* 4, 689–697. doi: 10.1002/mdc3.12522

Djukic, B., Casper, K. B., Philpot, B. D., Chin, L. S., and McCarthy, K. D. (2007). Conditional Knock-Out of Kir4.1 Leads to Glial Membrane Depolarization, Inhibition of Potassium and Glutamate Uptake, and Enhanced Short- Term

Synaptic Potentiation. *J. Neurosci.* 27, 11354–11365. doi: 10.1523/JNEUROSCI.0723-07.2007

Driessen, T. M., Lee, P. J., and Lim, J. (2018). Molecular pathway analysis towards understanding tissue vulnerability in spinocerebellar ataxia type 1. *Elife.* 7:e39981. doi: 10.7554/eLife.39981

Eiraku, M., Tohgo, A., Ono, K., Kaneko, M., Fujishima, K., Hirano, T., et al. (2005). DNER acts as a neuron-specific Notch ligand during Bergmann glial development. *Nat. Neurosci.* 8, 873–880. doi: 10.1038/nn1492

El Hajj, N., Dittrich, M., and Haaf, T. (2017). Epigenetic dysregulation of protocadherins in human disease. *Semin. Cell Dev. Biol.* 69, 172–182. doi: 10.1016/j.semcdb.2017.07.007

Escartin, C., Galea, E., Lakatos, A., O'Callaghan, J. P., Petzold, G. C., Serrano-Pozo, A., et al. (2021). Reactive astrocyte nomenclature, definitions, and future directions. *Nat. Neurosci.* 24, 312–325. doi: 10.1038/s41593-020-00783-4

Farmer, W. T., Chierzi, S., Lui, C., Zaelzer, C., Jones, E. V., Bally, B. P., et al. (2016). Neurons diversify astrocytes in the adult brain through sonic hedgehog signaling. *Science* 351, 849–854. doi: 10.1126/science.aab3103

Friedrich, J., Henzler, C., Orr, H. T., Friedrich, J., Kordasiewicz, H. B., Callaghan, B. O., et al. (2018). Antisense oligonucleotide–mediated ataxin-1 reduction prolongs survival in SCA1 mice and reveals disease- associated transcriptome profiles. *J. Clin. Investig.* 3:e123193. doi: 10.1172/jci.insight.123193

Funa, K., and Sasahara, M. (2014). The roles of PDGF in development and during neurogenesis in the normal and diseased nervous system. *J. Neuroimmune Pharmacol.* 9, 168–181. doi: 10.1007/s11481-013-9479-z

Furuichi, T., Shiraishi-Yamaguchi, Y., Sato, A., Sadakata, T., Huang, J., Shinoda, Y., et al. (2011). Systematizing and cloning of genes involved in the cerebellar cortex circuit development. *Neurochem. Res.* 36, 1241–1252. doi: 10.1007/s11064-011-0398-1

Gatchel, J. R., and Zoghbi, H. Y. (2005). Diseases of unstable repeat expansion: Mechanisms and common principles. *Nat. Rev. Genet.* 6, 743–755. doi: 10.1038/nrg1691

Grabert, K., Michoel, T., Karavolos, M. H., Clohisey, S., Baillie, J. K., Stevens, M. P., et al. (2016). Microglial brain region -dependent diversity and selective regional sensitivities to aging. *Nat. Neurosci.* 19:504. doi: 10.1038/nn.4222

Grosche, J., Matyash, V., Möller, T., Verkhratsky, A., Reichenbach, A., and Kettenmann, H. (1999). Microdomains for neuron–glia interaction?: Parallel fiber signaling to Bergmann glial cells. *Nat. Neurosci.* 2, 139–143. doi: 10.1038/5692

Habib, N., Avraham-Davidi, I., Basu, A., Burks, T., Shekhar, K., Hofree, M., et al. (2017). Massively parallel single- nucleus RNA-seq with DroNc-seq. *Nat. Methods* 14, 955–958. doi: 10.1038/nmeth.4407

Heneka, M. T., Kummer, M. P., and Latz, E. (2014). Innate immune activation in neurodegenerative disease. *Nat. Rev. Immunol.* 14, 463–477.

Herculano-Houzel, S. (2014). The Glia / Neuron Ratio?: How it Varies Uniformly Across Brain Structures and Species and What that Means for Brain Physiology and Evolution. *Glia* 62, 1377–1391. doi: 10.1002/glia.22683

Hook, G., Jacobsen, J. S., Grabstein, K., Kindy, M., and Hook, V. (2015). Cathepsin B is a new drug target for traumatic brain injury therapeutics: Evidence for E64d as a promising lead drug candidate. *Front. Neurol.* 6:178. doi: 10.3389/fneur.2015.00178

Ingram, M., Wozniak, E. A. L., Duvick, L., Yang, R., Bergmann, P., Carson, R., et al. (2016a). Cerebellar Transcriptome Profiles of ATXN1 Transgenic Mice Reveal SCA1 Disease Progression and Protection Pathways. *Neuron* 89, 1194–1207. doi: 10.1016/j.neuron.2016.02.011

Ingram, M., Wozniak, E. A. L., Duvick, L., Zoghbi, H. Y., Henzler, C., and Orr, H. T. (2016b). Cerebellar Transcriptome Profiles of ATXN1 Transgenic Mice Reveal SCA1 Disease Progression and Protection Pathways. *Neuron* 89, 1194–1207. doi: 10.1016/j.neuron.2016.02.011

Jacobi, H., Reetz, K., du Montcel, S. T., Bauer, P., Mariotti, C., Nanetti, L., et al. (2013). Biological and clinical characteristics of individuals at risk for spinocerebellar ataxia types 1, 2, 3, and 6 in the longitudinal RISCA study: Analysis of baseline data. *Lancet Neurol.* 12, 650–658. doi: 10.1016/S1474-4422(13)70104-2

Janeczko, K. (1993). Co-expression of gfap and vimentin in astrocytes proliferating in response to injury in the mouse cerebral hemisphere. A combined autoradiographic and double immunocytochemical study. *Int. J. Dev. Neurosci.* 11, 139–147. doi: 10.1016/0736-5748(93)90074-n

Kaur, G., and Levy, E. (2012). Cystatin C in Alzheimer's disease. *Front. Mol. Neurosci.* 5:79. doi: 10.3389/fnmol.2012.00079

Kim, J. H., Lukowicz, A., Qu, W., Johnson, A., and Cvetanovic, M. (2018). Astroglia contribute to the pathogenesis of spinocerebellar ataxia Type 1 (SCA1) in a biphasic, stage-of-disease specific manner. *Glia* 66, 1972–1987. doi: 10.1002/glia.23451

Klein, A. M., Mazutis, L., Akartuna, I., Tallapragada, N., Veres, A., Li, V., et al. (2015). Droplet barcoding for single-cell transcriptomics applied to embryonic stem cells. *Cell* 161, 1187–1201. doi: 10.1016/j.cell.2015.04.044

Kofuji, P., and Newman, E. A. (2004). Potassium buffering in the central nervous system. *Neuroscience* 129, 1045–1056.

Kozareva, V., Martin, C., Osorno, T., Rudolph, S., Guo, C., Vanderburg, C., et al. (2020). A transcriptomic atlas of the mouse cerebellum reveals regional specializations and novel cell types. *Biorxiv* [Preprint]. doi: 10.1101/2020.03.04.976407

Kuipers, H. F., Yoon, J., Van Horssen, J., Han, M. H., Bollyky, P. L., Palmer, T. D., et al. (2017). Phosphorylation of αB- crystallin supports reactive astrogliosis in demyelination. *Proc. Natl. Acad. Sci. U. S. A.* 114, E1745–E1754. doi: 10.1073/pnas.1621314114

Lacar, B., Linker, S. B., Jaeger, B. N., Krishnaswami, S., Barron, J., Kelder, M., et al. (2016). Nuclear RNA-seq of single neurons reveals molecular signatures of activation. *Nat. Commun.* 7:11022.

Liddelow, S. A., Guttenplan, K. A., Clarke, L. E., Bennett, F. C., Bohlen, C. J., Schirmer, L., et al. (2017). Neurotoxic reactive astrocytes are induced by activated microglia. *Nature* 541, 481–487. doi: 10.1038/nature21029

Liu, C. J., Rainwater, O., Clark, H. B., Orr, H. T., and Akkin, T. (2018). Polarization-sensitive optical coherence tomography reveals gray matter and white matter atrophy in SCA1 mouse models. *Neurobiol. Dis.* 116, 69–77. doi: 10.1016/j.nbd.2018.05.003

Liu, Y., Zhou, Q., Tang, M., Fu, N., Shao, W., Zhang, S., et al. (2015). Upregulation of alphaB-crystallin expression in the substantia nigra of patients with Parkinson's disease. *Neurobiol. Aging* 36, 1686–1691. doi: 10.1016/j.neurobiolaging.2015.01.015

Lobsiger, C. S., and Cleveland, D. W. (2007). Glial cells as intrinsic components of non-cell-autonomous neurodegenerative disease. *Nat. Neurosci.* 10, 1355–1360. doi: 10.1038/nn1988

Maria del Pilar, C. L., Marianna, S., Giusy, T., Shana, C., Defillipi, P., and Cabodi, S. (2017). P130CAS/BCAR1 scaffold protein in tissue homeostasis and pathogenesis. *Physiol. Behav.* 176, 139–148.

Mathis, C., Collin, L., and Borrelli, E. (2003). Oligodendrocyte ablation impairs cerebellum development. *Development* 130, 4709–4718.

Matson, K. J. E., Sathyamurthy, A., Johnson, K. R., Kelly, M. C., Kelley, M. W., and Levine, A. J. (2018). Isolation of adult spinal cord nuclei for massively parallel single-nucleus RNA sequencing. *J. Vis. Exp.* 2018:58413. doi: 10.3791/58413

Matsuda, K., Matsuda, S., Gladding, C. M., and Yuzaki, M. (2006). Characterization of the δ2 glutamate receptor- binding protein delphilin: Splicing variants with differential palmitoylation and an additional PDZ domain. *J. Biol. Chem.* 281, 25577–25587. doi: 10.1074/jbc.M602044200

McKenzie, I. A., Ohayon, D., Li, H., De Faria, J. P., Emery, B., Tohyama, K., et al. (2014). Motor skill learning requires active central myelination. *Science* 346, 318–322. doi: 10.1126/science.1254960

Mei, L., and Xiong, W. C. (2008). Neuregulin 1 in neural development, synaptic plasticity and schizophrenia. *Nat. Rev. Neurosci.* 9, 437–452.

Mellesmoen, A., Sheeler, C., Ferro, A., Rainwater, O., and Cvetanovic, M. (2018). Brain derived neurotrophic factor (BDNF) delays onset of pathogenesis in transgenic mouse model of spinocerebellar ataxia type 1 (SCA1). *Front. Cell. Neurosci.* 12:509. doi: 10.3389/fncel.2018.00509

Miyazaki, T., Yamasaki, M., Hashimoto, K., Kohda, K., Yuzaki, M., Shimamoto, K., et al. (2017). Glutamate transporter GLAST controls synaptic wrapping by Bergmann glia and ensures proper wiring of Purkinje cells. *Proc. Natl. Acad. Sci. U. S. A.* 114, 7438–7443. doi: 10.1073/pnas.1617330114

Moon, S., and Zhao, Y.-T. (2021). Spatial, temporal and cell-type-specific expression profiles of genes encoding heparan sulfate biosynthesis enzymes and proteoglycan core proteins. *Glycobiology* 31, 1308–1318. doi: 10.1093/glycob/cwab054

Moriarty, A., Cook, A., Hunt, H., Adams, M. E., Cipolotti, L., and Giunti, P. (2016). A longitudinal investigation into cognition and disease progression in spinocerebellar ataxia types 1, 2, 3, 6, and 7. *Orphanet J. Rare Dis.* 11:82. doi: 10.1186/s13023-016-0447

National Research Council (Us) Committee for the Update of the Guide for the Care and Use of Laboratory Animals (2011). *Guide for the Care and Use of Laboratory Animals*, 8th Edn. Washington, DC: National Academies Press.

Ng, S. Y., Bogu, G. K., Soh, B. S., and Stanton, L. W. (2013). The long noncoding RNA RMST interacts with SOX2 to regulate neurogenesis. *Mol. Cell.* 51, 349–359. doi: 10.1016/j.molcel.2013.07.017

Nicita, F., Tasca, G., Nardella, M., Bellacchio, E., Camponeschi, I., Vasco, G., et al. (2018). Novel Homozygous KCNJ10 Mutation in a Patient with Non-syndromic Early-Onset Cerebellar Ataxia. *Cerebellum* 17, 499–503. doi: 10.1007/s12311-018-0924-7

O'Leary, L. A., Davoli, M. A., Belliveau, C., Tanti, A., Ma, J. C., Farmer, W. T., et al. (2020). Characterization of Vimentin- Immunoreactive Astrocytes in the Human Brain. *Front. Neuroanat.* 14:31. doi: 10.3389/fnana.2020.00031

Ophir, G., Meilin, S., Efrati, M., Chapman, J., Karussis, D., Roses, A., et al. (2003). Human apoE3 but not apoE4 rescues impaired astrocyte activation in apoE null mice. *Neurobiol. Dis.* 12, 56–64.

Orr, H. T., and Zoghbi, H. Y. (2007). Trinucleotide Repeat Disorders. *Annu. Rev. Neurosci.* 30, 575–621.

Orr, H. T., Chung, M. Y., Banfi, S., Kwiatkowski, T. J. Jr., Servadio, A., Beaudet, A. L., et al. (1993). Expansion of an unstable trinucleotide CAG repeat in spinocerebellar ataxia type 1. *Nat. Genet.* 4, 221–226.

Ousman, S. S., Tomooka, B. H., Van Noort, J. M., Wawrousek, E. F., O'Conner, K., Hafler, D. A., et al. (2007). Protective and therapeutic role for αB-crystallin in autoimmune demyelination. *Nature* 448, 474–479. doi: 10.1038/nature05935

Parcerisas, A., Ortega-Gascó, A., Pujadas, L., and Soriano, E. (2021). The hidden side of ncam family: Ncam2, a key cytoskeleton organization molecule regulating multiple neural functions. *Int. J. Mol. Sci.* 22:10021. doi: 10.3390/ijms221810021

Park, Y. W., Joers, J. M., Guo, B., Hutter, D., Bushara, K., Adanyeguh, I. M., et al. (2020). Assessment of Cerebral and Cerebellar White Matter Microstructure in Spinocerebellar Ataxias 1, 2, 3, and 6 Using Diffusion MRI. *Front. Neurol.* 11:411. doi: 10.3389/fneur.2020.00411

Parkhurst, C. N., Yang, G., Ninan, I., Savas, J. N., Yates, J. R., Lafaille, J. J., et al. (2013). Microglia promote learning- dependent synapse formation through brain-derived neurotrophic factor. *Cell* 155, 1596–1609. doi: 10.1016/j.cell.2013.11.030

Pedroso, J. L., Braga-Neto, P., Felício, A. C., Aquino, C. C. H., do Prado, L. F. B., do Prado, G. F., et al. (2011). Sleep disorders in cerebellar ataxias. *Arq. Neuropsiquiatr.* 69, 253–257.

Pekny, M., Wilhelmsson, U., and Pekna, M. (2014). The dual role of astrocyte activation and reactive gliosis. *Neurosci. Lett.* 565, 30–38. doi: 10.1016/j.neulet.2013.12.071

Perea, G., Sur, M., and Araque, A. (2014). Neuron-glia networks: Integral gear of brain function. *Front. Cell. Neurosci.* 8:378. doi: 10.3389/fncel.2014.00378

Robeck, T., Skryabin, B. V., Rozhdestvensky, T. S., Skryabin, A. B., and Brosius, J. (2016). BC1 RNA motifs required for dendritic transport in vivo. *Sci. Rep.* 6:28300. doi: 10.1038/srep28300

Rosa, J., Hamel, K., Sheeler, C., Borgenheimer, E., Soles, A., Ghannoum, F., et al. (2021). Early stage of Spinocerebellar Ataxia Type 1 (SCA1) progression exhibits region- and cell-specific pathology and is partially ameliorated by Brain Derived Neurotrophic Factor (BDNF). *Biorxiv* [Preprint]. doi: 10.1101/2021.09.13.460129

Rothstein, J., Dykes-Hoberg, M., Pardo, C., Bristol, L., Jin, L., Kuncl, R., et al. (1996). Antisense knockout of glutamate transporters reveals a predominant role for astroglial glutamate transport in excitotoxicity and clearance of extracellular glutamate. *Neuron* 16, 675–686. doi: 10.1016/s0896-6273(00)80086-0

Rüb, U., Schöls, L., Paulson, H., Auburger, G., Kermer, P., Jen, J. C., et al. (2013). Clinical features, neurogenetics and neuropathology of the polyglutamine spinocerebellar ataxias type 1, 2, 3, 6 and 7. *Prog. Neurobiol.* 104, 38–66. doi: 10.1016/j.pneurobio.2013.01.001

Sakers, K., Liu, Y., Llaci, L., Lee, S. M., Vasek, M. J., Rieger, M. A., et al. (2021). Loss of Quaking RNA binding protein disrupts the expression of genes associated with astrocyte maturation in mouse brain. *Nat. Commun.* 12:1537. doi: 10.1038/s41467-021-21703-5

Saunders, A., Macosko, E. Z., Wysoker, A., Goldman, M., Krienen, F. M., de Rivera, H., et al. (2018). Molecular Diversity and Specializations among the Cells of the Adult Mouse Brain. *Cell* 174, 1015–1030.e16. doi: 10.1016/j.cell.2018.07.028

Sen, A., Nelson, T. J., and Alkon, D. L. (2017). ApoE isoforms differentially regulates cleavage and secretion of BDNF. *Mol. Brain* 10:19. doi: 10.1186/s13041-017-0301-3

Serra, H. G., Byam, C. E., Lande, J. D., Tousey, S. K., Zoghbi, H. Y., and Orr, H. T. (2004). Gene profiling links SCA1 pathophysiology to glutamate signaling in Purkinje cells of transgenic mice. *Hum. Mol. Genet.* 13, 2535–2543. doi: 10.1093/hmg/ddh268

Serra, H. G., Duvick, L., Zu, T., Carlson, K., Stevens, S., Jorgensen, N., et al. (2006). ROR a -Mediated Purkinje Cell Development Determines Disease Severity in Adult SCA1 Mice. *Cell* 1, 697–708. doi: 10.1016/j.cell.2006.09.036

Servadio, A., Koshy, B., Armstrong, D., Antalffy, B., Orr, H. T., and Zoghbi, H. Y. (1995). Expression analysis of the ataxin-1 protein in tissues from normal and spinocerebellar ataxia type 1 individuals. *Nat. Genet.* 10, 94–98.

Sheeler, C., Rosa, J., Borgenheimer, E., Mellesmoen, A., and Rainwater, O. (2021). Post-symptomatic Delivery of Brain- Derived Neurotrophic Factor (BDNF) Ameliorates Spinocerebellar Ataxia Type 1 (SCA1) Pathogenesis. *Cerebellum* 20, 420–429. doi: 10.1007/s12311-020-01226-3

Sheeler, C., Rosa, J., Ferro, A., Mcadams, B., Borgenheimer, E., and Cvetanovic, M. (2020). Glia in Neurodegeneration?:The Housekeeper, the Defender and the Perpetrator. *Int. J. Mol. Sci.* 21:9188. doi: 10.3390/ijms21239188

Sochacka, M., Opalinski, L., Szymczyk, J., Zimoch, M. B., Czyrek, A., Krowarsch, D., et al. (2020). FHF1 is a bona fide fibroblast growth factor that activates cellular signaling in FGFR-dependent manner. *Cell Commun. Signal.* 18:69. doi: 10.1186/s12964-020-00573-2

Soreq, L., Brain, U. K. C., North American, B. E., Rose, J., Patani, R., and Ule, J. (2017). Major Shifts in Glial Regional Identity Are a Transcriptional Hallmark of Human Brain Aging. *Cell Rep.* 18, 557–570. doi: 10.1016/j.celrep.2016.12.011

Tafti, M., and Ghyselinck, N. B. (2007). Functional implication of the vitamin A signaling pathway in the brain. *Arch. Neurol.* 64, 1706–1711.

Tejwani, L., Ravindra, N. G., Nguyen, B., Luttik, K., Lee, C., Gionco, J., et al. (2021). Longitudinal single-cell transcriptional dynamics throughout neurodegeneration in SCA1. *Biorxiv* [Preprint]. doi: 10.1101/2021.10.22.465444

Tohgo, A., Eiraku, M., Miyazaki, T., Miura, E., Kawaguchi, S. Y., Nishi, M., et al. (2006). Impaired cerebellar functions in mutant mice lacking DNER. *Mol. Cell. Neurosci.* 31, 326–333. doi: 10.1016/j.mcn.2005.10.003

Tsai, H. F., Chang, Y. C., Li, C. H., Chan, M. H., Chen, C. L., Tsai, W. C., et al. (2021). Type V collagen alpha 1 chain promotes the malignancy of glioblastoma through PPRC1-ESM1 axis activation and extracellular matrix remodeling. *Cell Death Discov.* 7:313. doi: 10.1038/s41420-021-00661-3

Verkhratsky, A., and Nedergaard, M. (2018). Physiology of Astroglia. *Physiol. Rev.* 98, 239–389.

Wang, X., Allen, M., Li, S., Quicksall, Z. S., Patel, T. A., Carnwath, T. P., et al. (2020). Deciphering cellular transcriptional alterations in Alzheimer's disease brains. *Mol. Neurodegener.* 15:38.

White, J. J., Bosman, L. W. J., Blot, F. G. C., Osório, C., Kuppens, B. W., Krijnen, W. H. J. J., et al. (2021). Region-specific preservation of Purkinje cell morphology and motor behavior in the ATXN1[82Q] mouse model of spinocerebellar ataxia 1. *Brain Pathol.* 31:e12946. doi: 10.1111/bpa.12946

Wieczorek, L., Majumdar, D., Wills, T. A., Hu, L., Winder, D. G., Webb, D. J., et al. (2012). Absence of Ca 2+-stimulated adenylyl cyclases leads to reduced synaptic plasticity and impaired experience-dependent fear memory. *Transl. Psychiatry* 2:e126. doi: 10.1038/tp.2012.50

Xin, W., Mironova, Y. A., Shen, H., Marino, R. A. M., Waisman, A., Lamers, W. H., et al. (2019). Oligodendrocytes Support Neuronal Glutamatergic Transmission via Expression of Glutamine Synthetase. *Cell Rep.* 27, 2262–2271.e5. doi: 10.1016/j.celrep.2019.04.094

Zawişlak, A., Jakimowicz, P., McCubrey, J. A., and Rakus, D. (2017). Neuron-derived transthyretin modulates astrocytic glycolysis in hormone-independent manner. *Oncotarget* 8, 106625–106638. doi: 10.18632/oncotarget.22542

Zhang, Y., Wang, J., Liu, X., and Liu, H. (2020). Exploring the role of RALYL in Alzheimer's disease reserve by network- based approaches. *Alzheimers Res. Ther.* 12:165. doi: 10.1186/s13195-020-00733-z

Zhong, J., Chuang, S. C., Bianchi, R., Zhao, W., Lee, H., Fenton, A. A., et al. (2009). BC1 regulation of metabotropic glutamate receptor-mediated neuronal excitability. *J. Neurosci.* 29, 9977–9986. doi: 10.1523/JNEUROSCI.3893-08.2009

Zhou, H., Lin, Z., Voges, K., Ju, C., Gao, Z., Bosman, L. W. J., et al. (2014). Cerebellar modules operate at different frequencies. *Elife.* 3:e02536.

Zhou, L., Tang, X., Li, X., Bai, Y., Buxbaum, J. N., and Chen, G. (2019). Identification of transthyretin as a novel interacting partner for the δ subunit of GABA A receptors. *PLoS One* 14:e0210094. doi: 10.1371/journal.pone.0210094

Zilionis, R., Nainys, J., Veres, A., Savova, V., Zemmour, D., Klein, A. M., et al. (2017). Single-cell barcoding and sequencing using droplet microfluidics. *Nat. Protoc.* 12, 44–73.

Zou, J., Chen, Z., Wei, X., Chen, Z., Fu, Y., Yang, X., et al. (2017). Cystatin C as a potential therapeutic mediator against Parkinson's disease via VEGF-induced angiogenesis and enhanced neuronal autophagy in neurovascular units. *Cell Death Dis.* 8:e2854. doi: 10.1038/cddis.2017.240

Zu, T., Duvick, L. A., Kaytor, M. D., Berlinger, M. S., Zoghbi, H. Y., Clark, H. B., et al. (2004). Recovery from polyglutamine- induced neurodegeneration in conditional SCA1 transgenic mice. *J. Neurosci.* 24, 8853–8861. doi: 10.1523/JNEUROSCI.2978-04.2004

Frontiers in
Systems Neuroscience

Advances our understanding of whole systems of the brain

Part of the most cited neuroscience journal series, this journal explores the architecture of brain systems and information processing, storage and retrieval.

Discover the latest Research Topics

See more →

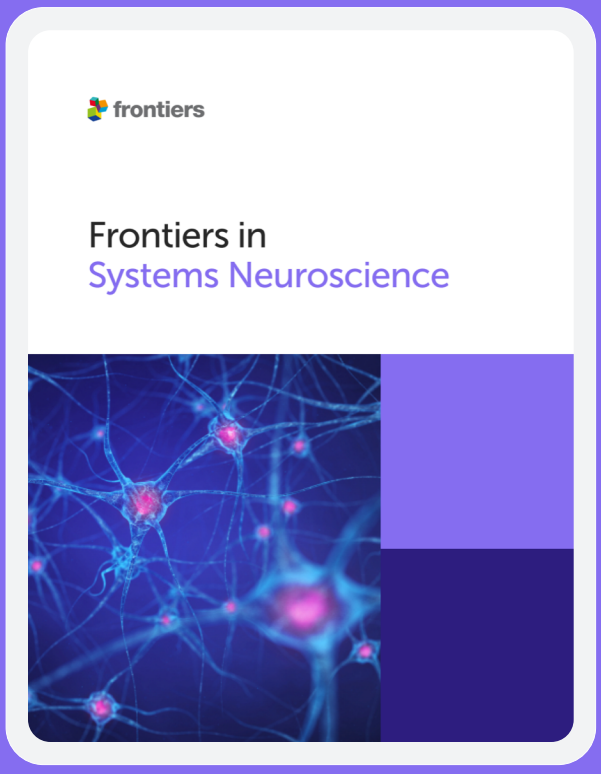

Frontiers

Avenue du Tribunal-Fédéral 34
1005 Lausanne, Switzerland
frontiersin.org

Contact us

+41 (0)21 510 17 00
frontiersin.org/about/contact